FZM-4572

17 FEBRUARY 1966

GPO PRICE $ _____

CFSTI PRICE(S) $ _____

Hard copy (HC) $7.00

Microfiche (MF) $2.00

ff 653 July 65

A STUDY OF
JUPITER FLYBY MISSIONS

N66-20904 (ACCESSION NUMBER)

377 (PAGES)

CR 71294 (NASA CR OR TMX OR AD NUMBER)

1 (THRU)

(CODE)

30 (CATEGORY)

FACILITY FORM 602

MID-TERM TECHNICAL PROGRESS REPORT

GENERAL DYNAMICS

Fort Worth Division

RE-ORDER NO. 66-101

FZM-4572
17 February 1966

NASA CR71294

MID-TERM TECHNICAL REPORT

OF

A STUDY OF JUPITER FLYBY MISSIONS

Prepared for

The Jet Propulsion Laboratory
California Institute of Technology
Pasadena, California

on

JPL Contract No. 951285

GENERAL DYNAMICS
Fort Worth Division

F O R E W O R D

This document is the Mid-Term Technical Report on a Study of Jupiter Flyby Missions. The study is being conducted by the Fort Worth Division of General Dynamics for the Jet Propulsion Laboratory of the California Institute of Technology on JPL Contract No. 961285, a subcontract under the National Aeronautics and Space Administration prime contract NAS7-100.

A C K N O W L E D G E M E N T S

Listed below are the personnel of the Fort Worth Division of General Dynamics who made primary contributions in the technical areas indicated:

L. E. Hove	Project Leader
G. F. Gibson	Spacecraft System Integration and Configuration Design
B. J. Csaszar	Configuration Design
J. C. Redmond	Science Subsystem Definition
B. A. Sodek	Science Subsystem Definition
S. W. Wilson	Mission Analysis
M. C. Poteet	Trajectory Analysis
E. R. Conrad	Communications Subsystem Studies
H. A. Shubert	Spacecraft Antenna Studies
C. D. Campebll	Data Management Subsystem Studies
M. B. Veal	Navigation & Guidance and Spacecraft Control Subsystem Studies
B. J. Ward	Spacecraft Control Subsystem Studies
C. W. Heller	Spacecraft Computer and Sequential Studies
G. P. Breaux	Attitude Control Studies
J. A. McCabe	Propulsion Subsystem Studies
J. S. Turner	Electrical Power Subsystem Studies
R. A. Knezek	Thermal Control Studies
D. E. Croy	Thermal Control Studies
L. E. Heyduck	Meteoroid Penetration Protection Studies

Professor Harlan J. Smith, Head of the Department of Astronomy at The University of Texas, contributed to the study in the role of consultant on Science Subsystem Definition.

TABLE OF CONTENTS

	Page
FOREWORD	
ACKNOWLEDGEMENTS	
SECTION 1 INTRODUCTION	1-1
1.1 Definition of Task	1-1
1.2 Constraints	1-2
1.3 Technical Approach	1-3
1.3.1 Mission Planning	1-3
1.3.2 Spacecraft Systems Design and Analysis	1-5
1.3.3 Spacecraft Concept Evaluation	1-5
1.4 Summary of Status and Results	1-6
SECTION 2 MISSION PLANNING	2-1
2.1 Science Subsystem Definition	2-1
2.1.1 Summary of Observations of the Planet Jupiter	2-1
2.1.2 Magnetic Field Measurements	2-5
2.1.3 The Detection of Charged Particles in Interplanetary and Planetary Regions	2-7
2.1.4 Solar Plasma Measurements	2-19
2.1.5 Cosmic Dust Measurements	2-21
2.1.6 Television	2-24
2.1.7 Photometric, Spectrometric, and Radiometric Measurements	2-28
2.1.8 Radio and Radar	2-33
2.1.9 Miscellaneous	2-34
2.1.10 Scientific Instrument Characteristics	2-35
2.1.11 Typical Mission Payloads	2-35
2.1.12 References	2-42

		Page
2.2	Energy Requirements and General Trajectory Characteristics	2-43
2.2.1	Launch Window Definition	2-43
2.2.2	Arrival Date Corrections	2-45
2.2.3	Mission Planning Charts	2-47
2.2.4	Conclusions	2-58
2.2.5	References	2-59
2.3	Launch Vehicle Evaluation	2-60
2.3.1	Basic Payload Capabilities	2-60
2.3.2	Payload Capabilities for Jupiter Missions	2-65
2.3.3	References	2-65
2.4	Detailed Mission Profile Analysis	2-79
2.4.1	Departure Phase	2-79
2.4.2	Heliocentric Phase	2-80
2.4.3	Encounter Phase	2-81
2.4.4	Post-Encounter Phase	2-81
2.4.5	References	2-81
SECTION 3	SPACECRAFT SYSTEMS DESIGN AND ANALYSIS	3-1
3.1	Communications	3-1
3.1.1	Functional Requirements	3-1
3.1.2	Identification of Trade-offs	3-2
3.1.3	Conclusions	3-13
3.1.4	References	3-14
3.2	Data Management	3-16
3.2.1	Functional Requirements	3-16
3.2.2	Possible Concepts	3-18
3.2.3	Analysés	3-19
3.2.4	Results	3-27
3.2.5	Conclusions	3-28
3.2.6	References	3-29

		Page
3.3	Spacecraft Control	3-31
3.3.1	Spacecraft Control Operations	3-32
3.3.2	Design of the Central Computer and Sequence	3-34
3.3.3	Design of the Attitude Control Electronics	3-36
3.3.4	Theory of Attitude Determination	3-37
3.4	Navigation and Guidance	3-41
3.4.1	The Guidance Requirement	3-41
3.4.2	Performance Analysis	3-42
3.4.3	Guidance Analysis	3-46
3.4.4	Self-Contained Terminal Navigation	3-49
3.5	Attitude Control	3-54
3.5.1	Configuration Concepts	3-54
3.5.2	Nominal Trajectory Characteristics	3-57
3.5.3	Considerations for Spin-Stabilization	3-60
3.5.4	Design Data for Gas Jet System	3-65
3.5.5	Design Data for Reaction Wheel System	3-67
3.5.6	Considerations for Three-Axis Stabilization	3-69
3.6	Propulsion	3-76
3.6.1	Midcourse Propulsion Subsystem	3-76
3.6.2	Attitude Control Propulsion Subsystem	3-95
3.7	Auxiliary Electric Power System	3-104
3.7.1	Scope and Requirements	3-104
3.7.2	Raw Power Generation	3-104
3.7.3	Power Management System	3-108
3.7.4	Energy Storage	3-115
3.7.5	Recommended Configuration	3-115
3.7.6	References	3-116
3.8	Thermal Control	3-117
3.8.1	Component Thermal Control Requirements	3-117
3.8.2	Concept Synthesis	3-117
3.8.3	Reference	3-123

		Page
3.9	Radiation Protection	3-125
3.10	Meteoroid Penetration Protection	3-126
3.10.1	Basic Relationships	3-126
3.10.2	Meteoroid Environment	3-128
3.10.3	Parametric Analysis	3-132
3.10.4	References	3-133
3.11	Structure	3-134
3.12	Configuration	3-134
3.13	Reliability	3-134
SECTION 4	SPACECRAFT CONCEPT EVALUATION	4-1
SECTION 5	SPACECRAFT DESIGN CONCEPTS	5-1
5.1	Spacecraft Design Concept A	5-1
5.1.1	Design Summary	5-1
5.1.2	Subsystem Design Information	5-3
5.2	Spacecraft Design Concept B	5-26
5.2.1	Design Summary	5-26
5.2.2	Subsystem Design Information	5-28
5.3	Spacecraft Design Concept C	5-46
5.3.1	Design Summary	5-46
5.3.2	Subsystem Design Information	5-48
5.4	Spacecraft Design Concept D	5-59
5.4.1	Design Summary	5-59
5.4.2	Subsystem Design Information	5-61
5.4.3	Reference	5-77
APPENDIX A - MISSION MAPS		A-1
APPENDIX B - METEROID DAMAGE TO SPACECRAFT ANTENNAS		B-1

Page

APPENDIX C - PARAMETRIC ANALYSIS OF THE BASIC HYDRAZINE PROPULSION SUBSYSTEM C-1

APPENDIX D - PARAMETRIC ANALYSIS OF A COLD GAS ATTITUDE CONTROL PROPULSION SUBSYSTEM D-1

LIST OF FIGURES

Number	Title	Page
1.3-1	Technical Approach	1-4
2.2-1	Launch Window Definition	2-44
2.2-2	Injection Energy as a Function of Window Width	2-44
2.2-3	Typical Launch Corridor	2-46
2.2-4	Jupiter Arrival Date Corrections	2-47
2.2-5	Mission Planning Chart, 1973 Launch	2-48
2.2-6	Mission Planning Chart, 1974 Launch	2-49
2.2-7	Mission Planning Chart, 1975 Launch	2-50
2.2-8	Mission Planning Chart, 1976 Launch	2-51
2.2-9	Mission Planning Chart, 1977 Launch	2-52
2.2-10	Mission Planning Chart, 1978 Launch	2-53
2.2-11	Mission Planning Chart, 1979 Launch	2-54
2.2-12	Mission Planning Chart, 1980 Launch	2-55
2.3-1	Summary of Launch Vehicle Payload Capability	2-61
2.3-2	Payload Curve Adjustments	2-63
2.3-3	Payload vs Flight Time,1973 Launch	2-66
2.3-4	Payload vs Flight Time,1974 Launch	2-67
2.3-5	Payload vs Flight Time,1975 Launch	2-68
2.3-6	Payload vs Flight Time, 1976 Launch	2-69
2.3-7	Payload vs Flight Time, 1977 Launch	2-70
2.3-8	Payload vs Flight Time, 1978 Launch	2-71

LIST OF FIGURES (Continued)

Number	Title	Page
2.3-9	Payload vs Flight Time, 1979 Launch	2-72
2.3-10	Payload vs Flight Time, 1980 Launch	2-73
2.3-11	Jupiter Mission Payload Capability, Saturn V/Centaur	2-74
2.3-12	Jupiter Mission Payload Capability, Saturn V	2-75
2.3-13	Jupiter Mission Payload Capability, Saturn IB/Centaur/HEKS	2-76
2.3-14	Jupiter Mission Payload Capability, Titan IIICx/Centaur	2-77
2.3-15	Jupiter Mission Payload Capability, Atlas SLV3x/Centaur/HEKS	2-78
2.4-1	Geocentric Distance vs Time, Typical Departure Trajectories	2-79
2.4-2	Heliocentric Geometry, Typical 500-Day Mission	2-80
2.4-3	Communications Parameters History, Spin-Stabilized Spacecraft, 1976 500-Day Mission	2-82
2.4-4	Communication Parameters History, Spin-Stabilized Spacecraft, 1974 600-Day Mission	2-83
2.4-5	Communications Summary, Spin-Stabilized Spacecraft, 1974 600-Day Mission	2-84
2.4-6	Jovicentric Distance vs Time, Typical Encounter Trajectories	2-85
2.4-7	Geometry of Typical Encounter Trajectories	2-86
3.1-1	Communications Interfaces	3-2
3.1-2	Communications Subsystem Trade-offs	3-3
3.1-3	Gain of Antennas with Toroidal Patterns	3-5

LIST OF FIGURES (Continued)

Number	Title	Page
3.1-4	Antenna Pointing Accuracy	3-11
3.1-5	Earth-Sun Position	3-11
3.1-6	PSK Transmission Chart	3-13
3.2-1	Data Management Subsystem	3-16
3.2-2	Fan Data Compression Technique	3-20
3.2-3	Zero Order Interpolator Data Compression Technique	3-22
3.2-4	Quantile Data Compression Technique	3-22
3.2-5	Stop-Scan Edge Detector Data Compression Technique	3-24
3.2-6	Ground Telemetry Demodulator	3-26
3.2-7	Command Word Format	3-27
3.3-1	Typical Mechanization-Central Computer and Sequencer	3-35
3.3-2	Typical Attitude Control Electronics	3-38
3.3-3	Determination of Spacecraft Heliocentric Attitude	3-39
3.4-1	Injection and Vernier Correction Geometry	3-44
3.4-2	Terminal Maneuver Geometry	3-45
3.4-3	State Estimation Flow Diagram	3-51
3.4-4	Self Contained Terminal Navigation (Sixteen Observations Per Day)	3-53
3.4-5	Self Contained Terminal Navigation (Thirty-Two Observations Per Day)	3-53
3.5-1	Configuration Concepts	3-55
3.5-2	Orbit Radius and Solar Pressure	3-59
3.5-3	Solar Aspect Angle for Earth Orientation	3-59

LIST OF FIGURES (Continued)

Number	Title	Page
3.5-4	Meteoroid Approach Conditions	3-60
3.5-5	Spin-Rate Limitations	3-62
3.5-6	Spin-Axis Precession Due to Solar Pressure	3-64
3.5-7	Allowable Moment - Area Unbalance	3-64
3.5-8	Limit-Cycle Characteristics	3-66
3.5-9	Reaction Wheel Design Data	3-68
3.5-10	Torque Due to Solar Pressure	3-70
3.5-11	Integrated Angular Momentum Due to Solar Pressure	3-71
3.5-12	Angular Impulse Due to Meteoroid Impact	3-74
3.6-1	Schematic Diagram of the Basic Hydrazine Subsystem	3-81
3.6-2	Weight of Hydrazine Required vs Total Propulsion Subsystem Weight	3-87
3.6-3	Spherical Tank Diameter vs Weight of Hydrazine Required	3-88
3.6-4	Propulsion Subsystem Weight vs Payload Weight	3-92
3.6-5	Propulsion Subsystem Weight vs Payload Weight	3-93
3.6-6	Propulsion Subsystem Weight vs Payload Weight	3-94
3.6-7	Propulsion System Concepts for Spacecraft Attitude Control	3-96
3.6-8	Schematic Diagram of Cold Gas Propulsion Subsystem - Configuration A	3-97
3.6-9	Schematic Diagram of Cold Gas Propulsion Subsystem - Configuration B	3-98

LIST OF FIGURES (Continued)

Number	Title	Page
3.6-10	Attitude Control Subsystem Weight vs Total Impulse Required	3-103
3.7-1	Requirement Schedule and AEC Programs	3-105
3.7-2	Thermocouple Interconnections	3-109
3.7-3	Thermocouple Failure Effects	3-110
3.7-4	Systems Configurations	3-111
3.7-5	McMurray-Bedford Inverter Circuit	3-112
3.7-6	Electric Power System Schematic Diagram	3-114
3.8-1	Estimated Louver Performance	3-120
3.8-2	Effect of Coating Properties on Thermal Control of Isothermal Module - Spacecraft Concept A	3-121
3.8-3	Effect of Solar Distance on Thermal Control of Isothermal Module Design with no Sidewall Insulation	3-122
3.8-4	Effect of Solar Distance on Thermal Control of Isothermal Module Design with no Sidewall Insulation	3-122
3.8-5	Effect of Deviation from Nominal Value of Emissivity on Heat Balance	3-124
3.8-6	Effect of Deviation from Nominal Value of Solar Absorptivity on Solar Heating	3-124
3.10-1	Meteoroid Velocity Determination	3-130
3.10-2	Summary of Meteoroid Environment	3-133
5.1-1	Spacecraft Design Concept A Configuration	5-2
5.1-2	Design Concept A Communications Subsystem	5-6

LIST OF FIGURES (Continued)

Number	Title	Page
5.1-3	Design Concept A Data Automation Element	5-10
5.1-4	Data Encoder Element for Design Concepts A, B, and C	5-12
5.1-5	Data Storage Element for Design Concepts A, B, C, and D	5-14
5.1-6	Command Detection Subelement for Design Concepts A, B, C, and D	5-15
5.1-7	Command Decoder Subelement for Design Concepts A, B, C, and D	5-16
5.2-1	Spacecraft Design Concept B Configuration	5-27
5.2-2	Design Concept B Communications Subsystem	5-30
5.2-3	Design Concept B Data Automation Element	5-33
5.3-1	Spacecraft Design Concept C Configuration	5-47
5.3-2	Design Concept C Communications Subsystem	5-50
5.3-3	Design Concept C Data Automation Element	5-54
5.4-1	Spacecraft Design Concept D Configuration	5-60
5.4-2	Design Concept D Communications Subsystem	5-64
5.4-3	Design Concept D Data Encoder and Data Storage Element Interface	5-64
A-1	Injection Energy and Asymptote Declination Mission Map, 1973 Launch	A-2
A-2	Injection Energy and Asymptote Declination Mission Map, 1974 Launch	A-3

LIST OF FIGURES (Continued)

Number	Title	Page
A-3	Injection Energy and Asymptote Declination Mission Map, 1975 Launch	A-4
A-4	Injection Energy and Asymptote Declination Mission Map, 1976 Launch	A-5
A-5	Injection Energy and Asymptote Declination Mission Map, 1977 Launch	A-6
A-6	Injection Energy and Asymptote Declination Mission Map, 1978 Launch	A-7
A-7	Injection Energy and Asymptote Declination Mission Map, 1979 Launch	A-8
A-8	Injection Energy and Asymptote Declination Mission Map, 1980 Launch	A-9
A-9	Hyperbolic Excess Speed Mission Map, 1973 Launch	A-10
A-10	Hyperbolic Excess Speed Mission Map, 1974 Launch	A-11
A-11	Hyperbolic Excess Speed Mission Map, 1975 Launch	A-12
A-12	Hyperbolic Excess Speed Mission Map, 1976 Launch	A-13
A-13	Hyperbolic Excess Speed Mission Map, 1977 Launch	A-14
A-14	Hyperbolic Excess Speed Mission Map, 1978 Launch	A-15
A-15	Hyperbolic Excess Speed Mission Map, 1979 Launch	A-16
A-16	Hyperbolic Excess Speed Mission Map, 1980 Launch	A-17
C-1	Ratio of Hydrazine Tank Weight to Hydrazine Volume Versus Ullage Factor	C-5

LIST OF TABLES

Number	Title	Page
2.1-1	Orbital and Physical Characteristics of Jupiter	2-2
2.1-2	Energy Ranges of Corpuscular Radiation	2-8
2.1-3	Energy Response of Trapped Radiation Detector	2-15
2.1-4	Intervals of Particle Energy	2-18
2.1-5	Television I	2-27
2.1-6	Television II	2-29
2.1-7	Scientific Instrument Characteristics	2-36
2.1-8	Scientific Experiment Packages	2-39
2.3-1	Payload Decrements	2-64
2.3-2	C_3 Decrements	2-64
3.6-1	Critical Failure Modes, Effects and Backup-First Maneuver Sequence	3-80
3.6-2	Weight Breakdown of Subsystem Fixed Hardware	3-83
3.6-3	Midcourse Correction Propulsion Subsystem - Nomenclature and Equation	3-84
3.6-4	Design Data	3-89
3.6-5	Attitude Control Propulsion Subsystem - Nomenclature and Equation Summary	3-100
3.7-1	60, 80, and 120 Watt RTG Geometry	3-107
5.1-1	Spacecraft Design Concept A Weight Summary	5-3
5.1-2	Design Concept A Communications Subsystem Gain-Loss Table	5-4

LIST OF TABLES (Continued)

Number	Title	Page
5.1-3	Design Concept A Antenna and Information Rate Schedule	5-5
5.1-4	Design Concept A Communications Subsystem Physical Characteristics	5-7
5.1-5	Anticipated Uncompressed Data Bit Rates For Design Concept A	5-8
5.1-6	Design Concept A Data Management Subsystem Physical Characteristics	5-13
5.1-7	Design Concept A Control Subsystem Physical Characteristics	5-19
5.1-8	Design Concept A Midcourse Propulsion Subsystem Physical Characteristics	5-24
5.1-9	Electric Power Subsystem Loads for Design Concept A	5-25
5.1-10	Design Concept A Electrical Power Subsystem Physical Characteristics	5-25
5.2-1	Spacecraft Design Concept B Weight Summary	5-28
5.2-2	Design Concept B Communications Subsystem Gain-Loss Table	5-29
5.2-3	Design Concept B Antenna and Information Rate Schedule	5-29
5.2-4	Design Concept B Communications Subsystem Physical Characteristics	5-30
5.2-5	Anticipated Uncompressed Data Bit Rates for Design Concept B	5-31

LIST OF TABLES (Continued)

Number	Title	Page
5.2-6	Design Concept B Data Management Subsystems Physical Characteristics	5-34
5.2-7	Design Concept B Spacecraft Control Subsystem Physical Characteristics	5-38
5.2-8	Design Concept B Midcourse Propulsion Subsystem Physical Characteristics	5-43
5.2-9	Electric Power Subsystem Loads for Design Concept B	5-44
5.2-10	Design Concept B Electrical Power Subsystem Physical Characteristics	5-45
5.3-1	Spacecraft Design Concept C Weight Summary	5-48
5.3-2	Design Concept C Communications Subsystem Gain-Loss Table	5-49
5.3-3	Design Concept C Antenna and Information Rate Schedule	5-49
5.3-4	Design Concept C Communications Subsystem Physical Characteristics	5-51
5.3-5	Anticipated Uncompressed Data Bit Rates For Design Concept C	5-52
5.3-6	Design Concept C Data Management Subsystem Physical Characteristics	5-53
5.3-7	Design Concept C Spacecraft Control Subsystem Physical Characteristics	5-55
5.3-8	Design Concept C Midcourse Propulsion Subsystem Physical Characteristics	5-56
5.3-9	Electric Power Subsystem Loads For Design Concept C	5-57

LIST OF TABLES (Continued)

Number	Title	Page
5.3-10	Design Concept C Electrical Power Subsystem Physical Characteristics	5-58
5.4-1	Spacecraft Design Concept D Weight Summary	5-61
5.4-2	Design Concept D Communications Subsystem Gain-Loss Table	5-62
5.4-3	Design Concept D Antenna and Information Rate Schedule	5-62
5.4-4	Design Concept D Communication Subsystem Physical Characteristics	5-63
5.4-5	Anticipated Uncompressed Data Bit Rates For Design Concept D	5-65
5.4-6	Design Concept D Data Management Subsystem Physical Characteristics	5-67
5.4-7	Design Concept D Spacecraft Control Subsystem Physical Characteristics	5-73
5.4-8	Design Concept D Midcourse Propulsion Subsystem Physical Characteristics	5-75
5.4-9	Electrical Power Subsystem Loads For Design Concept D	5-76
5.4-10	Design Concept D Electrical Power Subsystem Physical Characteristics	5-76

SECTION 1

INTRODUCTION

This report represents the work which has been accomplished during the first half of a six-month study of Jupiter flyby missions being conducted for the Jet Propulsion Laboratory by the Fort Worth Division of General Dynamics. Many of the results and conclusions reported here have been included for reasons of completeness and are subject to change during the last half of this study. In this section, the tasks, constraints, and technical approach are delineated in relation to the overall study. A summary of the status and results of the study to date is also included.

1.1 DEFINITION OF TASK

The objective of the study as it is described in the Jet Propulsion Laboratory Statement of Work No. 1285, 25 May 1965, is to

> ...perform a feasibility study to develop spacecraft design concepts for a 'flyby' mission of the planet Jupiter. The study shall consider a range of alternate design concepts for accomplishing the successive mission objectives listed below within the applicable design constraints:
>
> (1) Interplanetary and planetary measurements of the spatial distribution of particles and fields. Measurements shall include but not necessarily be limited to: (i) magnetic fields; (ii) solar plasma; (iii) dust and micrometeorites; (and) (iv) ionized radiation. The trapped radiation belts of Jupiter are considered a special case of particle and field measurements and shall be presented relative to the design complexity required for their measurement.
>
> (2) Measurements of the planetary atmosphere of Jupiter which shall include but not necessarily be limited to: (i) composition (and) (ii) temperature and pressure.
>
> (3) Measurements of the physical properties of Jupiter which shall include but not necessarily be limited to: (i) observation of the cloud cover and possibly gross features of the Jovian terrain.

Quoting again from the statement of work, the specific tasks to be completed during the course of the study are

(1) Develop the conceptual designs for spacecraft systems for each of the (mission) objectives listed....above by accomplishing the following: (i) establish the functional requirements for spacecraft systems to perform the mission; (ii) forecast the applicable state-of-the-art for the time period considered; (iii) perform design trade-offs as a basis of the rationale employed for design selection; (iv) synthesize the appropriate system concepts; (v) identify the problem areas and indicate approaches to their solution; (and) (vi) review the system concepts in terms of the Mariner Mars '64 spacecraft system design.

(2) Provide a description for each of the systems developed....above, which shall include, but not necessarily be limited to, the following: (i) system block diagrams; (ii) operational sequences; (iii) expected performance characteristics and design reliabilities; (and) (iv) weight and power estimates.

(3) Provide estimates of schedule, cost, and probability of success, including success of partial missions, for each of the systems developed....above, and indicate the trade-offs involved.

1.2 CONSTRAINTS

The constraints which are being observed in the study are as follows. (The first and third are quoted from the Jet Propulsion Laboratory Statement of Work No. 1285.)

(1) "Mission accomplishment shall be during the 1973 through 1980 time period. State-of-the-art applicability for design concepts evolved by this study shall consider development lead-time requirements for the time period of interest."

(2) Missions shall be compatible with at least one of the following launch vehicles: (i) Atlas SLV3x/Centaur/HEKS; (ii) Titan IIICx/Cenatur; (iii) Saturn IB/Centaur/HEKS; (iv) Saturn V; and (v) Saturn V/Centaur. The performance and physical characteristics of these vehicles to be used by this study shall be as described in the Jet Propulsion Laboratory Technical Direction Memorandum No. 1, Contract 951285, 7 January 1965.

(3) "Compatibility with the Deep Space Instrumentation Facility (DSIF), as described in the Jet Propulsion Laboratory Technical Memorandum 33-83, Revision 1, dated 24 April 1964 (shall be maintained)."

1.3 TECHNICAL APPROACH

The technical approach which was formulated by General Dynamics in order to meet the objectives and perform the tasks outlined in subsection 1.1 is illustrated in Figure 1.3-1. As indicated by those objectives and tasks, all aspects of a Jupiter flyby mission relative to launch vehicle requirements, scientific accomplishment, and spacecraft performance must be examined. Subsequently, spacecraft systems must be designed which are capable of carrying out selected groups of mission objectives. In the final phase of the study, each spacecraft concept must be evaluated in terms of its mission capabilities and the ramifications of its implementation. The plan of study shown in Figure 1.3-1 is based on the interpretation of the study objectives and tasks given here. The brief discussion of study objectives and tasks that follows complements the study task description in subsection 1.1.

1.3.1 Mission Planning

The Mission Planning phase is designed to supply the information required for spacecraft design. The primary objectives are (1) to describe possible scientific requirements in the Science Subsystem Definition task, and (2) to determine mission performance requirements in the Mission Analysis Task.

The definition of science subsystems is accomplished by considering as candidate experiments all interplanetary and planetary experiments which (1) have been previously established as feasible in existing literature, (2) satisfy one or more of the mission objectives outlined in subsection 1.1, and (3) are applicable to a Jupiter flyby mission. Each of these experiments is described in terms of the required instrumentation and the associated requirements of the various spacecraft subsystems. From these experiments, several "packages" are made up which are representative of different levels of scientific capability. These experiment packages are selected to provide design points for spacecraft subsystem studies.

The Mission Analysis task consists in identifying the characteristics of Earth-Jupiter heliocentric, ballistic transfer trajectories in order to (1) support spacecraft design studies, and (2) evaluate launch vehicle payload capabilities.

TECHNICAL APPROACH

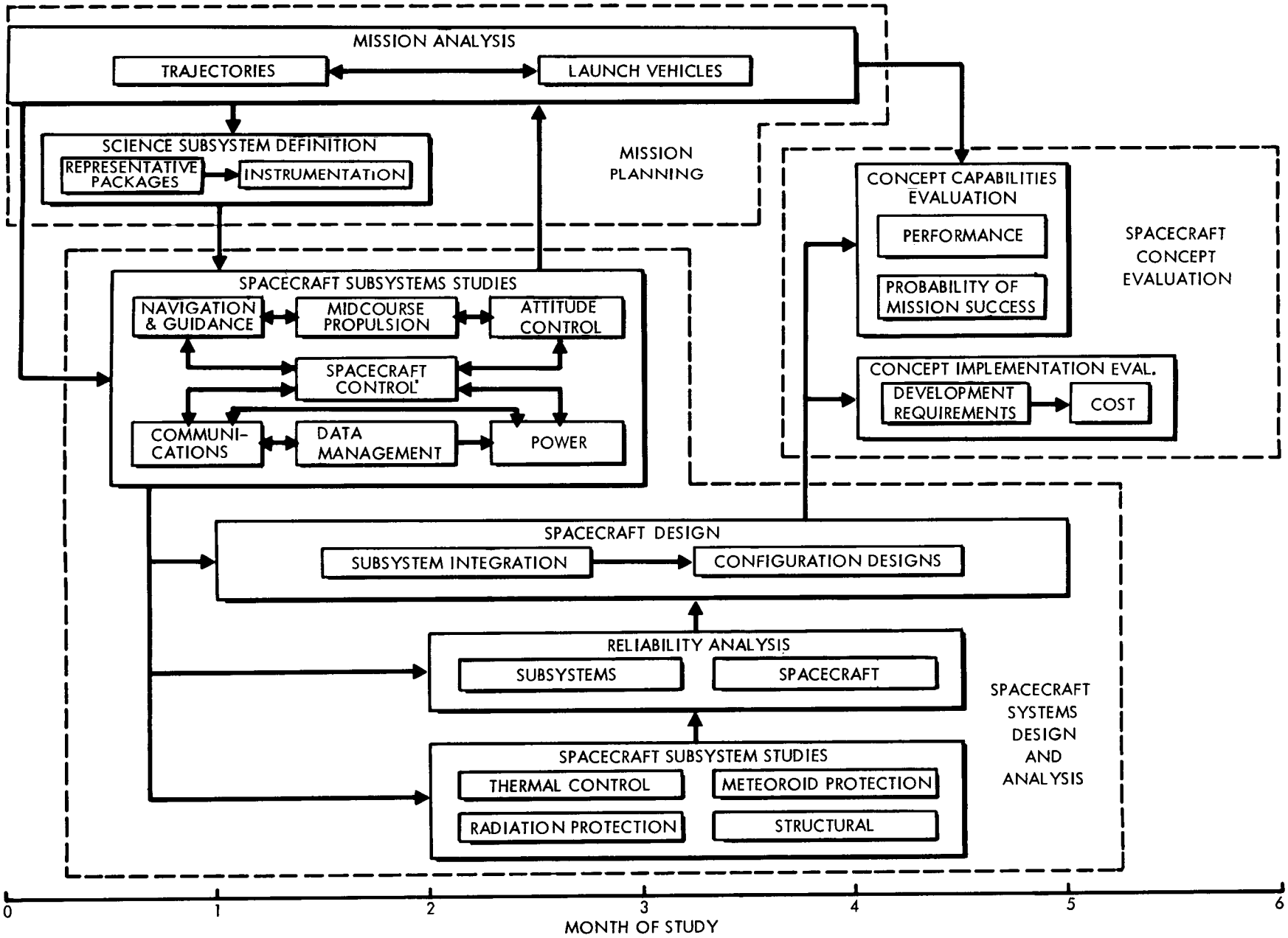


FIGURE I.3-1

In keeping with the constraints listed in subsection 1.2, this work is limited to launch dates in the 1973-1980 time period and to the Atlas SLV3x/Centaur/HEKS, Titan IIICx/Centaur, Saturn IB/Centaur/HEKS, Saturn V, and Saturn V/Centaur launch vehicles. Jupiter encounter and post-encounter trajectories are also analyzed to provide data pertinent to aim point selection.

1.3.2 Spacecraft Systems Design and Analysis

The study phase, Spacecraft Systems Design and Analysis, represents a design iteration loop, the results of which are spacecraft design concepts based on mission objectives and requirements defined in the Mission Planning Phase. The study tasks include Spacecraft Subsystems Studies, Reliability Analysis, and Spacecraft Design.

Spacecraft Subsystem Studies are conducted on each of the various subsystems which together comprise a complete spacecraft. This division of effort requires studies in the following technological areas: (1) communications, (2) navigation and control, (3) data management, (4) spacecraft control, (5) midcourse propulsion, (6) attitude control, (7) power, (8) thermal control, (9) radiation protection, (10) meteoroid protection, and (11) structure.

The Reliability Analysis is concerned with estimating and enhancing reliability at the subsystems level and finally at the integrated spacecraft level. The Reliability Analysis, although it is treated as a separate task, is an integral part of both the Spacecraft Subsystems Studies and the Spacecraft Design.

The task in Spacecraft Design is to integrate selected subsystem design concepts into spacecraft design concepts. Configuration designs for these concepts are then determined.

1.3.3 Spacecraft Concept Evaluation

In the third phase, Spacecraft Concept Evaluation, the spacecraft design concepts resulting from the second study phase are considered in terms of mission capability and implementation requirements. Specifically, this entails the evaluation of mission performance characteristics, the probability of mission success, development requirements, and cost. In each case, the activity is basically one of combining the appropriate results of mission and subsystems studies in order to obtain information relating to an integrated spacecraft. The results of these

studies are intended to provide an evaluation of the merits of each concept, not to provide a means of selecting one spacecraft design concept over another.

1.4 SUMMARY OF STATUS AND RESULTS

The status of the Jupiter Flyby Missions Study at the halfway point is indicated by the time scale in Figure 1.3-1. Definitions and descriptions of scientific experiments appropriate for Jupiter flyby missions have been completed. The investigations of the characteristics of Earth-Jupiter transfer trajectories during the time period 1973-1980 and the evaluation of the five launch vehicles of interest for Jupiter missions are completed. Analyses and designs in the areas of communications, data management, navigation and guidance, spacecraft control, midcourse propulsion, attitude control, and power are essentially complete. Design perturbations in the above areas are expected during the last half of this study from the studies now beginning of thermal control, radiation protection, meteoroid protection, spacecraft structure, and reliability. Spacecraft subsystem integration and configuration designs have been accomplished on the basis of the work completed, and these will continue to be iterated as the unfinished subsystem analyses proceed. No significant effort has been expended on spacecraft concept evaluation.

Four spacecraft design concepts have been evolved during the first half of the study. At the beginning of the study, no attempt was made to specify the number of concepts which would result from the study. It was felt that this number should be determined only after various levels of scientific capability, different design philosophies, and varying degrees of spacecraft complexity had been considered. These considerations, together with the study objective of covering a wide range of spacecraft design concepts and with appropriate consideration to the scope of the study, have led to the selection of the four concepts mentioned above which are designated by the letters A, B, C, and D.

Concept A is characterized by its method of stabilization. It is spin-stabilized, adaptable only to a limited number of scientific instruments, and consists of very simple subsystem design concepts. Consequently, in terms of mass, it is the smallest of the four concepts. Spacecraft design Concepts B, C, and D all embody a design philosophy of 3-axis stabilization, but differ in scientific capability, subsystem complexity, and total mass. In general, as either of these features increases, so do the others, so that Concept B can be described as a

minimal design, Concept C as an intermediate spacecraft, and Concept D as a full concept.

The remainder of this report consists of a detailed description of the technical progress made during the first half of the study. Sections 2, 3, and 4 report the general analyses and results which have been accomplished in the three study phases - Mission Planning, Spacecraft Systems Design and Analysis, and Spacecraft Concept Evaluation. Section 5 describes in detail the four spacecraft design concepts which have resulted from these analyses.

SECTION 2

MISSION PLANNING

In this section, the studies devoted to scientific endeavors, the trajectories, and the launch vehicles applicable to flyby missions to Jupiter are described. To a large degree, the results of these studies are indicative of the performance requirements for Jupiter flyby spacecraft.

2.1 SCIENCE SUBSYSTEM DEFINITION

As a part of the present study of flyby missions to Jupiter, a spectrum of scientific experiments has been defined in order to derive estimates of the engineering requirements and constraints imposed by the science payload on other spacecraft systems. Although the actual definition of the science payloads to be used in a mission of this type will be determined by NASA and NASA advisors at a later date, it is necessary to define relatively realistic approximations at the present time so that the effects of the science package on the other study parameters can be evaluated with reasonable confidence in their validity.

The following subsections contain descriptions of the physical phenomena to be studied, as dictated by the mission objectives identified in subsection 1.1, and the scientific investigations required to pursue such objectives. The characteristics of the instruments necessary to perform these investigations are described in both narrative and tabular form. To provide design points for spacecraft design, several instrument groupings are defined as possible mission payloads.

2.1.1 Summary of Observations of the Planet Jupiter

The orbital and physical characteristics of Jupiter have been determined from astronomical observations of the planet and its satellites. Some of these characteristics which are summarized in Table 2.1-1 are known with a fair degree of accuracy, e.g., the orbital period and the planetary mass. Others, such as the rotation rate of the solid planetary surface or the planetary flattening, are only approximate because Jupiter is obscured by cloud layers of indefinite thickness and no actual planetary surface is observed.

Table 2.1-1 ORBITAL AND PHYSICAL CHARACTERISTICS OF JUPITER

Distance, Jupiter to Sun (max.)	817×10^6 km	(508×10^6 miles)
Distance, Jupiter to Sun (min.)	740×10^6 km	(460×10^6 miles)
Distance, Jupiter to Earth (max.)	967×10^6 km	(601×10^6 miles)
Distance, Jupiter to Earth (min.)	591×10^6 km	(367×10^6 miles)
Angular Diameter, From Earth (max.)	50 sec	
Angular Diameter, From Earth (min.)	31 sec	
Eccentricity of Orbit	0.0484	
Inclination of Orbit to Ecliptic		1.03 deg
Inclination of Equator to Orbital Plane		3.01 deg
Orbital Period (sidereal)		11.86 years
Orbital Period (synodic from Earth)		399 days
Average Orbital Velocity	13.1 km (8.12 miles) per sec	
Radius (average), R_j	69×10^3 km (43×10^3 miles)	
Mass	1.902×10^{27} kg	
Average Density	1.35 gms/cm^3	
Gravitational Acceleration at Poles	26.0 meters (85.2 feet) per sec per sec	
Escape Velocity	61 km (38 miles) per sec	
Rotation Period	$\sim$9 hr 55 min	

All of the information concerning Jupiter has been gathered from visual observations, spectroscopic determinations in the visible and infrared, and detections of radio emission. These three regions of the spectrum can be observed from Earth, but the data obtained from these regions can probably be related to the upper levels of the atmosphere on Jupiter. More extensive measurements of the electromagnetic radiation in the ultraviolet, visible, and infrared portions of the spectrum could profitably be made above the atmosphere of the Earth.

The albedo of Jupiter is relatively high, about 0.4, and its angular diameter is relatively large, 31 to 50 seconds; therefore, the planet is easily seen. When the disc of Jupiter is observed by use of a telescope, it appears to be obviously flattened, and significant limb darkening is seen. Jupiter exhibits a number of alternate light and dark bands running parallel to the equator. The light-colored, yellowish regions are called zones, and the dark-colored bands are referred to as belts. The belts have been observed as being dark gray or brown, and occasional regions in these belts as blue, dark green, or red. A broad equatorial zone is bounded by north and south tropical belts which are followed by north and south tropical zones. There are then a temperate belt, a temperate zone, another temperate belt, and finally a polar region in each hemisphere.

The bands, which are believed to be clouds in the middle levels of the Jovian atmosphere, are quite irregular in their appearance. The temporary and variable nature of such features indicates that movements are taking place within the cloud system that surrounds the planet.

Most of the markings on Jupiter change fairly quickly. There are, however, some of a more permanent nature, lasting from periods of months to many years. One of the most striking is the Great Red Spot which lies mainly in the south tropical zone. It is an oval area, extending approximately 45,000 kilometers in length and 13,000 kilometers in width. The visibility varies in an irregular manner; at times the Red Spot is faintly pink, but there have been periods of one to three years when it has had a definite red color.

The nature of the cloud bands, of the Red Spot, and of other apparent markings is still the subject of considerable speculation.

The spectrum of the planet Jupiter has been extensively studied in the visible and infrared regions. Positive identifications of methane (CH_4), ammonia (NH_3), and the hydrogen molecule (H_2) have been made. The abundances of these and other possible constituents of the atmosphere are not well known.

Experiments involving the occultation of γ Arietis have been used to derive an atmospheric mean molecular weight of $\mu = 4.3 \pm 0.5$. Such a low value indicates that the bulk of the atmosphere is composed of hydrogen and helium. In most theoretical determinations of the Jovian atmosphere, neon and argon are also considered present.

Powerful radio emissions have been detected from Jupiter. The radiation falls into three wavelength regions: the centimeter region, the decimeter region, and the decameter region. In the first region, the radiation is believed to be mostly thermal; in the latter two, nonthermal.

The radiation from Jupiter in the decimeter region has been studied in the range from 10 to 68 centimeters. This radiation, which is characterized by long-term variations, is emitted continuously. The most satisfactory explanation of this radiation is that it is emitted by high-energy electrons spiraling around the lines of force of the Jovian magnetic field. The electrons responsible for the emission are trapped in radiation belts similar to the Van Allen zone in the Earth's magnetic field. The observations could be accounted for by synchrotron radiation if the strength of the magnetic field of Jupiter in the emitting region is on the order of 10 gauss. The main emission appears to come from the equatorial regions of Jupiter at distances from about 1.5 to 3.0 planetary radii.

The third type of radio-frequency emission from Jupiter is in the decameter range from 10 to 30 meters. The emission occurs in bursts. These bursts, which last a second or so, are generally observed in groups lasting for 5 or 10 minutes and occurring continually over a period of a few hours. There is as yet no satisfactory explanation of Jupiter's decameter radiation. Several theories have been proposed to explain this emission. The emission exhibits several of the characteristics associated with lightning on Earth, but the energy from Jupiter is on the order of a billion times greater. There is some evidence that the radiation is of the cyclotron type originating high in the Jovian atmosphere. Another possibility is that the bursts are caused by plasma oscillations in a Jovian ionosphere.

2.1.2 Magnetic Field Measurements

The strong magnetic field of Jupiter offers an interesting opportunity for investigation. The existence of a strong field has been inferred from the examination of the nonthermal radio emission from Jupiter, as discussed in the preceding section. The most plausible description of the magnetic field of Jupiter presently available is that the major part of the planetary field is caused by a dipole component aligned at an angle of about 10 degrees to the axis of rotation. The sense of the dipole moment is believed to be opposite to that of the Earth.

Jupiter is a large and rapidly rotating planet. Large-scale fluid or atmospheric motions are observed on the surface. If convective fluid motions occur in the core, a hydrodynamic dynamo may operate to produce a magnetic field. Accurate measurements of the magnitude and orientation of the Jovian magnetic field would contribute to a quantitative refinement of the dynamo theory.

The intensity and the spatial distribution of a planet's magnetic field control a number of important phenomena. The size and shape of the cavity in the solar wind containing the magnetosphere of a planet is determined by the deflection of the plasma flow by the planet's magnetic field. The energy distribution of energetic particles incident on a planet is also controlled by the planet's magnetic field. Many of the phenomena related to magnetic storms and auroras on Earth are related to the geomagnetic field. The latitude of maximum occurrence of auroras on the Earth is apparently determined by the outer boundary of the region of trapped radiation in the Earth's magnetosphere. Particles that enter the atmosphere to produce auroras are either accelerated within the magnetosphere or are injected into the magnetosphere from the solar plasma.

Knowledge of the distribution and variation of the magnetic fields of planets permits useful inferences concerning their interiors. For example, studies of geomagnetic data have shown that (1) motions of material are probably going on within the Earth; consequently the existence of a fluid core is suggested; (2) changing electric currents and winds in the upper atmosphere induce changing earth currents; consequently, the electrical conductivity of the Earth's crust is indicated; (3) parts of the Earth have different structures, i.e., mineral deposites, ocean floors, etc.; and (4) the field is self-maintained. Similar results should be obtained from measurements of the Jovian magnetic field.

A planetary magnetic field causes a transition region to exist between interplanetary space and the region close to the planet. In the generally accepted theories which are supported by a few measurements of the geomagnetic field at tens of earth radii, the existence of a characteristic transition region called the magnetopause is predicted. This magnetopause separates the planetary field from the ionized component of the interplanetary medium. The planetary magnetic field is confined to a tear-drop shaped cavity inside the interplanetary gas.

An estimate of the extent of Jupiter's magnetosphere can be made in the following way. If Jupiter were not rotating, and if the flow of the solar wind were laminar at Jupiter's orbit, then the magnetospheric envelope would be tear-drop shaped, with a stagnation point at the front. If an inverse square dependence upon distance is assumed, the energy density of the solar wind at the orbit of Jupiter is about 1/25 that at the orbit of Earth. Then, if the magnetic field near Jupiter's surface at the equator is in the vicinity of 20 gauss, the distance of the stagnation point from the center of the planet is 60 R_j, where R_j indicates a distance of one Jovian radius.

Actually, however, the rotation of the field must exert a great influence on the boundary location. If the solar-wind velocity is disregarded and it is assumed that Jupiter is rotating in a sea of stationary plasma, the plasma will possess an apparent circulatory motion relative to the field. At the magnetospheric boundary, the apparent kinetic energy density of the plasma must be approximately equal to the magnetic energy density:

$$\frac{R}{R_j} = \left(\frac{H_o}{\omega R_j}\right)^{1/4} (4\pi n m_p)^{-1/8}$$

where R is the approximate distance from the center of the planet to the magnetospheric boundary in the equatorial plane; H_e is the equatorial magnetic field at the Jovian surface; ω is the angular velocity of rotation; n is the number density of protons; and m_p is the mass of a proton.

If n at Jupiter's orbit = .4 cm^{-3}, then

$$R \approx 50 R_j$$

Although the actual situation is much more complicated, such an estimate seems reasonable.

A self-oscillating rubidium or cesium vapor magnetometer, may be developed which is capable of operating over the entire range of magnetic field encountered. Such a development is within the present state of the art if internal electronic switching is used. An instrument of this type may operate in a range of from 3 to 30,000 gammas with an accuracy and in a range of 0.25 to 10 gauss with an accuracy of about 3 to 20 gammas.

One objection to the use of this type of magnetometer is that the self-oscillation continues only under optimum conditions of vapor pressure temperature, 25° to 45°C; consequently, environmental temperature control within these limits is required.

Although it may become apparent that the advantages inherent in using a single instrument outweigh the present advantages of using two instruments (such as better accuracy), for purposes of this study two magnetometers, i.e., two separate sensors sharing a common electronics package, will be utilized in the scientific definition.

The electronics package may be mounted in the main part of the spacecraft. It would weigh about 5.0 pounds and require about 7.0 watts of power. The two sensing elements would weigh 1.5 pounds each.

In order to minimize the magnetic background from the spacecraft and its components, each of the two magnetometer sensors (with a weight of 1.5 pounds each) should be placed at an extreme extension of the spacecraft. As a general rule, the background field should be less than .5 gamma; consequently, every component placed on the payload should be magnetically checked and shielded if necessary. If absolutely necessary, highly coercive magnets may be appropriately located in the main body of the spacecraft to cancel the spacecraft field at the magnetometer.

2.1.3 The Detection of Charged Particles in Interplanetary and Planetary Regions

During a Jovian flyby mission, high-energy radiation will be measured over a relatively long time and over significantly varying spatial coordinates. These two features will allow the collection of information useful for understanding the nature, origin, and behavior of such radiation. An approximate classification of the energy ranges of corpuscular radiation is presented in Table 2.1-2. The extension and propagation of solar coronal material, i.e., the solar wind, would consist of ions and electrons exhibiting energies less than 30 keV, the mean thermal energy of the Sun.

Table 2.1-2 ENERGY RANGES OF CORPUSCULAR RADIATION

EXTRA - GALACTIC COSMIC RAYS		
Nucleonic	10^{17}	eV
GALACTIC COSMIC RAYS		
Nucleonic	10^{7} - 10^{16}	eV
Electronic	10^{5}	eV
SOLAR COSMIC RAYS		
Nucleonic	10^{12}	eV
Electronic	10^{3} - 10^{7}	eV
TERRESTIAL RADIATION BELTS		
Nucleonic	10^{3} - 10^{9}	eV
Electronic	10^{3} - 10^{7}	eV
JOVIAN RADIATION BELTS		
Nucleonic	10^{6} - 10^{9}	eV
Electronic	10^{6} - 10^{8}	eV
TERRESTIAL AURORAE		
Electronic	10^{3} - 10^{5}	eV
JOVIAN AURORAE (?)		
Electronic	10^{4} - 10^{6}	eV

The great strength of the Jovian magnetic field and the flyby trajectory should enable such measurements to be made at points well inside the magnetopause. Such measurements would be used to determine the geographic and altitude dependence of the undisturbed planetary field. It might then be possible to infer the multipolarity of the source and its orientation with respect to the planetary rotation axis.

A second objective set for a magnetometer experiment is the measurement of the interplanetary magnetic field. Preliminary measurements beyond the magnetopause of the Earth indicate that, approximately 20 percent of the time, magnetically quiet conditions prevail in the steady interplanetary field of approximately 3 gamma. Accurate measurements of this field will contribute to our understanding of the dynamics of the solar system. It will also be possible to study the long-period fluctuations in the interplanetary magnetic field. These data could lead to important information about solar disturbances and about the existence of hydromagnetic waves or magnetized plasmas in interplanetary space and to estimates of the kinetic energy density of the interplanetary plasma.

Ideally, a space magnetometer would be used to measure the magnitude and orientation of the magnetic field vector with an absolute accuracy of a fraction of 1 gamma. It would be used to provide measurements over a range in field magnitude between about 10 gauss near the Jovian surface to 1 gamma (10^{-5} gauss) in interplanetary space and to record fluctuations of the vector field over a frequency range between zero and several thousand cycles per second. This instrument would be light-weight, exhibit low power consumption, and be unaffected by shock, vibration, and extremes of temperature. Unfortunately, like most utopian designs, none of the instruments presently available meets all of these specifications. The magnetometers which seem most suited for use in a Jupiter flyby mission are the helium, rubidium, or cesium vapor-type magnetometers.

The physical principle underlying the operation of the helium magnetometer involves the transparency of a plasma of metastable helium atoms to a beam of resonant radiation at 1.083 μ wavelength and the dependency of this transparency on magnetic fields. Although this type of magnetometer is very accurate and stable, it has a relatively low dynamic range and, as such, its application is limited for a Jupiter flyby mission since it must be used with another instrument.

Much of the electromagnetic radiation and most of the particles emitted by the Sun and other sources never reach the surface of the Earth (or Jupiter) because of the protection of the atmosphere and magnetic field. Although the mechanisms of the trapping of charged particles are not well understood, extensive radiation belts around the Earth are believed to be caused by the interaction between the upper atmosphere of the Earth, the geomagnetic field, and the incoming corpuscular radiation. These trapped charged particles spiral back and forth along the lines of force of the magnetic field. The particles are predominantly, and perhaps exclusively, protons and electrons. From an analysis of radio emission from Jupiter, two radiation belts have been inferred. One is centered at a distance of 1.5 planetary radii from the center of Jupiter. The other extends from about 2 to at least 3.5 planetocentric radii. The most reasonable estimate is that the latter belt consists mostly of electrons with energies in the range of 1 to 10 MeV. Measurements of energy spectra in the Jovian radiation belts would provide a fruitful source of information in itself and also be applicable to still unresolved questions concerning the terrestrial radiation belts.

The corpuscular radiation, which is probably a source of the planetary radiation belts, is of primary interest in interplanetary space. Throughout the universe, certain physical processes result in the formation, ionization, and acceleration of matter. The motion of these charged particles results in the formation of magnetic and electric fields. The further interaction of these moving particles with other magnetic and electric fields results in their further acceleration. Consequently, there exists a whole continuum of charged particles which exhibit energies from thermal to at least 10^{21} eV and nuclear structures from that of hydrogen (single protons) to that of heavier materials (at least iron).

Galactic cosmic rays are those particles which are accelerated outside of our solar system and arrive with energies greater than about 10 MeV per nucleon. The features of galactic cosmic rays which are most easily investigated are (1) their energy and charge spectra and (2) the changes of their characteristics with time.

Th Sun is also a source of cosmic rays. When a solar flare occurs, a tongue of high-energy particles erupts from the Sun's surface. The charged particles drag along the lines of the solar magnetic field which become frozen into the cloud. As the force lines become distended, they lose their strength. The field is

still strong enough, however, to cause a partial screening of that portion of the solar system containing the Earth from the galactic cosmic rays.

The composition of the primary cosmic radiation striking the top of the Earth's atmosphere is approximately 85 per cent hydrogen; 12 percent helium; 1 percent in the carbon, nitrogen, and oxygen group; .25 percent in the lithium, beryllium, and boron group; and .25 percent in the neon and heavier groups. The flux of nuclei in the Li, Be, B, and C_1N and heavier groups is greater than would be expected from present estimates of stellar abundances. There are practically no data on the primary cosmic-ray electrons and positrons. Further measurements would help to differentiate solar and extrasolar abundances.

It appears reasonable to assume that the flux of cosmic rays incident on the solar system is constant. In the vicinity of Earth, however, large modulations are observed, and they appear to be controlled by solar activity. The two most important types of modulation are the 11-year variation and the Forbush decrease. It was first noted by Forbush that the cosmic-ray intensity varied inversely with the solar activity corresponding to an 11-year cycle. Forbush also observed the rapid worldwide decreases in cosmic-ray intensity associated with some types of solar magnetic flares.

The modulation effects are interpreted as being caused by large-scale variations of the solar magnetic field. Increases of the magnetic field strength near the Earth result in the deflection of the lower energy particles before they penetrate this field. This interplanetary field arises from two sources. A relatively steady magnetic field is the result of the streaming plasma from the Sun. The Forbush decreases are caused by somewhat more localized fields generated as a result of large solar flares.

Cosmic rays play a major role in the physical processes taking place in the Universe. The energy density of galactic cosmic rays is of the same order of magnitude as the kinetic energy of interstellar matter and the magnetic energy density in interstellar space.

One of the most fundamental questions to be answered by future exploration of interplanetary space is that of the galactic cosmic ray flux in interstellar space. It is now believed that these cosmic rays play a significant role in the dynamics of the universe, and a knowledge of their flux is required to construct a more realistic cosmological model.

In connection with the physics of the Sun and the circumsolar space, it will be interesting to determine (1) the conditions required for the propagation of galactic cosmic rays within the limits of the Solar System and (2) the mechanisms which are responsible for the generation, composition, and conditions of propagation of solar cosmic rays.

A cosmic-ray detector, i.e., a charged-particle detector, will be used

1. To monitor solar, galactic, and extragalactic cosmic rays in interplanetary space and provide data for the study of their angular distribution, energy spectra, and time histories.

2. To search for magnetically trapped particles in the vicinity of Jupiter and provide data for estimates of their spatial distribution, energy spectra, and identity.

3. To provide similar information concerning the Van Allen belts, if desired.

Estimates of the charge spectra and chemical composition would also be desirable, but these estimates could perhaps be obtained from circumterrestrial or lunar experiments.

2.1.3.1 Energetic Particle Detectors

A large number of physical techniques are required for the detection and analysis of the extreme energy scale of corpuscular radiation. The most efficient of terrestrial detectors, such as nuclear emulsion or electrostatic-magnetic analyzers, are ruled out because of weight limitations.

In all particle detectors, the interaction between a sample (with associated electronics) and an incoming particle is used as the basis of detection. The Cerenkov counter depends on the production of Cerenkov radiation by the passage of relativistic particles through a dielectric medium. Some variation of the particle-energy threshold is made possible by the choice of the gas or liquid used as a sample. This detector, as well as other detectors, is usually used in a coincidence arrangement in conjunction with one or more particle detectors to limit both the kinds of particles detected and their energy range. Such packages, which also restrict the physical path of detected particles, are called telescopes.

A similar detector, the scintillation counter, depends on the production of fluorescent radiation (which can be monitored by photomultipliers) by passing high-energy particles through a suitably chosen crystal. Again, when a choice is made from a number of organic or inorganic crystals, variations in energy thresholds can be attained.

A relatively simple instrument which contains a gold-silicon (Au - Si) surface barrier detector is available for measuring protons. The sensitive elements of such a solid-state detector are thin wafers of high-resistivity silicon with a very thin film of gold evaporated on the front surface. A space-charge region extends from the Au - Si interface into the bulk of the silicon. The thickness of this region is adjusted (by adjusting the potential difference across the wafer) to approximate equality with a particular proton energy range. A charged particle incident on the detector will penetrate the thin gold film and produce electron-hole pairs as it passes through the space-charge region. The liberated ion pairs are swiftly swept apart by the high electric field in the space-charge region; this action results in a measurable voltage pulse proportional to the amount of energy lost by the particle in passing through the sample.

A similar device is the semiconductor detector which is a small crystal of photoconductive cadmium sulfide (CdS). The sensitive element is approximately 2 millimeters square and between .1 and .3 millimeter thick. The electrical conductivity of such a sample is proportional to the rate of the deposition of energy of ionization in the crystal. If a constant voltage is applied, the current flow through the crystal can be calibrated in terms of energy flux.

A Neher-type ionization chamber consists of a spherical volume of argon gas contained by a thin steel wall. This detector is used to measure the ionization produced in the argon by all naturally occurring ionizing particles: those produced by secondary particles generated in the spacecraft which can penetrate the chamber walls, and those caused by secondary particles generated in the ion-chamber walls and gas. The flux of particles or current passing through the gas is easily measured and correlated with an ionizing particle.

In the Geiger-Muller counter,the ionizing power of nuclear radiations is also used as a basis for particle detection. Extensive variation in relations between response and detected particles are made possible through the use of various geometries, shielding, and kinds of wall material.

2.1.3.2 Low-Energy Particle Detector

In the case of planetary investigations, the energy range of most interest would comprise the regime of magnetically trapped particles, i.e., a few keV to a few MeV. Detectors which are operated in this area would also yield information on the space and time variation of galactic and solar cosmic rays in interplanetary space.

The Trapped Radiation Detector designed by Van Allen and used on Ranger and Mariner flights is an extremely useful and versatile instrument. A typical package for use in the measurement of energetic particles contains a system of five detectors. The following discussion is derived from the experiment as used on Mariner IV, but it can be regarded as representative of the use of a low-energy particle detector in a Jupiter flyby mission.

Three of the detectors, called A, B, and C, are Geiger-Muller end-window counters which measure the total number of charged particles passing through their sensitive volumes. The sensitive volume of each tube is shielded so that low-energy particles can enter only by passing through the window at the end of each tube. Only higher-energy particles can penetrate from other directions. If an allowance is made for the non-directional counting of higher energy particles, a directional measurement of the low-energy particles can be made.

The other two detectors, D_1 and D_2, are essentially one unit, a silicon surface barrier diode. The detector is virtually insensitive to electrons of any energy. Through amplitude discrimination in the associated electronics, two levels of proton energy discrimination are recognized.

A representative range of such an instrument is presented in Table 2.1-3. Within limits, shielding could be used to vary the listed operating regions.

In order to determine proper in-flight operation, the solid-state detector is equipped with a source of 5.5 MeV alpha particles. The counting rate of each of the three Geiger tubes is the sum of the rates caused by galactic cosmic rays, electrons, x-rays, protons, alpha particles, and other particles, which pass through their collimators; and, in some cases, by sidewall penetrations. Combinations of data from this system provide information on absolute intensities, particle identification, energy spectra, and angular distributions. In favorable cases, particle identification is conclusive.

Table 2.1-3 ENERGY RESPONSE OF TRAPPED RADIATION DETECTOR

Detector	Shielding	Energy(MeV)	
G-M Tubes			
A	1.4 mgm/cm^2 mica	Electrons	0.04
		Protons	0.50
B	1.4 mgm/cm^2 mica	Electrons	0.04
		Protons	0.50
C	+ 19. mgm/cm^2 Al	Electrons	0.13
		Protons	3.00
Solid State Detectors			
D_1	.242 mgm/cm^2 Ni	Protons	.5 - 11.
D_2	----------	Protons	.9 - 4.

The data channels are part of a commutated sequence of eight as follows: E, B, D_1, D_2, E, B, A, C (where E represents another detector). Unscaled counts from each channel are gated in turn into a shift register of 19 bits plus 2 overflow bits for a 45.0-second period and are read out through the telemetry system during the subsequent 5.4 seconds.

The five particle detectors of this low-energy particle experiment are combined in one package of a total weight of 2.5 pounds. The power required to operate the system is .4 watt. There are 4 sensors mounted on a magnesium chassis. Detector A will be constructed so that (1) the look-angle axis is directed at a 135-degree angle to the probe-Sun line, (2) the full-look angle will be 60 degrees, and (3) no payload structure will obscure its conical field of view. In Detectors B, C, and D, the look-angle axis will be directed at a 70-degree angle to the probe-Sun line, the full-look angle will be 60 degrees, and no payload structure will obscure their conical field of view. The counters must be protected from direct sunlight during the trip.

2.1.3.3 Ion Chamber

Another particle detector system used on Mariner vehicles consists of an ionization chamber, a Geiger-Muller tube, and associated electronics. This system is used to detect and measure the average omnidirectional flux of corpuscular radiation between Earth and Jupiter by determining the average specific ionization caused by this flux. It is also intended for the measurements of trapped particles in the vicinity of Jupiter.

Both the ionization chamber and the G-M tube detect particles of the same energy, i.e., electrons of energy greater than 0.5 MeV, and alpha particles of energy greater than 40 MeV. Both sensors have omnidirectional sensitivity.

The Ion Chamber unit weighs 2.6 pounds. The power required is 0.5 watt. The bit rate is 14 bits per sample. The two sensors should be mounted as close together as possible so that they receive a similar radiation flux. In order that the main body of the spacecraft subtend the minimum solid angle with regard to the detector, this unit should be mounted on a boom as far away from the main chassis as possible.

2.1.3.4 High-Energy Proton Directional Monitor

The high-energy proton directional monitor has been proposed for obtaining information regarding the temporal, spatial, and directional variations in galactic cosmic ray flux. A Cerenkov or scintillation counter would be used to measure the fluxes of particles which exhibit energy greater than 1 BeV.

The sensing units consist of four conical receptors; each unit is provided with a look angle of 60 degrees. While the location of this package is not critical, it must be mounted in such a way that the view of each sensor is not obstructed by the spacecraft.

The size of this unit has been estimated to be 3 by 4 by 4 inches. The weight is 4 pounds. The power required is 0.5 watt. Data handling is quite similar to that of the charged-particle telescope described below; however, the bit rate is 42 bits per sample. The reliability of Cerenkov and scintillation counters would probably ensure that no in-flight calibration is required.

2.1.3.5 Cosmic-Ray Spectrum Analyzer

The cosmic-ray spectrum analyzer is designed to be used in the study of the energy region of primary interest in the case of solar and galactic cosmic rays. The energy range would accept 1 to 400 MeV protons. The aim set for such an experiment is to determine the intensity and flux gradient of charged particles in interplanetary space as functions of nuclear species and time. In order to measure the mass, energy, and charge of high-energy particles, improved versions of integrating and differential Cerenkov counters of the type used in Russian satellites would have to be developed.

An estimate of the design characteristics of such an instrument has been made by Professor Simpson of the University of Chicago. The general design of the experimental package would be similar to that of the High-Energy Proton Directional Monitor. The 4 sensors of 60-degree look angle must be appropriately mounted. For the case of the Mariner B spacecraft, this cosmic-ray spectrum analyzer was to be 6 by 6 by 18 inches, the weight being 18 pounds. The power required is 2.0 watts. Data would be received at a rate of 98 bits per sample.

2.1.3.6 Medium-Energy Proton Directional Monitor

The medium-energy proton directional monitor is intended as a secondary detector to back up both investigations of cosmic rays and measurement to planetary radiation belts. The design range is intended for the measurement of particles of energy 10 to 30 MeV, but it can be easily extended to 3 to 50 MeV. The geometry and location requirements are identical to those of the Cosmic-Ray Spectrum Analyzer. The size of such an instrument, proposed for a Mariner B spaceflight, is 4 by 4 by 5 inches, the weight being 3 pounds and the power requirement 1.0 watt. Data would be taken at a rate of 84 bits per sample.

2.1.3.7 Charged-Particle Telescope

The charged-particle telescope was on board the Mariner IV and functioned according to design specifications. This unit consists of three Au-Si, surface barrier detectors, together with aluminum and platinum absorbers. Two circular detectors, D_1 and D_2, have surface areas of 2.4 square centimeters. The area of detector D_3 is 5 square centimeters. In detectors D_1 and D_2, an acceptance cone angle of 40 degrees is provided for

the charged particles that are arriving. The geometrical factor provided for D_3 is determined by the exact location of a necessary temperature control fin.

The counting rates of charged particles fall into three intervals of particle energy. The ranges are listed in Table 2.1-4.

Table 2.1-4 INTERVALS OF PARTICLE ENERGY

	1	2	3
Protons	15-80 MeV	15-80 MeV	80-190 MeV
Electrons	.18-.35 MeV	none	none
Alphas	2-60 MeV	60-320 MeV	320 MeV-

The instrument is able to separate protons from alpha particles. The complete package weighs 2.6 pounds; 0.6 watt is needed for operation. The average information-bit rate for this experiment is 0.4 bit per second. At periodic intervals, the instrument is switched to a "calibrate" mode in order to check the performance of individual detectors.

The charged particle telescope must be mounted so that a 60-degree opening angle with apex at the front detector is not obstructed in its view of space when it is pointed away from the Sun. Within this cone angle lies the 40-degree opening angle of the telescope. The package must be electrically isolated from the spacecraft chassis except for a single wire into the DAS. In the case of Mariner IV, a mechanical envelope was used to provide a circular hole in the frame so that a thermal radiating shield could maintain a low temperature for the telescope.

2.1.3.8 Triple-Coincidence Cosmic-Ray Telescopes

A similar but more versatile instrument has been flown successfully on Explorer VI and Pioneer V. This radiation detector consists of an assembly of seven proportional-counter tubes. Six of the counters are grouped in a concentric ring around the seventh counter; the outer counters are connected in two adjacent groups of three to form two triple-coincidence telescopes.

The high-energy unit has a threshold of 75 MeV for the case of a triple-coincidence count caused by protons and a threshold for the case of electrons of 13 MeV. The threshold for detection of electrons through their bremsstrahlung radiation is approximately 200 keV. The thresholds for particle detection by means of the low-energy telescope are approximately 10 MeV for the case of protons and 0.5 MeV for the case of electrons.

The total weight of the coincidence telescopes is 9 pounds and the total power requirement is 0.5 watt. For the Ranger probes a digital output was coupled to the 14-bit counters which were then read out by the DAS at a rate of one per minute.

Two telescopes are placed so that their axes are normal to the probe-Sun line in such a way that particles incident from the general direction of the Sun can be seen by both high- and low-energy telescopes.

2.1.4 Solar Plasma Measurements

In addition to the solar cosmic rays produced by large flares, a number of lower-energy charged particles are continuously given off by the sun. This production of plasma is essentially a hydrodynamic expansion of the solar corona. This stream of particles is termed the solar wind. An important effect of the solar plasma is the distortion of the shape of the geomagnetic cavity within which the earth is located. This boundary is a rather sharply defined surface separating the region within which the earth's magnetic field exerts primary control over the particle motion from the interplanetary region. A similar transition region should occur in the vicinity of Jupiter. This region would be one of the primary targets to be observed by means of a solar plasma detector.

The interplanetary plasma, which is the solar wind, consists of ionized hydrogen and helium whose energies range from a few keV to hundreds of keV. The flux decreases as the distance from the sun increases; probably as $1/r^2$.

Outside the magnetopause, the main field of the Sun, rather than the trapped field of the pasma, is dominant. The solar wind carries part of the solar field with it and stretches out the lines so that they are very nearly radial in the vicinity of the Earth. A more accurate picture is given by consideration of an Archimedean spiral, which results from the fact that the field lines are carried around by the rotation

of the Sun. This is analogous to a rotating lawn sprinkler, which squirts water out radially, but makes a spiral pattern in the air at any instant of time. It may be that the solar wind is not smooth and regular, but turbulent; in which case the magnetic field lines trapped within it will become distorted. This phenomenon should occur at some large distance from the Sun, probably well beyond the orbit of Earth. The time and space variation of the solar plasma between Earth and Jupiter would help to differentiate between several theories of solar wind propagation.

The solar plasma experiment is designed to measure the flux and energy spectrum of the positively charged components of streams of solar plasma. The plasma flux measured by Pioneer V, Mariner II, and IMP in the vicinity of 1 AU averaged about 10^8 ions per square centimeter-second; however, this value fluctuates one or two orders of magnitude. This value corresponds to an electrical current density of only 1.6 by 10^{-11} ampere per square centimeter. At 5 AU, currents would be expected to be lower by an order of magnitude; when the total current is divided into several angle and energy channels, individual currents (which are another order of magnitude below this level) could be expected. The instruments developed for use in Mariner II and Mariner IV exhibit a threshold sensitivity of 10^{-13} ampere per square centimeter. This value should be extended one or two orders of magnitude for the case of a flyby mission to Jupiter.

The plasma analyzer used on the Mariner IV was designed to sample the plasma energy spectrum from 10 eV to 10 KeV. This probe consists of a solar-oriented electrostatic particle-energy analyzer which selects the desired particles; a Faraday cup that collects the charge of the particles which traverse the electrostatic field; an electrometer circuit for measuring the current caused by this collected charge; and a high-voltage generating system, which consists of a programmer and a sweep amplifier and is used to apply a sequence of voltages to the analyzer plates.

Calibration signals are inserted into the sequence of level sampling. The number of bits per plasma probe cycle is estimated to be 56 per sample. The exact specifications depend on the number of levels in the analyzer. A complete cycle of measurements on the Mariner II spacecraft took 3.7 minutes.

The entire experiment is mounted on the main chassis of the spacecraft; the entrance end of the analyzer plates is extended and pointed toward the Sun. The weight of the unit is estimated to be about 7 pounds. The power required is 2.5 watts.

2.1.5 Cosmic Dust Measurements

A knowledge of the spatial and temporal density of cosmic dust between the Earth and Jupiter (particularly in the asteroidal and near-Jupiter regions) is of great importance, both for understanding the sources and dynamics of these interplanetary particles and for the design of future manned and unmanned spacecraft and equipment.

An understanding of the nature, origin, and dynamics of the cosmic dust in interplanetary space is helpful in formulating any theory of the origin and evolution of the solar system. There are at least four possible sources for these particles:

1. The disintegration of comets

2. The collisional fragmentation of larger solid bodies, such as the Moon, the asteroids, or other planetoids

3. Interstellar particles which move through the solar system

4. Primordial particles remaining from the formation process of the solar system.

Prior to space exploration, small solid extraterrestrial masses had been observed by recovering and examining meteors and meteoritic dust which penetrated the Earth's atmosphere; by visual and radar observations of meteor trails; and by measurements of the zodiacal light, gegenschein, and solar corona. With the advent of space flight, direct measurements of the dust were conducted by means of space probes. These initial studies revealed a higher concentration of very small particles in the vicinity of the Earth than had been predicted from the earlier studies. In addition, the existence of particle "streams" was indicated. Concentrations of cosmic dust (of the very small particles) are thought to be dispersed by the Poynting-Robertson and other drag effects, as well as by the cumulative effects of small differences in the orbital elements of the individual particles. Any large concentration of particles such as the "streams" should therefore be of relatively recent origin.

Measurement of the dust in interplanetary space, outside of the Earth-Moon system, has been relatively limited. In Mariner II, a crystal microphone detector measured only two

impacts on its interplanetary trip to Venus. This unit was capable of measuring particles with a momentum down to about 7 by 10^{-4} dyne-second (or to 1.4 by 10^{-10} grams), with an assumed relative velocity of 50 by 10^{5} centimeters per second. The flux was thus calculated to be 6 by 10^{-6} particles per square meter-second-steradian. Mariner IV was capable of measuring particles with a momentum of at least 6 by 10^{-5} dyne per second. The data taken by means of this probe, which included over two hundred impacts, indicated an increase in the flux level with an increase in heliocentric distance from the earth to a maximum of 3.3 by 10^{-4} particles per square meter-second-steradian at a distance of 1.36 to 1.43 AU from the sun to 1.8 by 10^{-4} particles per square meter-second-steradian in the vicinity of Mars.

The trajectory to Jupiter will extend a distance from the sun of about 5 1/2 AU, will involve a path through the asteroid belt, and will pass near to the planet, probably within the orbits of its moons. Present data are insufficient to predict what flux levels or average particle sizes will be encountered.

The cumulative influx rate of the micrometeoroids, as a function of particle mass, has been observed near the Earth to increase logarithmically with decreasing particle size down to the Poynting-Robertson limit of about 10^{-11} gram. Whether or not this relation, combined with the Mariner data, can be extrapolated to define the micrometeoroid environment of the asteroid belt and the Jupiter environs is not certain. It may well be that there is a higher relative concentration, especially of the larger particle sizes in the asteroidal region between Mars and Jupiter, than between Earth and Mars.

To date, most of the measurements of micrometeoroids have been made by means of a piezoelectric crystal microphone detector. Upon impact, the output of the microphone is proportional to the momentum of the impacting particle (except at extremely high velocities). Thus, if a velocity for the particle is assumed, its mass may be calculated. In another type of detector, a photomultiplier device is used to measure the light flash of an impact. This instrument, which is also used to measure a mass-velocity combination (energy), is capable of measuring a much smaller mass than the microphone detector, but it is not as simple in operation nor as reliable. There are other types of detectors which have been used or proposed, but they probably would not be as suitable for the first Jupiter mission. A possible exception may be devices

similar to those used on Explorer XVI to observe the larger particles.

In addition to the mass-velocity combination measurements, other information relevant to the particles would be useful; these include mass and velocity alone, penetrating and cratering ability, electrostatic charge, and composition and other physical properties. While instruments capable of performing these measurements will eventually be developed, a proven device is suggested for use in this study.

A suitable cosmic dust detector is one similar to the instrument used on the Mariner IV spacecraft. An advantage to using this instrument is that the data from the two probes would then be directly comparable. This device detects the impact of cosmic dust particles upon a sensor plate. This sensor is an aluminum plate .030 inch thick. A crystal acoustical transducer that yields a signal amplitude proportional to the momentum of the particle is bonded to one side of this plate. The sensor plate is coated on both sides with a dielectric material. A thin film of aluminum is then deposited over this dielectric. The combination of impact plate, dielectric, and aluminum film forms a penetration detection capacitor. When a static potential is connected across the capacitor, an impact will produce a voltage pulse across a connecting resistor. The films are over an order of magnitude more sensitive than the microphone; consequently, their primary function is to indicate the direction of the impacting particle and to detect particle hits below the microphone threshold.

The instrument would be in continuous operation throughout the duration of the mission. It is calibrated in flight, at time periods on the order of one day, by means of an acoustical transducer. Upon receipt of a command, the transducer imparts a mechanical shock to the input plate, producing an output from the detector microphone.

The plate is a bidirectional sensor. The particular plate on the Mariner IV was 22 by 22 centimeters and weighed 0.5 pound. The sensor may be mounted anywhere to provide approximately a π-steradian view (in the Mariner IV it was attached to the electronics chassis in the main part of the spacecraft). The total weight of sensor and associated electronics is 2.5 pounds. The power required is 0.2 watt. One side should look into the plane of the ecliptic (or the plane containing the Earth and Jupiter) in direct motion, and the other side should look into the same plane in retrograde motion.

2.1.6 Television

The obvious advantage of receiving pictures of Jupiter taken by a television camera in a near passage of the planet is an increase in the spatial resolution over that presently available from the Earth. What is not obvious, however, is the actual utility of such pictures.

At the present time, the maximum resolution of surface features on Jupiter, obtainable with large-aperture telescopes on the surface of the Earth, is close to 1000 kilometers. Therefore, only the grossest features, such as the latitude banding and the red spot, are discernable. Since the earth-based resolution of the large telescopes is limited by the atmosphere, telescopes placed in Earth orbit will allow an increase in the resolution. In the case of a diffraction-limited Earth-orbit telescope with an aperture of 40 inches, the resolution is about one-tenth of a second of arc, or approximately 200 to 300 kilometers at the surface of Jupiter.

It is difficult to predict what detailed information an increased spatial resolution will yield in terms of the data presently available on Jupiter. It is known that Jupiter is cloud-covered, yet these cloud systems are not featureless. Even in terms of the present data, it is possible to surmise, in general, what an increased resolution may yield about several of the visible features.

With a resolution of the order of several tens of kilometers, the fine structure of the features presently observed could be detected. The red spot, for example, may be seen to be characterized by smaller features, a knowledge of which would allow a better explanation of the spot's origin and existence, or the boundaries between the various latitude bands may be examined to establish their fine structure.

In addition, the pictures may provide information regarding the meteorology of the outer Jovian atmosphere. Cyclonic and anti-cyclonic-type features may be visible, and their size and distribution may be indicative of the dynamics of the meteorological processes operating on the planet.

With a resolution ranging from a few kilometers down to a few hundred meters, it may be possible to determine the fine structure of the upper cloud layers in order to establish whether Jupiter's atmosphere is the convective adiabatic or stratospheric isothermal-layer type. Thus, information about

the presence of an internal source of heat in the planet would be derived.

While the inspection of the light side of the planetary surface is the most important phase of the television camera mission, there are other observations that would yield useful information. A view of one of the Galilean satellites may provide information concerning the nature of its surface and the presence or absence of an atmosphere. On the dark side of the planet, the presence of large thunderstorms may be indicated by flashes of lightning that would be visible to the camera. Observations of the number and extent of these flashes would yield information concerning the nature and dynamics of the atmosphere. Near the limb of the planet, aurora may be seen, especially within about ten to thirty degrees of the magnetic poles.

In addition to the resolution discussed above, the importance of areal coverage must also be included in the consideration of gathering information by television pictures. The area covered must be sufficient to allow interpretation of the individual specific features or parts of such features observed as they are related to the larger features. Thus, if a requirement is warranted for obtaining an order of magnitude increase in the resolution over an earth-orbit telescope, this increase must be so effected that the fine structure observed can be interpreted in terms of the larger structure to which it is related.

The trade-offs between resolution and area covered are difficult to establish, but a general assumption of an order of magnitude increase in resolution to be used with two orders of magnitude decrease in areal coverage (actually one order of magnitude decrease in the radius of the areal coverage) is considered adequate for the purposes of this study. Thus, if the resolution of 200 to 300 kilometers is obtained of the whole planetary disc, a resolution of 20 to 30 kilometers is dependent on obtaining a picture (or composite of more than one picture) covering at least one-tenth of the planetary diameter. An apparently attractive, optional method of combining areal coverage with high resolution is to use an auxillary lens on the camera that would permit the taking of wide angle views intermixed every few frames with the high-resolution pictures. This type of data gathering would allow the orientation of the high-resolution pictures on the planetary surface.

For planning purposes, a general-purpose television camera with an angle of view of 1.5 degrees, a raster of 400 lines per frame, and thirty-two shades of gray is conceived. The pictures would be taken in overlapping triplets through three spectrally separated filters (e.g., 3000-5000-8000Å). A special constraint in using filters is to insure that their spectral response does not change appreciably or by an unknown amount as a result of exposure to the space and planetary radiation environment. The television package weighs 15 pounds, and 10 watts of power are required for operation. The approximate size is 4 by 4 by 10 inches.

Table 2.1-5 contains a list of the areas covered and the spatial resolutions for several distances from the planet in terms of the general-purpose camera specifications described above. The use of this general-purpose camera in a representative mission may be examined by considering a flyby of Jupiter with a closest approach of one-half of a planetary radius, a passage of thirty degrees from the south pole and a program of taking fifty pictures at one-minute intervals, starting at a planetocentric distance of two and one-third Jovian radii. The slant range of the picture series for a fixed-scan camera will vary from about 160,000 to 50,000 kilometers from the visible planetary surface. The resolution and areal coverage attained may be estimated from Table 2.1-5. It should be noted that this sequence will include some pictures of the dark side of the planet. The camera system may be roughly calibrated by taking pictures of free space prior or after the planetary encounter.

This mission may be considered to be representative and may be used in the considerations of mission planning and data handling. However, the actual spectrum of possibilities of various cameras, trajectories, and data handling capabilities is much more involved than is indicated in this description of a single mission. More complicated situations may be envisioned for the larger payloads when use will be made of more than one camera.

Table 2.1-5 TELEVISION I

Distance from Center of Jupiter (Jupiter Radii)	Distance from Visible Surface of Jupiter (km)	Area Covered* (km on a side)	Max. Theoretical Spatial Resolution* (km)
11.0	700,000	18,300	90
5.0	280,000	7,300	37
4.0	210,000	5,500	27
3.5	175,000	4,600	23
3.0	140,000	3,700	18
2.5	105,000	2,800	14
2.0	70,000	1,800	9
1.8	56,000	1,500	7
1.5	35,000	900	5
1.3	21,000	600	3
1.1	7,000	180	1

* On a plane surface normal to the pointing direction of the camera.

A television package consisting of two cameras, one for large areal coverage and one for high resolution, is described below:

Camera I - Raster of 1000 lines per frame
Angle of view of 10 degrees
Thirty-two shades of gray

Camera II - Raster of 400 lines per frame
Angle of view of 1 degree
Thirty-two shades of gray.

The pictures are so oriented that the area covered in pictures taken by Camera II are in known locations within the area covered by the pictures taken by Camera I.

The area covered and the resolution of these cameras for various distances from the planet are given in Table 2.1-6. The weight of this television package is taken as 30 pounds, and 20 watts of power are required for operation. The size is approximately 5 by 7 by 14 inches.

This camera package is considered for the "full" payload package.

A constraint relative to all of the cameras is that they must be mounted on the spacecraft in such a location that no light is reflected from any part of the spacecraft into the cameras.

2.1.7 Photometric, Spectrometric, and Radiometric Measurements

Photometric, spectrometric, and radiometric measurements made in a flyby mission of Jupiter have three distinct advantages over those made from the surface of the Earth. These advantages are (1) access to the entire Jovian phase angle; (2) freedom from the absorbing atmospheric envelope surrounding the Earth; and (3) an increase in the spatial resolution of measurements at the planetary surface (and also the greater angle subtended by the planet, which enables the use of a greater amount of energy flux available at the detector).

If the same comparison is made between measurements made in a flyby mission and an Earth-orbit location, it is seen that (1) the resolution advantage is reduced by about an order of magnitude (however, in the case of weak sources, the increase in

Table 2.1-6 TELEVISION II

Distance from Center of Jupiter (Jupiter Radii)	Distance from Visible Surface of Jupiter (km)	Area Covered* (km on a side)	Max. Theoretical Spatial Resolution* (km)
	Camera I		
11.0	700,000	114,000	228
5.0	280,000	48,200	96
4.0	210,000	36,200	72
3.5	175,000	30,200	60
3.0	140,000	24,200	48
2.5	105,000	18,200	36
2.0	70,000	12,000	24
1.8	56,000	9,600	19
1.5	35,000	6,000	12
1.3	21,000	3,600	7
1.1	7,000	1,200	2
	Camera II		
11.0	700,000	12,200	60
5.0	280,000	4,900	24
4.0	210,000	3,700	18
3.5	175,000	3,100	16
3.0	140,000	2,400	12
2.5	105,000	1,800	9
2.0	70,000	1,200	6
1.8	56,000	980	5
1.5	35,000	610	3
1.3	21,000	370	2
1.1	7,000	120	0.6

* On a plane surface normal to the pointing direction of the camera.

energy flux may be significant); (2) the advantage of freedom from the absorbing envelope is nearly eliminated; and (3) the advantage of access to the entire Jovian phase angle is retained.

In establishing a scientific payload for a Jupiter flyby at the present time, a decision is necessary regarding the assumption that astronomical earth orbit measurements will be possible at or before the time period for the flyby mission. Because of mission complexity and long duration, it will be assumed, for the purposes of this study, that higher priority will be given to experiments which can be performed to best advantage only on a mission to Jupiter instead of those which can be accomplished from or near the Earth. Therefore, experiments will be assigned a higher relative importance when they involve (1) the view of locations on the planet that are inaccessible to near-earth observations or (2) the use of a high spatial resolution.

2.1.7.1 Photometers

A photometer to measure the relative brightness reflected from Jupiter at various phase angles would allow a determination of the phase function for the planet $I(\alpha)/I(o) = \phi(\alpha)$. A relatively simple instrument could be used in a limited payload that would merely sample the brightness at a frequency near the solar maximum of around 5000Å at five-degree intervals around the planet. A slight modification to this experiment will include a filter wheel to look in a wide spectral region and also to make polarimetric measurements, thus allowing the definition of the polarimetric phase curve. A filter wheel with filters centered on wavelengths of 3000, 5000, 7000, and 9000 angstroms and two polarizers would provide suitable data.

It is envisioned that a simple instrument to measure only the brightness variation would weigh 2.0 pounds, would require 1.5 watts, and would provide a data output of 3 bits-per-second. With an increased capability of sampling at several wavelengths and measuring polarization, the instrument would weigh 6.0 pounds, would require 5.0 watts, and would provide a data output of 50 bits-per-second. These instruments, as with the TV system, will not yield reliable data if light is reflected from any part of the spacecraft into the sensing element. To aid in obtaining an accurate calibration of the data and to provide relative qualitative compositional information across a larger portion of the disk, the photometer would be programmed to scan the planet perpendicular to the flight path in addition to the traverse along the flight path during the measurements. This perpendicular scanning action is important to the calibration

of the total intensity measured, because the photometer integrates what it sees within its field of view. Thus, if there are variations within the field of view, an average value will be taken. Because the solid angle of view is constant and the distance from the visible planetary surface changes, that portion of the planet viewed by the photometer decreases as the probe gets closer to the planet. Although this will complicate the interpretation of the data, it is difficult to avoid. The use of a variable focal length lens would probably create more problems than it would solve.

An in-flight calibration of the instrument will have to be made at least twice, once prior to and once after the actual measurements. The calibration will require looking at a very stable internal radiation source (a Cherenkov source is suitable) through each of the filter wheels. Another method of calibration would be to look at a star of known brightness. In order to obtain really useful data, the measurements would have to be accurate to within one percent, or a few tenths of one percent would be especially desirable.

2.1.7.2 Radiometers

A radiometer may be used to measure the temperature distribution of the planet on both the light and dark sides. In addition to a general survey at various phase angles, specific locations on the surface could be examined. An especially interesting locale would be that in the vicinity of the poles where the clouds might be thin enough to permit the observation of the solid surface.

A single- or dual-channel instrument used in a mapping mode would provide significant information relative to compositional lateral distributions. A multichannel device, with wavelengths centered at absorption bands of ammonia and water and at wavelengths between, including the emission around the radiation temperature peak, would yield important data concerning composition, compositional abundances, and vertical compositional distributions.

A four-channel radiometer, as suggested in Reference 2.1-1, to measure the radiation at 4, 8, 13, and 20 microns is appropriate to the subject mission. The instrument would weigh 28 pounds, would require 6 watts of power, and the antenna would be about 30 centimeters in diameter. There would be a data output of 30 bits-per-reading. If a reading is made once every five minutes starting three hours prior to perijove, once every

minute one hour prior to and continuing until one hour after perijove, and then again every five minutes to three hours after perijove, sufficient data should be provided for this measurement. The instrument would be calibrated after each measurement by reference to an internal noise source.

An infra-red radiometer may be used to measure the thermal emission from the planet, and also to derive some information about the composition of the atmosphere. Although this instrument is somewhat redundant to the microwave radiometer, such redundancy is desirable on an extended mission. Mapping of the surface at at least two wavelengths would aid in the study of the unexplained radiation leak. A view near the poles is also suggested. A two-channel instrument operating at 10 to 20 microns is satisfactory. Such an instrument would weigh about 5 pounds, require 3 watts of power, and would have a data output of 15 bits-per-reading. The readings would be taken in the same schedule as given for the microwave radiometer. The instrument would in fact be mounted with the microwave radiometer antenna.

2.1.7.3 Spectrometers

An infra-red spectrometer should also be considered for use in obtaining data relevant to the planetary compositions and composition abundances. The device would operate in the region from approximately 5 to 30 microns, with a resolution of one micron. This range would allow scanning over bands of methane, ammonia, and water, and viewing of the spectral region of interest in order to obtain a better understanding of the nature of the unexplained thermal radiation leak. An instrument of this type would weigh about 16 pounds, require 5 watts of power, and have a data output of 5000 bits-per-scan and a scan rate of one per five or ten minutes. The instrument will start operation three hours prior to encounter and continue for three hours after encounter. It would take approximately one minute to complete one scan. A thermoelectric device or equivalent appears satisfactory for cooling the detector.

An ultra-violet-to-visible spectrometer may also be considered for the detection of minor constutuents of the Jovian atmosphere. A frequency range of 1000 to 6000 Å with a spectral resolution of 10 Å would be adequate. The instrument weighs 20 pounds and requires 10 watts. A bit rate of 10^4 bits per scan which would start at a distance of five planetary radii prior to encounter and continue until five planetary radii after encounter is planned with readings taken every 5 to 10 minutes.

2.1.8 Radio and Radar

A bistatic radar may be used (at a frequency above about 40 Mcs.) to measure the radar-scattering function at various phase angles. This measurement may also be made in interplanetary space to obtain information on the absolute electron density. One operational program that is envisioned involves an instrument with a weight of 15 pounds, a power requirement of 8 watts, a bit rate of 30 bits-per-sample, and which can be used to take samples every three minutes starting at three planetary radii from the surface prior to encounter and continuing to three planetary radii from the surface after encounter.

A null radio seeker may be used to determine the location of particular radio sources and may provide information relevant to the nature of the source of the electromagnetic disturbances. An instrument of about 5 pounds with a power requirement of 2 watts, a data rate of 50 bits-per-sample, and an operational program similar to that of the bistatic radar will be required. The procedure will thus probably involve taking measurements in and below the radiation belts. The directional antenna would have to be gimbled to move in any direction across the planetary disc.

A radio experiment designed to search for possible emission at low flux levels would provide information that would augment that available from measurements from the Earth. Measurements made in the decimeter wavelength region would be desirable. A representative instrument would weigh about 5 pounds, require 4 watts of power, and provide a data output of 50 bits-per-second during its program operation of three hours prior to encounter to three hours after encounter.

A radar altimeter may be used to obtain information about the planetary structure. Reflection off the solid planetary surface may be obtained with a wavelength of about one-half to one meter. Longer wavelengths reflections would be from the ionosphere, while shorter wavelengths would be affected by molecular absorption in the atmosphere. The instrument would weigh about 25 pounds, require about 10 watts of power, and provide a data rate of 50 bits-per-sample. An operational program of taking measurements every five minutes from three hours prior to encounter to three hours after encounter would be satisfactory. The antenna would have to point at the planet during the measurements.

2.1.9 Miscellaneous

In addition to the information obtained from the scientific instruments defined in the preceding sections, there are other means by which information may be generated. These are described in the following paragraphs:

1. The normal measurement of the position of the spacecraft as a function of time will yield data relevant to a more accurate determination of the orbital and gravitational parameters of Jupiter, (and probably the solar system, by a better determination of the astronomical unit). Increased accuracy in the values of the Jovian mass and second gravitational harmonic should result from the measurement of the spacecraft's hyperbolic orbit about the planet.

2. An occultation experiment, similar to the one performed with the Mariner IV spacecraft in its passage of Mars, should be performed in the Jupiter fly-by mission to obtain data relevant to the structure of the Jovian atmosphere and ionosphere. This measurement will require the reception at the spacecraft of a radio signal transmitted from the Earth, a coherent retransmission back to Earth, and the reception of the signal at the Earth station. The changes in the frequency, phase, and amplitude of the signal will provide the necessary information.

3. The feasibility of releasing a probe into the Jovian atmosphere should be examined. The capability of such a probe to yield direct, quantitative data may outweigh the problems involved in its operation. This probe could contain a mass spectrometer to give information about the relative compositional abundances of the planet. In particular, a determination of the relative abundance of deuterium would be especially valuable in providing information concerning the origin and history of the solar system and the universe. Determination of the existence and abundance of deuterium at Jupiter would aid in establishing whether or not this isotope had its origin as a remnant of the primordial atmosphere or is the result of a secondary nuclear process, as is probably the case for the Earth. Jupiter, unlike the Earth, is massive enough to retain its hydrogen and is large enough to have the element present in a relatively undiluted abundance. The relative abundance of deuterium may thus be indicative of the nuclear reactions involved in the very early formation of the universe. A probe

into the Jovian atmosphere could also measure such parameters as pressure, temperature, density, electric charge, and others.

It may be possible, although its feasibility is uncertain at the present time, to use an interferometer spectrometer that would scan a small wavelength region at a very high resolution to look for lines of HD, NH_2D, or CH_3D. This might be an optional method of detecting deuterium in the Jovian atmosphere.

4. Using Jupiter or one of its satellites to provide a turn-around so that the spacecraft would follow an out-of-the-ecliptic trajectory after planetary encounter would allow the continuation of the interplanetary measurements in a region of the solar system different from that encountered on the inbound path.

5. There should be at the same time as the Jupiter mission an Earth-orbiting satellite to gather radiation data similar to that obtained by the Jupiter spacecraft. This second satellite would allow a wide spatial separation in the data-gathering points and would yield information about the dynamics of these radiations as they propagate through the solar system.

2.1.10 Scientific Instrument Characteristics

In Table 2.1-7, the physical characteristics of the instruments necessary to perform the suggested scientific experiments are outlined.

2.1.11 Typical Mission Payloads

Typical scientific mission payloads ranging from a minimum instrument complement to a "full" package are represented in Table 2.1-8. The first package represents a payload that could be employed in a spin-stabilized spacecraft. The "full" experiment list represents a wide spectrum of investigations and would be expected to yield a relatively complete picture of the planet for the flyby mission. It is possible, however, that the individual instruments could be expanded in size and scope thus increasing the full payload size. It is suggested that, if a substantial increase in payload weight is available, it could best be utilized in putting the vehicle in an orbit around Jupiter rather than adding additional scientific payload weight.

Table 2.1-7 SCIENTIFIC INSTRUMENT CHARACTERISTICS
(Sheet 1)

Instrument	Weight (lbs)	Size (inches)	Power (Watts)	Data Requirements	Calibration	Location	Operating Regime	Special Considerations
Magnetometer	electronics 5.0 Two-sensor: 1.5 each	electronics 4 x 4 x 6 Two-sensor: 13 dia spheres	7.0	56 bits/ sample	on-off pulse from DAS	Sensor as far from bus as possible	Planetary & Inter-planetary	Remant magnetic field of bus should be reduced to a fraction of a gamma at the sensor. Temperature range of sensor 30 to 55° C.
Low Energy Particle Detector	2.5	electronics: 3 x 5 x 6 sensor: Four-5 x 1 dia.	0.4	45 bits/ sample	Internal Alpha Source	On bus, sensors exposed	Planetary & Inter-planetary	Sensors point in plane normal to Sun-probe line. Basic instrument of type used on Mariner IV.
High Energy Proton Directional Monitor	4.0	electronics 3 x 4 x 4 sensor: Four-5 x 1 dia.	0.6	42 bits/ sample		Sensors extend out of package on bus	Inter-planetary	Energy response variable over a wide range. Sensors not to point toward Sun.
Medium Energy Protron Directional Monitor	3.0	electronics 4 x 4 x 5 sensor: Four-5 x 1 dia.	1.0	84 bit/ sample	Pulses from DAS	Sensors extend out of package on bus	Inter-planetary & Planetary	Sensors not to point toward Sun
Ion Chamber	3.0	5 x 10 x 13	0.5	14 bit/ sample		On boom three feet from bus	Planetary & Inter-planetary	Basic instrument of type used on Mariner IV.
Plasma Probe	7.0	6 x 8 x 8	2.5	56 bits/ sample	Pulse from DAS	On bus, sensor exposed		Sensor to look toward Sun approximately 10 degrees above Sun-prove line.
Cosmic Ray Spectrum Analyzer	18	electronics: 6 x6 x 18 sensor: Four-5 x 1 dia.	2.0	98 bits/ sample	Internal Source	Sensors extend out of package on bus.	Inter-planetary & Planetary	Sensors not to point toward Sun.

Table 2.1-7 SCIENTIFIC INSTRUMENT CHARACTERISTICS
(Sheet 2)

Instrument	Weight (lbs)	Size (inches)	Power (Watts)	Data Requirements	Calibration	Location	Operating Regime	Special Considerations
Microwave Radiometer	28	6 x 10 x 14	6	30 bits/ reading	Internal noise source	Antenna to look at and scan planet, electronics in bus.	Planetary	Antenna is about 12 inches in diameter. Must only see planet (and reference horns if used).
Infrared Spectrometer	16	10 x 12 x 14	5	5000 bits/ scan	Internal comparison source spectra	Electronics in bus. Sensor to look at planet	Planetary	
UV-Visible Spectrometer	20	10 x 13 x 16	10	10,000 bits/scan	Internal comparison source spectra	Electro-nics in bus. Sensor to look at planet	Planetary	Cannot tolerate sunlight into instrument at any time, scattered light during measurements
Bistatic Radar	15	6 x 6 x 12	10	30 bits/ sample		Antenna visible to Earth and Jupiter	Planetary (Possibly alsof Inter-planetary)	
Null Radio Seeker	5.0	4 x 6 x 6	2	50 bits/ sample		Direction-al antenna looks at Jupiter	Planetary	
Radio Noise Detector	5.0	4 x 6 x 6	4	60 bits/ sample		Antenna looks at Jupiter	Planetary	
Radar Altimeter	25	6 x 10 x 12	10	50 bits/ sample		Antenna looks at Jupiter	Planetary	

Table 2.1-7 SCIENTIFIC INSTRUMENT CHARACTERISTICS
(Sheet 3)

Instrument	Weight (lbs)	Size (inches)	Power (Watts)	Data Requirements	Calibration	Location	Operating Regime	Special Considerations
Triple Coincidence Cosmic Ray Telescope	9.0	electronics: 2 x 6 x 6 Sensor: 5 x 3.5 dia.	0.5	112 bits/ sample		On bus, Sensor Exposed	Inter-planetary & Planetary	Axis of Sensor normal to Sun-probe line. Similar to instrument on Explorer VI
Charged Particle Telescope	3.0	2 x 6 x 6	0.6	56 bits/ sample	Internal Alpha Source	On bus, Sensor exposed	Inter-planetary & Planetary	Sensor to look away from Sun. Similar to instrument on Mariner IV.
Cosmic Dust Detector	2.5	electronics: sensor: 1 x 22 x 22	0.2	8 bits/ sample	One known acoustic pulse per day	Sensor plate perpendicular to ecliptic plane.	Inter-planetary & Planetary	Similar to instrument on Mariner IV.
Television I	15	4 x 4 x 10	10	calculated from camera description	Pictures of free spaces	On scanning platform on bus.	Planetary	Must not have scattered light into instruments.
Television II	30	5 x 7 x 14	20	calculated from camera description	Pictures of free space	On scanning platform on bus	Planetary	Must not have scattered light into the instrument.
Visible Photometer	2.0	2 x 3 x 6	1.5	30 bits/ sample	Standard brightness source	On scanning platform on bus	Planetary	Cannot have scattered light into instrument
Expanded Photometer	6.0	4 x 5 x 6	5.0	130 bits/ sample	Standard brightness source	On scanning platform on bus	Planetary	Cannot have scattered light into instrument

Table 2.1-8 SCIENTIFIC EXPERIMENT PACKAGES
(Sheet 1)

Spin-Stabilized Spacecraft Experiment Package

Instrument	Weight	Power
Extended Magnetometer	8 lbs.	7 watts
Low-Energy Particle Detector	2.5	0.4
Cosmic Dust Detector	2.5	0.2
	13 lbs.	7.6 watts

Minimal Scientific Experiment Package

Instrument	Weight	Power
Extended Magnetometer	8 lbs.	7 watts
Low-Energy Particle Detector	2.5	0.4
Cosmic Dust Detector	2.5	0.2
Expanded Photometer	2.0	1.5
TV Camera (TV-I)	15.0	10.0
Plasma Probe	7.0	2.5
	37 lbs.	21.6 watts

Table 2.1-8 SCIENTIFIC EXPERIMENT PACKAGES
(Sheet 2)

Intermediate Scientific Experiment Package - 1

Instrument	Weight	Power
Extended Magnetometer	8.0 lbs.	7.0 watts
Low-Energy Particle Detector	2.5	0.4
Cosmic Dust Detector	2.5	0.2
Expanded Photometer	6.0	5.0
TV Camera (TV-I)	15.0	10.0
Plasma Probe	7.0	2.5
Microwave Radiometer	28.0	6.0
Infrared Radiometer	5.0	3.0
Ion Chamber	3.0	0.5
	77.0 lbs.	34.6 watts

Intermediate Scientific Experiment Package - 2

Instrument	Weight	Power
Extended Magnetometer	8.0 lbs.	7.0 watts
Low-Energy Particle Detector	2.5	0.4
Cosmic Dust Detector	2.5	0.2
Expanded Photometer	6.0	5.0
TV Camera (TV-I)	15.0	10.0
Plasma Probe	7.0	2.5
Microwave Radiometer	28.0	6.0
Infrared Radiometer	5.0	3.0
Ion Chamber	3.0	0.5
Infrared Spectrometer	16.0	5.0
High Energy Proton Directional Monitor	4.0	0.6
Cosmic Ray Spectrum Analyzer	18.0	2.0
	115 lbs.	42.2 watts

Table 2.1-8 SCIENTIFIC EXPERIMENT PACKAGES
(Sheet 3)

Full Scientific Experiment Package

Instrument	Weight	Power
Extended Magnetometer	8.0 lbs.	7.0 watts
Low-Energy Particle Detector	2.5	0.4
Cosmic Dust Detector	2.5	0.2
Expanded Photometer	6.0	5.0
TV Camera (TV-II)	30.0	20.0
Plasma Probe	7.0	2.5
Microwave Radiometer	28.0	6.0
Infrared Radiometer	5.0	3.0
Ion Chamber	3.0	0.5
Infrared Spectrometer	16.0	5.0
High Energy Proton Directional Monitor	4.0	0.6
Cosmic Ray Spectrum Analyzer	18.0	2.0
UV - Visible Spectrometer	20.0	10.0
Medium Energy Proton Directional Monitor	3.0	1.0
Bistatic Radar	15.0	8.0
Radio Noise Detector	5.0	2.0
Null Radio Seeker	5.0	2.0
Radar Altimeter	25.0	10.0
	203.0 lbs.	85.2 watts

2.1.12 References

Numerous articles and reports relative to the scientific investigations of Jupiter were utilized in this report; however, a complete list is not being included. There were four references that were used extensively in defining the descriptions of the scientific instruments in this report. These are listed below:

2.1-1 "Survey of a Jovian Mission," Report No. M-1, Astro Sciences Center of IIT Research Institute, March 1964.

2.1-2 "Jupiter - Advanced Planetary Probe, Scientific Objectives and Typical Experiments," R. G. Brereton, JPL.

2.1-3 "Mariner C Reference Information for Future Mission Studies," JPL Engineering Planning Document No. 296, 15 April 1965.

2.1-4 "Design Data Information System," JPL, 1 October 1965.

2.2 ENERGY REQUIREMENTS AND GENERAL TRAJECTORY CHARACTERISTICS

The basic sources of information regarding energy requirements and general trajectory characteristics are the mission maps presented in Appendix A. In addition, certain other information, specifically guidance sensitivity parameters, were obtained from heliocentric conic trajectory data supplied by JPL. Data from these sources have been summarized in charts which are designed to aid the mission planner in the analysis of mission requirements. The methods used, the results obtained, and the conclusions reached in this process of summarizing mission characteristics are discussed in following paragraphs.

2.2.1 Launch Window Definition

The injection energy requirements and other characteristics of interplanetary missions are influenced by the ground rules for selecting launch windows. Since one of the primary objectives of mission analysis is to determine the relationship between flight time and the injection energy required for the mission, it would seem logical for this purpose to use fixed-flight-time windows of the type illustrated in Figure 2.2-1. The determination of energy requirements for such windows over a selected range of flight times would define a curve of energy requirement versus flight time. However, if flight time is held constant as the launch date is delayed, the time of arrival at Jupiter must also be delayed. In the areas of spacecraft design and mission operations, there are significant advantages in holding the encounter date constant for any launch date within the window. A number of important mission parameters, such as communication distance at encounter time, arrival hyperbolic excess velocity, size of the guidance error ellipse, etc., are either uniquely determined by the arrival date, or else they remain more nearly constant if the arrival date is held fixed than if the flight time is held fixed. For these reasons, fixed-arrival-date windows have been used for the purpose of defining mission requirements. Arrival dates themselves are of little interest to spacecraft designers, and mission requirements, although determined on the basis of arrival date, are commonly identified by reference to a characteristic flight time. The characteristic flight time used for this purpose is the mean flight time within the appropriate window. Actual flight times within the window differ from the characteristic flight time by as much as half the window width, but such variations are relatively small when compared to the overall flight time itself.

As illustrated in Figure 2.2-2, the injection energy requirement is strongly dependent on the width of the launch window. A nominal width of 20 days was selected for defining mission requirements in

LAUNCH WINDOW DEFINITION

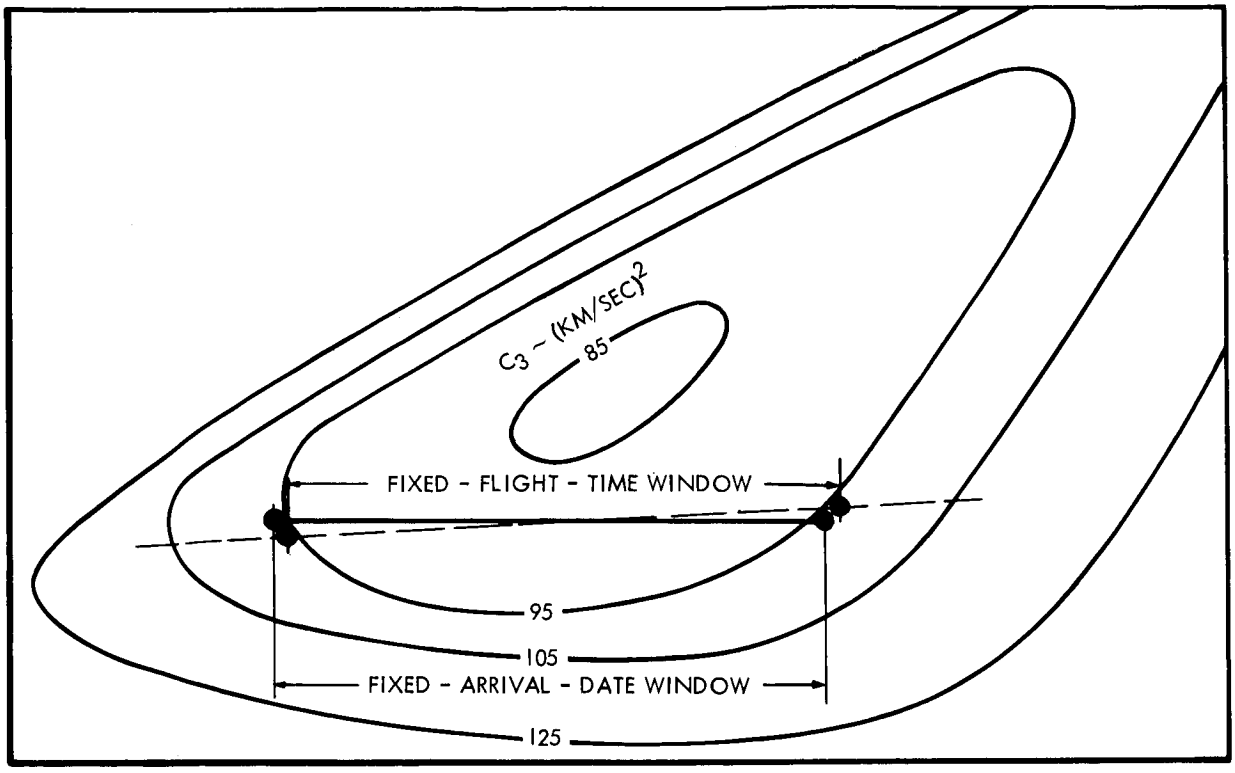


FIG. 2.2-1

INJECTION ENERGY AS A FUNCTION OF WINDOW WIDTH

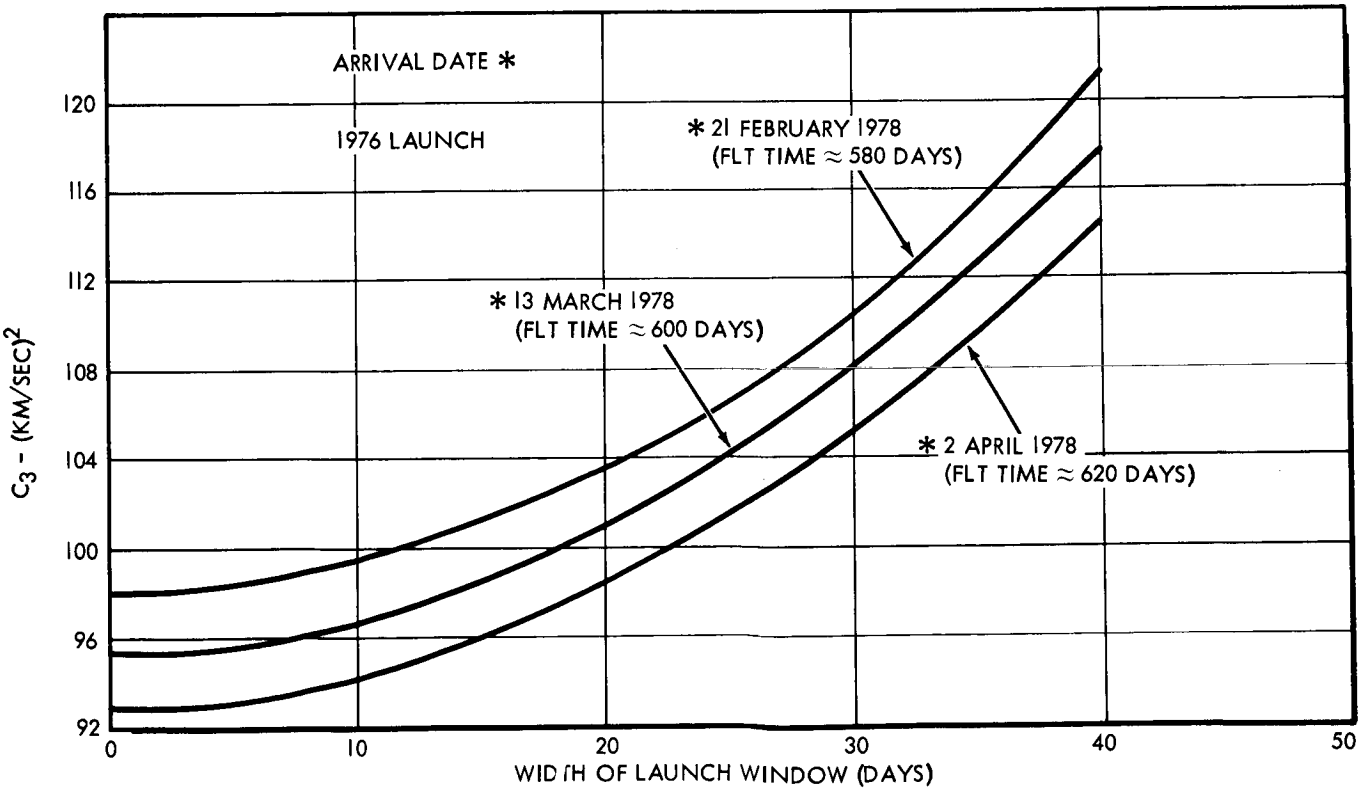


FIG. 2.2-2

this study. This is womewhat less than the width normally considered desirable for, say, Mars and Venus missions. However, injection energy "valleys" for Jupiter missions are considerably narrower than comparable valleys for Venus and Mars. Because Jupiter's synodic period (i.e., the interval between launch opportunities) is only about half as long as the synodic periods of Venus and Mars, the narrower window width is considered justifiable.

Another launch-window ground rule which has a significant effect on mission requirements in some launch years is the stipulation that the declination of the departure asymptote must fall within the range of $\pm$ 36 degrees for all nominal trajectories. This restriction was imposed in line with an overall policy of conservatism which is believed to be desirable in a feasibility study of this nature. Assuming a minimum acceptable daily lift-off window of approximately an hour, plus 36 degrees and minus 36 degrees represent the approximate limiting values of asymptote declination which can be realized (without an orbital plane change) by a launch from Cape Kennedy within the normal firing sector of 90- to 114-degree launch azimuths. Orbit determination during the first few days after injection into the interplanetary trajectory is another factor which was considered before selecting the asymptote declination limits. If the magnitude of the declination of the asymptote were very much greater than 36 degrees, DSIF stations in only one hemisphere (northern or southern) could be used to track the spacecraft during this critical period. Since a spread of tracking-station latitudes is desirable for accurate orbit determination, such a situation should be avoided if possible.

A launch "corridor", defined by the loci of launch-window boundary points, is shown in Figure 2.2-3. Although the figure is entitled "Typical Launch Corridor", the corridor is not typical in the sense that in most launch years the 36-degree asymptote declination constraint does not cause the corridor to swerve so drastically away from the minimum-energy region as indicated.

2.2.2 Arrival Date Corrections

The departure and arrival dates and flight times associated with heliocentric conic two-body trajectory computations are somewhat erroneous because the gravitational acceleration of the spacecraft caused by the planetary fields is ignored. The effect of Earth's gravity field is comparatively small, and the few hours error in departure date can be ignored for most purposes of mission analysis. However, Jupiter's gravity field is sufficiently strong to cause flight-time

TYPICAL LAUNCH CORRIDOR

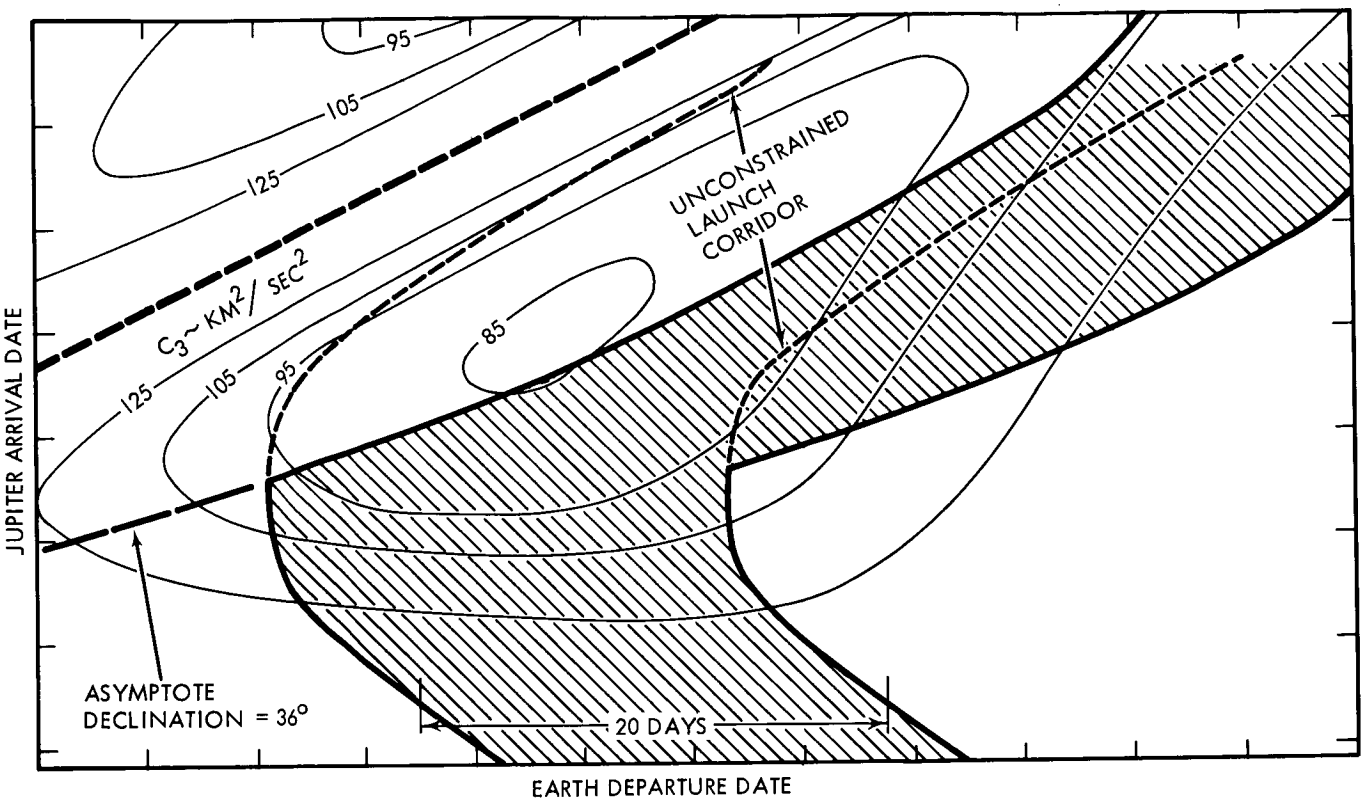


FIGURE 2.2-3

errors as great as 20 days. Essentially all of the flight-time error is built up within Jupiter's activity sphere, i.e., the volume of space in which Jupiter is the dominant gravitational body rather than the Sun.

The correction curve shown in Figure 2.2-4 was used to adjust the arrival dates and flight times associated with heliocentric conic data before they were incorporated in the mission planning charts which are discussed in paragraph 2.2.3. The corrections were computed by taking the difference between the "linear" flight time within Jupiter's activity sphere (i.e., the radius of the activity sphere divided by the appropriate hyperbolic excess speed) and the two-body hyperbolic flight time from the boundary of the activity sphere to perijove. For this purpose, the perijove altitude was taken to be one-tenth of Jupiter's surface radius. After adjustment, heliocentric conic arrival dates and flight times are accurate to within about 10 percent of the applied correction (i.e., to within $\pm$ 2 days or better), provided perijove altitude does not exceed about 10 planet radii.

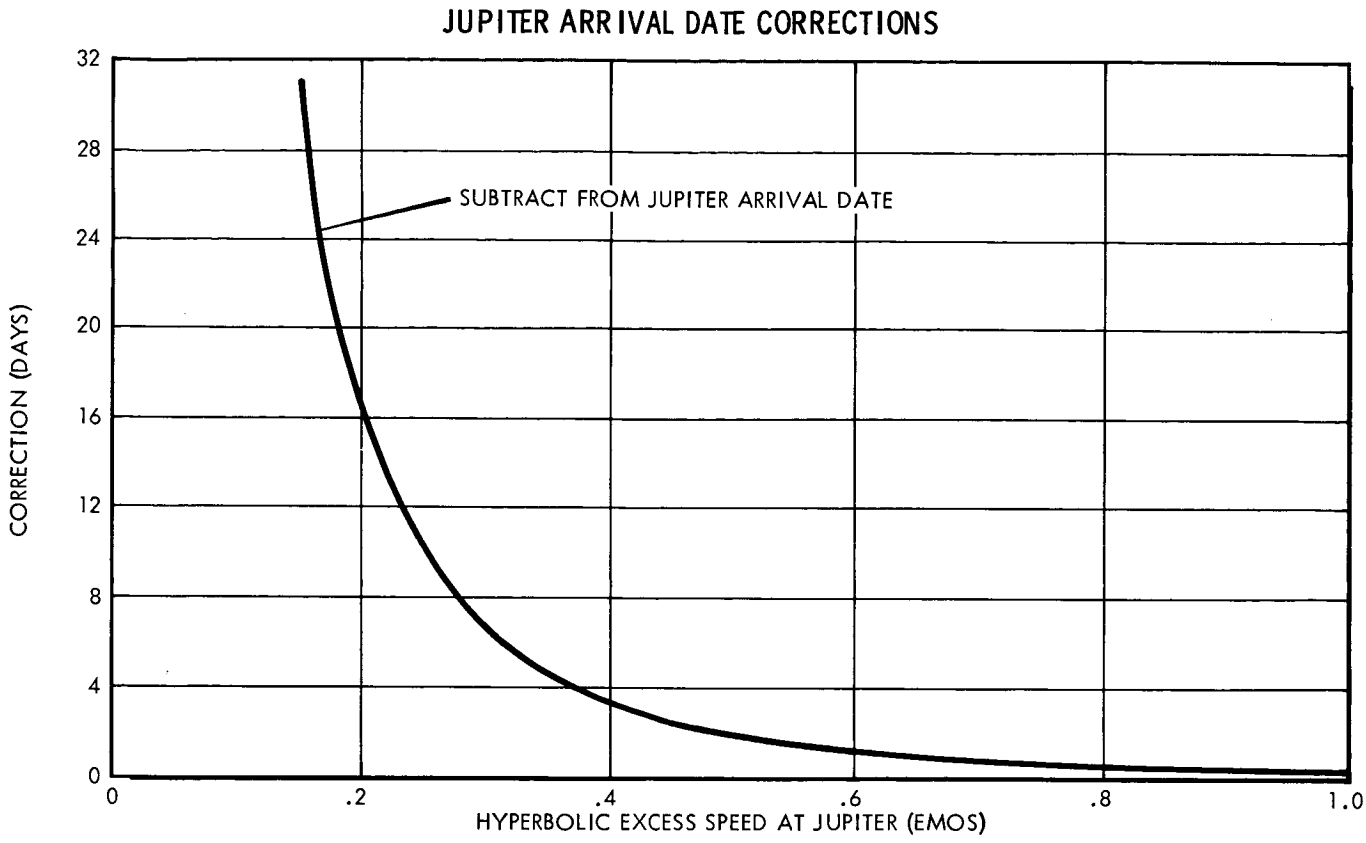


FIGURE 2.2-4

2.2.3 Mission Planning Charts

Mission planning charts applicable to each of the launch opportunities between 1973 and 1980 are shown in Figures 2.2-5 through 2.2-12. In these charts several important mission parameters are plotted as functions of arrival date.

2.2.3.1 Arrival Hyperbolic Excess Speeds

As previously stated, the heliocentric conic flight times and arrival dates appearing in these charts have been adjusted to account for Jupiter's gravitational attraction. For the purpose of making these adjustments, the hyperbolic excess speed at Jupiter on any given arrival date was taken to be equal to its mean value for the appropriate 20-day constant-arrival-date launch window. The curves of the mean hyperbolic excess arrival speed are shown on each of the charts.

2.2.3.2 Flight Time Curves

The distance between the two (minimum and maximum) total flight time curves corresponds to the 20-day width of the launch windows which were stipulated for the purpose of defining mission requirements.

MISSION PLANNING CHART, 1973 LAUNCH

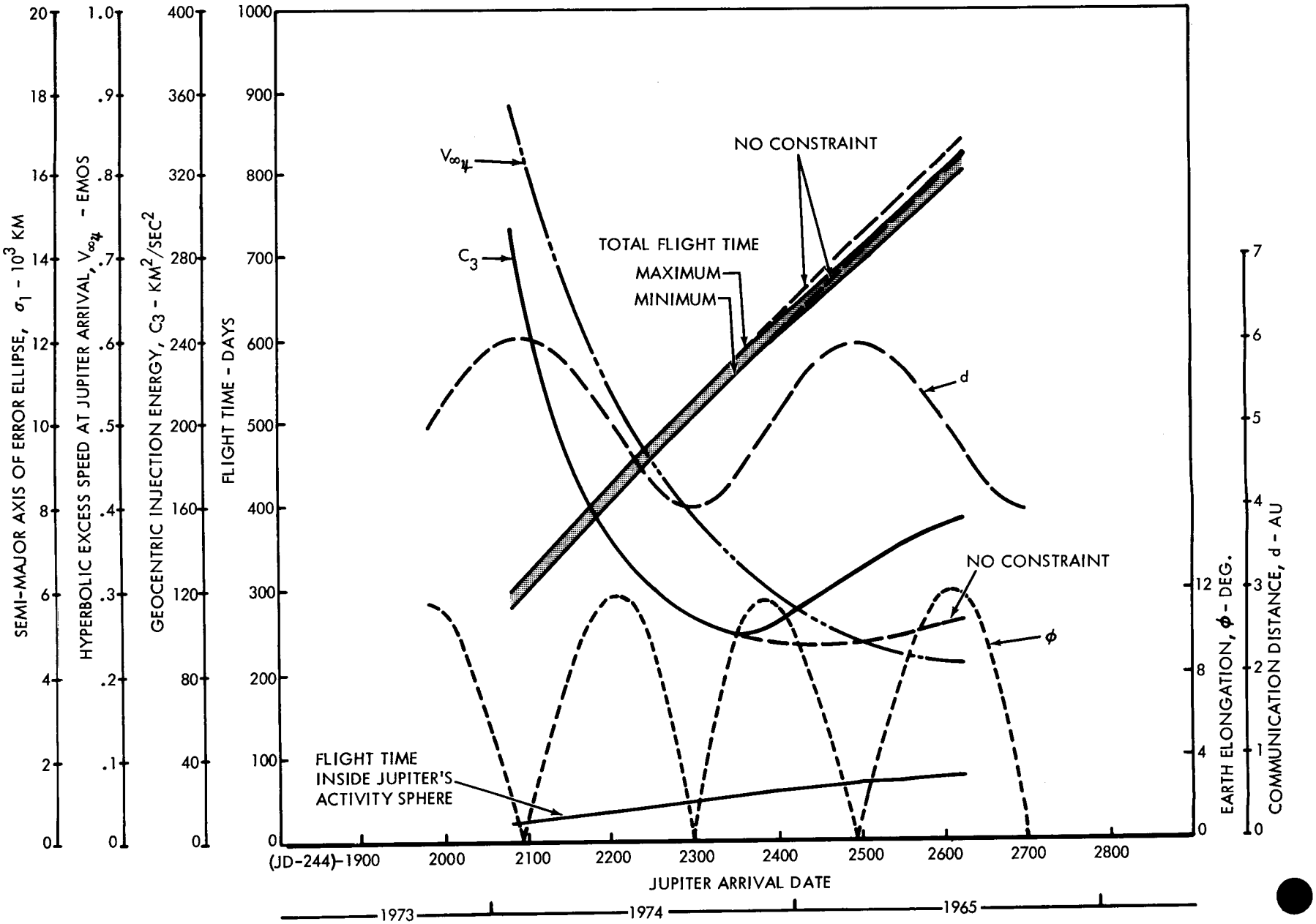


FIGURE 2.2-5

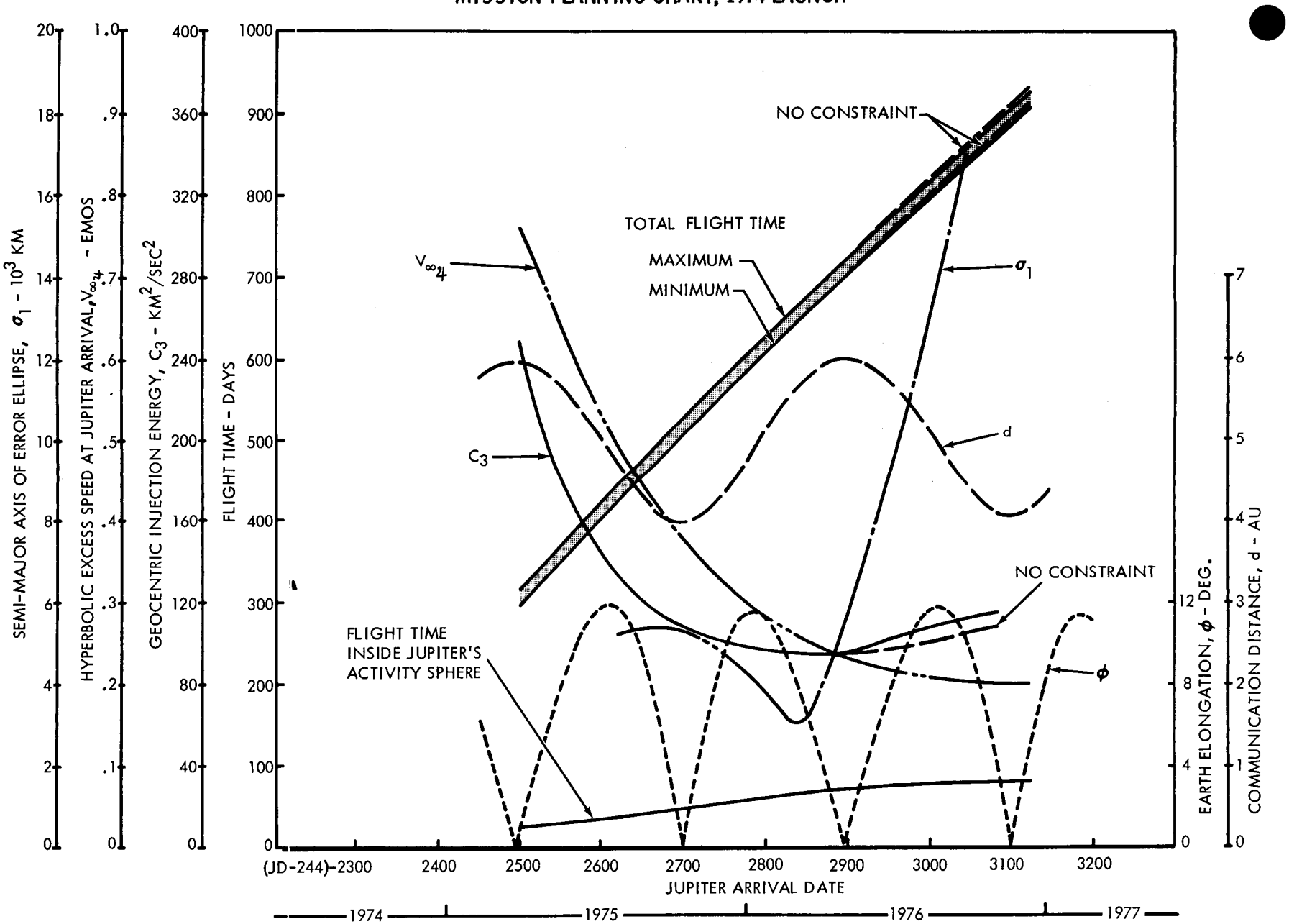

MISSION PLANNING CHART, 1974 LAUNCH
SEMI-MAJOR AXIS OF ERROR ELLIPSE, σ_1 - 10^3 KM
HYPERBOLIC EXCESS SPEED AT JUPITER ARRIVAL, V_{∞_4} - EMOS
GEOCENTRIC INJECTION ENERGY, C_3 - KM^2/SEC^2
FLIGHT TIME - DAYS
EARTH ELONGATION, ϕ - DEG.
COMMUNICATION DISTANCE, d - AU
NO CONSTRAINT
TOTAL FLIGHT TIME
MAXIMUM
MINIMUM
V_{∞_4}
σ_1
C_3
d
NO CONSTRAINT
FLIGHT TIME INSIDE JUPITER'S ACTIVITY SPHERE
ϕ
(JD-244)-2300
2400
2500
2600
2700
2800
2900
3000
3100
3200
JUPITER ARRIVAL DATE
1974
1975
1976
1977

FIGURE 2.2-6

MISSION PLANNING CHART, 1975 LAUNCH

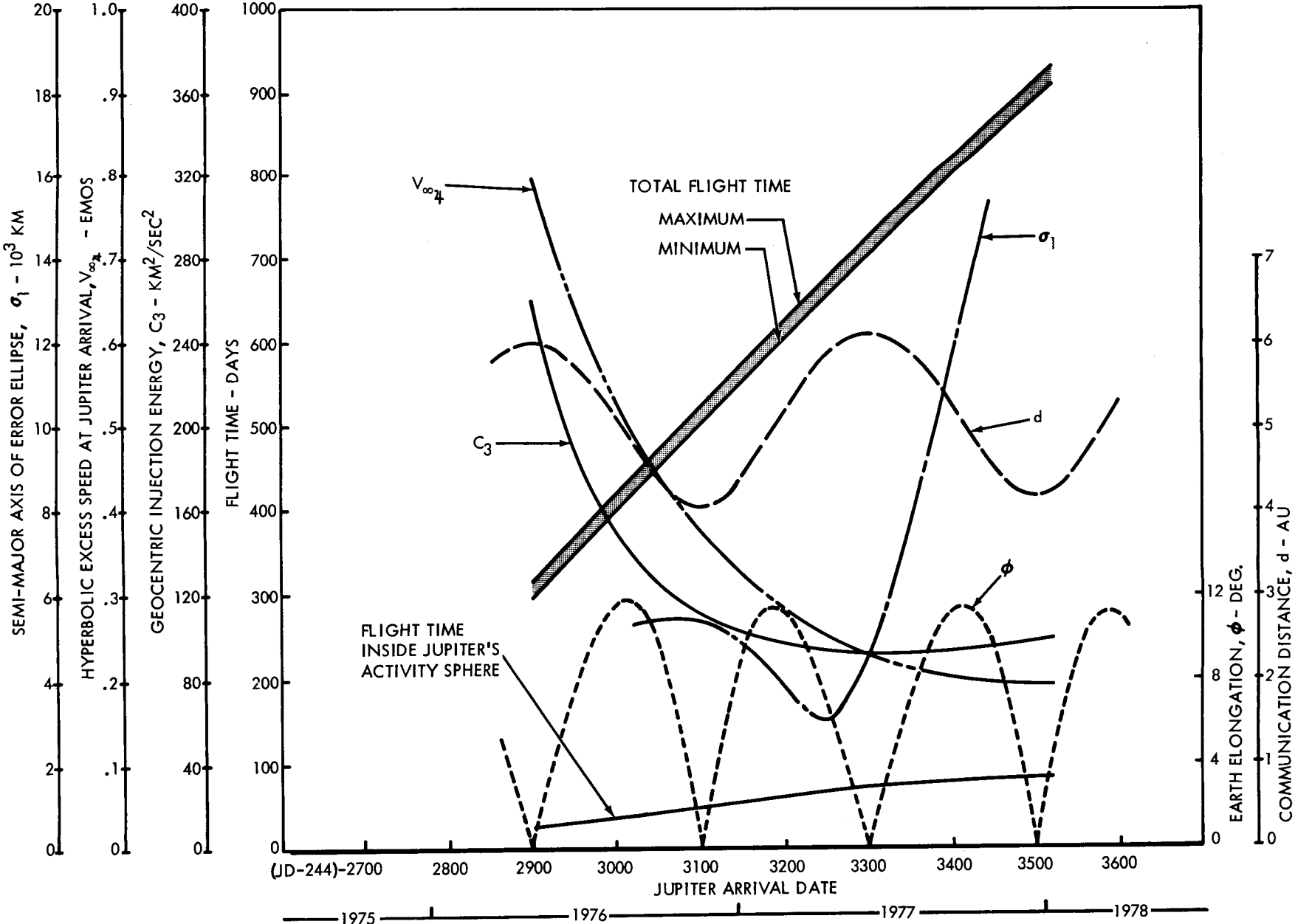


FIGURE 2.2-7

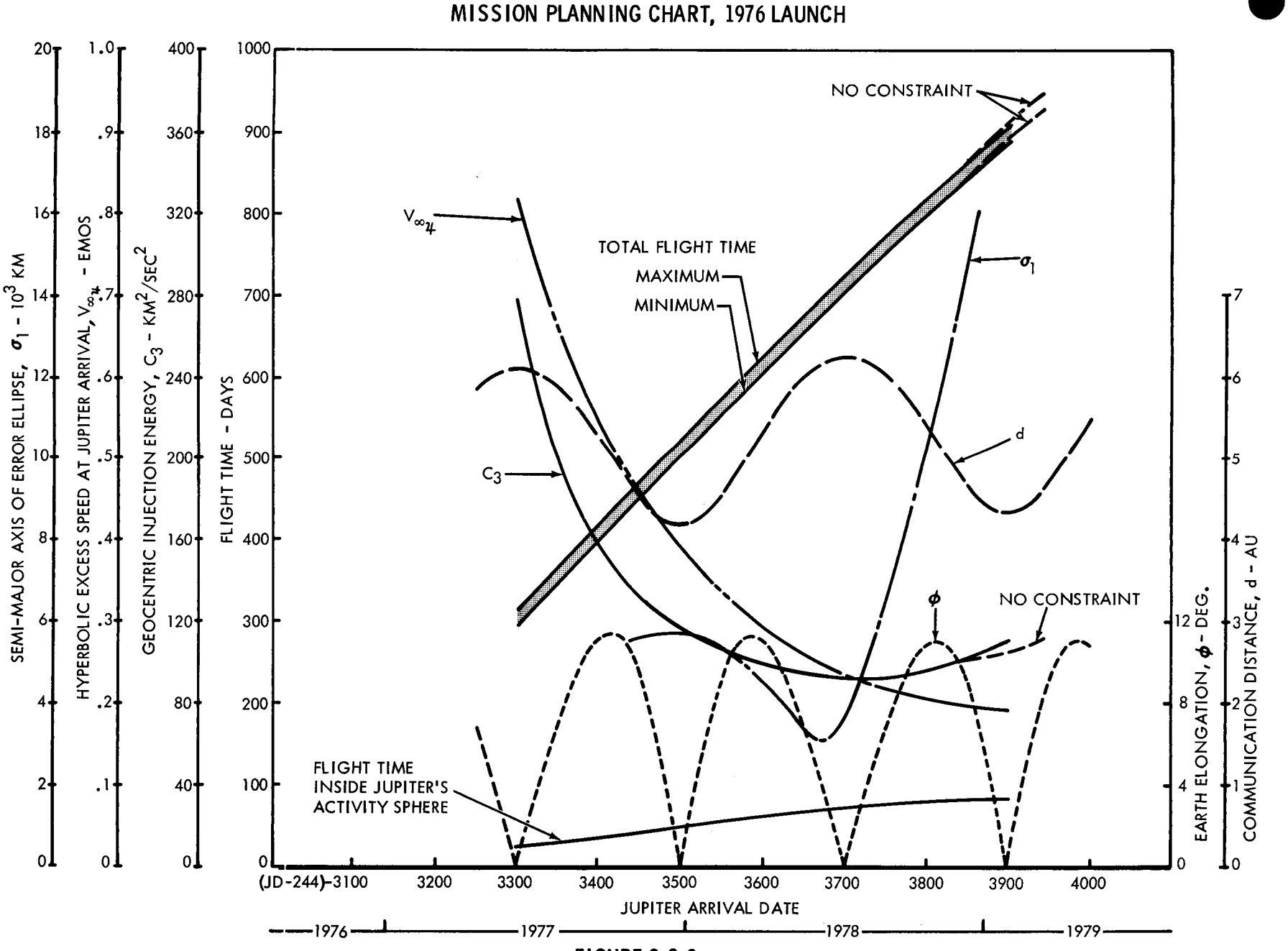

MISSION PLANNING CHART, 1976 LAUNCH
SEMI-MAJOR AXIS OF ERROR ELLIPSE, σ_1 - 10^3 KM
HYPERBOLIC EXCESS SPEED AT JUPITER ARRIVAL, V_{∞_4} - EMOS
GEOCENTRIC INJECTION ENERGY, C_3 - KM^2/SEC^2
FLIGHT TIME - DAYS
EARTH ELONGATION, ϕ - DEG.
COMMUNICATION DISTANCE, d - AU
NO CONSTRAINT
V_{∞_4}
TOTAL FLIGHT TIME
MAXIMUM
MINIMUM
σ_1
d
C_3
ϕ
NO CONSTRAINT
FLIGHT TIME
INSIDE JUPITER'S
ACTIVITY SPHERE
(JD-244)-3100
3200
3300
3400
3500
3600
3700
3800
3900
4000
JUPITER ARRIVAL DATE
1976
1977
1978
1979

FIGURE 2.2-8

MISSION PLANNING CHART, 1977 LAUNCH

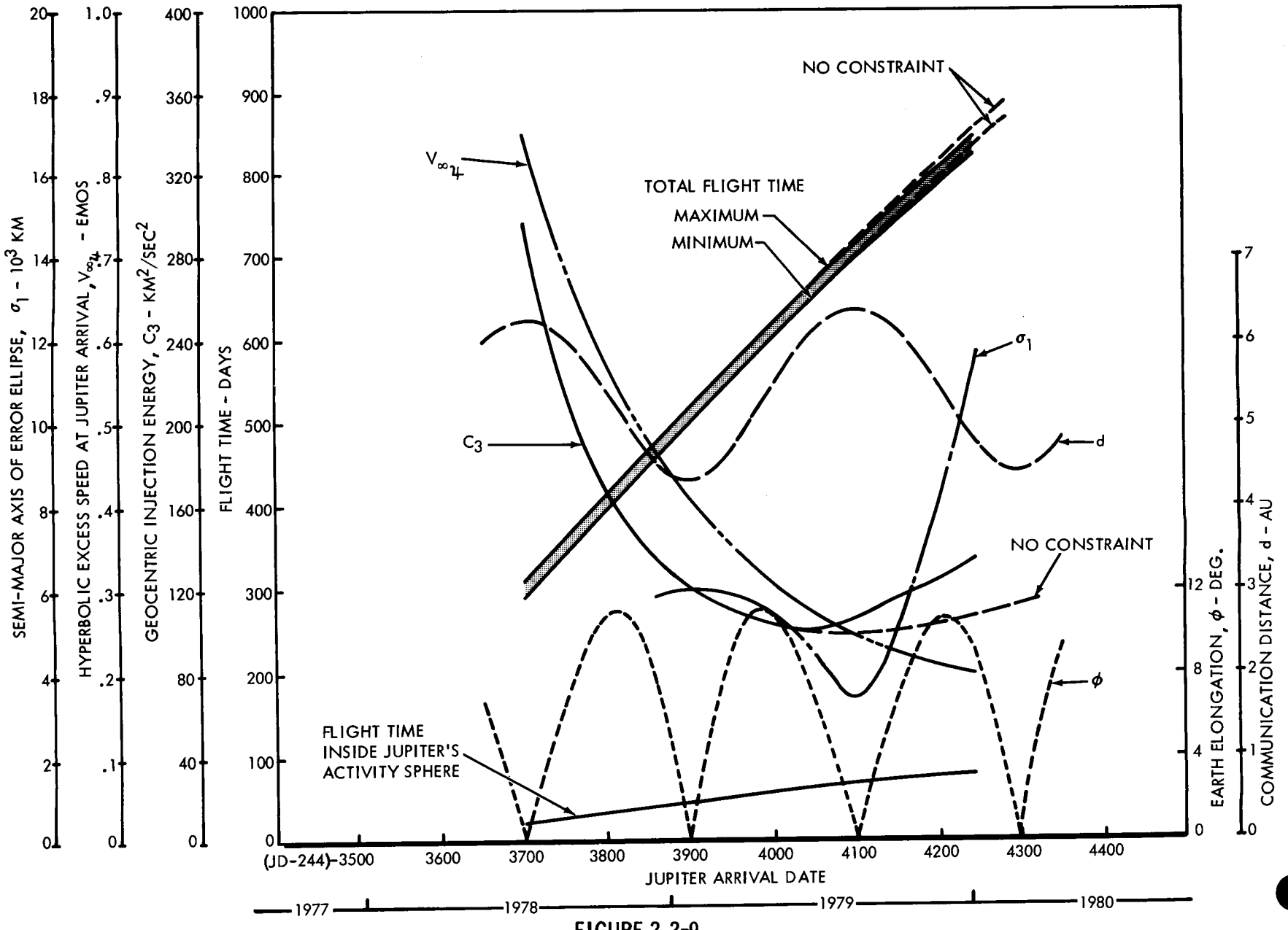


FIGURE 2.2-9

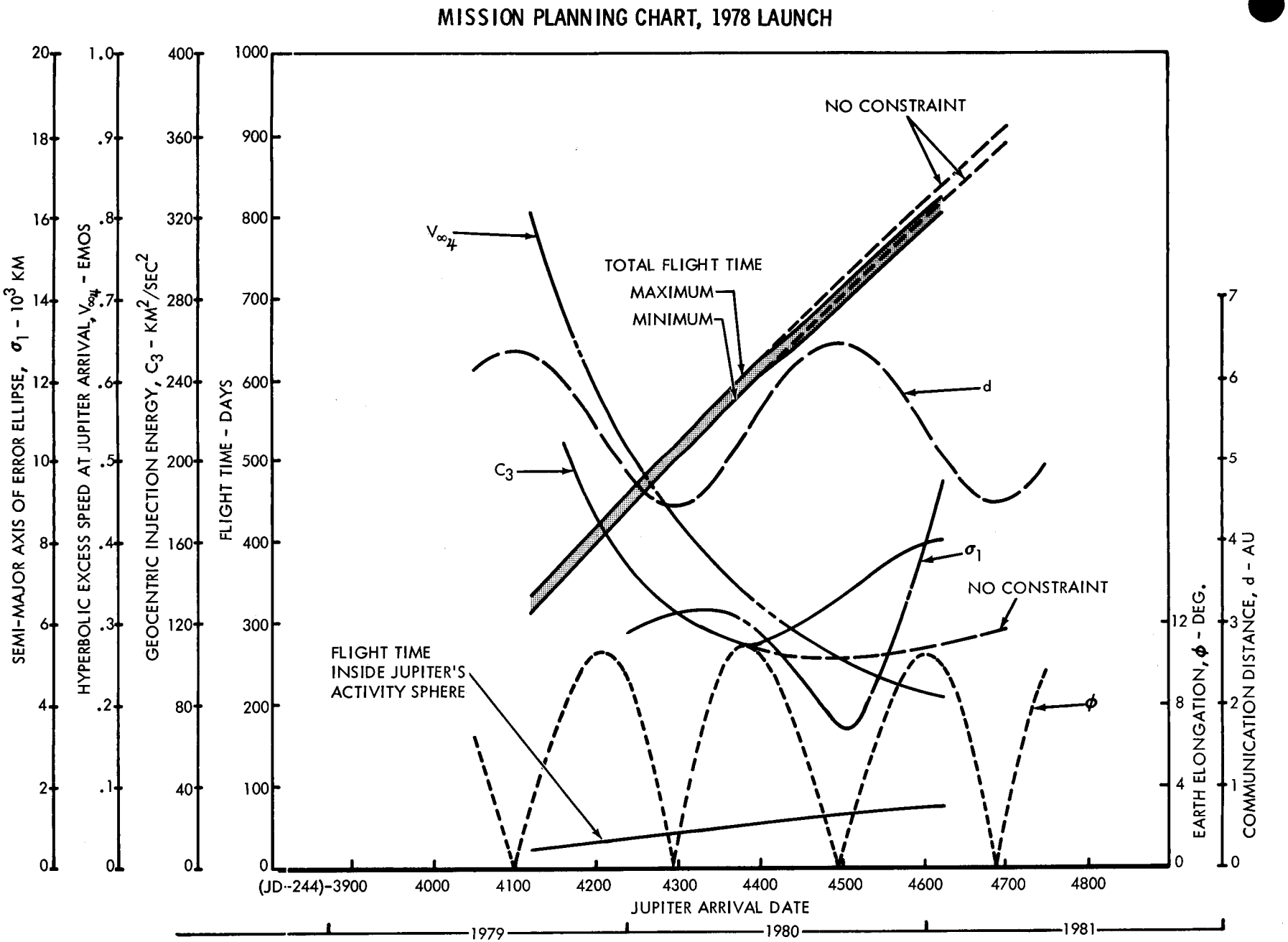

MISSION PLANNING CHART, 1978 LAUNCH
SEMI-MAJOR AXIS OF ERROR ELLIPSE, σ_1 - 10^3 KM
HYPERBOLIC EXCESS SPEED AT JUPITER ARRIVAL, V_{∞_4} - EMOS
GEOCENTRIC INJECTION ENERGY, C_3 - KM^2/SEC^2
FLIGHT TIME - DAYS
EARTH ELONGATION, ϕ - DEG.
COMMUNICATION DISTANCE, d - AU
NO CONSTRAINT
V_{∞_4}
TOTAL FLIGHT TIME
MAXIMUM
MINIMUM
d
C_3
σ_1
NO CONSTRAINT
FLIGHT TIME
INSIDE JUPITER'S
ACTIVITY SPHERE
ϕ
(JD--244)-3900
4000
4100
4200
4300
4400
4500
4600
4700
4800
JUPITER ARRIVAL DATE
1979
1980
1981

FIGURE 2.2-10

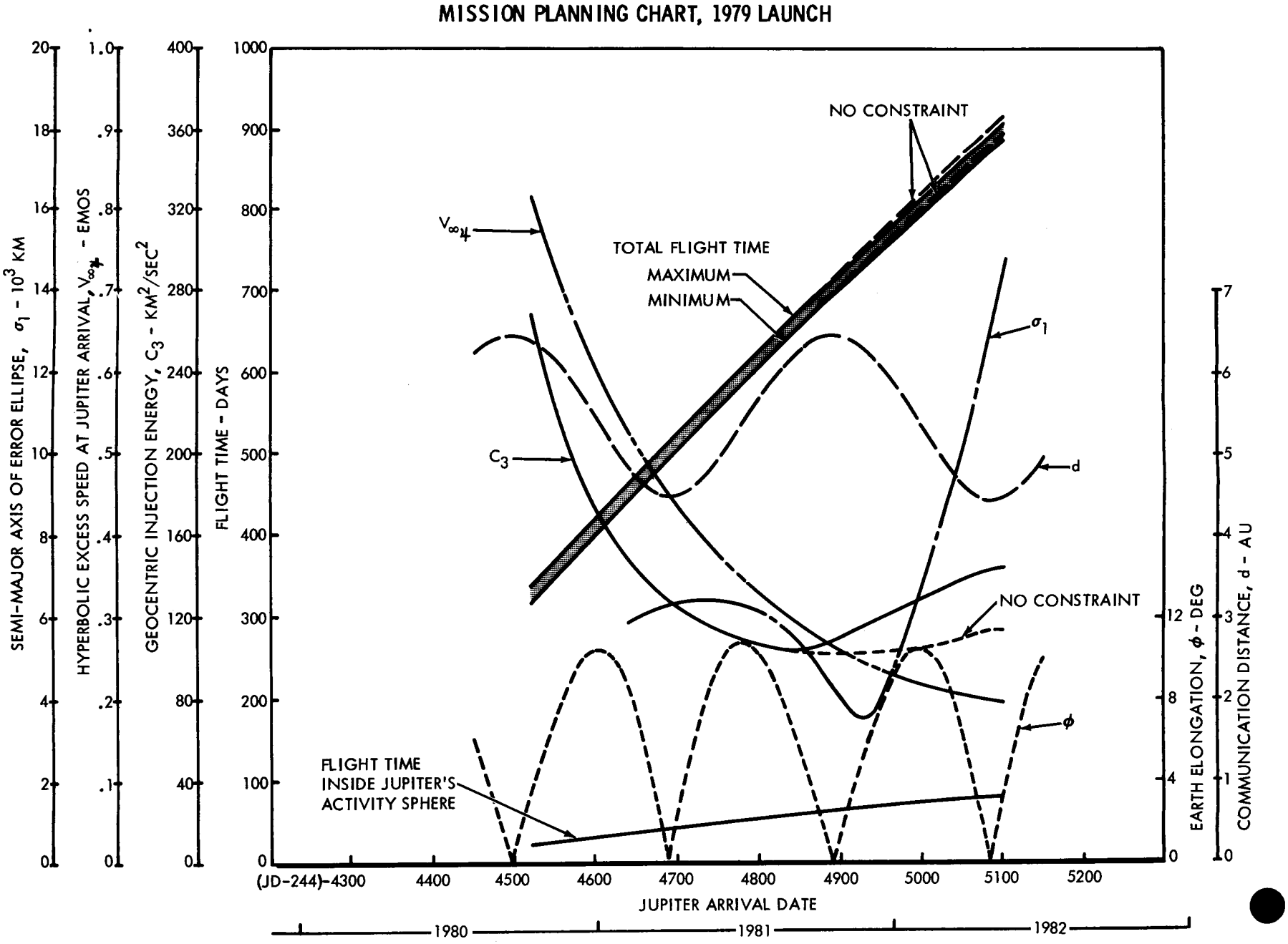

MISSION PLANNING CHART, 1979 LAUNCH
SEMI-MAJOR AXIS OF ERROR ELLIPSE, σ_1 - 10^3 KM
HYPERBOLIC EXCESS SPEED AT JUPITER ARRIVAL, V_{∞_4} - EMOS
GEOCENTRIC INJECTION ENERGY, C_3 - KM^2/SEC^2
FLIGHT TIME - DAYS
EARTH ELONGATION, ϕ - DEG
COMMUNICATION DISTANCE, d - AU
NO CONSTRAINT
V_{∞_4}
TOTAL FLIGHT TIME
MAXIMUM
MINIMUM
σ_1
C_3
d
NO CONSTRAINT
ϕ
FLIGHT TIME
INSIDE JUPITER'S
ACTIVITY SPHERE
(JD-244)-4300
4400
4500
4600
4700
4800
4900
5000
5100
5200
JUPITER ARRIVAL DATE
1980
1981
1982

FIGURE 2.2-11

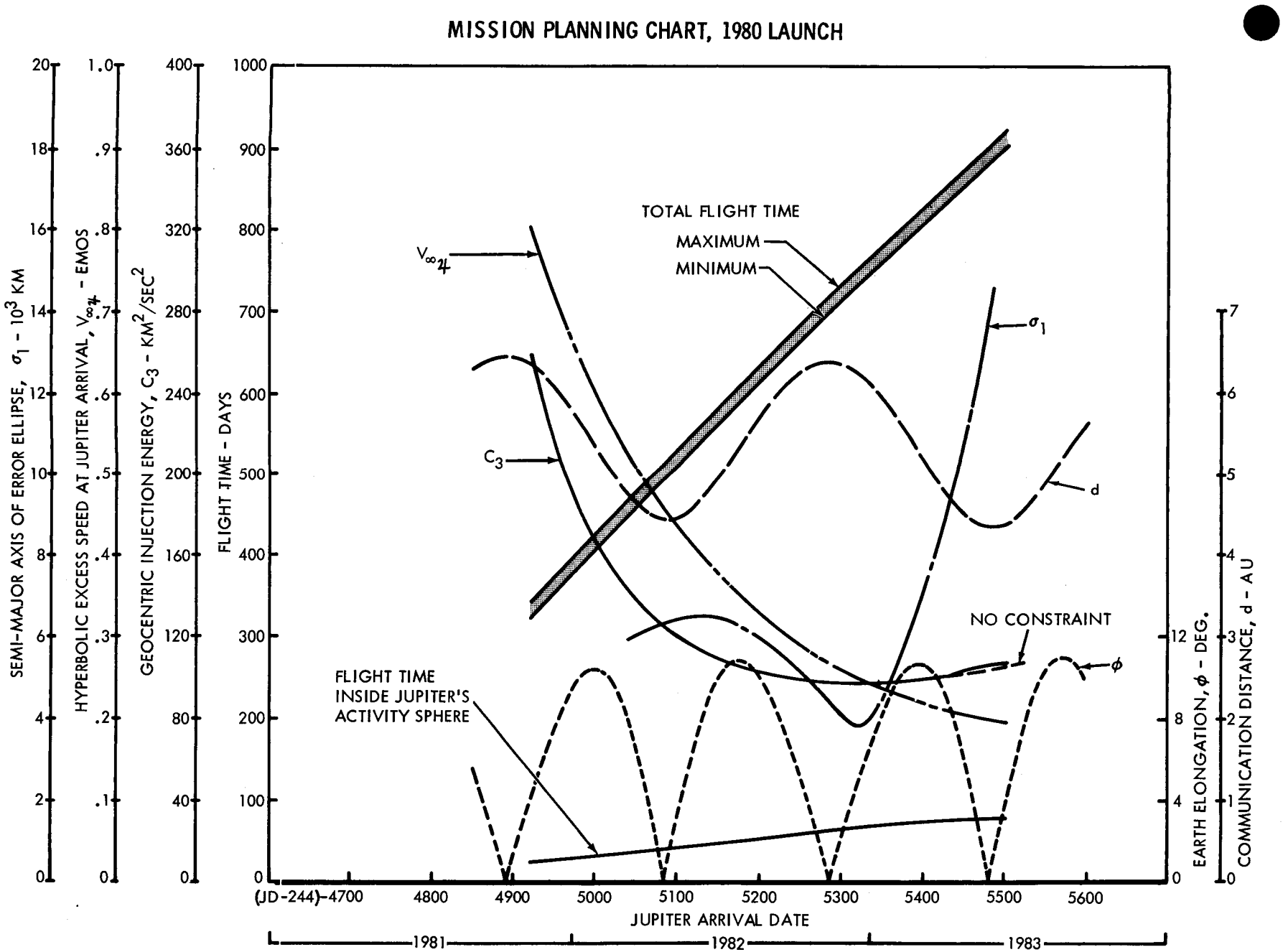

MISSION PLANNING CHART, 1980 LAUNCH
SEMI-MAJOR AXIS OF ERROR ELLIPSE, σ_1 - 10^3 KM
HYPERBOLIC EXCESS SPEED AT JUPITER ARRIVAL, V_{∞_4} - EMOS
GEOCENTRIC INJECTION ENERGY, C_3 - KM^2/SEC^2
FLIGHT TIME - DAYS
EARTH ELONGATION, ϕ - DEG.
COMMUNICATION DISTANCE, d - AU
TOTAL FLIGHT TIME
MAXIMUM
MINIMUM
V_{∞_4}
C_3
σ_1
d
ϕ
NO CONSTRAINT
FLIGHT TIME INSIDE JUPITER'S ACTIVITY SPHERE
(JD-244)-4700
JUPITER ARRIVAL DATE
1981
1982
1983

FIGURE 2.2-12

The curve showing flight time inside Jupiter's activity sphere at the bottom of each chart reflects the two-body hyperbolic flight time from the activity sphere boundary to perijove at an altitude of 0.1 planet radii.

2.2.3.3 Communication Distance and Earth Elongation Angle

The heliocentric configuration of the planets on the arrival date is defined by the communication distance, d, and the Earth elongation, Ø. The communication distance is the distance between the planets and the Earth elongation angle is the angular separation between Earth and the Sun, as seen from Jupiter. Conjunctions and oppositions of Jupiter are defined by maxima and minima respectively in the communication distance curve. These two types of events are accompainied and more sharply defined by local minima in the Earth elongation curve. Local maxima occur in the Earth elongation curve approximately 90 days before and after each opposition. The maximum Earth elongation just prior to opposition corresponds to a western quadrature of Jupiter, while the maximum immediately following opposition corresponds to an eastern quadrature.

Arrival at Jupiter on an opposition date is usually most desirable from the standpoint of radio tracking and communication for the simple reason that the communication distance is minimal. However, there may be situations in which arrival near the date of western or eastern quadrature would be more favorable for communication. For instance, one design concept for a minimal-capability spacecraft involves spin-stabilization for attitude control with the directional antenna beam aligned along the spin axis. The transmission of planetary encounter data to Earth would be accomplished by pointing the spacecraft spin vector at the time of spinup in the direction in inertial space where the Earth would appear at the time of encounter. For such a spacecraft, arrival on or near a date of quadrature would maximize the time period available for transmission of encounter data because the angular coordinates of Earth in inertial space (as seen from a spacecraft in the near vicinity of Jupiter) would be changing at a minimal rate.

Another mission-planning aspect related to the communication-distance and Earth-elongation curves is concerned with Earth-based optical telescopic observation of the target planet. The correlation of data received from the spacecraft with concurrently obtained Earth-based data would almost certainly improve the scientific value of the mission. Again, arrival on an opposition date would be most favorable for these purposes. This is true not only because the distance between planets is minimal at opposition, but also (and possibly of greater signficiance) because Jupiter rises at sunset, transits the local meridian at midnight, and sets at dawn;

thus, the daily observation period is maximized, and optimum viewing conditions are provided. From the standpoint of concurrent optical observation of Jupiter, arrival before the date of western quadrature or after the date of eastern quadrature would be highly undesirable because the planet would transit the local meridian during daylight hours, and less than half the nighttime hours would be available for observation.

One other mission-planning consideration which is related to the Earth-elongation curves in Figures 2.2-5 through 2-2-12 should be mentioned, although its significance has not been evaluated in this study. The Earth elongation angle is equal to the angular separation of the conical (almost cylindrical) Earth-occultation and Sun-occultation zones in jovicentric space. If scientific, operational, and/or environmental considerations relevant to a particular mission should require, for instance, that the spacecraft pass through one of these occultation zones and avoid the other (as in the Mariner 1964 mission), it would have to arrive on a date when the Earth elongation angle is significantly different from zero.

2.2.3.4 Guidance Sensitivity Curves

The σ_1 curves in Figures 2.2-6 through 2.2-12 (the data for the 1973 launch opportunity had not been received when the illustrations were prepared) which show the relationship between guidance sensitivity and arrival date are particularly significant for mission planning. The variable σ_1 is the length of the semi-major axis of the arrival position error ellipse which would result from a 0.1 meter per second spherically-distributed random velocity error in the execution of a guidance correction maneuver. The guidance correction maneuver is assumed to occur a few days after injection, and the gravitational effect of Jupiter is ignored in the computation of the arrival error ellipse. The effect of Jupiter's gravity field is to reduce the position error at perijove to something on the order of one-half to one-fourth of the values shown on the chart. The arrival position error is proportional to the midcourse execution velocity error, therefore an appropriate factor should be used to obtain arrival errors for a spacecraft guidance system whose execution accuracy is different than 0.1 meter per second.

The σ_1 values shown in the mission planning charts are the maximum values within the appropriate 20-day launch windows, and they were obtained from heliocentric conic trajectory data supplied by JPL. The minimum value of σ_1 occurs for arrival dates ranging from approximately 50 days before to 50 days after a conjunction of Jupiter with corresponding flight times ranging from 650 to 750 days depending on the launch year. The position error increase quite rapidly for longer flight times; whereas, in the case of shorter flight times, the

increase is more moderate and reaches a local maximum value less than twice as great as the minimum.

2.2.3.5 Geocentric Injection Energy

The single most important mission-planning parameter is the required injection energy, because it determines the payload capability of the launch vehicle for the mission. The geocentric injection energy C_3 is equal to the square of the departure hyperbolic excess speed, and actually corresponds to twice the Earth-relative kinetic energy per unit mass of the spacecraft when it is an "infinite" distnace from Earth. The injection energy curves shown in Figures 2.2-5 through 2.2-12 reflect the maximum values of C_3 within the appropriate 20-day launch windows. Only data for Type I heliocentric trajectories (having heliocentric transfer angles smaller than 180 degrees) are contained in these mission planning charts. This is in line with the results of earlier studies (Reference 2.2-1) which revealed that the reduction in C_3 which can be realized in some launch years by using Type II trajectories (having transfer angles greater than 180 degrees) is comparatively small in relation to the required increase in flight time.

Notable examples of the effect of the previously-described 36-degree asymptote declination constraint on injection energy requirements can be seen in the mission planning charts for the 1973 and the 1978 launch periods (Figures 2.2-5 and 2.2-10). In all of the mission planning charts, injection energy requirements for unconstrained launch windows are shown for reference. The greatest difference in miminum C_3 for constrained and unconstrained injection energy curves occurs in 1978, where the miminum-C_3 penalty is about 7 percent (i.e., 7 km^2/sec^2). The 36-degree declination constraint never causes a penalty for flight times shorter than 575 days.

Optimum flight times based on minimum injection energy requirement range from 575 to 750 days, depending on the launch year. For flight times shorter than about 400 days, the injection energy requirements increase very rapidly beyond the reasonable capabilities of chemically-propelled launch vehicles. The payload capabilities of 5 possible launch vehicles for Jupiter missions, based on the injection energy requirements shown in Figures 2.2-5 through 2.2-12, are discussed in subsection 2.3.

2.2.4 Conclusions

On the basis of the results of the investigation of energy requirements and general trajectory characteristics of Jupiter flyby missions discussed in the preceding paragraphs, the following major conclusions have been reached:

1. On the basis of minimum injection energy requirements, the nominal interplanetary flight time should never be longer than 750 days.

2. If good guidance accuracy is to be realized, interplanetary flight time should never exceed 800 days. If flight times are held below 700 days, the arrival position error will never be greater than twice the minimum value possible.

3. The use of chemically-propelled launch vehicles on missions with flight times shorter than 400 days will probably not be feasible.

4. From the standpoint of (1) radio tracking and communication, and (2) concurrent Earth-based optical observation of Jupiter, preferred arrival dates range from approximately 90 days before to 90 days after an opposition date (between the dates of western and eastern quadrature).

5. For a given launch year, there is only one 180-day arrival period which conforms to the conditions described in conclusion (4) and which also falls within the flight time limits described in conclusions (1), (2), and (3). The center of this arrival period is the date of the second opposition of Jupiter following the spacecraft's departure from Earth. The average interplanetary flight time for arrival on this opposition date is approximately 510 days. The average flight time for arrival on the date of western quadrature immediately preceding this opposition is about 420 days. The average flight time for arrival on the date of eastern quadrature immediately following this opposition is about 600 days.

6. In the case of missions arriving at perijove within the 180-day period described in conclusion (5), the stipulation that the departure asypmptote declination must lie in the range of ± 36 degrees has no effect on mission requirements in any launch year except 1973. The effect of the declination constraint in 1973 is minimal, causing only a slight increase in injection energy requirement for flight times between 575 and 600 days duration.

2.2.5 References

2.2-1 Wilson, S. W. Jr., et al., "Preliminary Analysis of One-Way Ballistic Flyby and Capture Missions to Jupiter", General Dynamics Corporation, Fort Worth Division, MR-FS-36, 11 November 1964.

2.3 LAUNCH VEHICLE EVALUATION

The payload capabilities of 5 launch vehicles were evaluated in relation to the energy requirements for Jupiter flyby missions. The following vehicles were specified by JPL:

1. Saturn V/Centaur
2. Saturn V
3. Saturn IB/Centaur/HEKS
4. Titan IIICx/Centaur
5. Atlas SLV3x/Centaur/HEKS.

A sixth vehicle, Atlas SLV3x/Centaur (without the high energy kick stage, HEKS) was determined to have no potential for a Jupiter mission early in the study and was considered no further.

2.3.1 Basic Payload Capabilities

The basic payload capabilities of the subject vehicles were defined by JPL in the form of curves of gross payload (including spacecraft adapter and aerodynamic fairing) versus C_3 attainable with a 90-degree launch azimuth on the Eastern Test Range (ETR). These curves were contained in a guideline document (Reference 2.3-1) in which it was pointed out that the indicated capabilities did not represent those of current vehicle configurations or of configurations currently being developed but that they represented the performance capabilities which would be technically feasible by the 1970 - 1980 time period with appropriate uprating and development programs. In this light, the payload data should be considered acceptable for long-range mission planning and conceptual design studies, but not necessarily so for other purposes.

The launch vehicle gross payload curves in Reference 2.3-1 were adjusted to reflect the performance capbilities that were more compatible with the probable operational modes and constraints associated with Jupiter flyby missions. Specifically, two adjustments were made (1) to account for the net payload decrement caused by carrying the mass of the payload aerodynamic fairing to 350,000 feet, and (2) to account for the injection energy decrement resulting from an ETR launch azimuth of 114 rather than 90 degrees. The adjusted curves for all 5 launch vehicles are shown in Figure 2.3-1.

SUMMARY OF LAUNCH VEHICLE PAYLOAD CAPABILITY

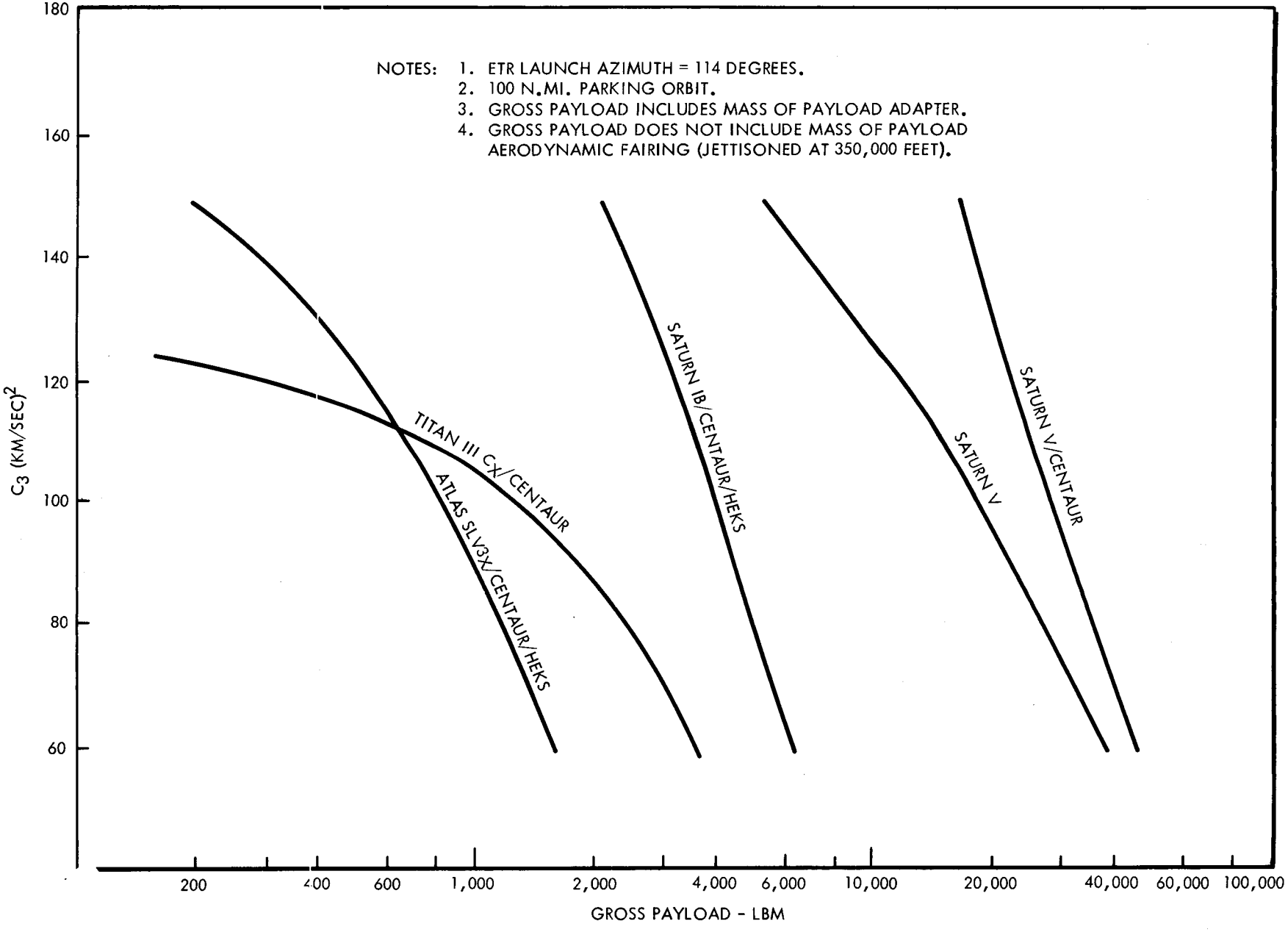


FIGURE 2.3-1

In Reference 2.3-1, it is stated that if the payload aerodynamic fairing is jettisoned at 350,000 feet (during ascent to the parking orbit), the interplanetary injection payload values shown in the curves in Reference 2.3-1 should be reduced by 10 percent of the actual fairing mass W_F. If the fairing is jettisoned in the parking orbit or after interplanetary injection, payloads should be decremented by 0.4 W_F or 1.0 W_F, respectively. Since aerodynamic effects are negligible above 350,000 feet, there appear to be only two plausible reasons for retaining the payload fairing beyond this point: (1) for thermal and meteoroid protection during the parking orbit coast and/or interplanetary injection phases, or (2) as an auxiliary load path for thrust acceleration loads. In view of the significant payload mass penalties involved in retaining the fairing, and the relatively short period (less than 2 hours) spent in the parking orbit as compared to the length of the interplanetary flight (several hundred days), retention of the fairing for thermal or meteoroid protection does not appear desirable.

Although a more thorough structural analysis is in order after launch vehicle/payload selections have been made, retention of the fairing for structural reasons does not appear to be a likely necessity. In the case of Saturn vehicles in which a Centaur stage is used, it is stated in Reference 2.3-1 that the load from the spacecraft and the HEKS (High Energy Kick Stage), when used, should be shared "approximately equally" between the fairing and the Centaur stage (i.e., about half of the load should be routed around Centaur, via the fairing, to the SIVB stage) during the boost phase of the trajectory. A check of thrust acceleration histories for typical Saturn IB/Centaur and Saturn V/Centaur boost trajectories indicates that the maximum acceleration experienced between 350,000 feet and SIVB burnout ranges from 50 to 67 percent of the peak acceleration which occurs below 350,000 feet. Therefore, jettisoning the fairing at 350,000 feet should not impose a much greater maximum load on Centaur than would result if the fairing were retained until final burnout of the SIVB stage. On the Atlas and Titan vehicles, there is no available load path around Centaur (i.e. all of the load from fairing, spacecraft, and kick stage must be routed through Centaur during the entire boost trajectory); hence, retention of the payload fairing on these vehicles above 350,000 feet would not be desirable from the structural standpoint.

Adjustment of the data in Reference 2.3-1 to a launch azimuth of 114 degrees was accomplished in line with the conservative overall policy which was adopted for the definition of launch vehicle capabilities for Jupiter missions. The 114 degree azimuth is the most severe azimuth from the standpoint of payload degradation due to non-Easterly launches within the normal ETR firing sector of 90 to 114

degrees. To assure maximum utilization of existing range facilities, only those interplanetary transfer trajectories which can be attained within the limits of the normal ETR firing sector were considered acceptable for the purpose of defining mission requirements. The effect of this constraint is to rule out any interplanetary transfer requiring a departure asymptote declination outside the range of ± 36 degrees. Therefore, when the geocentric injection energy C_3 required for a heliocentric trajectory which satisfies the cited asymptote declination constraint is used to find an allowable spacecraft-plus-adapter mass from the adjusted curves, the launch vehicle can be counted on to deliver the indicated payload (with some reserve in most cases).

Figure 2.3-2 schematically illustrates the procedure which was

PAYLOAD CURVE ADJUSTMENTS

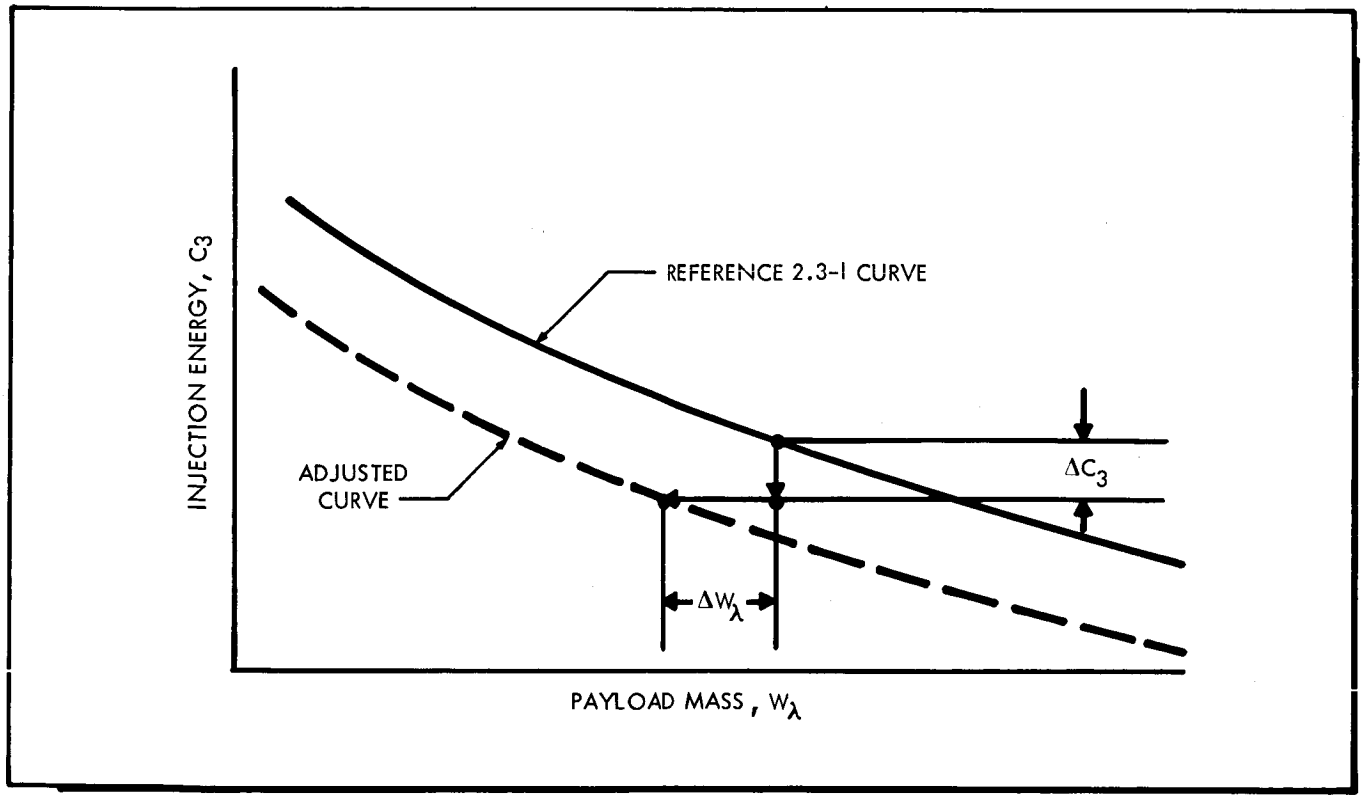


FIG. 2.3-2

followed in the adjustment of the payload curves. In line with the previous discussion, the payload decrement ΔW_λ was taken to be 10 percent of the estimated payload fairing mass given in Reference 2.3-1. The ΔW_λ values (constant for a given launch vehicle) are given in Table 2.3-1.

Table 2.3-1 PAYLOAD DECREMENTS

Launch Vehicle	ΔW_λ(lbm)
Saturn V/Centaur	330
Saturn V	750
Saturn IB/Centaur/HEKS	260
Titan $IIIC_x$/Centaur	185
Atlas $SLV3_x$/Centaur/HEKS	152

The injection energy decrements ΔC_3 were obtained by subtracting 36.6 meters per second (the difference between the components of Earth rotational velocity in the launch trajectory planes for ETR launch azimuths of 90 and 114 degrees) from the injection velocity required for the original value of C_3. Injection was assumed to occur at a geocentric distance of 8000 kilometers. Specifically, the equation

$$\Delta C_3 = C_3 - \left[\left(\sqrt{99.6508 + C_3} - .0366\right)^2 - 99.6508\right]$$

was used. The constant, 99.6508, is the square of the escape speed (in units of km/sec) at a distance of 8000 kilometers from the center of the Earth. The resulting values of ΔC_3 are shown in Table 2.3-2.

Table 2.3-2 C_3 DECREMENTS

C_3 $(km/sec)^2$	ΔC_3 $(km/sec)^2$
60	0.92
70	0.95
80	0.98
90	1.01
100	1.03
110	1.06
120	1.08
130	1.11
140	1.13
150	1.17

The method used to adjust the payload curves to account for the 114 degree launch azimuth is admittedly crude and may be somewhat in error. Point checks of actual payload decrements due to non-easterly launches in the case of a similar launch vehicle indicate that the ΔC_3 values possibly should be greater by a factor of two. Doubling the injection energy decrement would shift all the adjusted payload

curves downward by about 1.0 km^2/sec^2. The effective payload decrement resulting from such an additional shift would be less than 4 percent in all cases except for payloads smaller than 1600 lbm on the Titan $IIIC_x$/Centaur and smaller than 350 lbm on the Atlas $SLV3_x$/Centaur/HEKS launch vehicle.

2.3.2 Payload Capabilities for Jupiter Missions

In Figures 2.3-3 through 2.3-10, the payload capability of each launch vehicle is shown as a function of flight time in the case of each launch opportunity between 1973 and 1980. The flight times shown in these figures are mean values for 20-day fixed-arrival-date launch windows; therefore, the actual flight time within any launch window represented by a point on one of these curves varies by ± 10 days from the indicated value. The C_3 requirements which define the payload capability for a given vehicle and flight time were taken from the mission planning charts which were discussed in paragraph 2.2.3. It is noteworthy that although Titan IIICx/Centaur always has a greater maximum payload capability in any given launch year, below a certain flight time the Atlas SLV3x/Centaur/HEKS can deliver a greater payload. The break-even flight time varies from 490 to 565 days, depending on the launch year.

In Figures 2.3-11 through 2.3-15, payload capability as a function of flight time is summarized with respect to launch vehicle rather than launch year. It is not surprising that the payload capabilities of Saturn V/Centaur and Saturn IB/Centaur/HEKS, since they are rather efficient 4-stage vehicles, are relatively insensitive to variations in flight time and launch year. The Titan IIICx/Centaur is most sensitive to such variations, while Saturn V and Atlas SLV3x/Centaur/HEKS exhibit a moderate degree of sensitivity.

2.3.3 References

2.3-1 "Launch Vehicles Future Missions Study Guideline," Jet Propulsion Laboratory.

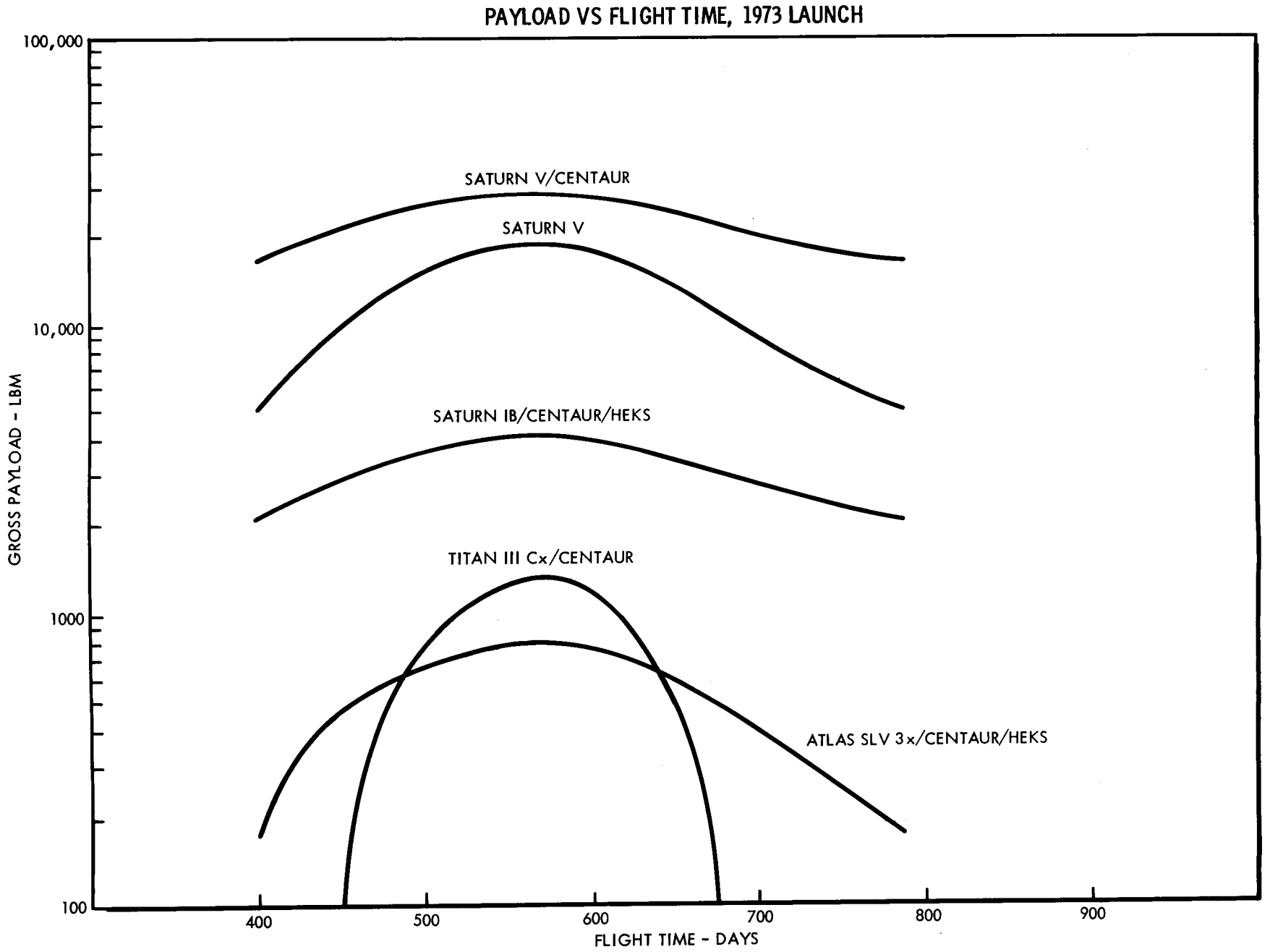

PAYLOAD VS FLIGHT TIME, 1973 LAUNCH
100,000
10,000
1000
100
GROSS PAYLOAD - LBM
SATURN V/CENTAUR
SATURN V
SATURN IB/CENTAUR/HEKS
TITAN III Cx/CENTAUR
ATLAS SLV 3x/CENTAUR/HEKS
400
500
600
700
800
900
FLIGHT TIME - DAYS

FIGURE 2.3-3

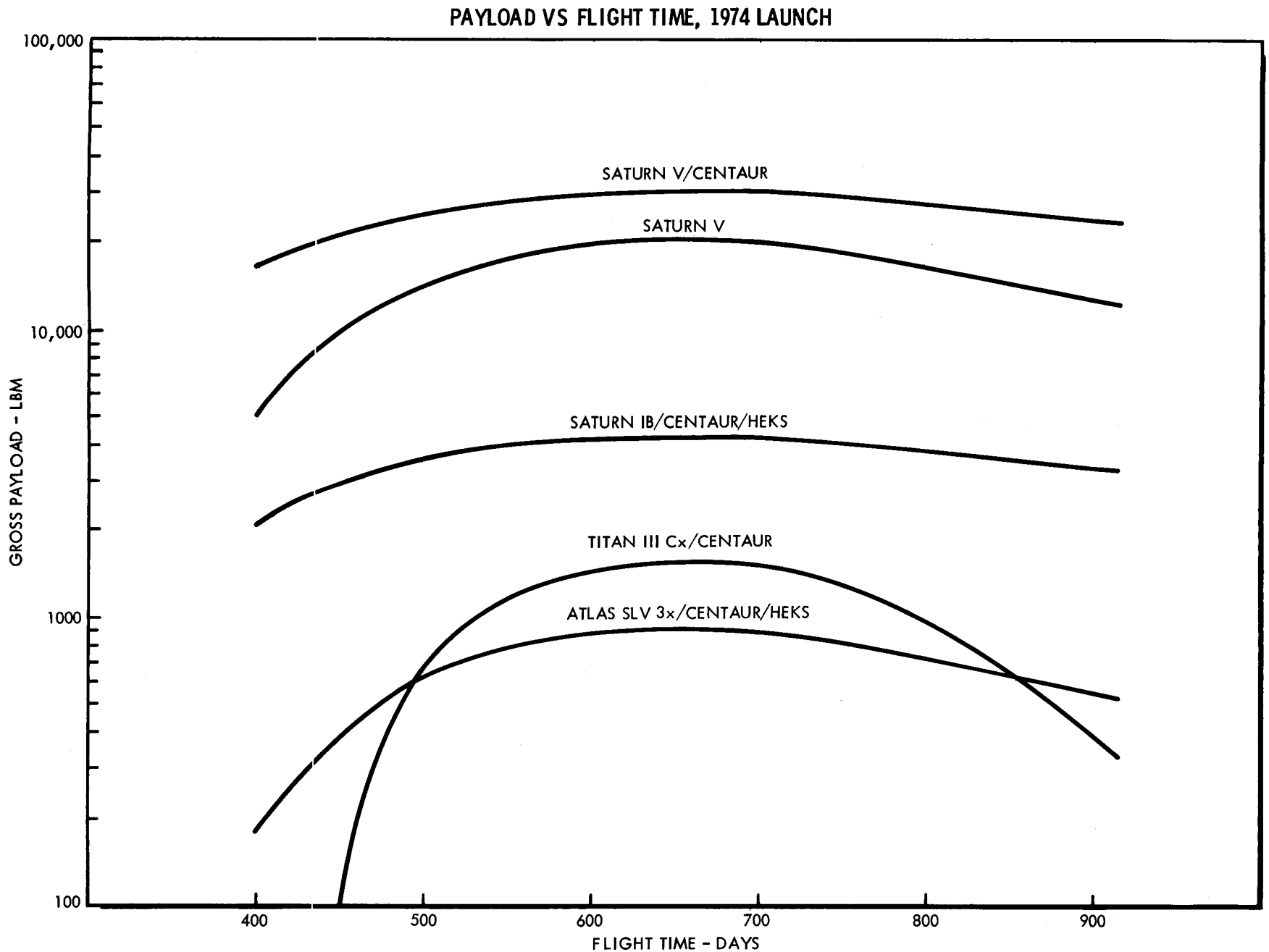

PAYLOAD VS FLIGHT TIME, 1974 LAUNCH
100,000
10,000
1000
100
GROSS PAYLOAD - LBM
SATURN V/CENTAUR
SATURN V
SATURN IB/CENTAUR/HEKS
TITAN III Cx/CENTAUR
ATLAS SLV 3x/CENTAUR/HEKS
400
500
600
700
800
900
FLIGHT TIME - DAYS

FIGURE 2.3-4

PAYLOAD VS FLIGHT TIME, 1975 LAUNCH

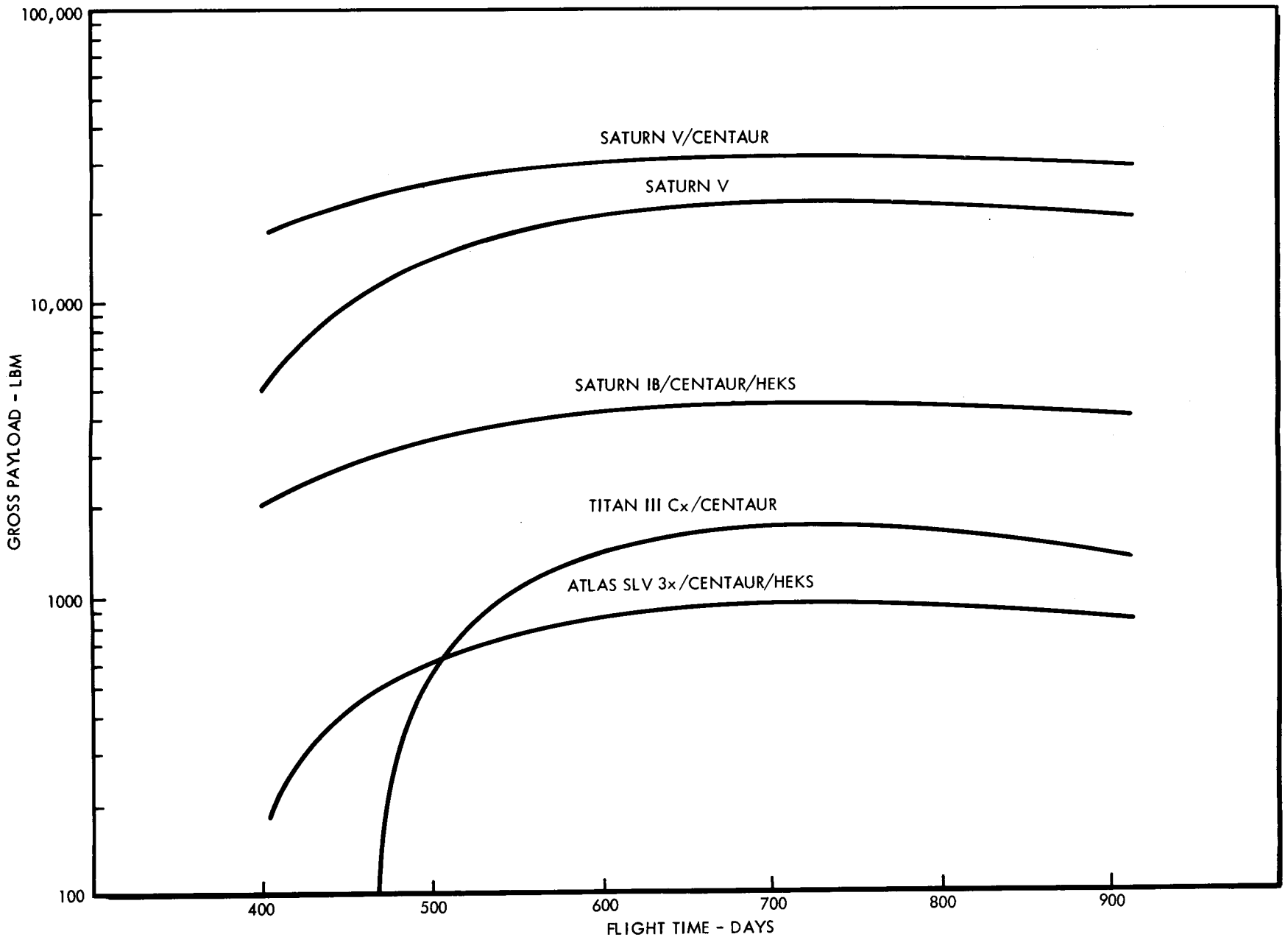


FIGURE 2.3-5

PAYLOAD VS FLIGHT TIME, 1976 LAUNCH

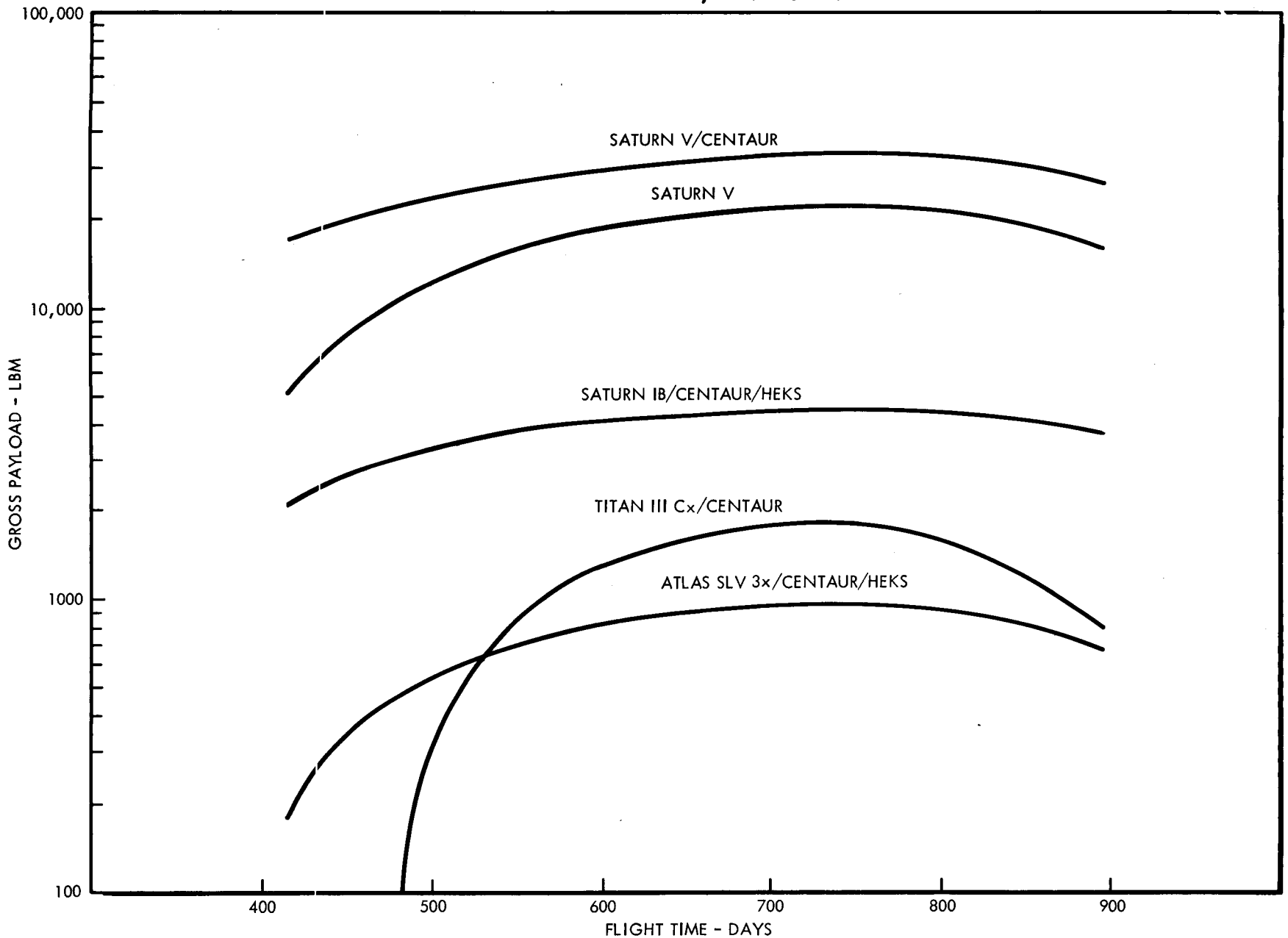


FIGURE 2.3-6

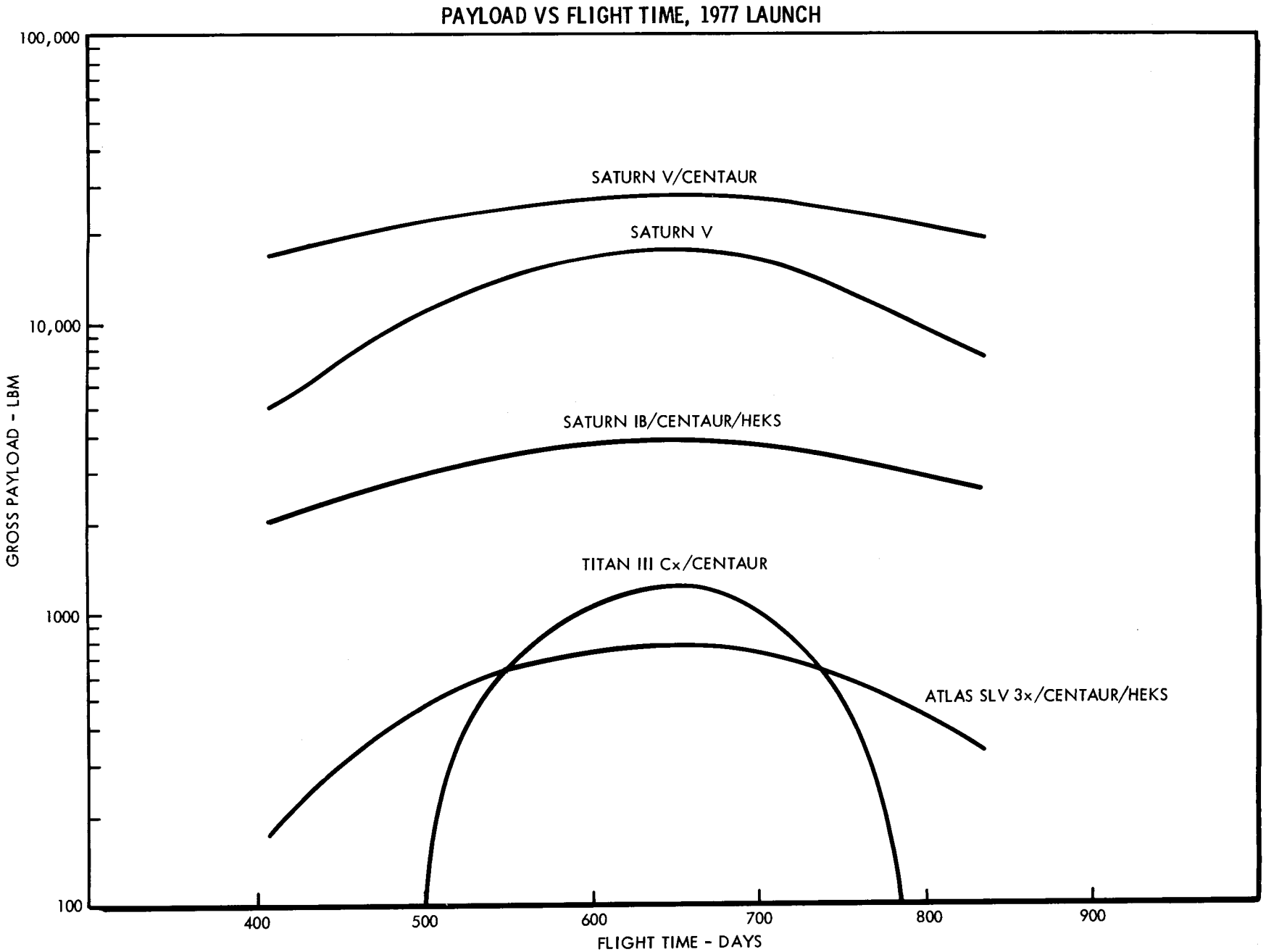

PAYLOAD VS FLIGHT TIME, 1977 LAUNCH
100,000
10,000
1000
100
GROSS PAYLOAD - LBM
SATURN V/CENTAUR
SATURN V
SATURN IB/CENTAUR/HEKS
TITAN III Cx/CENTAUR
ATLAS SLV 3x/CENTAUR/HEKS
400
500
600
700
800
900
FLIGHT TIME - DAYS

FIGURE 2.3-7

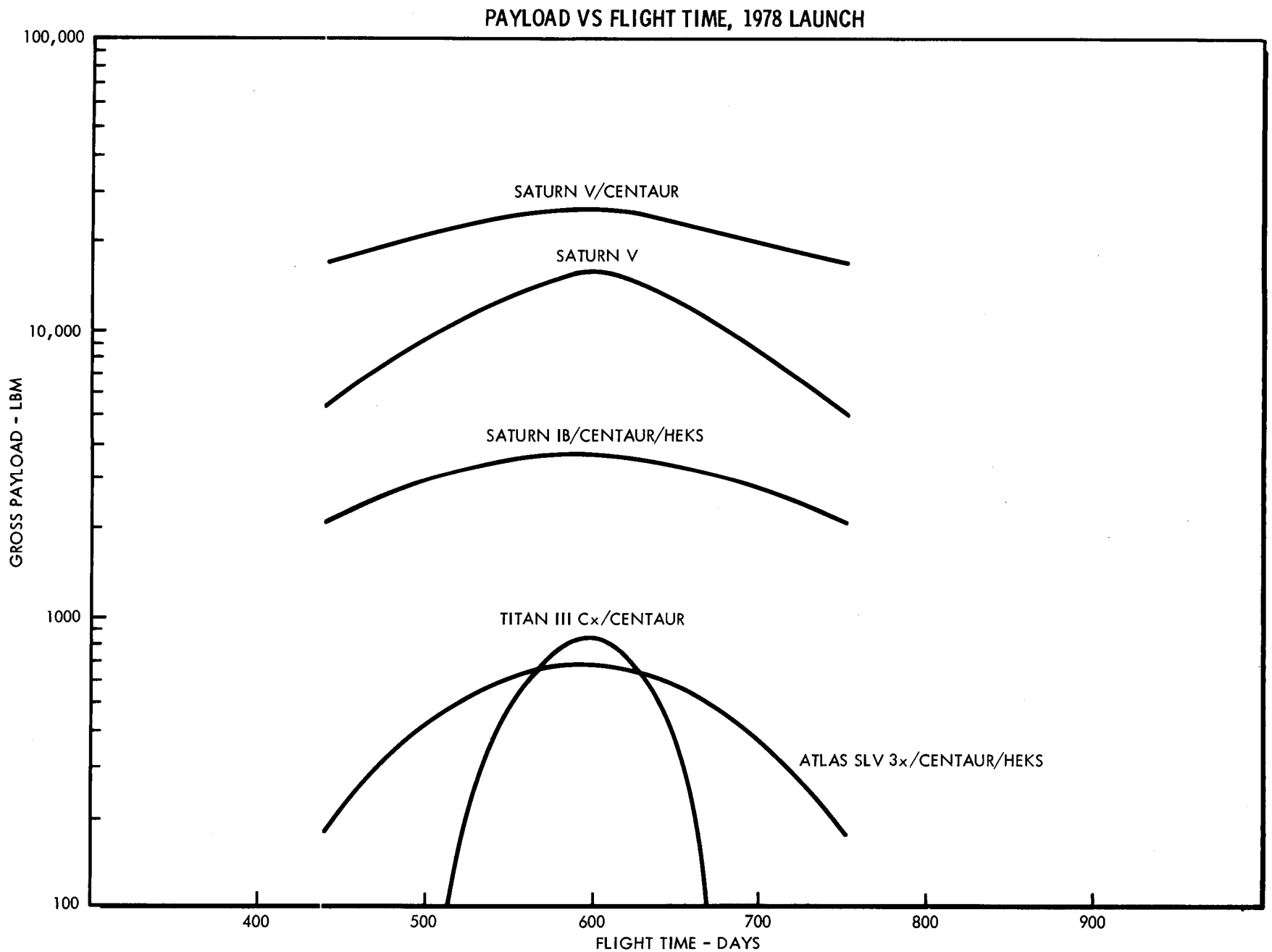

PAYLOAD VS FLIGHT TIME, 1978 LAUNCH
100,000
10,000
1000
100
GROSS PAYLOAD - LBM
SATURN V/CENTAUR
SATURN V
SATURN IB/CENTAUR/HEKS
TITAN III Cx/CENTAUR
ATLAS SLV 3x/CENTAUR/HEKS
400
500
600
700
800
900
FLIGHT TIME - DAYS

FIGURE 2.3-8

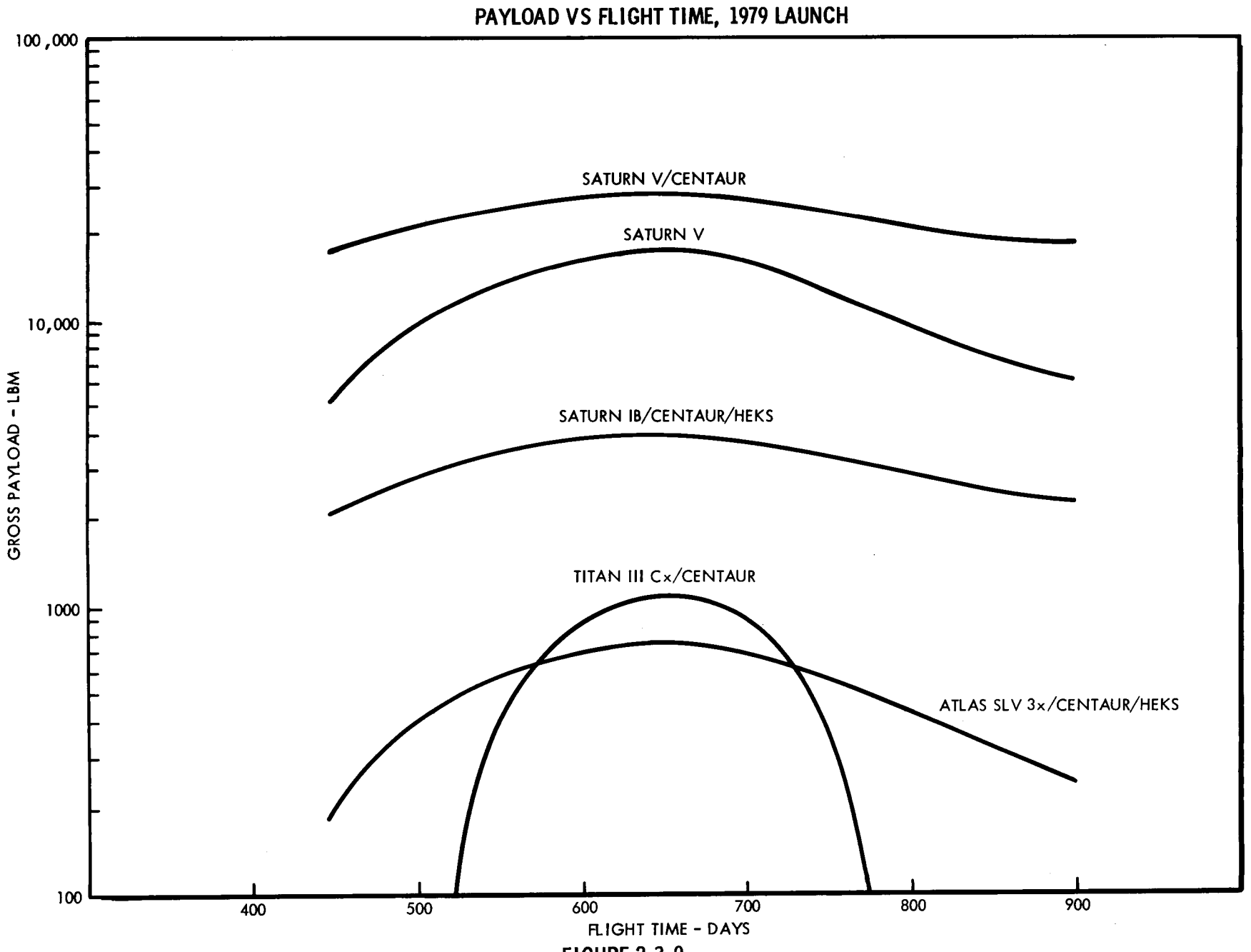

PAYLOAD VS FLIGHT TIME, 1979 LAUNCH
100,000
10,000
1000
100
GROSS PAYLOAD - LBM
SATURN V/CENTAUR
SATURN V
SATURN IB/CENTAUR/HEKS
TITAN III Cx/CENTAUR
ATLAS SLV 3x/CENTAUR/HEKS
400
500
600
700
800
900
FLIGHT TIME - DAYS

FIGURE 2.3-9

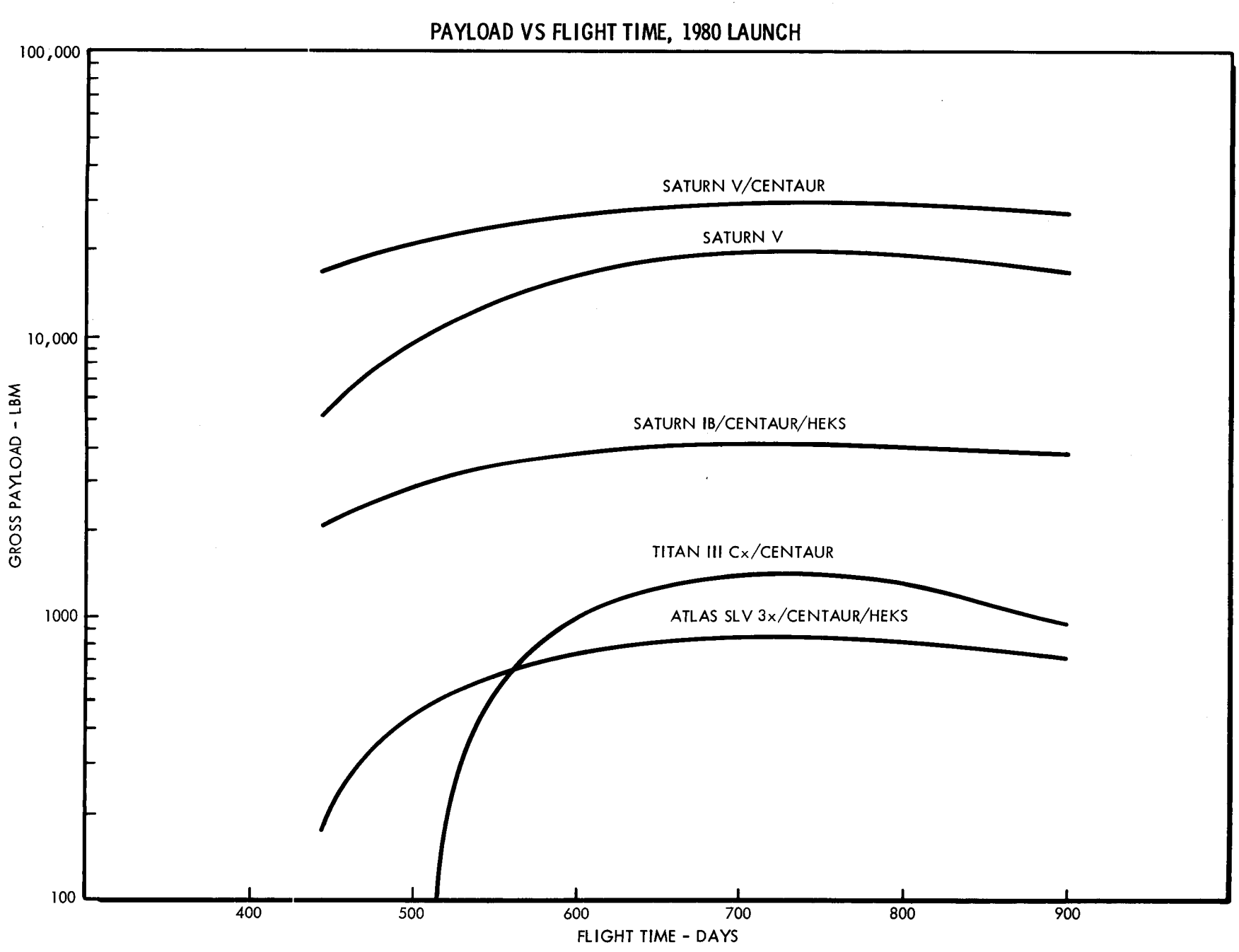

PAYLOAD VS FLIGHT TIME, 1980 LAUNCH
100,000
10,000
1000
100
GROSS PAYLOAD - LBM
SATURN V/CENTAUR
SATURN V
SATURN IB/CENTAUR/HEKS
TITAN III Cx/CENTAUR
ATLAS SLV 3x/CENTAUR/HEKS
400
500
600
700
800
900
FLIGHT TIME - DAYS

FIGURE 2.3-10

JUPITER MISSION PAYLOAD CAPABILITY, SATURN V/CENTAUR

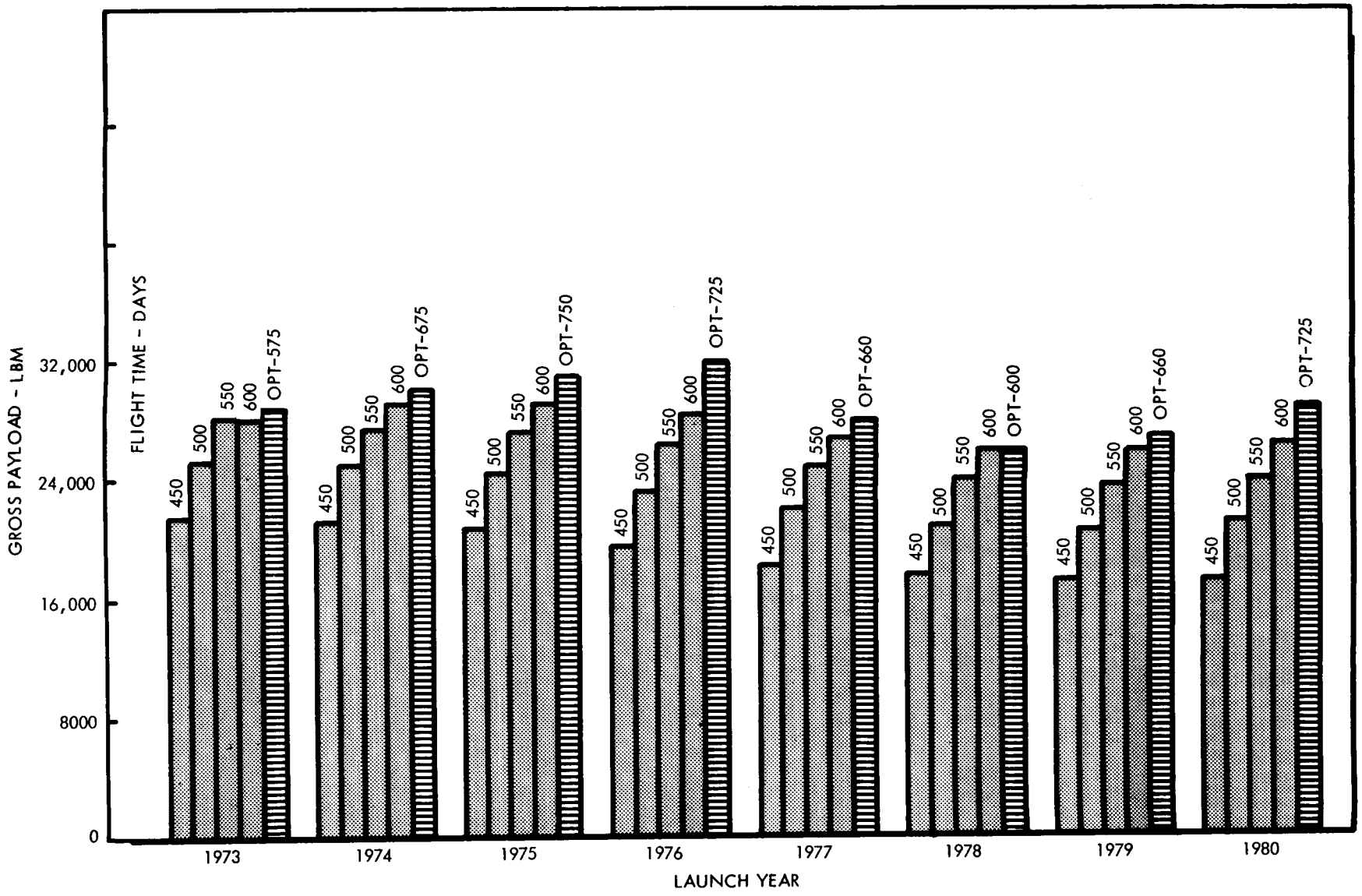


FIGURE 2.3-11

JUPITER MISSION PAYLOAD CAPABILITY, SATURN V

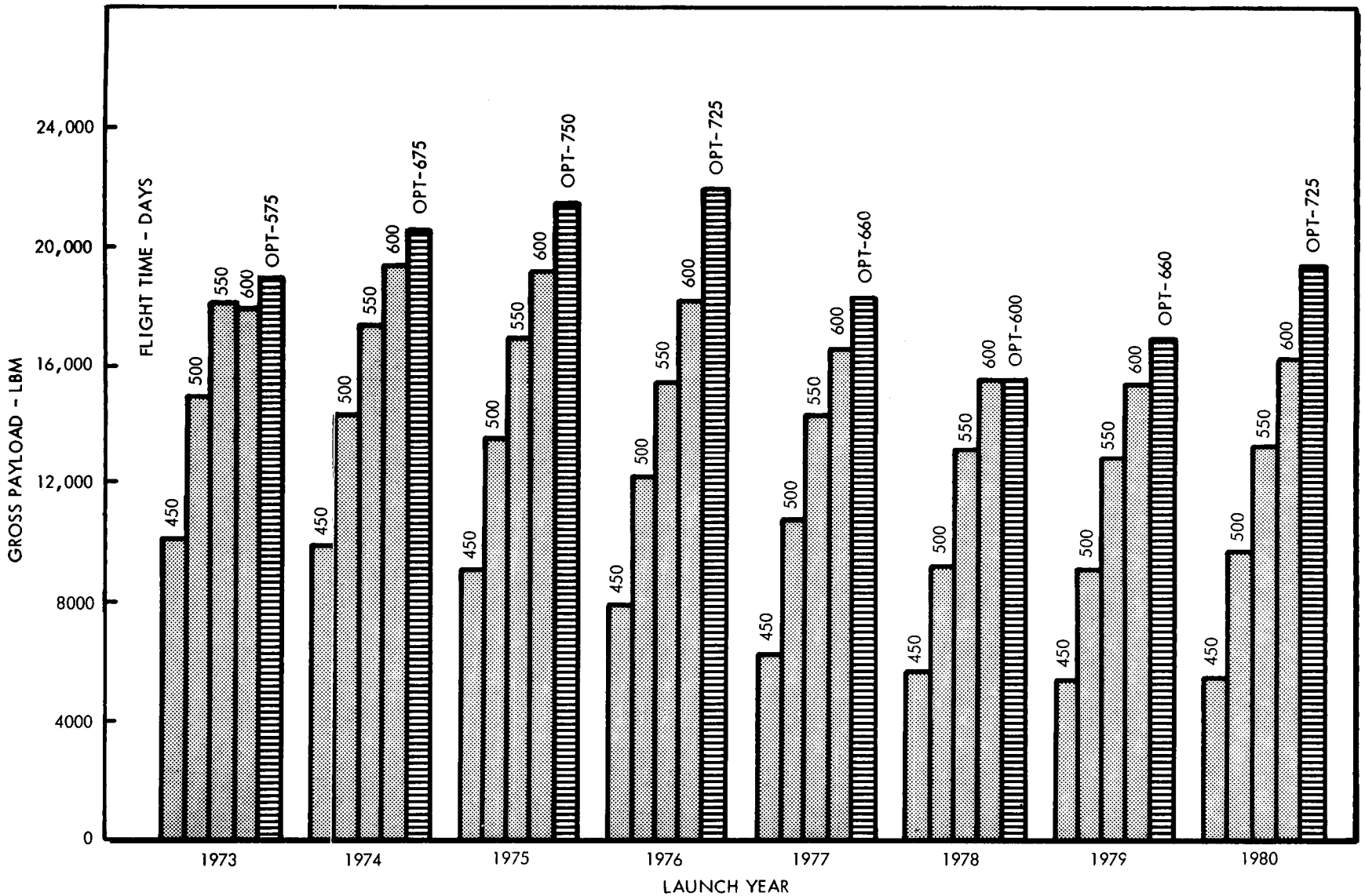


FIGURE 2.3-12

JUPITER MISSION PAYLOAD CAPABILITY, SATURN IB/CENTAUR/HEKS

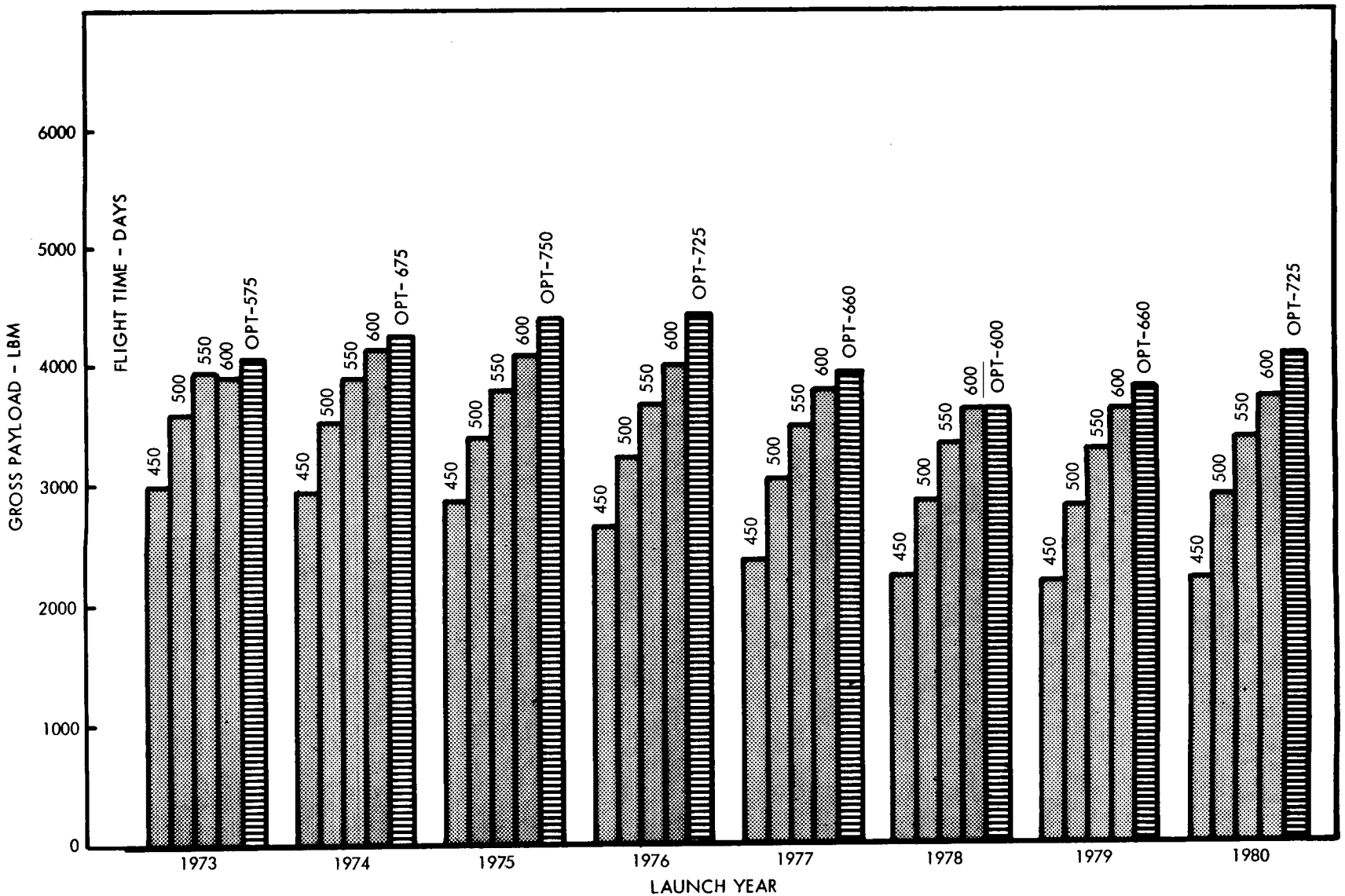


FIGURE 2.3-13

JUPITER MISSION PAYLOAD CAPABILITY, TITAN IIICx/CENTAUR

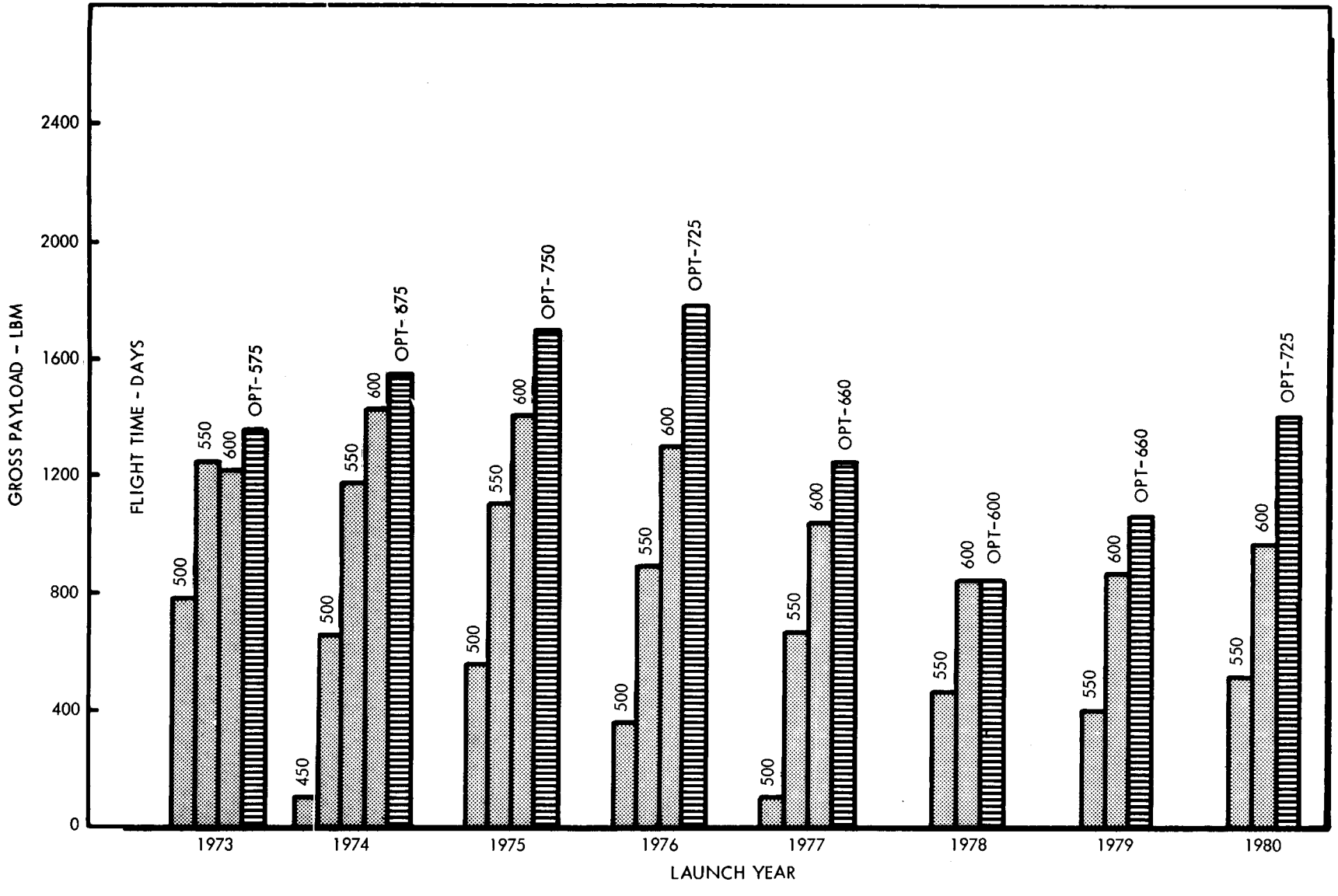


FIGURE 2.3-14

JUPITER MISSION PAYLOAD CAPABILITY, ATLAS SLV3x/CENTAUR/HEKS

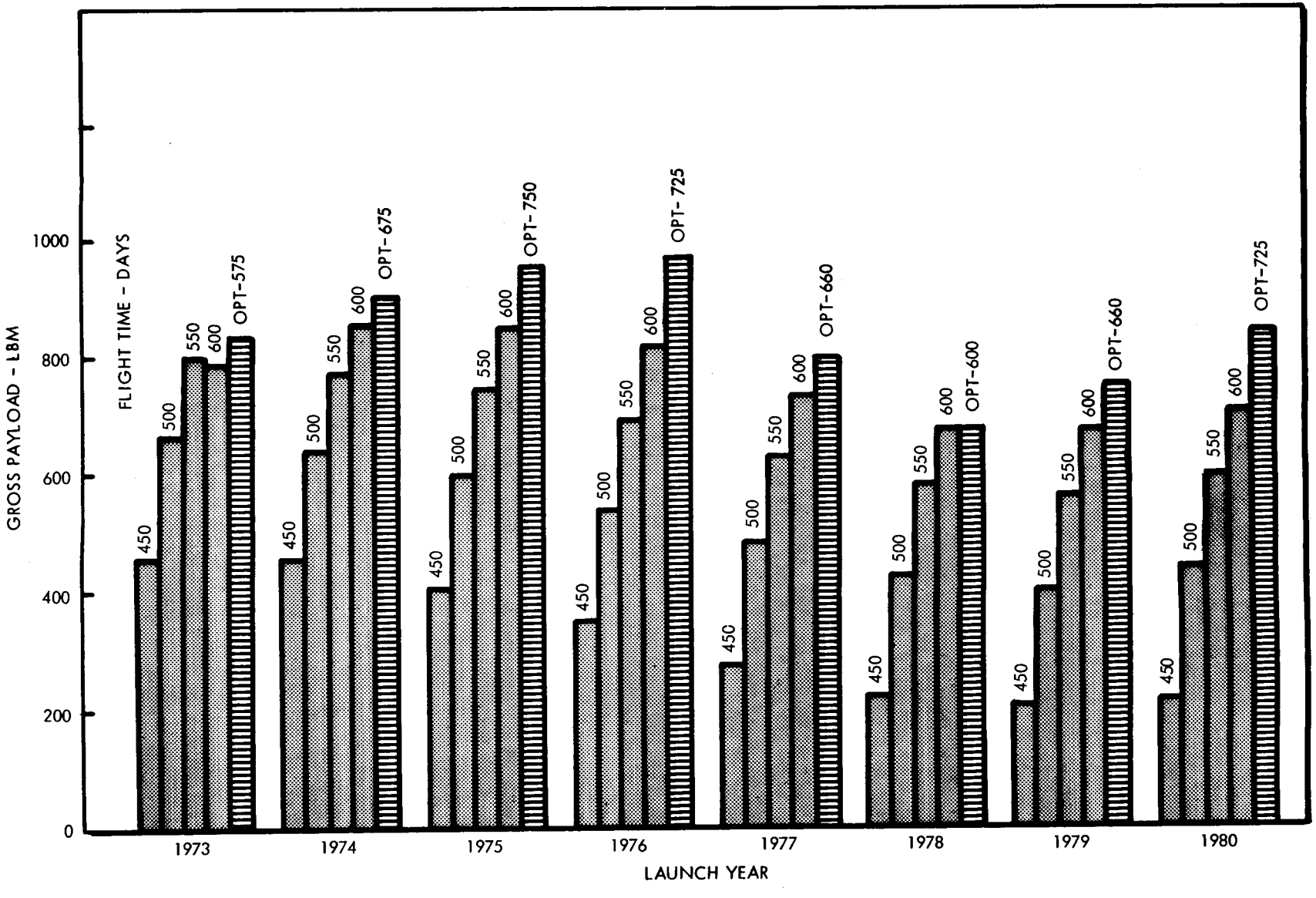


FIGURE 2.3-15

2.4 DETAILED MISSION PROFILE ANALYSIS

The portion of the study devoted to the detailed analysis of selected mission profiles has two primary objectives: (1) the generation of time histories of pertinent trajectory data for the use of the subsystem design groups in determining general operational requirements, environment, etc., and (2) the calculation of much more precise and extensive trajectory data (on a much more selective basis in terms of the number of cases considered) for the purpose of verifying the feasibility of spacecraft design/mission profile selections made on the basis of the earlier and less extensive calculations. Major emphasis to date has been placed on the first of these objectives. Since the data generated are in some cases quite voluminous, only representative samples of such data as are of greatest general interest will be presented in this subsection.

2.4.1 Departure Phase

Curves of geocentric distance versus time for typical Earth-departure hyperbolas are shown in Figure 2.4-1. The time required

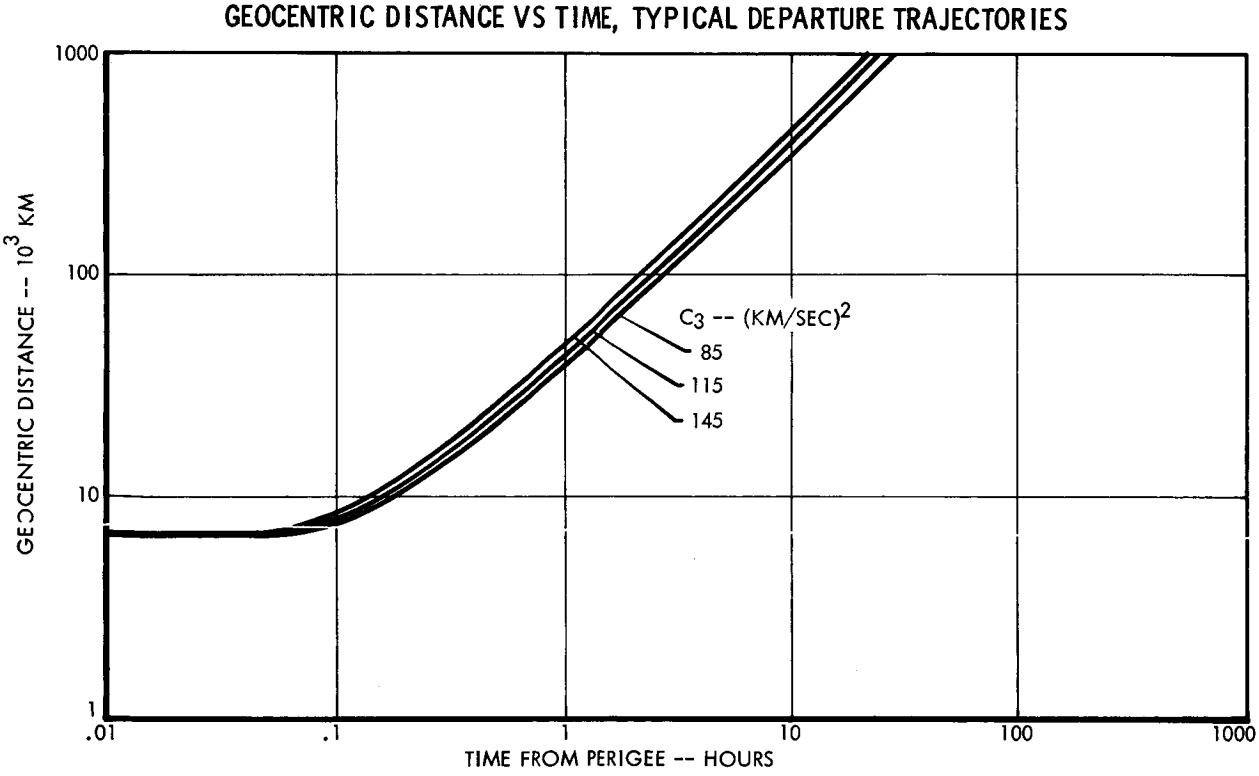


FIGURE 2.4-1

for the spacecraft to reach the boundary of Earth's activity sphere (≈925,000 kilometers) is typically on the order of one day for Jupiter missions, as compared to approximately three days for Mars and Venus missions. Assuming comparable DSIF tracking configurations,

this will mean that only about one-third as much close-in tracking data will be available for orbit determination prior to the execution of the first guidance correction maneuver. However, according to the heliocentric conic trajectory data supplied by JPL, the contribution of orbit determination errors to the arrival position error ellipse is roughly an order of magnitude smaller than the contribution of a nominal 0.1 meter per second execution error in the maneuver itself. Therefore, orbit determination accuracy during the departure (geocentric) phase of the mission does not appear to present a problem.

2.4.2 Heliocentric Phase

Two-body heliocentric trajectory data on a number of representative Earth-Jupiter transfers were published in Reference 2.4-1 for use by the subsystem design groups. The heliocentric geometry of one of the representative trajectories is shown in Figure 2.4-2. In

HELIOCENTRIC GEOMETRY, TYPICAL 500-DAY MISSION

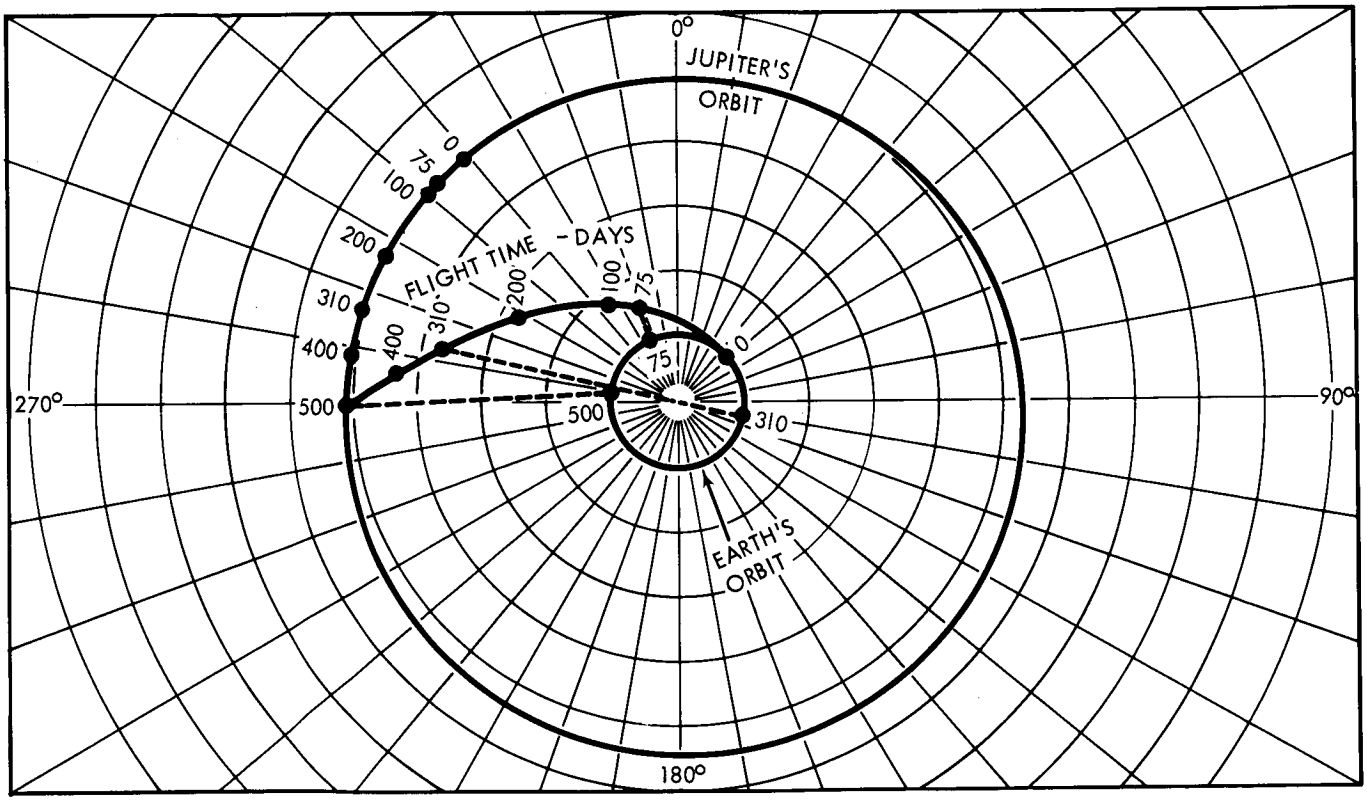


FIGURE 2.4-2

addition to the heliocentric and geocentric coordinates of the spacecraft, the referenced report contains spacecraft-centered coordinates (relative to a Mariner-type Sun-Canopus reference system) of Earth and Jupiter at 10-day intervals, as well as spacecraft-relative speed and impact direction for "average" meteroids.

Of particular interest are the histories of communication distance and Earth's out-of-beam-plane angle (Figures 2.4-3 through 2.4-5) which were prepared in order to investigate the feasibility of communication with a spin-stabilized minimal spacecraft. In this particular design concept, a bicone directional antenna was utilized for long-distance communication. In order to demonstrate feasibility, it was necessary to show that a direction in inertial space could be found such that, when the spacecraft's spin vector was oriented in such a direction, Earth (as seen from the spacecraft) would be located within a fraction of a degree of the antenna beam plane (normal to the spin axis) during the major portion of the mission when the communication distance is too great to use an omnidirectional antenna for down-link transmissions. The cited figures demonstrate that such a concept is feasible. One of the primary disadvantages of this concept is that the choice of jovicentric encounter trajectories is essentially limited to equatorial passages. This latter restriction is necessary if the communication link is to be maintained during the post-encounter phase of the mission.

2.4.3 Encounter Phase

In Figure 2.4-6, jovicentric distance versus time for representative encounter hyperbolas is shown. For the purpose of demonstrating the three-dimensional aspects of the encounter phase of the mission, relatively crude but effective 3-dimensional models, of which Figure 2.4-7 is a 2-dimensional representation, were prepared for typical approach conditions. These models have proved very helpful in visualizing the available alternatives with respect to the orientation of the encounter trajectory relative to the target planet.

2.4.4 Post-Encounter Phase

No detailed post-encounter profiles have been generated as yet.

2.4.5 References

2.4-1 Wilson, S. W., Jr. "Earth - Jupiter Heliocentric Transfer Trajectory Data," General Dynamics Corporation, Fort Worth Division, MR-A-2001, 13 December 1965.

COMMUNICATION PARAMETERS HISTORY, SPIN-STABILIZED SPACECRAFT, 1976 500-DAY MISSION

(ANTENNA BEAM PLANE NORMAL TO SPIN AXIS)

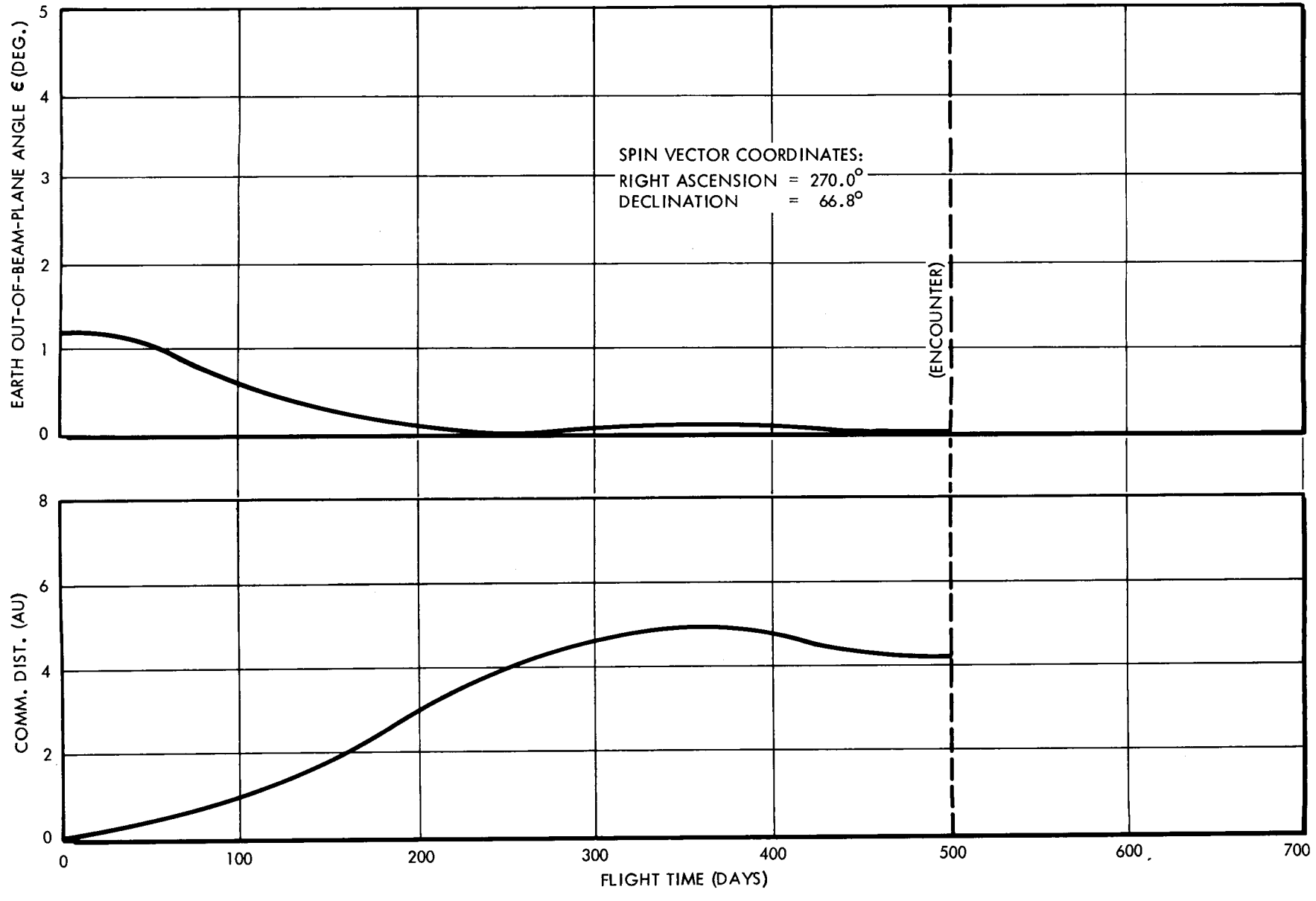


FIGURE 2.4-3

COMMUNICATION PARAMETERS HISTORY, SPIN-STABILIZED SPACECRAFT, 1974 600-DAY MISSION

(ANTENNA BEAM PLANE NORMAL TO SPIN AXIS)

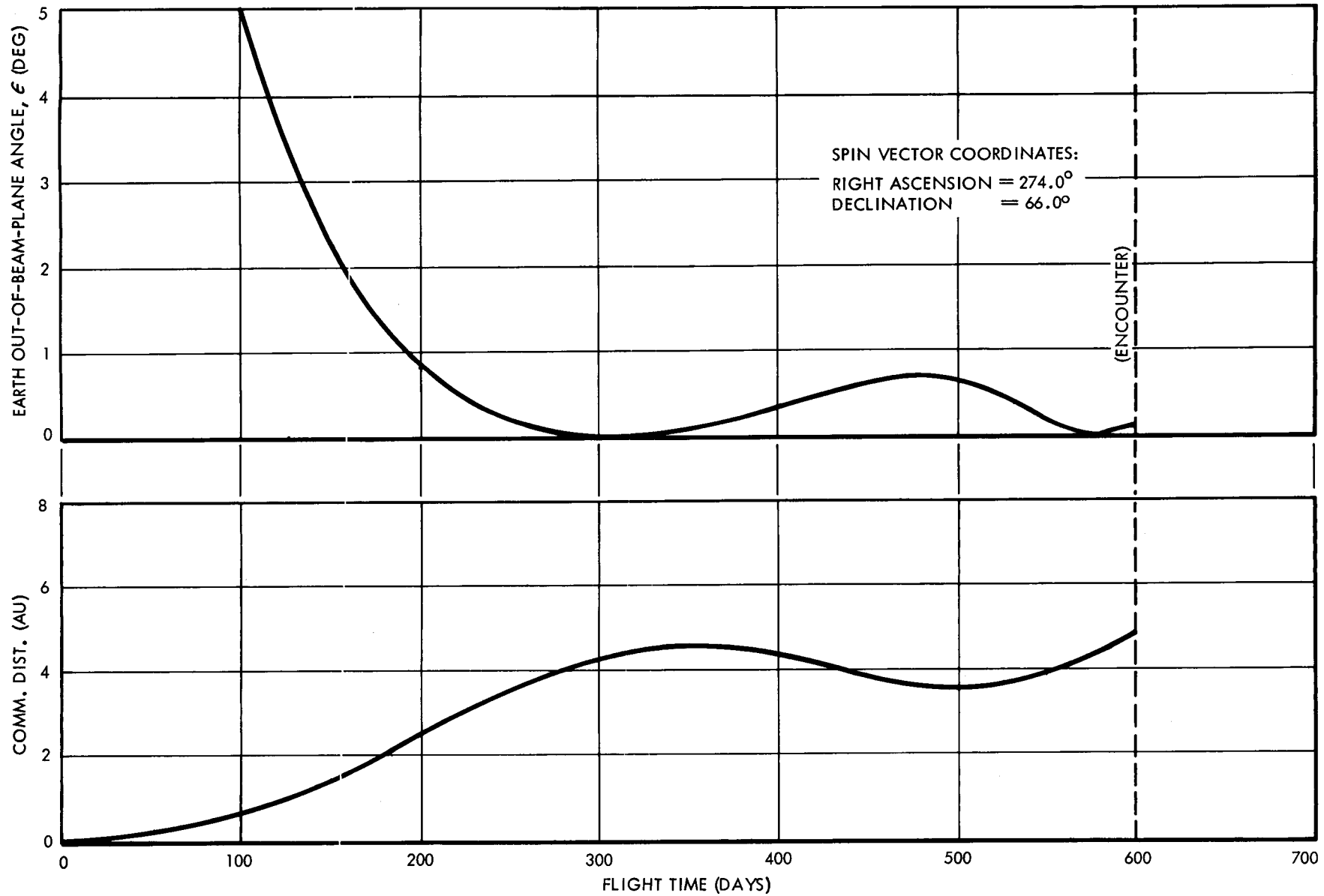


FIGURE 2.4-4

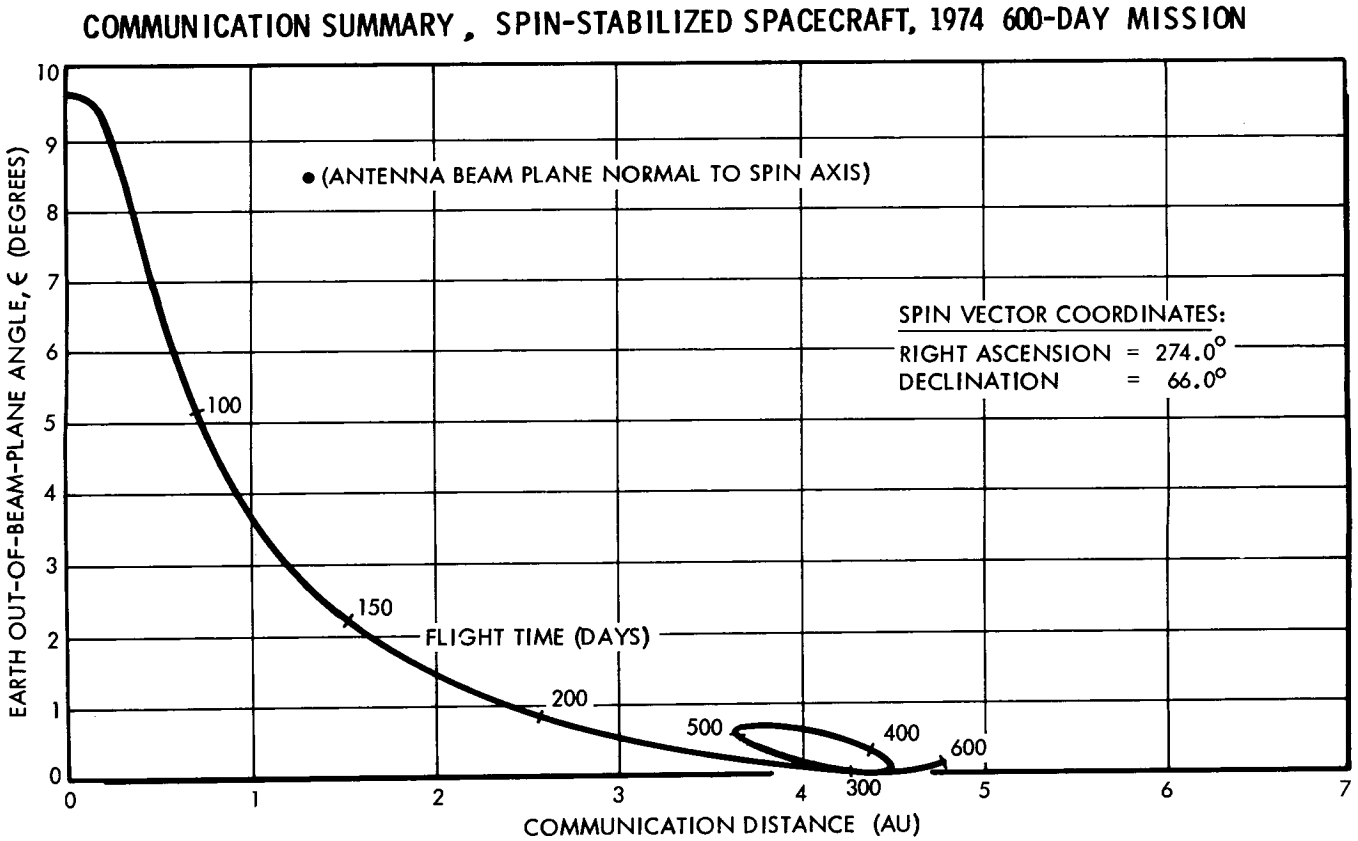

COMMUNICATION SUMMARY, SPIN-STABILIZED SPACECRAFT, 1974 600-DAY MISSION
EARTH OUT-OF-BEAM-PLANE ANGLE, ϵ (DEGREES)
10
9
8
7
6
5
4
3
2
1
0
• (ANTENNA BEAM PLANE NORMAL TO SPIN AXIS)
SPIN VECTOR COORDINATES:
RIGHT ASCENSION = 274.0°
DECLINATION = 66.0°
100
150
FLIGHT TIME (DAYS)
200
500
400
600
300
0
1
2
3
4
5
6
7
COMMUNICATION DISTANCE (AU)

FIGURE 2.4-5

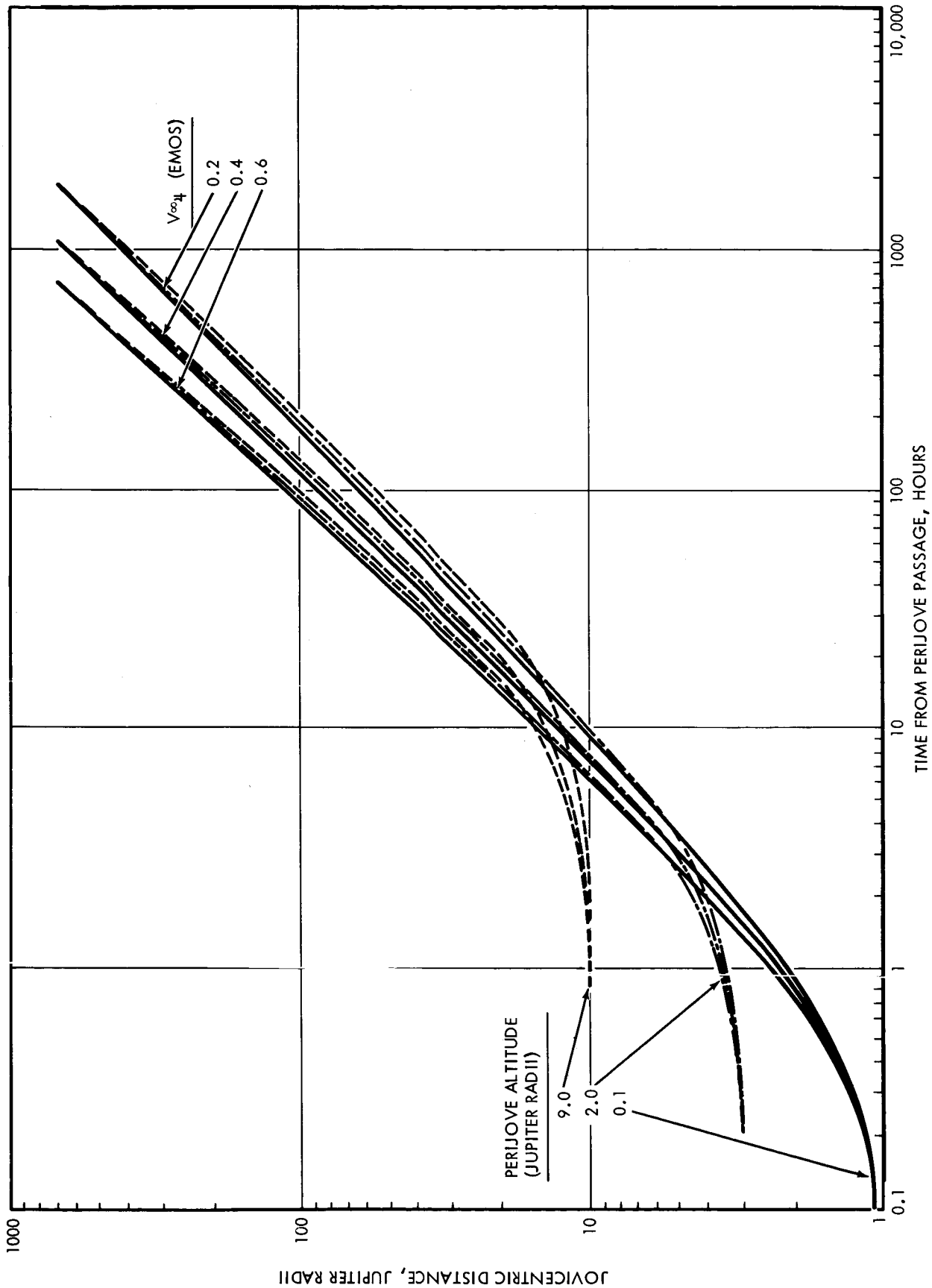

JOVICENTRIC DISTANCE VS TIME, TYPICAL ENCOUNTER TRAJECTORIES
JOVICENTRIC DISTANCE, JUPITER RADII
1000
100
10
1
0.1
TIME FROM PERIJOVE PASSAGE, HOURS
1
10
100
1000
10,000
V_{∞_4} (EMOS)
0.2
0.4
0.6
PERIJOVE ALTITUDE (JUPITER RADII)
9.0
2.0
0.1

FIGURE 2.4-6

GEOMETRY OF TYPICAL ENCOUNTER TRAJECTORIES

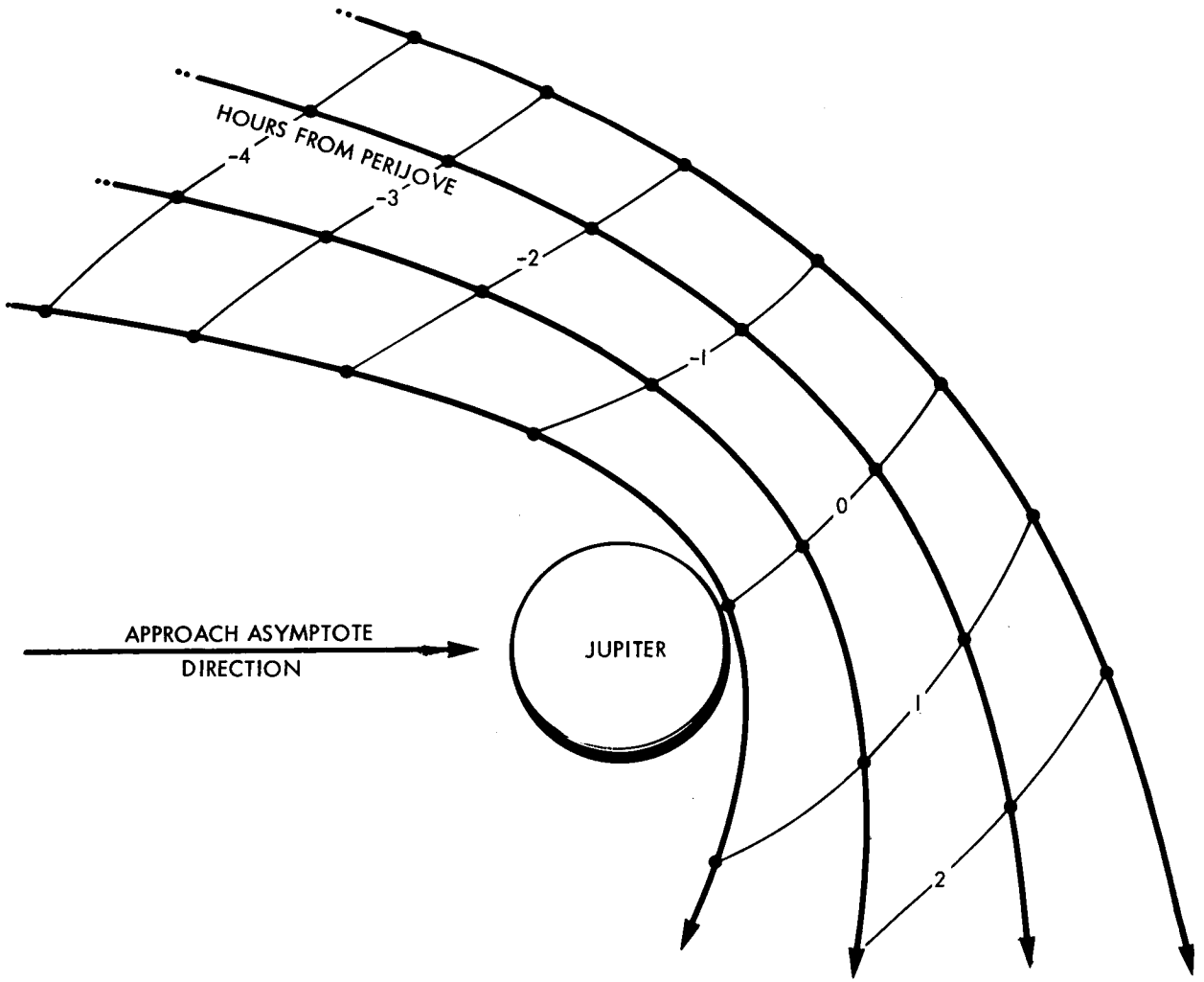


FIGURE 2.4-7

SECTION 3

SPACECRAFT SYSTEMS DESIGN AND ANALYSIS

In this section, the general aspects of the design and analysis of spacecraft subsystems which are intended to perform flyby missions of Jupiter are described. The analyses which are discussed are concerned with (1) communications, (2) data management, (3) spacecraft control, (4) navigation and guidance, (5) attitude control, (6) propulsion, (7) electrical power, (8) thermal control, (9) radiation protection, (10) meteoroid protection, (11) structure, (12) configuration, and (13) reliability. The section is arranged according to these topics and in this order.

3.1 COMMUNICATIONS

3.1.1 Functional Requirements

3.1.1.1 Basic Communications Requirements

The communications subsystem will be used to perform four basic functions: (1) transmission to Earth of scientific data gathered by the spacecraft; (2) transmission to Earth of engineering data, i.e., the condition of the spacecraft and its functions; (3) reception of command signals from Earth to direct the spacecraft and its subsystems to perform certain functions; and (4) retransmission of ranging interrogations to provide range information to the Earth. The communications subsystem, which will be used to accomplish these functions, will be considered as being composed of four components: (1) the antenna, (2) the receiver, (3) the transmitter, and (4) the modulator. The modulator can be considered as a part of the transmitter; but since it is used to add information to the radio signal returned to Earth, it will be considered as a separate subsystem component. In order to maintain communications with Earth properly, the communications subsystem must receive an adequate signal from Earth, receive data from the data management subsystem, modulate an rf signal by use of the data, amplify the modulated signal to the necessary power level, and transmit this signal to Earth through a properly oriented antenna.

3.1.1.2 Interfaces

A simple block diagram of the interfaces between the communications subsystem and other spacecraft subsystems is shown in Figure 3.1-1. The signal flow between the communications subsystem and other subsystems is as follows:

1. Data management will furnish communications with conditioned data at the proper information rate and in terms of a time schedule suitable for input to the modulator.

2. Communications will furnish data management with signals suitable for processing the communications engineering data.

3. Communications will furnish command and control with demodulated command signals received from DSIF.

4. Command and control will furnish communications with an antenna-positioning signal, if applicable.

5. Electrical power will be furnished by the power subsystem.

COMMUNICATIONS INTERFACES

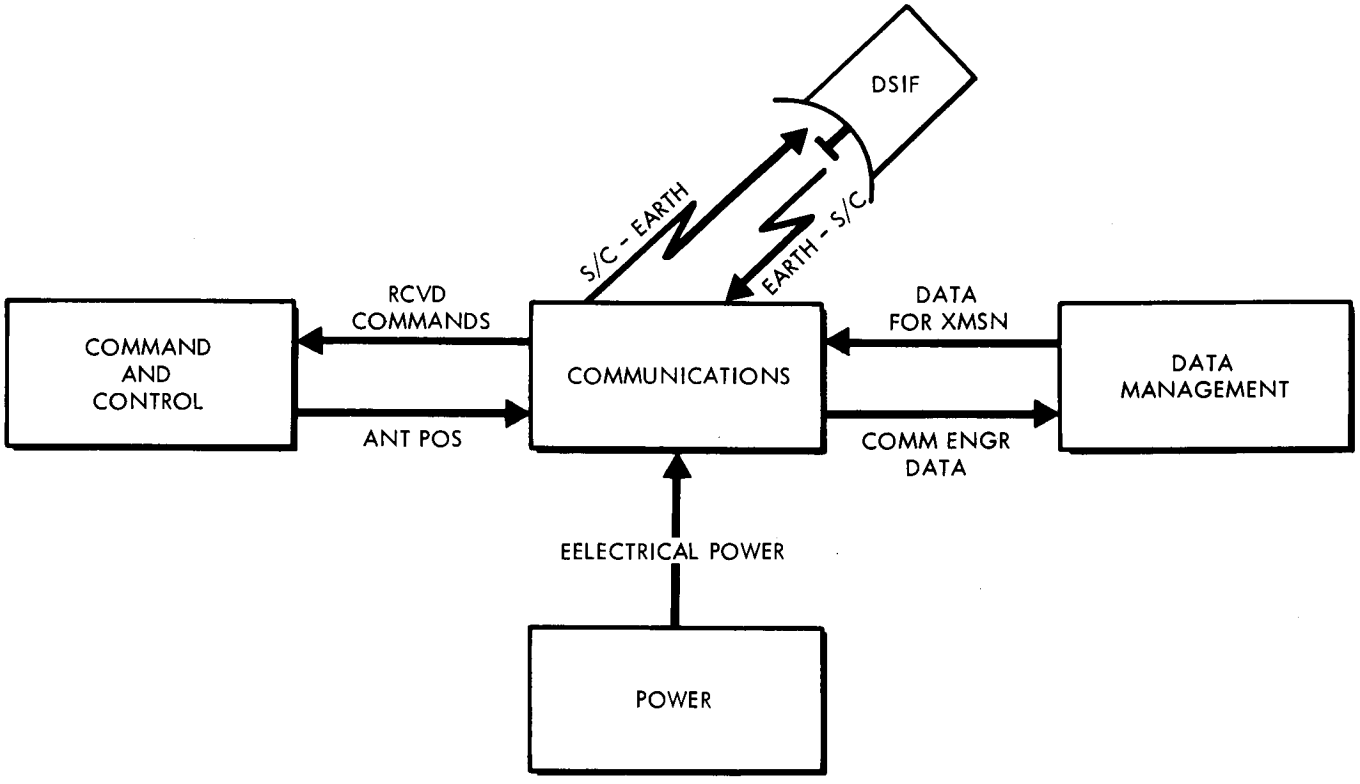


FIGURE 3.1-1

3.1.2 Identification of Trade-Offs

The trade-offs which are to be considered necessary for defining efficient systems are those between the various functional parameters, between the various physical parameters, and between the functional and physical parameters. The trade-offs to be made for the communications subsystem being considered in this study are shown diagrammatically in Figure 3.1-2. In this diagram, the antenna design is shown to be dependent upon the spacecraft stabilization, the point accuracy which can be provided by the command and control subsystem, and the transmitter power. Transmitter design is a function of the type amplifier selected, the electrical power required, and the antenna design.

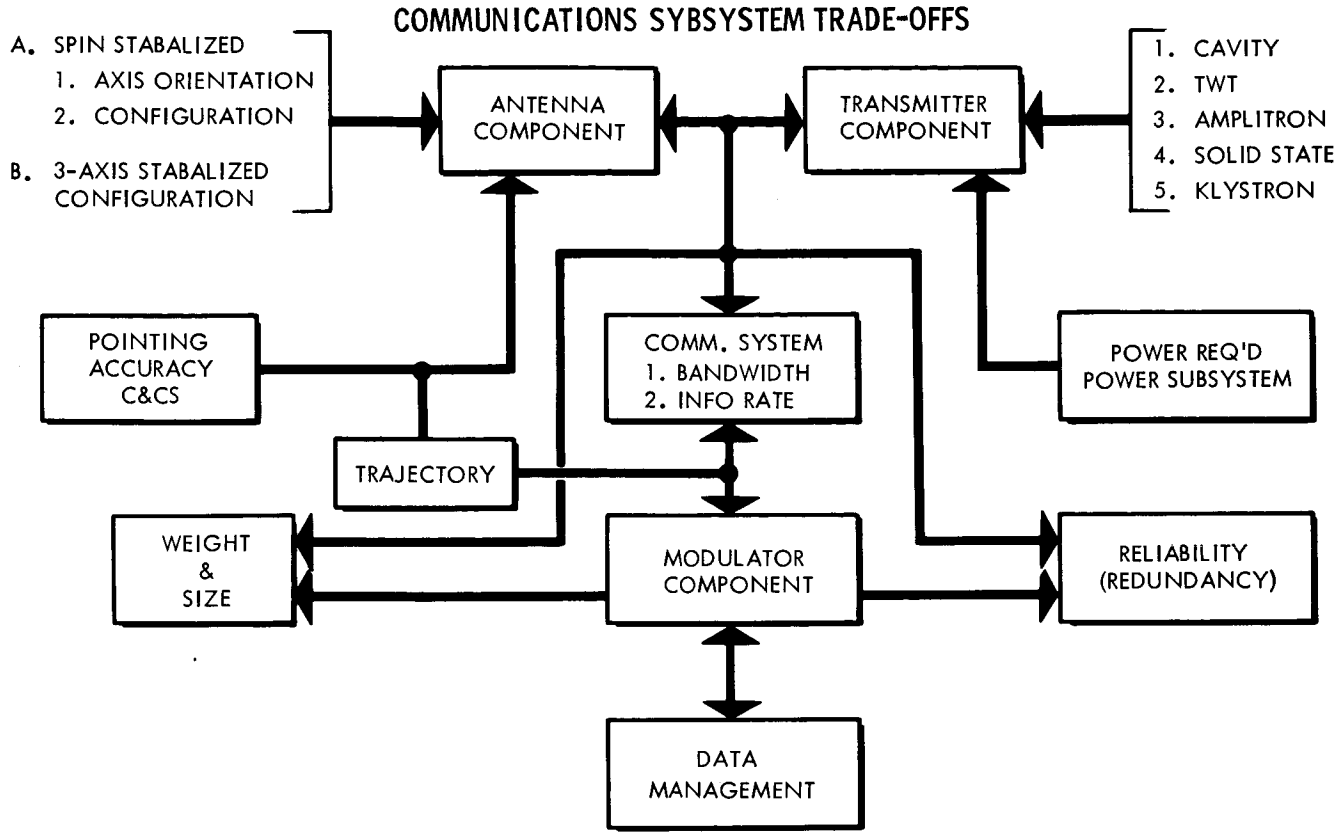


FIGURE 3.1-2

The information rate and rf bandwidth are dependent upon the effective radiated power (transmitter power multiplied by antenna gain) and the modulation scheme. Information rate is also dependent upon the coding technique and information storage capability of the data management subsystem. The spacecraft trajectory affects the entire subsystem, because it both determines the length of the spacecraft Earth link and defines the antenna-positioning requirements. Finally, the weight, size, and reliability of the entire subsystem must be considered.

3.1.2.1 Antenna Problems and Considerations

Before discussing specific problems, it is well to review possible antenna types. These fall into three major categories. Antennas such as bicones, round waveguide slot arrays, or collinear arrays produce toroidal patterns. Antennas which produce such patterns are used on spin-stabilized spacecraft and are always oriented normal to a given plane (approximately that of the Earth's orbit), and there is no need for steering. The second category is that of pencil beam antennas. Such antennas are used in conjunction with a spin-stabilized spacecraft that exhibits a

properly oriented spin axis or with a three-axis stabilized spacecraft. Finally, another category of antennas used with spin-stabilized spacecraft is that of electrically de-spun antennas. These antennas could be either arrays used in programmed scans or adaptive, self-focussing arrays. The use of a Luneberg lens in conjunction with multiple switched feeds, or some analogous device, is probably not practical but is not out of the question.

Since the antenna is physically located on the perimeter of the spacecraft, it will be susceptible to meteoroid damage. A discussion of the mechanics of the problem and of possible protective measures is presented in Appendix B. A solution to the problem presented is not considered unreasonable.

Consideration is now given to the relative merits of the use of various antenna types. The emphasis is on patterns, reliability, and other such considerations. Very little emphasis is placed on costs, difficulty of construction, or difficulty of initial alignment. It is assumed that the alignment can be done on the ground and that the cost and difficulty of construction is of secondary importance to reliability.

The first antennas to be discussed are those applicable to spin-stabilized spacecraft; the first of these is the biconical horn. Biconical antennas, being rotationally symmetric about an axis, naturally produce rotationally symmetric patterns. Perturbations such as changes in the antenna surface shape produce very little effect on this symmetric character. Bicones are quite rugged and can be confidently expected to survive a launch. On the other hand, there is a serious objection to using a bicone at the wavelength (13 centimeters) under consideration and for the gain and beamwidth desired (15 db and 3.6 degrees). The objection is that a biconical horn of even 180-inch diameter needs to be compensated by placing a lens in its mouth in order to obtain that desired gain and beamwidth (Reference 3.1-1). Such a compensated horn would be about 7 feet in height, as can be seen from Figure 3.1-3. Smaller diameter biconical horns exhibit even smaller maximum gain if they are uncompensated. In addition, circular polarization is difficult to obtain.

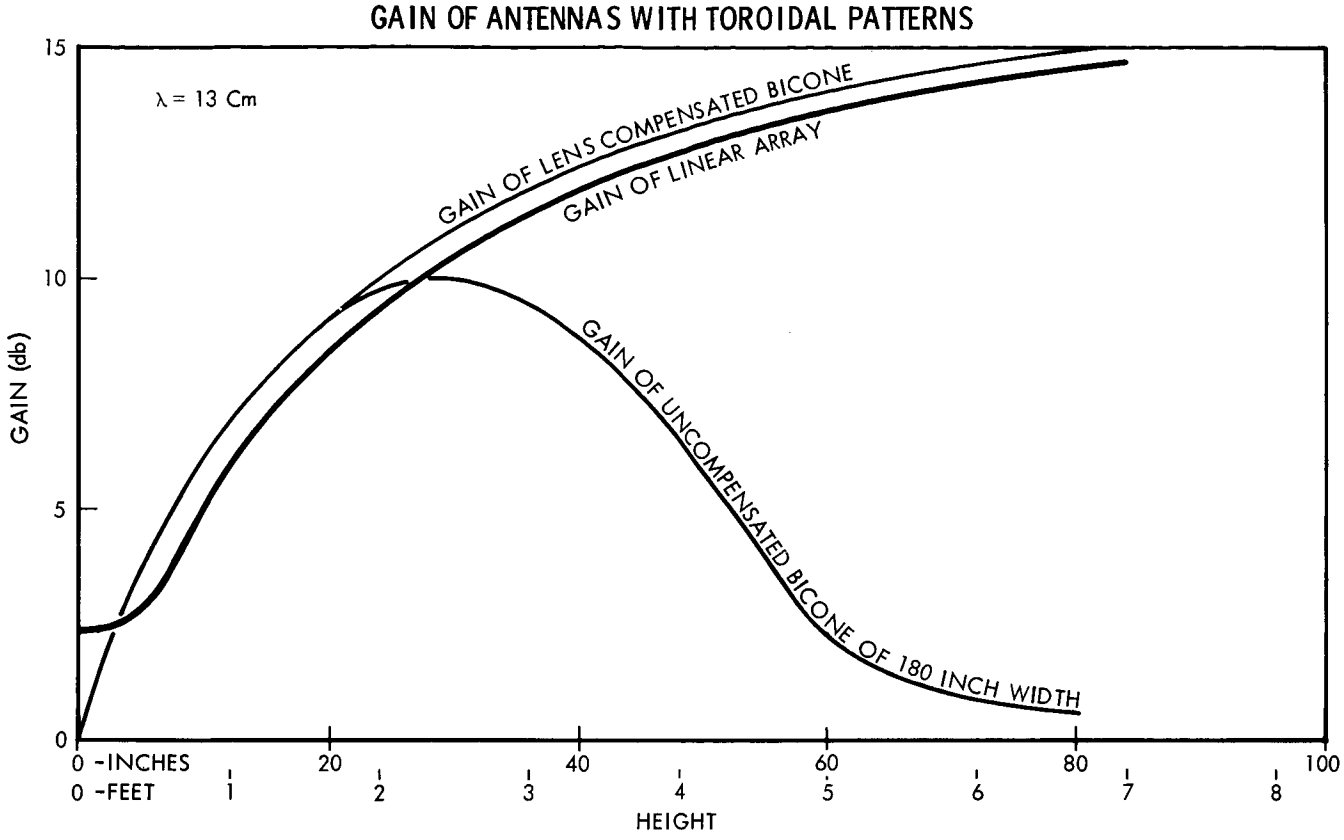


FIGURE 3.1-3

A collinear array, or any form of linear array of the same height as the compensated bicone, provides the same gain (Reference 3.1-2). However, for the case of the ordinary, simply fed collinear array (consisting of a line of end-fed halfwave dipoles separated by quarterwave sections), this gain is very difficult to obtain and is easily disturbed by vibrations, etc. The required gain is more easily obtained by using a broadside array instead. The problem of feeding such a broadside array without producing azimuthal variations in the pattern is difficult, but it could probably be solved by using cylindrical dipole elements and running the feed line inside them. It is then necessary either to run perhaps 16 feed lines or to provide baluns and power dividers along the length of the array. Such an array is also susceptible to vibrations. Also, for the case of both the above array types, circular polarization is difficult to obtain.

Most of the feed, ruggedness, and polarization problems are greatly simplified by use of a different design concept. Slots are cut in the wall of a circular waveguide and fed by waveguide mode fields. A sufficient number of slots, six or eight, cut around the circumference of the waveguide, produces pattern symmetry within any reasonable tolerance (Reference 3.1-3). Circular polarization is obtained by cutting cross-slots. Slot groups

are used to form a linear array and phased properly by proper spacing (Reference 3.1-4). From the above considerations, it appears likely that a slotted waveguide comprises the most practical antenna for producing an azimuthally symmetric pattern under the circumstances. Such an antenna, which is 4 inches in diameter and 7 feet tall, produces a gain of 15 db. If less gain is acceptable, the height can be correspondingly reduced as shown in Figure 3.1-3.

No form of de-spun antenna, either mechanical or electrical, is considered to be practical. The former because of obvious mechanical difficulties experienced in the use of bearings, rotary joints, etc.; the latter because of more subtle difficulties with timed switches (affecting reliability), accurate pointing, and many other problems. However, three possibilities present themselves. The simplest in concept is a pencil beam type array in which a clock and computer, or equivalent, is used to time the programmed beam scanning so that it points in the desired direction. This concept requires the use of not only a simple de-spin but also a changing de-spin to track the Earth in its orbit at different points in the spacecraft orbit. Such a setup seems impractical to build and program (though not impossible) and quite risky in view of the possibility of failure. In a more complicated concept, which might be called "crude electronic de-spin," a number of patterns are used. Each of these patterns covers one quadrant or one semicircle of azimuth. An example might be the use of four cardioid patterns. Such patterns can be obtained by using four collinear arrays, for example, or by use of a septated waveguide array, in which the waveguide is separated into four sections by walls and fed one section at a time (Reference 3.1-5). Simple switching is then used to select the pattern which provides the coverage of a full quadrant (for instance) at a time. The selected pattern is in the quadrant including Earth. The restriction of the radiated power to a segment of the full 360 degrees of azimuth thus produces additional gains on the order of 3 to 6 db. It should be possible to provide a simple program for the switching which will decide which of the four patterns to switch. Another concept which is really somewhat easier to implement is the concept of the adaptive or self-focussing array. Such an array works in the following way. Each individual element senses the phase of an incoming signal and sends out a transmitting signal with the opposite phase; consequently a transmitted wave is produced. This wave is focussed on the origin of the received wave. Thus, in effect, such an antenna produces a beam in the direction of the transmitter of a received wave. A pilot pointing wave is required for such an antenna to operate, but this is no serious disadvantage. The main problem is that each

individual element must receive (because of its own pattern gain) sufficient power for the phase of the incoming signal to be detected. It may be that a self-focussing or adaptive array would be more reliable than any other type if the individual elements could receive enough power. In the formulation of all the above de-spin concepts, it has been assumed that it was not feasible to de-spin anything but an array. It is felt that the case for such a statement is sufficiently well established that no other possibility will be discussed here. However, other possibilities, such as the use of Luneberg lenses in conjunction with multiple feed elements which can be switched in the proper sequence, do exist.

In regard to antennas for use with 3-axis stabilized spacecraft, it is clear that some form of reflector is the best choice. Reflectors are mechanically stable, simple to design and construct, almost invulnerable to meteoroids, and easy to make circularly polarized (by providing a circularly polarized feed). It is difficult to name any important disadvantage. Reflectors can be designed to produce any reasonable gain consistent with the area which is specified, and no other antenna type of the same size can be used to better advantage. It is also easy to provide beam shaping by use of reflectors.

3.1.2.2 Transmitter Amplifier Problems and Considerations

The type of transmitter amplifier which is considered as being compatible with DSIF at S-Band frequencies was limited to four types of vacuum tubes plus solid state. Solid-state amplifiers in general have exhibited excellent reliability and stability as compared to vacuum tube devices. The overall efficiency of a solid-state S-Band amplifier is comparable to that of the better vacuum tube devices. However, the power level deemed necessary in this study cannot be achieved by the use of the present solid-state S-Band equipment.

Of the vacuum tube devices, the negative grid tube is probably the most familiar. The tube elements can be configured to exhibit an acceptable cathode-to-plate transit time at S-Band, e.g., the planar triode. The amplifier is then a class C power amplifier with cavity resonators. There is no problem in attaining the required power levels or in building the tube and cavity ruggedly enough to achieve stability. However, cavity amplifiers in the 10- to 20-watt range typically attain overall efficiencies in the order of 15 to 20 percent (Reference 3.1-6); however, one manufacturer claims an overall efficiency of 28 percent for the case of

a 100-watt output. Unfortunately, operating these tubes under the conditions of maximum tube life results in roughly half the above stated efficiency.

The recently developed electrostatically focussed klystron has demonstrated overall efficiencies of about 30 percent. The conventional intermediate power klystron has demonstrated a life of 5000 hours. However, because of the significant difference between the conventional and electrostatically focussed klystron, one cannot assume a long life for the latter (Reference 3.1-7).

The traveling wave tube (TWT) has enjoyed considerable development work since the advent of space communications. Many reliable, efficient TWT's have been developed for space applications under NASA programs. Power levels of up to several hundred watts have been realized. It is not unreasonable to assume that an efficiency of 35 percent for the case of a 50-watt output can be readily attained.

The amplitron is a cross-field microwave tube. Its greatest attribute for space applications is its high efficiency which may run as high as 55 percent (Reference 3.1-7). Until recently, the amplitron was not considered suitable for space applications because of the large magnet needed as a part of the assembly. Recently, light-weight tubes have been developed. However, no reliability figures are available for the case of the light-weight tubes.

If it were necessary to provide a detailed transmitter amplifier design at this time, a TWT would be recommended because of the combination of reliability, efficiency, and power level. However, at the present pace of development, all microwave amplifiers should be surveyed before a design is finalized. In this study it is assumed that TWT's are used in the transmitter amplifier.

3.1.2.3 Modulation Systems

Two modulation systems were considered for use in the communications subsystem: the coherent phase-shift-keying (PSK) system which was used on Mariner IV and a non-coherent multiple frequency shift (MFS) system proposed by Goldstein and Kendall (Reference 3.1-8).

To analyze these two modulation systems, assume a transmitter power of 25 watts, an antenna gain of 14 db and a distance of 6AU. The basic transmission equation is well known and in logarithmic form is:

$$S/(N/B) = P_T - L_M + G_T + G_R - \Phi - L_S - L_M$$

where:

S = Received signal strength

N = Noise power per unit bandwidth

B = System bandwidth

P_T = Transmitted power

L_M = Modulation loss

G_T = Transmitted antenna gain

G_R = Receiving antenna gain

Φ = Receiver sensitivity per unit bandwidth

L_S = Space attenuation

L_M = Miscellaneous losses and tolerance.

Let us also assume the following receiving parameters:

G_R = 61 db

Φ = -186 dbm (40^oK)

at 6AU: L_S = 278 db

and let us further assume

L_M = 8 db.

Then for a phase coherent system assuming a modulation loss of 3 db,

$$S/(N/B) = 44 - 3 + 14 + 61 + 186 - 278 - 8$$

$$S/(N/B) = 16 \text{ db}$$

To transmit 1 bit per second with pseudo noise (PN) synchronization by use of a single-channel system that has a PN code length of 63 and

a word length of 7, the required bandwidth is 18.75 cps. Then the received signal-to-noise ratio will be

$$S/N = 16 - 10 \log 18.75 = 3.3 \text{ db.}$$

In the case of the MFS system, let us assume that all the power transmitted is in the sideband. Then applying the transmission equation

$$S/(N/B) = 44 + 14 + 61 + 186 - 278 - 8$$

$$S/(N/B) = 19 \text{ db.}$$

To receive a 3-db signal-to-noise ratio, the maximum bandwidth which can be used is 16 db or 40 cps. Therefore, to transmit eight bits per word, it would be necessary to have a mixer frequency stability in the receiver of better than 5 cps. While this may be attainable, its operations would be very delicate. Also, Goldstein and Kendall (Reference 3.1-8) show that for an error probability of 10^{-4}:

$$\frac{\frac{S}{N}(T)^{\frac{1}{2}}}{\pi (f)^{\frac{1}{2}}} = 3.1$$

where:

S/N is the signal-to-noise ratio

T is the time period per word

f is the frequency separation.

Then for the above system:

$$T = \left[\frac{\pi(3.1)\ (5)^{\frac{1}{2}}}{2}\right]^2$$

$$T = 119 \text{ seconds.}$$

So the information rate is $\frac{(2)^5}{119}$ or approximately 1/4 bit per second. The PSK system seems more desirable.

ANTENNA POINTING ACCURACY

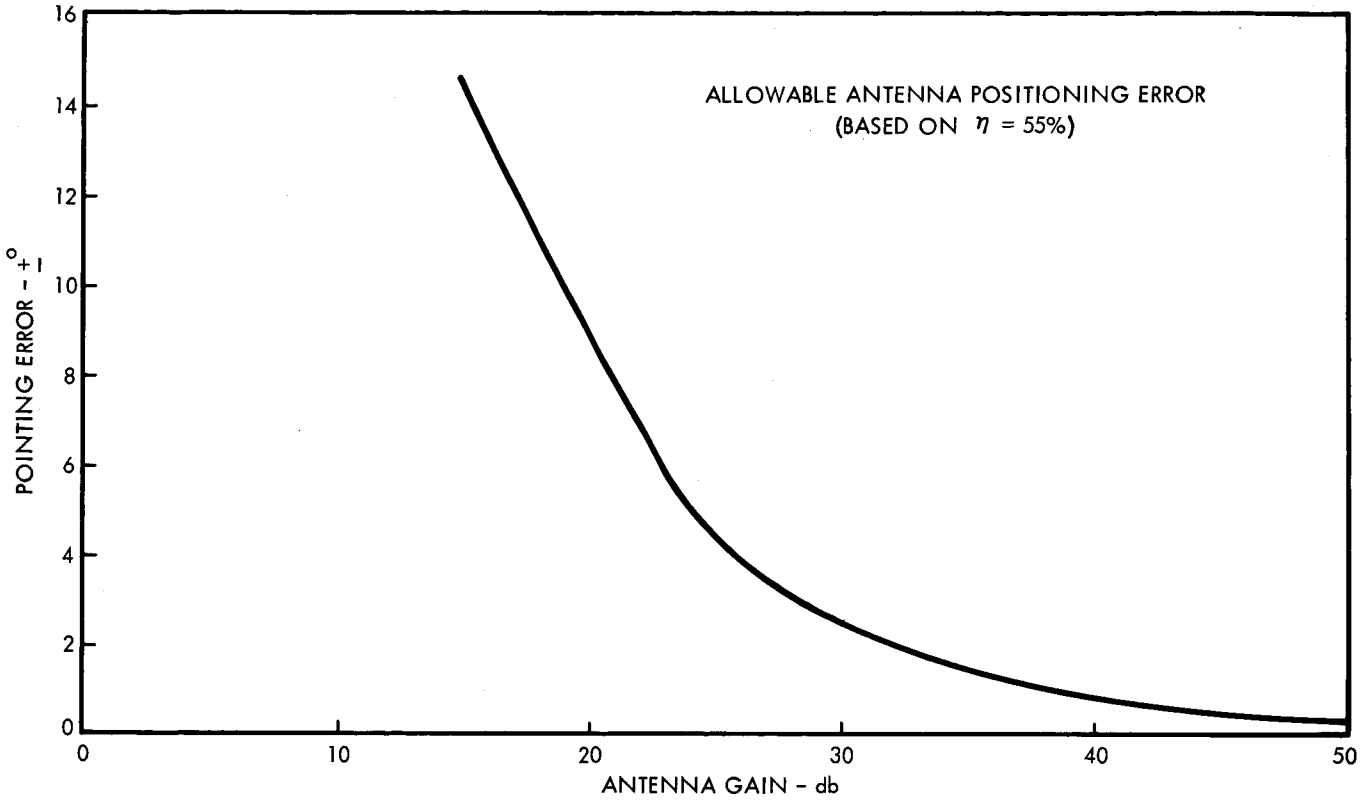


FIGURE 3.1-4

EARTH-SUN POSITION

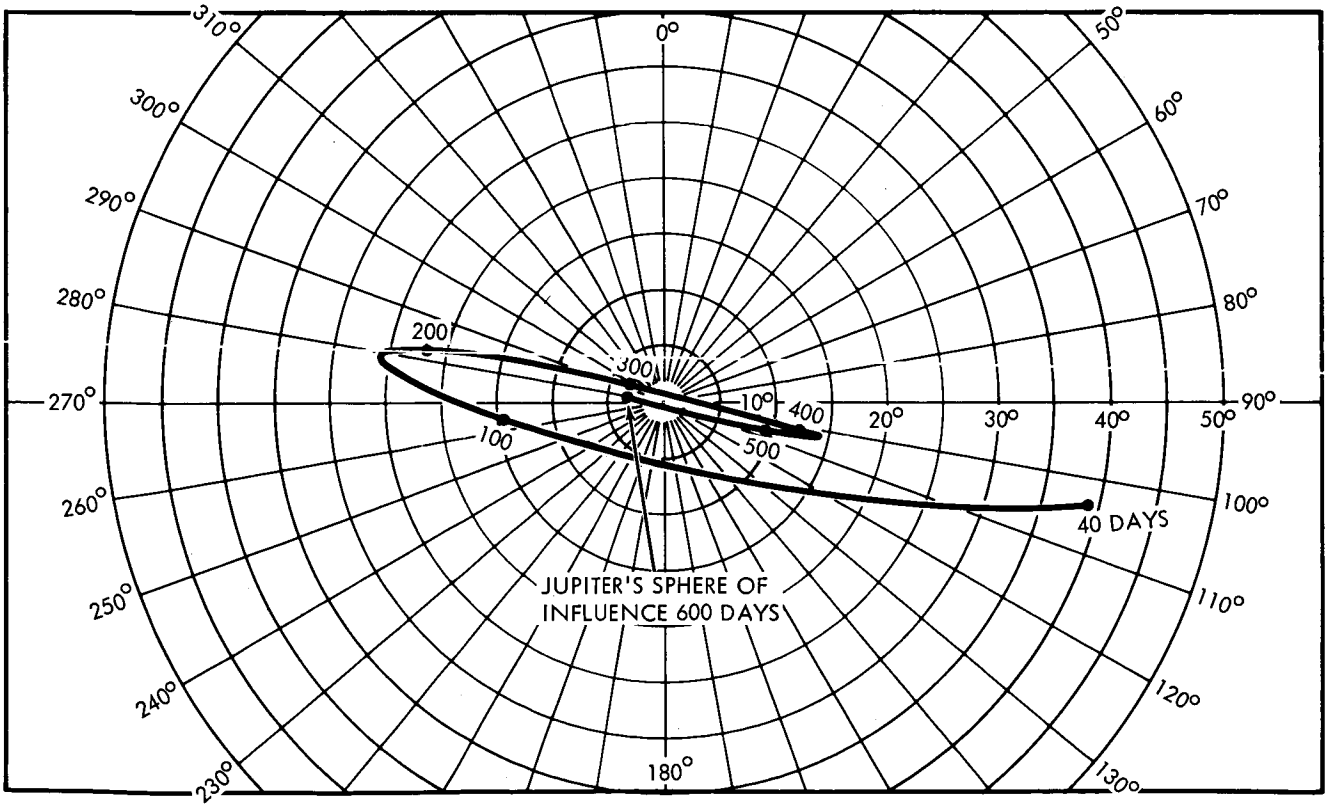


FIGURE 3.1-5

3.1.2.4 Earth System

Before examining the methods to be used in synthesizing a spacecraft communications subsystem, the characteristics of the Earth station should be defined.

For the purpose of this report, the full DSIF capability is assumed, i.e., a receiver noise temperature of 40°K, a receiving antenna gain of 61 db, a receiver frequency of 2295 mc, a transmitter power of 100 KW, a transmitting antenna gain of 51 db, and a transmitting frequency of 2113 mc. No attempt has been made to schedule communications with the spacecraft, and continuous communications capability is assumed except when the line-of-sight between Earth and the spacecraft is blocked. However, the scheduling of trans mission times would be a minor item.

3.1.2.5 Antenna Positioning

The problem of positioning pencil beam antennas must be discussed before continuing the discussion of the entire subsystem. Since a pencil beam antenna such as a parabolic reflector transmits energy only in a very small solid angle, it is necessary to point the antenna very accurately. Figure 3.1-4 shows a curve of necessary pointing accuracy versus antenna gain. To point the antenna with such an accuracy is probably most easily and reliably done by command from the ground, because the use of an elaborate on-board antenna pointing system is eliminated. Pointing can be achieved by means of steering either the spacecraft or the antenna alone. Steering is accomplished by changing the antenna position in discrete angular increments within two planes of freedom. When the antenna beamwidth and the Earth's position relative to the sun are known, the magnitude of these increments can be preselected. An example of Earth-Sun position is shown in Figure 3.1-5.

3.1.2.6 Spacecraft Subsystem

The spacecraft subsystem selection will basically require trade-offs between transmitter power, antenna gain and information rate. To aid in these trade-offs, Figure 3.1-6 was conceived. In this figure, antenna gain is shown as a function of the information rate and the transmitter power which is necessary to maintain an error probability not greater than 0.001. This requires the signal-to-noise per unit bandwidth times bit. (ST/N/B) to equal 6.8 db (Reference 3.1-9). The equation presented in paragraph 3.1.3.3, together with the DSIF parameters, was used to construct Figure 3.1-6.

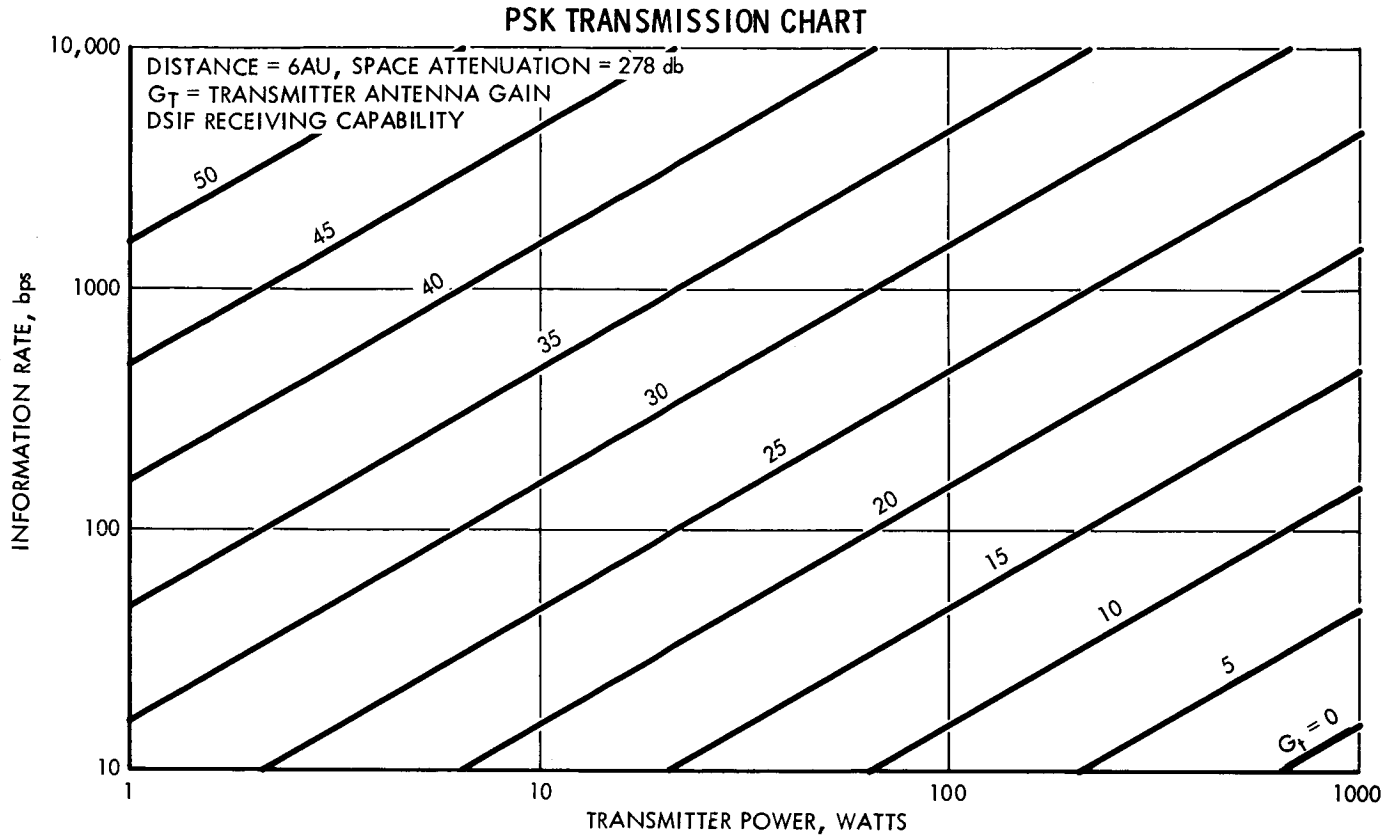


FIGURE 3.1-6

Antenna gain is considered first. Since increases in antenna gain increase the effective radiated power of the subsystem with no increase in electrical power input, the antenna gain is made as large as possible within physical and positioning limitations. After determining the attainable antenna gain, it is necessary to choose either a bit rate or transmitter power. Because the transmitter power necessary to transmit all the required data in real time is generally prohibitive, it is always necessary to store data. Therefore, the transmitter power is chosen to be compatible with equipment limitations and the electrical power subsystem. This choice then determines the bit rate. From the bit rate and modulation characteristics, the bandwidth is determined. Then by constructing a gain - loss chart, system operation will be confirmed.

3.1.3 Conclusions

3.1.3.1 Antennas

Thin double walls are recommended for antenna construction because of light weight and invulnerability to meteoroid damage. Slotted waveguide antennas are used on spin-stabilized vehicles. The concept of using pencil beam antennas pointed along the spacecraft spin axis was eliminated because of the added complexity in

continually controlling the spin axis orientation. This problem is discussed further in Section 1. The bicone antenna is more vulnerable to meteoroid damage than the slotted waveguide, and it also imposes the problem of manufacturing a precise compensating lens. Furthermore, circular polarization is readily obtainable from the slotted waveguide, while the bicone is basically a vertically polarized antenna.

It is recommended that parabolic high-gain antennas with Cassegrainian feed be used in all three-axis stabilized vehicles to protect the feed point. Two horn-type feeds are felt to be necessary: one to provide a normal antenna pattern and one which is an "off-focal point" feed to spoil the beamwidth and thereby provide a broader beamwidth. This feedpoint is used so that a wide beamwidth is available for reacquisition, in the event that communication with the spacecraft is lost.

3.1.3.2 Transmitters

At this point in time, the transmitter is considered to be a traveling-wave tube. However, the developments in the other types of microwave tubes must be monitored. The transmitter consists of two amplifiers and two exciters, any combination of which can be selected to meet the reliability requirements of the spacecraft.

3.1.3.3 Modulation

PSK modulation with PN synchronization is recommended on the basis of the discussion contained in paragraph 3.1.2.3. While this system falls very short of providing the theoretical maximum efficiency, it is the more efficient of the two systems investigated. It is also compatible with the present DSIF equipment. The synthesis of a new modulation system was not attempted.

3.1.4 References

3.1-1. Jakes, W.C., Jr., "Bi-conical Horns," Antenna Engineering Handbook, New York: McGraw-Hill (1961), pages 10-13.

3.1-2. Southworth, C.G., "Arrays of Linear Elements," Antenna Engineering Handbook New York: McGraw-Hill (1961), pages 5-14.

3.1-3. Galindo, V., and Green, K., "A Near Isotropic Circularly Polarized Antenna for Space Vehicles," Transactions of the Professional and Technical Group on Antennas and Propagation of the IEEE, Vol. AP-13, No. 6 (November 1965), pages 872-878.

3.1-4. Silver, S., "Microwave Antenna and Design," Radiation Laboratory Series, Vol. 12. McGraw-Hill (1949), pages 10-11.

3.1-5. Blass, J., "Slot Antennas," Antenna Engineering Handbook. New York: McGraw-Hill (1961), pages 8-6.

3.1-6. Sill, D., Webb, J., and Fairley, D., "A Survey of RF Power Sources for Telemetry," Proc. Nat. Telemetering Conference, (May 1961).

3.1-7. Feldman, N., "Communication Satellite Output Devices," Microwave Journal, (December 1965).

3.1-8. Goldstein, R., and Kendall,W., "Low Data Rate Telemetry," Symposium on Unmanned Exploration of the Solar System (February 8-10, 1965).

3.1-9 Springett, J., Telemetry and Command Techniques for Planetary Spacecraft. Technical Report No. 32-495. Pasadena, California: Jet Propulsion Laboratories (January 15, 1965).

3.2 DATA MANAGEMENT

The data management subsystem of a Jupiter flyby spacecraft is used to perform the following two significant functions:

1. Provide an efficient interface to encode data from the scientific and engineering sensors and to transfer these data to the communications subsystem for subsequent transmission.

2. Provide an efficient method of detecting and decoding ground commands received by the communications subsystem and to transfer these commands to the appropriate instrument for execution.

The four elements of the data management subsystem shown in Figure 3.2-1 are the data automation element (DAE), the data encoder element (DEE), the data storage element (DSE), and the command detector and decoder element (CDDE).

DATA MANAGEMENT SUBSYSTEM

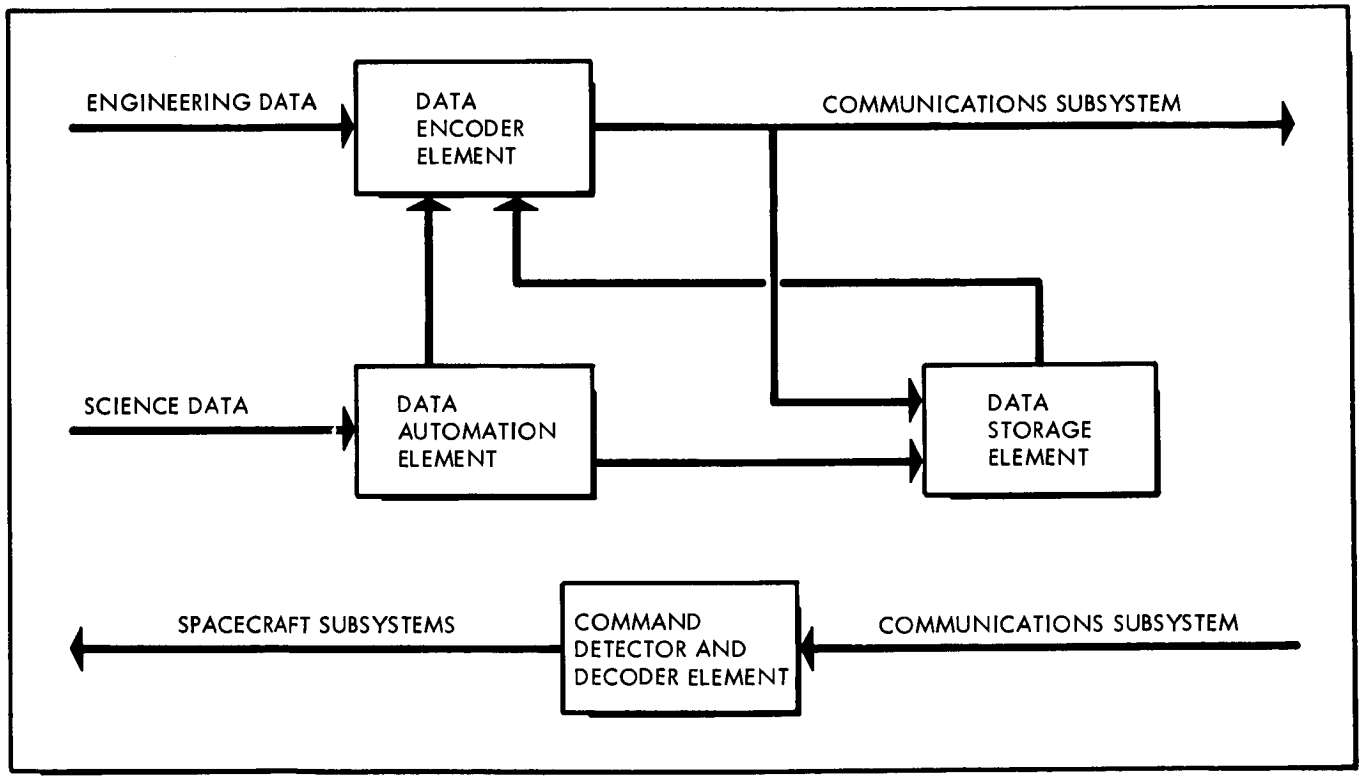


FIGURE 3.2-1

3.2.1 Functional Requirements

The elements contained in this subsystem are used to perform various functional requirements. These requirements for each element are listed in the following paragraphs.

The data automation element is used to perform the following functions:

1. To control and synchronize the scientific instruments within the DAE timing and format structure so that the instrument internal sequencing is known and to send commands to the instruments as required

2. Provide the necessary sampling rates, both simultaneous and variously sequential, to ensure meaningful scientific data

3. Perform the necessary conversions and encoding of the several forms of scientific data

4. Provide data compression for the scientific data and place them in a suitable format

5. Buffer the science data which occur at different and sporadic rates and send them to the DEE and the DSE at the desired rates and in the desired modes

6. Issue and receive from other subsystems aboard the spacecraft commands which pertain to the operation of the science subsystem.

The data encoder element is used to perform the following functions:

1. Control and synchronize the engineering measurement sensors within the DEE timing and format structure so that the measurement internal sequencing is known

2. Provide the necessary sampling rates to ensure meaningful engineering data

3. Perform the necessary conditioning, converting, and encoding of the engineering analog signals and event pulses

4. Provide data compression for the engineering data

5. Combine and put into format the engineering data with serial binary data inputs from the DAE

6. Transfer serial binary data from the DSE to the communications subsystem

7. Modulo 2 add the binary coded data to the synchronization code

8. Provide the various command-selectable data transfer rates to the communications subsystem in order to facilitate the optimum use of the available communications capability throughout the mission

9. Provide several command-selectable data modes to permit processing flexibility.

The data storage element is used to perform the following functions:

1. Provide the required data storage capacity to record scientific data from the DAE and engineering data from the DEE

2. Provide the capability to record data at the prescribed rate(s)

3. Provide the capability to play back data at the prescribed rate(s).

The command detector and decoder element is used to perform the following functions:

1. Detect commands in the form of binary PSK modulation on a sine wave subcarrier output of the spacecraft communications subsystem demodulator

2. Decode the digital commands, route discrete commands (DC) to spacecraft subsystems, and furnish quantitative commands (QC) to the CC&S.

3.2.2 Possible Concepts

Considering the types of data to be processed, the quantity of these data, and the available transmission data rates for each mission, several concepts must be investigated in order to provide the optimum data management subsystem operation. One concept is to use the Mariner IV equipment and techniques to the greatest extent possible and to make only those modifications which are required by the differing mission objectives. This concept will satisfy mission requirements with the least equipment development cost, but will not provide any important improvement in capability. Another concept is to undertake a large scale program to devise entirely new methods and designs for data management. The development cost will be high, but the possibility of lowering other costs and of accomplishing significantly more mission objectives is increased.

A third concept is a combination of the first two. Maximum use is made of Mariner designs, but at the same time, some development is undertaken. This development is concentrated in those areas which appear to offer the most opportunity for increasing the data management subsystem capability. In this way, capability can be improved without an unreasonably high development cost.

3.2.3 Analyses

The trade-off considerations are reliability, flexibility, efficiency, size, weight, and power. Because of the duration of a Jupiter flyby mission, reliability is considered the most important consideration. Flexibility and reliability can be achieved together in the case of interchangeable components which can replace each other in case of a malfunction. It has been necessary to sacrifice efficiency in order to obtain greater reliability and flexibility, but the significance of efficiency is still recognized. Weight, size, and power, though still important, are becoming less critical. Larger boosters and microminiaturization now permit greater latitude in the selection of equipment.

In order to select the most efficient data management subsystem for various Jupiter missions, several analyses were performed. A comparison was made between the engineering and science data-gathering requirements for the Jupiter flyby missions and the Mariner IV mission in order to assess the compatibility of the telemetry requirements for the two missions. Another comparison between the data-gathering rates and the available transmission rates during the various mission phases was made in order to determine the applicability of data compression and data storage. As expected, this analysis indicated that the maximum data-gathering rates occur at Jupiter encounter, when the allowable transmission rates are at a minimum. It was also found that the data-gathering rate is considerably more than the transmission rate at this point for all missions considered.

3.2.3.1 Data Compression

Data compression techniques for the various types of data were investigated as a mean of increasing the quantity of data which can be transmitted in real time. A literature survey indicates that satisfactory data compression techniques are available for both the engineering and the scientific measurements.

The fan method, developed and patented by Radiation, Incorporated of Melbourne, Florida, seems to be particularly applicable to engineering data (Reference 3.2-1). Figure 3.2-2 illustrates the logical operations performed by this technique. Basically, the fan method is used

FAN DATA COMPRESSION TECHNIQUE

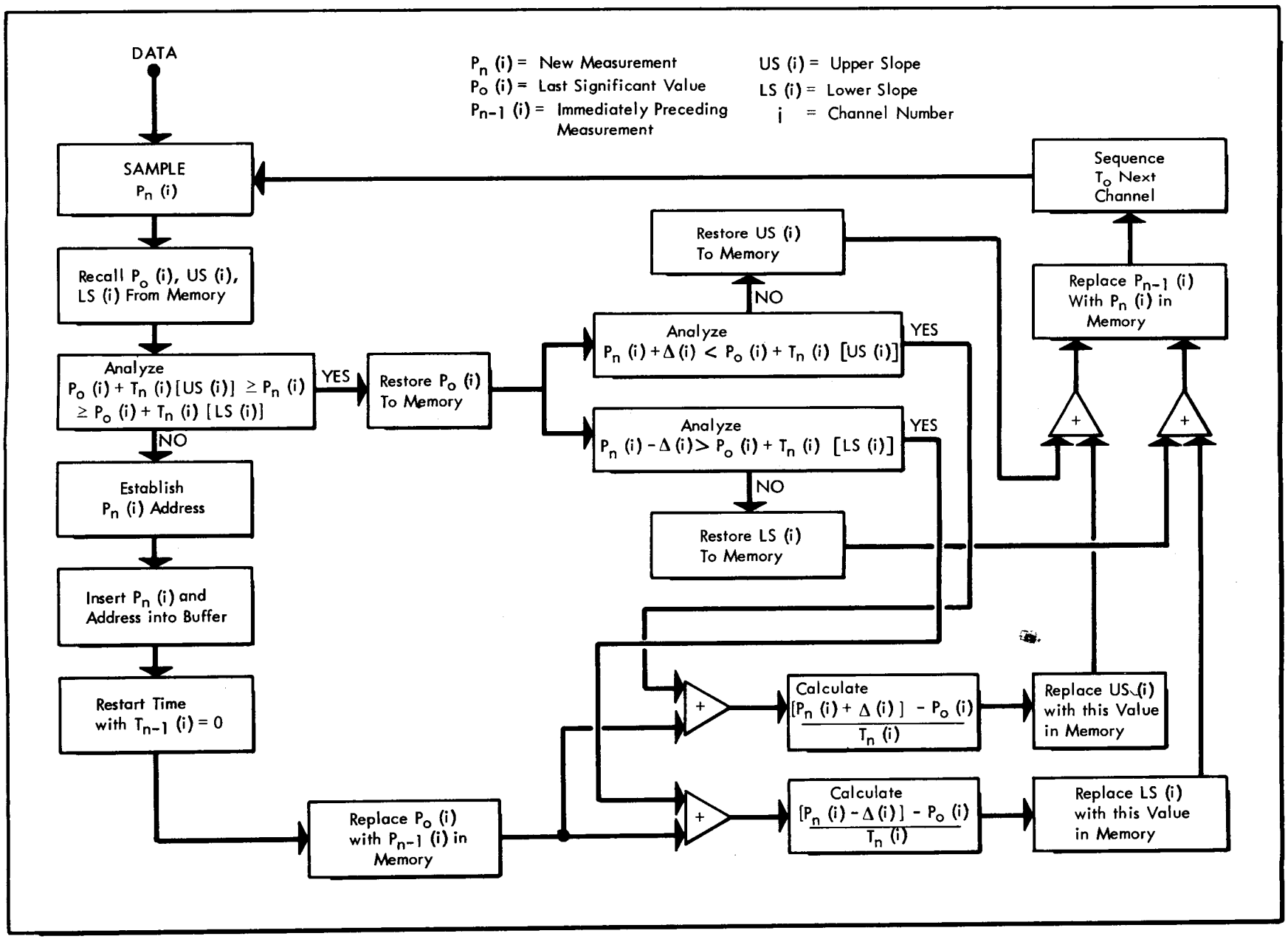


FIGURE 3.2-2

to project an angle from the last significant value and to determine if the current value falls within this angle. If the current value is located within these limits, the preceding point is discarded and the current value is stored until the following point has been tested. If the current value is located outside these bounds, the preceding value becomes the significant value, and it is transmitted. A compression ratio of approximately 150-to-1 is anticipated for the engineering data being considered.

Another much less complicated data compression scheme is the zero order interpolator (References 3.2-2 and 3.2-3). The logical operations performed by this technique are shown in Figure 3.2-3. In the zero order interpolator, the current value is compared with the last significant value. If the difference between the two samples is less than the preset upper and lower tolerances, the current sample is considered insignificant and is dropped. If this difference exceeds the tolerances, the current sample becomes the significant value, and it is transmitted. The implementation of this technique is simpler than the fan method, but a compression ratio of only 30-to-1 appears possible with engineering data.

A data compression technique which seems to be applicable to particle counter data is the quantile method (References 3.2-4, 3.2-5, and 3.2-6). Figure 3.2-4 shows the required equipment and the operations performed by this method of compression. A counter is sampled periodically and reset to zero so that the number of counts accumulated since the last sampling time can be determined. A one is placed in the storage register corresponding to this count. At the end of the total count interval, the storage registers are added sequentially into the accumulator. The cumulative sum after each addition is compared with the value in the comparator currently being used. As soon as the sum equals or exceeds this comparator value, the comparator value is transferred to its corresponding quantile register and the address of the current storage register and the comparison remainder are stored. After reseting the accumulator to zero, the addition of the storage registers is continued with the sum now being compared with next comparator value. This process continues until all of the storage registers have been summed. The compressed data is then transferred and a new total count interval is initiated by clearing the storage registers and accumulator and restarting with time equal to zero. A compression ratio of approximately 100-to-1 is expected for the data range considered.

Several techniques exist for compressing television picture data. Among these techniques are the fan, stop-scan edge detection, block coding, self-adaptive prediction, high information delta modulation, improved gray scale, course-fine, and pseudo-random noise methods

ZERO ORDER INTERPOLATOR DATA COMPRESSION TECHNIQUE

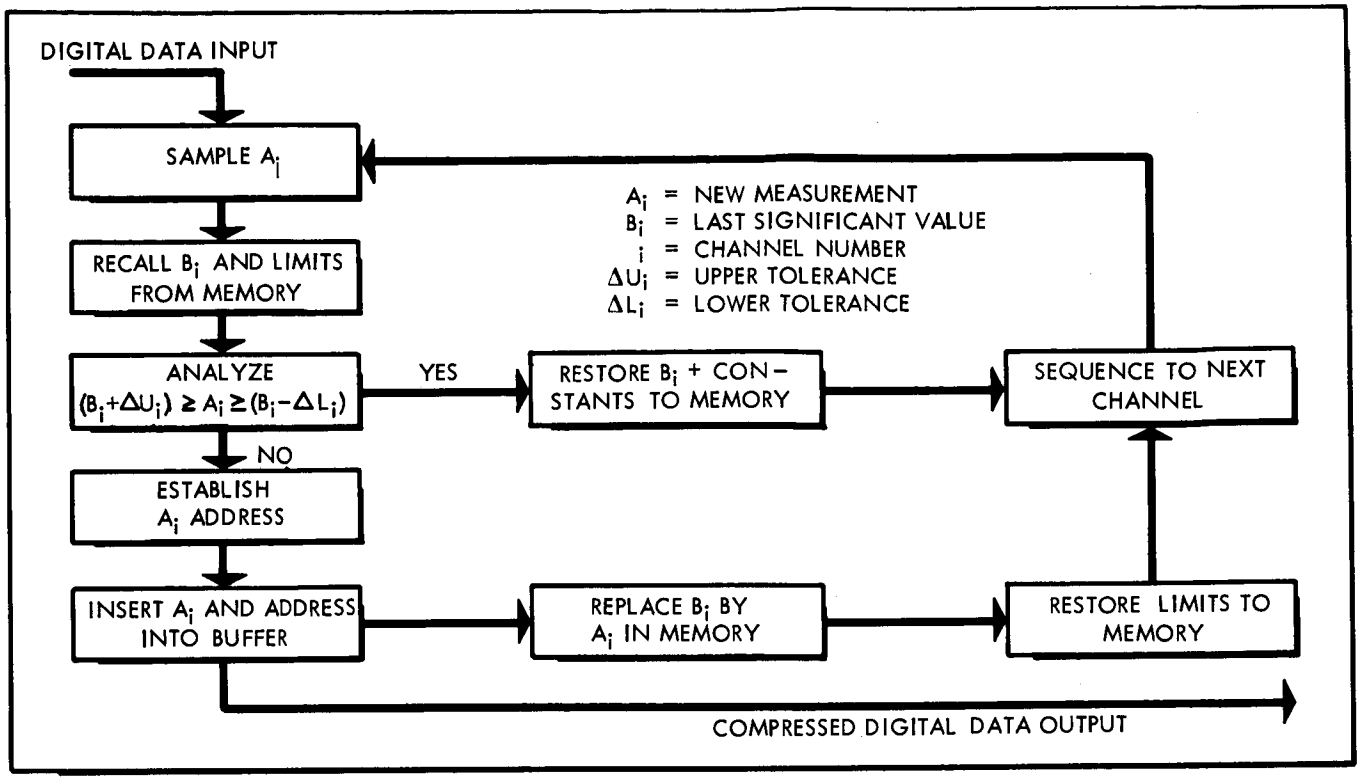


FIGURE 3.2-3

QUANTILE DATA COMPRESSION TECHNIQUE

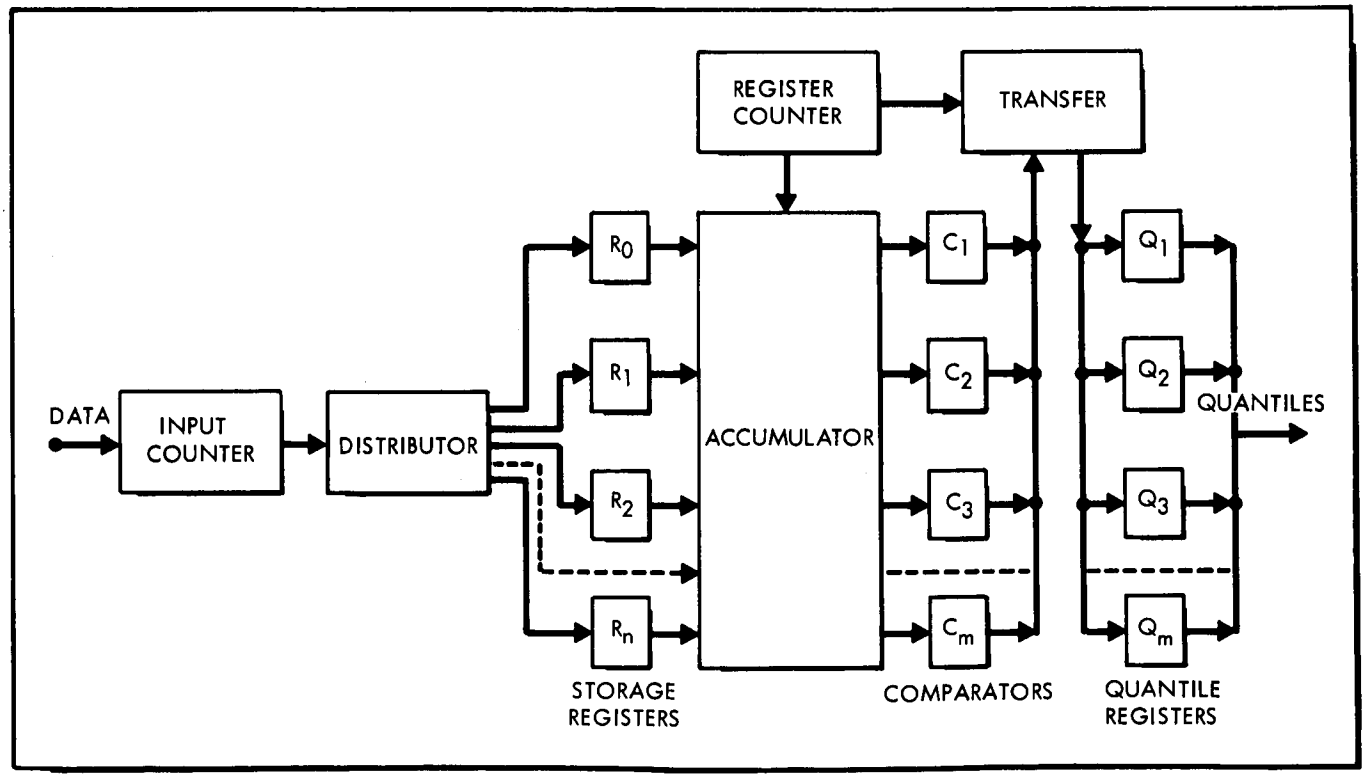


FIGURE 3.2-4

(References 3.2-7 through 3.2-13). The three techniques which seem to show the most promise are the fan method, the stop-scan edge detector, and the block coding.

The stop-scan edge detection technique shown in Figure 3.2-5 separates the television signal into a low frequency signal and a high frequency signal. The low frequency signal is used to perform a 2-bit delta modulation transformation and the high frequency signal is used to detect the location of picture edges (sudden changes in intensity) and to identify their intensity level. It is anticipated that a compression ratio of 5-to-1 can be obtained from both the fan method and the stop-scan edge detector for television pictures.

Block coding determines the correlation between the elements of a television picture and codes a block of elements according to its probability of occurrence. A method of achieving comma-free, variable-length code words has been developed (Reference 3.2-9). Compression ratios for this technique are highly dependent on the data, and the results of specialized tests on pictures applicable to this mission are not available at this time. However, this method is currently being investigated.

3.2.3.2 Data Storage

Another factor to be considered is the period of time that Jupiter will occlude the spacecraft as seen from Earth and prohibit communications. This consideration, the possibility of strong radio interference from the radiation belts of Jupiter, and the lack of sufficient data transmission rates for transmitting real time data during various mission phases indicate a need for data storage.

The following data storage devices are available: magnetic cores, magnetic drums, magnetic discs, and magnetic tape recorders. Of these four, only cores and tape recorders have been shown to be practical for a mission of the type being considered. Magnetic core buffers can be used to (1) accept small quantities of data at varying input rates, (2) temporarily store this data, and (3) later furnish this data to other equipment at a constant rate. Tape recorders on the Mariner IV and Tiros missions have been proved to be reliable and efficient devices for the storage of large quantities of data for indefinite time periods.

In the case of those missions which provide significantly greater transmission rates than the compressed data-gathering rates, the implementation of intermittent communications is considered feasible from the standpoint of data management. This is the case during the early portion of most missions, and during these non-critical periods tracking

STOP-SCAN EDGE DETECTOR DATA COMPRESSION TECHNIQUE

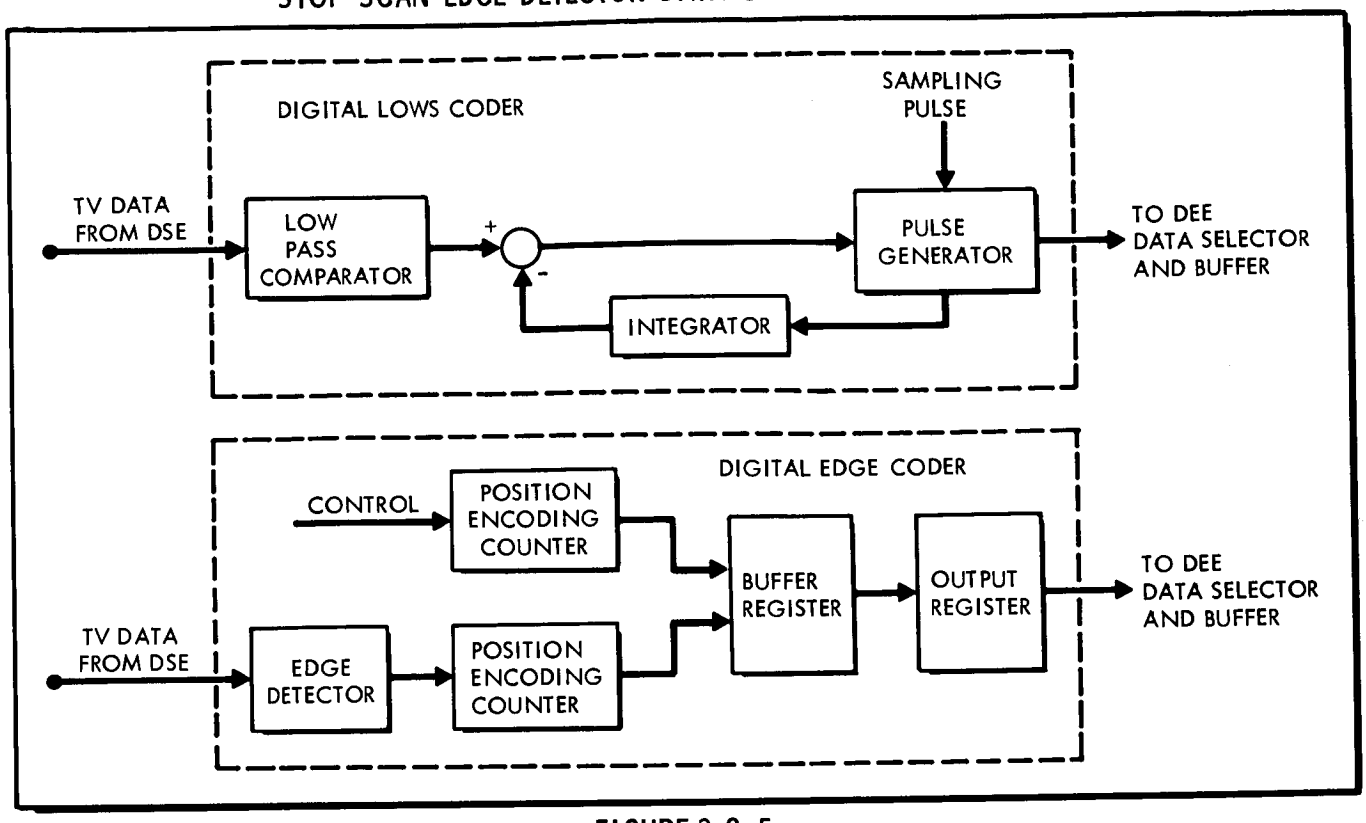


FIGURE 3.2-5

stations and the control center can be released to perform other tasks. Intermittent communications are enhanced further by the long delay between the spacecraft transmission of telemetry and Earth reception of the data. This delay, more than twenty minutes at 2.5 AU, indicates that real-time telemetry has little value in correcting immediate spacecraft problems. Therefore, onboard diagnostic routines are required to handle these problems. Telemetry data can be stored throughout the mission and played back periodically without affecting mission success.

3.2.3.3 Synchronization

A single channel synchronization data link is considered appropriate for all the design concepts being considered. Data is combined with the sync code in the DEE as discussed below.

A 63-bit pseudonoise code, PN, used to supply both bit and word synchronization, is continuously produced by a pseudonoise generator. This code is modulo 2 added to the clock frequency, 2 f_s. This modulo-2 sum, PN + 2 f_s, is then modulo 2 added to the data, D, from the data selector and buffer, and this combination is transmitted. So that data can be transmitted during prelaunch checkout and during boost, additional capability has been furnished to supply data to GSE and to the booster telemetry link.

The demodulator required on the ground to receive this telemetry data is shown in Figure 3.2-6. The following logical operations are performed by this demodulator to retrieve the data:

$$\pm \text{PN} \oplus 2f_s \oplus \text{PN}^* = \pm \text{PN} \oplus \text{PN} \oplus f_s \oplus 2f_s$$

$$\pm f_s \angle 90^\circ \oplus f_s \angle 90^\circ = \text{D}$$

Synchronization is maintained by the following logical operations performed by the phase-locked loop:

$$\pm \text{PN} \oplus 2f_s \oplus \text{PN}^* = \pm f_s \angle 90^\circ$$

$$\pm \text{PN} \oplus 2f_s \oplus \text{PN} = \pm 2f_s$$

$$\pm 2f_s \angle 90^\circ \oplus \pm 2f_s = f_s$$

$$2f_s \div 2 = f_s$$

$$\text{PN} + f_s = \text{PN}^*$$

$$2f_s \oplus f_s = f_s \angle 90^\circ$$

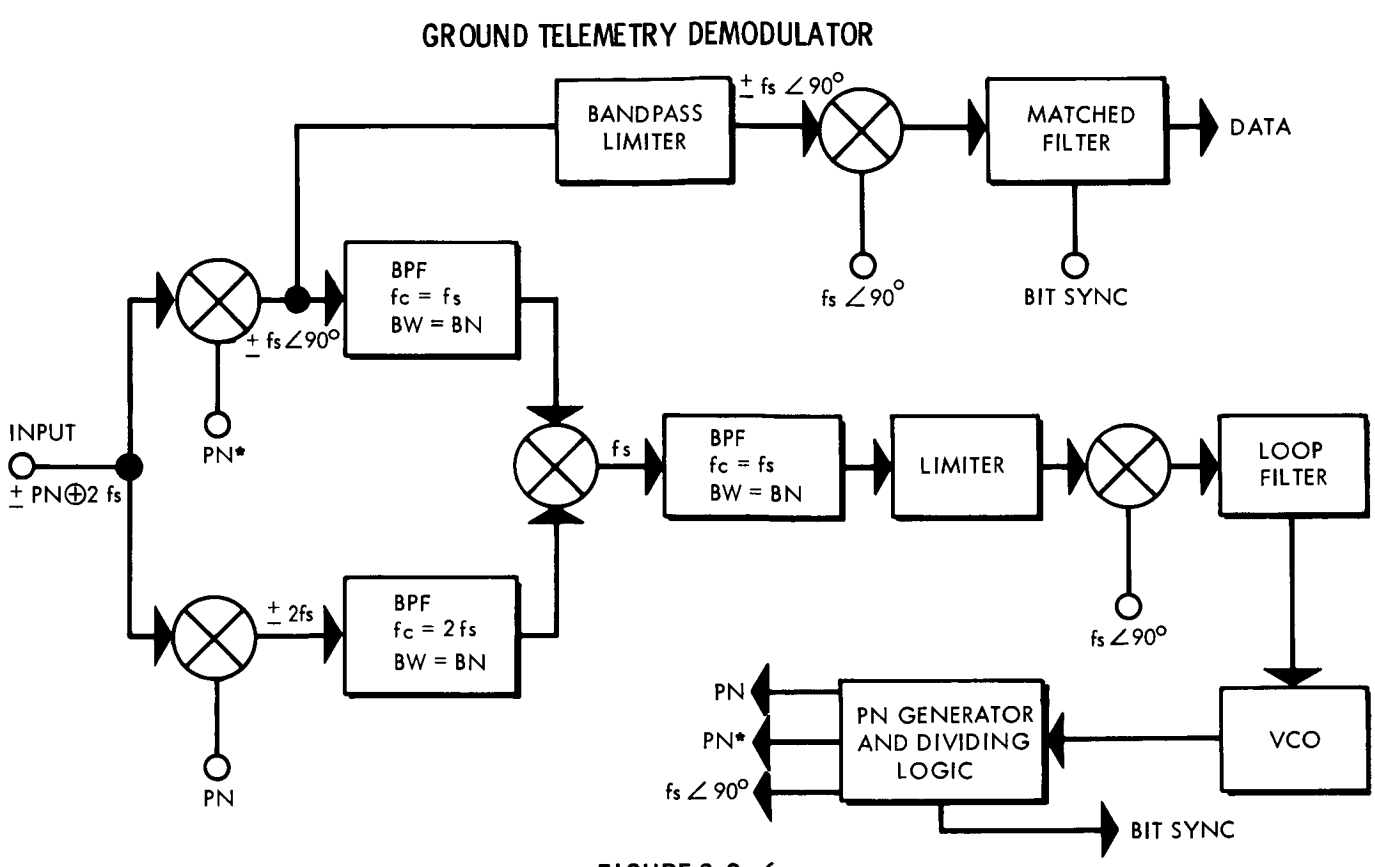


FIGURE 3.2-6

A 7-bit analog-to-digital conversion is provided for engineering analog data which yields one percent accuracy. The bit rates which have been supplied are related to the clock frequency $2f_s$ by the following formula:

$$\text{Bit rate} = \frac{2f_s}{9}$$

where 9 is the number of PN bits being generated per data word bit. This relationship permits bit rates to be changed by a simple division by two of the high accuracy frequency sources supplied by the power subsystem (References 3.2-14).

3.2.3.4 Command

The CDDE command word format for all Jupiter flyby spacecraft concepts is identical to that used for Mariner IV. The 26-bit command word format is given in Figure 3.2-7 (Reference 3.2-15.)

3.2.3.5 Reliability

Reliability is enhanced through the use of flight-tested Mariner designs and by the incorporation of micro-integrated circuitry whenever

MARINER C COMMAND WORD FORMAT

COMMAND BIT NO.	1	2	3	4	5	6	7	8	9	10	11	12	13	14	15	16	17	18	19	20	21	22	23	24	25	26
COMMAND BIT IDENTIFICATION	COM-MAND DECODER START			COMMAND ADDRESS						ADDRESS PARITY See Note 1		BITS 12–26 HAVE NO SIGNIFICANCE IN DC'S. IN QC'S THEY FORM PART OF THE CC&S COMMAND. REFER TO QUANTITATIVE COMMAND FORMAT														
COMMAND BIT VALUE	1	1	0	VARIABLE								ZERO FOR DC'S; VARIABLE FOR QC'S														

QUANTITATIVE COMMAND (QC) FORMAT

COMMAND BIT NO.		1	2	3	4	5	6	7	8	9	10	11	12	13	14	15	16	17	18	19	20	21	22	23	24	25	26
CC&S COMMAND BIT NO.										1	2	3	4	5	6	7	8	9	10	11	12	13	14	15	16	17	18
CC&S COMMAND BIT IDENTIFICATION										CC&S ADDRESS See Note 2			Register Selector		See Note 3 ODD PARITY	TIME VALUE See Note 5											See Note 4 POLARITY
QC COMMAND BIT VALUES	PITCH TURN	1	1	0	0	1	1	0	0	0	1	1	1	0		VARIABLE											
	ROLL TURN	1	1	0	0	1	1	0	0	0	0	0	0	1		VARIABLE											
	MOTOR BURN	1	1	0	0	1	1	0	0	0	1	0	1	1		VARIABLE											

1. COMMAND BIT NOS. 10 AND 11 ARE ADJUSTED TO ENSURE AGAINST SINGLE BIT ERRORS CAUSING AN INCORRECT COMMAND WORD OUTPUT.
2. COMMAND BIT NOS. 9–11 (CC&S COMMAND BIT NOS. 1–3) ARE NOT USED QUANTITATIVELY BY CC&S BUT ARE USED TO REMAIN COMPATIBLE WITH PREVIOUSLY DESIGNED HARDWARE (*MARINER R*)
3. COMMAND BIT NO. 14 (CC&S COMMAND BIT NO. 6) IS ADJUSTED IN QC'S TO GIVE AN ODD NUMBER OF *ONE* BITS IN COMMAND BIT NOS. 9–26 (CC&S BIT NOS. 1–18).
4. COMMAND BIT NO. 26 (CC&S COMMAND BIT NO. 18) MUST BE A *ONE* TO PRODUCE A CW (POSITIVE) SPACECRAFT ROTATION ABOUT THE SPECIFIED SPACECRAFT AXIS. A ZERO IN THIS BIT POSITION WILL RESULT IN A CCW (NEGATIVE) SPACECRAFT ROTATION ABOUT THE SPECIFIED SPACECRAFT AXIS. POLARITY BIT FOR MOTOR BURN COMMAND IS ALWAYS *ONE*.
5. COMMAND BIT NOS. 15–25 (CC&S COMMAND BIT NOS. 7–17) ARE A PSEUDO-BINARY CODE REPRESENTATION OF THE TURN OR MOTOR BURN DURATION.

FIGURE 3.2-7

possible. Redundancy is used in the more critical areas such as the analog-to-digital converters, PN generators, and data compressors. The capability to bypass data compression in the event of a malfunction is furnished to further increase the probability of reliable data handling. Whenever sets of redundant equipment are placed in series, separate switches initiated by separate DC's are provided to switch from one piece of equipment in a set to another in that same set. Further reliability analyses will be conducted during the last half of the study.

3.2.4 Results

The comparison of telemetry requirements between the Jupiter and Mariner spacecraft indicates that in most instances the required measurements are either identical or very similar. The data-gathering quantities and rates of Jupiter missions indicate a definite need to provide for bulk data storage and for the implementation of data compression techniques.

The storage of data, particularly during the critical phases of a mission (such as the encounter phase), increases the probability of obtaining reliable information. The stored data can be used, also, to fill in data gaps caused by interference or by occlusion and to double check questionable data points received in real time. Whenever

the rate of data acquisition exceeds the transmission rate, data storage can be used as a technique to provide a later replay of the data at a rate compatible with communications capability.

Magnetic tape recorders have proved to be the most efficient method of providing bulk storage of large quantities of data. In order to reduce power, weight, and size requirements, use of a television camera with a scan-converter tube is recommended. Through the use of a scan-converter tube, the data rate can be reduced to the extent that an audio recorder can be used to store television data instead of a larger, heavier video tape recorder which requires considerably more power. Intermittent communications are recommended as a good method of reducing mission support requirements.

Data compression is used to provide a method of obtaining the most efficient use of communications capability and will result in a reduction in ground processing time and cost. Because of the low transmission bit rates available on deep space probes, a choice of two undesirable alternatives usually develops: either data must be sampled at less than the optimum rate, or data must be stored and replayed later at a reduced bit rate. The data replay causes a loss of real time data during the playback interval. To overcome the undesirable effects of the alternative choices, data compression can be used to reduce the difference between the desired and the available transmission bit rates. The advantage of greatly increased communications efficiency provided by telemetry data compression is considered much more significant than its one major disadvantage: the fact that the effect of an error in a received data point is amplified by the compression ratio. To reduce the effects of this undesirable feature, uncompressed data blocks can be transmitted at specified intervals or whenever data is obviously incorrect.

It was determined that considerable micro-integrated circuitry can be incorporated into the data management subsystem; as a result, it is anticipated that reliability, flexibility, and efficiency can be greatly improved and that power, weight, and size requirements can be significantly reduced from current equipments without large scale development.

3.2.5 Conclusions

Because of the external importance placed on reliability, it is recommended that the third concept discussed in subsection 3.2.2 be implemented for all Jupiter spacecraft except the most advanced one. The probability of a successful mission will be greatly enhanced by the use of Mariner IV technology which has been thoroughly flight

tested on a successful mission. Concentrated development of the Mariner IV technology is then recommended in three areas; at the present time, there are indications that these three areas have the most potential for increasing the value of a mission: (1) the maximum incorporation of micro-integrated circuitry, (2) data storage improvements, and (3) the implementation of data compression techniques.

3.2.6 References

3.2-1 Bryan, J. A. and Stumpe, J. W., The Data Management Analyzer, A Laboratory Tool for Data Compression Analysis, 1965 PGAES Symposium, Miami Beach, Florida, November 2-4, 1965, pp. 11-A1 through 11-A13.

3.2-2 Morrison, W. L., Hogan, W. P., and Pentz, R. M., Application of Data Compression to Flight Data Processing, Western Electronic Show and Convention, Los Angeles, California, August 25-28, 1964, Section 19.3.

3.2-3 Medlin, J. E., Sampled Data Prediction for Telemetry Bandwidth Compression, Western Electronics Show and Convention, Los Angeles, California, August 25-28, 1964, Section 19.1.

3.2-4 JPL Technical Report No. 32-510, Jet Propulsion Laboratory, Pasadena, California, October 1, 1963.

3.2-5 JPL Technical Report No. 32-718, Jet Propulsion Laboratory, Pasadena, California, June 1, 1965

3.2-6 JPL Technical Report No. 32-772, Jet Propulsion Laboratory, Pasadena, California, December 1, 1965.

3.2-7 Pratt, W. K., Stop-Scan Edge Detection System for Interplanetary Television Transmission, 1962 PGSET Symposium, Miami Beach, Florida, October 2-4, 1962, Section 4.3.

3.2-8 Marggraff, W. A., and Klawa, R. F., Studies Related to Multi-Spectral Correlation: Error and Application Analyses of Satellite Television Camera Systems, General Dynamics/Convair, San Diego, California, December 15, 1965, pp. 20-31.

3.2-9 Fano, R. M., Transmission of Information, The MIT Press and John Wiley & Sons, Inc., New York, 1961.

3.2-10 Weber, D.R., and Wynhoff, F. J., The Concept of Self-Adaptive Data Compression, 1962 PGSET Symposium, Miami Beach, Florida, October 2-4, 1962, Section 4.1

3.2-11 Winkler, M. R., Pictorial Transmission with HIDM, 1965 IEEE International Convention, New York, New York, March 22-26, 1965, part 1, pp. 285-291.

3.2-12 Bisignani, W. T., Richards, G.P., and Whelan, J. W., The Improved Gray Scale and the Coarse-Fine PCM Systems, Two New Digital TV Bandwidth Reduction Techniques, 1965 IEEE International Convention, New York, New York, March 22-26, 1965, part 4, pp. 55-73.

3.2-13 Roberts, L. G., Picture Coding Using Pseudo-Random Noise, IRE Transactions on Information Theory, New York, New York, February, 1962, pp. 145-154.

3.2-14 JPL Technical Report No. 32-495, Jet Propulsion Laboratory, Pasadena, California, January 15, 1965, pp. 6-30.

3.2-15 JPL Space Programs Summary No. 37-29, Vol. II, Jet Propulsion Laboratory, Pasadena, California, September 30, 1964, pp. 37-42.

3.3 SPACECRAFT CONTROL

The spacecraft functions of interest in this section are (1) state estimation, (2) attitude determination, (3) prediction of terminal errors and steering, and (4) timing and sequencing of other spacecraft operations. These functions and the equipment required to perform them are referred to as "spacecraft control." Generally speaking, the implementation of control functions can be divided up many ways between systems on board the spacecraft and Earth-based tracking and data-processing facilities. It is possible to implement the entire control operation in a self-contained system on board the vehicle, or it is possible to perform a large part of the control from an Earth-based facility. Certain of the control functions, for example, the attitude sensing and vehicle maneuvering associated with guidance corrections or steering operations, are not suitable for any but "on board" control.

The choice of a control system for Jupiter flyby missions must be based on a careful examination of (1) operation and performance requirements, (2) the complexity and cost attendant to particular system concepts, and (3) the possibilities of using previously developed concepts such as those from the Mariner project. Using these guidelines, a single basic control concept has been worked out for the Jupiter flyby vehicles. This concept is characterized by several pertinent features. A group of optical sensors on board the vehicle are used to provide attitude reference. Earth-based facilities are used to determine the trajectory and to compute the required guidance corrections. A central computer and sequencer (CC&S) on the spacecraft provides master timing for all spacecraft systems and "translates" guidance commands into vehicle attitude changes and control signals to the midcourse propulsion system. The CC&S also provides pointing control for either the spacecraft itself or a high gain communications antenna.

Variations in the detailed design of the spacecraft control subsystem are present in each of the spacecraft design concepts. Of particular interest are the control system variations which provide self-contained, terminal navigation and guidance. This mode of operation yields the best terminal accuracy but at a significant cost in terms of increased system complexity. Such a mode of operation is possibly appropriate for a maximum capability spacecraft.

Another variation in possible design concepts arises from the requirement for accurate orientation of a communications antenna. One concept is to mechanically steer the antenna while keeping the orientation of the spacecraft axes fixed in a particular inertial frame. The alternative is to fix the antenna to the spacecraft and periodically change the orientation of the spacecraft. In either

case, the spacecraft control system must furnish angular control either to the antenna positioning device or the primary reference sensors. The latter case affects the spacecraft control system in more ways than the former, but the latter is considered less complex from the standpoint of the overall spacecraft.

3.3.1 Spacecraft Control Operations

The functions of the spacecraft control system vary among the several design concepts. In order to develop these concepts, the full list of control operations will be discussed individually with explanations to how these functions are traditionally divided between ground-based and on-board systems. These functions are grouped into four categories: (1) attitude determination, (2) navigation, (3) guidance, and (4) timing and sequencing for other vehicle systems.

3.3.1.1 Attitude Determination

Expressed in the most basic terms, attitude determination is the process which permits the orientation of the vehicle body axes to be known in relation to or as a function of unit vectors which define some primary coordinate system. This primary coordinate system may be either the heliocentric inertial frame defined by the eclipic and vernal equinox, some local vertical planetocentric frame, or some other convenient frame. The choice of a primary frame is based on the set of observables which will be used to establish the relationship between the primary and the vehicle axes. During the cruise phase of Jupiter missions, the trajectory is essentially heliocentric, and the convenient observables are the sun, stars, and perhaps planets; thus, the primary frame is the heliocentric inertial one because the observables are known in that system. When the vehicle is in the near field of a planet, and its motion is essentially planetocentric, a planet-centered primary coordinate system rotating with the vehicle offers many attractive features.

In the practical accomplishment of the attitude determination functions, it is not necessary that the transformation matrix relating the vehicle axes to the primary system be determined explicitly on board the spacecraft. The spacecraft can hold certain angular relationships with respect to the observables. Then, using the spacecraft position, the attitude transformation is explicitly determined at the Earth-based facility. Naturally, if the control philosophy calls for a self-contained operation, the entire attitude determination process can be mechanized in an on-board computer.

Once the attitude is determined, the vehicle can be accurately oriented for guidance maneuvers and other requirements and pointing angles for antennas and other sensors can be determined.

3.3.1.2 Navigation

The control functions which come under the heading "navigation" have to do with obtaining the best estimate of the spacecraft trajectory. This usually means successive estimates of position and velocity. Over a period of time, this successive state estimation permits a definitive trajectory to be determined which is the basis of subsequent guidance maneuvers. Navigation, as used herein, implies only state estimation and must be distinguished from the broader usage of some authors in which navigation includes guidance or steering maneuvers as well as state estimation.

The navigation function can be accomplished from the Earth by the use of optical or radar tracking, or it can be done on board the spacecraft by the use of some type of angular measurements. In either case, the actual navigation process probably involves the use of statistical filter methods. In this technique, navigational measurements are compared to their computed values corresponding to the expected state, and these residuals are optimally weighted to derive an estimated state. Details of the navigation processes are contained in subsection 3.4.

3.3.1.3 Guidance

As stated previously, the objective of the navigation function is to determine as accurately as possible the spacecraft position and velocity, either for comparison with some design point value or to predict the state at some future time. In both cases, the information gained is used to compute a guidance correction. The guidance function includes those operations performed on the estimated vehicle position and velocity which lead to the determination of a required maneuver as well as those operations concerned with the control of the correction maneuver itself.

The vernier correction, typically performed sometime during the first 10 days of the mission, is designed to correct for velocity errors in the injection maneuver. Thus, the estimated velocity is compared to the nominal or design point velocity at this time, and the vector difference becomes the required correction. Using the spacecraft attitude, this required change in velocity is resolved into a spacecraft attitude maneuver and a required number of accelerometer pulses.

Somewhat different considerations enter into the synthesis of a terminal guidance maneuver. Computation of the correction depends on what component of the terminal error is to be corrected. Generally, this maneuver is designed to null some part of the terminal position error. The terminal error may consist of any or all of the following:

(1) position components, (2) velocity components, or (3) time of arrival. A single impulsive velocity change can only correct three components of the total error vector. Thus, if complete, three dimensional position or velocity terminal errors are to be corrected, a midcourse velocity change is required for each. In practive, the terminal position error is expressed as a two dimensional vector in a plane perpendicular to the approach hyperbola. This two component position error alone, or the position error and the error in time of arrival, can be nulled with a single steering maneuver. Synthesis of the terminal correction is discussed further in subsection 3.4.

Having determined the required maneuver, the control system must implement the indicated velocity change. The vector velocity change expressed in the primary coordinate frame must be related to the vehicle body axes so that the vehicle can be aligned with this required velocity vector. The magnitude of the correction is monitored by an accelerometer. During the motor burn period, feedback from a system of gyros provides control to vanes in the rocket exhaust to maintain proper alignment.

3.3.1.4 Master Timing and Sequencing

In addition to all of the control operations identified or implied in the above discussions, certain timing and sequencing functions are also the responsibility of the spacecraft control system. A master frequency source in the control system provides the primary timing signal. Dividing circuits and other logic circuits are then used to generate signals for event sequencing throughout the spacecraft.

3.3.2 Design of the Central Computer and Sequencer

Control of the spacecraft systems is accomplished both automatically by spacecraft control and remotely via a radio command link. The central computer and sequencer (CC&S) furnishes the event signals required for automatic control and serves as a processor and sequencer for command data. Each of the CC&S concepts (Figure 3.3-1) considered are very nearly identical with the exception of a design concept which employs a computer in the more familiar sense which is used for on-board navigation, guidance, and sensor control. This concept is considered applicable only to very sophisticated spacecraft. All major events in less sophisticated spacecraft are controlled by the sequence timer. These events are, for example, initial attitude acquisition, high gain antenna turn on, and Jupiter encounter start.

In the less complex CC&S, command data and sync signals from the communication subsystem flow through the CC&S data encoder into the command data registers and sign flip flops. An address matrix and encoder logic direct the serial data into the proper register or sign

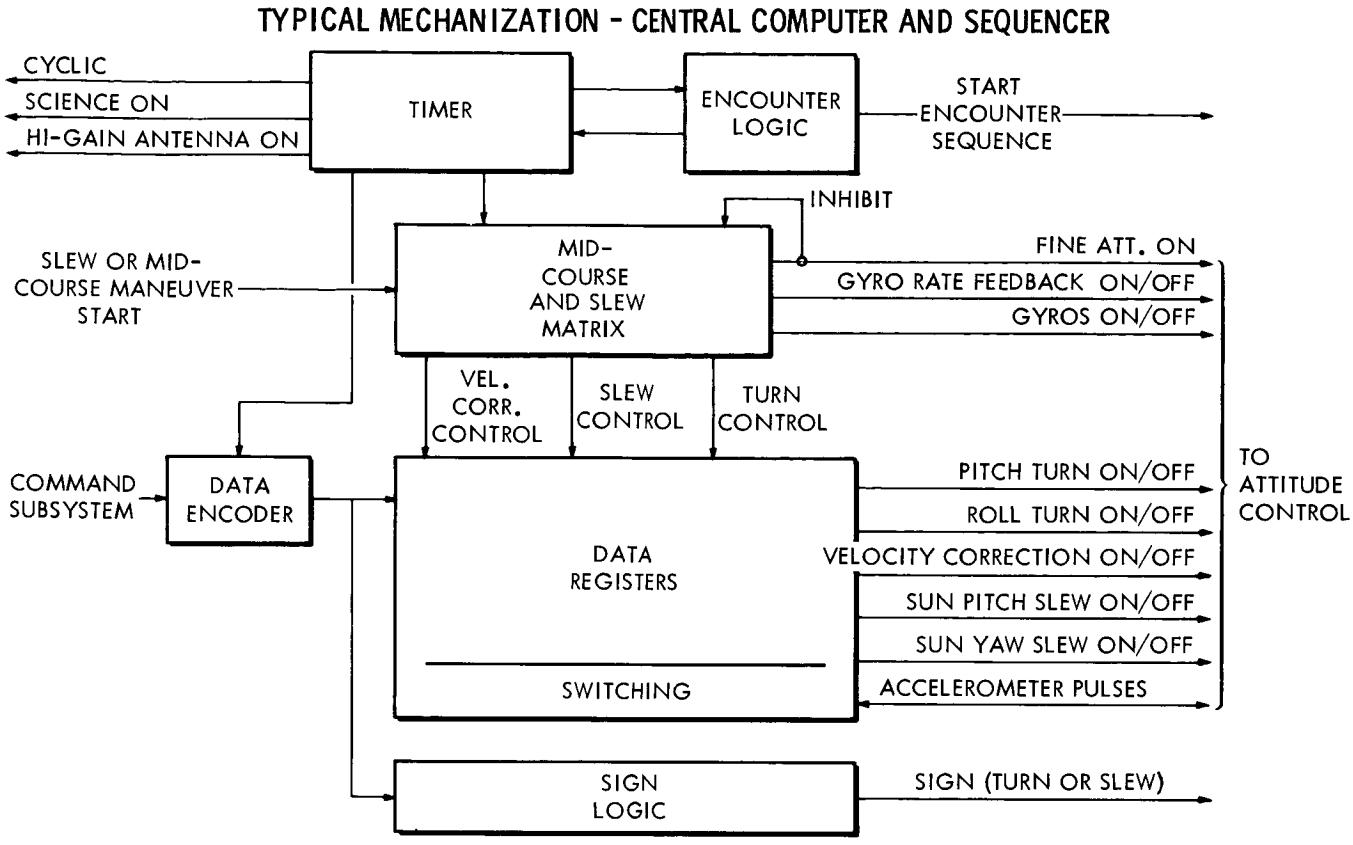


FIGURE 3.3-1

flip flop. When the correct data has all been stored, the maneuver (or sensor slew) sequence may begin. When the communication subsystem sends a maneuver start pulse, the gyro power is turned on in the attitude control subsystem by the CC&S and the fine attitude acquisition sequence begins. After a time interval, the roll turn sequence occurs, in which the one pulse per second signal drives the register as a counter as the spacecraft is turned in roll at a uniform rate. An overflow pulse from the roll turn register switches off the roll turn. The pitch turn and motor burn (or sun pitch slew and sun yaw slew) registers are pulsed in sequence in a similar manner. The fine limit cycle mode of attitude control is broken at the start of the roll maneuver. The coarse limit cycle mode of control is again used after the velocity correction. Since maneuver and sun slew sequences may not be performed at the same time, the undesired sequence can be suppressed by transmitting zero values for the parameters of that sequence (for example, to change spacecraft orientation, the command data is zeroed for the roll and pitch turns and motor burn, but the slew registers receive data). The gyros are then turned off if cruise attitude has been acquired.

The CC&S configuration which embraces a self-contained system philosophy includes a digital computer for on board sensor control, terminal navigation and guidance computation. These functions are additions to the master timing and sequencing functions which are required in all

spacecraft configurations. The computer will determine a terminal steering correction based upon on-board determination of the deviation between the actual and the design point trajectories. The state estimation function required for the above is based on angular measurements made and processed on board the spacecraft. These navigational measurements are made with respect to the target planet and a suitable set of stars. Pointing control of the required sensors is based on the spacecraft attitude and expected position and the coordinates of the observables in the primary reference frame. In addition, the computer may be utilized to perform certain computations for the science payload, malfunction isolation, switching, data compression, and computation of antenna pointing angles.

3.3.3 Design of the Attitude Control Electronics

The attitude control electronics in the proposed design concepts exhibit basic simularities. The attitude electronics utilizes signals from the sun and star sensors to furnish attitude control inputs to a cold gas system or reaction wheels. Planet sensors are used to verify star acquisition and to provide attitude signals during certain phases of the fly-by. There is a self-contained capability for acquisition of sun and star references after an attitude acquisition command or after some inadvertant loss of the references. Turning rate signals are supplied by body mounted gyros for rate control during timed turns, attitude stabilization during motor burn, and turn rate limiting during the search sequences. Control signals for the subsystem originate from the central computer and sequencer.

A signal from the CC&S timer initially starts the attitude acquisition sequence by turning on power to the attitude control electronics and the sensors. The search logic, located in the attitude control electronics is designed so that star search begins only after Sun acquisition and Canopus acquisition is checked by the Earth or Jupiter sensors. In each concept considered, there is also a roll override capability that can be activated through the command subsystem. The roll override signal is used for initiating another star search sequence. The CC&S may break the attitude acquisition sequence and restart the search sequence if required.

The gyros provide rate feedback for limiting turn rates during the search and maneuver sequences. Turns of any kind are accomplished by pulsing the gas jets (or utilizing reaction wheels). The attitude control electronics contain switching and compensation amplifier for control of the gas jets. These amplifiers complete the turn control loop (amplifier output, gas jets, gyro rate feedback to amplifier). In the event of gyro failure, the control system is to produce turns of a known rate on command so that open loop control is possible.

The attitude control electronics contains a turn command generator and logic for the maneuver mode. The turn command generator is a calibrated constant current source with two outputs, positive and negative. The turn command logic is driven by the CC&S such that the correct polarity current from this generator is switched to the appropriate gyro. The gyro is precessed at the calibrated rate. The control system seeks to null out movement between the gyro and the spacecraft. Therefore the gas jets pulse to turn the spacecraft so that there is no movement between the precessed gyro and the spacecraft. The calibrated turn continues until the calibrated current precessing the gyro is turned off.

When the spacecraft is turned by the gas jets, attitude reference is lost. Rate feedback is used in the axes which are not being turned by command to prevent undesired spacecraft turning rates to build up during the maneuver. The search sequence is begun by the attitude control electronics each time a motor burn stop signal is received from the CC&S.

Attitude control electronics contain Sun slew and star tracking circuits are shown in Figure 3.3-2. These permit the sensors to be pointed on command, thereby pointing a fixed high gain antenna (and the spacecraft) to Earth. The slew and tracking circuits use precision synchros, the outputs and inputs to which are controlled by the CC&S. Slew rates are controlled by a motor tachometer input to the slew amplifier which compares the rate input to a calibrated voltage. The polarity of the voltage is also controlled by the CC&S.

3.3.4 Theory of Attitude Determination

As stated above, the process of attitude determination amounts to defining the relationship between the spacecraft principal axes and some primary coordinate frame. Usually the coordinates of some set of objects (stars, planets, etc.) are known in primary reference frame: thus, when the spacecraft attitude is determined, the directions to these objects can be reduced to a pair of angles at the spacecraft. In order to determine attitude, it is necessary to view certain of these objects having known coordinates and relate unit vectors along these lines of sight to both the primary axis system and the vehicle axis system.

A single method will be demonstrated for determining vehicle attitude in heliocentric space. The primary frame in this case is a non-rotating one, centered at the Sun, and defined by the ecliptic and vernal equinox. Let the vehicle's heliocentric position and the direction cosines of a single star be known (see Figure 3.3-3). Sensors on board the vehicle then must view these two objects and view these two objects and record their azimuth and elevation

TYPICAL ATTITUDE CONTROL ELECTRONICS

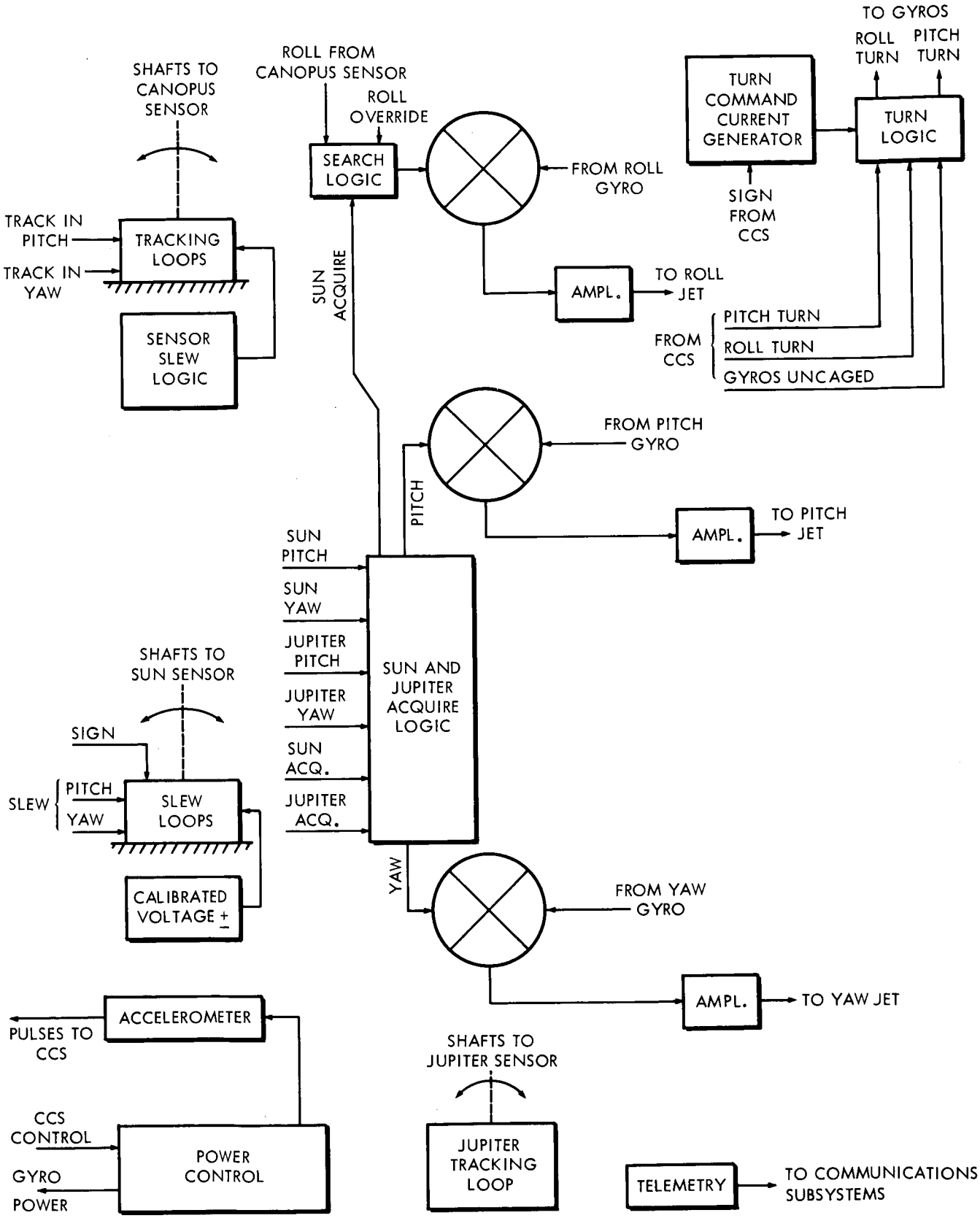


FIGURE 3.3-2

DETERMINATION OF SPACECRAFT HELIOCENTRIC ATTITUDE

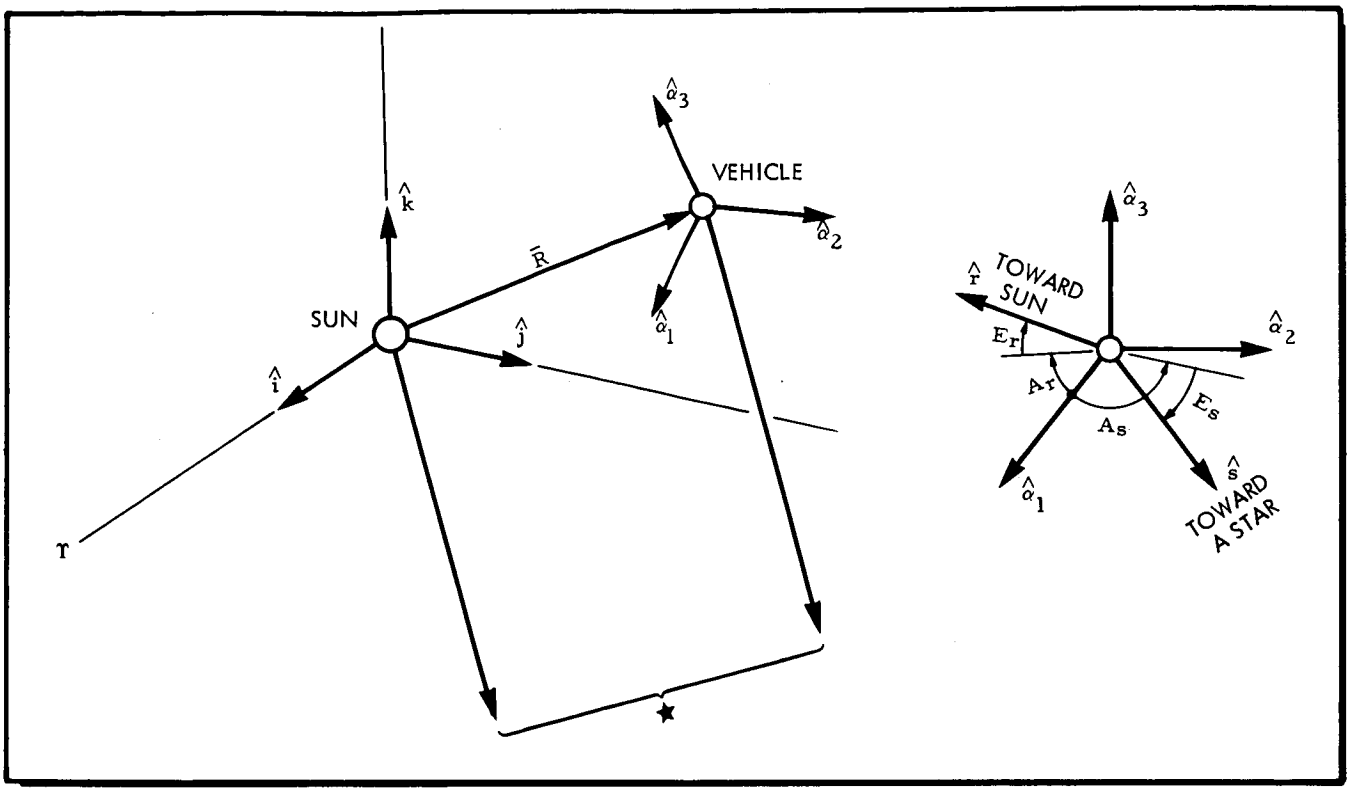


FIGURE 3.3-3

(as measured with respect to the vehicle axes). Next, unit vectors $\hat{r}$ in the direction of the sun and $\hat{s}$ in the direction of the star are defined. The star and sun azimuths and elevations are denoted by A_s, E_s, A_r, E_r. The primary frame is defined by unit vectors, $\hat{i}$, $\hat{j}$ and $\hat{k}$. The vehicle axes are defined by unit vectors $\hat{\alpha}_1$, $\hat{\alpha}_2$, and $\hat{\alpha}_3$. Let the vehicle position be x, y, z and the star direction cosines be β_1, β_2, and β_3. Then,

$$\hat{r} = -\frac{x}{R}\hat{i} - \frac{y}{R}\hat{j} - \frac{z}{R}\hat{k} \qquad R = \sqrt{x^2 + y^2 + z^2}$$

$$\hat{s} = \beta_1\hat{i} + \beta_2\hat{j} + \beta_3\hat{k}$$

Also

$$\hat{r} = l_1\hat{\alpha}_1 + l_2\hat{\alpha}_2 + l_3\hat{\alpha}_3$$

$$\hat{s} = m_1\hat{\alpha}_1 + m_2\hat{\alpha}_2 + m_3\hat{\alpha}_3$$

where

$l_1 = \cos E_r \cos A_r$ $\qquad$ $m_1 = \cos E_s \cos A_s$

$l_2 = \cos E_r \sin A_r$ $\qquad$ $m_2 = \cos E_s \sin A_s$

$l_3 = \sin E_r$ $\qquad$ $m_3 = \sin E_s$

Next, define $\hat{\rho}$ as the unit vector obtained from the cross product of $\hat{r}$ and $\hat{s}$. We may then write

$$\begin{bmatrix} \hat{r} \\ \hat{s} \\ \hat{\rho} \end{bmatrix} = M \begin{bmatrix} \hat{\imath} \\ \hat{\jmath} \\ \hat{k} \end{bmatrix} \quad \text{or} \quad \begin{bmatrix} \hat{r} \\ \hat{s} \\ \hat{\rho} \end{bmatrix} = N \begin{bmatrix} \hat{\alpha}_1 \\ \hat{\alpha}_2 \\ \hat{\alpha}_3 \end{bmatrix}$$

$$M \begin{bmatrix} \hat{\imath} \\ \hat{\jmath} \\ \hat{k} \end{bmatrix} = N \begin{bmatrix} \hat{\alpha}_1 \\ \hat{\alpha}_2 \\ \hat{\alpha}_3 \end{bmatrix} \quad \therefore \quad \begin{bmatrix} \hat{\alpha}_1 \\ \hat{\alpha}_2 \\ \hat{\alpha}_3 \end{bmatrix} = N^{-1} M \begin{bmatrix} \hat{\imath} \\ \hat{\jmath} \\ \hat{k} \end{bmatrix}$$

The transformation $C = N^{-1}M$ permits any vector given in the primary coordinate frame to be written as a vector in the frame $(\hat{\alpha}_1, \hat{\alpha}_2, \hat{\alpha}_3)$. The angles this vector makes with the spacecraft axes are immediately obtainable.

Except in the case of system concepts involving a fairly high level of on board computation, the process described above would not be carried out on board the vehicle. These calculations would be performed at an Earth-based facility using the vehicle position and the knowledge that the Sun sensor and star tracket form certain angles with respect to the body axes.

The role of the control system on board the spacecraft is then to insure that the sensor/spacecraft geometry remains fixed or is measured and relayed back to Earth as it changes. In carrying out this function, the attitude control subsystem comes into play. As the spacecraft drifts in attitude, error signals are produced in the sensors used to track the sun and a star. These error signals are used by the attitude control system to counteract the vehicle motion and keep the attitude within some allowable tolerance or dead band.

When it becomes necessary to reorient the vehicle, for example, prior to the vernier correction, commands are sent to the vehicle giving the duration of turns required (at fixed angular rates) to achieve the orientation. Rate sensing with body mounted gyroscopes are used in the control system to accurately maintain the specified vehicle angular velocities. An alternate mechanization would involve commanding the angular amount of each turn required. In this case, the gyro rate signals are integrated and the maneuver is terminated when the required total angle is achieved.

3.4 NAVIGATION AND GUIDANCE

3.4.1 The Guidance Requirement

In the years since the first artificial Earth satellites were orbited, the subject of space vehicle navigation and guidance has been the object of increasing amounts of research and development. The "state-of-the-art" in control system theory and technology can provide very accurate and sophisticated navigation and guidance system mechanizations. As has been mentioned before, navigation is concerned with determining the position and velocity of the vehicle so that the guidance function may be carried out more effectively. The guidance function is concerned with making corrections to the vehicle trajectory so that desired end conditions are met.

In the case of interplanetary missions between Earth and Jupiter, these functions are required to insure a reasonable probability of mission success. Starting with the fact that a satisfactory nominal trajectory has been chosen for the mission, the guidance functions begin during the launch and injection maneuvers. The booster control system attempts to place the space vehicle on the chosen trajectory. The deviation from the chosen trajectory near the target planet is largely dependent on errors in velocity near the departure planet. The degree of sensitivity of the terminal position to the initial velocity is dependent on the chosen trajectory, but for the typical Earth-Jupiter trajectories under consideration, this sensitivity is approximately 4000 km per 0.1 m/sec. Using figures of this type and the expected velocity dispersion at the end of the injection process, the RMS position error at the target is on the order of 5 to 6 Jupiter radii. This means that without any guidance correction after the injection maneuver, an aim point 10 to 12 Jupiter radii from the target must be chosen to give a 98 percent probability of not impacting the planet. Further, only very simple or crude experiments can be planned because of the large uncertainty in periapsis distance.

If a vernier correction is used to null the velocity error at a particular point early in the flight, an improvement of close to two orders of magnitude can be realized. If the allowable terminal error is less than 4000 km (one sigma), then the use of a second guidance correction later in the mission is indicated. To design for a second midcourse or terminal correction probably cannot be justified in view of the relatively simple scientific payloads under study for the early Jupiter flyby missions. To design for a second correction is to indicate that, in general, a higher terminal precision is required and/or the payload is important enough to warrant designing for an event having a low probability of occurrence. This event, that the effect of

all the mission uncertainties will produce a terminal error large enough to negate the scientific objective, could occur if the vernier correction should be badly in error or if some astrophysical phenomena should produce an unexpected effect on the vehicle trajectory.

Navigation prior to the vernier correction is accomplished through earth-based tracking and orbit determination. Terminal navigation can be done in the same way, however, with understandably larger errors. The use of direct sighting on the target from the vehicle itself offers a means for improving the terminal navigation process.

3.4.2 Performance Analysis

The performance of the booster system is given in terms of a figure of merit (FOM) which amounts to the RMS velocity error or the square root of the expected quadratic velocity error. This number is valid for a period of time ($\sim$2 weeks) early in the flight and is typically interpreted as the RMS error in departure hyperbolic excess velocity or in the initial heliocentric velocity. Using the booster FOM, the 1σ position errors at Jupiter can be found in several ways. The position errors are usually given in the target plane which is a plane defined by unit vectors $\bar{r}$ and $\bar{t}$ perpendicular to a unit vector $\bar{s}$ along the approach asymptote. The impact parameter B is the distance in the target plane (the $\bar{r}$ and $\bar{t}$ plane) from the center of the planet to the approach asymptote. The position error at the target (in so far as the heliocentric trajectory is concerned) is ΔB or the error in the impact parameter.

The booster FOM can be used to find the RMS dispersion in the injection energy ΔC_3 or can be converted into RMS injection velocity errors $\Delta \dot{X}_1$, $\Delta \dot{X}_2$, $\Delta \dot{X}_3$. Either course of action will lead to an estimate of the error at the target resulting from booster dispersions, given that no corrections are made. By using first the error in injection Vis Viva ΔC_3, the analysis proceeds as follows:

$$\Delta C_3 = \left| V_\infty^2 - (V_\infty + \text{FOM})^2 \right| \approx \left| 2\ \text{FOM}\ V_\infty \right|$$

Setting FOM = 15 m/s and V_∞ = 10km/sec results in $\Delta C_3 \cong .3 \left(\frac{\text{km}}{\text{sec}}\right)^2$

$$\Delta B = \frac{\partial B}{\partial C_3} \Delta C_3$$

If a value of 1.4×10^6 km/(km/sec)^2 is used for the partial derivative, ΔB is found to be $\sim$ 420,000 km. A similar result is found by the use of the following expression:

$$B = \sqrt{\left(\frac{\partial B}{\partial \dot{X}_1} \Delta \dot{X}_1\right)^2 + \left(\frac{\partial B}{\partial \dot{X}_2} \Delta \dot{X}_2\right)^2 + \left(\frac{\partial B}{\partial \dot{X}_3} \Delta \dot{X}_3\right)^2}$$

All necessary partial derivatives are generated by a digital computer program.

Because the vernier correction is designed to null the spacecraft initial velocity error, the magnitude of the velocity change capability to be provided is estimated from the booster FOM. The vernier correction capability is usually 5 or more times the FOM. The determination of the actual required velocity will be covered in subsection 3.4.3.

An analysis similar to the one outlined above can be used to find the heliocentric errors in the target plane which result from velocity error V_ϵ is to be nulled by the vernier correction ΔV. After the vernier maneuver, a residual error δV is left; this error is the result of several error sources. Principally, these are (1) error in the magnitude of ΔV, caused by thrust termination uncertainties, (2) spacecraft attitude control errors occurring prior to and during the vernier maneuver, and (3) orbit determination errors or errors in the estimation of V_ϵ . The individual velocity error components are represented as v_1, v_2, and v_3 respectively.

By using the expression $v_1 = \frac{\delta I}{W} g$, the error v_1 can be found from the spacecraft weight and the uncertainty in the vernier maneuver total impulse. For the vehicles under consideration, this error is approximately 0.06 m/sec. The one sigma value of v_2 will be approximately 0.125 m/sec, using ΔV = 15 m/sec and a vehicle alignment accuracy of 0.5 degrees. The value of v_3 based on DSIF projected capability should run about 0.005 m/sec (one sigma). Thus, the residual velocity error δV will be approximately 0.085 m/sec per axis (1σ). The error produced in the target plane due to this residual velocity error is found to be about 3800 km. The effect of Jupiter's gravity during the planetocentric phase of the flight will reduce the above RMS dispersion to approximately 2600 km at periapsis.

INJECTION AND VERNIER CORRECTION GEOMETRY

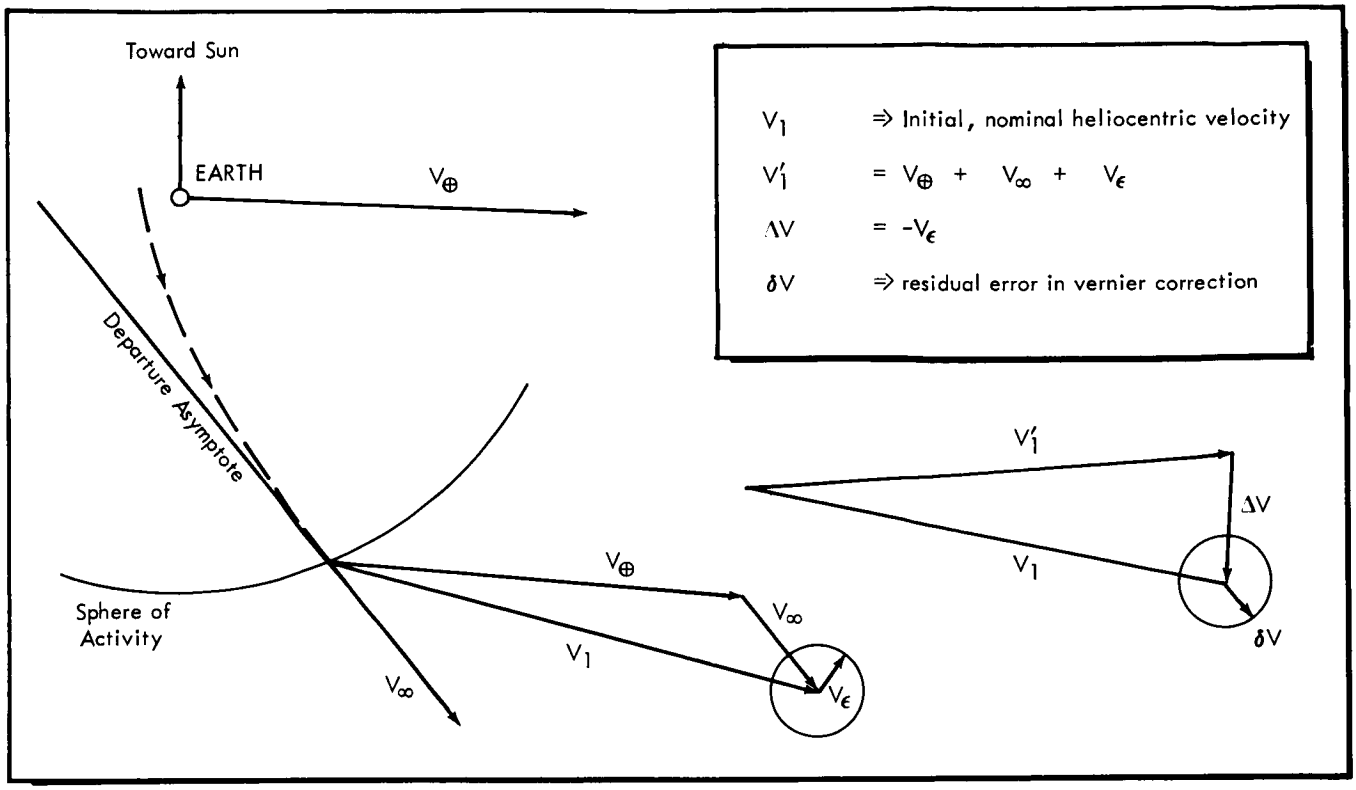


FIGURE 3.4-1

The velocity change capability to be designed into the system for terminal maneuvers can be estimated from the error ΔB. To correct for a given error, the ΔV requirement increases as the vehicle gets closer to the target. On the other hand, making the correction earlier will cause periapsis errors as a result of errors in the correction itself, to become larger. A more complete study of this trade-off is required in order to specify the optimum point for the terminal correction. In general, it should be made at a point where the required ΔV is very much greater than the expected velocity error in the guidance correction, and yet far enough away to produce the desired result with a reasonable ΔV expenditure. Assuming that the correction is made some 40-50 million km from Jupiter, the following ΔV estimate can be made. (See Figure 3.4-2.)

$$\Delta B \cong R \Delta \phi$$

$$\Delta \phi \cong \frac{\Delta V}{V_\infty}$$

$$\Delta B \cong R \frac{\Delta V}{V_\infty}$$

$$\frac{\partial B}{\partial V} \simeq \frac{\Delta B}{\Delta V} \cong \frac{R}{V_\infty} \cong 3000 \quad \frac{km}{m/sec}$$

TERMINAL MANEUVER GEOMETRY

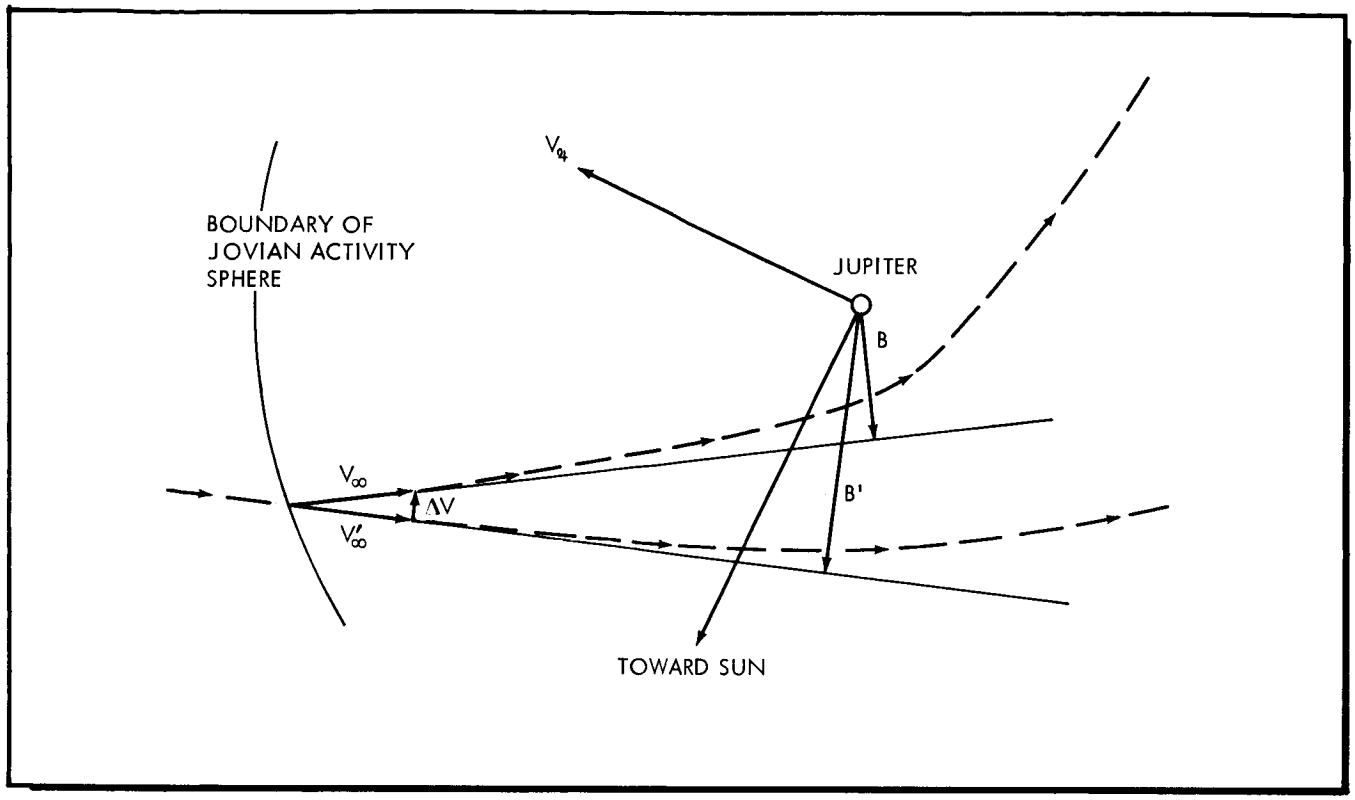


FIGURE 3.4-2

Using this value, a 5 sigma error in impact parameter can be corrected with a ΔV of less than 10 m/sec. An example can be used to show the effect of correction timing on the residual error in B. Assume that ΔB = 10,000 km and that the spacecraft has a correction capability of 15 m/sec. Further, assume that the RMS error in the terminal maneuver is approximately $\delta V = \left[.015\Delta V + .1\right]$ m/sec.

By postulating two points along the approach trajectory having different sensitivities of impact parameter to velocity changes orthogonal to the flight path, a reduction in residual error can be demonstrated which is the result of the timing of the terminal correction.

<u>point #1</u>

$$\frac{\partial B}{\partial V} = 3000 \frac{\text{km}}{\text{m/sec}}$$

$$\Delta V = \frac{10,000}{3,000} = 3.33 \text{ m/sec}$$

$$\delta V = 0.15 \text{ m/sec}$$

$$\delta B = 450 \text{ km}$$

point #2

$$\frac{\partial B}{\partial V} = 1000 \quad \frac{km}{m/sec}$$

$$\Delta V = \frac{10{,}000}{1{,}000} = 10.0 \text{ m/sec}$$

$$\delta V = 0.25 \text{ m/sec}$$

$$\delta B = 250 \text{ km}$$

3.4.3 Guidance Analysis

The nominal trajectory is the trajectory, determined in advance, which satisfies the desired terminal position and velocity. The guidance function is concerned with deriving one or more velocity corrections based on the difference between the best estimate of the actual position and velocity and the nominal trajectory position and velocity at this point. Applying these computed corrections, a new trajectory is gained which also nominally passes through the desired end state.

The terminal state is, generally speaking, very sensitive to initial errors in velocity. The proper choice of nominal trajectory can reduce this sensitivity somewhat, but the effect is still present. For this reason, a vernier correction is usually made early in the flight to correct for the injection velocity error. This should be made as soon as a good determination of the actual trajectory is available. Let the vector $\bar{\delta}(t_i)$ represent the difference between the nominal state and the best estimate of the actual position and velocity, i.e.,

$$\bar{\delta}(t_i) = \bar{X}(t_i) - \hat{X}(t_i)$$

$\bar{X}(t_i)$ = the best estimate of the actual state at time t_i

$\hat{X}(t_i)$ = the nominal state at time t_i

Therefore, the vernier correction is found as follows:

First the column vector $\bar{\delta}(t_i)$ is partitioned into position deviation and velocity deviation components.

$$\bar{\delta}(t_i) = \begin{bmatrix} \bar{r}(t_i) \\ \hline \bar{v}(t_i) \end{bmatrix}$$

The vernier correction amounts to the negative of the velocity deviation existing at the time of the correction.

$$\overline{\Delta V} = -\bar{v}(t_i)$$

The computation of the terminal correction proceeds in a different manner. It is assumed that linear perturbation theory applies to the column vector $\overline{\xi}(t_i)$. The linear perturbation equation

$$\frac{d\,\overline{\xi}(t_i)}{dt} = F\ \overline{\xi}(t_i)$$

has a solution of the following form:

$$\overline{\xi}(t_i) = \phi(t_i, t_{i-1})\ \overline{\xi}(t_{i-1})$$

The state transition matrix ϕ is evaluated for the proper interval through integration of the perturbation equation. Using ϕ, the expected terminal dispersion can be found.

$$\overline{\xi}(t_f) = \phi(t_f, t_i)\ \overline{\xi}(t_i)$$

Now by partitioning this matrix equation, the following is obtained:

$$\overline{\xi}(t_f) = \begin{bmatrix} \bar{r}(t_f) \\ \hline \bar{v}(t_f) \end{bmatrix} = \left[\begin{array}{c|c} \varphi_{rr} & \varphi_{rv} \\ \hline \varphi_{vr} & \varphi_{vv} \end{array}\right] \begin{bmatrix} \bar{r}(t_i) \\ \hline \bar{v}(t_i) \end{bmatrix}$$

The terminal deviation vector $\overline{\xi}(t_f)$ is made up of six elements. A single velocity change can null three of these at the most. Consider the computation of $\overline{\Delta V}$ required at t_i to null the terminal position error $\overline{r}(t_f)$.

$$-\bar{r}(t_f) = \varphi_{rv}\ \overline{\Delta V}$$

The elements of the three by three submatrix φ_{rv} have the form of partial derivatives of final position with respect to velocity components at t_i. Thus, we find

$$\overline{\Delta V} = \varphi_{rv}^{-1}\left[-\bar{r}(t_f)\right]$$

As far as the guidance computation is concerned, all that remains is to translate this vector representation of $\Delta\vec{V}$ (given in the primary coordinate frame) into attitude maneuver angles and a velocity change magnitude to be carried out by the spacecraft.

The terminal correction process described above is based on the use of an impulsive velocity change with three-dimensional freedom of the thrust vector orientation. Using a 50-pound thrust rocket, a velocity change of 10 meters per second can be made (in the intermediate and maximum payload vehicles) in something less than half a minute.

A second possibility for implementing the terminal maneuver involves the restriction of the thrust vector to the orbit plane and the use of a considerably longer rocket thrust time and associated low thrust. This approach exhibits several attractive features. When the terminal maneuver is intended to correct errors only in the magnitude of the impact parameter, the velocity correction can be made in the plane of the trajectory. The hyperbolic approach trajectory is essentially rectilinear from the entrance into the activity sphere to a point very near periapsis. A change in the magnitude of the impact parameter can be effected by a change in the direction of the velocity vector, which causes an angular change in the approach asymptote. The angular rotation of the approach asymptote for the typical range of correction required is small and can be accomplished with a small ΔV applied normal to the spacecraft velocity vector and in the plane defined by the approach asymptote and the center of Jupiter. A further simplification can be achieved by using thrusters mounted perpendicular to the spacecraft longitudinal axis and pointing this axis toward Jupiter with a suitable sensor. The velocity correction is then made normal to the spacecraft/Jupiter line of sight. In this way a simple roll maneuver is all that is required to place the thrust direction in the proper plane. A star tracker is used to define the plane of the approach trajectory. A pair of rockets on opposite sides of the vehicle will usually limit the required roll to a small angle and allow the use of a single star tracker for control during corrections to increase or decrease the impact parameter. Estimation of the error in impact parameter is accomplished at a distance on the order of 50 million kilometers from Jupiter; at this distance the duration of the velocity change maneuver is not critical. Thus, the terminal correction thrusters could be much smaller in size, requiring that the manuever itself occupy hours instead of minutes or seconds. This would eliminate the need for vane controls in the rocket exhaust. The small moments produced by the thrust-vector misalignments can be held by the attitude control system. The control signals would be generated by the Jupiter sensor pointed along the vehicle roll axis.

3.4.4 Self-Contained Terminal Navigation

For the sophisticated payloads, a terminal maneuver should be considered to compensate for the integrated effect of uncertainties in solar radiation pressure, solar plasma, meteoroid flux, the astronomical units, etc. or simply to improve the terminal precision over that obtainable with the vernier correction.

The nominal trajectory is the desired planetocentric trajectory at Jupiter. The reference trajectory is the best estimate of the spacecraft trajectory as it approaches Jupiter as determined by the DSIF. The objective of the terminal maneuver is to change the trajectory from the reference to a new trajectory which passes through the nominal or design point terminus.

In order to derive the most benefit from a terminal correction, the correction should be based on observations of the target planet. As the spacecraft approaches the planet, sensors will be used to search for and acquire the target planet. At this point, the operations depend on whether the navigation and guidance computations are accomplished on Earth or on the spacecraft.

In the case of Earth-based navigation and guidance, the reference trajectory determined from Earth-based tracking can be improved (i.e., a better estimate is made) by using measurements made of the target planet from the spacecraft. These measurements are transmitted back to Earth with a time index. They may consist of stadiometric measurements, angular rate measurements, or measurements of the angular distance between Jupiter and the Sun, other stars, or one of Jupiter's moons. With the improved estimate of the reference trajectory, the terminal error can be predicted by a comparison of nominal and reference trajectories. The correction maneuver is computed and the proper commands sent to the spacecraft.

It is possible to design the spacecraft navigation and control system so that the terminal correction is computed on board. Essentially, this amounts to providing sufficient computer and sensor control functions so that Earth-based data processing is not required. To implement this, the same observations are made as in previous case, but they are used on board the spacecraft in a navigation routine in the central computer.

The terminal navigation phase, which precedes the terminal guidance maneuver, is initiated at a point some 60×10^6 km from Jupiter. Earth-based tracking and orbit determination has been engaged in the determination of the spacecraft position and velocity in heliocentric space. From this information and the knowledge of Jupiter's location with respect to the Earth, the position of the

spacecraft with respect to Jupiter can be estimated. Tracking errors plus errors in Jupiter's ephemeris combine to produce an error in the knowledge of the spacecraft's planetocentric position and velocity. It is this error which is to be reduced by direct observations of Jupiter from the spacecraft and with on board trajectory determination and guidance computations based on these observations.

In the past several years researchers in the field of space navigation have applied the theory of statistical estimation to the problems of position and velocity estimation on board a space vehicle. The problem amounts to estimating the six components of the vehicle state vector from a sequence of angular measurements made on board the spacecraft with imperfect instruments. This problem and its solution has been formulated in the notation of modern control system theory, i.e., the state vector and state transition concepts. Although the spacecraft trajectory obeys nonlinear equations of motion, the state estimation process can be linearized by assuming the validity of a first order Taylor's expansion of the actual trajectory about the reference or nominal trajectory. From this, the state transition concept follows whereby the deviations from the reference state at one point may be written as linear functions of these deviations at a prior time.

The statistical filter is an estimator which makes an optimal estimate of this deviation vector based on a set of observations made from the spacecraft. This estimator minimizes the effects of the sensor noise. It can be proven that the best estimate of the deviation vector (in the least squares sense) is the conditional expectation of the deviation vector given the sequence of observables on which the estimate is to be based. The observables are the angular residuals obtained by comparison of measured angles from the actual but unknown spacecraft position and the computed angles based on the expected spacecraft position.

A concept of navigation has been developed which encompasses the statistical filter estimation method. The entire logic flow for this method of navigation is shown in Figure 3.4-3. The numbers appearing on this figure correspond to the sequence in which the operations are carried out.

STATE ESTIMATION FLOW DIAGRAM

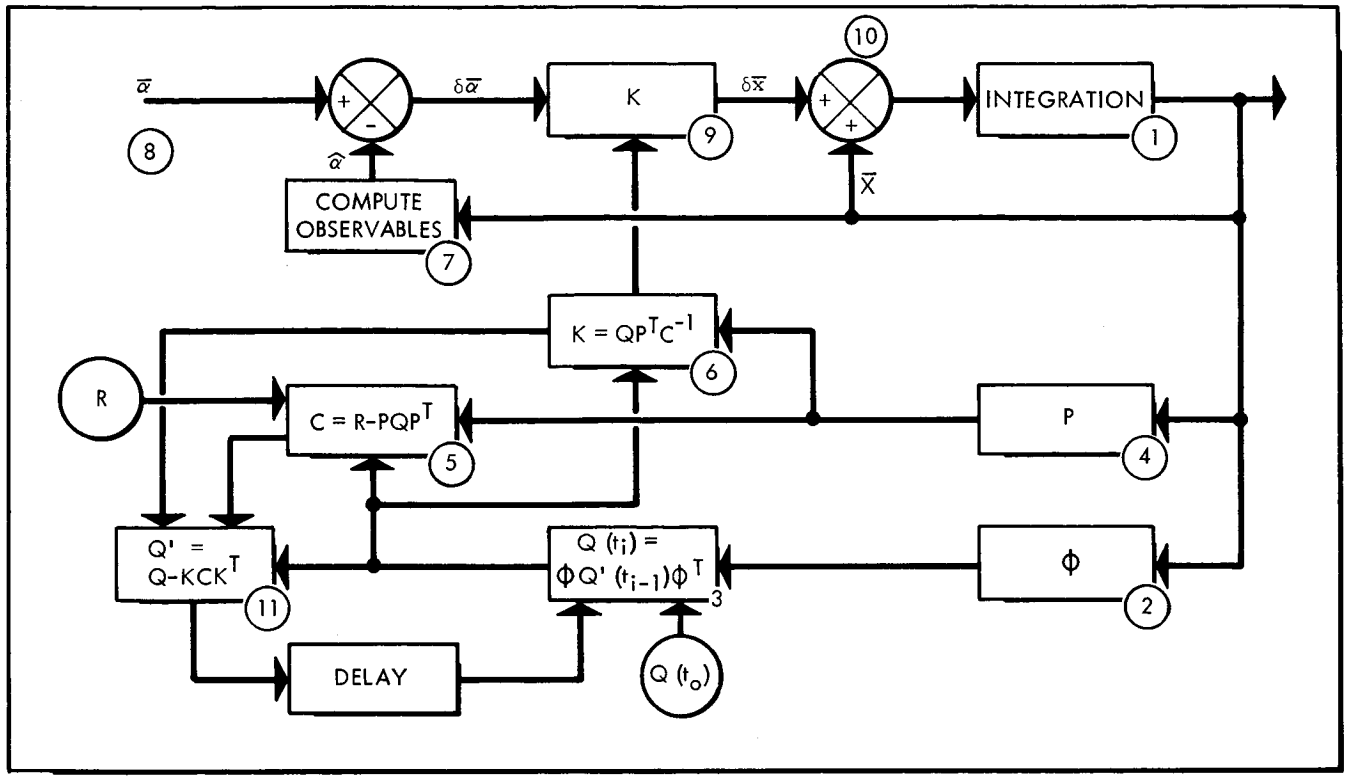


FIGURE 3.4-3

These operations are as follows:

Operation 1: In anticipation of the ith group of observations and the ith estimate of the spacecraft position and velocity, the navigation computer is used to integrate the equations of motion from the previous best estimated state to the time t_i.

Operation 2: The state transition matrix Φ, which links the state at t_{i-1} to the state at t_i, is evaluated.

Operation 3: The corrected covariance matrix of estimation errors at t_{i-1} is updated to t_i by the use of the Φ matrix. The new matrix, $Q(t_i)$, reflects the state uncertainty just prior to the ith estimation.

Operation 4: The matrix P, which relates the angular residuals to the state, is evaluated.

Operation 5: The covariance matrix of the observation residuals C is formed with inputs $Q(t_i)$, $P(t_i)$ and R, the covariance matrix of sensor noise.

Operation 6: The optimum estimator K is computed.

Operation 7: The expected values of the observables (space angles) are computed on the basis of the reference position and velocity at the time of the ith estimation.

Operation 8: The observations are made from the spacecraft actual but unknown position. The actual values of the angles being measured are corrupted with sensor noise during the observation process, thus the sensor outputs are imperfect.

Operation 9: The computed space angles are subtracted from the observed angles. The angular residuals, including the noise component, are operated upon by the optimal estimator K.

Operation 10: The best estimate of the state is added to the reference position and velocity to form the initial condition for the next trajectory integration.

Operation 11: The covariance matrix of estimation error is corrected to reflect the ith estimation.

A computer simulation of this state estimation method was carried out in order to get a feel for its performance capability. Initial uncertainties were assumed in the planetocentric position and velocity of the spacecraft at a point 60 million km from Jupiter. These RMS errors were assumed to be 5000 km per axis and 0.2 meters/second per axis. Separate computer runs were made with instrument error standard deviations of 5, 10, and 30 arc seconds. The observables used were the Jovian angular diameter and the included angles between lines of sight from the spacecraft to Jupiter and from the spacecraft to 3 different stars. The results for two different observation rates are shown in Figures 3.4-4 and 3.4-5. The plots show the resultant total position error as a function of time.

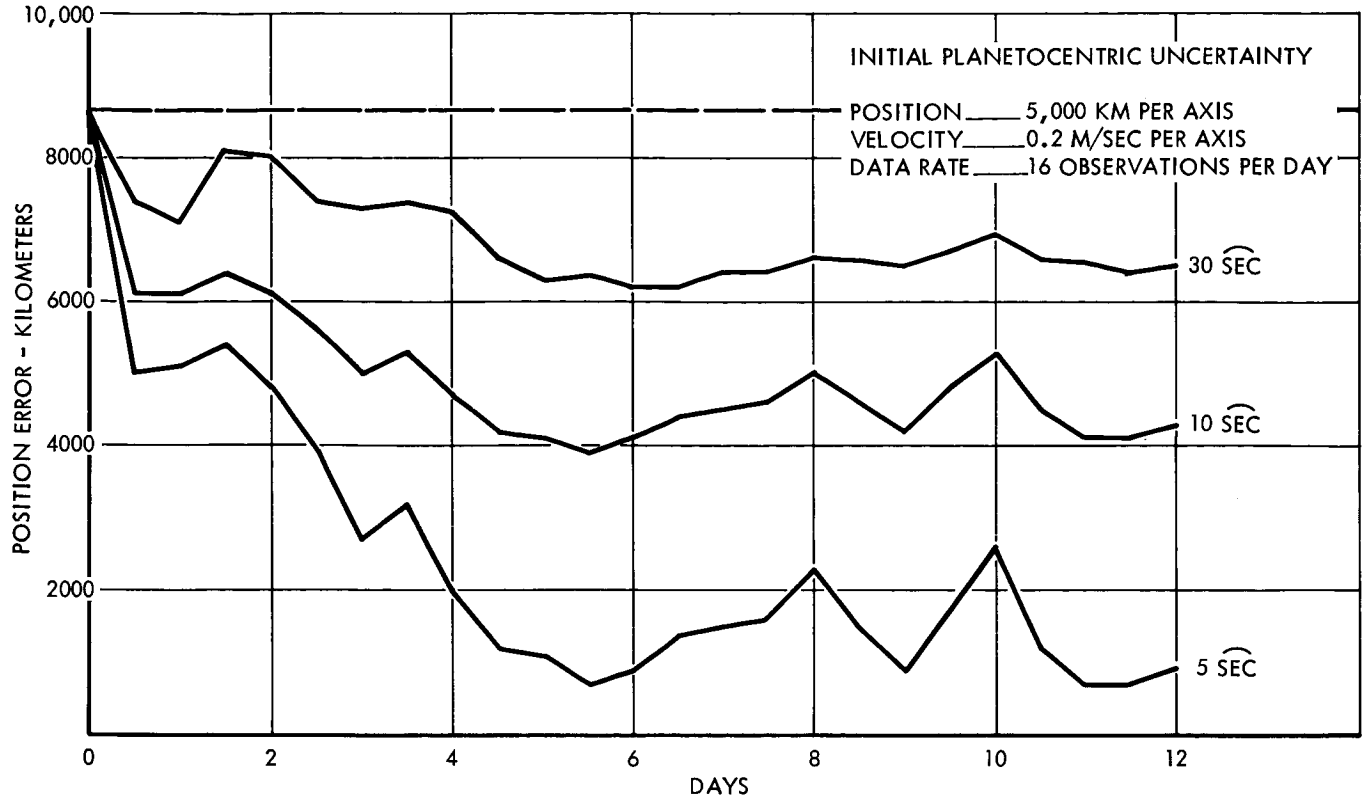


FIGURE 3.4-4

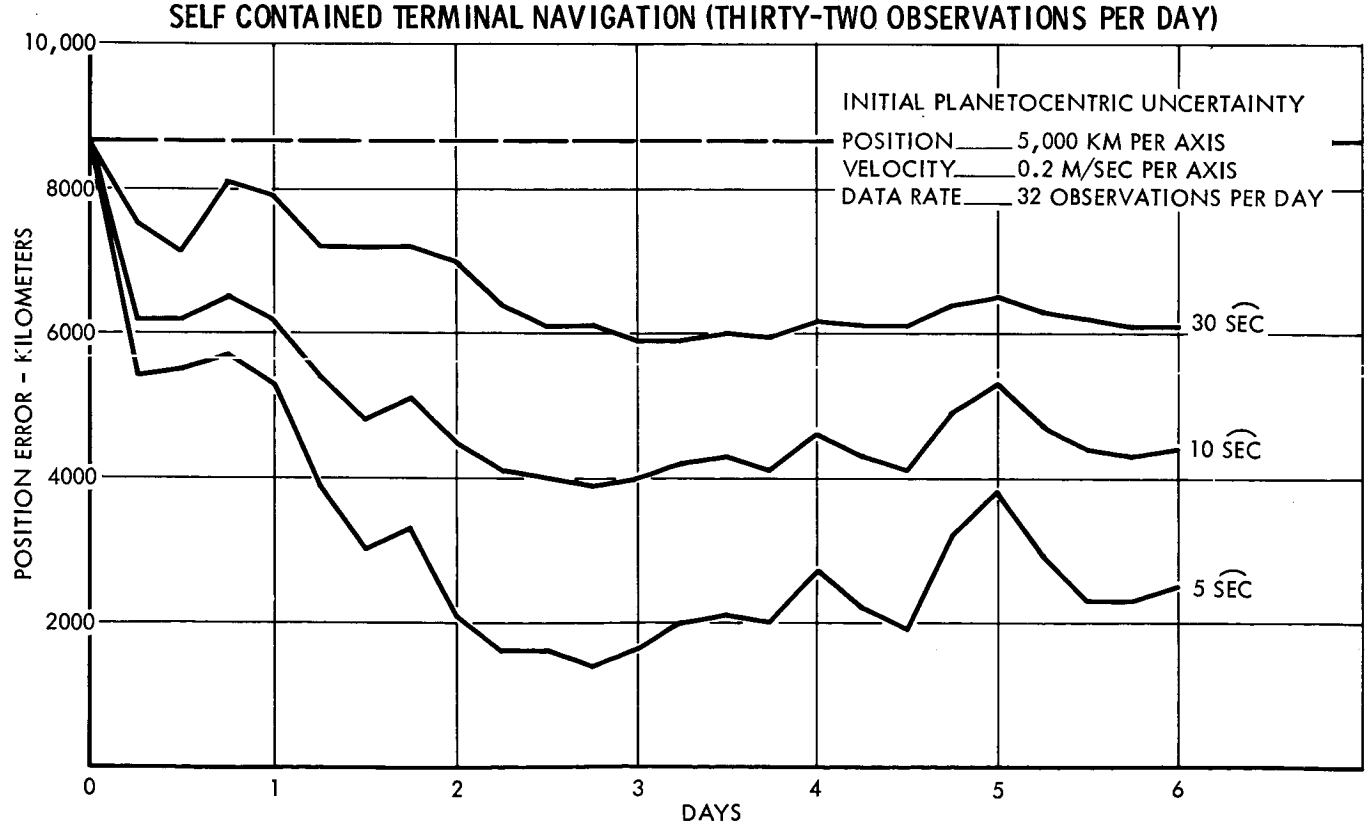


FIGURE 3.4-5

3.5 ATTITUDE CONTROL

The term"attitude control system"as used herein refers to the group of actuation devices and associated electronics which are employed to generate torques about the spacecraft axes for controlling the orientation to some desired condition. The sensors used to generate the attitude-error signals are considered part of the spacecraft control system and are discussed in subsection 3.3. However, many of the requirements of the attitude control system stem directly from the specific control objectives to be attained, so that guidance considerations are not entirely separable.

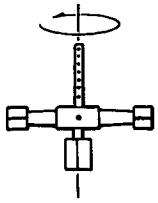
There are many possible methods and combinations of methods of achieving attitude control, and any specific mission will require a succession of different modes of control. This problem will be limited or influenced to some degree by many design considerations. Communications requirements are critical because of the long ranges involved in a Jupiter mission, and they largely dictate the configuration features. Design constraints in the form of geometric and physical limitations (or preferences) resulting from booster features and capabilities are also important. The usual requirements to accomplish maneuvers, perform scientific experiments, overcome external moments, and permit other functions associated with the mission must also be met. Because of the extended period of time over which the system must operate, reliability considerations are paramount.

In this section, attention will be given to general considerations and design criteria associated with the attitude control problem. The application of these results to the design of specific spacecraft is considered subsequently in Section 5. By this process, the influence of each requirement upon the final result is made clearer, and the effect of future modifications can be more easily assessed.

3.5.1 Configuration Concepts

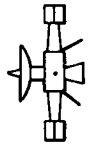
Although many attitude control approaches can be postulated, various compromises tend to reduce the number to a few categories offering the greatest potential. For the purposes of this investigation, three basic configuration concepts were defined, and each concept depends upon a different control arrangement. These configuration types are summarized in Figure 3.5-1. The distinctions between these approaches will be described before considering the detailed requirements of each. The classifi-

CONFIGURATION CONCEPTS



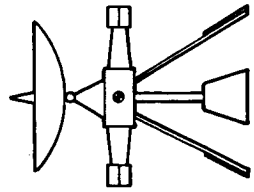
- MINIMUM WEIGHT AND SCIENTIFIC PAYLOAD CAPABILITY.
- SPIN AXIS NORMAL TO ECLIPTIC.
- INTERIM GAS JET SYSTEM REQUIRED TO ACCOMPLISH VERNIER INJECTION CORRECTION AND INITIATE SPIN-UP.
- PRECESSION DUE TO SOLAR TORQUE MINIMIZED BY AREA BALANCE.
- SPIN STABILITY MAXIMIZED BY PROPER INERTIA DISTRIBUTION.

(A) SPIN STABILIZED



- MINIMUM TO INTERMEDIATE WEIGHT AND SCIENTIFIC PAYLOAD CAPABILITY.
- MAINTAINED IN EARTH-POINTING ATTITUDE PRIOR TO JUPITER ENCOUNTER.
- SWITCHED TO JUPITER-POINTING ATTITUDE FOR ENCOUNTER PHASE, WITH COMMUNICATIONS INTERRUPTION.
- BALANCED TO MINIMIZE SOLAR TORQUES.
- CONTROL CONCEPTS INCLUDE GAS JETS AND REACTION WHEELS.

(B) 3-AXIS STABILIZED; FIXED ANTENNA



- MAXIMUM WEIGHT AND SCIENTIFIC PAYLOAD CAPABILITY.
- MAINTAINED IN NEAR SOLAR-POINTING ATTITUDE WITH EARTH-TRACKING ANTENNA.
- SOLAR TRIM PANELS PROVIDE STABILIZING TORQUES USEFUL IN CONTROL CONCEPT.
- REACTION WHEELS AND/OR GAS JETS USED TO SUPPLEMENT SOLAR TORQUES.
- LITTLE OR NO COMMUNICATIONS INTERRUPTION, DEPENDING ON TRAJECTORY.

(C) 3-AXIS STABILIZED; MOVABLE ANTENNA

FIGURE 3.5-1

cation is intended to infer different levels of complexity as well as reflect different control concepts. It should be emphasized, however, that the classification is primarily a conceptual guide, and many valid offshoots can be postulated (such as spacecraft design concept C in Section 5).

The spin-stabilized configuration represents the simplest control concept, and it is herein associated with a case of minimum weight and scientific payload capability. The spin axis is to be oriented approximately normal to the ecliptic plane with communications accomplished through a slotted-waveguide type of antenna located along the spin axis. An interim gas jet system is required to accomplish the attitude changes associated with the vernier injection correction and with the orientation of the spacecraft prior to firing the spin rockets. After spin-up, all control functions are terminated and the stabilization becomes completely passive. Spin stability is designed into the configuration by proper inertia distribution, with nutation damping provided either by natural structural flexure or specially designed dampers, as required. The effect of solar torques on the precession of the spin axis is minimized to a tolerable level by proper attention to balancing the moment-area about the axes normal to the spin axis.

The capacity of the communications system is greatly improved by the use of a parabolic antenna which is maintained in a nominal Earth-pointing attitude. Theoretically, this concept could be implemented under the spin-stabilization approach by choosing the antenna axis as the spin axis and maintaining it along the Earth-spacecraft line by an active precession control system. However, this control requirement would seemingly defeat the desire for simplicity which was the inspiration for spin stabilization in the first place. Also, this concept is not directly applicable to a Jupiter mission because it is impractical to directly sense the Earth at the large separation distances involved. It would be necessary to utilize a Sun-pointing attitude with sufficient antenna sweep to encompass the Earth throughout the mission. Because of these considerations, this version of spin stabilization was regarded as less favorable than the previous one, and it was not pursued.

The use of Earth-pointing parabolic antennas was restricted to a 3-axis stabilization approach using two basic configuration types identified here as "fixed antenna" or "movable antenna". The fixed-antenna design is the least complex, and it is identified with the case of minimum to intermediate weight and scientific payload capability, which requires an antenna of only moderate size. Fixing the antenna avoids the bearing problems and reliability reduction associated with an antenna control mechanism, but it constrains the vehicle attitude because of the Earth-pointing requirement. The main consequence of this condition is the necessity to counteract the torques due to solar pressure which vary with solar aspect angle. The importance of this requirement depends upon the control concept. However, it is considered a design objective to obtain a condition of "neutral stability" (i.e., the center of pressure of the solar force coincident with the center of gravity at reasonable aspect angles) through the use of fixed solar vanes for balance. Two control concepts are postulated for this configuration: (1) the use of gas jets alone, and (2) the use of reaction wheels in conjunction with the gas jets. A major limitation associated with the fixed antenna approach is the necessity to interrupt the communications link in the planetary encounter phase when a Jupiter-pointing mode of control is required for experiments. After the encounter, the spacecraft must be re-oriented to transmit the stored data to the Earth.

The movable-antenna design represents an increase in complexity because of the required antenna control mechanism. However, it also offers the possibility of using solar torques as part of the control concept. It is identified with the case

of maximum weight and scientific payload capability, which utilizes the largest antenna size that can be practically accommodated. In this approach, the spacecraft axis of symmetry is to be maintained in a nominal solar-pointing attitude while the antenna is allowed the necessary relative motion to maintain its Earth-pointing orientation. The design objective is to provide the spacecraft with positive stability about the solar-pointing attitude by means of fixed solar vanes. The control system would allow the vehicle to seek its natural trim point (attitude for zero moment), which will vary somewhat with antenna position. A reaction wheel system is most consistent with this concept and would be the primary control mode. The solar torques would be used primarily to accomplish continuous de-saturation of the wheels. A gas jet system would also be provided to meet other requirements and would be available either as a back-up or as an integral part of the overall control concept. In principle, this control concept offers an almost unlimited lifetime and may be most useful when the mission is extended beyond the point of a Jupiter encounter. The movable antenna also eliminates or minimizes the communications interruptions at planetary encounter, depending on the encounter trajectory and the limits of antenna motion.

The front-mounted antenna location compromises the problem of sun sensor placement as well as limiting the antenna motion. These problems could be circumvented by moving the antenna to an eccentric location on the top, bottom, or either side of the spacecraft. However, this idea was discarded as impractical because of the size of the antenna and the difficulty of balancing the solar torque caused by an asymmetrical arrangement.

Consideration was also given to the idea of obtaining favorable gravity-gradient torques in the Jupiter-pointing attitude through a proper distribution of mass in the spacecraft design. However, such a condition would be difficult to realize without unduly compromising the design approaches suggested by booster mounting considerations. It appears more reasonable to approach the condition of zero gravity-gradient torque so that the effect is, at least, not unfavorable.

3.5.2 Nominal Trajectory Characteristics

In order to assess the attitude control requirements, it is necessary to specify certain trajectory characteristics. However, because the results of an attitude control analysis are not especially sensitive to small variations in the trajectory, preliminary studies can be based on one representative case. The example chosen for this work corresponds to a

600-day mission with departure on 30 July 1976, and its pertinent characteristics are presented in Figures 3.5-2 through 3.5-4.

The variation of orbital radius with time is presented in Figure 3.5-2. The solar radiation pressure is also shown in this figure and is an inverse square function of orbital radius. The value of the solar radiation pressure at the Earth's location (1 au) was assumed to be 9.4×10^{-8} pounds per square foot (0.45 dynes per square meter), which is for the case of normal impingement upon a completely absorbing surface. The location of the asteroid belt, which extends from about 2.2 to 3.6 au, is indicated in the figure. These limits define a period which begins at about 150 days after launch and extends to about 330 days after launch, or approximately 180 days out of the total mission time of 600 days (30 percent).

The variation of solar aspect angle along the trajectory is shown in Figure 3.5-3 for the case of an Earth-pointing spacecraft. The net solar torque will be dependent upon this angle as well as the magnitude of the solar pressure.

Finally, the meteoroid approach conditions relative to the spacecraft are presented in Figure 3.5-4. These results were computed under the assumption that the meteoroids move in circular orbits about the Sun with characteristic velocities corresponding to local circular satellite velocity, so that the spacecraft velocity must be vectorially subtracted to yield the relative velocity vector. The approach angle of the meteoroids is shown for both Earth-pointing ($\bar{\alpha}$) and Sun-pointing ($\bar{\alpha}'$) conditions. In both cases, the approach is seen to be essentially from the rear. The average approach velocity in the asteroid-belt region is seen to be about 14.5 kilometers per second.

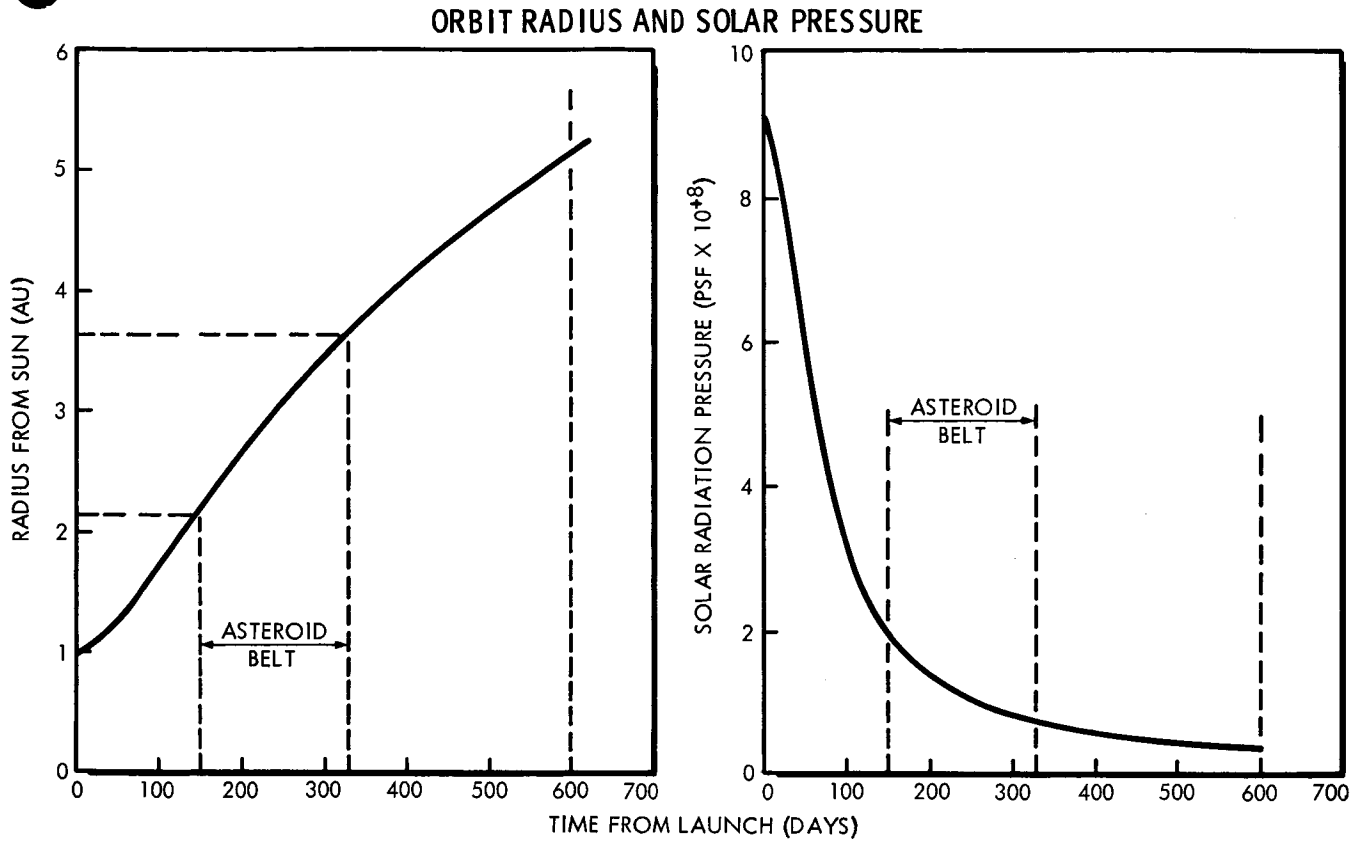


FIGURE 3.5-2

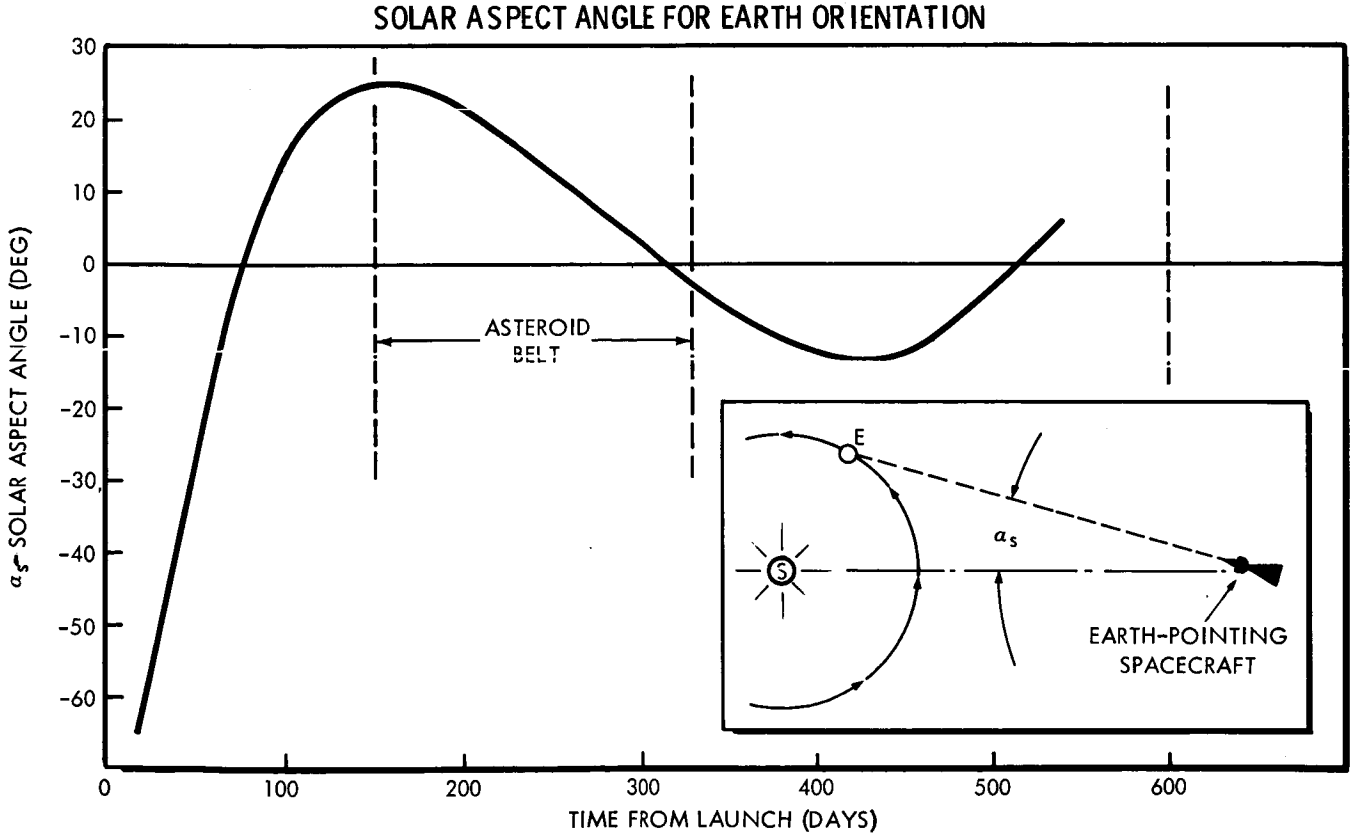


FIGURE 3.5-3

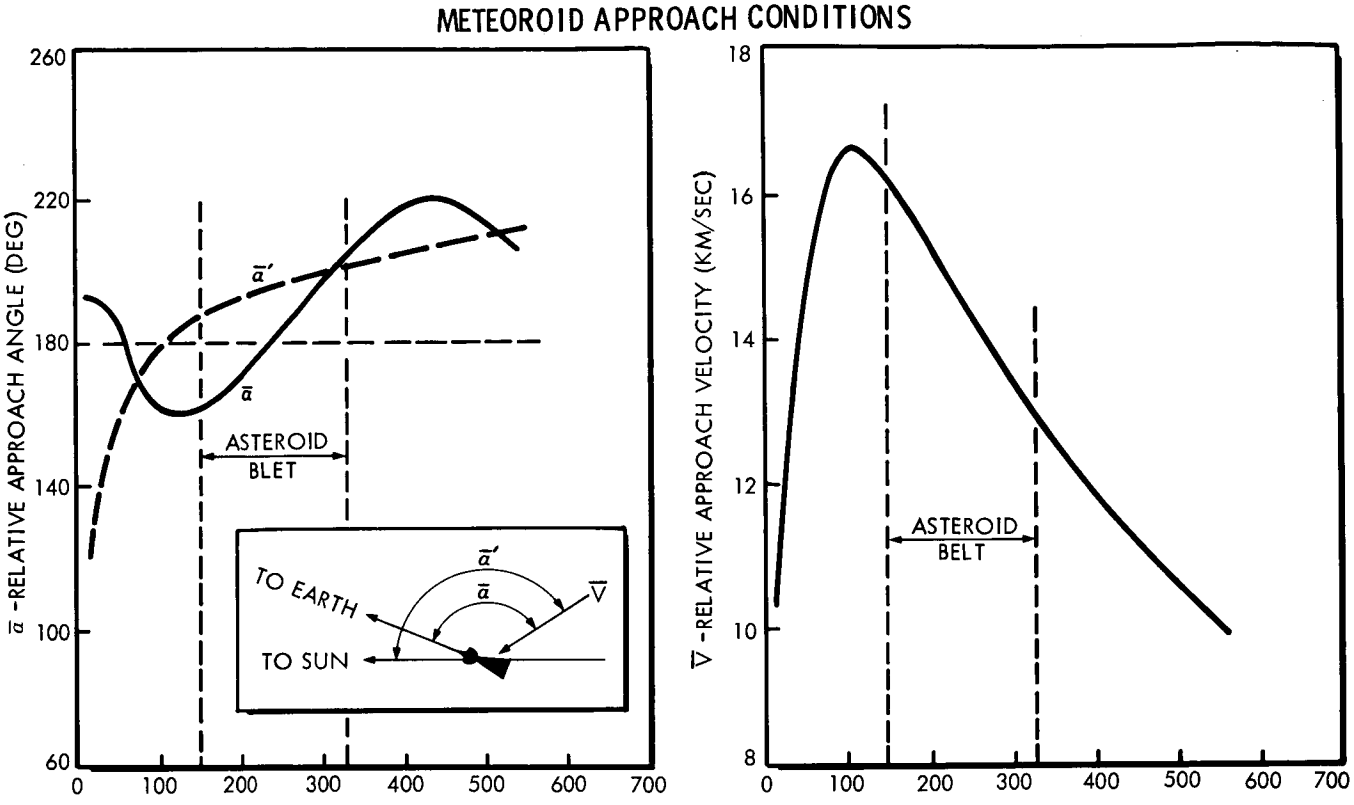


FIGURE 3.5-4

3.5.3 Considerations For Spin-Stabilization

Spin-stabilization is a simple approach to the problem of attitude control when only one axis of the spacecraft must be oriented in some inertial direction with relatively low accuracy. However, it is not generally possible to spin an arbitrary spacecraft design and expect satisfactory results. As in any engineering problem, spin stabilization is circumscribed by certain minimum requirements, with the possibility of approaching optimum conditions by proper attention to design parameters.

The stability of a spinning body is defined by its behavior under conditions of no external torques, and is concerned with the problem of nutation about the spin axis. This problem is described in many reports and textbooks and is a function of the relative values of the moments of inertia. For a non-rigid body (such as the spacecraft under consideration), it is necessary that the spin axis coincide with the principal axis of the maximum moment of inertia. The vehicle would be either statically or dynamically unstable for any other spin condition. This requirement leads to disk-like configurations with the spin axis normal to the disk plane. By placing the maximum amount of mass near the periphery, the effect is to maximize the spin stability as well as the moment of inertia about the spin axis.

For symmetrical configurations of the type under consideration, two of the moments of inertia are essentially equal, and the spin stability is measured by the following factor:

$$\underline{\text{let}}: \quad K = \text{Spin stability factor} = \left[\frac{I_{spin}}{I_{normal}} - 1\right]$$

where: I_{spin} = Moment of Inertia about spin axis

I_{normal} = Moment of Inertia about axis normal to spin axis

The condition of $K = 0$ corresponds to neutral stability and is obtained when all moments of inertia are equal. The maximum value of K is 1.0, and it corresponds to the case of a thin, flat disk which has a spin moment of inertia that is twice as large as that about the other two axes. A design objective was to achieve values of $K = 0.4$ or greater (i.e. $I_{spin} = 1.4\ I_{normal}$). This criteria was selected as a reasonable compromise for holding the steady-state nutation motion to the smallest value for a given spin rate. However, this problem requires much additional study, and is influenced by system damping, spin rocket burn time, thrust misalignment, manner of spin-up, etc.

The spin rate to be used for a given configuration will most likely be determined by centrifugal force limitations. The spin moment of inertia must then be large enough to yield the required angular momentum for counteracting the precession resulting from external torques. The variation of spin rate with allowable centrifugal force level and radius arm is presented parametrically in Figure 3.5-5. For a 10-g limitation at a 35-inch radius arm, the allowable spin rate is only 100 RPM. A design value somewhat lower than this figure is more probable, but the final result will depend upon an analysis of the "g" tolerances due to structural strength and equipment operating limits.

SPIN-RATE LIMITATIONS

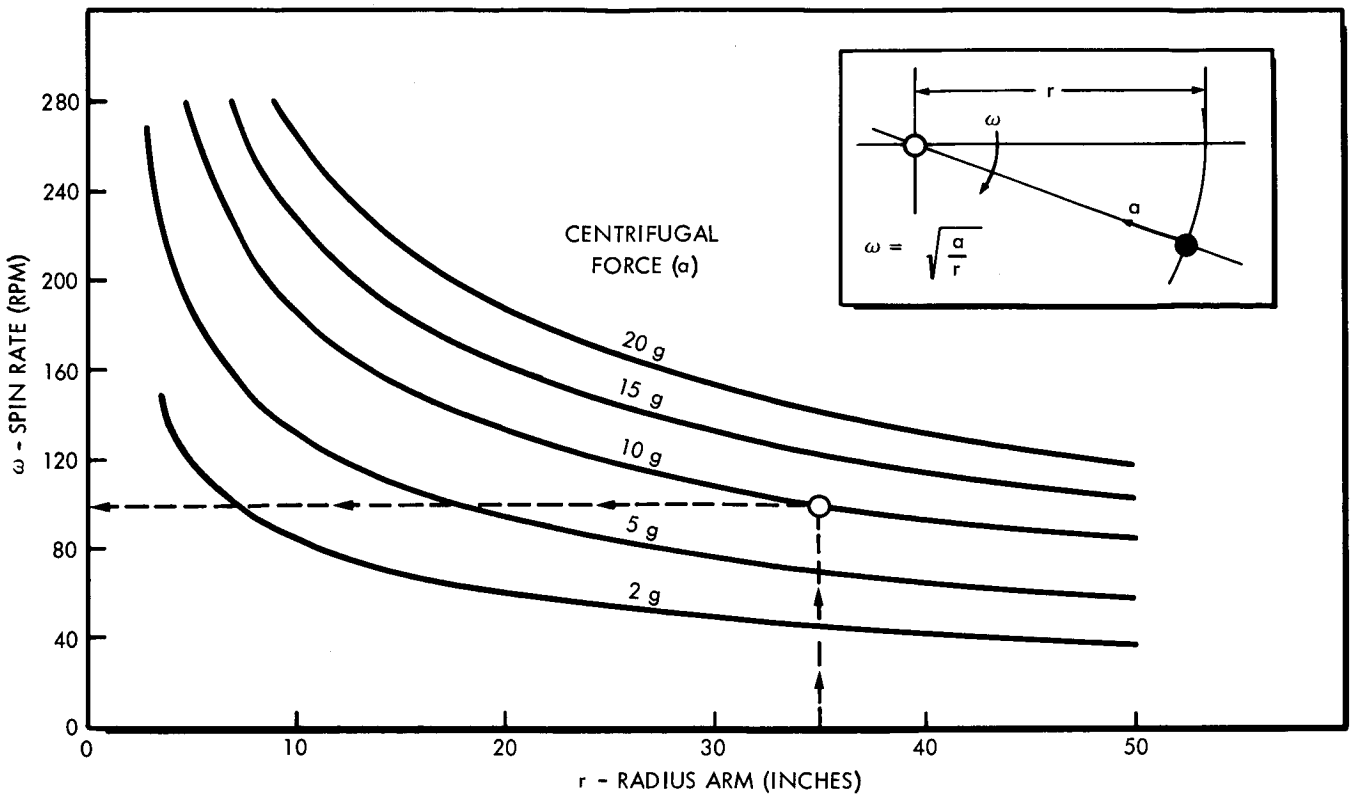


FIGURE 3.5-5

The spin rate in itself is not the fundamental quantity in spin stabilization; it is, rather, the angular momentum that is important. The angular momentum is defined as follows:

$$H = (I)\ \ (\omega)$$

H = Angular Momentum (ft-lb-sec)

where:

I = Moment of Inertia (slug-ft^2)

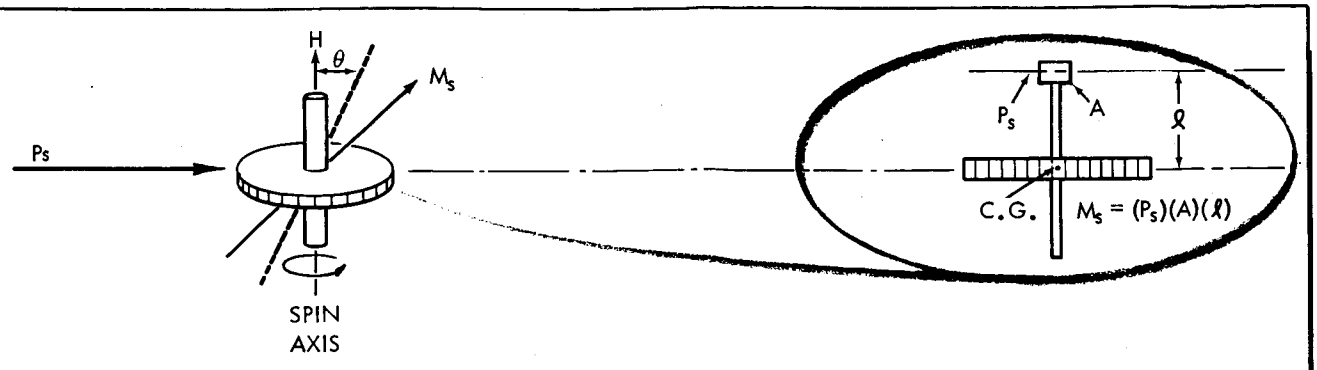
ω = Spin Rate (Rad/Sec)

In the configuration arrangements under study, the value of H is maximized by locating the RTG units at the largest possible radius consistent with design limitations. The allowable spin rate would reduce as the radius is increased (for a given "g" tolerance) but the moment of inertia contribution would increase faster. Under these assumptions the contribution of the RTG units to H would increase as the 3/2 power of their radius arm. The attainable values of H are believed to be in the region of about 500 to 1000 ft-lb-sec for the configuration studied.

In order to meet the objectives of the communications system, the precession of the spin axis due to external torques must be held to the lowest possible value. The effect of spin-up errors and errors associated with the inertially-fixed spin axis (which arise because of the slight difference between the plane of the ecliptic and the plane of the spacecraft's orbit) are expected to account for the major part of the tolerable inaccuracy. Because there is an upper limit to the amount of spin angular momentum that can be provided, design efforts to minimize the magnitude of the disturbance torques are important.

The most significant source of disturbance torque is the effect of solar radiation pressure. This problem can be reduced by designing a balanced configuration - that is, making the moment-area zero about the axes normal to the spin axis. However, because of practical limitations and unknowns, a certain amount of unbalance is unavoidable. This small discrepancy can be important because of the long time period over which the resultant torque acts. An approximate analysis of this effect may be constructed by considering the analogy of the spinning spacecraft to a simple gyro, as indicated in Figure 3.5-6. By assuming that the moment vector is inertially fixed so that two-dimensional precession takes place, a simple expression for the precession angle, θ, is obtained. This expression involves the time integral of the solar pressure (K_1), which is evaluated from the data presented in Figure 3.5-2. The results are presented parametrically in Figure 3.5-7, which shows the allowable moment-area unbalance as a function of H and θ. In a typical example (H=750 ft-lb-sec; θ=.25 deg), the allowable value of unbalance is about 4 feet cubed. This corresponds to an area of one square foot at a moment arm of 4 feet. Although this allowable error is believed to be well within the tolerance, it indicates that the effect could become significant if the balance requirement is overlooked or if the value of H is not sufficiently high.

SPIN-AXIS PRECESSION DUE TO SOLAR PRESSURE



P_s = Solar Radiation Pressure (Lbs/Ft^2)

A = Net Unbalance Area (Ft^2)

ℓ = Moment Arm of A (Ft)

M_s = Moment of Solar Force about c.g. (Ft-Lb)

H = Spin Angular Momentum (Ft-Lb-Sec)

θ = Precession Angle (Rad)

PRECESSION EQ: $M_s = H\dot{\theta}$ or $\dot{\theta} = \left(\frac{M_s}{H}\right)$

INTEGRATING: $\theta = \int_0^{T_F} \left(\frac{M_s}{H}\right) dt = (K_1)\ \frac{(A)(\ell)}{H}$ (RAD)

WHERE: $K_1 = \int_0^{T_F} (P_s)\, dt = .90\left(\frac{LB\text{-}SEC}{FT^2}\right)$

FIGURE 3.5-6

ALLOWABLE MOMENT - AREA UNBALANCE

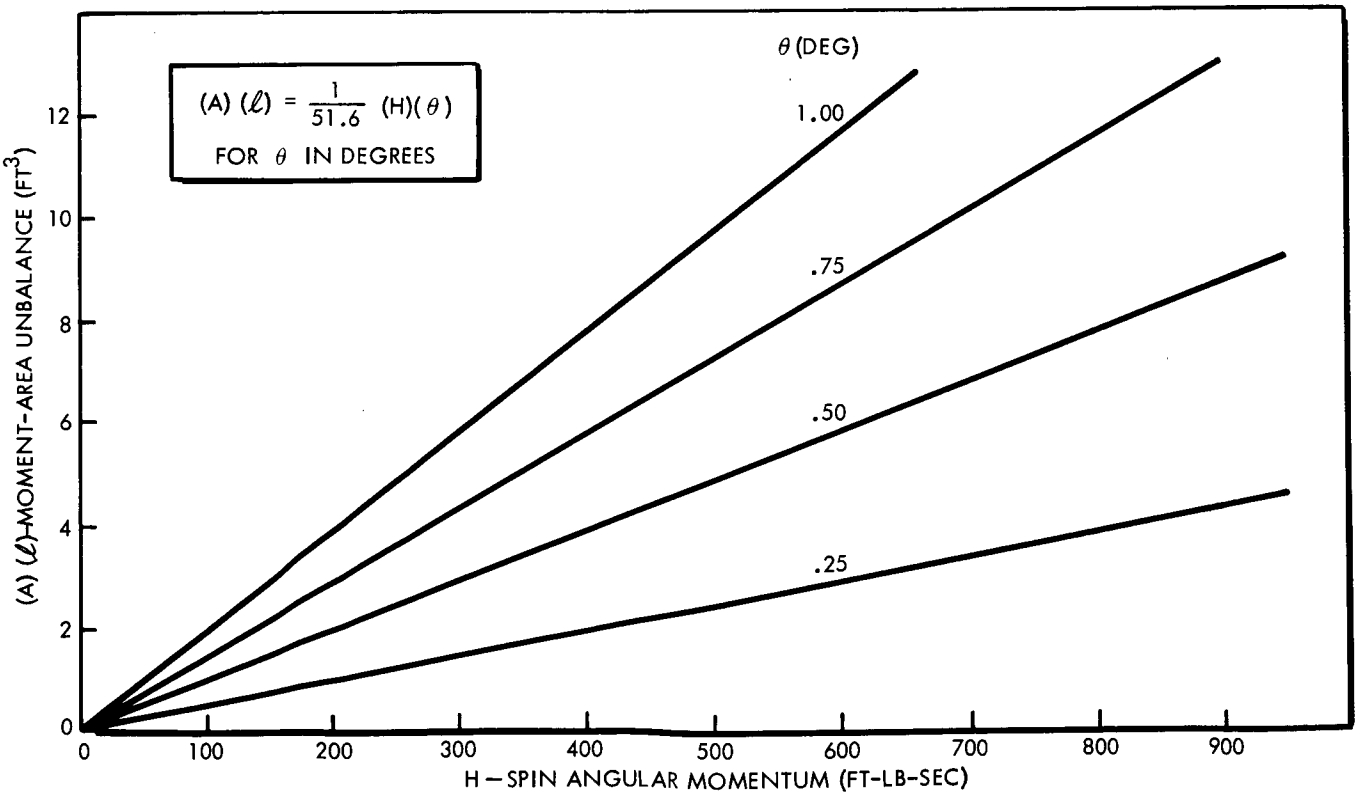


FIGURE 3.5-7

3.5.4 Design Data For Gas Jet System

In this study, consideration was given only to the stored-gas type of mass expulsion system because of its superior reliability and performance capabilities for attitude control applications. The total impulse requirements computed for the various cases of interest are low enough so that monopropellant or bipropellant systems are not believed to be justifiable, considering the various compromises involved.

The weight requirements for a stored-gas system using nitrogen are analyzed in the Propulsion section (Section 3.6) and curves are presented showing the variation of system weight with total impulse. Two basic system configurations are considered: (1) a single gas tank with one set of twelve jet nozzles, and (2) dual gas tanks with two sets of jet nozzles. Configuration (1) represents a minimum approach with no redundancy but some fail-safety protection afforded for each control axis by the use of four jet nozzles which normally operate to generate a torque couple. Configuration (2) represents a concept with redundancy and it provides the capability of tolerating a stuck-open valve in one system. Configuration (1) is proposed for short-life systems such as that required for the spin-stabilized approach, while Configuration (2) is proposed for all long-life systems associated with the 3-axis stabilized approach. The referenced curves include an allowance for residuals and the redundant tank, so that the impulse ordinate refers to the actual requirement in both cases.

The total impulse requirement of a gas jet system is determined primarily by the fuel usage on the limit-cycle mode. Maneuvering requirements may influence the system design in other ways, but the amount of gas required to perform maneuvers is generally small. The characteristics of the idealized, symmetrical limit-cycle are presented in Figure 3.5-8. With these relationships, the required impulse to support the limit-cycle for each of the three control axes may be determined. The required system impulse is then the sum of these results multiplied by an appropriate factor of safety. The effect of external torques may actually tend to reduce the limit-cycle fuel requirements by lengthening the pulse spacing on one side of the deadband. Accordingly, the limit-cycle fuel requirement is a conservative estimate of the overall requirements, unless unusually large external torques are expected.

LIMIT-CYCLE CHARACTERISTICS

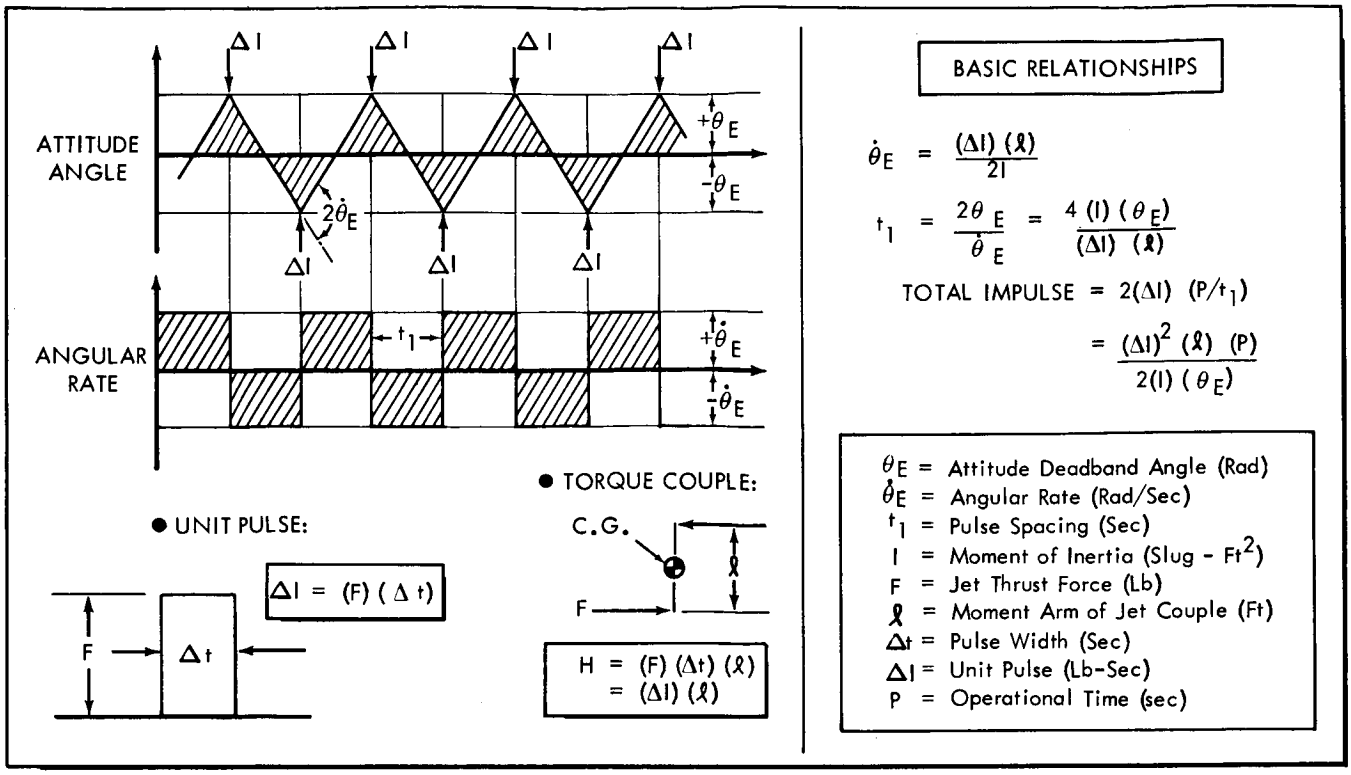


FIGURE 3.5-8

As noted in Figure 3.5-8, the limit-cycle impulse requirement is dependent upon a number of parameters which are under the control of the designer. The most important of these parameters is the unit pulse, ΔI, since it appears as a squared term in the impulse formula. Thus, long-life systems depend upon the achievement of small unit pulses in order to keep the fuel usage to a tolerable level. The requirements to perform manuevers and develop a peak torque for other control purposes generally specifies the jet thrust level, F, so that the unit pulse is dependent upon the pulse width, Δt, that is utilized. For the solenoid-operated valves used on stored gas attitude control thrusters, it is possible to achieve very small pulse widths down to about 0.005 seconds or lower. However, in order to reduce valve power requirements and solenoid weight, and to reduce the gas leakage problem, it is not practical to plan on the lowest value. A pulse width of 0.02 seconds is used herein as a more realistic lower limit.

The moments of inertia and jet moment arms depend upon the configuration approach, and the designer should seek to obtain optimum arrangements. The required lifetime and deadband angle are usually specified as part of the mission requirements.

However, for critical cases where the unit pulse cannot be further reduced, it may be possible to increase the deadband angle over selected regions to alleviate the problem of limit cycle fuel usage.

3.5.5 Design Data For Reaction Wheel System

As the required lifetime of the attitude control system increases, the suitability of the gas jet approach diminishes, at least as a single mode of control. This is due not only to the increased fuel weight required, but also to the greater number of pulses that must be demanded of the system hardware. One possible solution to this problem is the use of a reaction wheel system operating in conjunction with the gas jet system. In this approach, the limit cycle requirement of the gas jet system is removed and it operates mostly on a standby basis and for occasional wheel desaturation. The reaction wheel also provides continuous control to a much finer degree than is possible under the limit cycle concept. It is basically an electric motor with a high-inertia rotor, and designs of satisfactory reliability should be realizable. The bearing problem is a basic limiting factor, but the problems can be reduced by utilizing low RPM, brushless motors, and hermetic sealing.

The reaction wheel system can be designed to give the same peak torque achievable with the limit-cycle gas system, but the peak power requirement will be much larger. This feature may be prohibitive in instances where power is at a premium (i.e., systems relying on batteries or solar panels), but it is not considered a serious drawback in the present concept. Because the large power capacity provided to meet the requirements of the communications and guidance systems is not required continuously, the reaction wheel system will probably require no increase in overall capacity.

The determination of reaction wheel weight and power requirements can be accomplished by the use of generalized data presented in the literature. However, there is sufficient data available on actual designs to constitute a more realistic point of reference. The characteristics of eight designs representative of the type required in this application were used to construct the curves presented in Figure 3.5-9. The weight of a reaction wheel unit is primarily a function of its momentum storage capacity, and the power requirement is primarily a function of its maximum torque capability. The data points indicated in this figure bear out this generalization. Actually, a more accurate analysis

of the problem would indicate that weight and power are each a function of the two basic parameters (momentum and maximum torque). All the data points in this figure are for sealed units with maximum speeds in the range from 900 to 1250 RPM. They range in size from a 6-inch diameter casing with 3-inch thickness to a 12-inch diameter casing with 5-inch thickness. The data refer to a single wheel only, and it is noted that three identical wheels will be required to accomplish 3-axis control. Provision should also be made for additional control electronics and power to accompany each wheel. An allowance of three pounds of electronics weight and one watt of power is recommended for each wheel control.

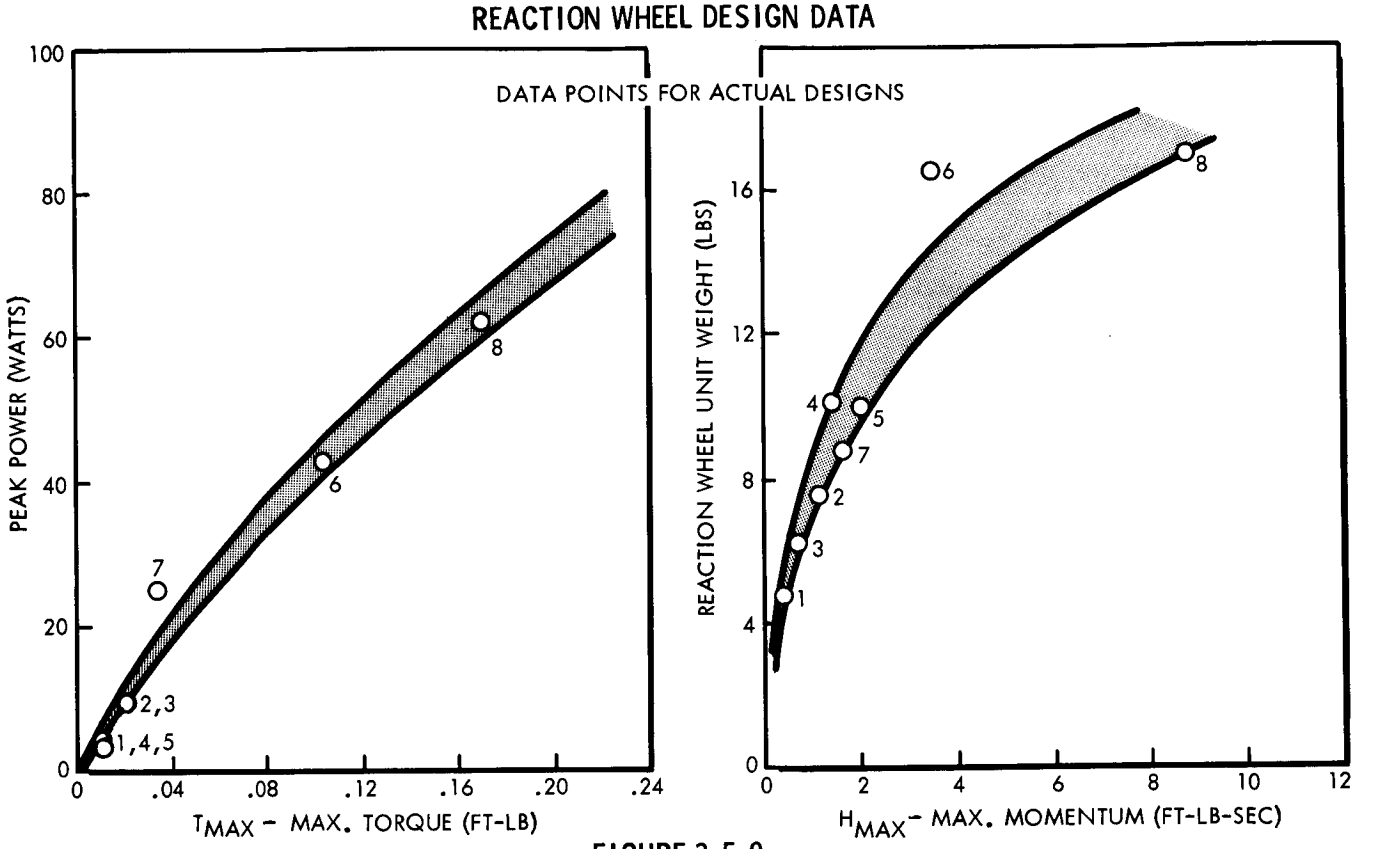


FIGURE 3.5-9

In some quarters, the fluid flywheel has been proposed as a substitute for the reaction wheel. This concept depends on the circulation of a dense liquid, mercury, through a closed-circuit tube so that angular momentum is absorbed in the same manner as in the reaction wheel. The main advantage claimed is improved reliability because of the lack of moving parts; however, there is no apparent weight advantage to be realized. This idea is worth following, but it is considered "novel" at the present time and requires further development. Reaction wheels are presently being used in a number of satellites and are in an advanced stage of development. Thus, they may be considered "state-of-the-art."

3.5.6 Considerations For Three-Axis Stabilization

Three-axis stabilization is required for the more ambitious missions which depend upon orientation control to accomplish navigation, data gathering, communications, and other functions in the most efficient manner. The disturbance torques in interplanetary space are few and relatively insignificant compared to ordinary measures, but they assume importance because of the long time periods over which they act. Therefore, the problem of three-axis stabilization is characterized by its delicacy, and the most important requirement is the achievement of long-term reliability.

The disturbance torques of primary importance in interplanetary space arise because of solar radiation pressure and meteoroid impacts. The solar pressure is an electromagnetic phenomenon and may be thought of as the impingement of photons on an absorbing surface. The Sun also emits a stream of protons moving at velocities that are less than the velocity of light and which constitute the "solar wind". However, the pressure due to total momentum transfer of the solar wind is much smaller than the solar radiation pressure and may be ignored. The meteoroids are mass particles moving in orbits around the Sun and are of primary concern in the region of the Asteroid Belt which must be traversed in a Jupiter mission.

The configuration concept based on the fixed antenna is the most susceptible to the effects of solar torques because of the attitude constraint associated with maintaining the Earth-pointing attitude. For preliminary purposes this problem may be treated in the manner indicated in Figure 3.5-10. The configuration may be envisioned as an equivalent sphere such that the solar force is equal to the product of solar pressure and the spherical area. The design objective is to make the center of pressure of this solar force coincident with the center of gravity so that the torque is nominally zero in all attitudes of interest. However, this objective can only be approached in practice, and it is necessary to make allowances for a certain amount of error. Because of the symmetry of the configuration, it is assumed that both the center of gravity and center of pressure lie on the spacecraft centerline, but with a small offset, $\bar{X}$, between them. The solar torque is then a function of solar aspect angle, α_s, as well as solar radiation pressure, P_s. The magnitude of this torque is small in itself, and it is the time integral of the torque (angular momentum) that is important.

TORQUE DUE TO SOLAR PRESSURE

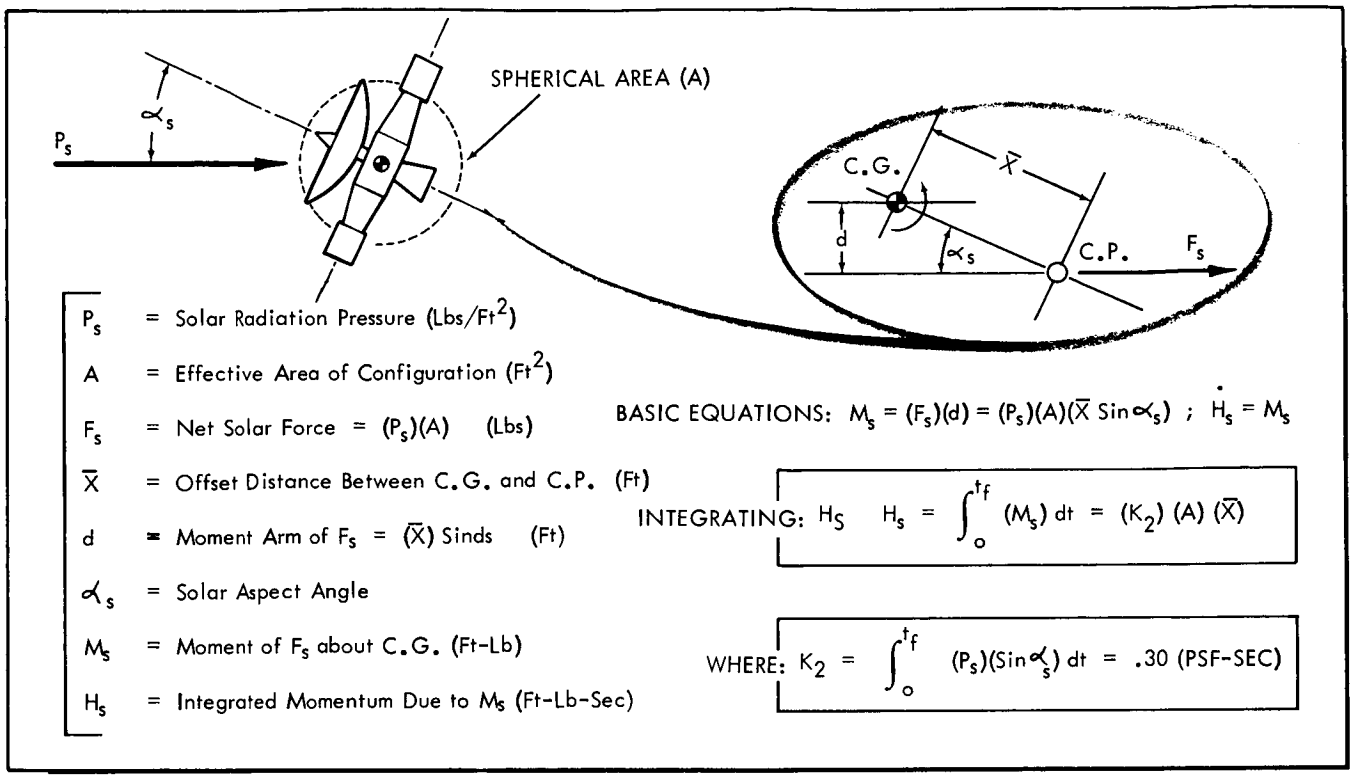


FIGURE 3.5-10

As indicated in Figure 3.5-10, the problem is expressed by the quantity, K_2, which may be evaluated from the trajectory data presented in Figures 3.5-2 and 3.5-3. The integrand of K_2 consists of both plus and minus area contributions because of the fact that α_s changes sign several times during the course of the trajectory. Since the results of this analysis are most applicable to the reaction wheel approach, the value of K_2 was chosen as the largest area segment, irrespective of sign. This value occurs during the first portion of the trajectory (up to about 75 days), and it is about three times larger than the next segment. The rapidly decreasing value of P_s is primarily responsible for this diminishing effect.

The variation of H_s with the parameters A and $\bar{X}$, according to the above result is presented in Figure 3.5-11. In the case of a gas jet system on the limit cycle mode, this requirement would be insignificant and would be lost in the limit cycle impulse. However, for a reaction wheel system, these results are very important, and they determine the momentum storage capacity required of the wheel if saturation is to be avoided. The value of H_s for a typical example is just within the range of a moderate-sized reaction wheel. This result indicates the importance of balancing the configuration to alleviate the solar torque effects when this type of attitude control system is considered.

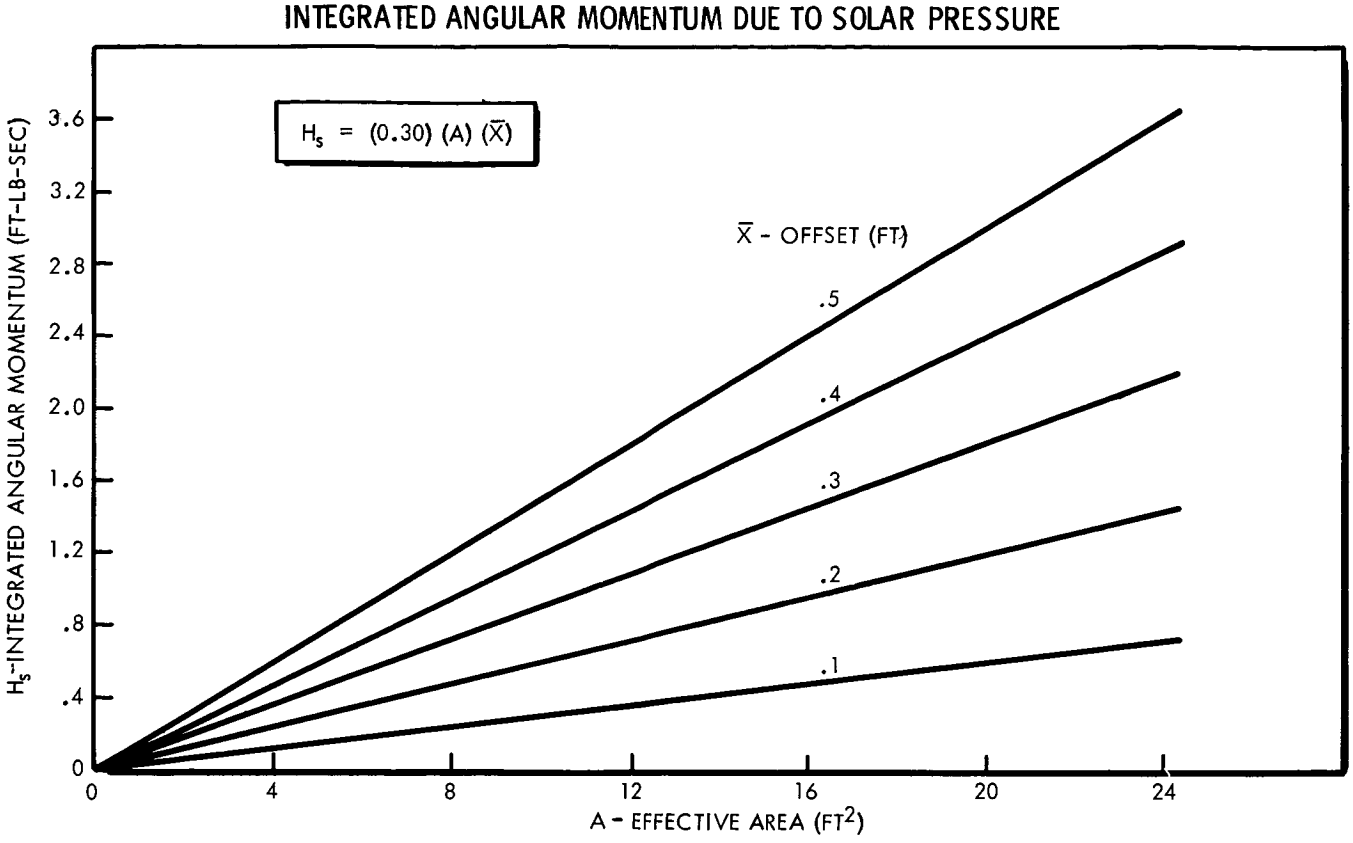


FIGURE 3.5-11

The meteoroid problem is very uncertain because of the lack of direct data on the meteoroid flux and the existence of widely differing assessments of the problem. The impact of a meteoroid with a mass greater than some limiting value must be assumed to be catastrophic, but it is generally agreed that this is a low-probability occurrence. Of greater concern for attitude-control considerations are the more numerous impacts of small particles which do not disable the spacecraft but which introduce disturbance torques. This problem is apparently most pronounced in the Asteroid Belt, but is to be expected throughout the entire mission. Cometary debris constitute the most important source of interplanetary matter outside the Asteroid Belt.

Present estimates of meteoroid flux in the Asteroid Belt are based on extrapolations of the data available from observable objects together with various theoretical guidelines. However, there is room for considerable disagreement, and the minimum and maximum estimates of the meteroid flux differ by many orders of magnitude. This problem is discussed in detail in Section 3.10 where meteoroid protection requirements are considered. Using the most severe predictions presented there, the small-particle flux is predicted to be no greater than about 10^{-9} grams per square meter per second. These particles are assumed to be moving in circular orbits around the Sun, so that their average velocity in the Asteroid Belt region is about 17.5 kilometers per second. The average density of this meteoroid "cloud"

is then given as follows:

$$\rho = \text{Density} = \frac{\text{Mass Flow}}{\text{Velocity}} = \frac{10^{-9}\ g/m^2\text{-sec}}{17.5 \times 10^3\ \text{m/sec}} = .57 \times 10^{-13}\ g/m^3$$

The spacecraft moves through this cloud at some velocity, $\bar{V}$, relative to the particles. This velocity is indicated in Figure 3.5-4 to be about 14.5 kilometers per second (average) for the Asteroid Belt region. Assuming total momentum transfer at impact, the pressure that would be experienced by a flat plate normal to $\bar{V}$ would be defined as follows:

$$\text{Pressure} = (\text{Mass Flow}) \times (\text{Velocity})$$

$$\text{or} \quad P = (\rho\bar{V})\ (\bar{V}) = \rho\ (\bar{V})^2$$

This result is familiar to aerodynamicists and corresponds to the "dynamic pressure". It is seen that the pressure increases as the square of $\bar{V}$, so that results may vary significantly with the particular trajectory. This effect is unlike the solar pressure, which is essentially unaffected by the motion of the spacecraft, because the impinging photons move at a velocity greatly in excess of the spacecraft velocity. Using the figures presented above, the meteoroid pressure is as follows:

$$P = (.57 \times 10^{-13}\ g/m^3)(10^{-6}\ m^3/cm^3)(14.5 \times 10^5\ cm/sec)^2$$

$$= 1.22 \times 10^{-7}\ \text{dynes/cm}^2$$

$$= 1.22 \times 10^{-3}\ \text{dynes/m}^2$$

$$= 2.55 \times 10^{-10}\ \text{lbs/ft}^2$$

For comparison, the value of solar radiation pressure in the Asteroid Belt is about 1.1×10^{-8} pounds per square foot (see Figure 3.5-2). Thus, the solar radiation pressure is greater than the meteoroid dynamic pressure by a factor of about 43.

On the basis of these results, the effect of micrometeoroids on the attitude control problem is small enough to be ignored. It should be noted, however, that if the meteoroid flux is revised upward several orders of magnitude, the reverse is true. It is likely that this situation will not be further clarified until the first probe is launched, and actual measurements are undertaken. In the meantime, the designer should make whatever allowances are permissible without undue compromise and take comfort in the fact that the most reasonable estimates of the problem indicate no cause for concern.

Although the integrated effect of micrometeoroids is apparently unimportant, the effect of discrete, non-destructive impacts by particles of larger size constitutes an important criteria in the control system design. It is desired that the control system have the capability of responding to such an occurrence without losing the "lock" of its electromagnetic sensors (Sun sensors, Canopus star-tracker, and Jupiter sensor). This requirement specifies the maximum control system torque capability that must be provided.

It is assumed that the impact phenomenon is described by the case of simple momentum transfer, or:

Angular Impulse = (Linear Impulse) x (Moment Arm)

= (Mass) x (Velocity) x (Moment Arm)

Values of meteoroid mass in the region around 1/10 gram are of primary interest for this problem, with an impact velocity of about 14.5 kilometers per second. Figure 3.5-12 presents the variation of angular impulse, according to this formula, as a parametric function of meteoroid mass and moment arm between the spacecraft center of gravity and the point of impact. The results were converted to engineering units for ease in use. The recommended design value for angular impulse, H_M, is 0.7 foot-pound-seconds, which corresponds approximately to the impact of a mass of 1/10 gram at a distance of 2 feet from the center of gravity. This value was selected somewhat arbitrarily and is subject to future modification.

The meaning of the above result in terms of the maximum torque requirement can be determined by a simple response analysis. The meteoroid impulse corresponds to an initial angular rate which varies with the spacecraft moment of inertia. It is assumed that maximum control system torque will be commanded immediately after the disturbance, and that this torque is maintained until the angular rate is reduced to zero. The attitude excursion associated with this maneuver is not to exceed some specified limit, θ_F. The value of torque required to meet these conditions is found to be as follows:

$$T_{MAX} = \frac{H_M^2}{2\,(I)\,(\theta_F)}$$

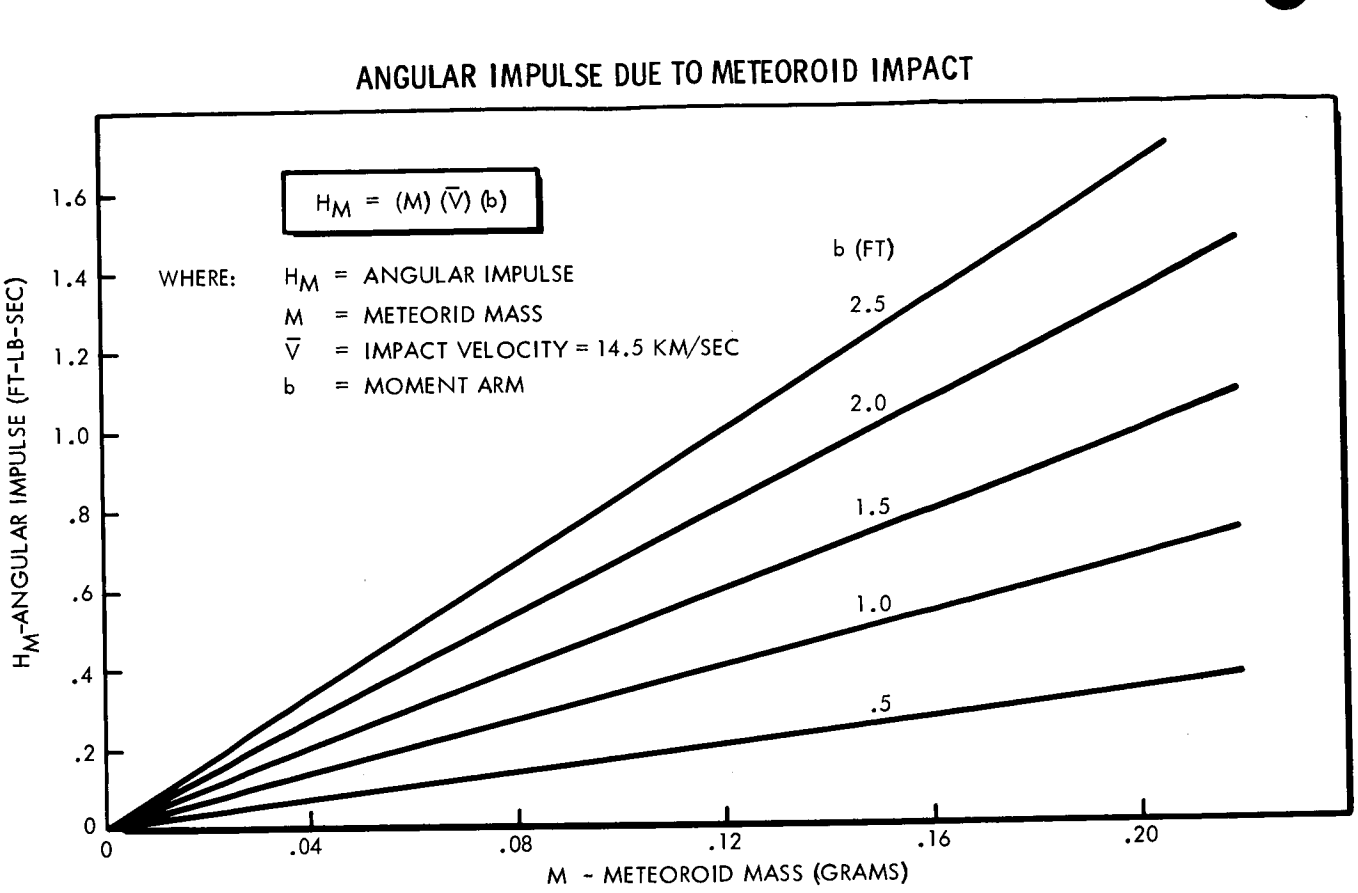


FIGURE 3.5-12

where: T_{MAX} = Maximum Torque (Ft-lbs)

H_M = Angular Impulse (Ft-lb-sec)

I = Moment of Inertia (Slug-Ft^2)

θ_F = Attitude Angle Limit (Rad)

It is to be noted that the torque requirement varies with the square of the meteoroid angular impulse, so that the result is sensitive to the particular assumptions made in regard to meteoroid mass and impact moment arm.

For the reaction wheel system, the above-described torque requirement directly affects the peak power requirement and indirectly affects the wheel weight requirement through motor size. For the gas-jet system, the torque requirement determines the thrust level of the gas jets, which indirectly affects the whole system design. The maximum torque for a pulse-jet system of the type contemplated is realized when maximum pulse rate is commanded. An effective torque must be dealt with in this case because of the discontinuous operation of the jets. In this study, it is assumed that the interval between

successive pulses is about twice the pulse width (for the short pulse widths of interest) so that the maximum torque is given as follows, using the terms defined in Figure 3.5-8:

$$T_{MAX} = \frac{1}{3} (F) (\ell)$$

$$\text{or } F = \frac{3 (T_{MAX})}{\ell}$$

By using this as a starting point, the remaining characteristics of the gas jet system may easily be determined.

One final item of interest is the disturbance torque that is likely to be encountered in the vicinity of Jupiter due to interaction between Jupiter's magnetic field and that of the spacecraft. It was assumed in a preliminary estimate that the magnetic field of Jupiter is 10 Gauss with the spacecraft field set at 50×10^{-6} Gauss (50 γ). The magnetic torque for a spacecraft volume of 1 cubic meter is thus calculated to be 5×10^{4} Dyne-centimeters, or 4×10^{-3} foot-pounds. The maximum control torque capability to be provided is almost two orders of magnitude greater than the above figure, as indicated in Section 5. Thus, this problem is not regarded as important, especially since the disturbance torque is only of short duration.

3.6 PROPULSION

In this subsection the results of the studies of the two propulsion subsystems required to perform Jupiter Flyby Missions are described. These are the midcourse correction propulsion and the attitude control propulsion subsystems.

3.6.1 Midcourse Propulsion Subsystem

The functional requirements of a Jupiter flyby spacecraft midcourse propulsion subsystem are similar in most respects to the functional requirements for the Mariner IV midcourse propulsion subsystem. Like its Mariner predecessor, the Jupiter Flyby propulsion subsystem must be capable of (1) providing a desired velocity increment to the vehicle, (2) operating at a predictable thrust level, and (3) providing two controlled-interval thrusts. The unit must be capable of repeatable ignition, operation, and shutdown in a hard vacuum and gravity-free environment, and must be able to satisfy space storage requirements with regard to materials compatibility, propellant stability, negligible fluids leakage and avoidance of vacuum cold welding of movable component parts. In addition, it is required that proper orientation of the thrust vector be maintained during a propulsion maneuver so that trajectory errors arising from the maneuver itself are held to a minimum.

A number of propulsion system types are theoretically capable of satisfying the functional requirements of the Jupiter flyby midcourse maneuver. Such types might be broadly categorized according to their primary energy source as electrical, nuclear, or chemical. Within each of these major categories, a great number of propulsion options exist. The typical electrical types would include the electrostatic (ion) engine, electrothermal (arcjet or resistojet) engine, and the electromagnetic (plasma) engine. Nuclear types include the nuclear reactor and radioisotope-heated units, and the chemical types include cold gas, mono-, bi- and tri-propellant, hybrid, hypergolic subliming solids and thixotropic gel systems.

Each of the above systems has its own peculiar advantages and disadvantages, and each was evaluated on the basis of its applicability to the Jupiter flyby midcourse maneuver. From an evaluation on the basis of current development status, proven performance, power required, simplicity, and cost, the monopropellant hydrazine and earth-storable liquid bipropellant systems were determined to be most suitable. Of these two systems, the monopropellant

hydrazine unit is clearly superior both in weight and simplicity to a typical bipropellant unit for applications where the spacecraft mass is low and the velocity increments required are small. For applications where larger total impulses are involved, a bipropellant system offers potential weight and volume savings, but compromises simplicity. These statements are admittedly very general. It is interesting to note, however, that the hydrazine propulsion systems aboard all Mariner and Ranger vehicles weighed in each case less than 10 percent of the total payload weight. Viewed in this context, it is reasonable to inquire whether weight savings obtained by the use of a bipropellant system can ever be justified in comparable Jupiter flyby vehicles when the overall reliability is impaired as a result. It is an objective of this study, nevertheless, to investigate both a hydrazine and a typical bipropellant system in order to (1) provide individual system design data and (2) illuminate those criteria which could influence the selection of one or the other type system.

At this point in the study, investigation of the hydrazine system is essentially complete. A basic hydrazine system configuration was defined, analyses were performed, and system sizing data were generated. These efforts are reported in the paragraphs which follow. An analogous investigation of a conservative bipropellant system (IRFNA-MMH) is currently in progress. The results of this investigation will be submitted in the final report.

3.6.1.1 Description of the Basic Hydrazine Subsystem

The basic hydrazine configuration adopted for this study is shown schematically in Figure 3.6-1 together with an itemized listing of pertinent components and instrumentation. The configuration shown is based largely on the successful Mariner IV design with some notable exceptions that will be described later.

A provision is made in the basic design for two controlled-interval thrusts. This is accomplished by the inclusion of two full-on, full-off flow control channels in both the propellant pressurization and propellant feed subsystems. For each thrust application (start and shutdown), four squib valves must be activated. Thus, a requirement for an additional thrust maneuver (three in all) would necessitate the addition of four more squib valves to the basic design along with associated accessory equipment. Because of the comparatively low weight of each additional squib, a modification of this type would have slight effect on the overall subsystem weight estimates in this report.

The basic subsystem in the schematic is a prepressurized, gas-pressure-regulated, constant-thrust device employing nitrogen as the pressurant and hydrazine as the propellant. During operation, nitorgen passes through a pressure regulator and displaces propellant from the propellant tank by the deformation of a butyl rubber bladder. The hydrazine flows to the rocket motor where it is decomposed spontaneously into thrust gases upon surface contact with a Shell 405-type catalyst mounted in the chamber. No auxiliary injection of a liquid propellant start slug (such as nitrogen tetroxide) is required to initiate hydrazine decomposition.

In a typical operation of the basic system, the sequence of events involved in the initial rocket firing would be as follows:

1. Upon the receipt of a start signal from the onboard computer, the normally closed, explosively actuated squib valves (7) and (19) (see Figure 3.6-1) are simultaneously activated, resulting in regulated pressurization of the hydrazine tank and a flow of hydrazine to the thrust chamber.

2. Catalytic decomposition of the hydrazine takes place in the chamber, and thrust is produced.

3. At a signal from the onboard computer to terminate rocket thrust, the normally open, explosively actuated squib valves (5) and (17) are simultaneously activated, resulting in isolation of the high pressure gas reservoir from the primary pressure regulator (9) and termination of propellant flow to the thrust chamber.

Should a second propulsion maneuver be required, the sequence of events is functionally the same. In this case, the normally closed squib valves (6) and (22) are activated in order to start thrusting, and the normally open squib valves (4) and (20) are activated to terminate thrust.

It should be noted that because the propellant tank is prepressurized only one start signal is required to commence the first maneuver. This signal activates valves (7) and (19) simultaneously, and the result is an almost immediate production of nominal thrust.

If the tank were not prepressurized, sequencing would be required to allow for regulator flow to increase the pressure in the tank up to the working level before the propellant start valve could be activated.

During each maneuver of the basic subsystem, only four valves are fired to accomplish complete engine start and shutdown as compared to the five valves required for the same purpose on Mariner IV. This is due to the fact that an additional valve was required on Mariner IV for flow control of the N_2O_4 start slug used to commence hydrazine decomposition. Use of the recently developed Shell catalyst in the present design obviates the need for hypergolic slug starting and thereby eliminates the need for a slug control valve, the slug propellant itself, and its supporting flow and sequencing circuitry.

Substantial redundancy for the first propulsion maneuver is provided by the two-start capability of the basic configuration and by the inclusion of certain additional features not found on Mariner IV. In effect, the failure of a valve to open or close during the first maneuver may be remedied by the activation of an analogous valve in the second maneuver circuit. This is demonstrated in Table 3.6-1, which lists some critical failure modes of components involved in the first maneuver together with their effects and backup measures afforded by the present design. Of course, by implementing the second maneuver circuitry as backup against a valve failure during a first maneuver, the capability for a second maneuver is either impaired or lost. This fact would probably necessitate additional redundancy within the subsystem for those applications where a second firing, such as a terminal maneuver, is mandatory.

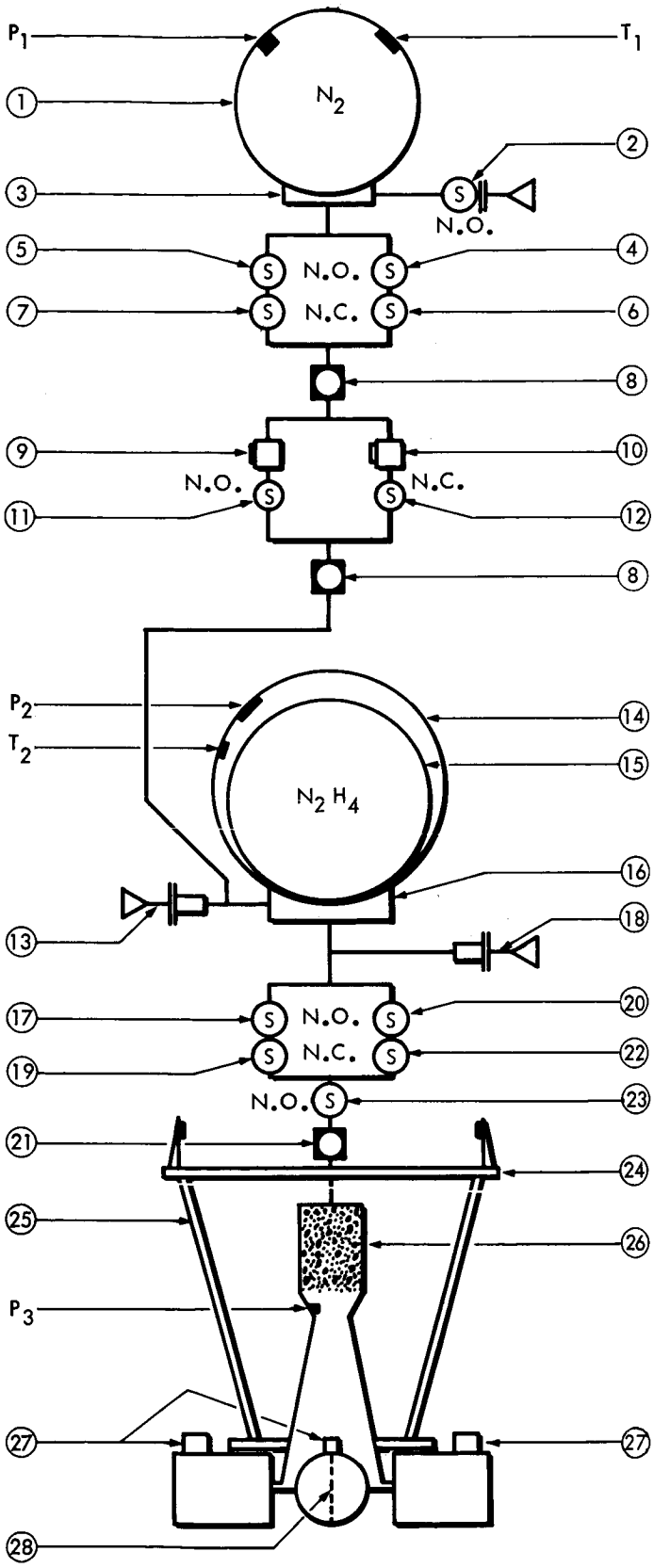
The basic propulsion subsystem, as in the Mariner IV system, would employ nitrogen gas pressurant, gas pressure regulation, hydrazine propellant, bladder expulsion, and jet vane thrust vector control. Considerations of performance and reliability justify the retention of these features. The present design would also employ, as did Mariner, a number of "ganged" explosive-actuated squib vanes, characterized by parallel branches of normally closed (start) and normally open (shutdown) squib valves mounted in series (see Figure 3.6-1). This type of valve arrangement is recommended because it provides positive isolation of both pressurant and propellant flow, contributes to overall system reliability, and precludes, at least in the propellant feed circuit, the hazard of vacuum cold welding.

The most significant difference between the two propulsion subsystems lies in the means employed to initiate hydrazine decomposition. The basic subsystem presented here would use the spontaneous Shell hydrazine catalyst (now at an acceptable level of development) in lieu of the JPL type H-7 catalyst used on Ranger and Mariner. Use of the former catalyst would eliminate

Table 3.6-1 CRITICAL FAILURE MODES, EFFECTS AND BACKUP - FIRST MANEUVER SEQUENCE

No.	Failure Mode	Effect	Backup
	Start No. 1		
1	Valve (7) fails to open	No regulated pressurization of propellant tank	Activate second start valve (6)
2	Valve (19) fails to open	No propellant flow to rocket motor	Activate second start valve (22)
3	Regulator (9) malfunction	Regulates too high or too low, sticks closed	Activate valves (11) and (12)
	Shutdown No. 1		
4	Valve (5) fails to close	Potential pressure buildup in propellant tank due to gas seepage across regulator	Activate primary regulator close valve (11)
5	Valve (17) fails to close	Propellant flow (and thrusting) continues via propellant tank blowdown. Excessive ΔV produced.	Activate redundant shutdown valve (23)

SCHEMATIC DIAGRAM OF THE BASIC HYDRAZINE SUBSYSTEM



COMPONENTS

1	High pressure gas reservoir
2	N_2 fill port and closure valve
3	High pressur e reservoir manifold
4	N.O. squib valve, N_2 shutdown No. 2
5	N.O. squib valve, N_2 shutdown No. 1
6	N.C. squib valve, N_2 start No. 2
7	N.C. squib valve, N_2 start No. 1
8	Filter
9	Pressure regulator, primary
10	Pressure regulator, secondary
11	N.O. squib valve, primary reg. close
12	N.C. squib valve, secondary reg. start
13	Propellant prepressure, fill port
14	Propellant tank
15	Propellant bladder
16	Propellant tank manifold
17	N.O. squib valve, prop. shutdown No. 1
18	Propellant fill and drain port
19	N.C. squib valve, prop. start No. 1
20	N.O. squib valve, prop. shutdown No. 2
21	Filter
22	N.C. squib valve, prop. start No. 2
23	N.O. squib valve, prop. shutdown
24	Thrust plate & tank support structure
25	Jet vane actuator support structure
26	Rocket motor and catalyst bed
27	Jet vane actuators (4)
28	Jet vanes (4)

INSTRUMENTATION

P_1	Nitrogen tank pressure
P_2	Propellant tank pressure
P_3	Thrust chamber pressure
T_1	Nitrogen tank temperature
T_2	Propellant tank temperature

FIGURE 3.6-1

the cumbersome start apparatus associated with the Ranger and Mariner systems and provide some gain in system weight and operational simplicity.

Additional differences between the basic propulsion subsystem design and that of Mariner IV take the form of the following:

- A redundant pressure regulator (10) (see Figure 3.6-1) and squib valves (11) and (12) would be incorporated in the pressurization subsystem. The squib valves would be used to transfer nitrogen gas regulation from the primary regulator (9) to regulator (10) in the event of primary regulator malfunction. Valve (11) could also be activated independently to isolate the high pressure reservoir from the propellant tank in the event that shutdown valve (5) failed to close at the conclusion of the first propulsion maneuver.

- Incorporation of a redundant propellant shutdown valve (23) in the propellant feed system. This feature would provide backup against the failure of shutdown valve (17) to close at the conclusion of the first maneuver. Following a successful first maneuver, backup would then be available also against failure of valve (20) to close at the conclusion of a possibly required second maneuver.

A weight breakdown of the fixed hardware in the basic hydrazine subsystem is presented in Table 3.6-2. The term "fixed hardware" comprises those components whose weights are not drastically altered by changes in the total impulse required. Stated differently, the weight of a fixed hardware component is considered essentially constant for a given thrust level or for a particular design parameter such as operating pressure, line size, or rate of flow. The constituents of the subsystem whose weights are not fixed but vary with total impulse include the propellant, pressurant, bladder, and all tankage.

By using this technique of isolating subsystem elements into either fixed hardware or total impulse-variant categories, the subsystem sizing effort presented in the next paragraphs was greatly simplified. Weight estimates of all fixed hardware contained herein were obtained from in-house and Mariner IV experience, as well as manufacturers' published data.

Table 3.6-2 WEIGHT BREAKDOWN OF SUBSYSTEM FIXED HARDWARE

Item	Estimated Weight - lb
Nitrogen fill port and closure valve	0.10
High pressure reservoir manifold	0.50
Squib valve, nitrogen shutdown, No. 2	0.13
Squib valve, nitrogen shutdown, No. 1	0.13
Squib valve, nitrogen start, No. 2	0.13
Squib valve, nitrogen start, No. 1	0.13
Filter (2)	0.20
Pressure regulator, primary	1.20
Pressure regulator, secondary	1.20
Squib valve, primary regulator shutdown	0.13
Squib valve, secondary regulator start	0.13
Prepressurization fill port	0.10
Propellant tank manifold	1.10
Squib valve propellant shutdown, No. 1	0.13
Propellant fill and drain port	0.10
Squib valve, propellant start, No. 1	0.13
Squib valve, propellant shutdown, No. 2	0.13
Filter	0.15
Squib valve, propellant start, No. 2	0.13
Squib valve, propellant shutdown (redundant)	0.10
Thrust plate and tank support structure	3.70
Jet vane actuator support structure	0.80
Rocket motor and catalyst bed	2.50
Jet vane actuators (4)	2.10
Jet vanes (4)	0.20
Cabling	2.10
Misc. mounting brackets, fasteners, etc.	1.30
Pressure (3) and temperature (2) transducers	1.15
Total Weight	19.90

3.6.1.2 Parametric Analysis

A detailed parametric analysis of the monopropellant hydrazine subsystem is presented in Appendix C. This analysis forms the basis for the propulsion subsystem weight and volume data which are presented in subsection 3.6.1.3. Table 3.6-3 contains the nomenclature to be used and a summary of the primary equations that are developed in Appendix C.

Table 3.6-3 MIDCOURSE CORRECTION PROPULSION SUBSYSTEM - NOMENCLATURE AND EQUATION SUMMARY

Nomenclature

Symbol	Description	Units
W_{system}	Total weight of the subsystem	lb_m
W_H	Total weight of hydrazine required	lb_m
W_{H_1}	Expected hydrazine consumption	lb_m
W_{H_2}	Hydrazine contingency for I_{sp} degradation	lb_m
W_{H_3}	Hydrazine contingency for ΔV reserve	lb_m
W_{H_4}	Hydrazine contingency for bladder expulsion inefficiency	lb_m
$W_{S/C}$	Total weight of the spacecraft	lb_m
W_{H_T}	Weight of hydrazine tank	lb_m
W_{ACC}	Weight of tank accessories (welds, bosses, etc.)	lb_m
W_{weld}	Weight due to weldment	lb_m
W_{PG}	Weight of pressurant gas	lb_m
W_{PG_T}	Weight of pressurant gas tank	lb_m
W_B	Weight of expulsion bladder	lb_m
W_{COM}	Total weight of fixed hardware (i.e., valves, regulators, tubing, etc.)	lb_m

Table 3.6-3 MIDCOURSE CORRECTION PROPULSION SUBSYSTEM - NOMENCLATURE AND EQUATION SUMMARY

(Sheet 2)

Symbol	Description	Units
W_{PL}	Weight of non-propulsive payload	lb_m
I_T	Total impulse required	$lb_f \cdot sec$
I_{SP}	Specific impulse	$lb_f \cdot sec/lb_m$
ΔV	Velocity increment required	ft/sec
g	Gravitational constant	$lb_m \cdot ft/lb_f \cdot sec^2$
α_H	Contingency factor for I_{SP} degradation	--
$(\frac{\delta \Delta V}{\Delta V})$	Contingency factor for ΔV reserve	--
ϵ	Bladder expulsion efficiency	--
P_D	Hydrazine or pressurant tank design pressure (at maximum anticipated temperature)	$lb_f/in.^2$
P_{PPG}	Initial pressure of the prepressurant gas in the hydrazine tank	$lb_f/in.^2$
P_T	Hydrazine tank working pressure	$lb_f/in.^2$
P_{PG_i}	Initial storage pressure of pressurant gas	$lb_f/in.^2$
P_{PG_f}	Final storage pressure of pressurant gas	$lb_f/in.^2$
V_H	Hydrazine volume (at 70°F)	$in.^3$
V_{H_T}	Hydrazine tank volume	$in.^3$
V_{UL}	Ullage volume	$in.^3$
V_B	Bladder material volume	$in.^3$

Table 3.6-3 MIDCOURSE CORRECTION PROPULSION SUBSYSTEM - NOMENCLATURE AND EQUATION SUMMARY

(Sheet 4)

Symbol	Description	Units
R	Pressurant gas constant	in. lb_f/lb_m ^oR
k	Ratio of specific heats of pressurant gas	--

Equation Summary

(1) $$W_{SYSTEM} = W_H + W_{H_T} + W_{PG} + W_{PG_T} + W_{COM} + W_B$$

(2) $$W_H = \frac{W_{S/C}}{\epsilon}\left[1 - e^{-\frac{\Delta V}{I_{SP} g}}\right]\left\{1 + \alpha_H + \left(\frac{\delta \Delta V}{\Delta V}\right)\frac{\left(\frac{\Delta V}{I_{SP} g}\right)}{\left(e^{\frac{\Delta V}{I_{SP} g}} - 1\right)}\right\}$$

(11) $$W_{H_T} = 1.5 P_{PPG}\left(\frac{T_{MAX}}{T_o}\right)\left(\frac{\rho}{\sigma}\right)_{MAT}(S.F.)V_H\left\{\frac{1.02 + \chi}{1 - \left(\frac{\Delta N}{N_o}\right)\frac{1}{\chi}}\right\}\left[1 + \frac{22.7(S.F.)P_{PPG}T_{MAX}}{\left\{1 - \left(\frac{\Delta N}{N_o}\right)\frac{1}{\chi}\right\}T_o \sigma_{MAT}}\right] + 0.35$$

(12) $$W_{PG} = \frac{P_T W_H}{R T_o \rho_H}\left[\frac{K}{1 - \left(P_{PG_f}/P_{PG_i}\right)}\right]$$

(14) $$W_{PG_T} = 1.5 W_{PG} R T_{MAX}\left(\frac{\rho}{\sigma}\right)_{MAT}(S.F.)\left[1 + \frac{8.5(S.F.)P_{PG_i}T_{MAX}}{T_o \sigma_{MAT}}\right] + 0.35$$

(16) $$W_B = 44.3 (W_H)^{0.667} t_B \rho_B$$

$$W_{COM} = 19.90 \text{ lb}_m$$

3.6.1.3 Subsystem Parametric Sizing

Parametric sizing of the basic hydrazine subsystem was undertaken to accomplish two main objectives: (1) to provide immediate support for spacecraft weight, packaging, and conceptual design studies, and (2) to provide a format for the comparison of the basic hydrazine subsystem with any alternate propulsion concepts.

Sizing of the basic hydrazine subsystem proceeded in three discrete steps from the equations presented in subsection 3.6.1.2. First, a required weight of hydrazine was postulated, and from the appropriate equations, the estimated weight of subsystem fixed hardware and pertinent design data, a corresponding total subsystem weight was derived. This procedure was repeated for several values of required hydrazine weight and resulted in the graphical plot presented in Figure 3.6-2. The use of appropriate equations and design data resulted also in the tank size information presented graphically in Figure 3.6-3.

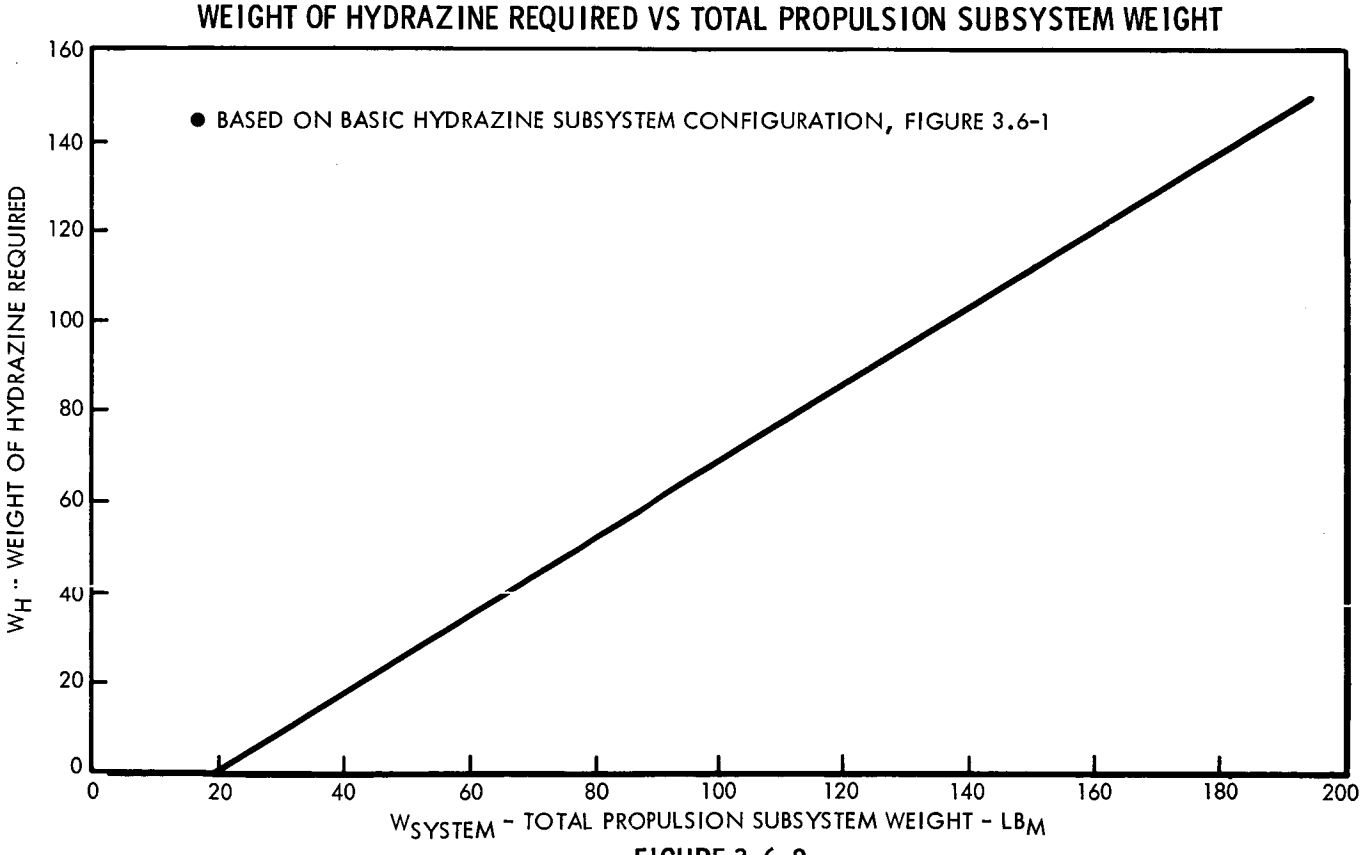


FIGURE 3.6-2

SPHERICAL TANK DIAMETER VS. WEIGHT OF HYDRAZINE REQUIRED

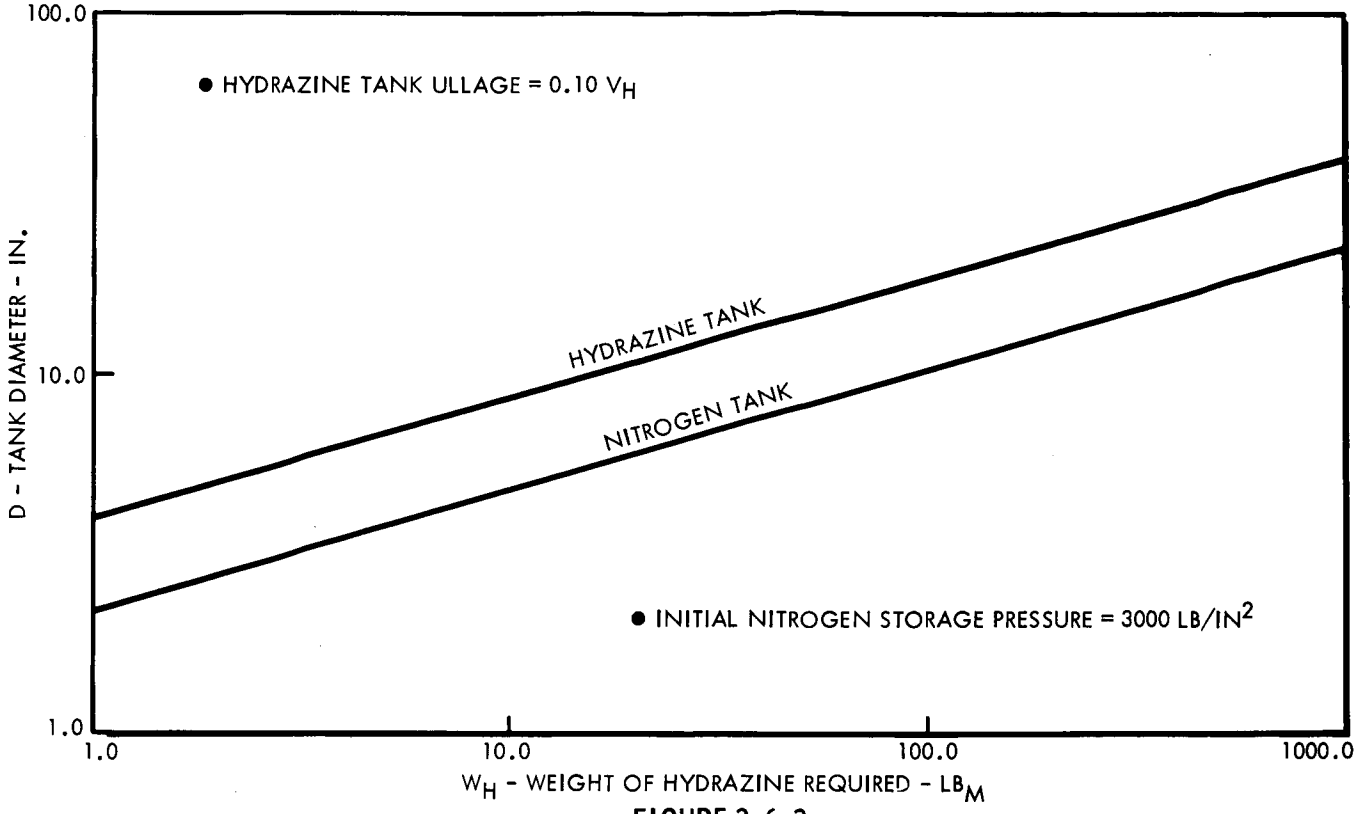


FIGURE 3.6-3

Second, the equation expressing the ratio of required hydrazine weight to total spacecraft weight was solved for a series of total velocity increments ranging from 100 to 500 feet per second. This equation, identified as Equation (2) in the earlier analysis, is rewritten below.

$$\frac{W_H}{W_{S/C}} = \frac{1}{\epsilon}\left[1 - e^{\frac{-\Delta V}{I_{sp} g}}\right]\left\{1 + \alpha_H + \left(\frac{\delta \Delta V}{\Delta V}\right)\frac{\left(\frac{\Delta V}{I_{sp} g}\right)}{\left(e^{\frac{\Delta V}{I_{sp} g}} - 1\right)}\right\}$$

Next, total spacecraft weights ranging from 200 to 2000 pounds were assumed, so that the weight of hydrazine required to attain a particular velocity increment was determined. With the required weight of hydrazine known, Figure 3.6-2 provided the total weight of the subsystem which, in turn, provided the weight of the non-propulsive payload from the relation:

$$W_{PL} = W_{S/C} - W_{System}$$

The results of the preceding effort are presented graphically in Figures 3.6-4, 3.6-5, and 3.6-6 for the range of values investigated.

The design data presented in Table 3.6-4 were adopted for sizing of the basic hydrazine subsystem.

Table 3.6-4 DESIGN DATA

GENERAL

Nominal thrust	50 lb_f
Propellant	Anhydrous Hydrazine
Specific impulse (area ratio 44:1)	233 $lb_f \cdot sec/lb_m$
Pressurant	Nitrogen
Fixed hardware weight	19.90 lb_m
Thrust vector control	Jet vanes

MATERIALS

Propellant tank	Titanium Alloy 6AL-4V
Pressurant tank	Titanium Alloy 6AL-4V
Propellant bladder	Butyl rubber compound
Tank configurations	Spherical
Rocket nozzle	Haynes Alloy No. 25
Catalyst bed	Iridium on Alumina (Shell 405)

Constants

Symbol	Description	Assigned Value
α_H	I_{sp}	0.05
$(\frac{\delta \Delta V}{\Delta V})$	ΔV reserve contingency factor	0.05

Table 3.6-4 DESIGN DATA

(Sheet 2)

Symbol	Description	Assigned Value
P_{PPG}	Pressure of prepressurant gas	270 $lb_f/in.^2$
P_T	Hydrazine tank working pressure	320 $lb_f/in.^2$
P_{PG_i}	Initial nitrogen tank pressure	3000 $lb_f/in.^2$
P_{PG_f}	Final nitrogen tank pressure	600 $lb_f/in.^2$
P_D	Nitrogen tank design pressure (at maximum anticipated temperature)	3540 $lb_f/in.^2$
P_D	Hydrazine tank design pressure (at maximum anticipated temperature)	513 $lb_f/in.^2$
P_C	Chamber pressure	200 $lb_f/in.^2$
(S.F.)	Design safety factor	2.2
χ	Ullage factor (fraction of hydrazine volume)	0.10
T_{max}	Maximum anticipated temperature	165°F
T_o	Initial temperature	70°F
ϵ	Bladder expulsion efficiency	0.98
R	Nitrogen gas constant	660 in. lb_f/lb_m °R
ρ_{mat}	Density of tank material (Ti-6AL-4V)	0.16 $lb_m/in.^3$
σ_{mat}	U.T.S. of tank material (Ti-6AL-4V)	16500 $lb_f/in.^2$
ν_o	Hydrazine specific volume at 70°F	27.70 $in.^3/lb_m$
$\Delta\nu$	Change in hydrazine specific volume due to thermal expansion (from 70°F to 165°F)	1.053 $in.^3/lb_m$
t_B	Bladder material thickness	0.030 in.
ρ_B	Density of bladder material	0.05 $lb_m/in.^3$

Table 3.6-4 MIDCOURSE CORRECTION PROPULSION SUBSYSTEM - NOMENCLATURE AND EQUATION SUMMARY

(Sheet 3)

Symbol	Description	Units
V_{PG}	Pressurant gas volume	$in.^3$
ΔV_{EXP}	Change in hydrazine volume due to thermal expansion	$in.^3/lb_m$
Δv	Change in hydrazine specific volume due to thermal expansion (to max. temp.)	$in.^3/lb_m$
v_o	Hydrazine specific volume (at 70^oF)	$in.^3/lb_m$
χ	Ullage factor = $\frac{V_{UL}}{V_H}$	--
(S.F.)	Design safety factor	--
T_{max}	Maximum anticipated temperature	^oR
T_o	Initial temperature	^oR
ρ_H	Hydrazine density (at 70^oF)	$lb_m/in.^3$
ρ_{mat}	Density of tank material	$lb_m/in.^3$
ρ_B	Density of bladder material	$lb_m/in.^3$
σ_{mat}	Ultimate tensile strength of material	$lb_f/in.^2$
t_T	Nominal tank wall thickness	in.
t_W	Maximum thickness of weld buildup	in.
t_B	Bladder material thickness	in.
K_1	Arbitrary constant	--
θ	Taper angle of weld buildup	deg
w	Width of weld buildup section	in.
D_B	Bladder diameter	in.
D	Tank diameter	in.

PROPULSION SUBSYSTEM WEIGHT VS PAYLOAD WEIGHT*

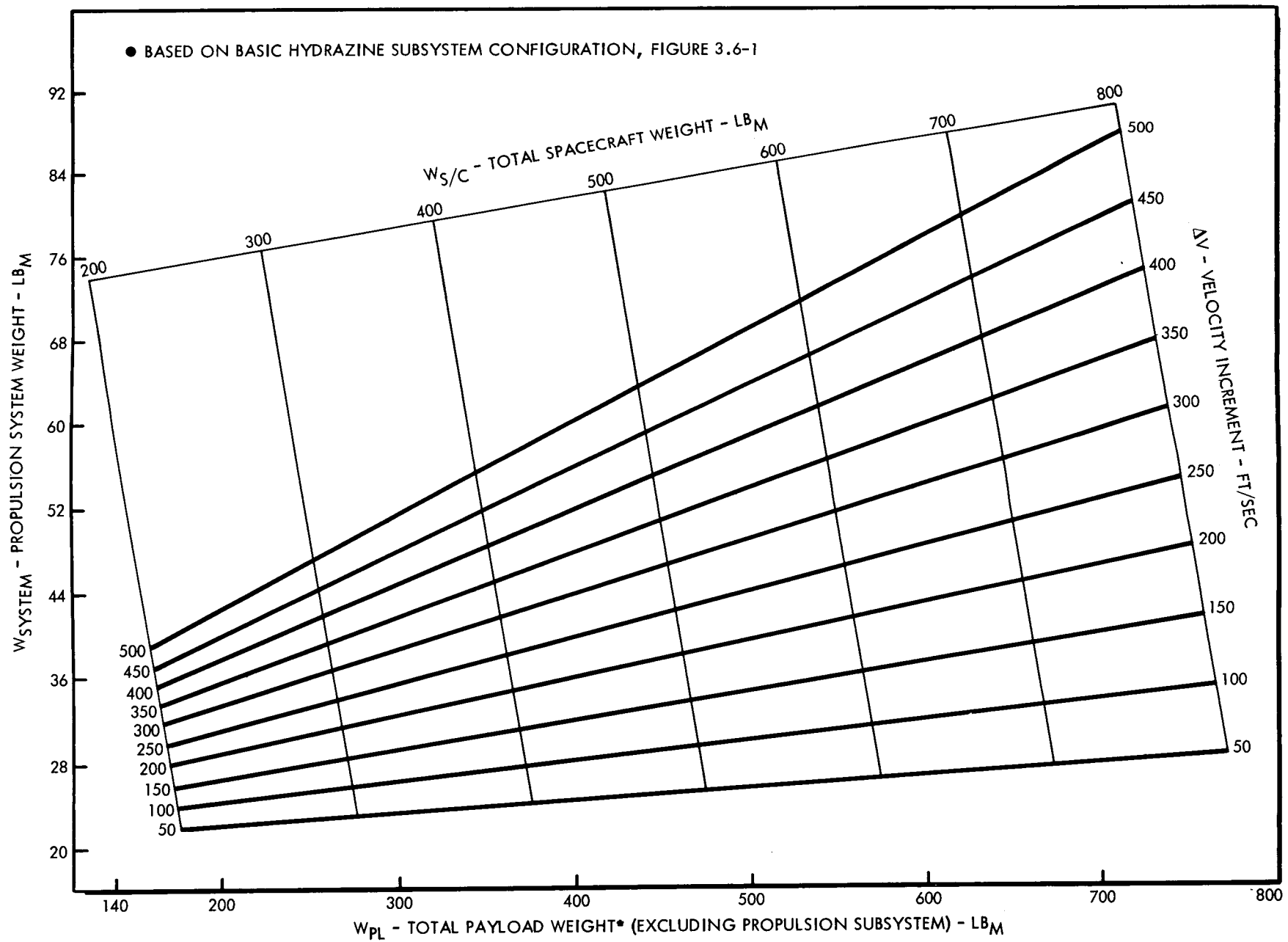


FIGURE 3.6-4

PROPULSION SUBSYSTEM WEIGHT VS. PAYLOAD WEIGHT*

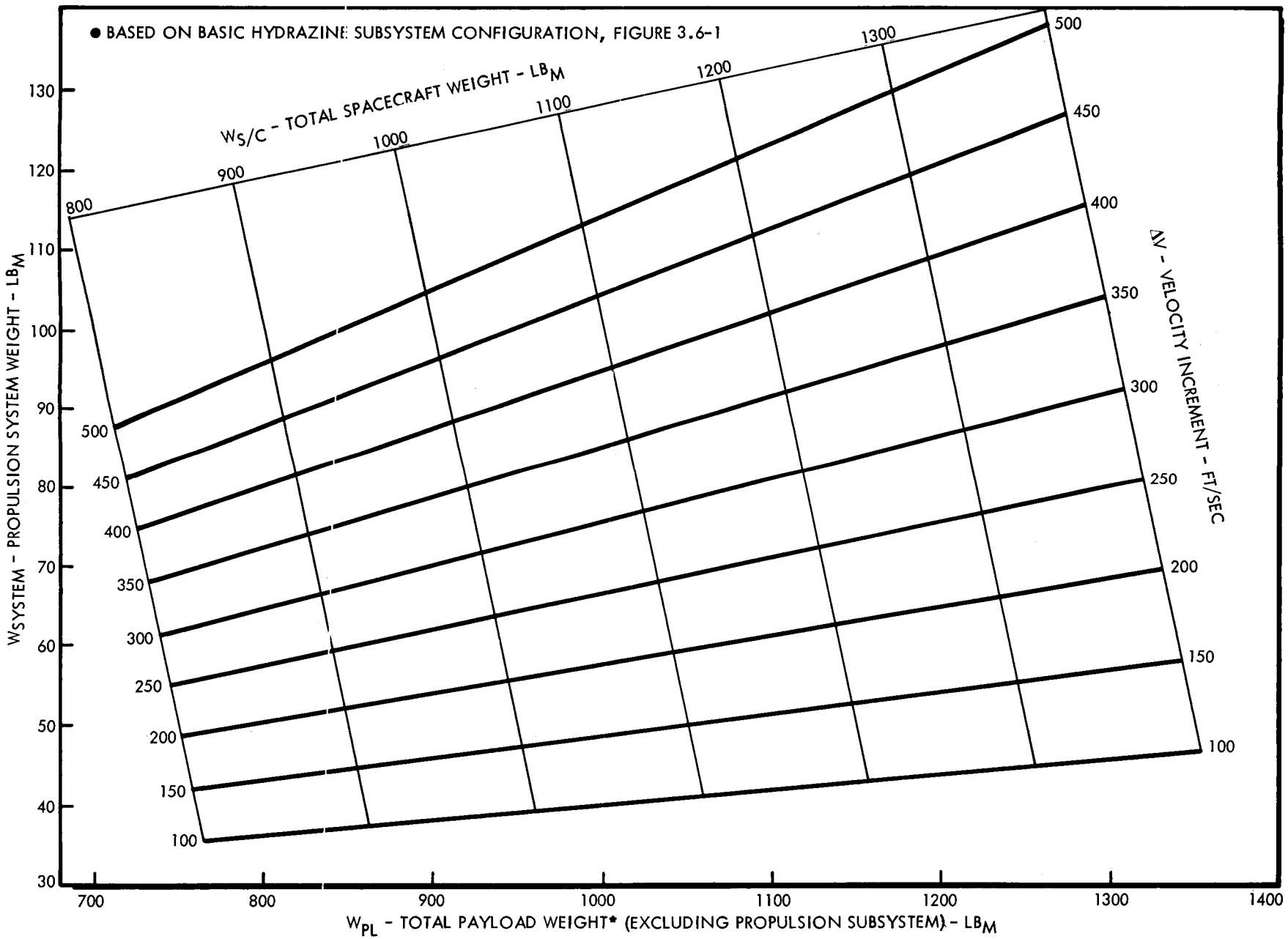


FIGURE 3.6-5

PROPULSION SUBSYSTEM WEIGHT VS. PAYLOAD WEIGHT*

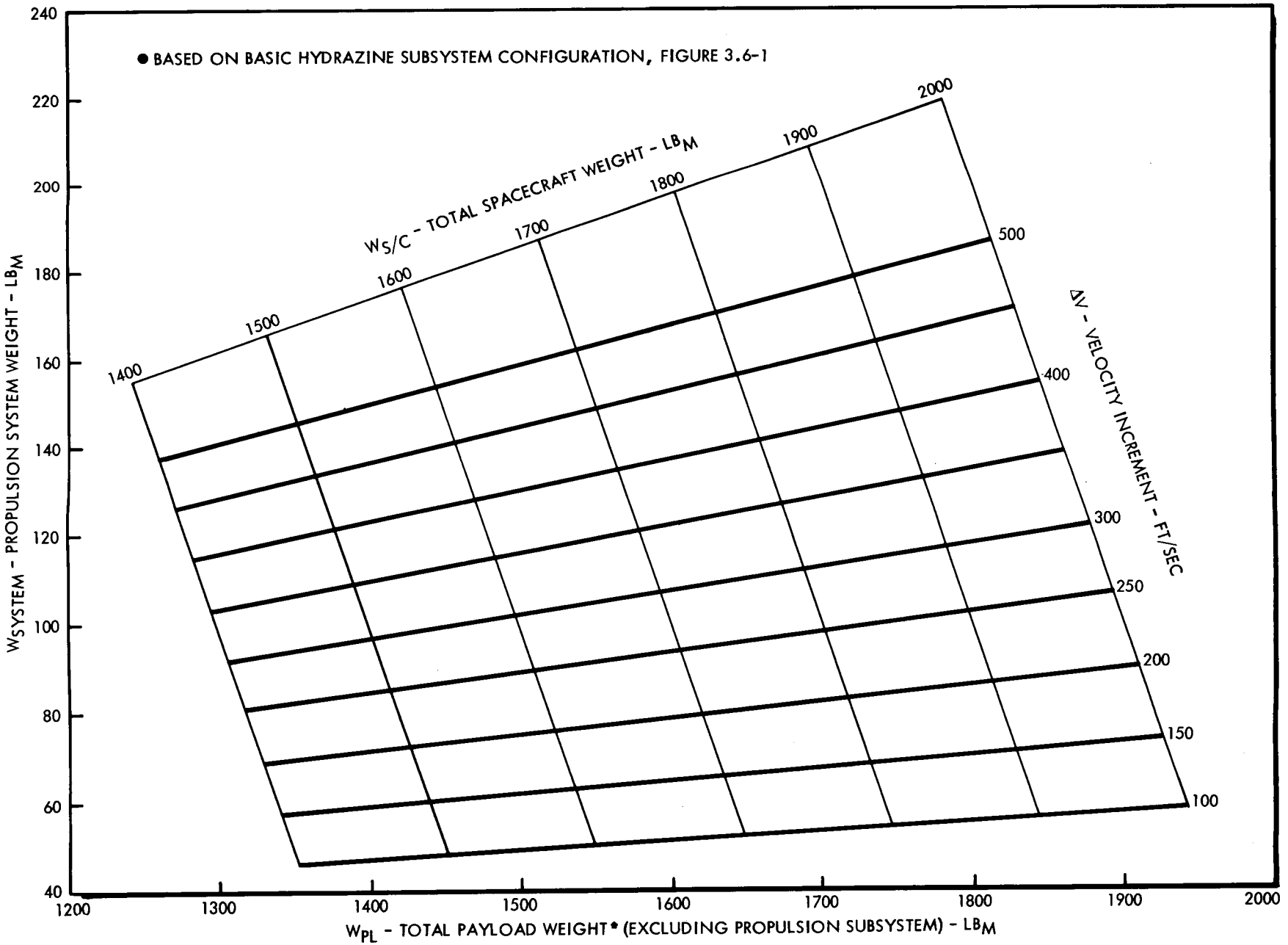


FIGURE 3.6-6

3.6.2 Attitude Control Propulsion Subsystem

3.6.2.1 Functional Requirements

The primary functional requirement of the attitude control propulsion subsystem is to provide control torques to the vehicle in response to processed information from the guidance and control computer. In order to achieve three-axis stabilization, the propulsion subsystem must be capable of imparting a control torque about either of the three vehicle-centered axes. When reaction jets are employed, this torque is accomplished by the simultaneous expulsion of mass from two opposing nozzles. Simultaneous operation of two opposing nozzles is required to assure a pure moment about any one axis; and two nozzle pairs are required for each axis to provide control capability in both the clockwise and counter-clockwise direction. Thus, a minimum of 12 nozzles is usually prescribed to obtain complete, pure-moment, three-axis control.

In addition to the requirements mentioned above, it is imperative that propellant leakage from the propulsion subsystem be held to a minimum. Propellant leakage is undesirable because it leads to a premature depletion of the propellant supply. Not only does leakage represent an unscheduled loss of propellant, but it can impart a continuous disturbing torque to the vehicle, which accelerates propellant consumption even further. Because of the long durations associated with Jupiter flyby missions, propellant leakage must be regarded as a critical problem area and accommodated as such in the design and quality control phases of the attitude control propulsion subsystem development.

3.6.2.2 Possible Propulsion System Concepts

A variety of propulsion system concepts are technically capable of providing attitude control of space vehicles. Among these are systems which derive their exhaust kinetic energy from electrical, nuclear, or chemical sources or combinations of each. Figure 3.6-7 illustrates this idea and identifies some typical propulsion system concepts which could be employed for attitude control. In the figure, the electrical and electrical/chemical devices such as the ion engines, resistojet, arcjet, hydrolysis rocket, and plasma accelerator all require considerable use of onboard electrical power and at present are not as technically advanced or as simple as their chemical competitors. Among the chemical devices, the bipropellant systems would be expected to pose some operational difficulties at the low thrust levels envisioned for attitude control of Jupiter flyby vehicles. The subliming solid systems appear promising for volume-limited situations, but these are unfortunately characterized by a tendency towards recondensation in flow channels and component volumes which compromises their reliability.

PROPULSION SYSTEM CONCEPTS FOR SPACECRAFT ATTITUDE CONTROL

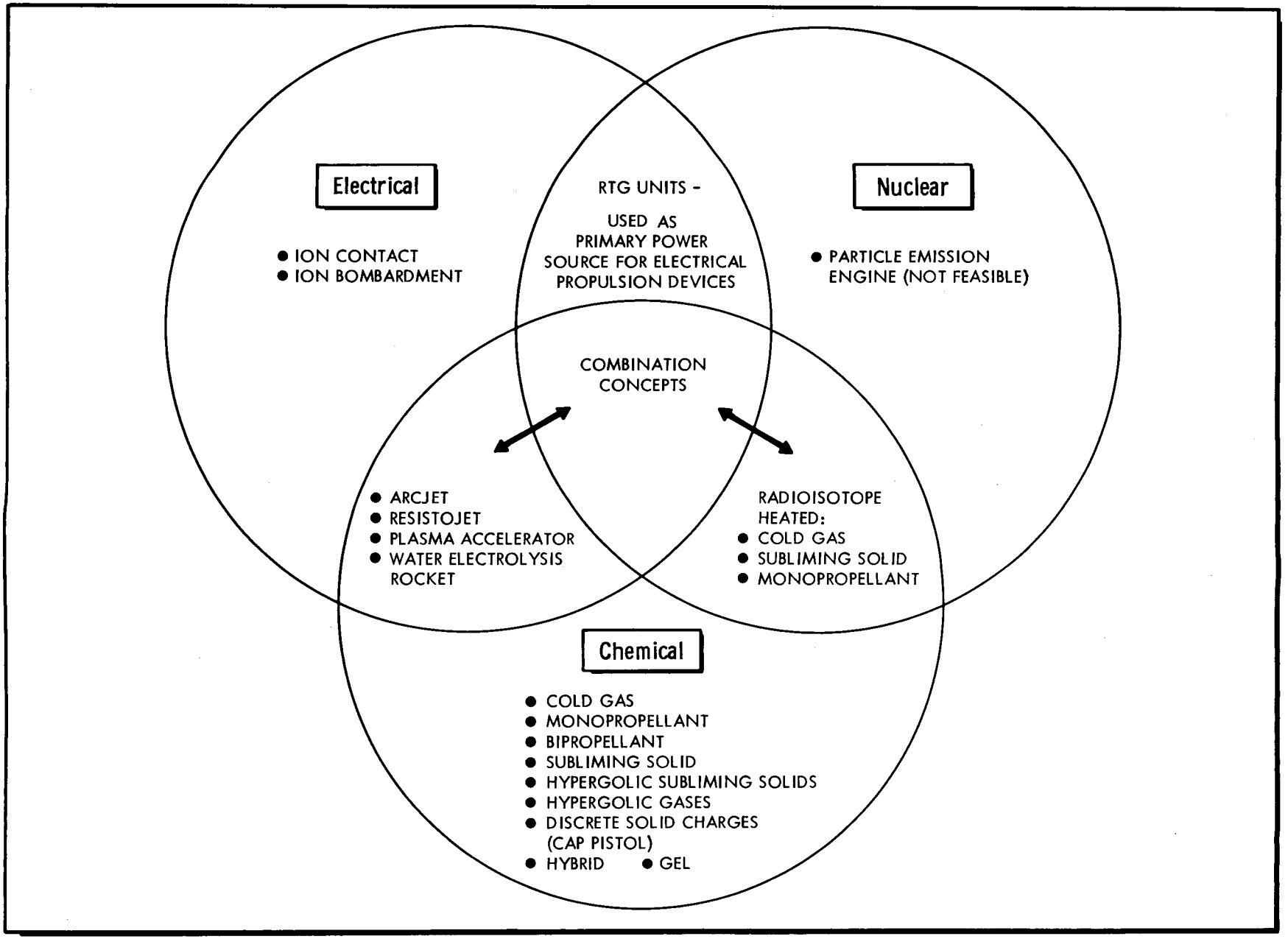


FIGURE 3.6-7

Among the remaining devices, the cold gas and monopropellant systems appear best suited for the Jupiter flyby mission by virtue of their innate reliability and adaptability to the requirements for rapid response, minimum impulse bit, and reproducible operation at low thrust levels. As a design option, either of these system types could be integrated with a radioisotope heat source or possibly the on board RTG units to improve system performance. For example, the cold gas system could be improved by directly heating the gas to increase the specific impulse. With a monopropellant system (such as hydrazine), performance could be improved by heating the catalyst bed to reduce I_{sp} losses due to start transients and assure uniform propellant decomposition. A number of design options are available in this area which warrant further study.

In the interests of a simple and conservative design, however, the propulsion system selected for the attitude control of all Jupiter flyby vehicles is a cold gas system employing nitrogen as propellant. This system is described and analyzed in the paragraphs which follow.

3.6.2.3 Description

In this study, two cold gas propulsion subsystem configurations were defined. These are illustrated in Figures 3.6-8 and 3.6-9. The first, identified as Configuration A, is typical of a system which is recommended to provide three-axis attitude control for short periods of time. As a result, the system is characterized by minimum redundancy.

SCHEMATIC DIAGRAM OF COLD GAS PROPULSION SUBSYSTEM - CONFIGURATION A

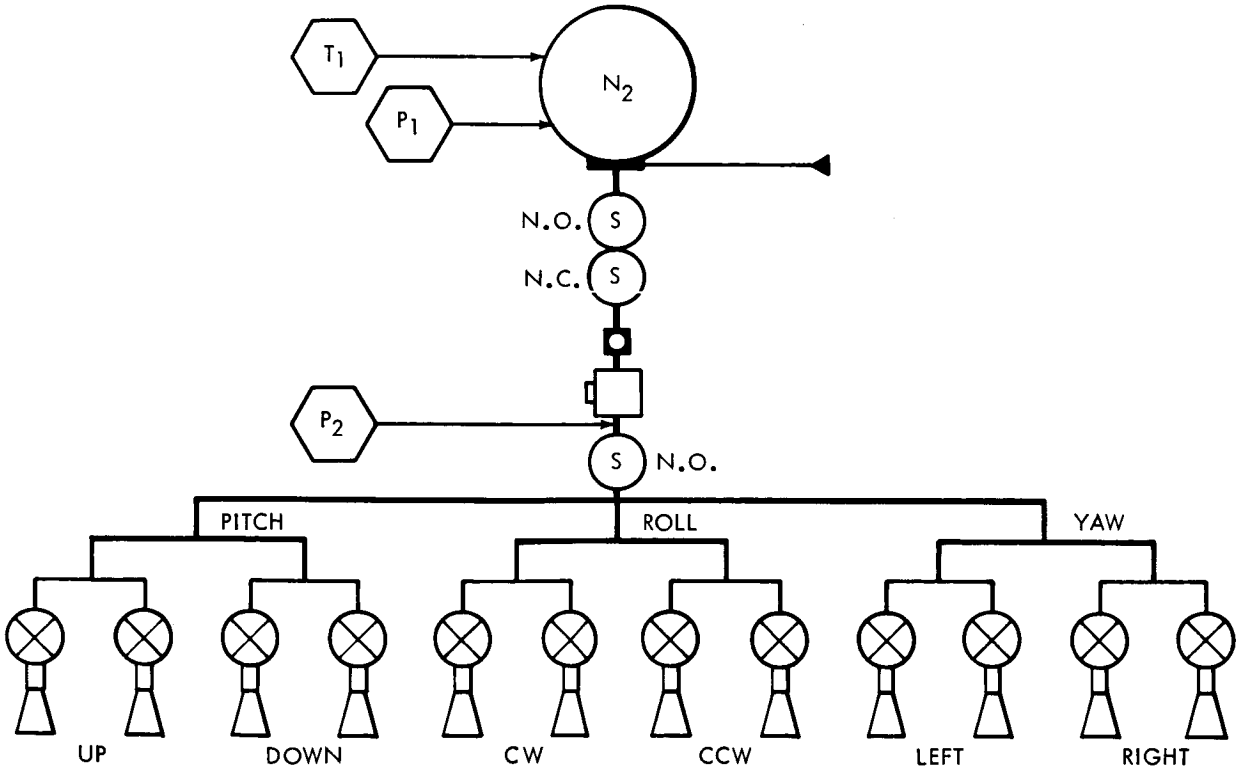


FIGURE 3.6-8

SCHEMATIC DIAGRAM OF COLD GAS PROPULSION SUBSYSTEM - CONFIGURATION B

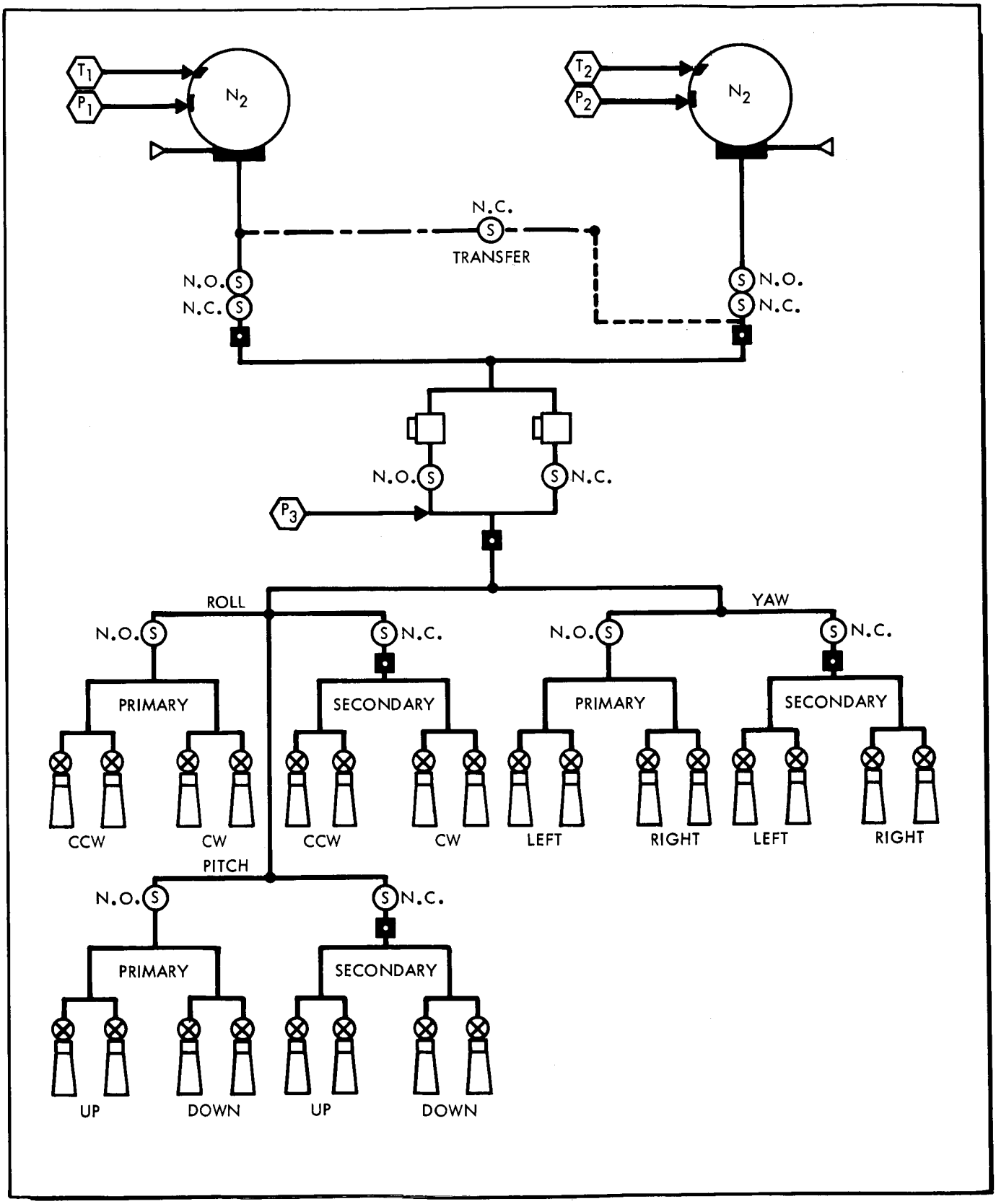


FIGURE 3.6-9

The second configuration, identified as Configuration B, is typical of a system which is recommended for three-axis attitude control of Jupiter flyby vehicles for the entire duration of the mission. For such durations as these (400 to 800 days), it is felt that operational redundancy is necessary in order to increase the probability of mission success. The redundant features provided by Configuration B include (1) a redundant propellant supply, that is, at least twice the nominal propellant necessary to complete the mission is carried in separate propellant tanks, (2) a redundant gas pressure regulator, and (3) a redundant set of nozzle assemblies, each assembly consisting of a solenoid on-off valve and a rocket nozzle.

3.6.2.4 Weight Breakdown of Fixed Hardware

A common problem in predicting the weight of attitude control systems is the uncertainty associated with the weights of the fixed hardware components. Items such as solenoid valves, regulators, etc., which collectively form a significant portion of overall system weight, are found to vary considerably in weight from one manufacturer to another, even when each item is ostensibly capable of the same application. Recognizing this, it was decided to investigate a large sample of vendor's data for the purpose of isolating fixed hardware component weights into conservative (heavy weight) and optimistic (light weight) categories. The results of this effort are tabulated below.

Weight Breakdown of Subsystem Fixed Hardware

	Configuration A	Configuration B
Conservative Estimate	16.50 lbm	34.73 lbm
Optimistic Estimate	6.74 lbm	15.43 lbm

This information was combined with the propellant and tank weight data developed in the following subsection to provide relationships for estimating overall system weight.

3.6.2.5 Parametric Analysis

A detailed parametric analysis of a cold gas attitude control propulsion subsystem is presented in Appendix D. This analysis forms the basis for the propulsion subsystem weight data which is presented in subsection 3.6.2.6. The nomenclature to be used is listed below, followed by a summary of the primary equations which were developed.

Table 3.6-5 ATTITUDE CONTROL PROPULSION SUBSYSTEM - NOMENCLATURE AND EQUATION SUMMARY (Sheet 1)

Nomenclature Symbol	Description	Units
W system	Total Weight of the Subsystem	lbm
Wp	Total Weight of Propellant Required	lbm
W_t	Weight of Propellant Tank	lbm
W_{com}	Total Weight of Fixed Hardware (i.e., valves, regulators, tubing etc.)	lbm
Wp_1	Expected Propellant Consumption	lbm
Wp_2	Propellant Contingency for Isp Degradation	lbm
Wp_3	Residual Propellant at Termination of Thrust Program	lbm
I_t	Total Impulse Required	lbf.sec
I_{sp}	Specific Impulse	lbf.sec/lbm
α_p	Contingency Factor for Isp Degradation	---
P_i	Initial Propellant Tank Pressure	$lbf/in.^2$
P_f	Final Propellant Tank Pressure	$lbf/in.^2$
P_D	Propellant Tank Design Pressure (at maximum anticipated temp.)	$lbf/in.^2$
T_{max}	Maximum Anticipated Temperature	^oR
T_i	Initial Propellant Temperature	^oR
T_f	Final Propellant Temperature	^oR
V_{tank}	Volume of Propellant Tank	$in.^3$

Table 3.6-5 ATTITUDE CONTROL PROPULSTION SUBSYSTEM - NOMENCLATURE AND EQUATION SUMMARY
(Sheet 2)

Symbol	Description	Units
R	Propellant (gas) Constant	in.-lbf/lbm·°R
S.F.	Design Safety Factor	---
ρ_{mat}	Density of Tank Material	lbm/in.^{3}
σ_{mat}	U.T.S of Tank Material	lbf/in.^{2}

Equation Summary

(1) $$W_{SYSTEM} = W_P + W_t + W_{COM}$$

(3) $$W_P = \frac{I_t}{I_{SP}} \frac{(1+\alpha_P)}{\left\{1-\left(\frac{P_f}{P_i}\right)\left(\frac{T_f}{T_i}\right)\right\}}$$

(7) $$W_t = 1.5\, W_P R T_{MAX} \left(\frac{\rho}{\sigma}\right)_{MAT} (S.F.)$$

(8) $$W_{SYSTEM} = I_t \left[\frac{(1+\alpha_P)}{I_{SP}} \frac{\left\{1 + 1.5 R T_{MAX} \left(\frac{\rho}{\sigma}\right)_{MAT} (S.F.)\right\}}{\left\{1 - \left(\frac{P_f}{P_i}\right)\left(\frac{T_i}{T_f}\right)\right\}} \right] + W_{COM}$$

3.6.2.6 Subsystem Sizing

The sizing of the two attitude control configurations A and B is accomplished by combining the fixed hardware weights of each configuration with the appropriate equation form developed in the preceding paragraph.

For Configuration A, which is non-redundant with respect to propellant supply and tankage, the basic equation (8) for subsystem weight is valid. Thus, in calculating the total subsystem weight,

$$W_{\substack{SYSTEM \\ A}} = I_t \left[\frac{(1+\alpha_P)\left\{1+1.5\,R\,T_{MAX}\left(\frac{\rho}{\sigma}\right)_{MAT}(S.F.)\right\}}{I_{SP}\left\{1-\left(\frac{P_f}{P_i}\right)\left(\frac{T_i}{T_f}\right)\right\}} \right] + W_{COM}$$

where Wcom, the weight of fixed hardware, is either 16.50 pounds (conservative estimate) or 6.74 pounds (optimistic estimate).

In the case of Configuration B, which is assumed to carry twice the nominal supply of propellant (contained in two equivalent tanks), the basic equation (8) is modified in the first term to read:

$$W_{\substack{SYSTEM \\ B}} = 2I_t \left[\frac{(1+\alpha_P)\left\{1+1.5\,R\,T_{MAX}\left(\frac{\rho}{\sigma}\right)_{MAT}(S.F.)\right\}}{I_{SP}\left\{1-\left(\frac{P_f}{P_i}\right)\left(\frac{T_i}{T_f}\right)\right\}} \right] + W_{COM}$$

Where W_{com} is estimated at 34.73 pounds (conservative) and 15.43 pounds (optimistic). Using the design data listed below, both of these equations were plotted as a function of the total impulse required for both the conservative and optimistic estimates of fixed hardware. These results appear in Figure 3.6.10.

The following design data have been adopted for sizing the attitude control propulsion subsystems.

General

Propellant	Nitrogen
Specific Impulse	56.6 lb_f. sec/lbm

Materials

Propellant Tank	Titanium Alloy 6 AL-4V
Configuration	Spherical

Constants

Symbol	Description	Assigned Value
α_p	Contingency Factor for Isp Degradation	0.10
P_i	Initial Propellant Tank Pressure	3000 $lb_f/in.^2$
P_f	Final Propellant Tank Pressure	150 $lb_f/in.^2$
P_D	Propellant Tank Design Pressure (at maximum anticipated temperature)	3540 $lb_f/in.^2$
T_{max}	Maximum Anticipated Temperature	165°F
T_i	Initial Propellant Temperature	70°F
T_f	Final Propellant Temperature	70°F
R	Propellant (Gas) Constant	660 $in.lb_f/lbm°R$
S.F.	Design Safety Factor	2.2
ρ_{mat}	Density of Tank Material	0.16 $lbm/in.^3$
σ_{mat}	U.T.S. of Tank Material	165000 $lb_f/in.^2$

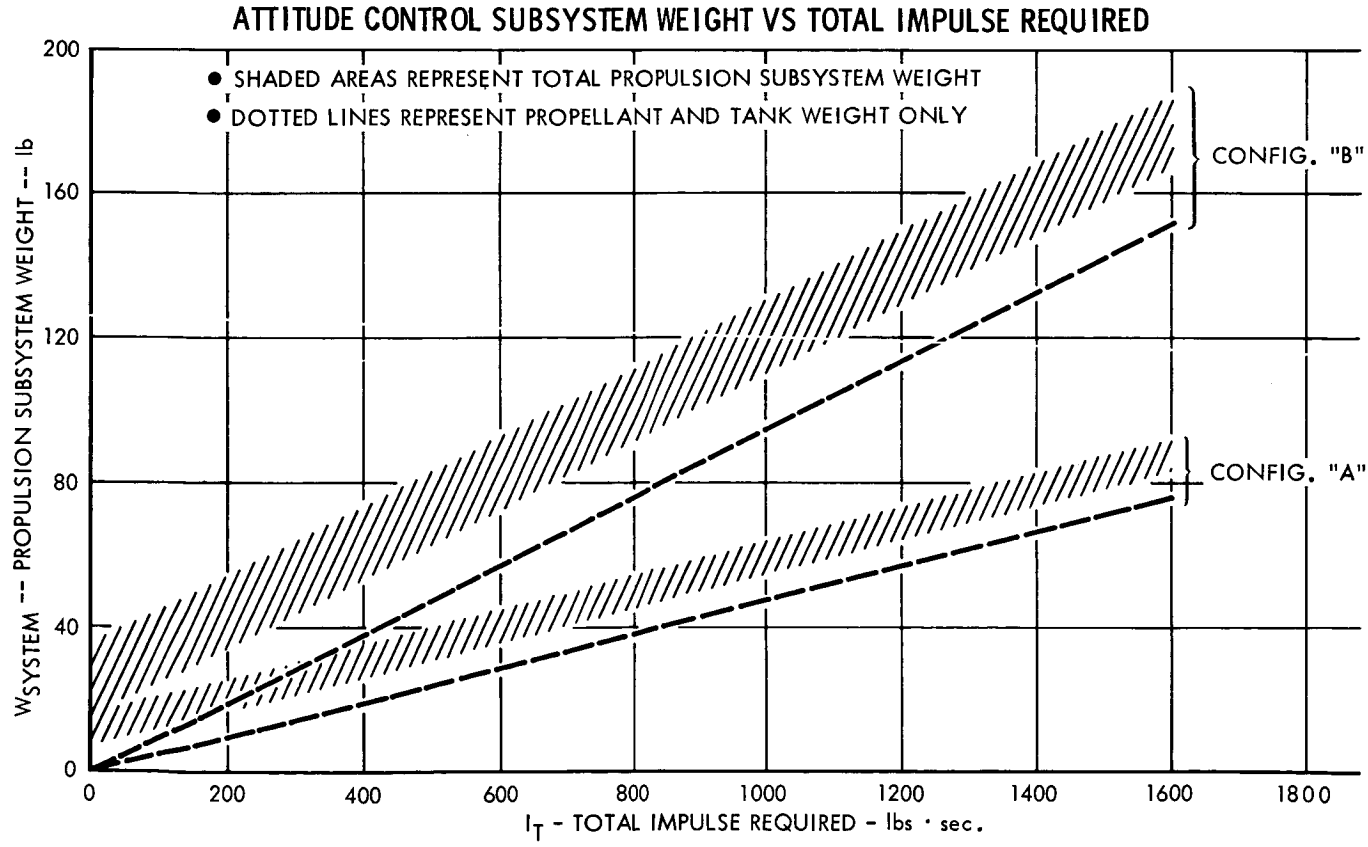


FIGURE 3.6-10

3.7 AUXILIARY ELECTRIC POWER SYSTEM

3.7.1 Scope and Requirements

The scope of the Jupiter flyby electrical system study includes the organization of applicable data on current power systems, a projection from such data to that anticipated during the early 1970's, coordination of various trade-off analyses which are expressed in terms of parametric systems configurations, and the designation of four specific design configurations. The requirements and constraints imposed upon the power system by the Jupiter flyby mission profile include: (1) temperature, vibration, atmospheric, and space vacuum environment of all the mission phases, (2) the volume and weight limitations of the launching system, (3) the power requirement profile, (4) the weight, volume, and reliability trade-offs, (5) the availability and cost considerations, and (6) interface coordination with other spacecraft systems. Item (6) includes the following: structural aspects; view angle restrictions of optical navigation devices, communications antennas, and thermal radiation; vehicle inertial dimensions; and nuclear irradiation effects.

3.7.2 Raw Power Generation

3.7.2.1 Energy Sources

Selection of the energy source and conversion process are the first consideration of the power system study. Mission durations in the 400- to 1000-day range immediately restrict considerations to solar, nuclear reactors, or radioisotopes thermal energy sources. Solar thermal energy intensity at Jupiter's orbit is approximately 4 percent of that at Earth's orbit which is in the order of 5 watts per square foot. The low level negates any practical consideration of employing any form of currently envisioned solar energy collection system. Nuclear reactors have a minimum critical size and weight required to maintain a controlled nuclear reaction. The minimum weight is currently approximately 250 pounds. Reactor radiation effects further complicate the matter to the point of eliminating any consideration of nuclear reactors as an energy source for the subject application.

Isotopes alone remain as a candidate energy source. Isotope fuel selection is based on considerations of half-life, availability, cost, radiation characteristics, energy density, handling, and safety aspects. Strontium 90, Cesium 137, and possibly Promethium 147 can be used to meet the first three requirements. However, safety considerations, beta radiation effects on scientific instruments, shielding mass penalties, and lack of experience

with their application combine to make their successful application extremely unlikely. Plutonium 238 and Currium 244 are long half-life alpha emitters. Of the two, Plutonium 238 is more favorable in terms of cost, availability, and safety; hence, it is recommended for this application.

3.7.2.2 Energy Converters

Candidate thermal to electric converters include thermionic, Rankine and Brayton dynamic, and thermoelectric. Thermionic systems, although they show great promise, are not sufficiently advanced to warrant consideration for the early 1970 time period. The dynamic systems are not competitive weight wise in the subkilowatt range. Information in Figure 3.7-1 (Reference 3.7-1) supports the conclusion that the RTG (Radioisotope-Thermalelectric-Generator) is best suited to provide power for the subject application.

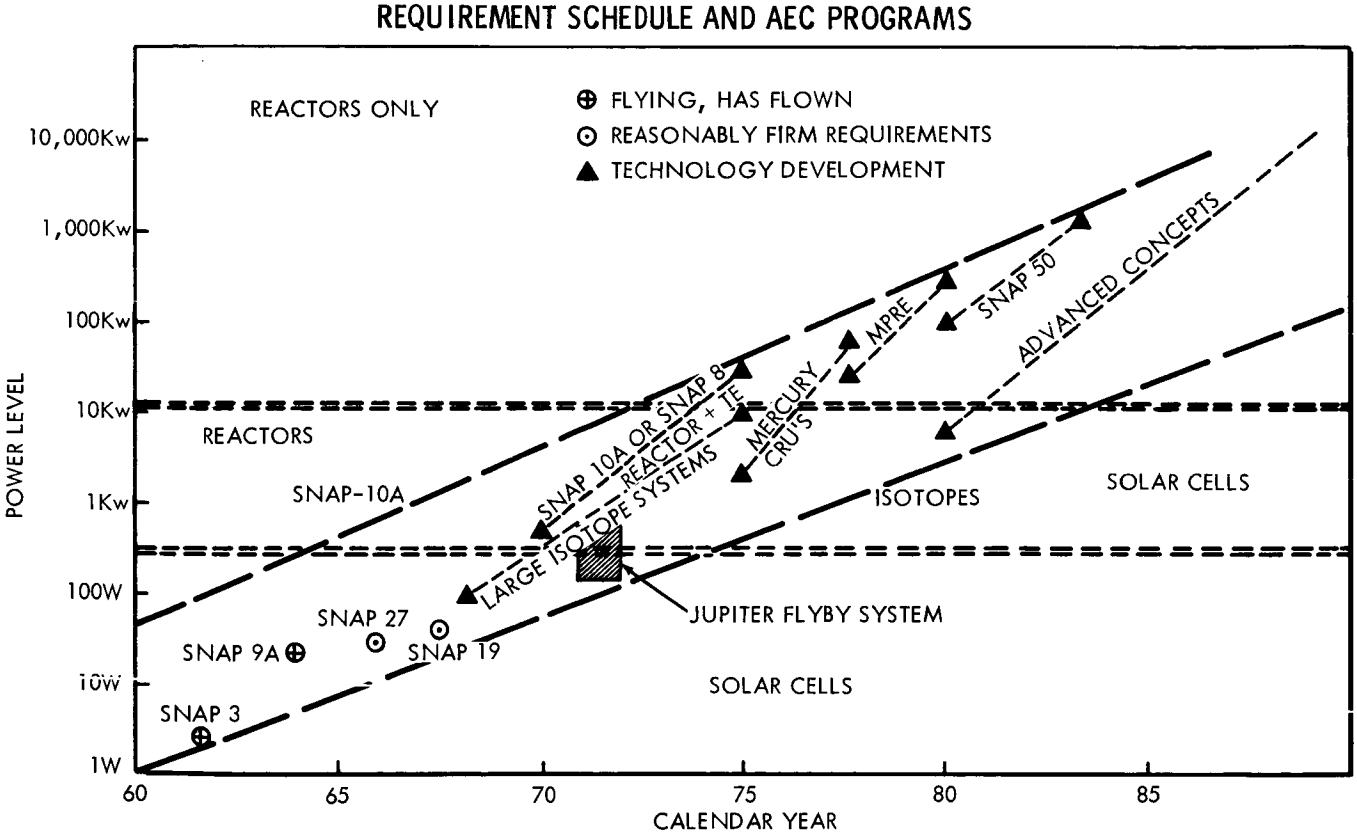


FIGURE 3.7-1

3.7.2.3 RTG Configurations

The RTG design configurations set forth herein are based upon (1) unclassified oral communications with Germantown AEC personnel, Dr. Fred Schulman, and other personnel of NASA Headquarters, (2) the classified reports on Advanced Space Radioisotope Studies on a 250-watt Sr-90 system (References 3.7-2, -3, -4, and -5), and (3) the classified study performed by the General Electric Company on a

40-watt Pu-238 Unit (Reference 3.7-6). The latter includes a projected analysis of a 100-watt unit which is within the range of the units recommended in this study. Security classifications rigidly restrict the extent to which such data may be set forth in this report. However, based upon information received in the AEC unclassified communications and their guidelines pertaining to the security classification of RTGs, the following tabulation of parameters are set forth and employed in this study:

. Fuel	Pu-238
. Specific Power Density	2 watts/pound
. Radiation temperature	500° F
. Physical Size	
Diameter over fins	19 inches
Length	0.02 inches/watt
. Thermocouple	
Material	Lead-Teluride
Open circuit voltage	0.166 volts
Max power voltage	0.083 volts
. Overall efficiency	5 percent

Thermal power level decay of the Pu-238 fuel over a 600-day period is small due to its 86.4 year half life. The combined degradation of the RTG assembly due to deterioration of couples, interconnectors, heat transport system, thermal radiation effectiveness, and the fuel is less than 2 percent. The application in this study of the criteria listed above has been a part of the evaluation of the three RTG configurations. The physical configuration data for the 60-, 80-, and 120-watt units as applied are listed in Table 3.7-1.

3.7.2.4 RTG Internal Interconnections

The RTG is composed of a large number of electrically independent, low voltage power converters. The manner in which they may be interconnected to enhance overall reliability is described herein. Each thermocouple, when operated at a specific thermal environment, exhibits a linear voltage versus current relationship

Table 3.7-1

60, 80, and 120 WATT RTG GEOMETRY

Rating, watts	60	80	120
RTG total weight, pounds	30	40	60
Nominal potential, volts	28	28	28
Number of groups, Ng	14	14	14
Series couples per group, Ns	24	24	24
Parallel strings per group, Np	2	2	3
Thermocouples per group	48	48	72
Total couples for RTG	672	672	1008
RTG nominal current	2.14	2.86	4.28
Couple nominal current	1.07	1.43	1.43
Couple nominal volts	0.083	0.083	0.083
Couple nominal watts	0.089	0.119	0.119

as illustrated in Figure 3.7-2a. Maximum power output occurs when the internal and external impedances are balanced as illustrated in Figure 3.7-2b. The simplist RTG interconnector is a series string as illustrated in Figure 3.7-2c. However, one open couple or interconnection disables the entire RTG. The effect of open circuits can be minimized by a parallel interconnection as illustrated in Figure 3.7-2d. However, in such a case the total output voltage is in the order of 0.1 volt at a current of several hundred amperes, and this produces an unmanageable power conditioning task. A compromise which combines the advantages of both schemes is illustrated in Figure 3.7-2e. Here the couples are arranged in a number of groups, Ng, with the groups connected in series. Each group is composed of a number of parallel strings, Np. The string consists of Ns couples connected in series.

The effects of open and shorted couples are illustrated by an analysis of the 120-watt RTG unit in Figure 3.7-3. As listed in Table 3.7-1, the proposed 120-watt unit is made up of 14 series-connected groups, each group of which is composed of 3 parallel strings of 24 couples giving in each case a total of 1008 couples for the complete RTG. Part a, Figure 3.7-3, applies to the individual couple. Part b illustrates the series string with 24 functional couples and a series string with 23 couples representing the situation with one couple shorted. Part c applies to a fully functional group, a group with one string containing a shorted couple, and a group with one open-circuited string. Part d illustrates the performance of the complete RTG with all couples functioning properly and a situation in which 12 groups are functioning properly; one group contains a string with a shorted couple and one group has an open string. Note that with two such internal failures the RTG maintains an output power of 95 percent normal.

3.7.3 Power Management System

3.7.3.1 Functions

The functions of a spacecraft power management system include conditioning, distribution, and control. The power conditioning system accepts raw electrical energy and converts it to ac or dc of the quality required by the utilization systems. The distribution system transmits power to each load device while minimizing spurious coupling effects. The control function includes switching action to apply and interrupt power flow. Circuits are switched to obtain a more favorable diversity function and to remove faulty devices from the system.

THERMOCOUPLE INTERCONNECTIONS

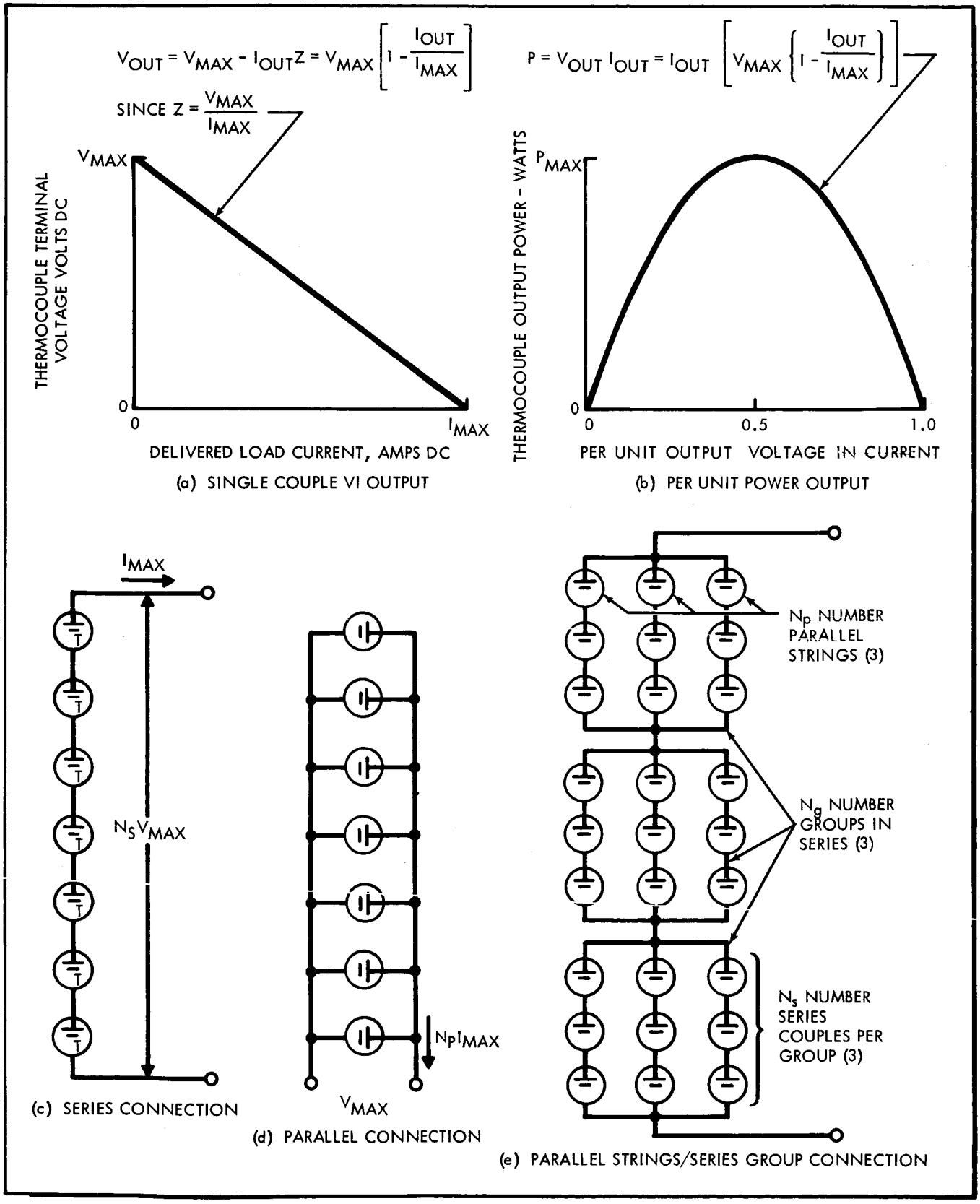
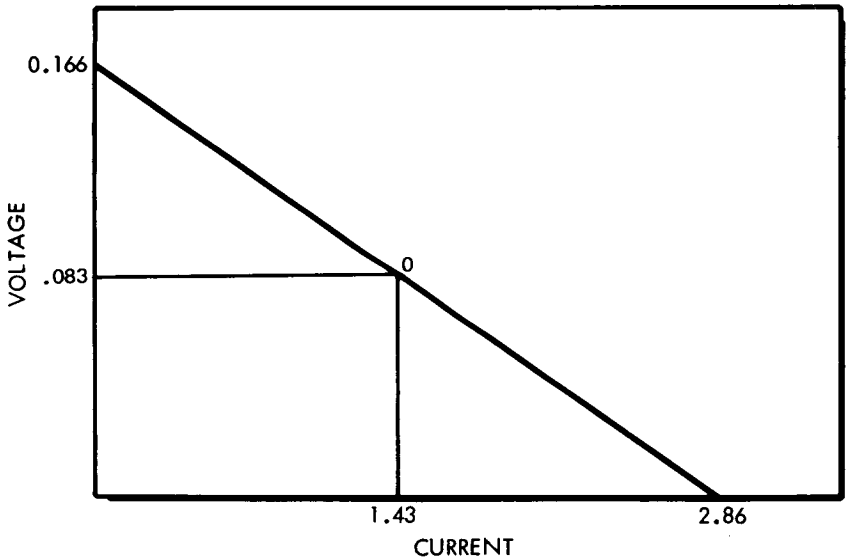
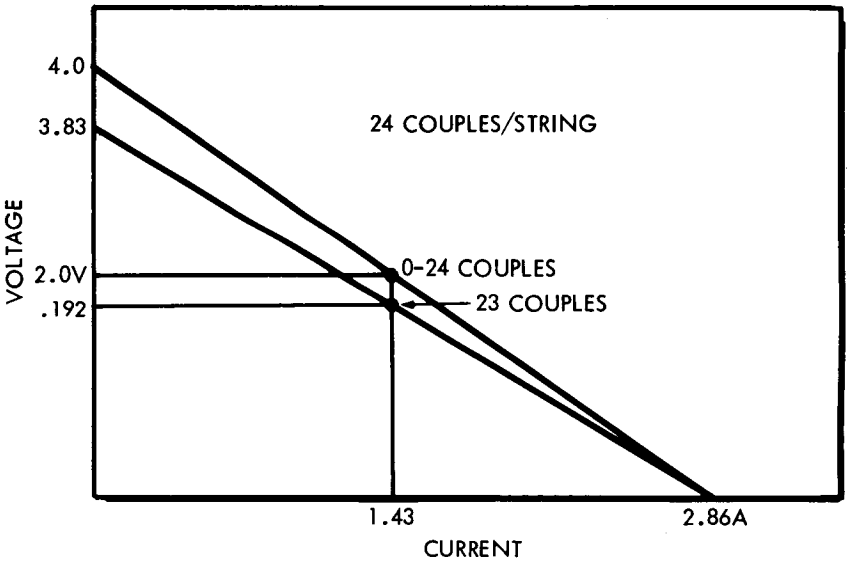


FIGURE 3.7-2

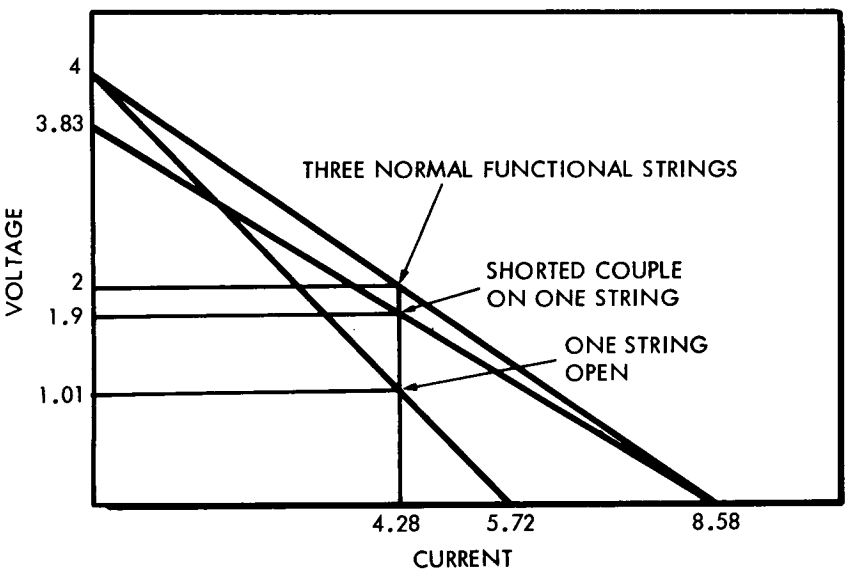
THERMOCOUPLE FAILURE EFFECTS



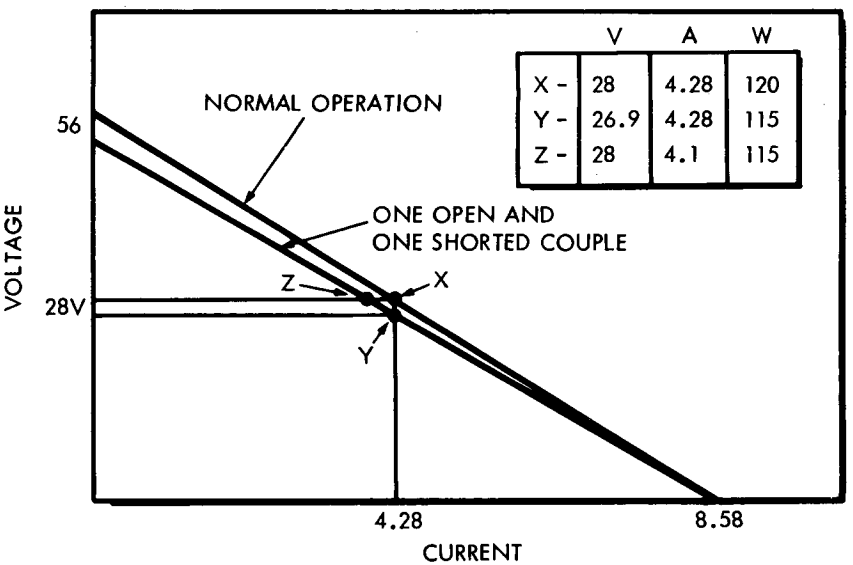
A. SINGLE THERMO COUPLE



B. STRING PERFORMANCE



C. GROUP PERFORMANCE



D. RTG PERFORMANCE

FIGURE 3.7-3

The overall management function is arranged to provide an assurance of success based upon total power system unit weight. Configuration optimization involves the judicious value assessment of partial versus total mission success and of light weight system sophistication versus rugged brute force approach. Three basic approaches to system configurations are illustrated in Figure 3.7-4, Nonredundant Single Channel System; Modular System Configuration and Selective Redundancy.

SYSTEMS CONFIGURATIONS

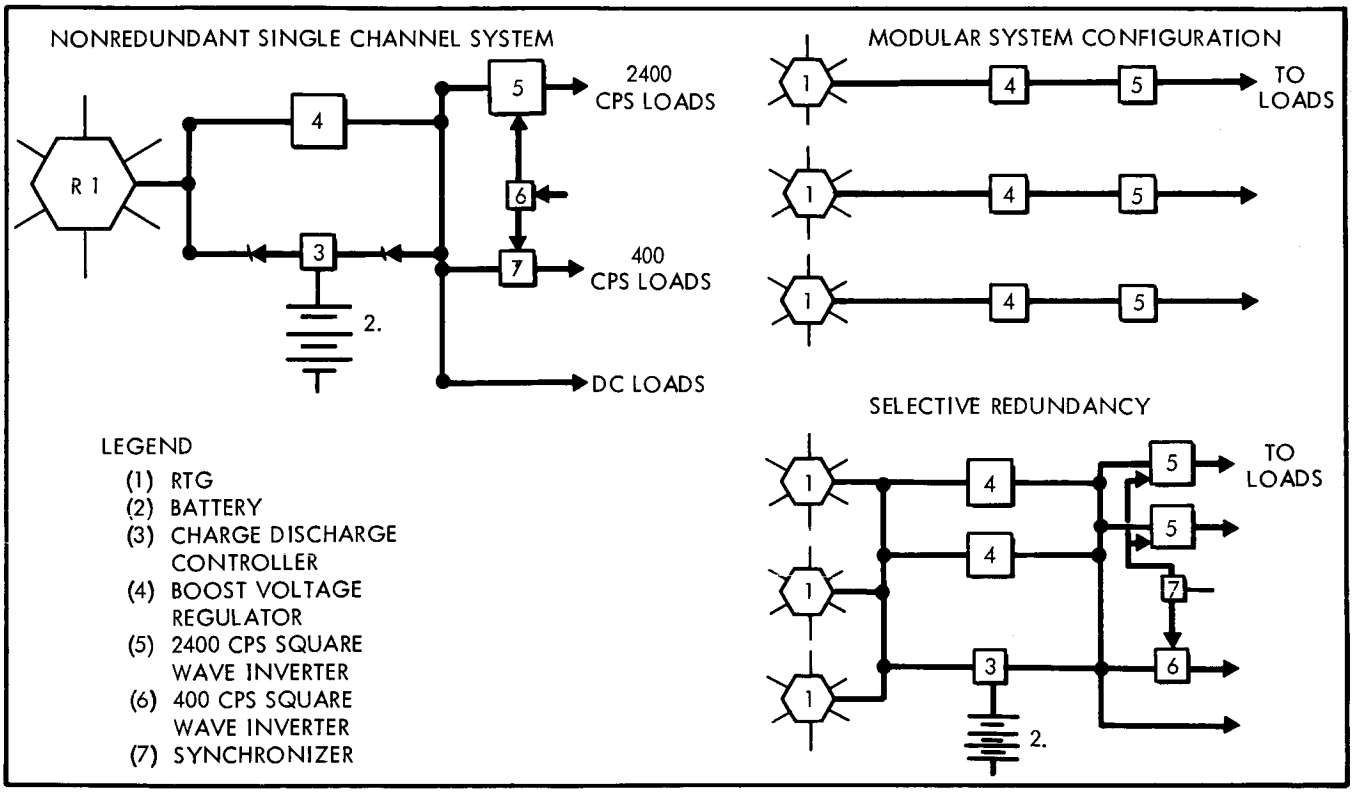


FIGURE 3.7-4

On the basis of relative degrees of reliability, operational flexibility, and considerations of packaging, it has been concluded that the selective redundancy configuration is best suited to the subject application.

3.7.3.2 Form of Conditional Power

After the raw power generation system has been designated, the selection of the most suitable form of power distribution is made. The choice rests essentially between ac and dc. The dc system is the most simple. The possibility exists of arranging the utilization equipment to operate directly from the raw power source with a minimum amount of conditioning and losses. However, as the systems become more complex, as larger loads of various types are added, as the requirement for voltage boost functions are included, as motors are added to the system, and as the advantages of flexibility become greater, the

merits of the ac system increase. Therefore, primary power is distributed as square wave 2400 cps. Direct current is produced by transformer-rectifiers at the point of utilization. DC voltage regulation is achieved by high efficiency phase width control silicon control rectifiers (SCR) operating as both the rectifier and control element. A 400 cps supply is provided to operate gyros and synchros.

3.7.3.3 Inversion

The recommended inverter circuit was developed by the General Electric Company (Reference 3.7-7) and is illustrated in Figure 3.7-5. The circuit has substantially a square-wave output under all load conditions and does not create high voltage across the SCR's under lightly loaded or no-load conditions.

McMURRAY-BEDFORD INVERTER CIRCUIT

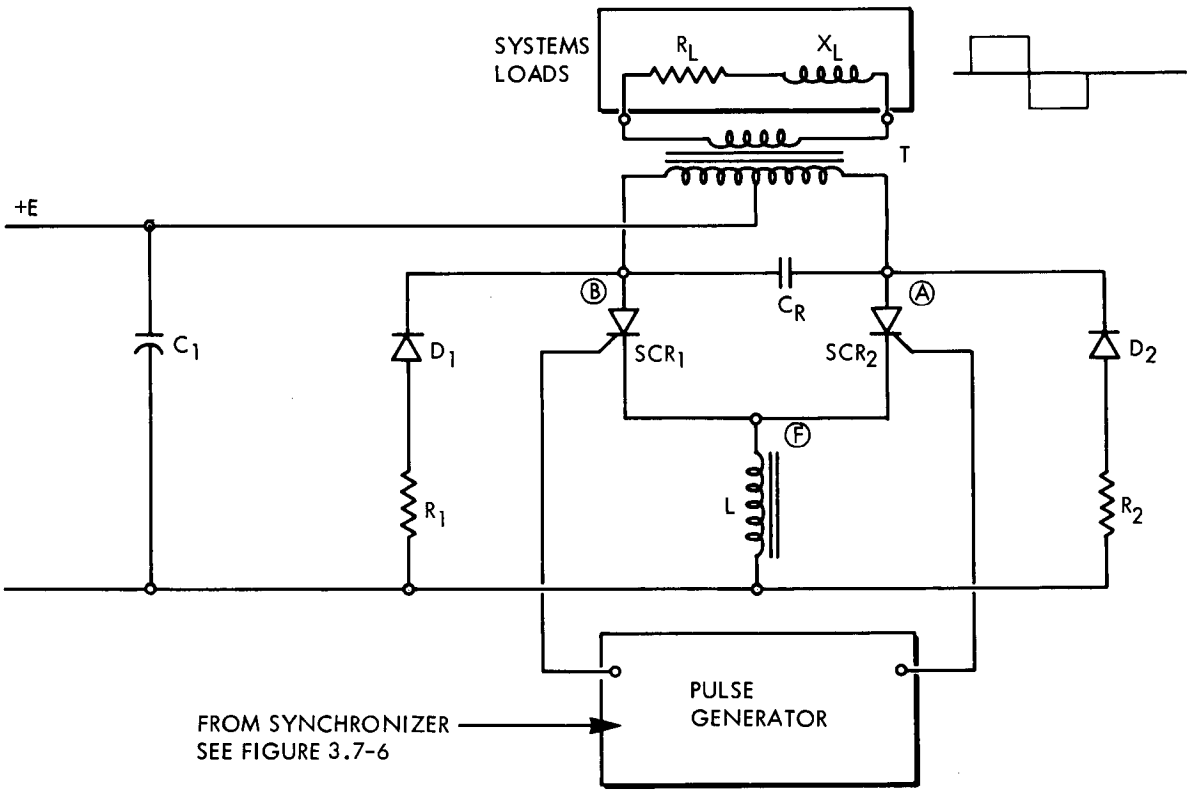


FIGURE 3.7-5

A major advantage of the circuit is its ability to operate under lightly loaded or open-circuit conditions. In the circuit shown in Figure 3.7-5, the feed-back diodes prevent the voltage across either half of the primary winding from exceeding the supply voltage. These diodes not only maintain a square wave output under all load conditions but also permit the use of lower break-over voltage SCR's. The diodes also compensate for leading or lagging power factor loads by feeding reactive power back into the supply. This permits the commutating capacitor C_2 to be much smaller since its value depends on

the maximum current to be commutated and does not have to correct for the reactive load current. The RTG raw power source is complimented by the battery to reduce transient impedance. Capacitor C_1 is arranged to accept power from the raw power generation source as well as supply power to the inverter.

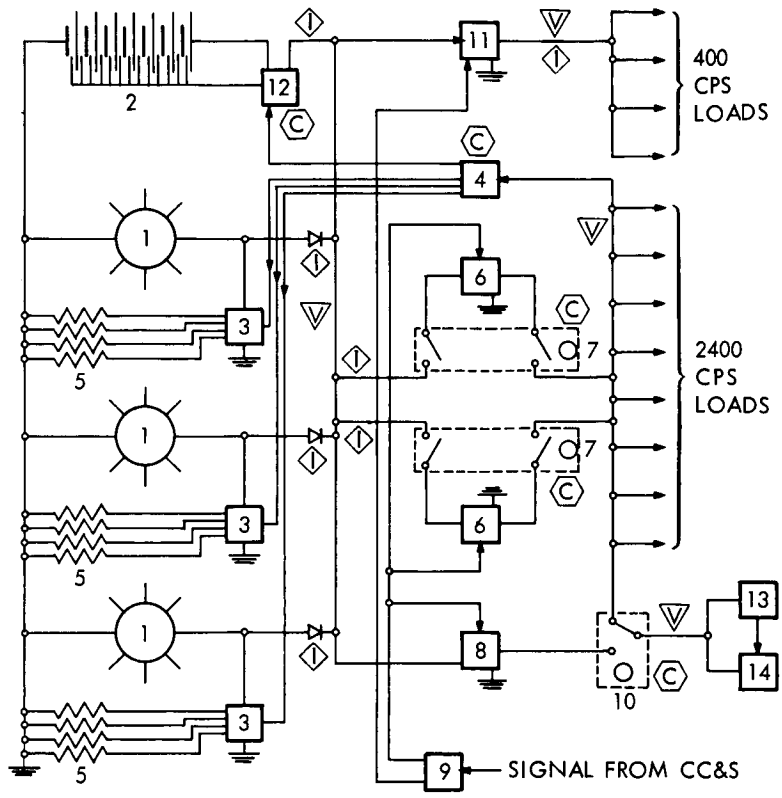
The series inductance L of Figure 3.7-5 is quite small (compared to that used in conventional parallel inverters) and chosen to resonate with C_2 to create a short impulse to turn off the conducting SCR. The values of C and L are determined by the maximum current to be commutated, the dc supply voltage, and the turn-off time of the SCR's.

The operation of this inverter can best be understood by a detailed explanation of one complete cycle. Assume that SCR1 is conducting. The anode voltage of SCR2 and the right-hand side of capacitor C_2 will be at twice the supply voltage E due to the autotransformer action of T. When voltage is applied to the gate of SCR2, it will turn "on" and the top end of L, point "F," will rise momentarily to twice the supply voltage. Capacitor C is thereby connected directly across SCR1, and its voltage back-biases SCR1. The capacitor discharge through L is oscillatory, and when the anode of SCR2 goes below ground, diode D2 conducts and the oscillation is damped out by R2. C and L are chosen so that the SCR being turned "off" is back-biased a sufficient length of time for it to recover its blocking characteristics. With a purely resistive load, D2 and D1 conduct only during the commutation interval and short turn-on pulses applied alternately to the gates would insure proper operation.

With an inductive load, the operation of the inverter is more complex. Based on the assumption that SCR1 is conducting, turning "on" SCR2 will turn SCR1 off as described previously. An inductive load prevents the main load current from reversing instantaneously. Transformed load current must flow through diode D2 back into the DC supply until the load current reverses. During this feedback interval, the current through SCR2 will fall to zero and SCR2 will actually become back-biased so that it will have to be refired when the load current reverses. After being refired, SCR2 will continue conduction for the rest of the half cycle. SCR2 can be refired either by supplying another pulse at the proper time or more easily by maintaining gate drive for the full half cycle.

As illustrated in the Electric Power System Schematic Diagram of Figure 3.7-6, a signal from the power synchronizer controls the inverter square wave output to 2400 cps.

ELECTRIC POWER SYSTEM SCHEMATIC DIAGRAM



1. MULTIPLE RADIOISOTOPE THERMOELECTRIC GENERATORS
2. NICKEL CADMIUM BATTERY, WITH THIRD ELECTRODE
3. SHUNT VOLTAGE REGULATORS
4. VOLTAGE SENSOR AND SHUNT REGULATOR MODE CONTROLLER
5. SHUNT POWER DISSIPATION RESISTORS
6. 2400 CPS SOLID STATE CHOPPER
7. TRANSFER RELAY
8. EMERGENCY INVERTER
9. INVERTER SYNCHRONIZER
10. EMERGENCY TRANSFER RELAY
11. 400 CPS SOLID STATE CHOPPER
12. BATTERY CHARGE - DISCHARGE CONTROLLER
13. COMMAND RECEIVER
14. COMMAND CONTROL SYSTEM

CURRENT MONITORED POINT
VOLTAGE MONITORED POINT
COMMAND CONTROLLED

FIGURE 3.7-6

3.7.3.4 Voltage Regulation

The shunt regulator is more advantageous for this application because at the end of life, under maximum load conditions, the losses are essentially zero. The shunt regulator draws the amount of extra current required to cause the excess voltage to be dropped across the internal resistance of the source, thereby adjusting the voltage to the desired point. The shunt regulator functions to maintain a constant load on the RTG. The continuous drain of a fixed level of electrical energy from the couples stabilize the energy balance and temperature.

The Power System Schematic Diagram, Figure 3.7-6, shows the shunt regulation system as consisting of three separate parts. The shunt power dissipation resistors, item 5, are shown relative to each RTG. Each group of resistors is rated to accept the full output of the RTG. Item 3 is the switching unit arranged to switch individual resistors on and off the line. The resistors are sized to permit a step regulation function to maintain voltage within tolerances. The transistor switches of item 3 are arranged to operate in the saturated mode thereby decreasing their heat rejection requirement, reducing their temperature, and prolonging their life. Separate items 3 and 5 operate with each RTG such that a failure within one unit does not impare the full raw power generation system.

Item 4 senses voltage on the 2400 cps bus and produces signals to each switching unit to maintain voltage at the 2400 cps bus within tolerance. This removes any requirement for the inversion unit to include regulation functions.

Item 4 serves also as a mode of operation selector. To prevent the occurance of instability between the separate voltage controllers, one RTG control unit is selected as the master voltage controller. The remaining units operate in a slave mode as a function of both output current and bus voltage. A command link permits the selection of a mode for each of the RTG units.

3.7.4 Energy Storage

An energy storage system performs two functions. One, it provides a high capacity source of transient energy which is not available from the RTGs. Second, it permits short duration load peaks to exceed the capacity of the RTG's. The unit recommended for the application is a nickel cadmium three electrode battery which is floated on the system at all times. A command link is available to permit remote selection of other charge-discharge operation modes.

From the standpoint of parts population, the battery adds considerably to the unreliability of the prolonged space mission. Hence, considerable analytic study and laboratory tests are required to define the extent to which the total power systems operation should be made dependent on the continued operation of the battery element.

3.7.5 Recommended Configuration

The application of principals set forth above evolved into the recommended system configuration as shown in Figure 3.7-6.

3.7.5.1 Operation

Raw power generator and inverter currents are monitored by the data management system. Raw power and conditioned power bus voltages are monitored in a similar manner. Command control functions include (1) the turn-on and turn-off of loads individually and in groups, (2) the operational mode selection of individual RTG shunt voltage regulators, (3) the function selection of the battery charge-discharge controller, and (4) the application and removal of the redundant 2400 cps inverters.

The command receiver and control system is normally powered from the main 2400 cps load bus. However, a transfer switch is provided to automatically shift the essential command functions to the emergency

bus upon a failure of the normal source. Command override is provided for the transfer function. Voltage control is as described in section 3.7.3.4.

3.7.5.2 Efficiency

As stated in section 3.7.3.4, the shunt regulator consumes only surplus power as required to reduce the voltage to the desired point. Hence, losses occurring under light load situations do not enter into efficiency considerations. The component efficiencies are as follows: (1) blocking diode on RTG output, 96 percent, (2) inverter switching SCR's, 96 percent, (3) inverter transformation and control, 92 percent, (4) distribution, 97 percent, and (5) control elements, 98 percent. The total system efficiency is therefore the product of component efficiencies, i.e., 80.5 percent.

3.7.6 References

3.7-1 The Nuclear Space Power Program, Paper presented by Dr. J. D. Lafleur and R. T. Carpenter, 12th Nuclear Science Symposium, 18 October 1964 (Unclassified)

3.7-2 Design Study for an Advanced RTG Power Supply, General Atomics/ GA-500, July 17, 1964 (Confidential)

3.7-3 Advanced SR-90 Space Power Supply Study, Martin Company, MND-3393, August 1964, (Confidential)

3.7-4 Engineering Study of an Advanced 250 Watt, SR-90 Fueled Thermoelectric Power Supply, Hittman Associates, HIT-143, August 14, 1964 (Confidential)

3.7-5 Advanced Space RTG Study, General Electric Co., GEMS-NS-107, August 1964, (Confidential)

3.7-6 40-Watt PU-238 Power Supply Engineering Study, General Electric Company, GEMS-NS-111, January 1965, (Confidential)

3.7-7 Voltage Regulation and Power Stability in Unconventional Electrical Generating Systems, Quarterly Progress Report No. 3, General Electric Company, ASTIA No. 282718.

3.8 THERMAL CONTROL

Only a limited amount of detailed thermal control analyses have been conducted during the reporting period. The preliminary spacecraft design concepts generated to date have been reviewed and suggestions have been made which will have the effect of minimizing the most obvious thermal control problems. Further effort has been directed toward establishing an approach for thermal control and conducting generalized analyses leading toward concept development. The general thermal control requirements and the approach to concept synthesis are discussed in the following paragraphs.

3.8.1 Component Thermal Control Requirements

Equipment thermal control requirements deal primarily with operating and storage temperature limits and the dissipation of waste heat. An environmental (cold plate) operating temperature range of 14 to 100°F is suitable for virtually all components. Some items have a considerably wide range of temperature limits and a broader range of non-operating temperatures can be tolerated. Propellant for the midcourse correction (hydrazine) on the other hand should not be allowed to drop below 40°F. The ultimate layout of equipment requires a consideration of the temperature limits of individual components for optimum placement.

The power dissipation of individual components is generally small except for the communication transmitter. This is an important consideration in providing sufficient heat flow paths from the power dissipating equipment to the heat sink (radiating surface). This problem will be analyzed for the individual experiment configurations.

3.8.2 Concept Synthesis

3.8.2.1 Design Considerations

The design considerations for the synthesis of thermal control concepts for each spacecraft configuration include equipment requirements, mass penalty, and operational factors. Equipment thermal control requirements can be further grouped into three categories: (1) those associated with the RTG's, (2) the items located on extensions from the central equipment bay, and (3) equipment located in the central bay area.

A ground-rule defining RTG size and exterior temperature was established for the synthesis of thermal control concepts in other areas. The surface temperature is considered to be 510°F and the size-capacity relations are discussed in subsection 3.7.

The temperatures of the components located on extensions from the spacecraft are controlled largely by radiant interchange between them and the RTG's and the space environment. It is difficult to identify specific problem areas until an analysis of the specific components is made. The temperature limits of these components are generally broad, and the thermal control problem is not expected to be unusually difficult. One problem area which may require some special consideration, however, is the effect of thermal gradients on high-gain antenna performance.

Of the components located in the central equipment bay area, the chemical propellant for the midcourse correction will probably have the most stringent temperature limitations. This propellant, however, may be consumed during the early part of the mission, and the temperature control requirement will be relaxed for the remainder of the mission. If installation proves practical, the time-varying power dissipation of the electronic equipment may be offset by an appropriate placement of the voltage regulator shunt resistors of the power conditioning system. Consideration must also be given to the possible use of RTG heating to stabilize the bay component temperatures.

The actual mass penalty for thermal control may be manifested in several ways. These include mass of insulation, mass penalty for louvers, increased structural mass (to obtain desired heat conduction paths and thermal radiation environment), and restrictions on component design. Thermal control concepts are largely dictated by performance and operational requirements and do not readily lend themselves to mass optimization in a strict sense. Due consideration of mass penalty is required, however, in the synthesis of thermal control concepts.

The operational factors which must be considered in concept synthesis include (1) predictability of performance, and (2) reliability, both in terms of active thermal control elements and in terms of the effect of environmental extremes on other component reliability, and flexibility of design. Excellent thermal performance can sometimes be predicted theoretically by the use of special devices such as reflective finishes, solar reflective paints and controlled heat shorts. While such devices may be required in any design, they are readily affected by surface condition, prior handling, etc. Such uncertainties must be minimized in concept synthesis and design.

Flexibility in thermal control design is required so that changes in power dissipation, temperature limits, and trajectory parameters will have a minimum effect on the spacecraft. Power loads will probably

be uncertain until the spacecraft is well into the design phase or even into manufacture because operating conditions may change or components may be substituted.

High reliability in thermal control elements requires that a minimum of active interdependent components be used. Louvers, which are simple and highly reliable mechanisms, may be required to maintain adequate control during variations in power dissipation and changing space environment. The Mariner type louver arrays are particularly well suited, because the louvers operate independently or in small sets so that failure of one set does not completely upset the thermal control function.

3.8.2.2 Isothermal Module

The only thermal control concept that has been analyzed sufficiently to be discussed in this report is what will be termed the "isothermal module." In this concept, the vehicle surface is made of a highly conductive material, such as aluminum, so that the temperature variations over the surface are small.

This concept permits the designer to take advantage of the constant heating from the RTG's as a temperature stabilizing effect over the entire mission. The amount of heating by the RTG's is controlled by the proper selection of coatings on the sides of the spacecraft exposed to the RTG's, by insulation of spacecraft surfaces, and by shielding the RTG's from the spacecraft. Correspondingly, heat dissipation and temperature control is achieved by the selection of proper coatings on the surfaces not seen by the RTG's and by the use of louvered surfaces.

In all of the spacecraft concepts studied to date, it is possible to locate louvered surfaces so that they are essentially in the shadow of sunlight for the entire mission, at least after earth escape. The estimated performance of a practical louver design was determined from the work of Plamondon (Reference 3.8-1) and from analyses conducted at the Fort Worth Division of General Dynamics. Figure 3.8-1 was constructed for the preliminary sizing of louver areas with no solar irradiation. The effects of solar radiation will also be analyzed when the operational sequence is better understood.

The initial analyses conducted to establish the feasibility of an isothermal module concept without exterior insulation were conducted with reference to spacecraft concept A. These results, however, are expected to be generally applicable to the other configurations.

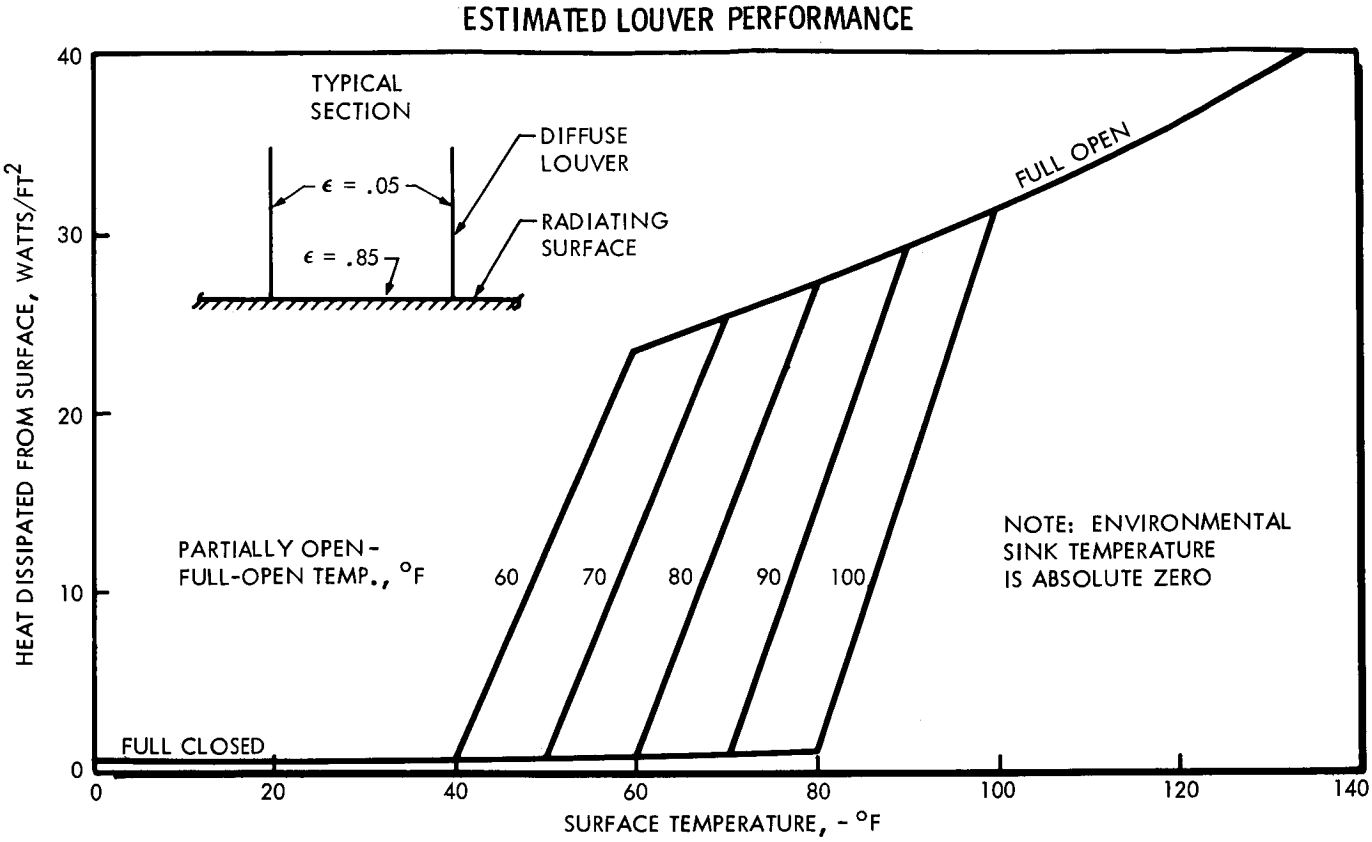


FIGURE 3.8-1

The spacecraft configuration is illustrated in Figure 5.1-1 of Section 5. The central equipment bay is characterized thermally by two regions: (1) the side surfaces, and (2) the upper and lower surfaces in the direction of the spin axis. Because the spin axis is oriented nominally perpendicular to the solar vector, the sides are the primary surfaces affected by solar radiation. These sides also receive heating from the RTG's. The upper and lower surfaces receive very little heating from the sun and RTG's and are a logical location for thermal control louvers.

Considering the three characteristic surface areas--louvered area, unlouvered area on top and bottom, and side area--there is an indefinite number of combinations of surface properties and insulation applications that can be evaluated for thermal control. The approach selected for this analysis is to initially assume no insulation on the spacecraft surfaces, use the louver area provided by initial configuration development, and then analyze the effect of various surface properties on the other two surface areas. In order to make the analysis more realistic, the coating properties are assumed to be those of a mosaic of low emittance aluminum and white silicone paint. This combination yields a wide range of emissivities while retaining a low solar absorptivity. For a particular mosaic on the sides of the spacecraft, the heat rejected from the spacecraft can be calculated as a function of the emissivity of the upper and

lower surfaces. The rejection of heat over a range of mosaic properties with louvers full open is shown in Figure 3.8-2.

EFFECT OF COATING PROPERTIES ON THERMAL CONTROL OF ISOTHERMAL MODULE - SPACECRAFT CONCEPT A

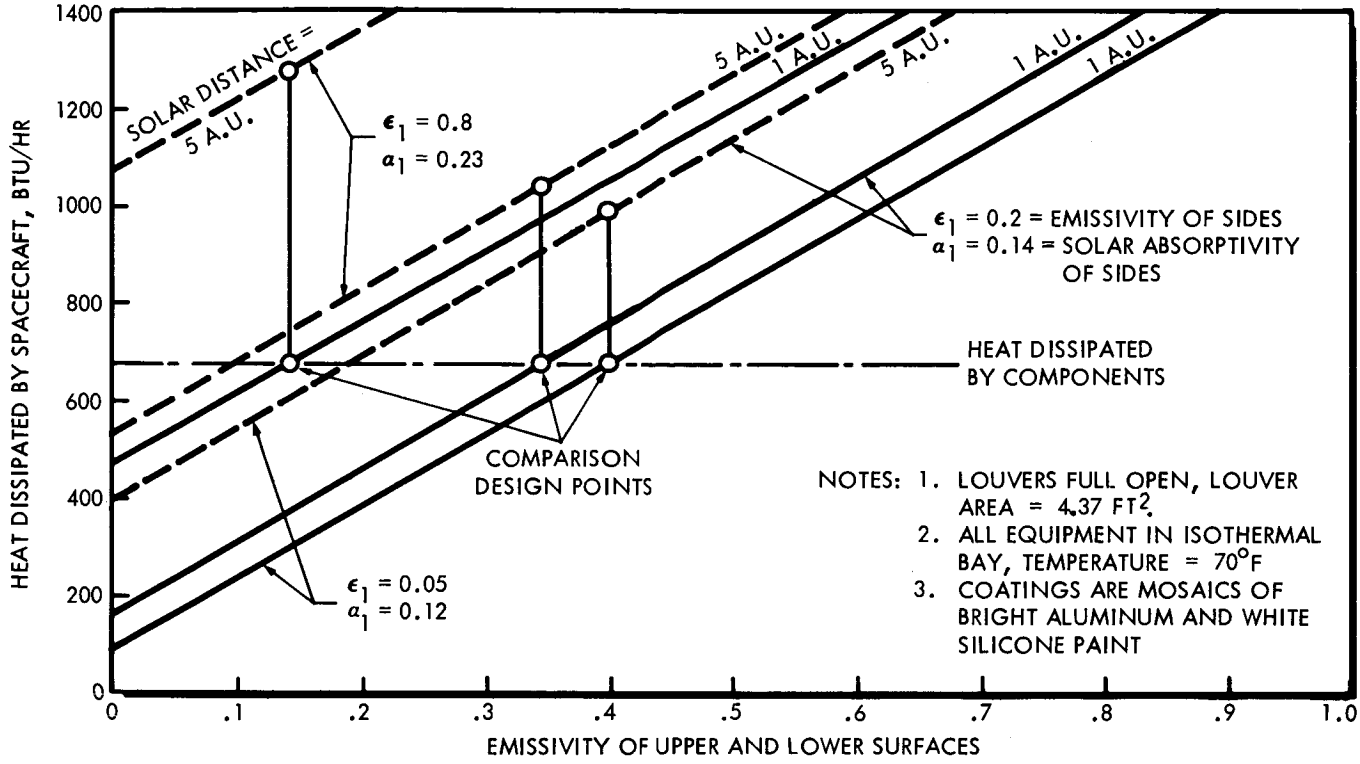


FIGURE 3.8-2

If the voltage regulator shunt resistors are designed to dissipate heat within the central bay, the total component heat dissipation remains essentially constant. Considering the design point to be the louver full open position at a solar distance of 1 A.U., the variation in the heat dissipation capability for a mission is indicated by performance at 5 A.U. It is noted from the curve that as the side surface emittance decreases (lower percentage of white silicone paint), the variation in heat dissipation also decreases, thereby requiring less control by the louvers. The capability of Mariner-type louvers with a side wall coating of low emissivity aluminum to control the heat dissipation is illustrated in Figure 3.8-3.

The trend of decreasing louver requirements with a decrease in emissivity suggests the possible advantages of insulating the sidewall surfaces. Figure 3.8-4 shows the capability of the louvers to control heat dissipation with the sides fully insulated (negligible heat flow).

Another consideration in the use of low emissivity and low solar absorptivity surfaces is the sensitivity of these properties to surface condition. The effect of deviation from the nominal or predicted

EFFECT OF SOLAR DISTANCE ON THERMAL CONTROL OF ISOTHERMAL MODULE DESIGN WITH NO SIDEWALL INSULATION

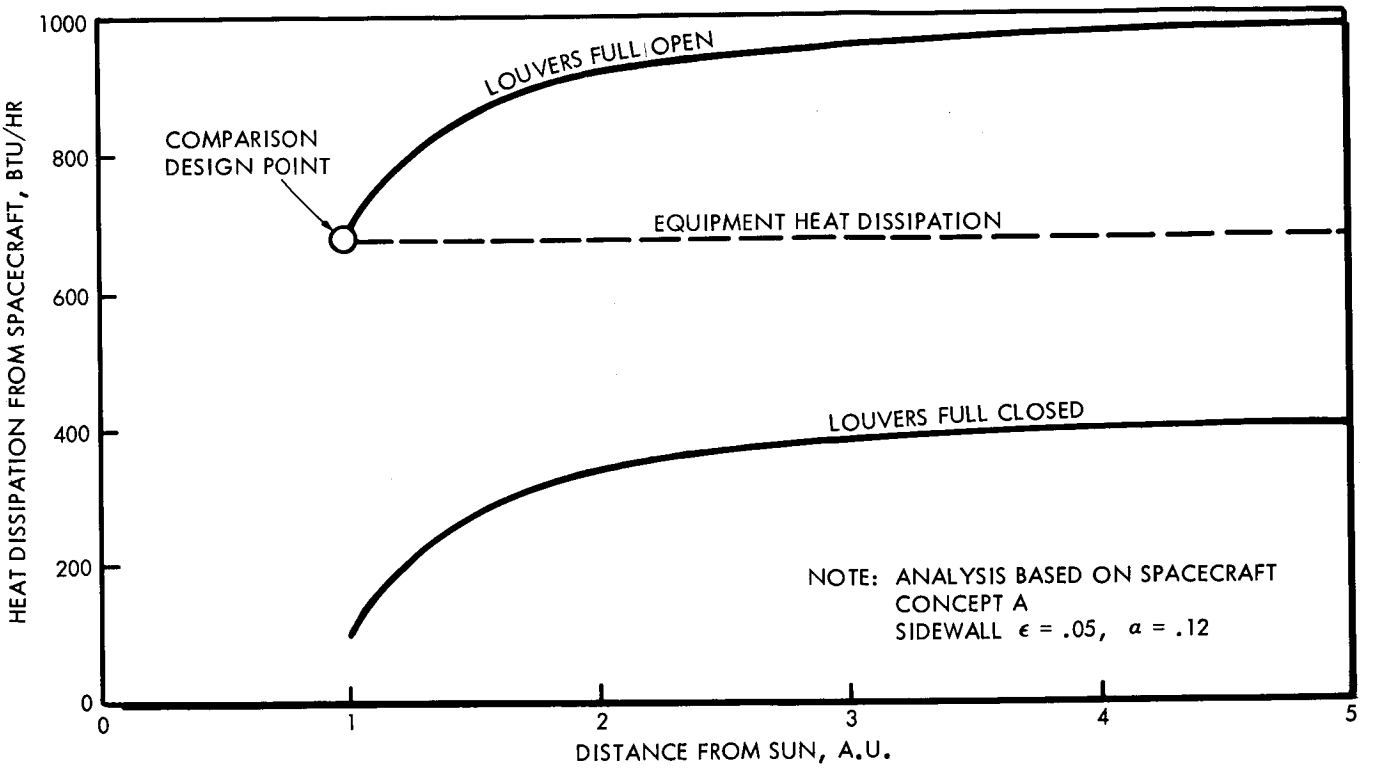


FIGURE 3.8-3

EFFECT OF SOLAR DISTANCE ON THERMAL CONTROL OF ISOTHERMAL MODULE DESIGN WITH NO SIDEWALL INSULATION

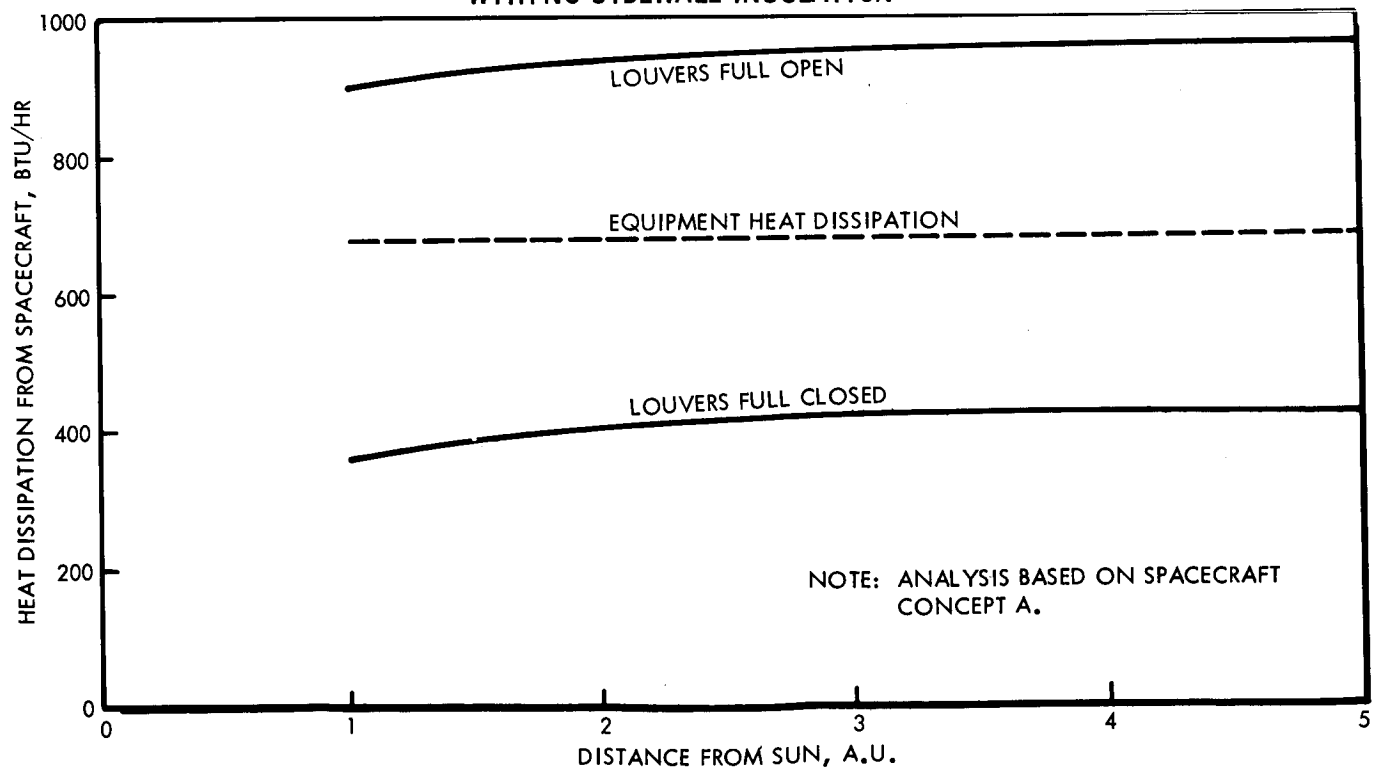


FIGURE 3.8-4

value of emissivity on heat dissipation from the spacecraft is shown in Figure 3.8-5. Similarly, the effect of deviation in solar absorptivity is shown in Figure 3.8-6. A maximum expected deviation is difficult to predict accurately, but it is not expected to be more than about 0.02 with proper handling procedures. Such a deviation would result in a significant error in predicted heat dissipation, but the louvers can be designed to handle it. If the sides of the spacecraft are insulated, the deviation in absorbed solar energy is considerably reduced.

On the basis of thermal control capability, it appears that the sides of the spacecraft should be insulated where an isothermal module concept is used. This insulation would also reduce environmental problems during the launch phase of the mission. However, the extra difficulty in installing the insulation and the delicate nature of high performance insulations may make their use undesirable. Further analyses must be performed before more exact louver area requirements and mass penalty trade-offs can be known.

3.8.3 Reference

3.8-1 Plamondon, J. A., "Analysis of Movable Louvers for Temperature Control," Journal of Spacecraft and Rockets, September-October, 1964.

EFFECT OF DEVIATION FROM NOMINAL VALUE OF EMISSIVITY ON HEAT BALANCE

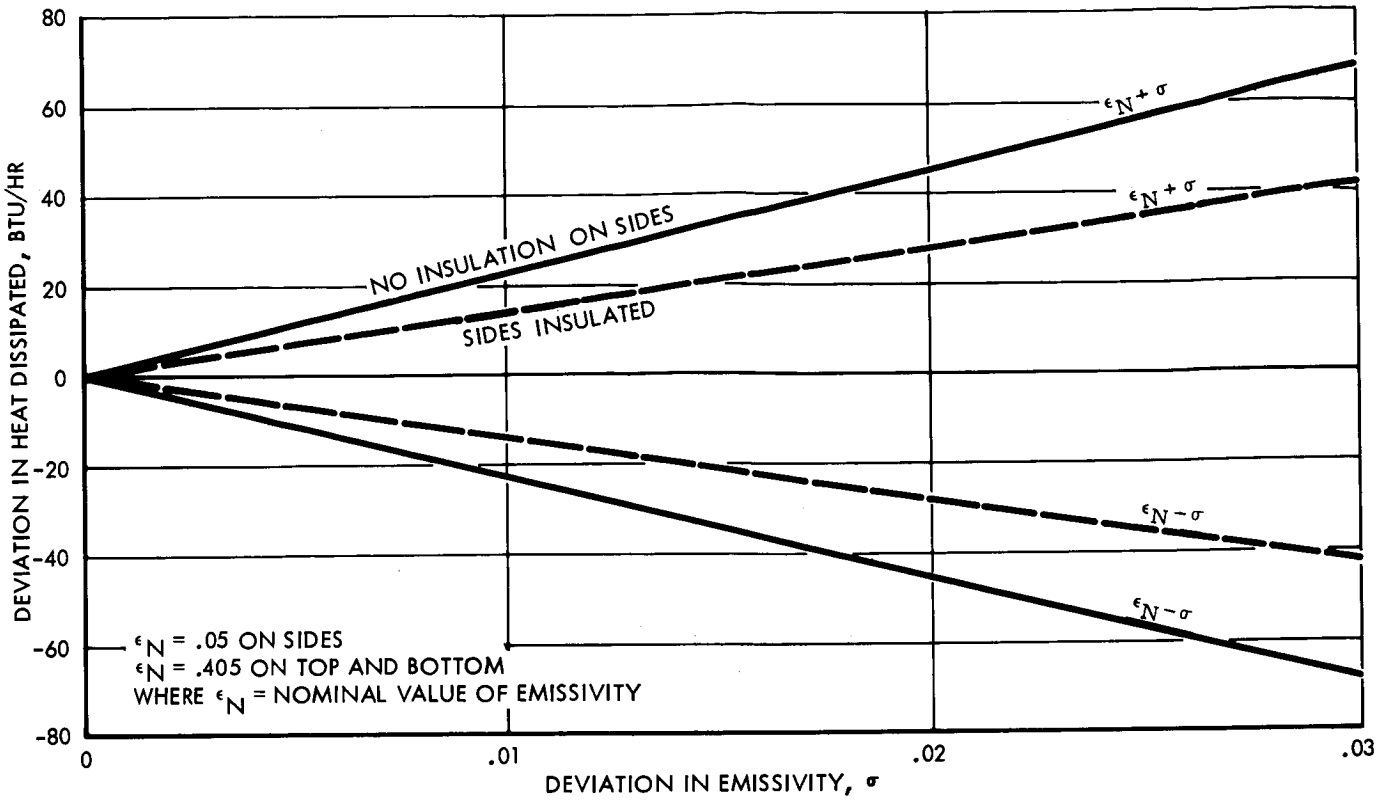


FIGURE 3.8-5

EFFECT OF DEVIATION FROM NOMINAL VALUE OF SOLAR ABSORPTIVITY ON SOLAR HEATING

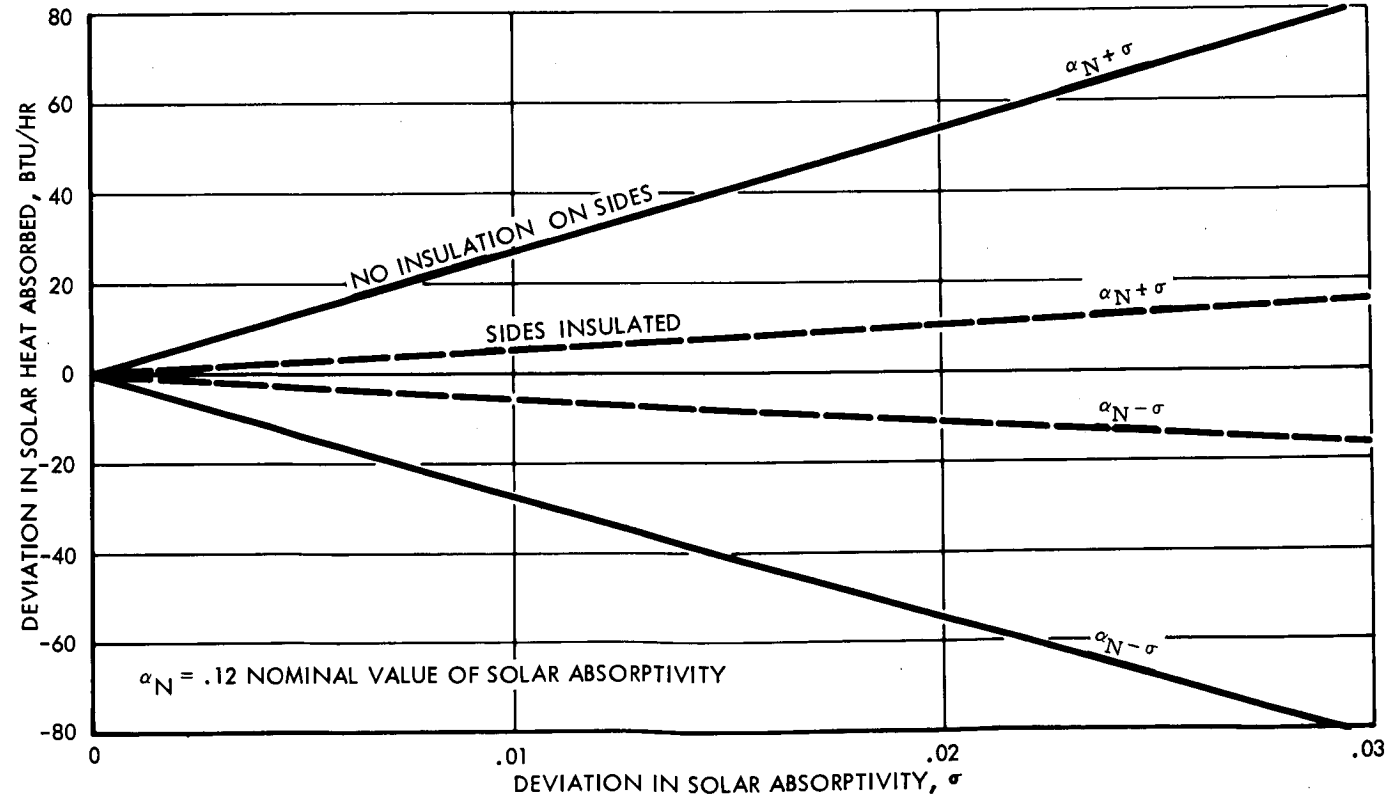


FIGURE 3.8-6

3.9 RADIATION PROTECTION

The results of the radiation protection study will be presented in the final report.

3.10 METEOROID PENETRATION PROTECTION

The objective of this analysis is to provide spacecraft design information pertaining to the protection of the spacecraft subsystems from meteoroid damage. The basic approach is to provide armor-type shielding that will prevent meteoroid penetration. It is well known that this type of information will be questionable because of the nature of its origin. The two factors contributing to the uncertainty of the analysis are (1) the lack of a physical description of impacts between appropriately sized particles and targets at velocities of interest, and (2) the lack of data on the number and size of meteoroids in space, particulatly outside the immediate vicinity of Earth. The first uncertainty is the result of present day incapabilities to accelerate particles of mass 0.1 to 1 gram to velocities of 10 km/sec and greater. The latter uncertainty results from the absence of in situ measurements of the meteoroid population in space or the lack of a significant statistical sample.

Because of these unknowns and the scope of the task, the meteoroid penetration protection analysis is based on information contained in existing literature. A consensus is used if the resulting design requirements are affected only a little by differences of opinion. The analysis attempts to consider both conservative and liberal viewpoints in matters which significantly affect the penetration requirements.

3.10.1 Basic Relationships

Although laboratory data which describe hypervelocity impact in the momentum range of interest are not available, several theoretical descriptions have been postulated in the form of mathematical equations (Reference 3.10-1). All have merit, but none yield significantly different results. The hypervelocity impact equation predicted by Herrmann and Jones (Reference 3.10-1) has been selected for use in the analysis, i.e.,

$$(1) \quad t_T = 1.119\, \rho_T^{-2/3}\, \rho_P^{1/3}\, m^{1/3} \ln\left(1 + \frac{\rho_P^{2/3}\, \rho_T^{1/3}\, V^2}{39.23\, H_T}\right)$$

where t_T (meters) is the maximum thickness of a target having a density ρ_T (g/m^3) and Brinell hardness H_T (g/m^2) that will be penetrated by a particle of mass m (grams) and density ρ_P (g/m^3) that is moving at a velocity V (m/sec) relative to the target.

A relationship such as the one described in Equation (1) provides a means of obtaining the thickness of a specific shielding material that will prevent penetration by a meteoroid of a particular mass, density, and relative velocity. The analysis is then applied to the determination of these unknowns--mass, density, and velocity. The selection of a worst-case set of values for these meteoroid parameters would constitute a design point, and such a selection must be made for any ultimate design application. The usual approach (Reference 3.10-2) is to delay the decision at this point and bring in another meaningful consideration, namely, the effect that the amount of spacecraft exposed area and the length of time it is in the meteoroid environment has on the realization of meteoroid impacts.

The proposed analysis defines a meteoroid flux for a given portion of space, i.e., the expected number of meteoroids of mass m or greater passing through a unit area of the particular region of space in unit time. This flux ϕ is expressed as (e.g., Reference 3.10-2)

$$(2) \qquad \phi = \alpha m^{-\beta} = \frac{\text{number of particles of mass m or greater}}{m^2\text{-sec}}$$

where α and β are constants. Thus, if the flux is multiplied by the spacecraft exposed area and the spacecraft flight time in the particular region, the number of expected impacts I on the spacecraft of particles having mass m or greater will be the result, i.e.,

$$(3) \qquad I = \phi AT = \text{number of impacts of particles having mass m or greater}$$

where A is the spacecraft exposed area and T is staytime.

If Equation (1) is solved for m, and m is substituted into Equation (2), and the resulting ϕ is subsequently included in Equation (3), the expected number of penetrations N of spacecraft exposed area A during time T will be determined, i.e.,

$$(4) \qquad N = \alpha \left[\frac{t_T \rho_T^{2/3}}{1.119 \rho_P^{1/3} \ln\left(1 + \frac{\rho_P^{2/3} \rho_T^{1/3} V^2}{39.23 H_T}\right)} \right]^{-3\beta} AT .$$

The parameter N will be used as a basic measure of the meteoroid hazard to spacecraft. It is noted that the parameter "probability of penetration" (or "probability of no penetration") will not be employed, because it is felt that the use of this parameter only further complicates an already complicated picture. If its use is required for the calculation of the probability of mission success, such a number can be obtained at a later date; but N is considered a more meaningful design parameter.

Reflecting on the number of meteoroid environment parameters that appear in Equation (4), it becomes apparent that a completely parametric analysis is prohivitively large, and that any uncertainty in these parameters is increased by orders of magnitude in the ultimate answer. On these grounds, "average" values of the parameters α, β, ρ_p, and V are defined for each of four meteoroid environments. These values and their origins are discussed in the following subsection.

3.10.2 Meteoroid Environment

The portion of space through which a Jupiter spacecraft must pass is considered to present four different meteoroid environments, namely, the near-Earth, interplanetary, asteroid, and near-Juipter environments. As implied, these refer to different regions of the spacecraft trajectory with the exception of the asteroid environment which is considered to be superimposed on a portion of interplanetary trajectory.

3.10.2.1 Near-Earth

The data presented by Whipple (Reference 3.10-3) on meteoroid flux, density, and velocity have generally been accepted for near-Earth criteria, and they are used in this study. Data concerning the extent of the near-Earth region are those suggested by Volkoff (Reference 3.10-2).

The summation of the near-Earth parameters is as follows:

1. The near-Earth region starts at a geocentric distance of 1.0 Earth radius (6436 km) and extends to 65 Earth radii (414,115 km).

2. The near-Earth flux intensity α and flux gradient β are $\alpha = 5 \times 10^{-15}$ and $\beta = 1.34$.

3. Particle density is 0.443 g/cc.

4. Particle velocity relative to the spacecraft is 22 km/sec.

3.10.2.2 Interplanetary

It is generally agreed that the comentary flux away from Earth and in the plane of the ecliptic decreases from that found near Earth. Estimates vary from 10^{-3} to 10^{-5} of the near-Earth flux intensity. Volkoff (Reference 3.10-2) writes that, for the particle size range of importance, the flux at 1.0 a.u solar distance and away from Earth is 10^{-3} of that of near-Earth, and that it varies inversely with solar distance to the 3/2 power. He also postulates that the mean flux gradient for the interplanetary region lies between 1.0 and 0.7. This study conservatively adopts the average interplanetary cometary flux intensity as 10^{-3} of the unshielded near-Earth value and the flux gradient as 1.34. Reference 3.10-2 also indicates that the cometary particle density is the same as the near-Earth particle density.

In order to obtain an average relative particle velocity, all particles were assumed to move in direct circular orbits. Relative velocities at regular time intervals were then calculated from trajectory data for 500-, 600-, and 700-day transfers in 1976. Figure 3.10-1 shows the variation in relative velocity and heliocentric distance with time for these trajectories. The average relative particle velocity for each trajectory was obtained, and the arithmetic mean of these three averages is the value used in the subject analysis.

The summation of the interplanetary parameters is as follows:

1. The interplanetary region extends from 1.0 a.u. to 5.2 a.u.

2. The interplanetary flux intensity α and flux gradient β are $\alpha = 10^{-18}$ and $\beta = 1.34$.

3. Cometary particle density is 0.443 g/cc.

4. Relative particle velocity is 12.1 km/sec.

METEOROID VELOCITY DETERMINATION

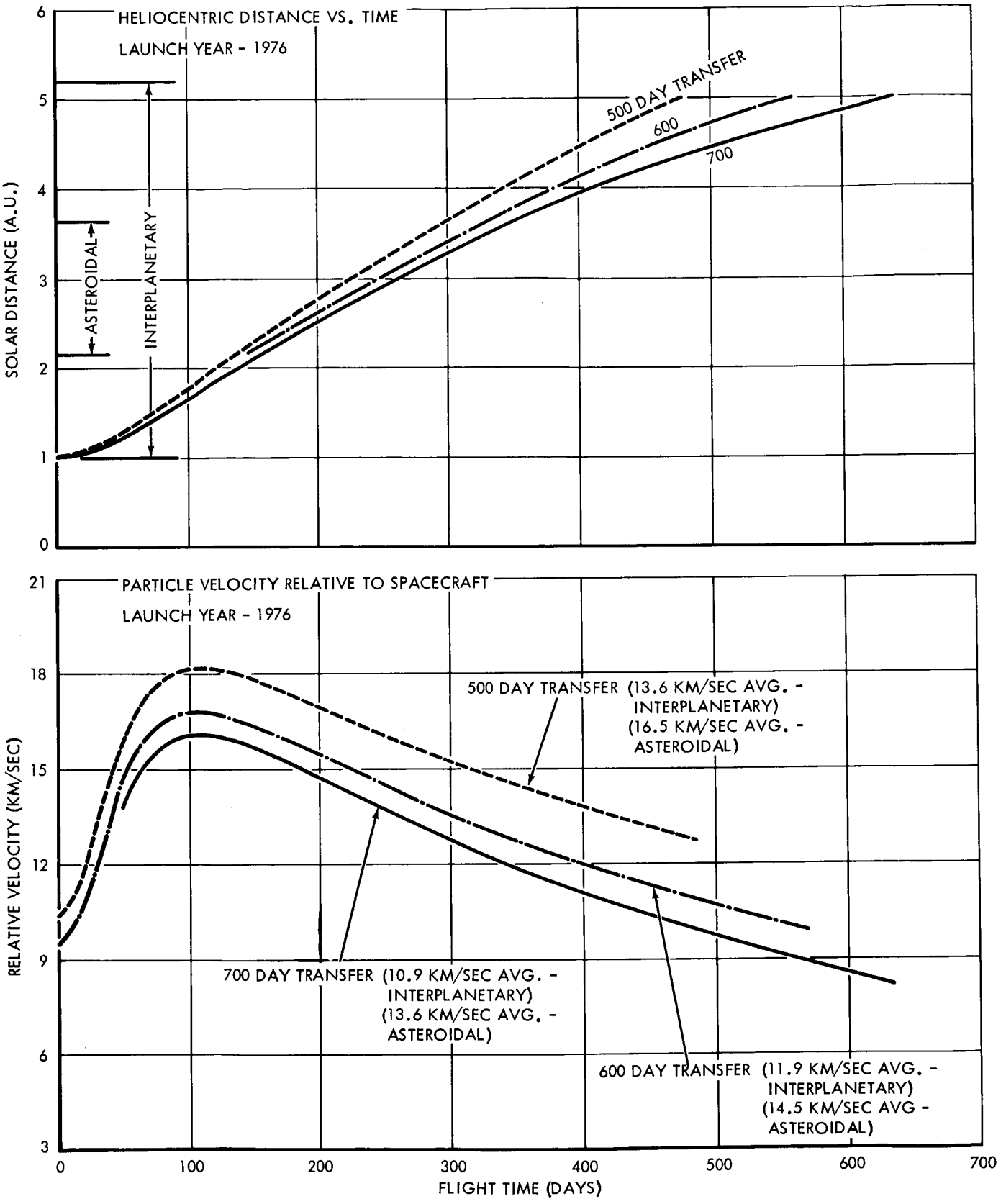


FIGURE 3.10-1

3.10.2.3 Asteroidal

The most logical studies of the hazards to spacecraft in the Asteroid Belt are based on extrapolations of data points obtained from visual observations (References 3.10-4 and 3.10-5). Objects in the Asteroid Belt that have an absolute photographic magnitude greater than 18 can be observed from Earth, and extrapolations of these data can be done on various theoretical grounds (Reference 3.10-4). It is felt that the most extreme environment that could possibly be postulated corresponds to an α of 10^{-9} and a β of 1.0, and a nominal environment corresponds to an α of 10^{-5} and a β of 0.67. Both of these environments are considered in the analysis of protection requirements.

Most of the literature defines the Asteroid Belt as having the shape of a torus with a major radius of approximately 2.90 a.u. and a minor radius of approximately 0.75 a.u. There is also general agreement that the particle densities range from 1.0 to 7.0 g/cc with 3.0 to 3.5 g/cc generally used as average. Some uncertainty exists as to whether asteroidal particles travel in circular orbits, but relative velocities will be determined here as they were in the case of the interplanetary region (see Figure 3.10-1).

The summation of the asteroidal parameters is as follows:

1. The asteroidal region extends from 2.15 to 3.65 a.u.

2. Two asteroidal flux intensities and flux gradients are considered. They are $\alpha = 10^{-15}$, $\beta = 0.76$ and $\alpha = 10^{-9}$ and $\beta = 1.0$.

3. Particle density is 3.0 g/cc.

4. Relative particle velocity is 14.9 km/sec.

3.10.2.4 Near-Jupiter

Very little information is available on the meteoroid environment in the vicinity of Jupiter. The environment employed here is based on the postulations described by Volkoff (Reference 3.10-2). The particle flux intensity is conservatively defined as 10^{-15}. The flux gradient is taken to be 1.34. The particle density is assumed to be 0.443 g/cc, but there is reason to believe the density may

be slightly higher near Jupiter because of the contribution made by the asteroids. Jupiter's meteoric debris is believed to extend to the planet's tidal radius which is approximately equal to 400 Jupiter radii.

Generally, particle impact velocity in the vicinity of a planet is assumed to be the larger of the planet's escape velocity or heliocentric velocity. In the case of Jupiter, the escape velocity at the surface is 61 km/sec and is the larger. However, because on a flyby mission the spacecraft is in the near-surface area for only a short span of the total Jupiter influence time, an average relative particle velocity of 40 km/sec is assumed for the entire near-Jupiter region. This is approximately equal to averaging the escape and heliocentric velocities.

The following is a summation of the near-Jupiter parameters:

1. The near-Jupiter region extends from the surface (69892 km) to 400 Jupiter radii (27956800 km).

2. The near-Jupiter flux intensity α and flux gradient β are $\alpha = 10^{-15}$ and $\beta = 1.34$.

3. Particle density is 0.443 g/cc.

4. Relative particle velocity is 40 km/sec.

3.10.2.5 Environment Summary

The meteoroid environment that is used in the penetration protection requirements analysis is summarized in Figure 3.10-2.

3.10.3 Parametric Analysis

This work will be accomplished during the last half of the study.

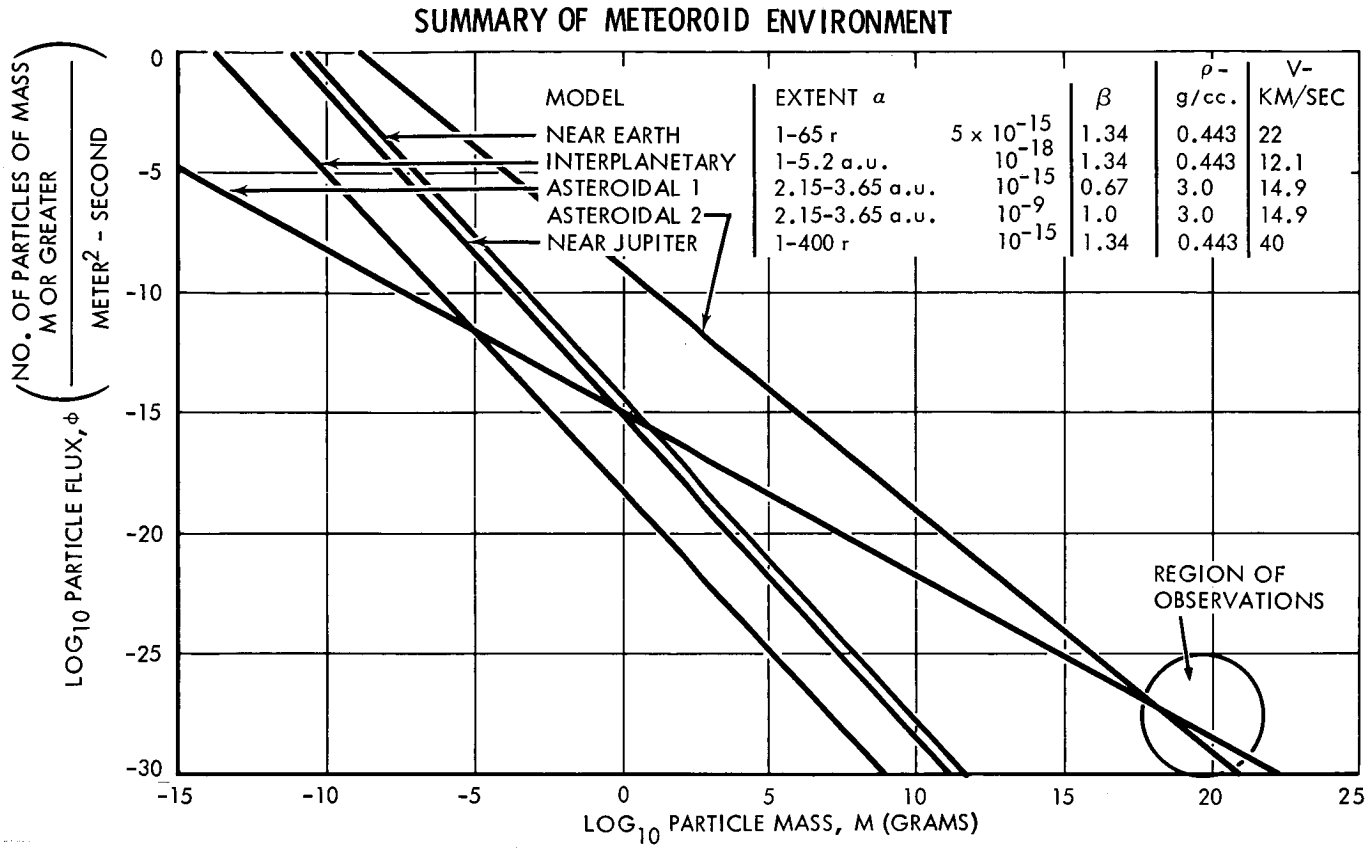


FIGURE 3.10-2

3.10.4 References

3.10-1 Procedings of the Fifth Symposium on Hypervelocity Impact, Vol. 1 - Part 2, April 1962.

3.10-2 Volkoff, John J., Protection Requirements for the Resistance of Meteoroid Penetration Damage of Interplanetary Spacecraft Systems, Technical Report No. 32-410, 1 July 1964.

3.10-3 Whipple, Fred L., "On Meteoroids and Penetration," The Journal of the Astronautical Sciences, Vol. X, No. 3, Fall 1963.

3.10-4 "Advanced Pioneer-Synthesis of System Concepts for a Mission to 10 AU," AAS Symposium on Unmanned Space Exploration, 1965, General Electric Co.

3.10-5 Bradford, D., and Martin, C. O., "Meteoroid Environment," North American Space and Information Systems Division Report SID 64-1-2, July 1963.

3.11 STRUCTURE

The study results will be presented in the final report.

3.12 CONFIGURATION

The study results will be presented in the final report.

3.13 RELIABILITY

The study results will be presented in the final report.

SECTION 4

SPACECRAFT CONCEPT EVALUATION

In the first half of the Jupiter Flyby Missions Study, no results were obtained in this study area. This section of the final report will be devoted to the guidelines, assumptions, and approach used to evaluate the spacecraft design concept synthesized during the study. The evaluation comprises four categories - Performance, Probability of Mission Success, Development Requirements, and Cost.

SECTION 5

SPACECRAFT DESIGN CONCEPTS

This subsection contains the design details of four Jupiter flyby spacecraft design concepts as evolved during the first half of the study. Specifically, design concepts for each spacecraft's science, communications, data management, spacecraft control, attitude control, propulsion, and electrical power subsystems are described. For completeness, integrated spacecraft characteristics, such as total mass and vehicle configuration, are estimated. All results reported herein are subject to revision during the last half of the study.

5.1 SPACECRAFT DESIGN CONCEPT A

In this section, a spin-stabilized Jupiter flyby spacecraft, denoted as Design Concept A, is described.

5.1.1 Design Summary

A configuration of Spacecraft Design Concept A is illustrated in Figure 5.1-1. The concept is governed by a philosophy of spin-stabilization, and its scientific capability is limited. The injected weight of the spacecraft is approximately 470 pounds. When the Atlas SLV3x/Centaur/HEKS booster is used, potential Earth-Jupiter flight times range upwards from 450 days for missions in the 1973-1980 time period. Use of the Titan IIICx/Centaur makes possible flight times equal to or greater than approximately 480 days for missions in the 1973-1980 time period.

The salient characteristics of the spacecraft are (1) interim 3-axis, reaction jet stabilization, (2) spin-stabilization, (3) a science capability on the order of 20 pounds and 10 watts, (4) a slotted waveguide antenna and a 25-watt transmitter, (5) data compression and tape storage, (6) Mariner IV-type midcourse propulsion, and (7) Plutonium-238 radioisotope-thermalelectric generators and a nickel-cadmium battery. The spacecraft performance is indicated by the following: (1) A one-bit-per-second information rate at maximum communications distance, (2) an overall data compression ratio of 15 to 1, (3) data storage for 43 K bits, (4) a vernier correction capability of 60 m/sec, and (5) 200 watts of available electrical power.

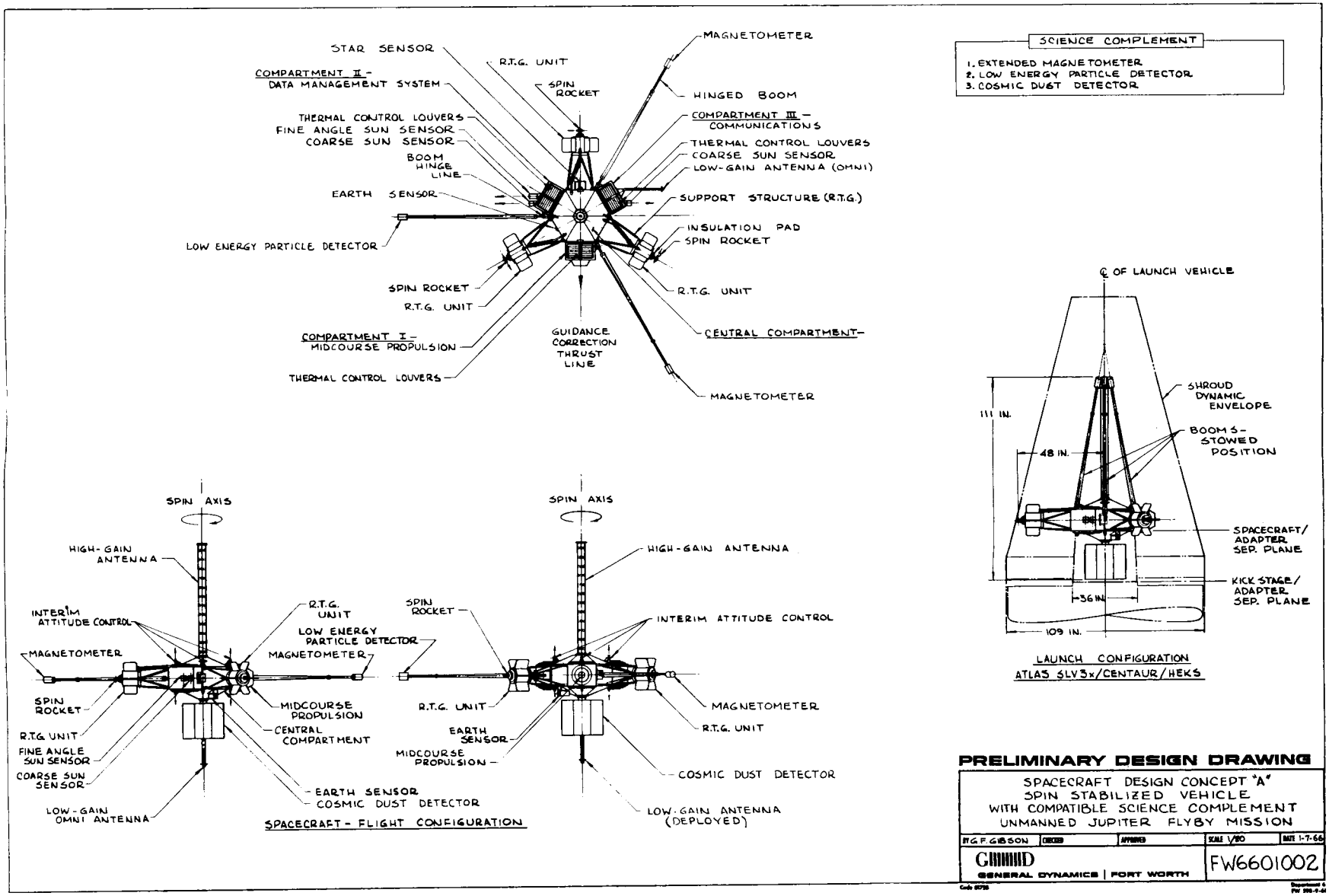


FIGURE 5.1-1 SPACECRAFT DESIGN CONCEPT A CONFIGURATION

The 3-axis stabilization system provides spacecraft attitude control between the times of spacecraft injection and completion of the vernier correction. All science is turned on prior to the maneuver and operates throughout the mission. The spacecraft is spun up by solid-propellant rocket motors following the correction. The high/medium-gain slotted waveguide antenna provides the primary communications downlink. Omni antennas are available for two-way communications during near-Earth operation and for command capability throughout the mission. The data management subsystem compresses and stores scientific and engineering data in addition to converting data to a telemetry signal. For good power management, a Ni-Cd battery is employed in conjunction with RTG units. The spacecraft is expected to pass by the planet Jupiter within approximately 4,000 km of any selected periapsis. The spacecraft weight is summarized in Table 5.1-1.

Table 5.1-1

SPACECRAFT DESIGN CONCEPT A WEIGHT SUMMARY

Subsystem	Weight, lbs.
Science	15
Communications	52
Data Management	21
Spacecraft Control	45
Attitude Control Propulsion	25
Spin Rockets	6
Midcourse Propulsion	39
Electrical Power	209
Structural and Mechanical Provisions (est.)	60
Meteoroid Protection, Thermal Control, Radiation Protection, and Reliability Enhancement	?
Total Spacecraft	472
Adapter (0.065 x Spacecraft Weight)	31
Launch Weight	503

5.1.2 Subsystem Design Information

5.1.2.1 Science

The design philosophy of Spacecraft Design Concept A imposes the following limitations on its scientific capability.

1. The requirement for simplicity implies incorporation of only a few scientific instruments.

2. Planetary instruments which must be pointed at Jupiter are not compatible with spin-stabilization.

3. The communications subsystem applicable to spin-stabilization limits data rate. It also restricts encounter trajectories to essentially equatorial flybys.

The scientific experiment package selected for design concept A is defined in Table 2.1-8, and details of the instruments are discussed in subsection 2.1. The total weight of this package is 15.0 pounds.

5.1.2.2 Communications

The communications subsystem to be used in the spin stabilized spacecraft is limited by the antenna configuration presented in subsection 3.1. The recommended antenna is a slotted waveguide which will radiate a toroidal pattern with a gain of 14 db in the plane normal to the spin axis and a half beamwidth of 2°. The minimum transmitter power necessary to maintain communications is 25 watts (see Figure 3.1-6). Because the spacecraft design philosophy is to provide minimum capability, the 14 db antenna in conjunction with a 25-watt transmitter is used as a starting point. A gain-loss table for this system is presented in Table 5.1-2.

Table 5.1-2

DESIGN CONCEPT A COMMUNICATIONS SUBSYSTEM GAIN-LOSS TABLE

	Gain	Loss
Transmitter Power	44 dbm	
Modulation		3 db
S/C Ant Gain	14 db	
Space Attenuation		278 db
Receiver Ant Gain	61 db	
Receiver Sens (40°K)		-186 dbm
Misc. Loss		2 db
System Tolerances		6 db
Totals	119	103

S/(N/B) = 119 - 103 = 16 db

If an information rate of one bit per second is assumed, the required bandwidth is 16.75 cps. Therefore, the received signal to noise rate is S/N = 16 - 10 log 16.75, and S/N = 3.8 db.

This is an acceptable signal-to-noise ratio. In practice it should be somewhat better. The 40°K receiver is a conservative estimate for the 1970 to 1980 time period, and the 6 db system tolerance is somewhat conservative.

Now that a system has been defined that will operate at maximum communications distance, consideration will be given to transmission during other phases of the mission. In the parking orbit and prior to spinning the spacecraft, the attitude is such that the slotted waveguide antenna is not usable. During this period, two turnstile antennas are used to provide omnidirectional coverage. After the spacecraft is spun, the expected trajectories do not allow the earth to fall within the $\pm$ 2° of the slotted waveguide antenna beamwidth for approximately the first 100 days of the mission. However, if the antenna gain is reduced by 4 db, the beamwidth is widened to $\pm$ 5.7 degrees. This gain reduction is accomplished by placing a shutter in the waveguide.

As calculated by use of the signal-to-noise ratio equations presented in Paragraph 3.1.4, a schedule for antennas, information rate, and signal-to-noise ratio at maximum distance is given in Table 5.1-3.

Table 5.1-3

DESIGN CONCEPT A
ANTENNA AND INFORMATION RATE SCHEDULE

Distance (au)	Antenna (type)	Information Rate (bps)	S/N (db)
0 - 0.2	Omni	8	2
0.2 - 0.5	Med. Gain	8	4
0.5 - 1.5	Hi Gain	8	5
1.5 - 3	Hi Gain	4	2
3 - 4	Hi Gain	2	3
4 - 6	Hi Gain	1	3

Note: All decimals are dropped in S/N column.

The subsystem which is recommended is shown in Figure 5.1-2.

DESIGN CONCEPT A COMMUNICATIONS SUBSYSTEM

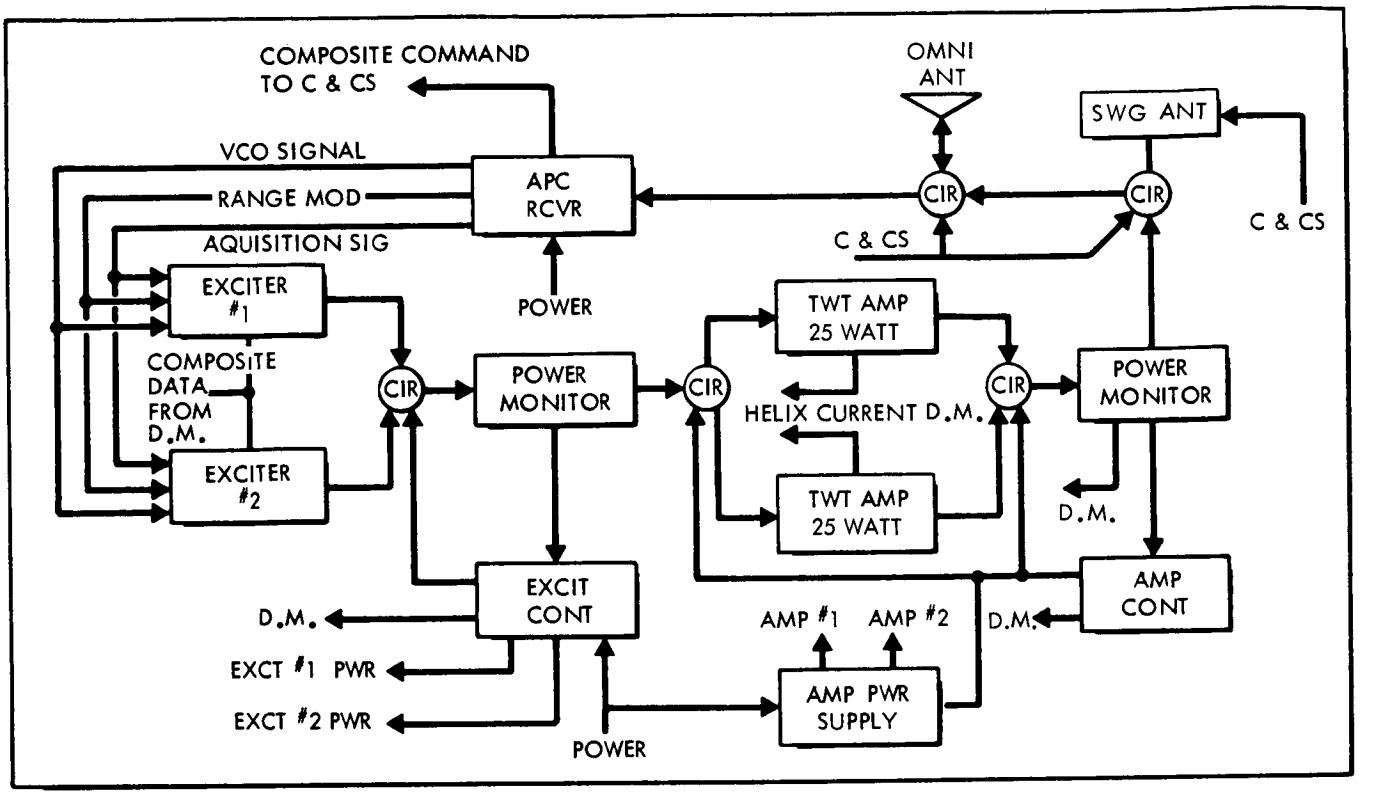


FIGURE 5.1-2

The command and control subsystem selects the proper transmitting antenna in accordance with the schedule in Table 5.1-3. The automatic phase control receiver demodulates the signal received from Earth which is of the form: $A = \sin(\omega_0 t + \phi_c + \phi_r)$ where

A = amplitude
$\omega_0 t$ = carrier angular velocity
ϕ_c = command phase modulation
ϕ_r = range code phase modulation.

The receiver tracks the phase of the component, translates it at a known ratio, and uses it as an input to the exciter. (In the event the signal from Earth is lost, a crystal oscillator feeds the exciter, and noncoherent data is received.) This signal is then phase-modulated by the composite data and transmitted back to Earth. In this manner, data transmission and two-way doppler range tracking is achieved. The receiver also demodulates the command signal and feeds it to the command and control subsystem.

The power output of the exciter and the TWT amplifier are monitored. If either of these fall below a specified level, the control circuit switches to the other unit. In this way, any combination of

two exciters and two amplifiers can be used. This is deemed satisfactory from a reliability viewpoint. No other redundancy is recommended. All other active circuits are operated at low power levels, except the high-voltage power supply, and all are solid state. Temperature limits will be maintained between -54 and + 95°C.

A list of physical characteristics is presented in Table 5.1-4.

Table 5.1-4

DESIGN CONCEPT A COMMUNICATIONS SUBSYSTEM
PHYSICAL CHARACTERISTICS

Component	Weight, lbs.
Amplifier (2)	4
Power Monitor (2)	2
Circulator (5)	5
Exciter (2)	7
APC Rcvr	9
Exctr Cont	2
Amp Cont (2)	2
Omni Ant (2)	4
S.W.G. Ant	6
Power Supply, Amp	7
Cabling, etc.	4
Total	52

5.1.2.3 Data Management

The elements and functional requirements of the data management subsystem have been discussed generally in subsection 3.2. It is expected that the subject mission can be accomplished so that a minimum of modification to equipment used for the Mariner IV is required. Maximum use of integrated circuits will increase equipment reliability and reduce size, weight, and power requirements. Data storage is required during the encounter phase of the mission when Jupiter will occlude the spacecraft. A tape recorder is employed for this purpose. Data storage at other times during the mission is a possibility.

The available transmission rates for various portions of the mission have been identified in Table 5.1-3. The anticipated uncompressed data bit rates are given in Table 5.1-5. The large difference between the anticipated data rates and the available transmission

rates indicates the need for data compression. The fan method appears to be the most applicable data compression technique for the engineering data, and a compression ratio of approximately 150 to 1 is anticipated. The zero order interpolator method, which requires less complex equipment, is also a possibility, but a compression ratio of only 30 to 1 appears feasible. For the case of magnetometer data, the fan method appears to be the only significant data compression technique. Since magnetometer measurements are expected to show considerable variation between samples, a compression ratio of only 5 to 1 is anticipated. The quantile method is the most applicable to the cosmic dust detector and the trapped radiation detector and will give a compression ratio of 100 to 1.

Table 5.1-5

ANTICIPATED UNCOMPRESSED DATA BIT RATES FOR DESIGN CONCEPT A

Type	Rate
Engineering	33.3
Magnetometer	9.5
Cosmic Dust Detector	0.6
Trapped Radiation Detector	1.6
Housekeeping	3.2
Total	48.2

When these compression techniques are used, the science data rates can be reduced to just over 2 bits per second, and the main contributor to this value is the magnetometer data. When the engineering data is considered, the total bit rate will be approximately 2½ bits per second if the fan method is employed, or the total bit rate will be approximately 3½ bits per second if the zero order interpolator method is used. Since both of these values exceed the 1 bit per second transmission rate, other methods for reducing the quantity of the data must be considered. One method, which was used by the Mariner IV, is to neglect the engineering data during the period of 1 bit per second transmission. This would still leave a data rate of approximately 2 bits per second.

Rather than reducing the actual data-gathering rates, it is recommended that data storage be used and that there be a playback of non-real-time information. This, of course, will still mean that half of the actual data must be lost during real time transmission, but all data will be received during playback. Since the most important data is that collected during the encounter phase of the

mission it is recommended that storage be provided for all scientific data which will be obtained during a nominal 6-hour encounter period (including spacecraft occulation). That is, 6 hours x 3600 seconds per hour x 2 bits per second = 43,200 bits. This storage can also be used intermittently at various times in the mission when solar interference causes the loss of communications, but the inclusion of this feature will reduce the probability of successful planetary operations. It is not felt that a redundant tape recorder is justified.

Since the total compressed data rate is less than 4.1 bits per second, consideration was given to disregarding the 8.3 bits per second transmission capability. It is recommended that this rate be included, however, to assist in verifying the validity of the data compression techniques during this early portion of the flight. Blocks of uncompressed data will be transmitted at periodic intervals, and comparisons between compressed and uncompressed data can be made.

The following specific functions of the data management subsystem elements are recommended. The DAE of the data management system buffers science data and inputs them to the DEE and the DSE at the specified rates of 1, 2, 4, and 8 bits per second. The DEE provides 4 interdependent commutator rates for 90 analog measurements. The sampling speeds of these commutators are determined by the 4 command-selectable data-transfer rates, and the DEE provides data to the communication system at 1, 2, 4, and 8 bits per second. The 4 command-selectable data modes are as follows:

- Mode I - Engineering Data Only (RT)
- Mode II - Engineering and Science Data (RT)
- Mode III - Science Data Only (RT)
- Mode IV - Science Data Only (NRT).

The data storage element provides data storage of 43.2 K bits of information at a recording rate of 2 bits per second and a playback rate of 1 bit per second. In the following paragraphs, each element of the data management subsystem is discussed in detail.

The basic differences between the DAE recommended for this mission (Figure 5.1-3) and the DAE used on Mariner IV are (1) the combination of the real-time and non-real-time sequencer into a single sequencer, (2) the implementation of data compression for the science data, and (3) a magnetometer data comparator for automatic selection of the magnetometer to be used. The combination of the two sequencers into a single unit is possible because all science sensors

DESIGN CONCEPT A DATA AUTOMATION ELEMENT

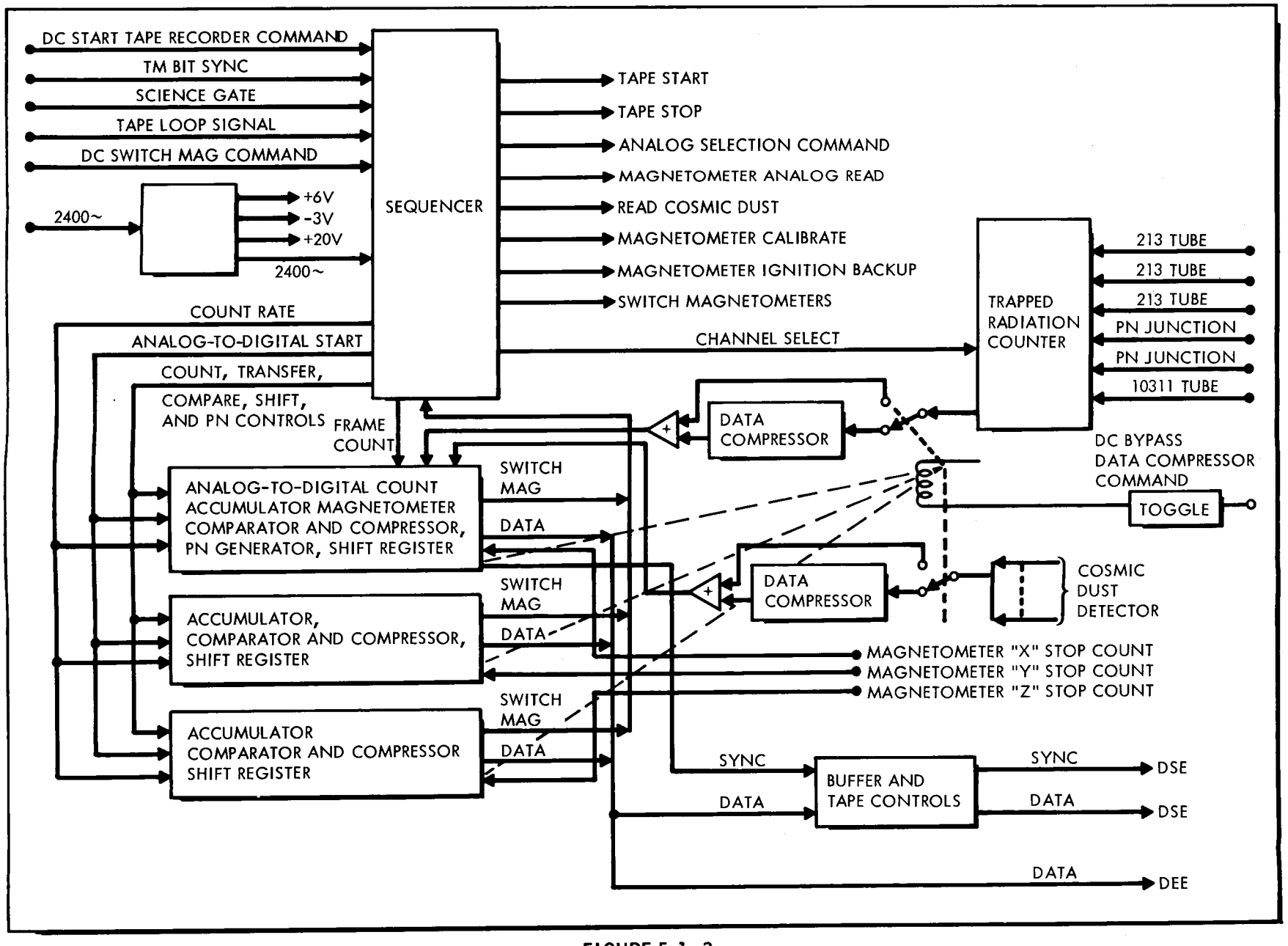


FIGURE 5.1-3

operate throughout the mission. In order to provide a means of automatic switching between the high- and the low-range magnetometer, the comparator is included to monitor constantly the difference between magnetometer current readings and preset switchover tolerances.

Basically, data from the cosmic dust detector and the trapped radiation detector enter the DAE where they are routed through two experiment-unique data compressors based on the quantile method. Magnetometer data is accepted in the form of pulse width modulated data because of the long distance between the sensor and the DAE. The pulse width data is converted into digital form, compared with the tolerances, and compressed. Three separate count accumulators are provided so that data from all three magnetometer axes can be sampled simultaneously. All science data is then combined and sent to the DEE or to the buffer and tape controls subelement for subsequent transfer to the DSE.

The capability to bypass the data compressors has been provided to enable operation if a malfunction occurs and to permit transmission of uncompressed data blocks for data compression accuracy verification. Also, the capability to override automatic magnetometer switching control has been supplied through an additional ground command.

The primary differences between the Spacecraft Design Concept A DEE (Figure 5.1-4 without modifications 1, 2, and 3) and the Mariner IV DEE are (1) data compression is included for the engineering measurements and (2) a single-channel synchronization data link replaces the Mariner IV channel link. The one-channel transmission link provides a better (S/T)/(N/B) ratio for the data.

Functionally, analog data from the engineering sensors are sampled at one of four rates:

(1) 1/20 of the basic word time by the "100" decks

(2) 1/200 of the basic word time by the "200" decks

(3) 1/2000 of the basic word time by the "300" decks

(4) 1/4000 of the basic word time by the "400" decks

This data is conditioned, multiplexed, and converted into digital format before being compressed. At the compressor, data from the event registers is combined with the commutator data. From the compressor, this combined data is directed to the data selector and buffer where it is further combined with data from the DAE. During

DATA ENCODER ELEMENT FOR DESIGN CONCEPTS A, B, AND C

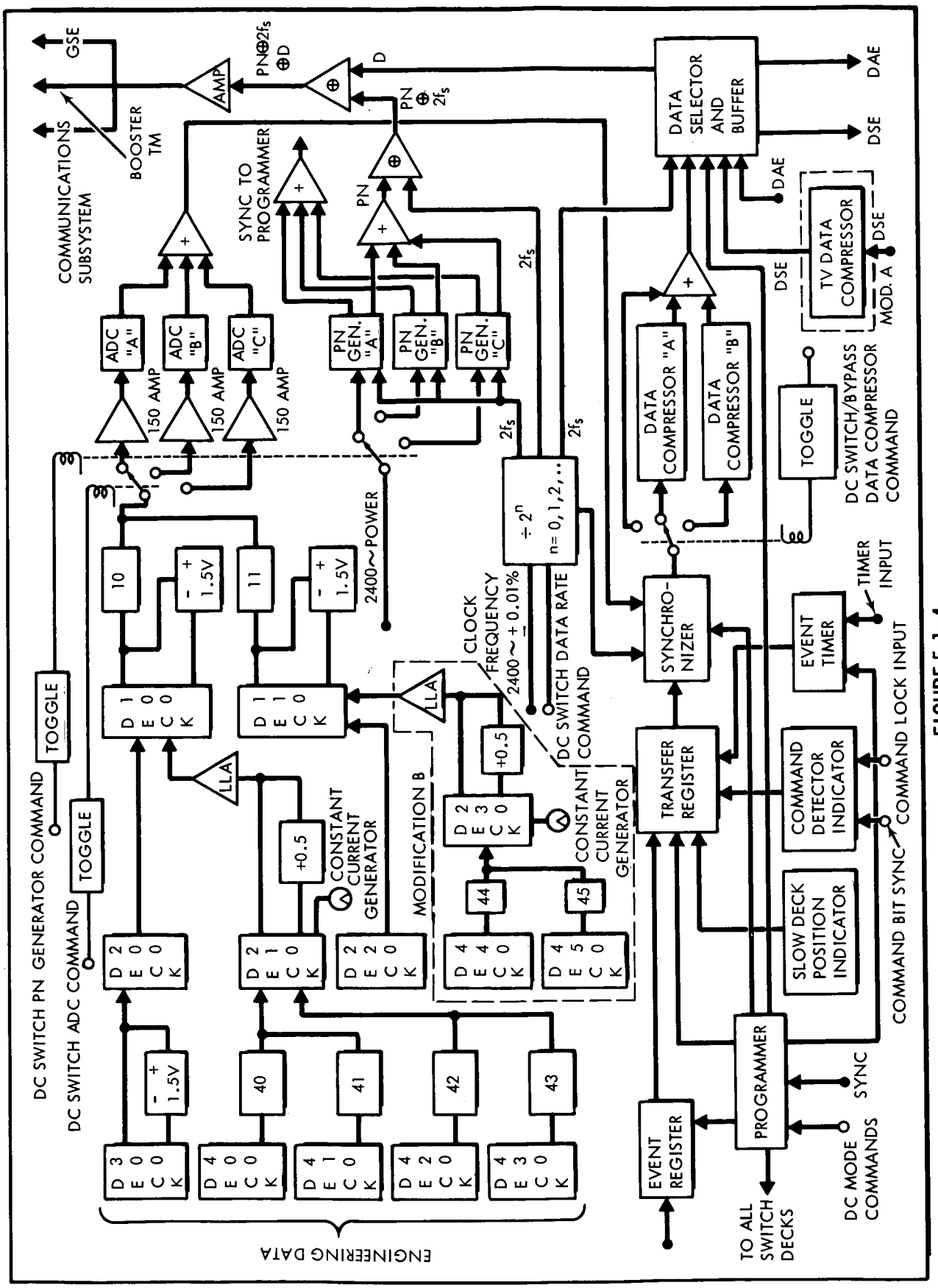


FIGURE 5.1-4

DSE playback, these previous functions continue; however, the DEE data is discarded, and only the stored DSE data is transferred to the communications subsystem.

The DSE (Figure 5.1-5) is functionally the same unit which was provided for Mariner IV except for reduced data storage capacity and decreased bit rates for recording and playback. To provide sufficient playback, it is recommended that either an endless loop tape recorder be used or that the capability to playback data in both forward and reverse directions be included.

The CDDE (Figures 5.1-6 and 5.1-7) is functionally identical to the Mariner IV CDDE. The 29 DC's and 3 QC's which were used for the Mariner IV should be adequate to accomplish the mission objectives.

The physical characteristics of the data management subsystem are given in Table 5.1-6.

Table 5.1-6

DESIGN CONCEPT A DATA MANAGEMENT SUBSYSTEM
PHYSICAL CHARACTERISTICS

Component	Weight, lbs.
DEE	7.5
DAE	4.0
DSE	5.0
CDDE	4.0
Total	20.5

5.1.2.4 Spacecraft Control

The function of the spacecraft control subsystem for the spin-stabilized Jupiter flyby vehicle is to perform master timing and sequencing for other vehicle subsystems, to sense vehicle attitude, to control vehicle maneuvers in anticipation of the vernier correction, and to control the thrust duration during the correction itself. In addition, the control subsystem properly orients the vehicle spin axis prior to spin up, and acts to null angular rates about axes other than the spin axis during the initial phase of spin up. During the initial phase of spin up, the roll channel of the cold gas attitude control system is used to begin spin up. While

DATA STORAGE ELEMENT FOR DESIGN CONCEPTS A, B, C, AND D

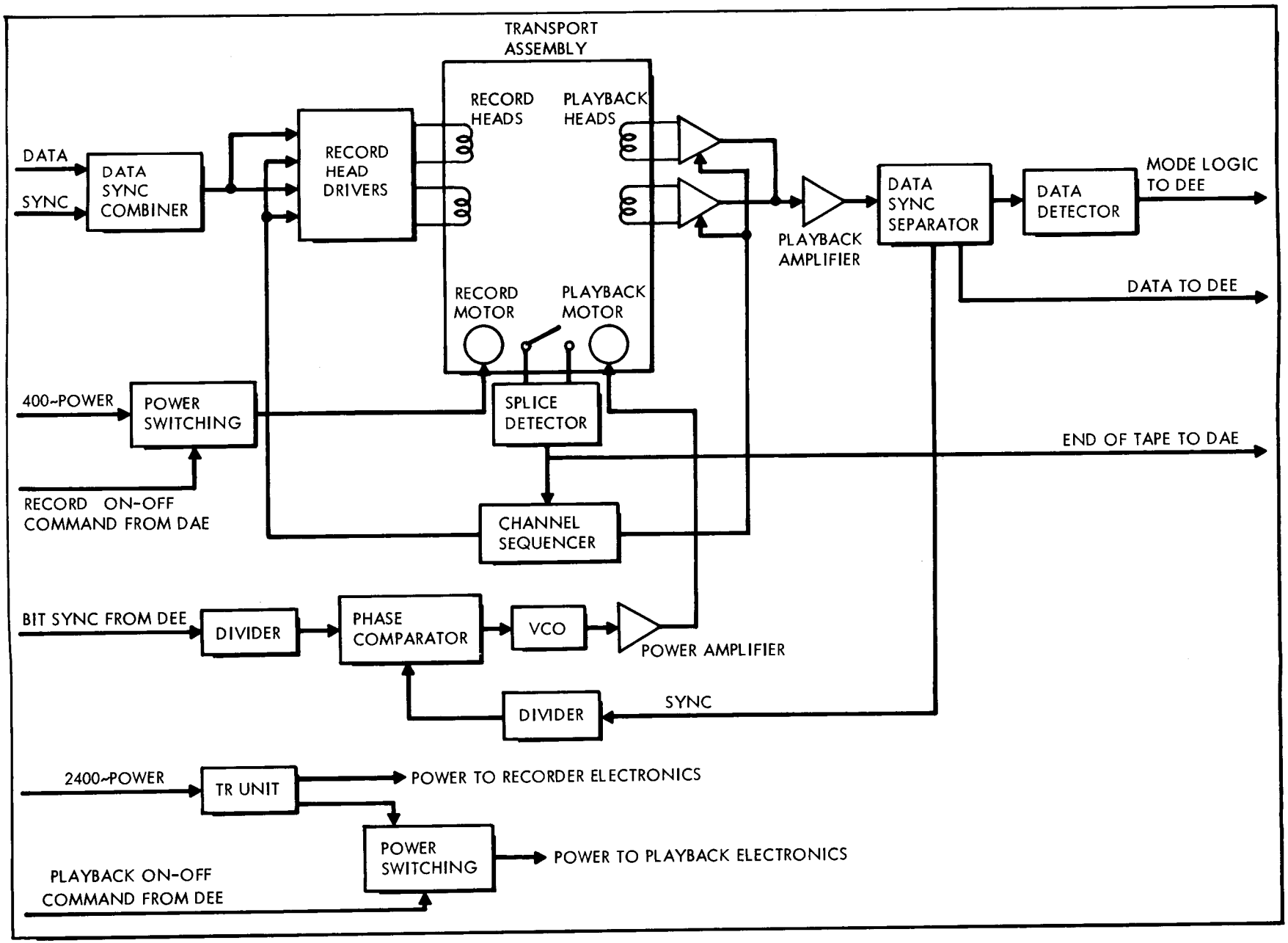


FIGURE 5.1-5

COMMAND DETECTION SUBELEMENT FOR DESIGN CONCEPTS, A, B, C, AND D

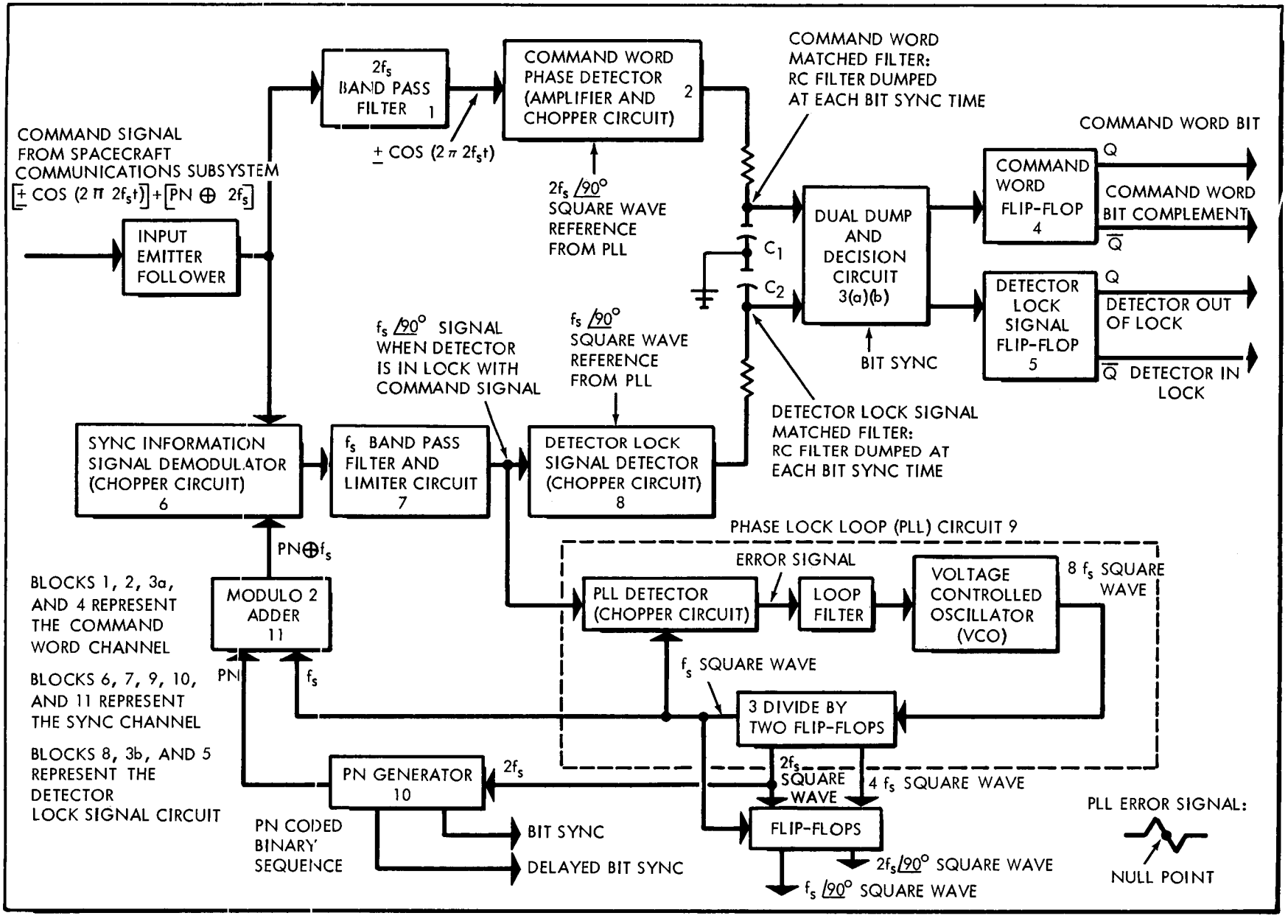


FIGURE 5.1-6

COMMAND DECODER SUBELEMENT FOR DESIGN CONCEPTS, A, B, C, AND D

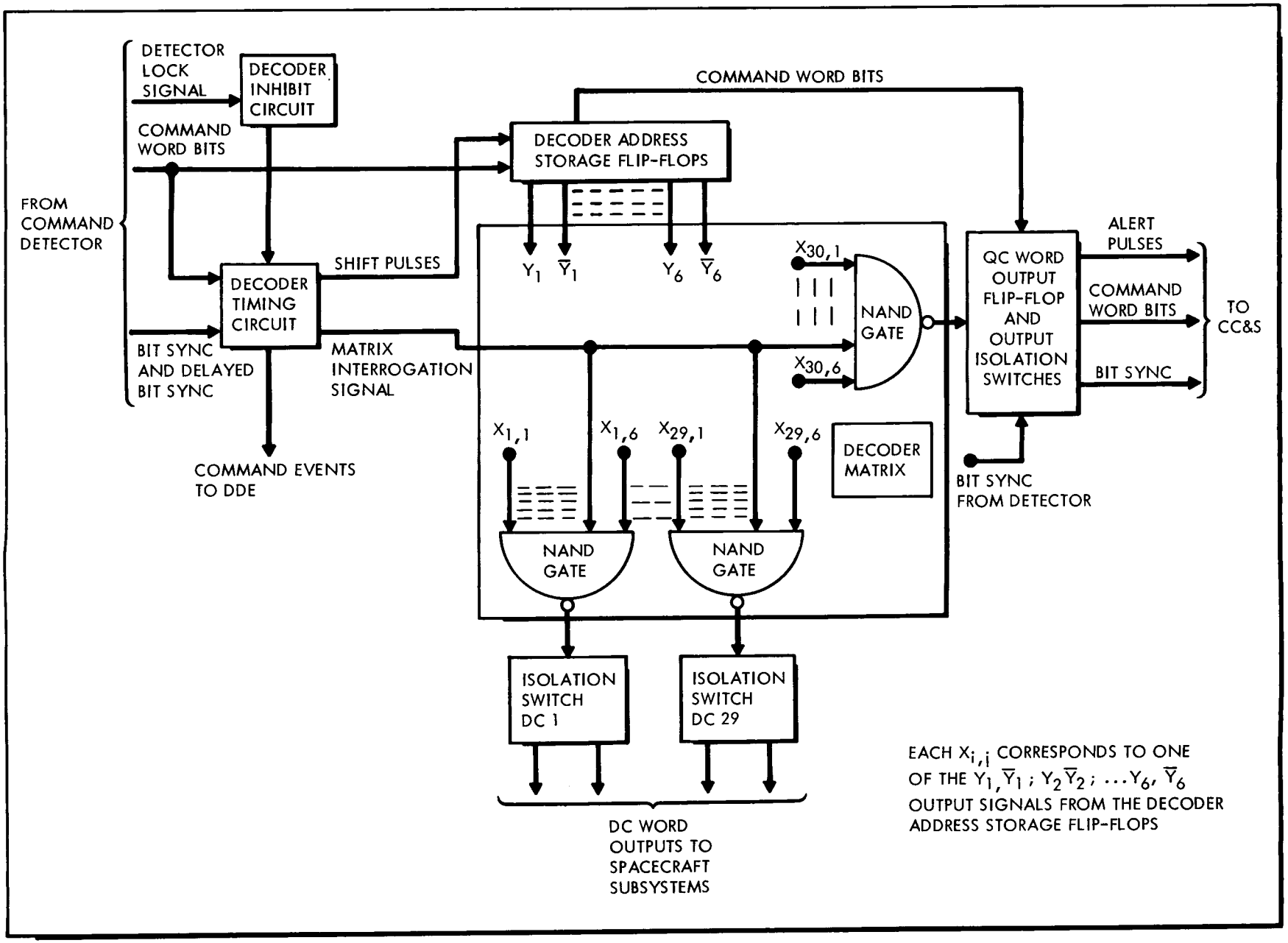


FIGURE 5.1-7

the roll rate is increasing, wobble of the spin axis is sensed with rate gyros and nulled through the attitude control subsystem.

Of fundamental importance to this vehicle configuration is the achievement of very high probability of mission success in conjunction with relatively low cost and low system complexity. To meet this basic objective, the specific functions of the control subsystem are established to reflect high reliance on available Earth based facilities. Thus, the orbit determination and the determination of the vernier correction will be implemented by means of Earth based tracking and data processing. In so far as the vernier correction is concerned, the on board control system merely orients the thrust vector and measures the velocity change.

The control system is also dependent on the choice of a terminal control concept. Basically, two concepts which involve the question of despin prior to encounter, present themselves. To despin and stabilize about 3 axes for the Jupiter encounter provides a more satisfactory platform from which to gather the encounter scientific data and from which to point a suitable antenna toward Earth for transmission of this information. The drawbacks to this approach are the requirements for (1) the despin mechanism, (2) the attitude sensing and control equipment which must now function through the encounter phase, and (3) antenna pointing during encounter and post-encounter phases. If the scientific payload is such that 3-axis attitude control is not a requirement during encounter, then despin and control mechanisms are not required to operate after the initial spin up. The spacecraft attitude control system and the control electronics are then very light in weight and require only moderate reliability because there are only ten to fourteen days between injection and spin up. Considerations such as those mentioned above led to the decision not to include any despin maneuver in the spin-stabilized vehicle configuration.

The guidance and attitude control system proposed for the spin-stabilized vehicle consists of the sensors, attitude jets, and necessary electronics needed to stabilize the vehicle, carry out the vernier correction, and properly orient the spin axis prior to spin up (see Figure 3.3-2). Spin axis orientation and spin rate are chosen to provide the proper communications geometry through the flight and to hold this orientation within some tolerance against expected en-route disturbance. These basic functions are completed in 10 to 14 days following the injection maneuver. When spin up is complete, no further use of the attitude control system is anticipated. The central computer and sequencer (CC&S) (see Figure 3.3-1) will continue to perform in its capacity as master timer and sequencer for other spacecraft systems.

The first operation following injection of the spacecraft into the transfer trajectory is to stabilize the craft with respect to the Sun and a star in anticipation of the vernier correction.

The three orthogonal rate gyros which have been running for some time begin to feed rate signals to the attitude control electronics. The coarse and fine Sun sensors are turned on. The above sequence is initiated by a signal from the CC&S. Pitch and yaw rates will be reduced to 0.5 deg/min through a loop involving the gyros and the pitch and yaw thrusters. Signals from the coarse Sun sensor are used to null the vehicle roll rate leaving the Sun in the plane of the pitch and roll axes. Error signals from the Sun sensor next control the yaw channel to position the vehicle pitch axis directly toward the Sun. The remaining task is to pitch about the Sun/vehicle line to orient the roll axis approximately normal to the ecliptic. This is controlled by setting a star tracker to the declination of a suitable star (traditionally Canopus) and pitching slowly until the star tracker indicates that it has acquired the star. A feedback loop including the star tracker and the pitch thrusters refines the vehicle attitude.

As a check on the star tracker, an Earth sensor is oriented so that, if the attitude is right, it will view the Earth and produce a suitable signal. If the Earth is not directly in view of the Earth sensor, then the star tracker has acquired the wrong star and the star acquisition sequence must be repeated.

A coarse limit cycle operation is maintained from this point until time for the vernier correction. On the basis of tracking and orbit determination, a vernier correction is computed to reduce the injection velocity errors. The correction velocity vector is reduced to a vehicle roll and pitch sequence and to a magnitude described by so many accelerometer pulses. These commands are sent to the spacecraft along with the time at which the correction is to be made.

Prior to the correction, the gyros are turned on and the attitude control is switched to a fine limit cycle. From this attitude the roll and pitch maneuvers are carried out. These maneuvers are timed, while the gyros and attitude thrusters control the angular rates. At the proper time, the vernier engine is turned on, and accelerometer pulses which measure the velocity change are used to control the velocity magnitude. During motor burn, rate error signals are sent to the propulsion unit thrust vector control vanes to keep the line of thrust constant in space. At the end of the vernier maneuver, the attitude control system reacquires the Sun and a star for attitude reference much as it did at the end of the injection.

Prior to spin up the fine attitude control is used, and the roll axis is oriented in the direction which it is to hold throughout the mission. It appears to be desirable to begin the spin up with the roll attitude jets while the pitch and yaw gyros and jets are used to damp out any wobble of the spin axis. At this point the spin jets are fired.

As discussed in subsection 3.4, the vernier correction performed prior to spin up is expected to yield a terminal position accuracy of better than 0.1 Jupiter radii. It is unlikely that any component redundancy will be required in the spacecraft control subsystem, with the exception of some parts of the CC&S. Table 5.1-7 gives the physical characteristics of the spacecraft control subsystem to be used in Design Concept A.

Table 5.1-7

DESIGN CONCEPT A CONTROL
SUBSYSTEM PHYSICAL CHARACTERISTICS

Component	Weight, lbs.
Fine Sun Sensor	1
Coarse Sun Sensor (2)	2
Earth Sensor	6
Star Tracker	10
Attitude Control Electronics	10
CC&S	12
Gyros & Accelerometers	4
Total	45

5.1.2.5 Attitude Control

An active attitude control system is required on this configuration to accomplish the various functions occurring between injection and spin up. During this period of about two weeks, the spacecraft is tracked from the Earth to determine its exact trajectory and compute the required vernier correction. After the correction has been applied, the spacecraft is oriented in the desired final attitude and spun up. All attitude control functions will cease at that point.

The attitude control problems encountered here are similar to those in the case of the Mariner spacecraft (except for spin up); and

it is intended to utilize the same general techniques, except where experience has indicated desirable modifications. Control torques will be provided by a gas jet system in which stored nitrogen gas is used. Twelve gas jets will be utilized; these jets will be operated in pairs to produce a couple about each control axis.

Following separation from the booster, any residual disturbances are removed by driving the angular rates to zero, as measured by the body-mounted rate gyros. The spacecraft then enters into the acquisition mode to activate its sensors; the spacecraft acquires first the Sun, and then the star, Canopus. Three-axis stabilization in the Sun-pointing attitude is then maintained under the limit-cycle mode of operation. The control system switches to an inertial reference in order to accomplish the attitude changes and control functions associated with the vernier correction. Control during the thrusting phase is accomplished by use of jet vanes to counteract the effect of thrust misalignments. After thrusting, the spacecraft is returned to the Sun-pointing attitude, and control is re-established by use of the Sun-sensor and Canopus star tracker. An attitude change relative to this condition is relayed to the spacecraft to orient the spin axis in the desired final attitude. This attitude change is executed by use of the inertial reference in the same manner employed for the thrusting phase. Spin-up is initiated by means of the roll jets. The pitch and yaw jets are also operated to keep the pitch and yaw rate at zero during spin up. At some preset time, the attitude control system is shut down, and the spin rockets are fired to attain final spin rate.

The design of the gas jet system is determined as a compromise between the desire to keep the total system impulse to a minimum level and to provide maximum control torque to accommodate the spin-up functions. In order to analyze this problem, the following estimates of moments of inertia and gas jet moment arms are utilized:

$$I_{ROLL} = 100 \text{ slug-ft}^2$$

$$I_{PITCH/YAW} = 70 \text{ slug-ft}^2$$

$$\text{Moment Arms} = 33 \text{ inches} = 2.75 \text{ ft.}$$

The roll axis corresponds to the spin axis, which is made the axis of maximum inertia to meet the stability criteria described in subsection 3.5.3. The pitch and yaw axes are assumed to have identical moments of inertia, although there may actually be a slight difference involved. The moment arm for the case of all gas jets is the same, and it refers to the distance between matching jets in the couple (i.e., the quantity, ℓ , defined in Figure 3.5-8). It is assumed that the gas jets are all identical.

For the case of the limit-cycle calculations, the following values of deadband angle and limit-cycle time period are postulated:

θ_E = Deadband Angle = 1 degree = .01745 radian

P = Limit-cycle Time Period = 2 weeks = $1.2. \times 10^6$ seconds

This value of deadband angle is fairly large because the spacecraft is not subject to any stringent attitude requirements during the major part of the control period. However, it is considered that the deadband is switched out, or reduced, when maximum accuracy is required during the thrusting and spin-up maneuvers. During these periods, the spacecraft can be controlled to the sensor threshold, if desired.

It remains to specify the thrust level and pulse width. The pulse width is set at 0.02 seconds, which is considered to be the minimum practical value for the stored gas system. It is desired to make the thrust level as high as possible without causing excessive fuel usage on the limit cycle mode. After some iteration, the following design point is selected:

F = Jet Thrust Force = 0.30 lb

Δt = Pulse Width = 0.02 sec

ΔI = Unit Pulse = (F) (Δt) = 0.006 lb-sec

This thrust level is considerably above the minimum value (about .005 lb.) that is attainable for a stored gas system, but it is below the maximum value (1 to 5 lbs) that can be achieved if necessary. For this data, the characteristics of the limit cycle about each axis are computed by use of the formulas presented in Figure 3.5-8, with the following results:

Control Axis	$\dot{\theta}_E$ (deg/min)	t_1 (min)	Impulse (lb-sec)
ROLL	0.283	7.06	34
PITCH/YAW	0.405	4.93	49

Thus, the total impulse required for the 3-axis limit cycle is computed as follows:

$$\text{LIMIT-CYCLE IMPULSE} = 1.5 \left[34 + 2(49) \right] \approx 200 \text{ lb-sec}$$

The factor of safety of 1.5 is considered to account for variations in the unit pulse and other deviations from the idealized assumptions used in the limit-cycle analysis. The total system impulse is obtained by adding to the above figure an allowance for maneuvering and initiation of spin up, as follows:

3-AXIS LIMIT CYCLE	200 lb-sec
MANEUVERING ALLOWANCE	25 lb-sec
SPIN UP ALLOWANCE	75 lb-sec
Total ----------	300 lb-sec

Large attitude changes may be required to accommodate the vernier correction. These maneuvers are governed by the inertial reference unit (body-mounted gyros operating in conjunction with a computer) on a rate-command mode. It is assumed that a maximum rate of 1.0 degree per second is utilized, a 180-degree attitude change requires about 3 minutes to accomplish. The impulse required to achieve this rate about the roll axis (worst case) is defined as follows:

$$\text{Angular Impulse} = (I)(\dot{\theta})$$

$$= (100) \times \left(\frac{1.0}{57.3}\right) = 1.745 \text{ ft-lb-sec}$$

The number of pulse pairs required to obtain this result is:

$$\text{No. of Pulse pairs} = \frac{(I)(\dot{\theta})}{2(\Delta I)(\ell)} = \frac{1.745}{2(.006)(2.75)} \approx 53$$

If a spacing of two pulse widths between pulses (i.e., maximum pulse rate) is assumed, the time required to achieve this rate is thus about 3.2 seconds. The amount of gas used in this process is very small, corresponding to only .64 pound-seconds of impulse. The number of pulses required is indicative of the accuracy to which the commanded rate can be maintained by the control system. For the above case, this result is 1/53 or about 1.9 per cent. This accuracy is approximately equivalent to the rate gyro resolution.

For the spin up process, it is assumed that the roll-jet valves are held open so that maximum continuous roll acceleration is applied. It is further assumed that the gas jets are required to achieve a spin rate of 1.0 radians per second, which is about 10 RPM. This initial rate reduces the effects of misalignments in the more efficient spin rockets, which are subsequently utilized to achieve final spin rate. The time required to attain this initial rate by means of the gas jets is computed as follows:

$$\text{Thrust Time} = \frac{\text{Angular Momentum}}{\text{Control Torque}} = \frac{I\dot{\theta}}{F\ell}$$

$$= \frac{(100)\ (1.0)}{(.30)\ (2.75)} = 121 \text{ seconds} = 2.0 \text{ minutes}$$

During this time, the spacecraft completes about 10 revolutions. The amount of gas impulse required for this operation is:

$$\text{Gas Impulse} = (2) \times (.30) \times (121) \approx 75 \text{ lb-sec}$$

This value corresponds to the value used earlier to determine the total system impulse requirement. Under the present concept, the attitude control system is permanently shut down after spin up by positive action squibs, which prevent the possibility of gas leakage.

For a maximum spin rate of 72 RPM (or about 7.5 radians per second) the spin angular momentum is approximately 750 foot-pound-seconds for the case of the assumed inertias. The precession due to solar radiation pressure, indicated by Figure 3.5-7, is only about 0.25 degrees if the moment area unbalance is as high as 4 feet cubed. A preliminary analysis of attitude control sensor errors and spin rocket thrusting errors shows the expected error in spin axis orientation to be on the order of 0.5 degrees. These figures indicate that precession is well within tolerable limits for the communications requirement. However, it is not known what damping torques (magnetic fields or unknown phenomena) will act on the spacecraft to reduce its spin rate during the mission.

5.1.2.6 Propulsion

The midcourse propulsion subsystem is the basic hydrazine system described in subsection 3.6.1. The system design has the capability of imparting a total velocity increment of 60 meters per second (200 feet per second) to a spacecraft mass of about 470 pounds. This corresponds to approximately a 5 σ design criteria for a launch vehicle FOM of 10-15 m/sec. Table 5.1-8 contains a summary of the physical characteristics of the midcourse propulsion system.

The attitude control propulsion system is that identified and described as Configuration A in subsection 3.6.2. In subsection 5.1.2.5, the need for a 300 lb-sec total impulse capability is indicated. As shown in Figure 3.6-10, the total system weight is estimated as being 25 pounds; this weight includes gas, tankage, and components.

The spin rockets are small, solid propellant thrusters. The approximate required impulse is 75 lb-sec. Based on manufacturer's data, the weight of the rockets is estimated as being 1 to 2 pounds. The placement of the rockets on the periphery of the vehicle is necessary, and Figure 5.1-1 shows them mounted on the RTG units. The resulting thermal considerations are obvious, and an analysis of the feasibility of this configuration is to be made during the last half of the study. A total weight of 6 pounds is estimated for the rockets, mountings,and thermal control provisions.

Table 5.1-8

DESIGN CONCEPT A MIDCOURSE PROPULSION SUBSYSTEM
PHYSICAL CHARACTERISTICS

Component	Weight, lbs.
Hydrazine	15.0
Hydrazine tank	1.3
Nitrogen	0.7
Nitrogen Tank	1.7
Bladder	0.4
Fixed Hardware	19.9
Total	39.0

Hydrazine Tank Diameter	9.6 in.
Nitrogen Tank Diameter	5.4 in.

5.1.2.7 Electric Power

The Design Concept A electric power subsystem arrangement is illustrated by the schematic diagram of Figure 3.7-6. The subsystem load profile is set forth in Table 5.1-9. The critical power situation occurs during the trajectory correction operations period when the spacecraft control system requirements are maximum. If data transmission is continued during that event, the peak load is 202 watts. By terminating data transmission for intervals of up to ten minutes out of two hours during the period, the peak is avoided as shown by the load tabulation. Peak power duty of 172 watts then occurs during the parking orbit period.

Total raw power capacity is 240 watts initially and 235 at the end of the mission. Table 5.1-10 lists ratings, numbers of component

devices, and weights. Functional aspects are described in subsection 3.7.

Table 5.1-9

ELECTRIC POWER SUBSYSTEM LOADS FOR DESIGN CONCEPT A

Subsystem / Mission Phase	Data Management	Spacecraft Control	Communications	Experiments	Total
Prelaunch	11.5	54	100	7.6	173.1
Boost	8	54	100	7.6	169.6
Parking Orbit	10	54	100	7.6	171.6
Cruise	10	10	100	7.6	126.6
Trajectory Correction	10	84	20	7.6	121.6
Encounter	11	10	100	7.6	128.6
Post Encounter	10.5	10	100	7.6	128.6

Table 5.1-10

DESIGN CONCEPT A ELECTRIC POWER SUBSYSTEM PHYSICAL CHARACTERISTICS

Component (no.)	Rating	Weight, lbs.
Radioisotope Thermalelectric Generator (3)	80 watt, 28 volt	120.00
3 Electrode Ni-Cd Battery	15 ampere-hour	21.00
Shunt Volt. Reg. Switch (3)	Eight .5a channels	1.80
Volt. Reg. Mode Controller	Signal Device	.75
Shunt Dissipation Resistors (3)	112 watts	6.00
Main 2400 cps Inverter (2)	10 ampere input	4.00
Transfer Relay (2)	10 ampere dpst	1.00
Emergency 2400 cps Inverter	2 ampere input	.50
Inverter Synchronizer	Signal device	.50
Emergency Transfer Unit	5 ampere spdt	.50
400 cps Inverter	2 ampere input	4.00
Battery Charge-Discharge Controller	2 amp. chg, 5 amp discharge	9.00
Power Distribution and Wiring		40.00
Total		209.05

5.2 SPACECRAFT DESIGN CONCEPT B

Spacecraft Concept B, which is a 3-axis stabilized, minimal capability Jupiter flyby vehicle, is described in this subsection.

5.2.1 Design Summary

A configuration of Spacecraft Design Concept B is illustrated in Figure 5.2-1. The design philosophy for this concept is to provide minimal capability and complexity in both the science package and supporting subsystems. The injected weight of the spacecraft is approximately 670 pounds. Flight times of 550-600 days are possible with the Atlas SLV3x/Centaur/HEKS or the Titan IIICx/Centaur for most launch opportunities in the time period 1973-1980.

The salient characteristics of the spacecraft are (1) a science capability of approximately 40 pounds and 25 watts, (2) a fixed,4-foot parabolic antenna and a 25-watt transmitter, (3) data compression and tape storage, (4) 3-axis stabilization using a reaction jet system, (5) periodic changing of the spacecraft attitude orientation to point the parabolic antenna at Earth, (6) Mariner IV-type midcourse propulsion, and (7) Pu-238 RTG's and a Ni-Cd battery. The spacecraft performance is indicated by the following: (1) A 17 bit per second information rate at maximum communications distance, (2) an overall data compression ratio of approximately 10 to 1, (3) data storage for 32 M bits, (4) a vernier correction capability of 60 m/sec, and (5) 200 watts of available electrical power.

Following injection into a transfer trajectory, the spacecraft acquires 3-axis stabilization using the Sun and Canopus as primary references. The cruise science is turned on. A vernier correction is executed utilizing computations and commands transmitted from Earth. The primary communications downlink is the high-gain parabolic antenna. Omni antennas are provided for two-way communications during the early part of the mission and for uplink communications throughout the mission. The high gain antenna is pointed at the Earth by periodically changing the orientation of the spacecraft axes. This is done on an average of every two weeks by computations and commands from Earth. At encounter, the spacecraft attitude is reoriented using Jupiter and Canopus as primary references. Encounter science is turned on, and encounter data is stored on tape. The expected deviation from the nominal periapsis altitude is 4000 km. Following encounter, cruise attitude is reacquired, and the encounter data is played back. The spacecraft is then switched to cruise mode operations.

A weight summary for Design Concept B is given in Table 5.2-1.

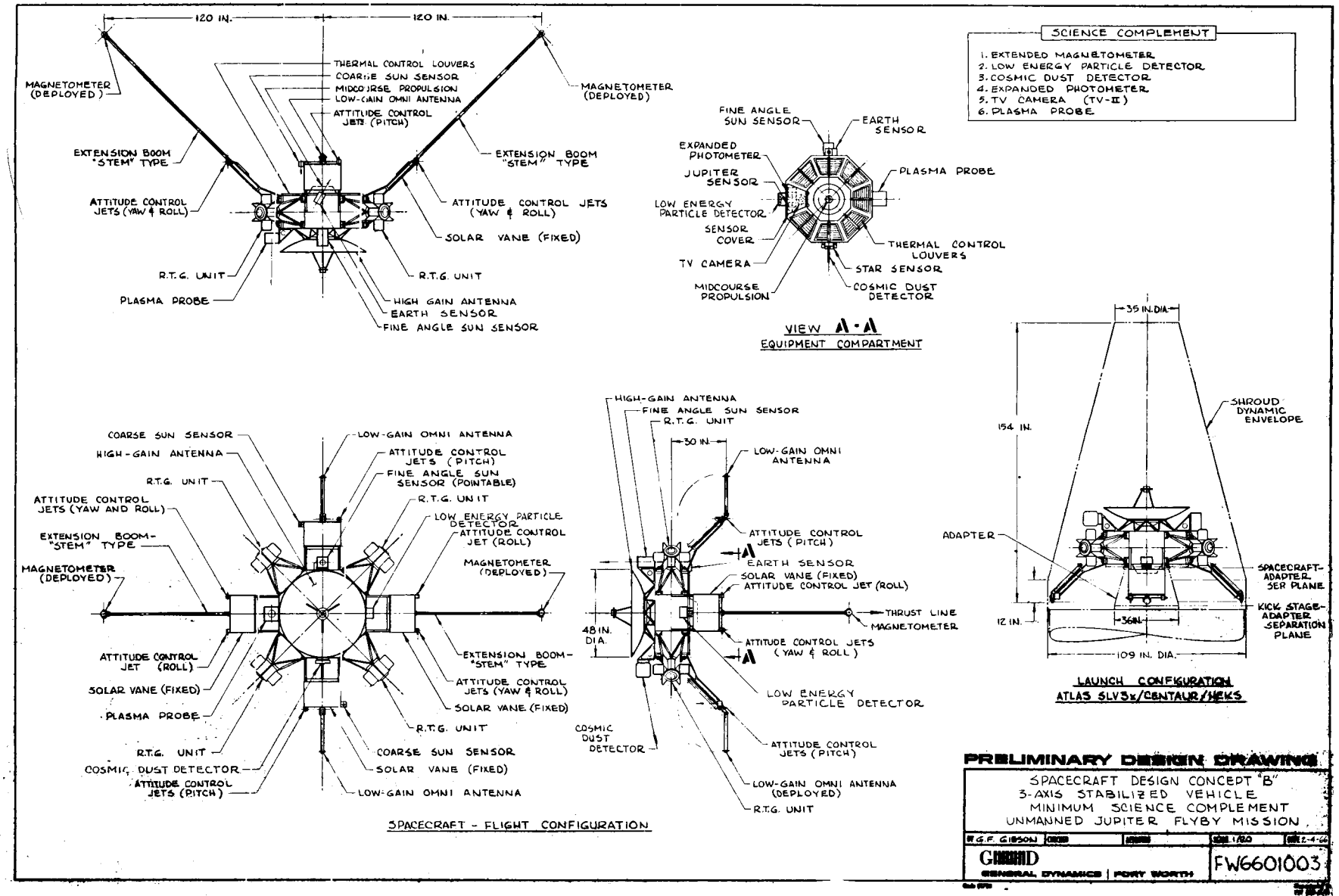


FIGURE 5.2-1 SPACECRAFT DESIGN CONCEPT B CONFIGURATION

Table 5.2-1

SPACECRAFT DESIGN CONCEPT B WEIGHT SUMMARY

Subsystem	Weight, lbs.
Science	37
Communications	62
Data Management	23
Spacecraft Control	72
Attitude Control Propulsion	110
Midcourse Propulsion	46
Electrical Power	210
Structural and Mechanical Provisions (est.)	111
Meteoroid Protection, Thermal Control, Radiation Protection, and Reliability Enhancement	?
Total Spacecraft	671
Adapter (0.065 x Spacecraft Weight)	44
Launch Weight	715

5.2.2 Subsystem Design Information

5.2.2.1 Science

Spacecraft Design Concept B incorporates a scientific instrument complement of minimal capability. A definition of the minimal scientific experiment package is presented in Table 2.1-8, and the individual instruments are described in subsection 2.1. The total weight of this package is 37 pounds.

5.2.2.2 Communications

The communications subsystem to be used in Spacecraft Design Concept B is very similar to the subsystem recommended for Design Concept A. The most important difference is the use of a four-foot parabolic antenna. The gain of this antenna is 27 db. When this antenna and the 25-watt transmitter which was used for the spin-stabilized vehicle are employed, an information rate of 17 bps is available at maximum communications distance. Table 5.2-2 is a gain-loss chart for the case of communications from 6 a.u.

Table 5.2-2

DESIGN CONCEPT B COMMUNICATIONS SUBSYSTEM GAIN-LOSS TABLE

	Gain	Loss
Transmitter Power	44 dbm	
Modulation		3 db
S/C Ant. Gain	27 db	
Space Attenuation		278 db
Rcvr. Ant. Gain	61 db	
Rcvr. Sens (40°K)		-186 dbm
Misc. Loss		2 db
System Tolerances		6 db
TOTALS	132	103

S/(N/B) = 132 - 103 = 29 db

At 17 bps, the necessary bandwidth is 300 cps. Therefore, the signal-to-noise ratio received is S/N = 29 - 10 log 300 = 4 db.

During the early part of the flight, it is not practical to point the parabolic antenna at Earth because of the large spacecraft-to-Earth cone angle. Therefore, for about the first 60 days of the flight, two turnstile antennas with zero db gain are used. These omnidirectional antennas are always used for receiving signals from Earth.

An antenna and information rate tabulation is presented in Table 5.2-3. Signal-to-noise ratios have been calculated as described in subsection 3.1.4.

Table 5.2-3

DESIGN CONCEPT B ANTENNA AND INFORMATION RATE SCHEDULE

Distance (a.u.)	Antenna	Info. Rate (bps)	S/N (db)
0 - 0.2	Omni	67	4
0.2 - 2	Parabola	133	4
2 - 3	Parabola	67	3
3 - 4	Parabola	33	4
4 - 6	Parabola	17	4

A block diagram of the recommended subsystem is shown in Figure 5.2-2. The operation of this subsystem is identical to that of Design Concept A described earlier with the exception of antenna pointing. The parabolic antenna is pointed by proper orientation of the entire spacecraft. This orientation is accomplished by command from Earth. This

scheme is proposed over one in which the antenna is steered mechanically in order to decrease overall spacecraft complexity. The parabolic antenna will have an off-focus feed in addition to its normal feed. If communications with the spacecraft is lost, the off-focus feed can be switched in for reacquisition. Table 5.2-4 gives the system physical characteristics.

DESIGN CONCEPT B COMMUNICATIONS SUBSYSTEM

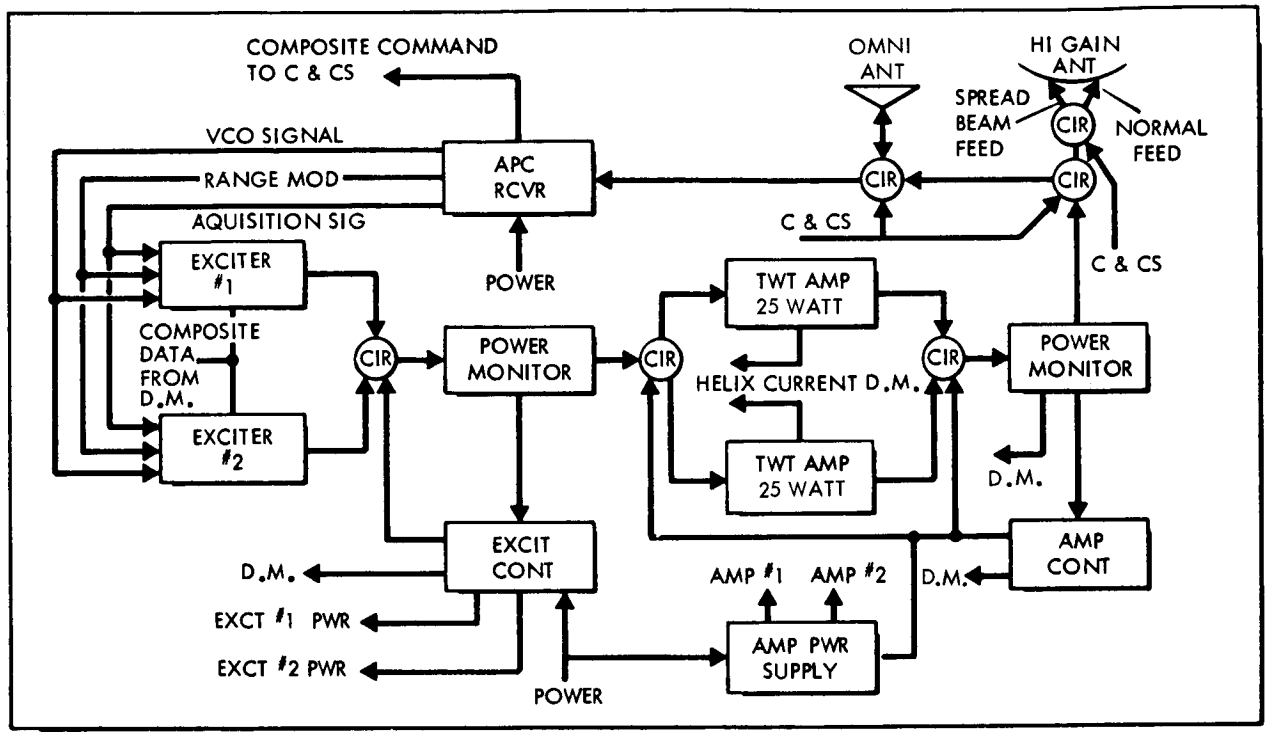


FIGURE 5.2-2

Table 5.2-4

DESIGN CONCEPT B COMMUNICATIONS SUBSYSTEM PHYSICAL CHARACTERISTICS

Component	Weight, lbs
Amplifier (2)	4
Circulator (6)	6
Power Monitor (2)	2
Exciter (2)	7
APC Rcvr.	9
Exciter Control	2
Amp. Control	2
Omni Ant. (2)	4
Parabolic Ant.	15
Power Supply HV	7
Cabling, etc.	4
Total	62

5.2.2.3 Data Management

The requirements of the elements and functions of the data management subsystem have been discussed generally in subsection 3.2. As in the case of Design Concept A described in subsection 5.1.2.3, microintegrated circuitry is incorporated whenever possible, and a tape recorder is employed to store data at Jupiter encounter.

The transmission rates available for various portions of the mission have been previously given in Table 5.2-3, and the anticipated uncompressed data bit rates for Design Concept B are given in Table 5.2-5. Examination of these two tables indicates that data compression is required for at least half of the flight. Either the fan method or zero order interpolator can be applied to the engineering data to supply compression ratios of 100-to-1 and 30-to-1, respectively. A compression ratio of 5-to-1 can be obtained for the magnetometer, plasma probe, and visible photometer data by using the fan method, and a similar compression ratio is made possible for television data by use of either the fan or stop-scan edge detector. The quantile technique will yield a compression ratio of 100-to-1 for the data from the cosmic dust detector and the trapped radiation detector.

Table 5.2-5

ANTICIPATED UNCOMPRESSED DATA BIT RATES FOR DESIGN CONCEPT B

Type	Cruise Rate (bps)	Encounter Rate (bps)
Engineering	33.3	33.3
Magnetometer	9.5	9.5
Cosmic Dust Detector	0.6	0.6
Trapped Radiation Detector	1.6	1.6
Plasma Probe	3.2	3.2
Visible Photometer		3.0
Television		20000.0
Housekeeping	3.2	5.2
Total	51.4	20056.4

Compressed data rates for scientific data, excluding television pictures, were calculated to be approximately 2 2/3 bits per second during cruise and 3 3/4 bits per second during encounter. Since compression of television data will still not allow real-time transmission, greater reliability is provided by recording the entire set of television picture elements and compressing this data during playback. Therefore,

when the fan technique is used for compressing engineering data, the total of real-time compressed data rates are just under 3 bits per second for cruise and just under 4 bits per second for encounter. If the zero order interpolator is used, the data rates are approximately 3 3/4 bits per second for cruise and just over 4 3/4 bits per second for encounter. Either rate permits combined real-time transmission of both engineering and science data, excluding television pictures, throughout the flight.

Since the most important data of the mission will be collected at encounter, it is recommended that storage be provided for all data which is obtained during a nominal 6-hour encounter period (including spacecraft occulation). Two rates of recording are necessary so that a slow rate can be used for recording the data, without television pictures, and a much higher rate can be used for recording the data in conjunction with television pictures. The capacity required for a tape recorder to store this data is 32.1 M bits. While data compression deletes the requirement to provide several of the transmission bit rates, these are included for verification and reliability purposes. Calculations were performed to ensure that the playback of encounter data would not require an excessive length of time. When a television picture compression ratio of 5-to-1 is assumed and the bit rate which is available after encounter is used, one complete playback requires only 4 1/2 days. Thus, if two playbacks are required and 1 hour out of every 6 is used to transmit real time data, the time period is less than 11 days. This length of time is considered satisfactory. If the playback interval becomes excessive, a decrease in picture resolution or intensity levels is required.

The following specific functions of the data management subsystem elements are recommended. The DAE buffers scientific data for input to the DEE and DSE at the specified rates of 8, 17, 33, 67, and 133 bits per second. The only differences between the DEE recommended for this mission and the one recommended for Design Concept A are the data rates described above and inclusion of modifications 1 and 2 shown in Figure 5.1-4. Three modifications are for recording engineering data at encounter and compressing the television data. The data storage element provides storage for 32.1 M bits of information at recording rates of 8 and 20,000 bits per second and a playback rate of 17 bits per second. In the following paragraphs, each element of the data management subsystem is discussed in detail.

The basic differences between the DAE recommended for this mission, Figure 5.2-3, and the DAE used on Mariner IV are (1) the implementation of data compression for scientific data and (2) a magnetometer data comparator for automatic selection of the particular magnetometer to be used. The operation of this element is very similar to that

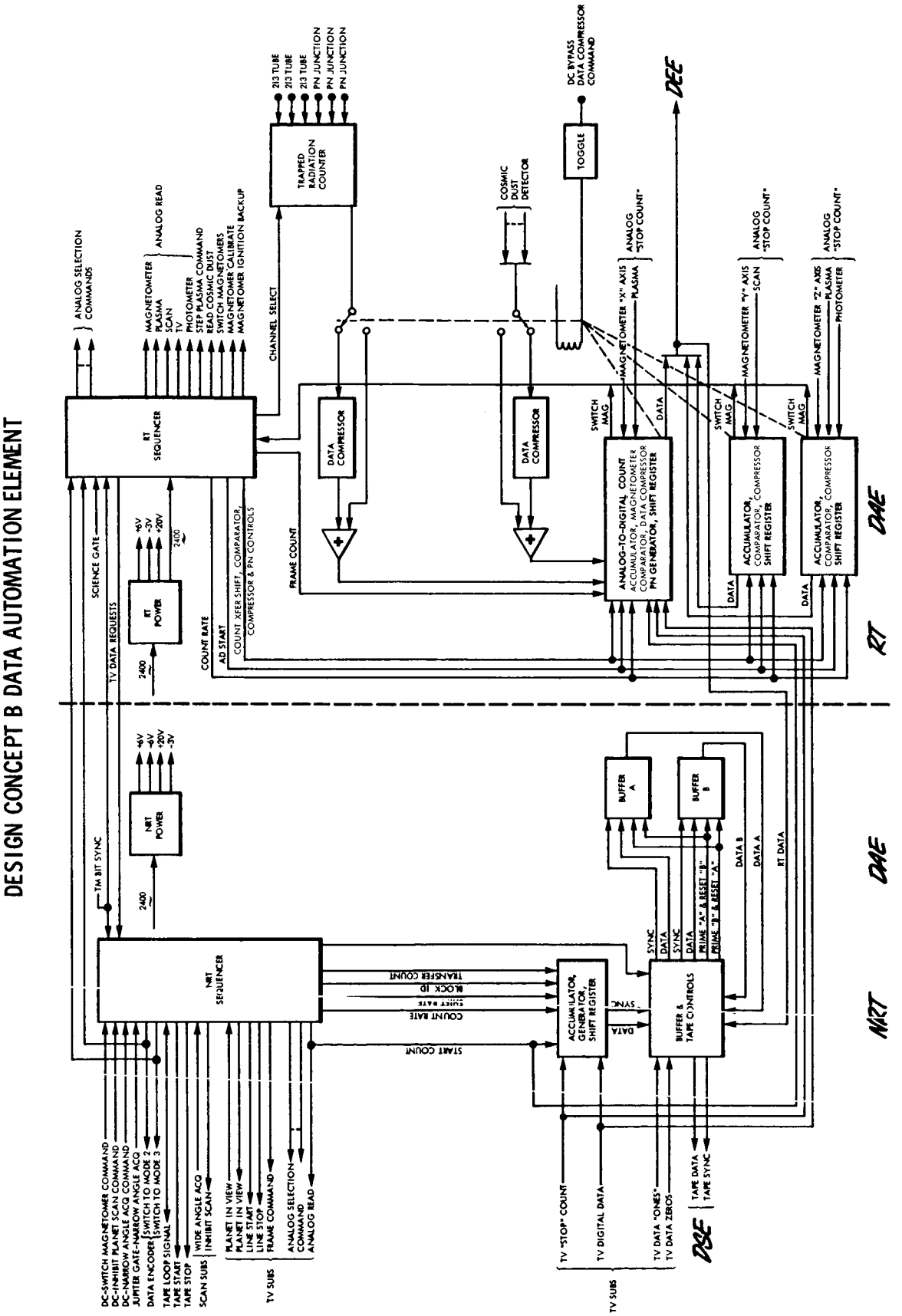

DESIGN CONCEPT B DATA AUTOMATION ELEMENT
DEE
DAE
RT
DAE
MRT
DSE
ANALOG SELECTION COMMANDS
MAGNETOMETER
PLASMA
SCAN
PHOTOMETER
STEP PLASMA COMMAND
READ COSMIC DUST
SWITCH MAGNETOMERS
MAGNETOMER CALIBRATE
MAGNETOMER IGNITION BACKUP
ANALOG READ
CHANNEL SELECT
213 TUBE
213 TUBE
213 TUBE
PN JUNCTION
PN JUNCTION
PN JUNCTION
TRAPPED RADIATION COUNTER
COSMIC DUST DETECTOR
DC BYPASS DATA COMPRESSOR COMMAND
TOGGLE
ANALOG "STOP COUNT"
MAGNETOMETER "X" AXIS
PLASMA
ANALOG "STOP COUNT"
MAGNETOMETER "Y" AXIS
SCAN
ANALOG "STOP COUNT"
MAGNETOMETER "Z" AXIS
PLASMA
PHOTOMETER
RT SEQUENCER
DATA COMPRESSOR
DATA COMPRESSOR
SWITCH MAG
DATA
SWITCH MAG
SWITCH MAG
ANALOG-TO-DIGITAL COUNT ACCUMULATOR, MAGNETOMETER COMPARATOR, DATA COMPRESSOR PN GENERATOR, SHIFT REGISTER
ACCUMULATOR, COMPARATOR, COMPRESSOR SHIFT REGISTER
ACCUMULATOR, COMPARATOR, COMPRESSOR SHIFT REGISTER
DATA
DATA
+6V
-3V
+20V
2400
RT POWER
SCIENCE GATE
TV DATA REQUESTS
COUNT RATE
AD START
COUNT XFER SHIFT, COMPARATOR, COMPRESSOR & PN CONTROLS
FRAME COUNT
+6V
-6V
+20V
-3V
2400
MRT POWER
TM BIT SYNC
MRT SEQUENCER
BUFFER A
BUFFER B
DATA B
DATA A
RT DATA
SYNC
DATA
SYNC
DATA
PRIME "A" & RESET "B"
PRIME "B" & RESET "A"
ACCUMULATOR, GENERATOR, SHIFT REGISTER
BUFFER & TAPE CONTROLS
SYNC
DATA
TRANSFER COUNT
BLOCK ID
SHIFT RATE
COUNT RATE
START COUNT
DC-SWITCH MAGNETOMER COMMAND
DC-INHIBIT PLANET SCAN COMMAND
DC-NARROW ANGLE ACQ COMMAND
JUPITER GATE-NARROW ANGLE ACQ
DATA ENCODER SWITCH TO MODE 2
SWITCH TO MODE 3
TAPE LOOP SIGNAL
TAPE START
TAPE STOP
SCAN SUBS
WIDE ANGLE ACQ
INHIBIT SCAN
PLANET IN VIEW
PLANET IN VIEW
LINE START
LINE STOP
FRAME COMMAND
TV SUBS
ANALOG SELECTION COMMAND
ANALOG READ
TV "STOP" COUNT
TV DIGITAL DATA
TV SUBS
TV DATA "ONES"
TV DATA ZEROS
TAPE DATA
TAPE SYNC

FIG. 5.2-3

described for Concept A in subsection 5.1.2.3. The plasma probe and visible photometer data are processed in a manner similar to that used in processing the magnetometer data. The main difference between the DAE's used in Concepts A and B is the incorporation of a non-real-time sequencer (similar to the one used in Mariner IV) which is connected to the scan and television camera equipment to provide automatic camera and tape recorder operation.

The only differences between the DEE's used in Concepts A and B have been discussed earlier. Greater storage capacity, two record rates, and faster record and playback data rates are the only modifications to the DSE described for Concept A; while an increase in the number of DC's from 29 to 34 is the only change to the CDDE.

The physical characteristics of the data management subsystem are given in Table 5.2-6.

Table 5.2-6

DESIGN CONCEPT B DATA MANAGEMENT SUBSYSTEM
PHYSICAL CHARACTERISTICS

Component	Weight, lbs
DEE	7.5
DAE	6
DSE	5
CDDE	4
Total	22.5

5.2.2.4 Spacecraft Control

The functions of the Design Concept B spacecraft control system are identical to those outlined for Design Concept A through the time of the vernier correction maneuver. Following the maneuver, the system continues to maintain 3-axis stabilization throughout the mission. The orientation of the spacecraft sxis is changed periodically during the mission so that the communication antenna pattern is pointed properly. This means that the primary reference (Sun) sensor must be gimballed.

The experiments to be performed at Jupiter encounter require only a 6,000 - 8,000 km accuracy in periapsis distance. Analysis shows that this accuracy can be achieved with a single vernier correction which is based on tracking and commands from Earth based facilities. During

Jupiter encounter, the primary attitude reference is Jupiter. This allows all planetary scan instruments to be boresighted along the sensor line of sight, and it removes the requirement for a scan platform. One disadvantage in the design philosophy is that the fixed high gain antenna is not generally pointed at Earth during this phase, and spacecraft-Earth communications are not possible.

The recommended CC&S for Design Concept B is illustrated by Figure 3.3-1. The proposed attitude control electronics are shown in Figures 3.3-2. A sequence of events for the operation of the subsystem is narrated below.

The sequence timer in the central computer and sequencer (CC&S) is started before lift-off. The gyros are supplied with power. The booster places the payload into an Earth orbit and then into a Earth-Jupiter transfer trajectory. The sequence timer then activates the attitude control system which promptly acquires a three-axis stabilized attitude. This is initiated by supplying the Sun sensors with power. The gyros are uncaged and the Sun search begins. When the Sun gate indicates Sun acquisition, the Sun gate acquisition signal turns on the star tracker power and a search signal to the roll switching amplifier. The spacecraft rolls about the Sun axis until a star is acquired by the star tracker. If the star acquired is not Canopus, the Earth gate interrupts the star acquisition and initiates another search. When Canopus is acquired, the Earth gate sends a no interrupt signal, the star tracker continues to track Canopus, and the Earth sensor beings tracking Earth. The gyros are caged and turned off.

The gyros, having been warmed up prior to attitude acquisition, are used for supplying control system rate feedback to limit turning rates in the Sun and star search sequences. The turn jets also emit calibrated amounts of gas in a series of very short pulses to obtain the torque for turn execution. The number of gas pulses emitted are preset so that the spacecraft turns at the limiting rate set by the gyros. This mechanization serves as a back-up event of failure of a gyros, and this back-up capability is especially important in the maneuver sequence.

The next event depends upon telemetered Earth commands. Earth tracking stations track the spacecraft, and this data is used to calculate the trajectory of the spacecraft, its position, and the parameters required for the midcourse correction maneuver. After these parameters are determined, the data is transmitted to the spacecraft. The data consists of pitch (one pulse equals one second of pitch turn at a calibrated rate), roll (one pulse equals one second of roll turn at a calibrated rate), and velocity correction (one pulse equals one pulse from a cliabrated accelerometer output). This data

is stored in the CC&S registers. At the appropriate point in time, the Earth command for execution of the midcourse maneuver is sent.

The CC&S sequence timer then controls the maneuver sequence. The attitude control system receives a fine attitude acquisition signal. This causes the Sun and Canopus sensor deadbands to narrow so that attitude is kept within narrower limits. Power to the gyros is turned on to warm up the gyros, and the sequence timer starts the roll maneuver, allowing time for the gyros warm-up. The roll gyro is uncaged so that rate feedback is provided in that channel. The spacecraft is moved in pitch in a similar manner.

The start thrust signal from the sequence timer turns on the rocket motor, and the overflow pulse from the velocity register turns off the rocket motor. The velocity register receives a pulse train from the accelerometer, which measures the Δ V correction. Roll, pitch, and yaw gyros remain uncaged and send rate signals to thrust vector control vanes in the rocket motor. The vanes deflect exhaust gases to obtain sufficient torque which opposes moments caused by uneven motor burn or other causes. This is necessary, because the gas jets do not generate enough torque to oppose attitude perturbations caused by uneven motor burning. At the end of the velocity correction, the sequence timer commands acquisition of coarse attitude in a manner similar to that used in the post-injection attitude acquisition.

Use of the fixed high-gain antenna begins at a preset time on command from the sequence timer. It is expected that the high-gain antenna will be fixed to the spacecraft along the initial Sun line axis. Therefore, either before or after antenna switch-over, the Sun and star sensors are slewed so that the spacecraft points the fixed antenna at Earth. The Sun sensor slew commands are stored in registers in the CC&S, by means of the same logic as that used in the maneuver sequence. The fine attitude acquire sequence and attitude break is inhibited, but the gyros are turned on for roll rate feedback during Sun sensor slew. On slew command, the gyros are warmed up. Then the Sun sensor slews in pitch while the star sensor tracks Canopus in pitch but continues to furnish roll information. After the pitch slew, the Sun sensor slews along the yaw axis while the star sensor tracks Canopus in yaw. The roll gyro is uncaged to supply roll rate feedback in the roll channel, preventing any movement in roll which would result in an antenna pointing error. It should be noted that the Sun slewing sequence is identical to the midcourse maneuver sequence. Here the roll, pitch, and velocity registers are supplied with zero information, whereas in the midcourse correction, the slew registers are supplied with zero information. This

slew sequence is exercised at intervals short enough to keep the antenna pointing within 2 degrees of Earth.

The Earth sensor eventually turns off when the Earth signal is too weak to permit tracking. At some point during cruise, the sequence timer turns on the Jupiter sensor. The Jupiter sensor line of sight is preset at a correct angle so that Jupiter acquisition will be immediate, and tracking can begin.

After Juipter acquisition, the sequence timer switches pitch and yaw output from the Jupiter sensor into the pitch and yaw attitude control channels and switches the respective Sun sensor outputs out. This is done without loss of Canopus. The CC&S then turns on a slew loop on the Jupiter sensor which nulls out the pitch and yaw angles between the direction of Jupiter and the line of sight of the science sensors. A pulse from the sequence timer begins the encounter mode of operation.

At the end of encounter, the sequence timer switches off the Jupiter output and switches the Sun pitch and yaw information back into the pitch and yaw channels. The Sun sensor line-of-sight is turned by the spacecraft pitch and yaw jets until it is on the Sun. The Sun and star sensors have already been slewed so that the high gain antenna is pointed at Earth before Jupiter flyby, and these slew angles are sufficiently close for the antenna to point at Earth when normal attitude is acquired. When spacecraft-Earth communications are established, the high-gain antenna pointing angles can be changed by Earth commands as desired.

Analyses,which are presented in subsection 3.4, show that the vernier correction will place the spacecraft on a trajectory having an error in the impact parameter of approximately 4,000 km RMS. Coarse attitude control throughout the mission will hold vehicle orientation to within $\pm$ 0.5 degrees. The fine mode of attitude control allows the spacecraft axes to be held close to the threshold accuracy of the sensors and control system combination, which is on the order of $\pm$ 0.1 degree.

Since the duration of the mission planned for the Jupiter flyby spacecraft is long, reliability of components parts is an extremely important consideration in the design of the subsystems. For this reason, proven techniques and high reliability components are chosen whenever possible. Since adequate sensors having large predicted MTBF's are available, the acquisition of such components is not expected to be a major problem.

Table 5.2-7 contains a summary of the physical characteristics of the control system.

Table 5.2-7

DESIGN CONCEPT B SPACECRAFT CONTROL SUBSYSTEM
PHYSICAL CHARACTERISTICS

Component (no.)	Weight, lbs.
Fine Sun Sensor	12
Coarse Sun Sensors (2)	2
Earth Sensor	6
Jupiter Sensor	6
Canopus Star Tracker	10
Attitude Cont. Electronics	20
CC&S	12
Gyros (3) and Accel. (1)	4
Total	72

5.2.2.5 Attitude Control

For Spacecraft Design Concept B, the attitude control requirements up through the vernier injection phase are similar to those previously described for Design Concept A. These requirements are to be met in the same general manner, i.e., by use of a nitrogen gas jet system. Any differences are of secondary importance, and are mostly caused by the modified capabilities of the gas jet system. The present discussion deals with the attitude control problem during that part of the mission following the vernier correction.

The design concept is considered to be the simplest case of 3-axis stabilization, because the communications antenna is fixed. This means that the whole spacecraft is maintained in a unique Earth-pointing attitude. However, the generation of the required attitude-error signals by the guidance system is made difficult by the fact that an Earth sensor which can be used at sufficient range is not available. Earth-based facilities must compute the position of the Earth by use of the data obtained from the Sun sensor and Canopus star tracker, and then command inertial rotations of the spacecraft.

Two control concepts were considered in this spacecraft: (1) the use of gas jets only, and (2) the use of reaction wheels operating in conjunction with the gas jets. The studies which are related to this spacecraft were conducted to define the basic features, requirements,

and capabilities of each approach rather than to evaluate their relative worth. The latter factor depends upon subsequent reliability comparisons of the two as well as detailed performance comparisons.

The following values of moments of inertia and gas jet moment arms were estimated for the spacecraft:

I_{ROLL} = 130 slug-ft^2

$I_{PITCH/YAW}$ = 110 slug-ft^2

Moment Arms = 100 inches = 8.4 ft

The roll axis corresponds to the antenna axis in this case, and it is to be kept pointing at the Earth. The fact that the roll axis has the largest moment of inertia is a consequence of the preferred configuration arrangement based on booster mounting considerations and is not the result of any specified criteria (as in the spin-stabilized case). It would be preferable from the standpoint of attitude control considerations that all three inertias be approximately equal in order to neutralize the gravity gradient torques near Jupiter. The moment arm for all gas jets is the same, and it refers to the distance between matching jets in the couple. This moment arm is large, because the jets are located on booms which serve as mountings for solar balance panels. The increased control efficiency associated with this large moment arm is very desirable in this case because of the long lifetime requirement. As before, all jets are assumed to be identical.

A major design consideration for this configuration is the torque requirement to counteract the effect of a discrete meteoroid impact, as described in subsection 3.5.6. Assuming a meteoroid angular impulse (H_M) of 0.70 ft-pound-seconds and an attitude angle limit (θ_F) of 1.0 degrees, the required maximum torque capability for the pitch/yaw axis (worst case) is calculated to be:

$$T_{MAX} = \frac{H_M^2}{2(I)\ (\theta_F)} = \frac{(0.7)^2}{(2)(110)(0.01745)} = 0.125 \text{ ft-lbs}$$

This requirement is applicable to both the gas jet and reaction wheel systems.

Another design requirement is the necessity to account for the effect of solar torques arising because of the Earth-pointing requirement and the unavoidable discrepancies between the center of pressure and center of gravity. This problem is described in subsection 3.5.6. Assuming an effective area A of 20 square feet (which corresponds to

a sphere about 5 feet in diameter) and an offset distance $\bar{X}$ of 0.30 feet, the value of H_s indicated by Figure 3.5-11 is 1.8 foot-pound-seconds. This quantity is important only to the reaction wheel system and represents the minimum momentum storage capability that must be provided if desaturation is to be avoided. As an additional margin of safety, it is desired that the reaction wheel be capable of absorbing one discrete meteoroid hit as well as the integrated solar torque. Thus, the wheel momentum capability should be the sum of H_M and H_s, or

$$H_{WHEEL} = H_M + H_s = 1.8 + .7 = 2.5 \text{ ft-lb-sec}$$

Although these requirements are subject to variations from individual assessments of the problem, they are believed to constitute a reasonable starting point.

For the gas jet system, the above maximum torque requirement sets the thrust level of the gas jets, as indicated in subsection 3.5.6. The following thrust level is thus obtained:

$$F = \frac{3\ (T_{max})}{\ell} + \frac{(3)(.125)}{(8.4)} = 0.045 \text{ lb.}$$

The unit pulse characteristics, assuming minimum pulse width, are thus:

$$F = \text{Jet Thrust Force} - 0.045 \text{ lb}$$

$$\Delta t = \text{Pulse Width} = 0.02 \text{ sec}$$

$$\Delta I = \text{Unit Pulse} = (F)(\Delta t) = 0.0009 \text{ lb-sec}$$

The fuel requirements for the gas jet system are defined primarily by the 3-axis limit cycle, since maneuvering requirements and external torque requirements are small. The following deadband angle and limit-cycle time period were assumed:

$$\theta_E = \text{Deadband Angle} = 0.5 \text{ degrees} = 0.00873 \text{ Radians}$$

$$P = \text{Limit-Cycle Time Period} = 600 \text{ days} = 5.2 \times 10^7 \text{ sec}$$

This value of deadband angle is consistent with the antenna pointing requirements, and the time period is simply the duration of a nominal mission. With this data, the characteristics of the limit cycle about each axis were computed using the formulas presented in Figure 3.5-8, with the following results:

Control Axis	$\dot{\theta}_E$ (deg/min)	t_1 (min)	Impulse (lb-sec)
ROLL	0.100	10.00	156
PITCH/YAW	0.118	8.46	184

Thus, the total impulse required for the 3-axis limit cycle is computed as follows:

$$\text{LIMIT-CYCLE IMPULSE} = 1.5 \left[156 + 2\,(184) \right] = 786 \text{ lb-sec}$$

On the basis of this result, a system design impulse of 900 pound-seconds is chosen to provide an added margin of safety for maneuvering, leakage, and unknowns. The system weight for this total impulse is obtained from Figure 3.6-10 for the system arrangement identified as Configuration B. This weight is estimated to be 110 pounds, which includes gas, tankage, and hardware components. This system contains dual tanks, each of which has the fuel capacity to meet the total system requirement. It also includes a dual set of jet nozzles with a switch-over capability.

In the alternate approach, the reaction wheel is the primary means of control during the long cruise period, with the gas jet system on a back-up basis. Control torques are obtained in reaction to the acceleration and deceleration of each of three wheels through the application of voltages to the control motors. There is no limit-cycle on this system comparable to that of the gas jet system, and fine control (to the sensor threshold) is possible without the expenditure of fuel. When the wheel speed reaches some predetermined limit, the gas jets are commanded to torque the vehicle in such a fashion that the response of the reaction wheel system causes a reduction in wheel speed. This desaturation is necessary whenever the integrated angular momentum of the external torque exceeds the momentum storage capacity of the wheel. As indicated earlier, a wheel with a momentum storage capability of 2.5 foot-pound-seconds would normally not require desaturation for this mission. This design criteria, in conjunction with the peak torque requirement of 0.125 foot-pounds, yields the following single wheel features; on the basis of data shown in Figure 3.5-9:

Weight of Wheel Unit = 12 lbs

Peak Power Requirement = 50 Watts

This peak power is required only when maximum torque is called for, and the average operating power will be much less. If it is assumed that three identical wheels are provided along with required additional electronics, the total weight and power requirements of the reaction wheel system are estimated as follows.

WEIGHT:	3 Wheel Units	36 lbs
	Electronics	9 lbs
	TOTAL	45 lbs
POWER:	Peak Requirement	50 watts
	Continuous	10 watts

These figures do not include the back-up gas jet system that must be provided along with the reaction wheel system.

In order to provide a system redundancy comparable to that required of the simple gas jet approach, it is necessary that the back-up gas jet system be capable of handling the mission in the event the reaction wheel system fails. This requirement means that the back-up jet system must be of identical design to that described earlier. However, the required system impulse may now be cut in half, since there will be enough fuel in the two tanks (Configuration B) to meet the mission requirement. In other words, the redundant fuel originally provided in the gas jet approach is now traded for the reaction wheel system. The weight of the back-up gas jet system is thus defined by the impulse requirement of 450 pound-seconds, and it is estimated to be 65 pounds. Thus, the total weight of the reaction wheel/gas jet system is 110 pounds. The fact that this weight is identical to the figure obtained for the simple gas jet approach is not entirely due to manipulation, for the results naturally tend this way under the given assumptions. A small weight difference in either direction could be obtained by variations in the numerous parameters involved in the calculations, but such a result would be more artificial than the condition of identical weight. The latter eliminates weight as a basis for comparison of the two approaches.

In summary, the reaction wheel system provides a finer control capability but at the cost of higher power requirements. The lifetime of the reaction wheel system is not limited by the fuel available, since saturation should be infrequent and requires negligible fuel to accomplish. For this application, the fine control capability

would be a definite advantage to the communications system, and the power requirement does not appear to be a limitation. It appears, then, that the reaction wheel system is to be preferred, unless the reliability assessment is adverse. For purposes of subsystem integration, attitude control for Design Concept B is considered to be implemented by only the gas jet system.

5.2.2.6 Propulsion

The midcourse propulsion subsystem for Design Concept B is the basic hydrazine system described in subsection 3.6.1. The subsystem design has the capability of imparting a total velocity increment of 60 meters per second (200 feet per second) to a spacecraft mass of about 670 pounds. This corresponds to approximately a 5 σ design criteria for a launch vehicle FOM of 10-15 m/sec. Table 5.2-8 summarizes the physical characteristics of the midcourse propulsion subsystem.

Table 5.2-8

DESIGN CONCEPT B MIDCOURSE PROPULSION SUBSYSTEM PHYSICAL CHARACTERISTICS

Component	Weight, lbs.
Hydrazine	21.0
Hydrazine Tank	1.5
Nitrogen	0.9
Nitrogen Tank	2.2
Bladder	0.5
Fixed Hardware	19.9
Total	46.0
Hydrazine Tank Diameter	10.8 in.
Nitrogen Tank Diameter	6.0 in.

The attitude control propulsion system is that identified and described as Configuration B in subsection 3.6.2. In subsection 5.2.2.5, a need for 900 lb-sec total impulse capability is indicated. From Figure 3.6-10, the total system weight is estimated as 110 pounds which includes gas, tankage, and components.

5.2.2.7 Electric Power

The Design Concept B electric power subsystem arrangement is illustrated by the schematic diagram of Figure 3.7-6. The subsystem load profile is set forth in Table 5.2-9. The critical power situation

occurs during trajectory correction operations of the cruise period when the spacecraft control system requirements are maximum. If data transmission is continued during that event, the peak load is 194 watts. By terminating data transmission for intervals of up to ten minutes out of two hours during the period, the peak is avoided as shown by the load tabulation. Peak power duty of 174 watts then occurs during the parking orbit period.

Total raw power capacity is 240 watts initially and 235 watts at the end of the mission. In Table 5.2-10, ratings, numbers of component devices, and weights are listed. Functional aspects are described in subsection 3.7.

Table 5.2-9

ELECTRIC POWER SUBSYSTEM LOADS FOR DESIGN CONCEPT B

Subsystem / Mission Phase	Data Management	Spacecraft Control	Communications	Experiments	Total
Prelaunch	18	54	100	10.1	182.1
Boost	8	54	100	10.1	172.1
Parking Orbit	10	54	100	10.1	174.1
Cruise	10	16	100	10.1	136.1
Trajectory Correction	10	84	20	10.1	124.1
Encounter	16	28	100	21.6	165.6
Post Encounter	10.5	16	100	10.1	136.6

Table 5.2-10

DESIGN CONCEPT B ELECTRIC POWER SUBSYSTEM
PHYSICAL CHARACTERISTICS

Component (no.)	Rating	Weight, lbs.
Radioisotope Thermoelectric Generator (4)	60 watts, 28v	120.00
3 Electrode Ni-Cd Battery	15 ampere hour	21.00
Shunt Volt. Reg. Switch (4)	Six 0.5a channels	1.80
Volt. Reg. Mode Controller	Signal Device	.75
Shunt Dissipation Resistors (4)	84 watts	6.00
Main 2400 cps Interter (2)	10 ampere inputs	4.00
Transfer Relay (2)	10 ampere dpst	1.00
Emergency 2400 cps Inverter	2 ampere input	0.50
Inverter Synchronizer	Signal Device	0.50
Emergency Transfer Unit	5 ampere spdt	0.50
400 cps Inverter	2 ampere input	4.00
Battery Charge-Discharge Controller	2 amp. chg. 5 amp disc.	9.00
Power Distribution and Wiring		41.00
TOTAL		210.05

5.3 SPACECRAFT DESIGN CONCEPT C

A 3-axis stabilized Jupiter flyby spacecraft of intermediate capability, which is referred to as Design Concept C, is described in this subsection.

5.3.1 Design Summary

A configuration of Spacecraft Design Concept C is illustrated in Figure 5.3-1. The concept design philosophy is one of intermediacy in both scientific and subsystem capability. That is, the capabilities of the subsystem design concept are somewhere between the most capable and least capable of the candidate concepts. The injected weight of the spacecraft is approximately 900 pounds. Flight times upwards from 510 days are possible during the period 1973-1980 when the Titan IIICx/Centaur is used. Use of the Saturn IB/Centaur/HEKS makes 400 day flight times possible in any of the launch years 1973-1980.

The salient characteristics of Design Concept C are (1) a science capability of approximately 115 pounds and 45 watts, (2) a steerable, 6-foot parabolic antenna and a 35-watt transmitter, (3) data compression and tape storage, (4) 3-axis attitude stabilization implemented by gas jets or reaction wheels, (5) Mariner IV-type midcourse propulsion, and (6) Pu-238 RTG's and a Ni-Cd battery. The spacecraft performance is indicated by the following: (1) a 33 bit per second information rate at maximum communications distance, (2) an overall data compression ratio of approximately 15 to 1, (3) data storage for 33 M bits, (4) a vernier correction capability of 90 m/sec, and (5) 260 watts of available electric power.

Following spacecraft injection, 3-axis attitude stabilization is acquired. Cruise science is then activated. Approximately one week following injection, a vernier correction maneuver is executed. The capability is provided to make a second correction during later portions of the mission. The parabolic antenna provides the primary communications downlink, and it is pointed at Earth by means of a mechanical steering device which is positioned on command from Earth. Omni antennas are used for near-Earth communications and for command capability throughout the mission. Spacecraft attitude is held during encounter by use of Jupiter and Canopus as primary references. Encounter science is turned on by Earth command. Data is stored intermittently throughout the mission and during encounter. The expected error in periapsis altitude is approximately 4000 km. Playback of the television picture is accomplished following encounter and after reacquisition of cruise altitude. The spacecraft then assumes its cruise mode of operation.

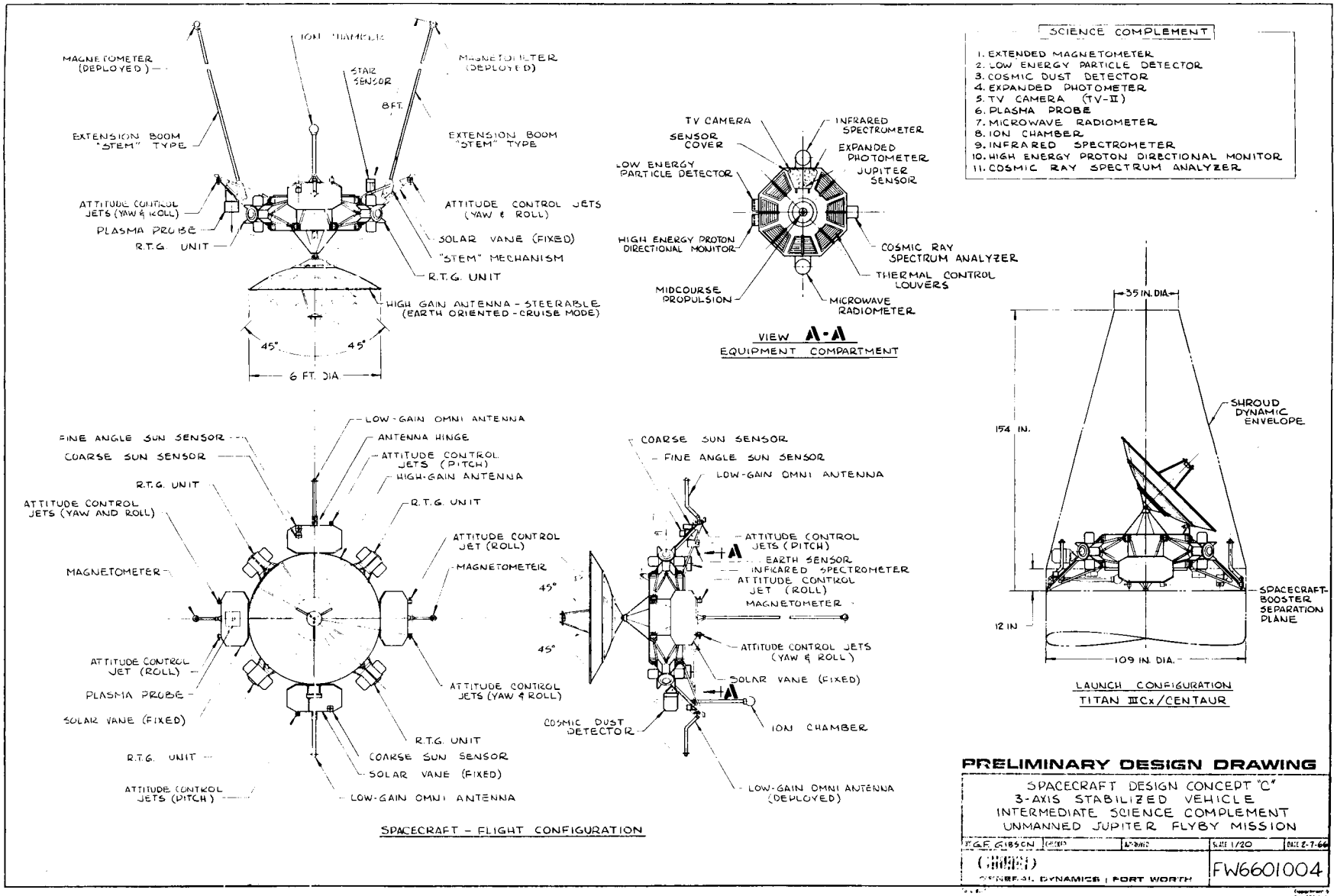


FIGURE 5.3-1 SPACECRAFT DESIGN CONCEPT C CONFIGURATION

A weight summary of Spacecraft Design Concept C is presented in Table 5.3-1.

Table 5.3-1

SPACECRAFT DESIGN CONCEPT C WEIGHT SUMMARY

Subsystem	Weight, lbs.
Science	115
Communications	73
Data Management	35
Spacecraft Control	57
Attitude Control Propulsion	120
Midcourse Propulsion	70
Electrical Power	286
Structural and Mechanical Provisions (est.)	148
Meteoroid Protection, Thermal Control, Radiation Protection, and Reliability Enhancement	?
Total Spacecraft	904
Adapter (0.065 x Spacecraft Weight)	59
Launch Weight	963

5.3.2 Subsystem Design Information

5.3.2.1 Science

Spacecraft Design Concept C incorporates a scientific instrument complement of intermediate capability. A definition of this experiment package (Intermediate Scientific Experiment Package - 2) is presented in Table 2.1-8, and the individual instruments are described in subsection 2.1. The total weight of this package is 115 pounds.

5.3.2.2 Communications

In the communications subsystem for Design Concept C, a six-foot parabolic antenna is used. Since the amount of data gathered by means of this spacecraft is greater than that gathered by Design Concept B, a 35-watt transmitter is recommended so that a higher data rate can be used. At maximum communications distance, the available data rate is 33 bits per second. A gain-loss chart at 6 a.u. is presented in Table 5.3-2.

Table 5.3-2

DESIGN CONCEPT C COMMUNICATIONS SUBSYSTEM GAIN-LOSS TABLE

	Gain	Loss
Transmitter Power	45.5 dbm	
Modulation		3 db
S/C Ant. Gain	30 db	
Space Attenuation		278 db
Rcvr. Ant. Gain	61 db	
Rcvr. Sens. ($40^{o}K$)		-186 dbm
Misc. Loss		2 db
System Tolerances		6 db
TOTALS	136.5 db	103 db

S/(N/B) = 33.5 db

At an information rate of 33 bits per second, the required bandwidth is 600 cps. Therefore, the received signal-to-noise ratio is:

S/N = 33.5 - 10 log 600

S/N = 5.7 db

A transmission schedule for the entire flight is shown in Table 5.3-3. Signal-to-noise ratios are obtained from the equations presented in subsection 3.1.4.

Table 5.3-3

DESIGN CONCEPT C ANTENNA AND INFORMATION RATE SCHEDULE

Distance (a.u)	Antenna	Info. Rate (bps)	S/N (db)
0 - 0.2	Omni	8	4
0.2 - 2	Parabola	267	5
2 - 3	Parabola	133	5
3 - 4	Parabola	67	5
4 - 6	Parabola	33	5

A block diagram of the communications equipment recommended for the spacecraft is presented in Figure 5.3-2. The operation of the

DESIGN CONCEPT C COMMUNICATIONS SUBSYSTEM

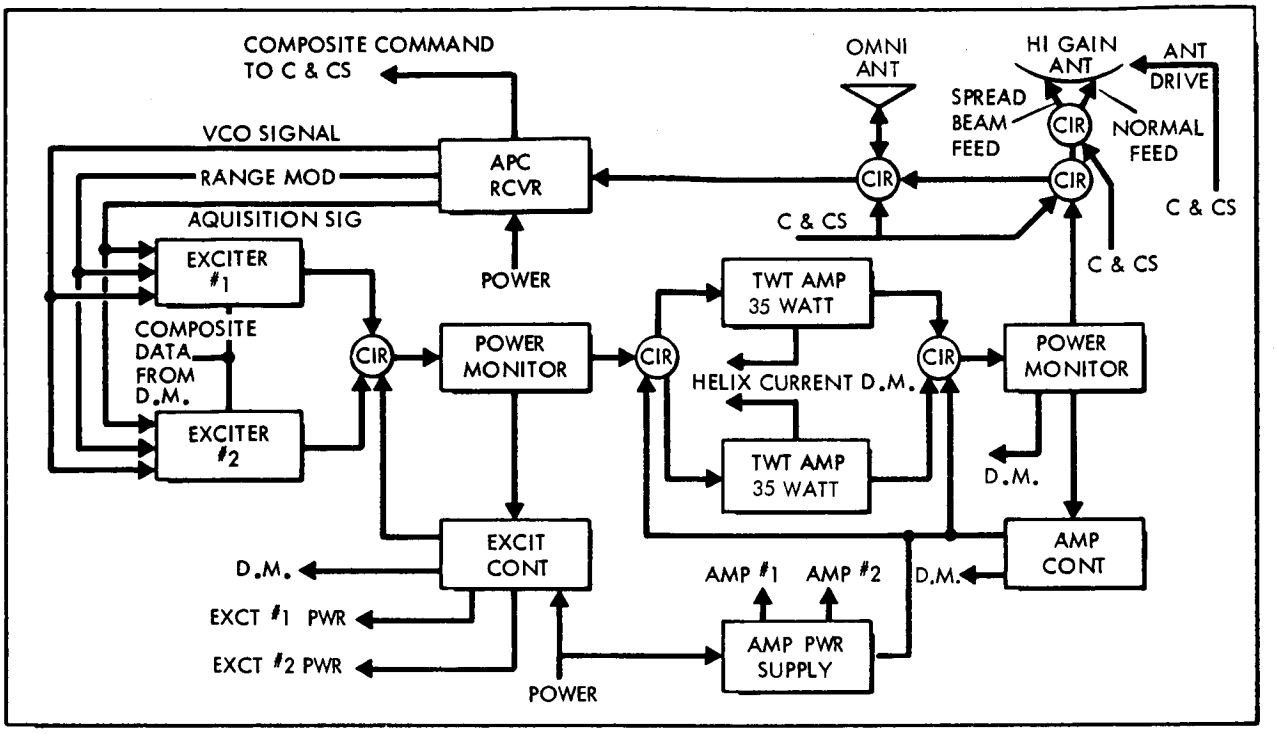


FIGURE 5.3-2

equipment is the same as that in the case of Design Concept A with the exception of the antenna circuitry. The parabolic antenna is positioned by a drive mechanism. The position of the high-gain antenna is stepped in small angular increments upon command from Earth. Also, the high-gain antenna is equipped with an off-focus feed which widens the beamwidth. This feed can be switched in if communications with the spacecraft is lost. After communications is reacquired using the off-focus feed, the antenna can be properly positioned and switched back to the narrow beam feed.

A summary of the physical characteristics of this system is shown in Table 5.3-4.

Table 5.3-4

DESIGN CONCEPT C
COMMUNICATIONS SUBSYSTEM PHYSICAL CHARACTERISTICS

Component (no.)	Weight, lbs.
Amplifier (2)	6
Power Monitor (2)	2
Circulator (6)	6
Exciter (2)	9
Receiver	9
Exctr. Cont.	2
Amp. Cont.	2
Omni Ant. (2)	4
Parabolic Ant.	20
Power Supply-HV	9
Cable and Wave guide	4
TOTAL	73

5.3.2.3 Data Management

The elements and functional requirements of the data management subsystem have been discussed generally in subsection 3.2. Two interchangeable tape recorders have been provided to permit intermittent recording of data during cruise without degrading the probability of successful recording during encounter. Whenever possible, micro-integrated circuitry is used.

The available transmission rates for various portions of the mission have been previously given in Table 5.3-3, and the anticipated uncompressed data bit rates are given in Table 5.3-5. Data compression is used to permit real-time transmission of all data, except television data, throughout the mission and also to allow intermittent communications. For intermittent communications, compressed data is recorded at low bit rates during periods of no communications, and later played back at higher rates during contact periods. In addition to the compression capability discussed for Design Concept B in subsection 5.2.2.3, the fan technique is used to provide 5-to-1 compression ratios for the microwave radiometer, high-range interferometer spectrometer, high-energy proton directional monitor, and cosmic ray spectrum analyzer measurements; and the quantile method is used to provide 100-to-1 compression ratios for the ion chamber data.

Table 5.3-5

ANTICIPATED UNCOMPRESSED DATA BIT RATES FOR DESIGN CONCEPT C

Type	Cruise Rate (bps)	Encounter Rate (bps)
Engineering	33.3	33.3
Magnetometer	9.5	9.5
Cosmic Dust Detector	0.6	0.6
Trapped Radiation Detector	1.6	1.6
Plasma Probe	3.2	3.2
Visible Photometer	---	3.0
Microwave Radiometer	---	0.5
Ion Chamber	0.8	0.8
HR Interferometer Spectrometer	---	0.6
HE Proton Directional Monitor	0.7	0.7
CR Spectrum Analyzer	1.6	1.6
Television	---	20000.0
Housekeeping	3.2	5.2
TOTAL	54.5	20060.6

Excluding television pictures, the compressed data rates for scientific measurements are just under 3 1/4 bits per second for cruise and 4 1/2 bits per second during encounter. Compression for television pictures is implemented during playback so that the total real time compressed data rates using the fan technique for compressing engineering data is approximately 3 1/3 bits per second during cruise and around 4 2/3 bits per second during encounter. If the zero order interpolator is employed for compressing engineering data, the data rates are about 4 1/4 bits per second for cruise and just over 5 1/2 bits per second during encounter. All data, excluding television pictures, can therefore be transmitted in real time during the entire mission.

It is recommended that data storage be provided for all data which is obtained during encounter and that two record rates be implemented. The tape recorder capacity is sufficient to store 32.2 M bits. The length of time required for data playback is virtually the same as that required for the case of Design Concept B discussed in subsection 5.2.2.3 (less than 11 days).

Few changes are made to the data management system elements described previously for Design Concept B. The data rates are increased to 8, 33, 67, 133, and 267 bits per second. The DAE (Figure 5.3-3) processes the microwave radiometer, high-range interferometer spectrometer, high-energy proton directional monitor, and cosmic ray spectrum analyzer data in a manner similar to the magnetromer measurements of Concept B. Likewise, the ion chamber data is processed in a manner similar to that used for the trapped radiation detector data of Design Concept B. The DEE capability is increased so that 120 analog measurements can be processed as indicated by modification 3 in Figure 5.1-4. The capacity of the tape recorder is slightly increased to 32.2 M bits, and the playback rate is doubled to 33 bits per second. The number of DC commands is increased to 39 for this concept.

The physical characteristics of the data management subsystem are given in Table 5.3-6.

Table 5.3-6

DESIGN CONCEPT C DATA MANAGEMENT SUBSYSTEM
PHYSICAL CHARACTERISTICS

Component	Weight, lbs.
DEE	9
DAE	8
DSE	12
CDDE	6
TOTAL	35

5.3.2.4 Spacecraft Control

The function of the spacecraft control subsystem for Spacecraft Design Concept C is essentially the same as that for Design Concept B. Two differences which should be pointed out are the basic attitude orientation of the vehicle in the cruise phase, and the possible use of a terminal guidance correction. For this design concept, the high-gain antenna is moveable with respect to the spacecraft, and a general Sun pointing attitude is held by the spacecraft. The antenna is moved periodically by commands from the CC&S operating on instructions received from ground control.

The terminal guidance capability is provided for back up use. This offers an additional margin for error, rather than being a design necessity to achieve an acceptable RMS error at the target. This second maneuver is implemented in the same manner as the vernier

DESIGN CONCEPT C DATA AUTOMATION ELEMENT

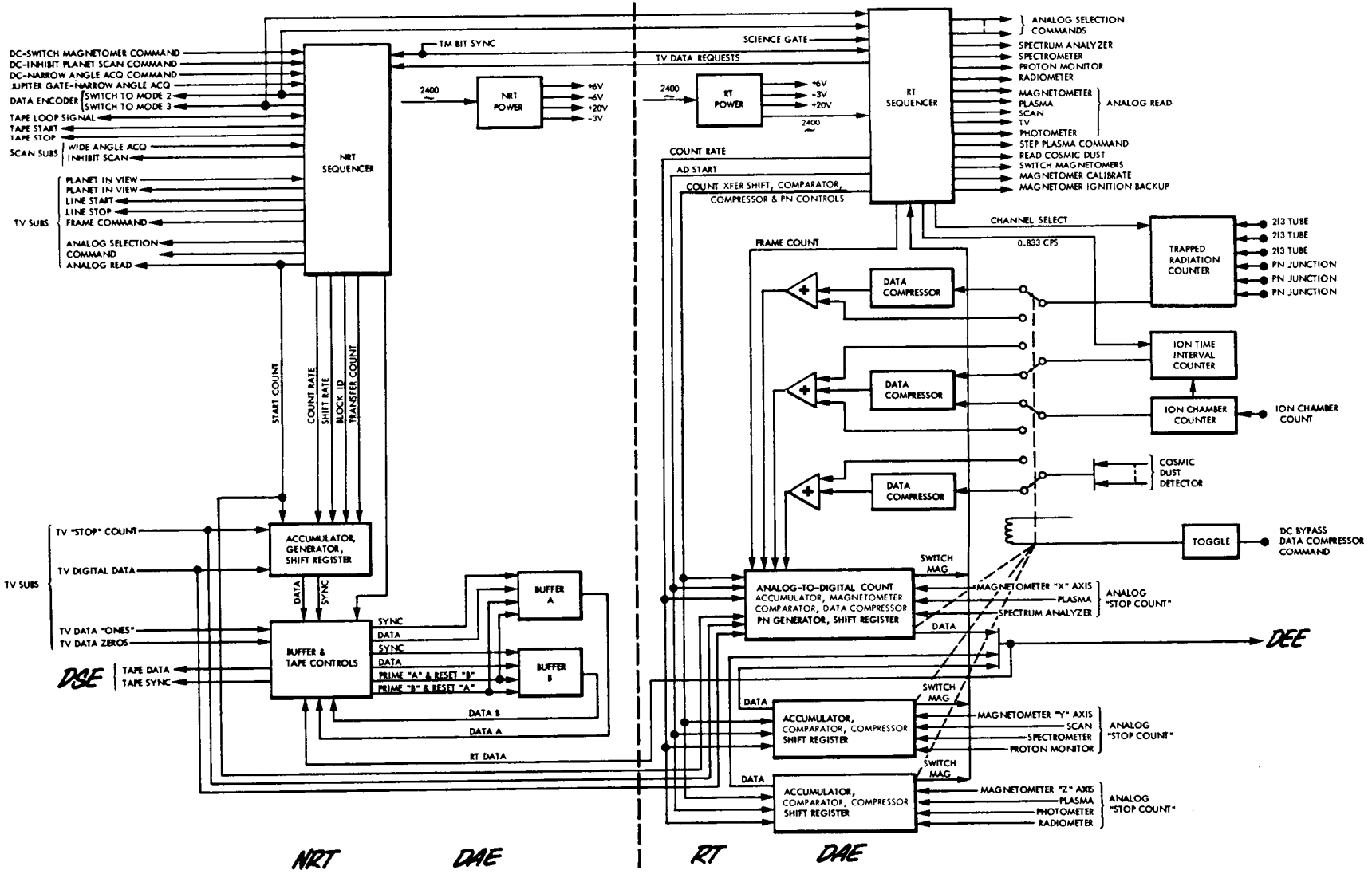


FIG. 5.3-3

correction, i.e., attitude and velocity change commands received from ground control will be carried out, and all orbit determination and guidance computations will be done on Earth. The one vernier correction reduces the RMS error in impact parameter to less than 4000 km.

The proposed spacecraft control system physical characteristics are shown in Table 5.3-7. The general configuration of the CC&S and the attitude control electronics are shown in Figures 3.3-1 and 3.3-2.

Table 5.3-7

DESIGN CONCEPT C SPACECRAFT CONTROL SUBSYSTEM
PHYSICAL CHARACTERISTICS

Component (no.)	Weight, lbs.
Fine Sun Sensor	1
Coarse Sun Sensors (2)	2
Earth Sensor	6
Star Tracker	6
Jupiter Tracker	6
CC&S	12
Attitude Control Elect.	20
Gyros and Accelerometers	4
TOTAL	57

5.3.2.5 Attitude Control

The attitude control Design Concept C is essentially a growth version of Concept B. The primary difference between the two cases is in the manner of generating the attitude-error signals. In the present case, the spacecraft centerline axis is to be maintained in a nominal Sun-pointing attitude rather than an Earth-pointing attitude. This approach reduces the weight and complexity of the Sun sensor and Canopus star tracker.

In order to accommodate the communications requirements, the antenna is movable (universal joint) relative to the spacecraft, and it is positioned to maintain a nominal Earth-pointing orientation. The antenna control mechanism functions on a periodic stepping basis rather than a continuous basis. This avoids the possibility of adverse dynamic coupling with the spacecraft attitude control system. Thus, as far as the attitude control system is concerned, the antenna is essentially fixed and causes only periodic disturbances because of its movements.

It remains a design objective to minimize the effects of torques due to solar radiation pressure. However, the problem is somewhat different in this case since the solar aspect angle is nominally zero. The solar torque will vary with antenna position, and it is nominally zero only for the case of the neutral position. Since the antenna is large and has been placed forward from the center of gravity to accommodate the motion requirement, a problem is created. This problem could be significant for the reaction wheel system. It may be possible to reduce the torque contribution of the antenna by the use of balance surfaces located on the antenna periphery. The use of coatings to modify the reflectivity of special areas may also be advantageous. These ideas constitute areas for future study.

The attitude control requirements for Design Concept C are not analyzed in detail, but the mechanics are identical to those outlined in subsection 5.2.2.5. The control possibilities are again either a gas jet system or a reaction wheel/gas jet system. For performing spacecraft integration, a gas jet system is assumed for primary control. The estimated weight of the system is 120 pounds including gas, tankage, and components.

5.3.2.6 Propulsion

The midcourse propulsion subsystem for Design Concept C is the basic hydrazine system described in subsection 3.6.1. It has the capability of imparting a total velocity increment of 90 meters per second (300 feet per second) to a spacecraft mass of about 915 pounds. This corresponds to approximately a 5 σ design criteria for a launch vehicle FOM of 10-15 m/sec and a capability for a second maneuver. Table 5.3-8 contains a summary of the physical characteristics of the midcourse propulsion system.

Table 5.3-8

DESIGN CONCEPT C MIDCOURSE PROPULSION SUBSYSTEM
PHYSICAL CHARACTERISTICS

Components	Weight, lbs.
Hydrazine	41.0
Hydrazine Tank	2.8
Nitrogen	1.8
Nitrogen Tank	3.8
Bladder	0.7
Fixed Hardware	19.9
TOTAL	70.0
Hydrazine Tank Diameter	13.5 in.
Nitrogen Tank Diameter	7.5 in.

The attitude control propulsion system is that identified and described as Configuration B in subsection 3.6.2. The estimated weight of the system necessary to meet the projected requirements of Spacecraft Design Concept C is 120 pounds (see Figure 3.6-10).

5.3.2.7 Electric Power

The Design Concept C electric power subsystem arrangement is illustrated by the schematic diagram of Figure 3.7-6. The subsystem load profile is set forth in Table 5.3-9. The critical power situation occurs during the trajectory correction operations period when the spacecraft control system requirements are maximum. If data transmission is continued during that event, the peak load is 289 watts. By terminating data transmission for intervals of up to ten minutes out of two hours during the period, the peak is avoided as shown by the load tabulation. Peak power duty of 255 watts then occurs during the encounter period.

Total raw power capacity is 320 watts initially and 314 watts at the end of the mission. Table 5.3-10 lists ratings, numbers of component devices, and weights. Functional aspects are described in subsection 3.7.

Table 5.3-9

ELECTRIC POWER SUBSYSTEM LOADS FOR DESIGN CONCEPT C

Subsystem / Mission Phase	Data Management	Spacecraft Control	Communications	Experiments	Total
Prelaunch	22.5	59	160	13.2	254.7
Boost	9.5	59	160	13.2	241.7
Parking Orbit	13.5	59	160	13.2	245.7
Cruise	16	20	160	13.2	209.2
Trajectory Correction	16	95	25	13.2	149.2
Encounter	21.5	32	160	42.2	255.7
Post Encounter	16	20	160	13.2	209.2

Table 5.3-10

DESIGN CONCEPT C ELECTRIC POWER SUBSYSTEM
PHYSICAL CHARACTERISTICS

Component (no.)	Rating	Weight, lbs.
Radioisotope Thermoelectric Generator (4)	80 watt, 28 volt	160.00
3 Electrode Ni-Cd Battery	20 ampere hour	28.00
Shunt Volt. Reg. Switch (4)	Eight .5a Channels	1.60
Volt. Reg. Mode Controller	Signal Device	.75
Shunt Dissipation Resistors (4)	112 Watt	12.00
Main 2400-cps Inverter (2)	15 ampere input	6.00
Transfer Relay (2)	15 ampere dpst	1.00
Emergency 2400-cps Inverter	2 ampere input	.50
Inverter Synchronizer	Signal device	.50
Emergergency Transfer Unit	5 ampere spdt	.50
400-cps Inverter	2 ampere input	4.00
Battery Charge-Discharge Controller	3 amp chg, 7.5 amp. disc.	12.00
Power Distribtuion and Wiring		59.00
TOTAL		285.85

5.4 SPACECRAFT DESIGN CONCEPT D

In this subsection, a Jupiter flyby spacecraft is described which has "full" capability and is denoted as Design Concept D.

5.4.1 Design Summary

A configuration of Design Concept D is illustrated in Figure 5.4-1. The design philosophy is one of maximum capability in both scientific instrumentation and subsystem performance. The injected weight of the spacecraft is approximately 1300 pounds. A flight time of around 600 days is possible in most years when the Titan IIICx/Centaur is used. Use of the Saturn IB/Centaur/HEKS makes possible 400-day missions launched in any of the years 1973-1980.

The salient characteristics of the spacecraft are (1) a science capability on the order of 200 pounds and 85 watts, (2) a steerable, 10-foot parabolic antenna and a 50-watt transmitter, (3) data compression and tape storage, (4) an on board, self-contained spacecraft control system, (5) 3-axis stabilization implemented by gas jets and reaction wheels, (6) Mariner-IV type midcourse propulsion, and (7) Pu-238 RTG's and a Ni-Cd battery. The spacecraft performance is indicated by the following: (1) a 133 bit per second information rate at maximum communications distance, (2) an overall data compression ratio of approximately 20 to 1, (3) data storage for 232 M bits, (4) a trajectory correction capability of 90 m/sec, and (5) 385 watts of available electric power.

Following spacecraft injection, spacecraft attitude is stabilized by use of the Sun and Canopus as primary references. Cruise science is turned on. A vernier correction is made using Earth-based navigation, computation, and command facilities. The parabolic antenna is the primary communications downlink. Omni antennas are used for two-way communications during early portions of the mission and for uplink communications throughout the mission. The parabolic antenna is mechanically positioned by means of angular computations made on board the spacecraft. If necessary, a terminal trajectory correction is made by use of navigation measurements, computations, and commands generated on board. Encounter attitude is acquired by use of Jupiter and Canopus as primary references. Encounter science is turned on. The expected periapsis miss distance at Jupiter is 400 km. Data storage is implemented intermittently during cruise and continuously during encounter. Playback of encounter data is performed following reacquisition of cruise attitude. Following playback, the spacecraft reverts to its cruise mode of operation.

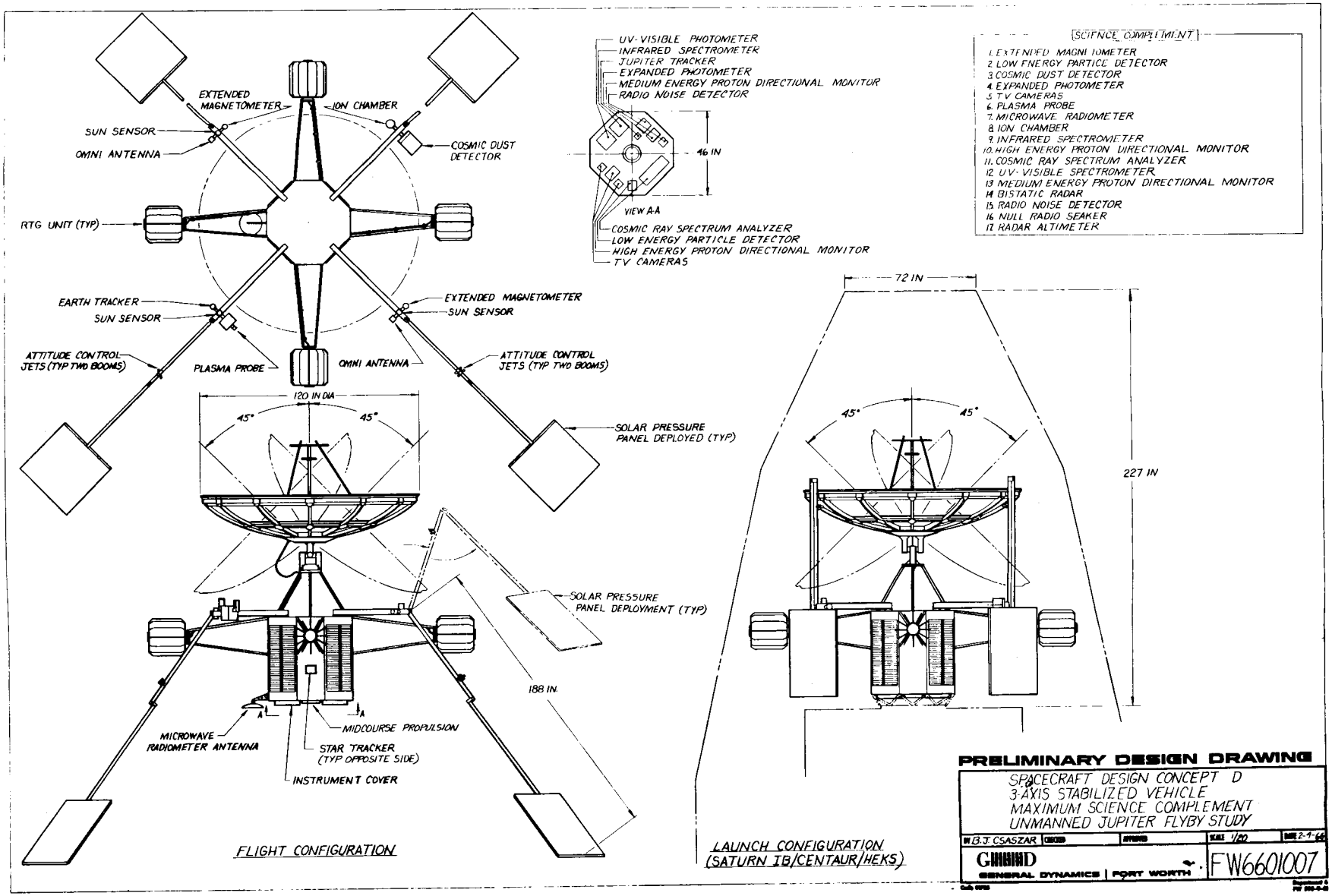


FIGURE 5.4-1 SPACECRAFT DESIGN CONCEPT D CONFIGURATION

The weight of Spacecraft Design Concept D is summarized in Table 5.4-1.

Table 5.4-1

SPACECRAFT DESIGN CONCEPT D WEIGHT SUMMARY

Subsystem	Weight, lbs.
Science	203
Communications	82
Data Management	76
Spacecraft Control	110
Attitude Control Propulsion	130
Midcourse Propulsion	89
Electrical Power	413
Structural and Mechanical Provisions (est.)	191
Meteoroid Protection, Thermal Control, Radiation Protection, and Relaibility Enhancement	?
Total Spacecraft	1294
Adapter (0.065 x spacecraft weight)	85
Launch Weight	1379

5.4.2 Subsystem Design Information

5.4.2.1 Science

Spacecraft Design Concept D incorporates a scientific instrument complement of full capability. A definition of the full experiment package is presented in Table 2.1-8, and the individual instruments are described in subsection 2.1. The total weight of this package is 203 pounds.

5.4.2.2 Communications

The communications subsystem for Spacecraft Design Concept D is the same as the subsystem for Concept C with the exception that the transmitter has a 50-watt power output, and the antenna has a gain of 35 db. The proposed antenna is a ten-foot parabola. With this configuration, the information rate at maximum communications distance is 133 bits per second. A gain-loss chart for communications from 6 a.u. is shown in Table 5.4-2.

Table 5.4-2

DESIGN CONCEPT D COMMUNICATIONS SUBSYSTEM GAIN-LOSS TABLE

	Gain	Loss
Transmitter Power	47 dbm	
Modulation		3 db
S/C Ant. Gain	35 db	
Space Attenuation		278 db
Rcvr. Ant. Gain	61 db	
Rcvr. Sens. ($40^{o}K$)		-186 dbm
Misc. Loss		2 db
System Tolerances		6 db
Total	143	103

$S/(N/B) = 143 - 103 = 40$ db

For an information rate of 133 bps, the necessary bandwidth is 2400 cps. Therefore, the received signal-to-noise ratio is:

$S/N = 40 - 10 \log 2400 = 6.2$ db

For the flight to Jupiter, a transmission schedule is presented on Table 5.4-3.

Table 5.4-3

DESIGN CONCEPT D ANTENNA AND INFORMATION RATE SCHEDULE

Distance (a.u.)	Antenna	Info. Rate (bps)	S/N (db)
0 - 0.2	Omni	8	5
0.2 - 1.5	Parabola	2133	4
1.5 - 2	Parabola	1067	6
2 - 3	Parabola	533	5
3 - 4.5	Parabola	267	5
4.5 - 6	Parabola	133	6

A block diagram of the recommended equipment is shown in Figure 5.4-2. The operation of the equipment including antenna

pointing is the same as for Concept C. A summary of the system physical characteristics is contained in Table 5.4-4.

Table 5.4-4

DESIGN CONCEPT D COMMUNICATIONS SUBSYSTEM PHYSICAL CHARACTERISTICS

Component (no.)	Weight, lbs
Amplifier (2)	8
Power Monitor (2)	2
Circulator (6)	6
Exciter (2)	10
Receiver	9
Exciter Control	2
Amp. Control	2
Omni Ant. (2)	4
Parabolic Ant.	25
Power Supply, HV	10
Cable & Waveguide	4
Total	82

5.4.2.3 Data Management

The integration of the DAE and DEE into a single DEE is the only modification to the data management subsystem elements and functional requirements discussed generally in subsection 3.2. However, a design which exhibits considerably more flexibility is proposed for use in this concept.

A telemetry command word to be used in each scientific and engineering measurement is supplied by the CC&S portion of the central digital computer (discussed in the next subsection) and is 12 bits in length. One bit is used to indicate direct or indirect addressing; four bits are used to specify the sampling rate; five bits are used to indicate the converted word length; and two bits are used to specify the routing. Five interchangeable buffers are supplied in the DEE, and four interchangeable tape recorders are provided in the DSE to permit processing flexibility throughout the mission. In Figure 5.4-3, one arrangement which can be used is indicated (Reference 5.4-1). Scientific and engineering data is temporarily stored in buffer A while data is being placed on tape

DESIGN CONCEPT D COMMUNICATIONS SUBSYSTEM

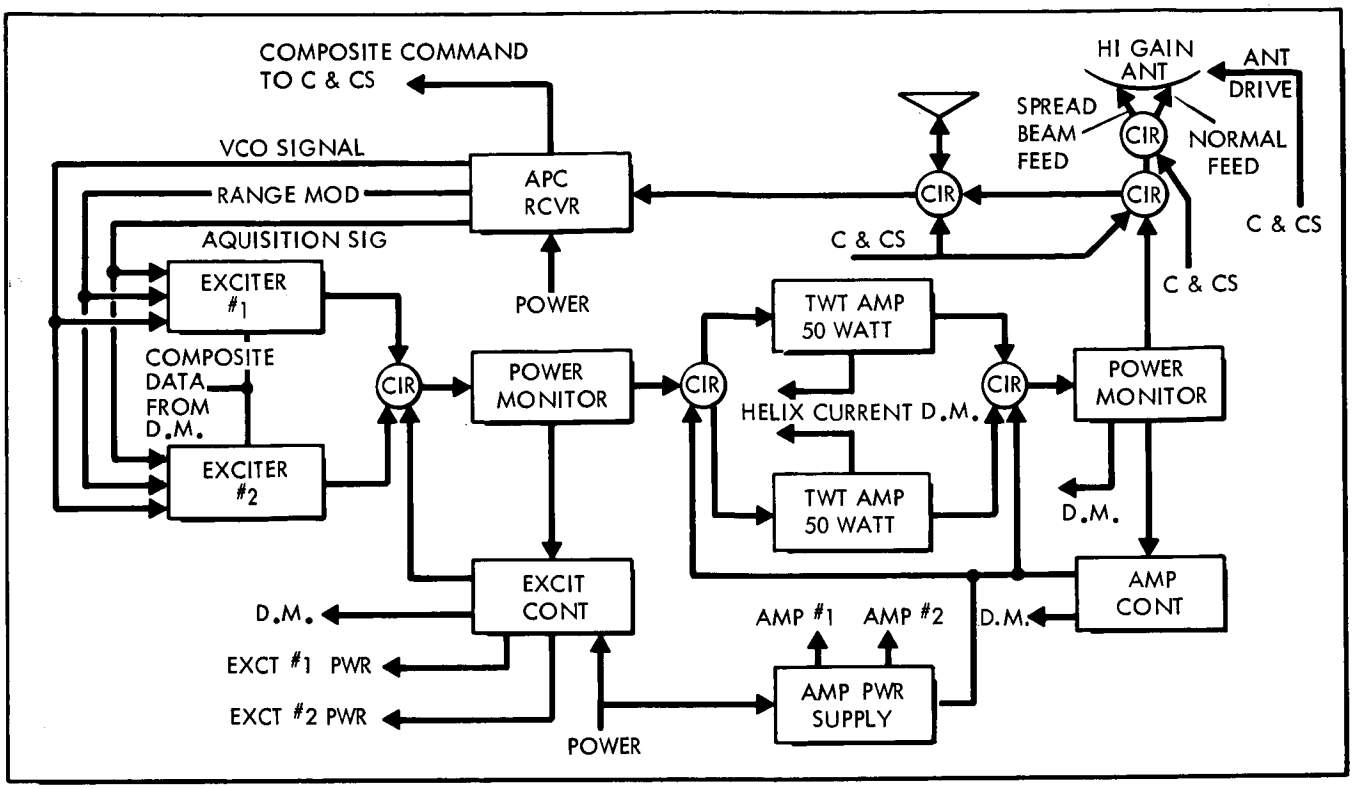


FIGURE 5.4-2

DESIGN CONCEPT D DATA ENCODER AND DATA STORAGE ELEMENT INTERFACE

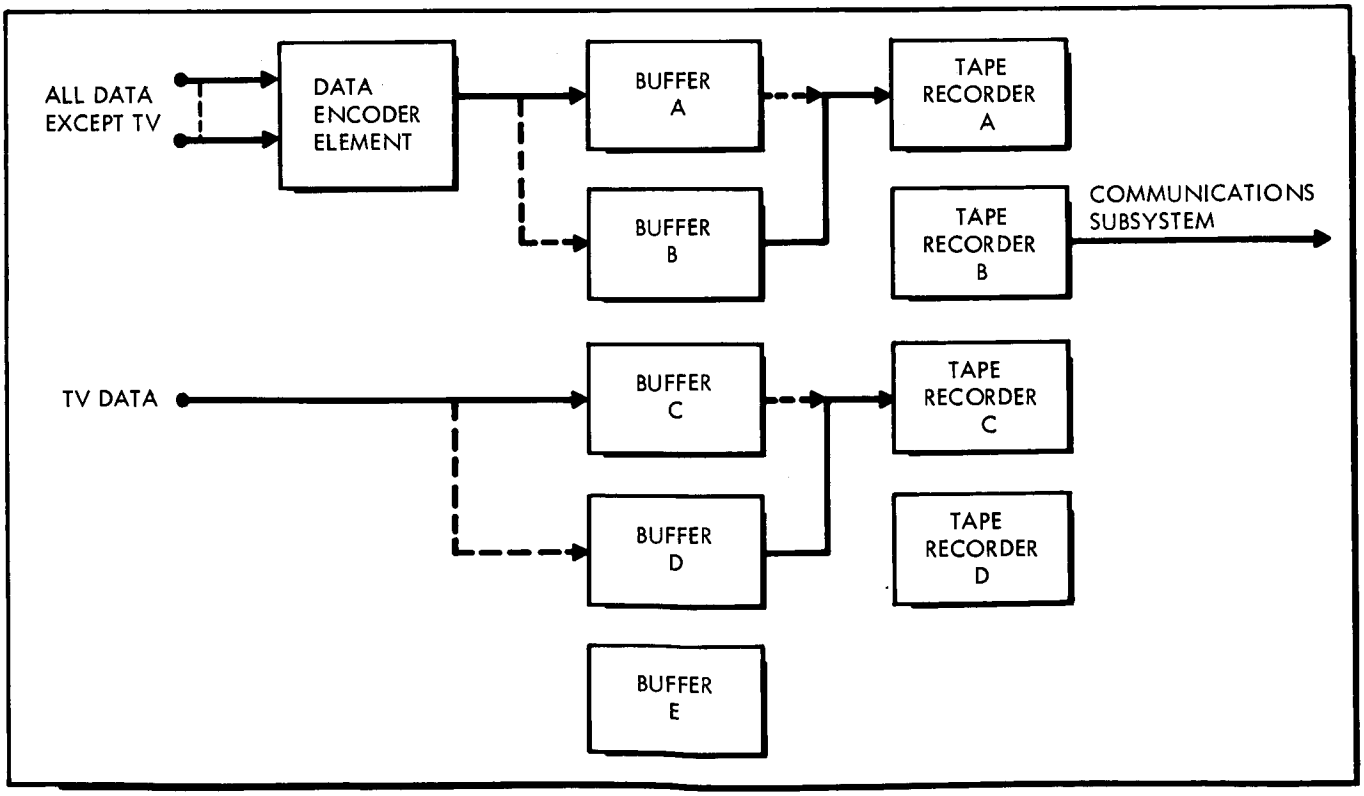


FIGURE 5.4-3

recorder A from buffer B. When buffer B is empty, buffers A and B are interchanged. Meanwhile, the same procedure is used for the television data in buffers C and D and tape recorder C. Also, previously recorded data is being transferred from tape recorder B to the communications subsystem for transmission. Tape recorder D and buffer E are redundant components.

Other arrangements permit data to be routed to two buffers so that one buffer is used to transfer this data to the communications subsystem for real-time transmission, and the other buffer is used to transfer data to a tape recorder for playback later. Additionally, it is planned to record redundant and modified sets of command words for the CC&S on the beginning of the tape in each tape recorder as well as to provide the capability to modify these words by ground command through two redundant CDDE's. In this way, sampling rates can be modified on the basis of mission performance, and useless measurements from malfunctioning equipment or limited-use equipment can be deleted.

The general purpose computer was considered for use in data management, and the results indicated that greater efficiency can be currently obtained by use of tape recorders, buffers, and special purpose data compression equipment.

The available transmission rates for various portions of the mission have been previously given in Table 5.4-3. The anticipated uncompressed data bit rates are given in Table 5.4-5. Data compression is used (1) to provide real-time transmission of all data during the initial portion of the mission out to 0.2/a.u. when the omni antenna is in use, and (2) to make possible intermittent communications during other phases of the mission. In addition to the data compression capability discussed in the description of Concept C, the fan technique will be used to provide 5-to-1 compression ratios for the intermediate range spectrometer, the medium energy proton directional monitor, the bistatic radar, and the radio noise detector data.

Table 5.4-5

ANTICIPATED UNCOMPRESSED DATA BIT RATES FOR DESIGN CONCEPT D

Type	Cruise Rate	Encounter Rate
Engineering	33.3	33.3
Magnetometer	9.5	9.5
Cosmic Dust Detector	0.6	0.6
Trapped Radiation Detector	1.6	1.6

Table 5.4-5
(Cont'd.)

ANTICIPATED UNCOMPRESSED DATA BIT RATES FOR DESIGN CONCEPT D

Type	Cruise Rate	Encounter Rate
Plasma Probe	3.2	3.2
Visible Photometer	---	5.0
Microwave Radiometer	---	0.5
Ion Chamber	0.8	0.8
HR Interferometer Spectrometer	---	0.6
HE Proton Direction	0.7	0.7
CR Spectrum Analyzer	1.6	1.6
IR Spectrometer	---	2.8
ME Proton Directional Monitor	1.4	1.4
Bistatic Radar	---	0.2
Radio Noise Detector	---	50.0
Television	---	120000.0
Housekeeping	3.2	5.2
Total	55.9	120117.0

Excluding television pictures, the compressed data rates for scientific measurements are 3 1/2 bits per second for cruise and 15 1/3 bits per second during encounter. Compression for television pictures is implemented during playback so that the total real-time compressed data rates are approximately 3 3/4 bits per second during cruise and 15 1/2 bits per second during encounter when the fan technique is used for compressing the engineering data. Using the zero order interpolator technique for engineering data, data rates are just over 4 1/2 bits per second for cruise and 16 1/2 bits per second during encounter. During the entire mission, all data except the television pictures can be transmitted in real time.

However, it is recommended that data be compressed and stored throughout the mission. The availability of high communications data rates permits non-real-time data to be played back much more rapidly than real-time data is gathered. Seven record rates of 8, 133, 267, 533, 1067, 2133, and 0.12 M bits per second and playback rates corresponding to the first six record rates are required. The storage capacity required to record this data is 232 M bits. If it is assumed that the compression specifications for Design Concept B and a 10-to-1 compression ratio for television data (on the basis of improvement in existing techniques) are used,

playback of this data takes 48 days. This interval is longer than is desired but is not considered unreasonable for this concept.

The following specific functions of the data management subsystem elements are proposed. The DEE is able to process 200 analog and digital measurements at sampling intervals between 0.01 to 4096 seconds and to transfer these measurements to the communications subsystem at rates of 8, 133, 267, 533, 1067, and 2133 bits per second. Word length of up to 32 bits per channel are accommodated. Each buffer has a capacity of 50 K bits, and each tape recorder has a capacity of 10^9 bits. Data from the additional science sensors over those noted in Concept C are processed in a manner similar to that used for magnetometer data. The physical characteristics of the data management subsystems are given in Table 5.4-6.

Table 5.4-6

DESIGN CONCEPT D DATA MANAGEMENT SUBSYSTEM PHYSICAL CHARACTERISTICS

Component (no.)	Weight, lbs.
DEE	40
DSE	24
CDDE (2)	12
Total	76

5.4.2.4 Spacecraft Control

For the spacecraft control subsystem used in Design Concept D, consideration is given to performing any or all of the following tasks: (1) attitude control computations, (2) sensor control, (3) event sequencing, (4) navigation computations, (5) guidance computations for midcourse and/or terminal maneuvers, (6) execution of midcourse and/or terminal maneuvers, (7) malfunction isolation, (8) malfunction mode switching decisions, (9) computations necessary for antenna pointing, and (10) compression of data prior to transmittal. Since the spacecraft design concept is postulated not to be severely weight limited, it is conceivable that most of these tasks should be performed on board the spacecraft. Considerations which influence the decision as to which tasks are to be performed on board are (1) whether adequate sensors for navigation measurements will be available, (2) whether sufficiently accurate measurements can be made by Earth-based equipment, (3) whether a computer large enough to perform

the navigation and/or guidance computations can be placed aboard the spacecraft (considering all aspects of systems integration), (4) whether malfunction isolation should be Earth-based or self-contained, (5) what provisions, if any, are to be made for alternate operational modes in case of malfunction, and (6) the effect of increased (or decreased) complexity of each added function on the probability of mission success.

The considerations and functions enumerated must be weighed with respect to their relationship to the requirements of the mission. The most basic requirement of any mission is the provision for a high probability of mission success. This probability is to be made as large as possible under the constraints imposed upon the design philosophy under consideration. The success of a spacecraft concept having maximum capability is heavily dependent on the following aspects of spacecraft control: (1) the miss distance at the target planet must be kept within the prescribed limits, (2) the encounter trajectory of the spacecraft and its orientation with respect to the target planet, must be controlled, and (3) the recorded data must be transmitted back to Earth. Naturally, these three aspects are interrelated. The first and second are dependent on the accuracy of midcourse and terminal corrections. These, in turn, are largely dependent on the accuracy with which spacecraft attitude can be determined and controlled. If accurate determination of attitude is required, then the success of the third aspect is enhanced. Although data transmission per se is not a function of the spacecraft control subsystem, the computation of pointing angles for the antenna is. These pointing angles, in conjunction with accurate attitude determination and control, permit more accurate pointing of the antenna; thus, higher antenna gain may be used, and higher data rates are possible. This improves the probability of data recovery.

Another factor which greatly influences the accuracy with which trajectory corrections can be made is the computation of the corrections themselves. In order to determine the magnitude and direction of the corrections, the position and velocity of the spacecraft must be known. These are obtained from processing Earth-based tracking data or from processing measurements made on board the spacecraft. In the latter case, accurate attitude determination and control is required for the pointing of the sensors which make the on-board measurements.

Thus, it is seen that, other than such reliability oriented measures as redundancy and choice of high-reliability components, the foremost requirement of a complex on board spacecraft control subsystem is accurate attitude determination.

Although most of the functions listed in the preceeding paragraphs can be carried out either on Earth or on board the spacecraft, some must be performed on board if they are included at all. These functions are sensor control, maneuver execution, and data compression. Of the remaining functions, the attitude control computations, event sequencing, and malfunction isolation present no problems in their implementation on board a spacecraft containing a computer which is capable of performing a modest amount of computation.

It is proposed that the functions enumerated above be performed on board, thus only the navigation and guidance computations, malfunction mode switching, and the antenna pointing computations must be assigned. Of these, malfunction mode switching presents the fewest problems. The chief reason for performing this function on Earth is simply that more consideration can be given to the selection of alternate modes. However, an automatic system in which there is a provision for override commands, can be used to accomplish the same purpose. Therefore, this function is included in the list of functions which are to be performed on board.

In light of the previous discussion, four alternate philosophies of spacecraft control can be outlined. They are:

1. Navigation and guidance computations and antenna pointing computations done on Earth.

2. Navigation and guidance computations done on Earth, and antenna pointing computations done on board the spacecraft.

3. Navigation and guidance computations and antenna pointing computations done on board the spacecraft with back-up computations done on Earth.

4. A combination of concepts 2 and 3. That is, all antenna pointing computations are done on board, and the navigation and guidance computations for the midcourse (vernier) correction (if any) are done on board.

Note that all other functions are to be performed on board the spacecraft, and override commands are provided from Earth when they are necessary or more expedient. From the following examination of the advantages and disadvantages of each of these concepts will come a recommended subsystem for the Spacecraft Concept D.

The first concept offers three distinct advantages: (1) the spacecraft is less complex; consequently, the probability that the subsystem will operate during the entire mission is increased;

(2) the peak power required is low compared to that required in concepts 3 and 4; therefore a smaller load is placed on the power subsystem; and (3) proven components and techniques can be used; thus the probability of subsystem operation for the duration of the mission is enhanced. Also, no appreciable state-of-the art advances are required. A factor which is of somewhat unknown importance is the smaller system weight. This system weighs fifty to sixty pounds less than the next smallest competitive system. This difference is principally caused by differences in computer size and the absence of the requirement for additional sensors.

However, there is a significant problem with this concept. It is expected that the vernier correction will place the spacecraft on a trajectory which exhibits a standard deviation of approximately 4000 km from the desired impact parameter. In the estimation of this standard deviation, no uncertainties in astrophysical phenomena were considered. Such perturbations as solar pressure, meteoroid impacts, and uncertainties in the knowledge of the Jovian gravitational field could easily increase this deviation beyond the tolerances imposed by the scientific payload. Compensation for these unknown effects can best be made by means of a provision for a terminal correction. Thus, not only can miss distance be more accurately controlled, but a high degree of control over the orientation of the trajectory with respect to the target planet can be exercised.

The above consideration of planetary control is not a completely obvious one. If on board control is not provided, such parameters as antenna pointing angles and maneuver commands must be transmitted over vast distances so that there is the attendant uncertainty of reception and verification. Added restrictions are placed on selection of launch windows so that the Earth is in a favorable position for tracking and maneuver command generation and transmission. Also, the maneuver must be timed so that a DSIF station which has command capability, probably Goldstone, is in position to track and transmit the commands. Another significant consideration is spacecraft navigation during the terminal portion of the mission. The generation of spacecraft steering commands for the terminal correction is dependent on the determination of spacecraft position and velocity with respect to the target planet which is, in turn, dependent on tracking accuracy and an accurate knowledge of the astronomical unit. These parameters are discussed further in subsection 3.4.

The second design concept is very similar to the first and has essentially the same advantages and disadvantages. The difference is that the added complexity of antenna pointing angle computation capability must be added to the computer. This modification proves advantageous in that spacecraft-Earth communications are no longer as

dependent on the Earth-based computations. The slight increase in complexity is not expected to materially affect the probability of mission success.

The third concept includes almost all of the features of self-contained interplanetary navigation and control theory. Since a completely self-contained system is employed, many of the disadvantages previously enumerated are dispensed with. In this concept, the potential for more accurate navigation information is provided; therefore, more accurate guidance commands can be computed. The spacecraft becomes essentially independent of the long communication link to Earth during the terminal phase of the mission. This concept imposes fewer restrictions on the selection of launch windows, and it allows both the vernier and terminal corrections to be made at or near the optimum times. The navigation and guidance technique employed in this concept was discussed in subsection 3.4.4.

The disadvantages attendant to this concept are few, but they are of considerable importance. The first of these is the inevitable increase in complexity of the subsystem. The computer itself can be designed for high reliability or can be made somewhat failure tolerant, but the reliability of the associated equipment necessary to make adequate stellar measurements can only be estimated at present. These instruments do not have an "off the shelf" availability; thus, new instrument designs are required to make this concept feasible. If highly reliable, suitable instruments can be developed, this concept should have a high probability of successfully performing the mission objectives. Even if reliability remains questionable, a back-up mode is readily available, i.e., measurements and computations are made by Earth-based equipment, and the associated maneuver commands are transmitted to the spacecraft control subsystem. Another disadvantage is that a relatively large amount of power, approximately two hundred to two hundred fifty watts is required to operate this subsystem. However, this power requirement only occurs for short periods of time over a 10 to 20 day time span piror to each correction. The control system power requirement for the other portions of the mission would be approximately forty to fifty watts.

The fourth concept is a hybrid system which is composed of the more attractive features of concepts 2 and 3. Since Earth-based tracking and computations are used to make the vernier correction, the advantage of using the DSIF in the region of its maximum accuracy is gained. The inaccuracy in the knowledge of the astronomical unit is not a factor in this correction, because the velocity of the spacecraft relative to the earth is the dominant parameter in this computation. The accuracy of the self-contained system in the terminal phase is retained. Although the power drain is still high for this

concept, it occurs only for one period during the mission. The disadvantages of using this concept are: (1) the system is still complex (2) although the power requirement has been reduced, this requirement is still large and (3) advanced sensor designs and control concepts must be developed in order to implement the concept.

On the basis of the arguments presented in the preceding section, the logical choice for the spacecraft Design Concept D control system is the hybrid concept. This concept employs the most successful of present techniques, yet allows for the expected improvements of the 1973 to 1980 time period. There is some risk involved in the area of sensor development, but the gain in navigation and guidance accuracy in the terminal mission phase is appreciable when this technique is used.

The performance of a system similar to the recommended system was discussed in subsections 3.4.2 and 3.4.4. The analysis and data presented in those subsections show that one vernier correction will place the spacecraft on a trajectory which is expected to deviate 3000-4000 km from the nominal trajectory at periapsis. The self-contained terminal navigation and a single terminal correction is expected to reduce this deviation by approximately an order of magnitude. This places the spacecraft well within tolerable periapsis altitudes for scientific experimentation.

The spacecraft control subsystem sequence of operations has several subsequences as integral parts. These subsequences are: (1) pre-launch, (2) acquire cruise attitude (Sun and Canopus) (3) acquire encounter attitude (Jupiter and Canopus) (4) execute correction maneuver, and (5) execute navigation measurements. The first four subsequences are very much like those described for use in Design Concepts A, B, and C. The execution of navigation measurements is described in the following paragraphs.

The Jupiter tracker first acquires Jupiter. Acquisition of a desired star and verification of the acquisition is then performed. The included angle between the lines of sight to the star and Jupiter is computed. Finally, the system prepares to make the next measurement.

The measurement cycle is repeated until the required number of measurements has been made. The computer processes the measurements in groups using a statistical filter method to estimate the spacecraft position and velocity on the basis of these filtered measurement residuals. The required steering command is computed from the current estimate of the spacecraft state (see subsection 3.4.4). The Concept D spacecraft control subsystem sequence of operation is

(1) start pre-launch operations, (2) acquire cruise attitude, (3) turn on cruise science, (4) execute correction maneuver (using information from Earth), (5) acquire cruise attitude, (6) initialize for antenna pointing computations (this information is received from Earth), (7) compute antenna pointing angles and turn on high-gain antenna, (8) begin navigation (command from Earth), (9) execute navigation measurements, (10) compute terminal correction and transmit to Earth for verification (an execute command will be received from Earth if the computed correction is deemed accurate), (11) execute correction maneuver, (12) acquire encounter attitude, (13) turn on encounter science, (14) turn off encounter science, (15) turn on gyros, (16) acquire cruise attitude, (17) commence data playback, (18) end data playback, (19) turn on cruise science.

The most critical component system is the computer. Without the computer, many of the spacecraft subsystems would, in effect, cease to function. For this reason, the computer must be made as reliable as possible. Fortunately, there are techniques which improve the probability of computer operation for the duration of the mission. The computer can be made to be self-reorganizing and/or to possess redundant logic, circuitry, and critical components.

The physical characteristics of the recommended control subsystem are summarized in Table 5.4-7.

Table 5.4-7

DESIGN CONCEPT D SPACECRAFT CONTROL SUBSYSTEM
PHYSICAL CHARACTERISTICS

Component (no.)	Weight, lbs.
Fine Angle Sun Sensor	1
Coarse Sun Sensors (2)	2
Earth Sensor	6
Startrackers (2)	20
Jupiter Sensor	6
Computer	45
Attitude Control Electronics	20
Gyros (3)	3
Accelerometer	1
Jupiter Moon Tracker*	6
Total	110

*Optional

5.4.2.5 Attitude Control

This spacecraft design concept embodies a large movable antenna and has the same basic requirements as Concept C, but the requirements are of increased magnitude. However, the idea of minimizing the effect of solar torque is now discarded since the size of the spacecraft makes it impractical. It is proposed instead to make use of the solar torque as part of the control concept.

The requirement in this case is to make the spacecraft statically stable about the solar-pointing attitude through the use of large, fixed solar vanes protruding aft. These vanes are sized so that a restoring torque due to solar pressure is developed for an angular error between the spacecraft centerline axis and the Sun-spacecraft line. The exact trim point, or attitude for zero torque, varies with antenna position angle: but the variations are kept within reasonable bounds by the proper choice of stability level and the use of antenna balancing.

A reaction wheel system is assumed to be the primary means of control in this design concept. The wheels are operated by attitude-error signals obtained from a passive, wide-angle Sun sensor. This sensor is aligned along the spacecraft centerline axis and generates a control signal proportional to the angular position of the Sun relative to the sensor boresight. This control signal is combined with an adjustable bias signal before being used as an attitude-error signal. By allowing the bias signal to vary as some function of reaction wheel speed, the spacecraft is made to seek its trim point automatically and to accomplish continuous desaturation. This technique is not applicable to the roll control since the spacecraft has no stability about that axis. A constant roll torque would eventually lead to saturation of the roll wheel. The occurrence of this problem can possibly be prevented by use of a controllable surface to accomplish roll trim.

This concept has not been investigated in detail at the present time, but the mechanics of such a study are similar to those outlined in subsection 5.2.2.5. Because of the complexity of a system in which gas jets, reaction wheels, and solar radiation pressure are used, a great deal of study is required before its feasibility can be assured. System stability and interactions between the various torque sources constitute potential problem areas. An allowance of 130 pounds is made for the reaction wheel and gas jet portions of this system. Power requirements for the reaction wheels are estimated at 10 watts continuous and 60 watts peak (required for meteoroid impacts, etc.).

5.4.2.6 Propulsion

The midcourse propulsion subsystem is the basic hydrazine system described in subsection 3.6.1. The subsystem is designed to impart a total velocity increment of 90 meters per second (300 feet per second) to a spacecraft mass of about 1280 pounds. This corresponds to approximately a 5σ design criteria for a launch vehicle FOM of 10-15 m/sec and a capability for a terminal correction. Table 5.4-8 contains a summary of the physical characteristics of the midcourse propulsion subsystem.

Table 5.4-8

DESIGN CONCEPT D MIDCOURSE PROPULSION SUBSYSTEM PHYSICAL CHARACTERISTICS

Component	Weight, lbs.
Hydrazine	57.0
Hydrazine Tank	3.7
Nitrogen	2.5
Nitrogen Tank	5.0
Bladder	0.9
Fixed Hardware	19.9
Total	89.0
Hydrazine Tank Diameter	15.0 in.
Nitrogen Tank Diameter	8.4 in.

The attitude control propulsion system is that defined as Configuration B in subsection 3.6.2. As stated in the subsection 5.4.2.5, 130 pounds is estimated to be the weight of the attitude control system which includes both the propulsion system and a reaction wheel system.

5.4.2.7 Electric Power

The electric power arrangement for use in Design Concept D is illustrated by the schematic diagram of Figure 3.7-6. The subsystem load profile is set forth in Table 5.4-9. The critical power situation occurs during the trajectory correction operations period when the spacecraft control system requirements are maximum. If data transmission is continued during that event, the peak load is 497

watts. By terminating data transmission for intervals of up to ten minutes out of two hours during the period, the peak is avoided as shown by the load tabulation. Peak power duty of 384 watts then occurs during the encounter period.

Total raw power capacity is 480 watts initially and 470 watts at the end of the mission. Table 5.4-10 lists ratings, numbers of component devices, and weights. Functional aspects are described in subsection 3.7.

Table 5.4-9

ELECTRIC POWER SYSTEM LOAD FOR DESIGN CONCEPT D

Mission Phase \ Subsystem	Data Management	Spacecraft control	Communications	Experiments	Total
Prelaunch	30.5	42	205	85.2	362.7
Boost	11	42	205	14.2	272.2
Parking Orbit	18	42	205	14.2	279.2
Cruise	20.5	60	205	14.2	299.7
Trajectory Correction	20.5	257	30	14.2	321.7
Encounter	32	62	205	85.2	384.2
Post Encounter	20.5	62	205	14.2	301.7

Table 5.4-10

DESIGN CONCEPT D ELECTRICAL POWER SUBSYSTEM PHYSICAL CHARACTERISTICS

Component	Rating	Weight, lbs.
Radioisotope Thermoelectric Generator (4)	120W, 28V	240.00
3 Electrode Ni-CD Battery	20 ampere-hour	42.00
Shunt Volt. Reg. Switch (4)	Ten .5a channels	3.60
Volt. Reg. Mode Controller	Signals device	.75
Shunt Dissipation Resistors (4)	140 watt	12.00
Main 2400 cps Inverter (2)	20 amperes input	8.00
Transfer Relay (2)	20 ampere dpst	1.00
Emergency 2400 cps Inverter	2 ampere input	.50
Inverter Synchronizer	Signal device	.50
Emergency Transfer Unit	5 ampere spdt	.50
400 cps Inverter	2 ampere input	4.00

(Cont'd.)

Table 5.4-10
(Cont'd.)

DESIGN CONCEPT D ELECTRICAL POWER SUBSYSTEM PHYSICAL CHARACTERISTICS

Component	Rating	Weight, lbs.
Battery Charge-Discharge Controller	5 a chg.10 a dischg	16.00
Power Distribution and Wiring		84.30
Total		413.15

5.4.3 Reference

5.4-1 Tooley, J. R. and Sarrafian, G. P., A Programmable Spacecraft Data Handling System, Las Vegas, Nevada, 1964 PGSET Symposium (October 6-9, 1964), pages 2-c-1 through 2-c-12.

APPENDIX A

MISSION MAPS

The basic working charts which were used to determine mission requirements are the hybrid digital/contour mission maps which are shown in Figures A-1 through A-16. Although only four trajectory parameters (geocentric injection energy, departure asymptote declination, and departure and arrival hyperbolic excess speeds) are shown in these high-resolution maps, low-resolution maps of 11 other mission parameters that are adequate for most mission planning purposes have been published in Reference 2.2-1. The parameters contained herein are those for which high-resolution maps were deemed necessary.

In the first set of maps (Figures A-1 through A-8), only injection-energy contours were drawn. Since the digital values of the trajectory parameters are retained in this type of display, asymptote declination contours (or additional energy contours) can be drawn on the map for any desired value of the parameter. For reference, the injection energy contours were transferred from the first set of maps (Figures A-1 through A-8) to the second set of maps (Figures A-9 through A-16). Because injection energy is directly related to hyperbolic excess speeds, the injection energy contours which were transferred to the hyperbolic excess speed maps also represent contours of constant departure hyperbolic excess speed, albeit the contours do not represent round-number values of hyperbolic excess speed. The dashed contours on Figures A-9 through A-16 represent constant values of the arrival hyperbolic excess speed.

For convenience, curves of communication distance and Earth elongation angle as functions of Jupiter arrival date are included in Figures A-1 through A-8. In like manner, interplanetary flight times have been indicated in the margins of Figures A-9 through A-16.

The trajectory data contained in Figures A-1 through A-16 are based on heliocentric conic calculations and mean planet orbit elements. As pointed out in paragraph 2.2.2, the Jupiter arrival dates corresponding to heliocentric conic trajectory computations can be in error by as much as 20 days. To obtain more accurate arrival dates and flight times, the corrections described in the cited paragraph should be applied.

INJECTION ENERGY AND ASYMPTOTE DECLINATION MISSION MAP, 1973 LAUNCH

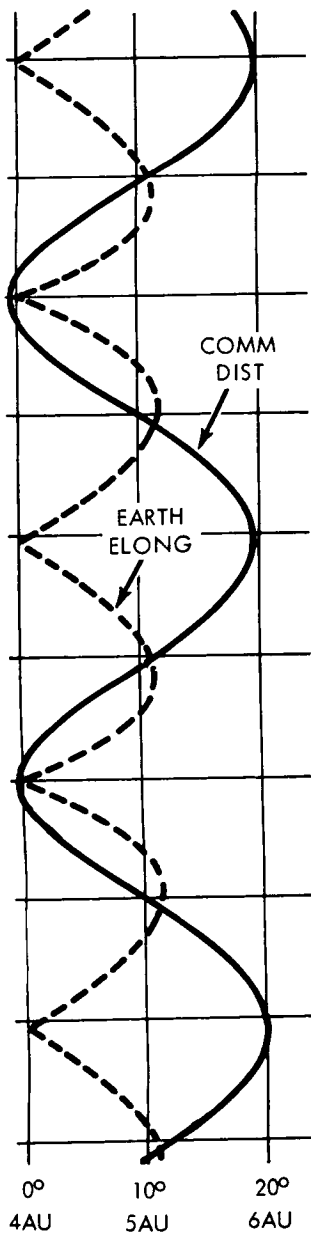


FIGURE A-1

INJECTION ENERGY AND ASYMPTOTE DECLINATION MISSION MAP, 1974 LAUNCH

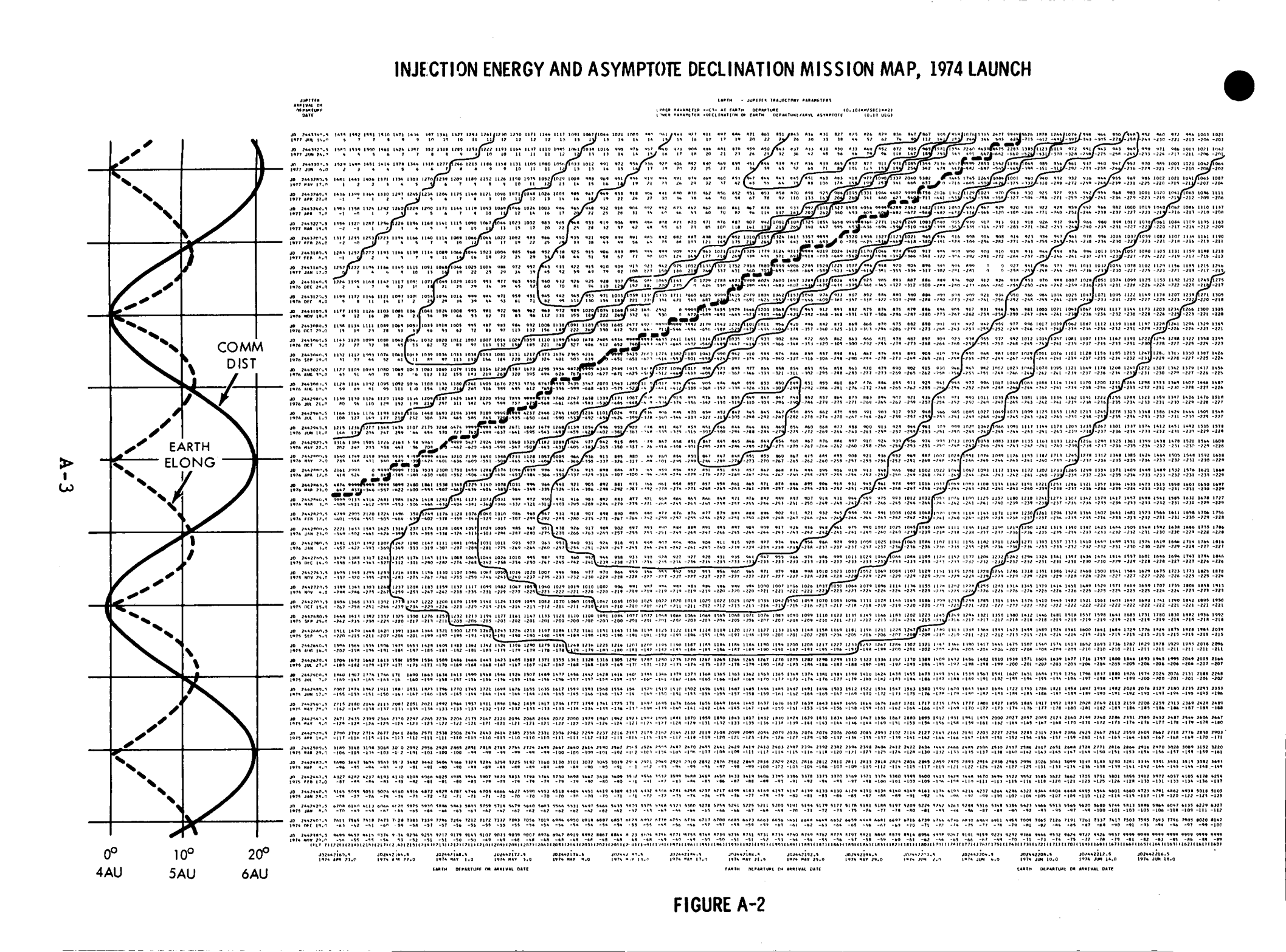
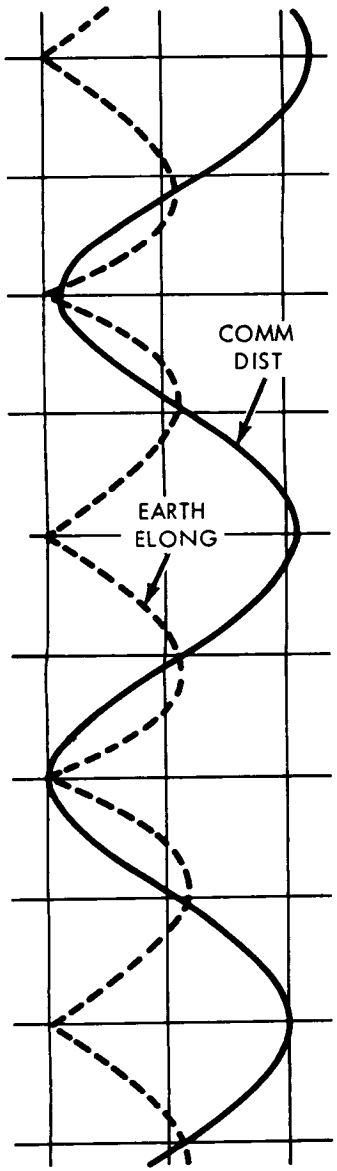


FIGURE A-2

INJECTION ENERGY AND ASYMPTOTE DECLINATION MISSION MAP, 1975 LAUNCH



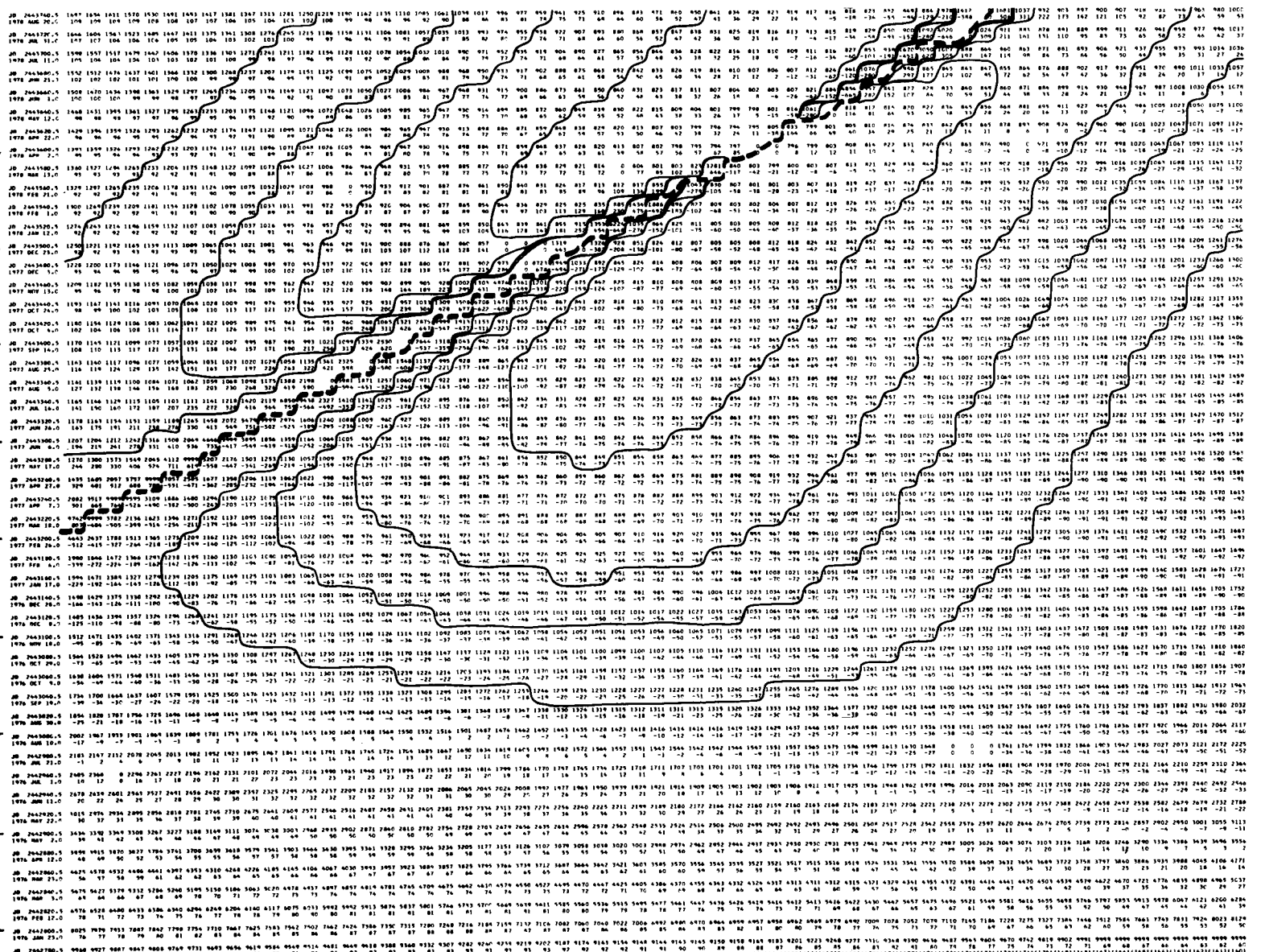


FIGURE A-3

INJECTION ENERGY AND ASYMPTOTE DECLINATION MISSION MAP, 1976 LAUNCH

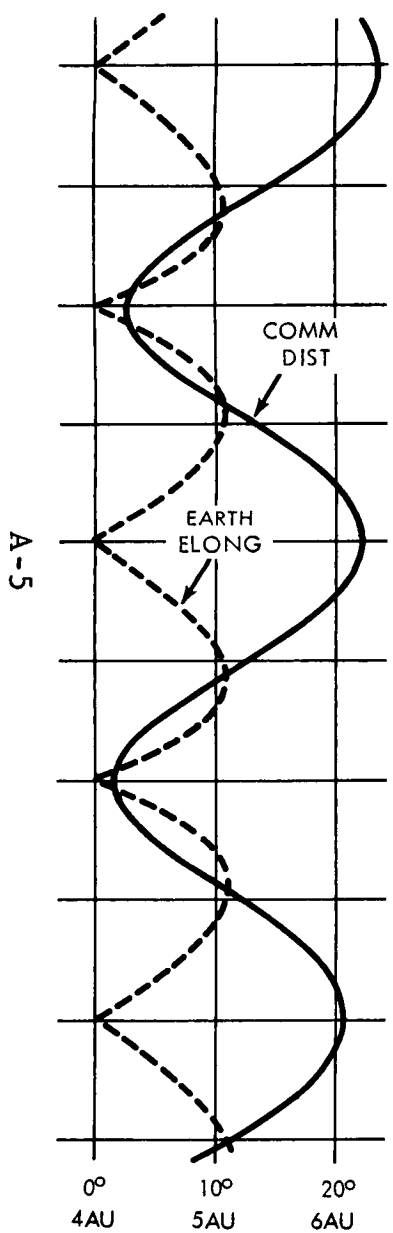
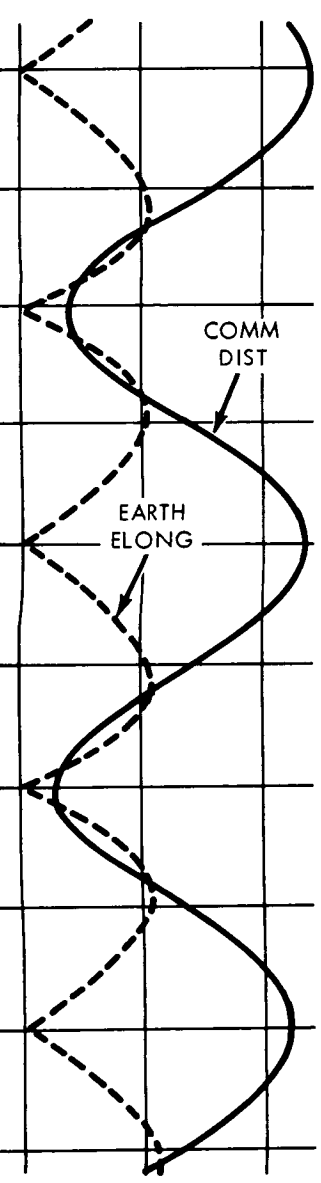


FIGURE A-4

INJECTION ENERGY AND ASYMPTOTE DECLINATION MISSION MAP, 1977 LAUNCH



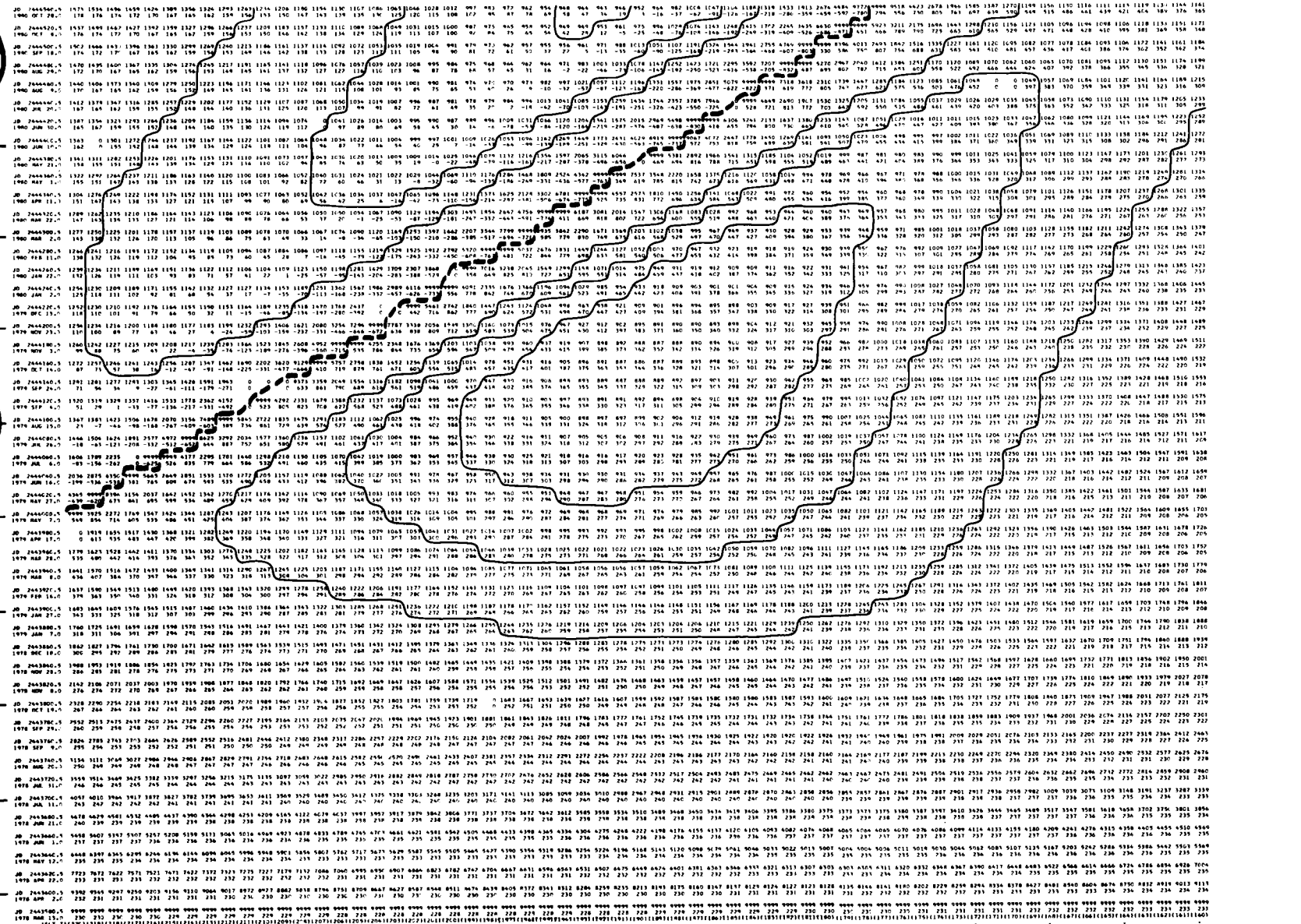


FIGURE A-5

INJECTION ENERGY AND ASYMPTOTE DECLINATION MISSION MAP, 1978 LAUNCH

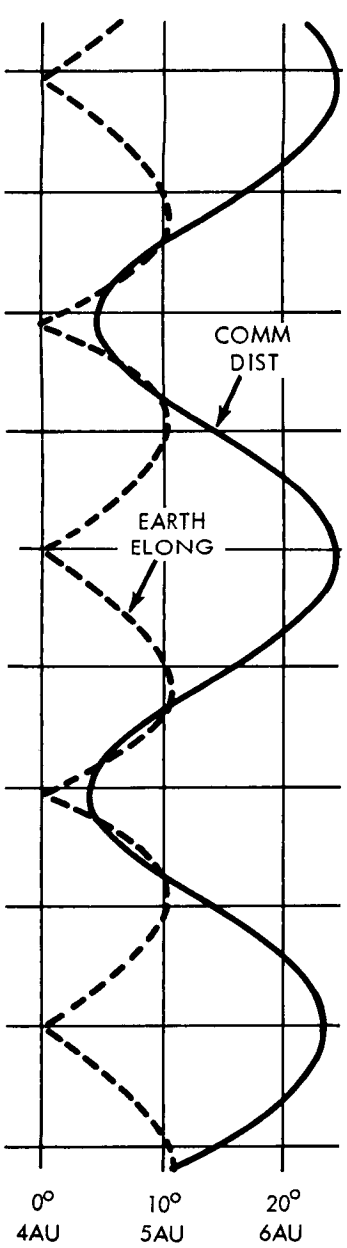


FIGURE A-6

INJECTION ENERGY AND ASYMPTOTE DECLINATION MISSION MAP, 1979 LAUNCH

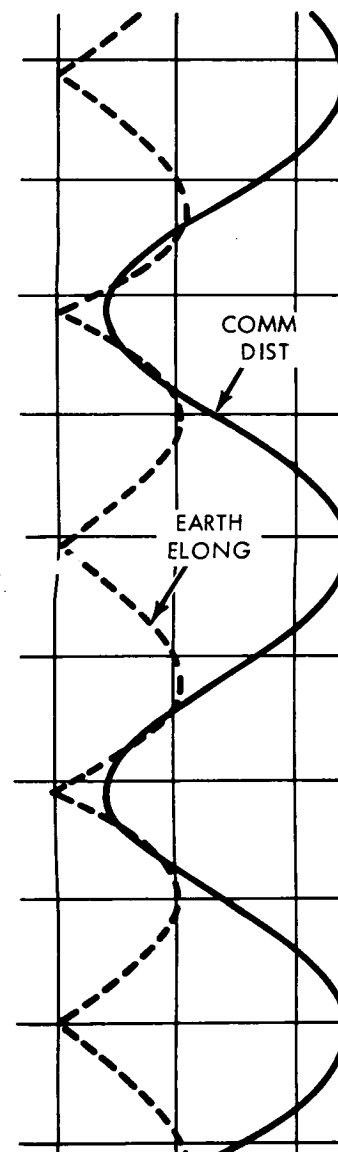
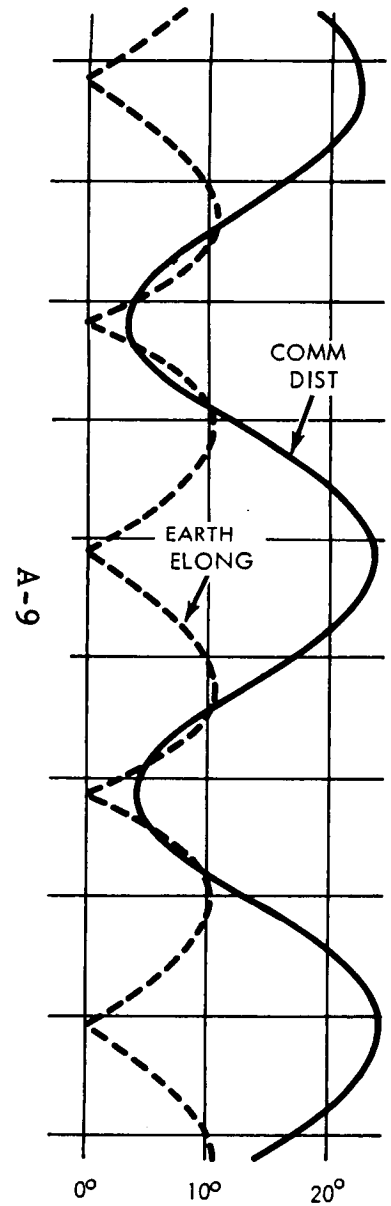
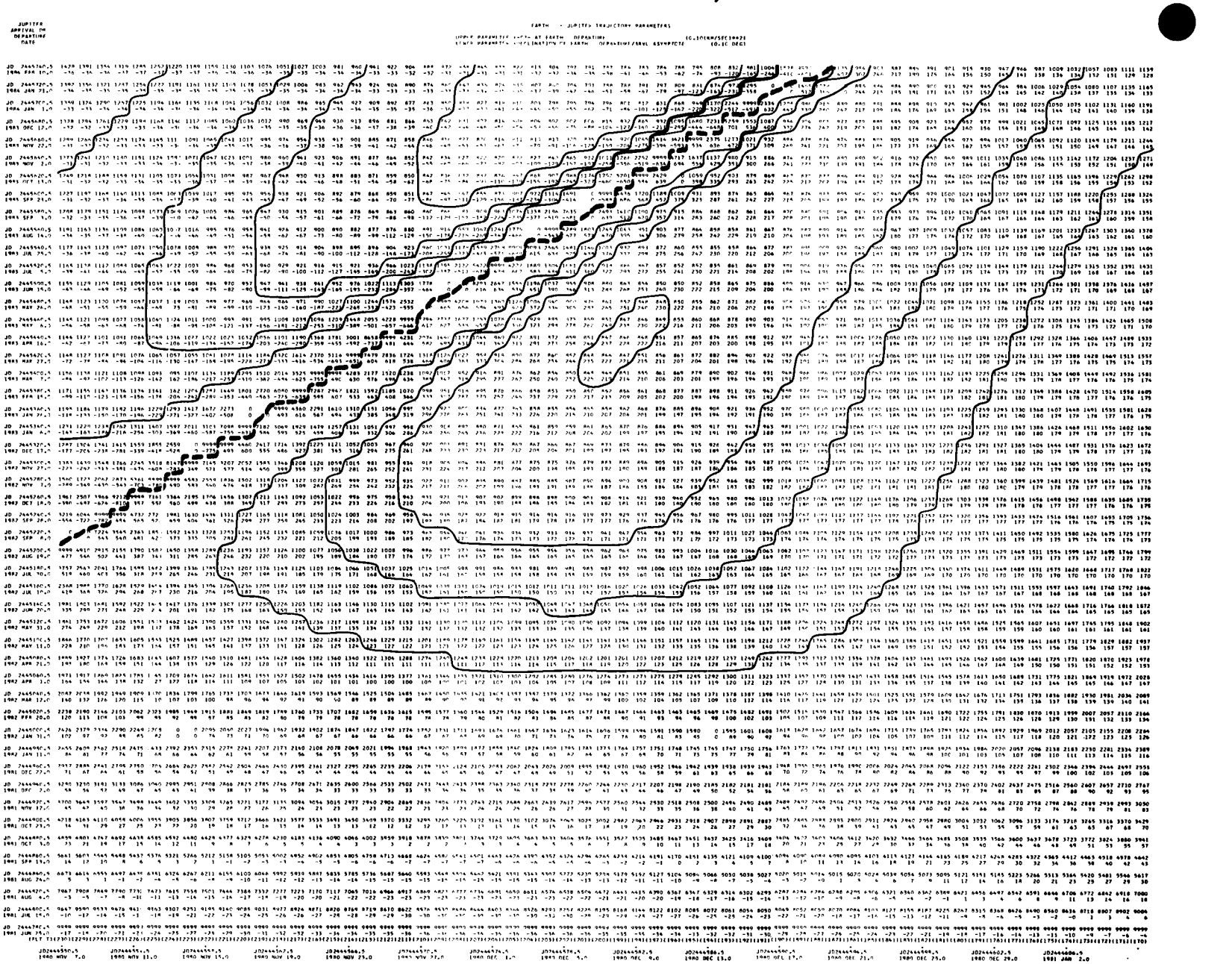


FIGURE A-7

INJECTION ENERGY AND ASYMPTOTE DECLINATION MISSION MAP, 1980 LAUNCH





A-9

FIGURE A-8

HYPERBOLIC EXCESS SPEED MISSION MAP, 1973 LAUNCH

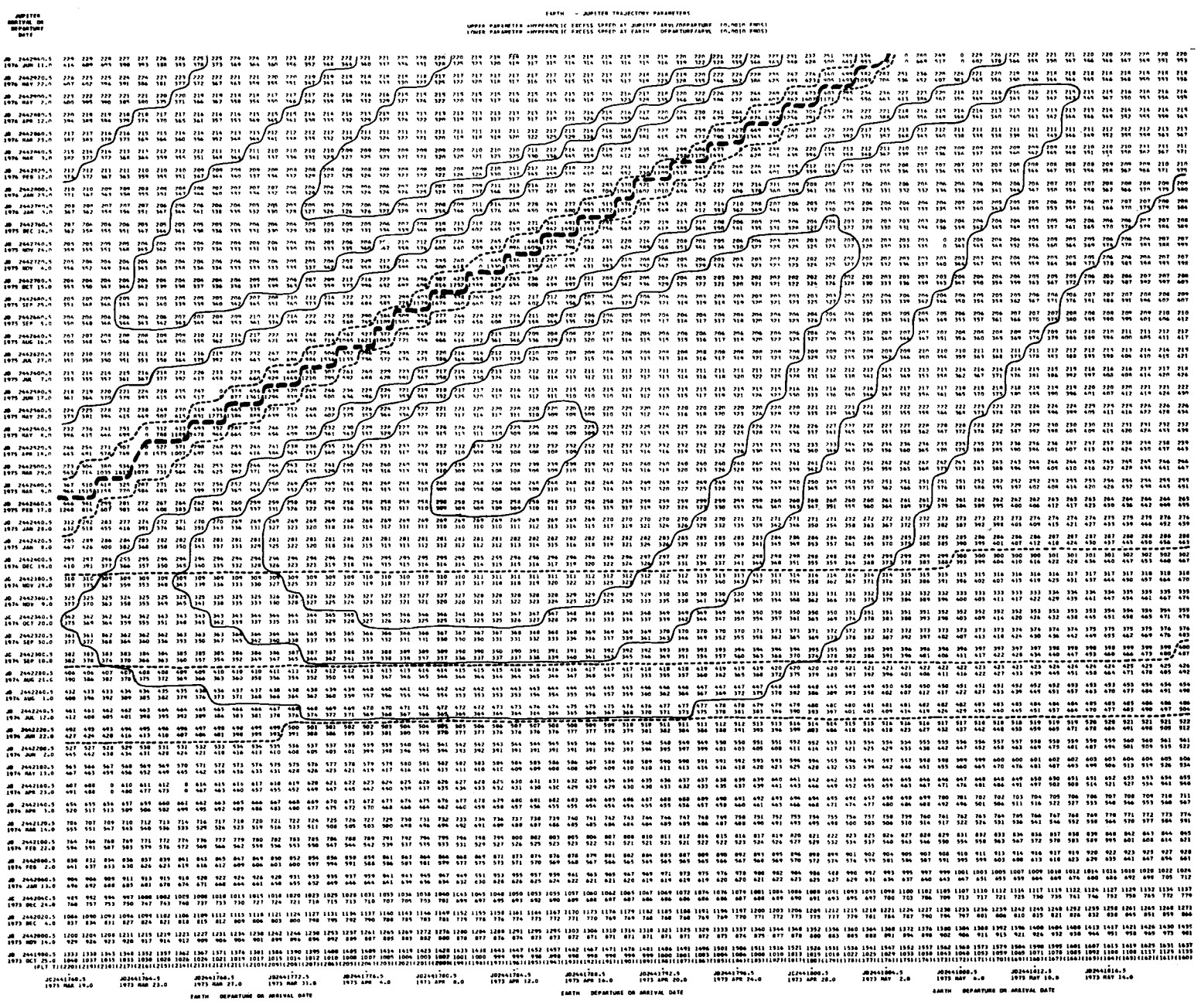


FIGURE A-9

HYPERBOLIC EXCESS SPEED MISSION MAP, 1974 LAUNCH

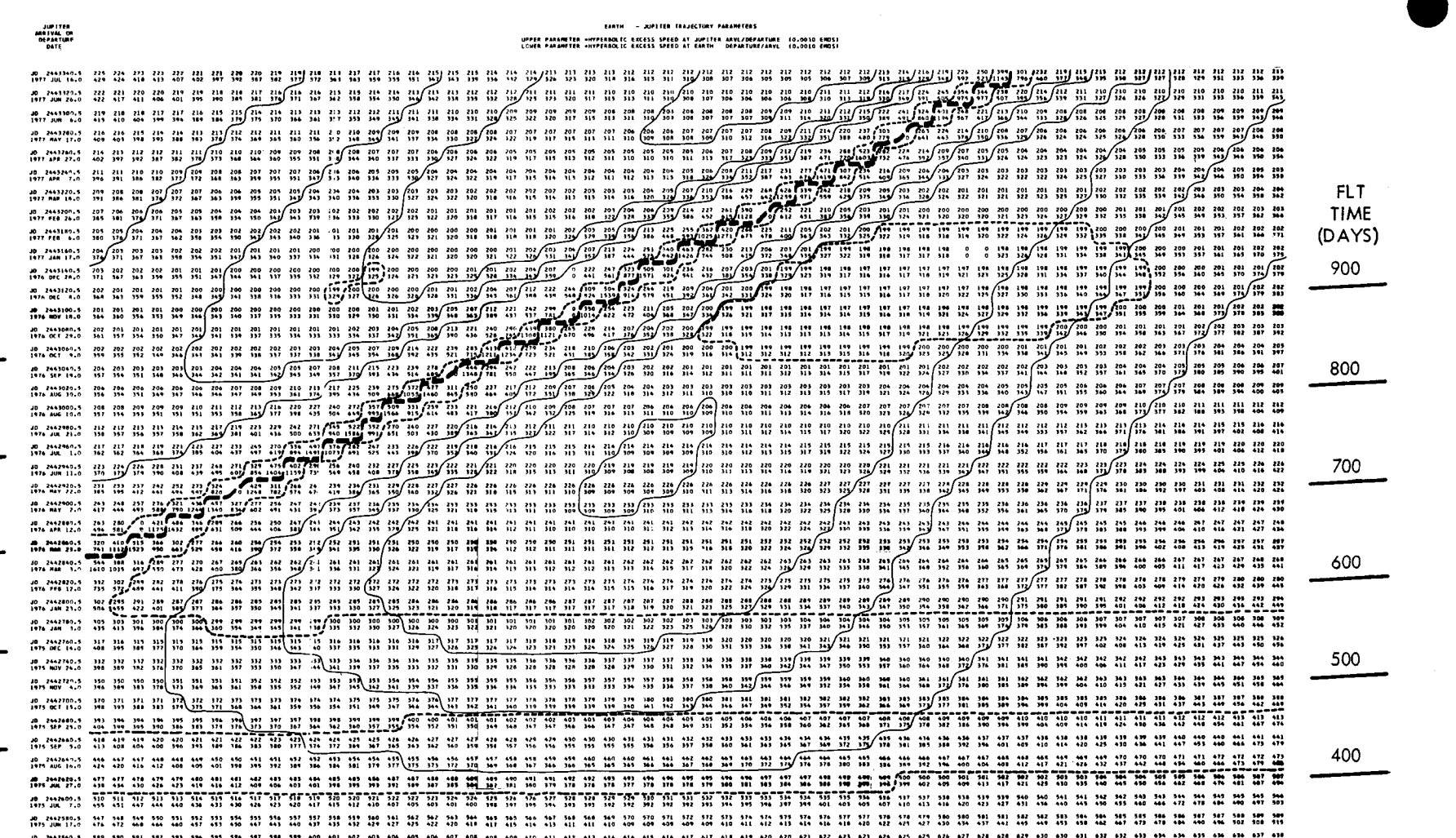
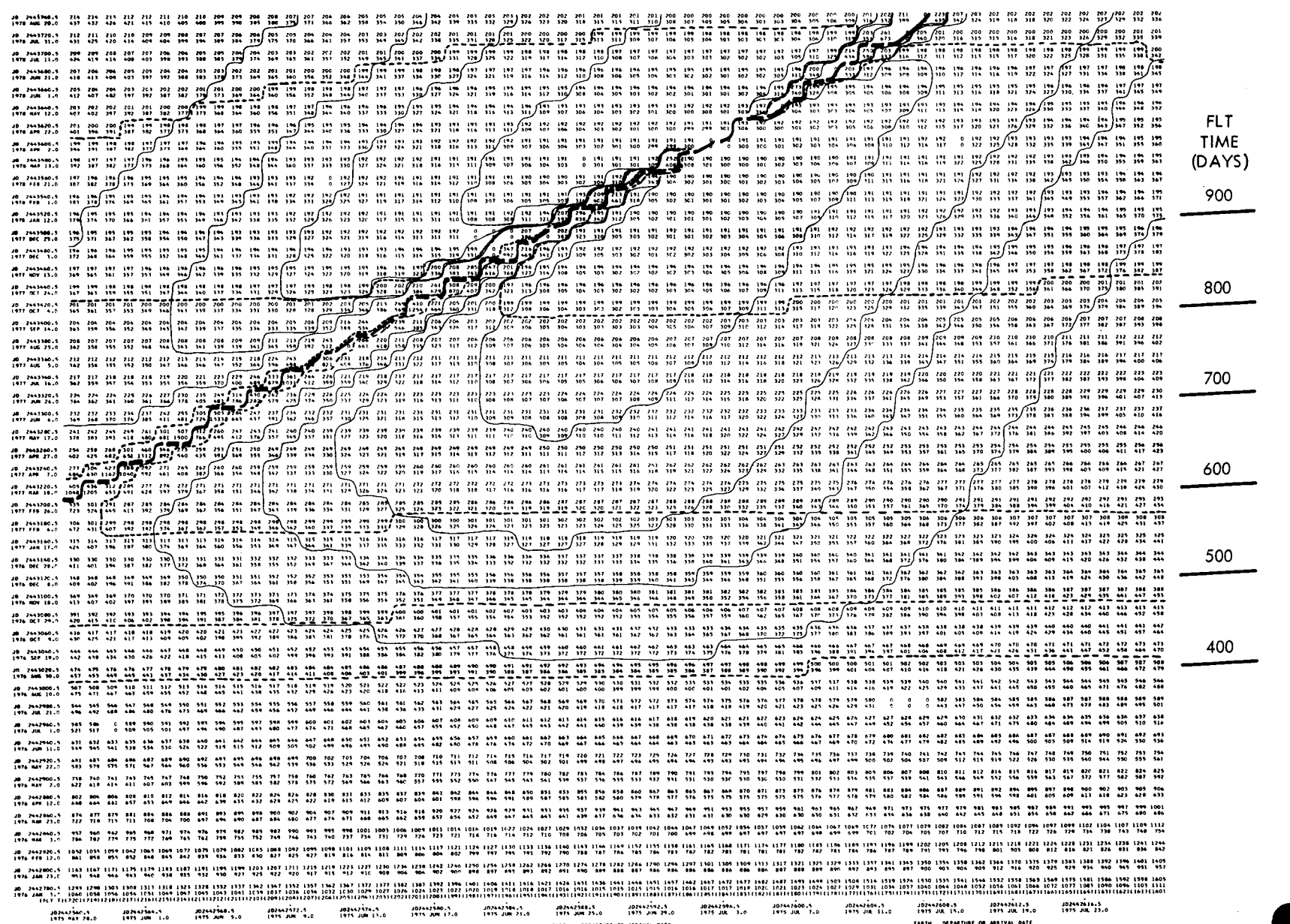


FIGURE A-10

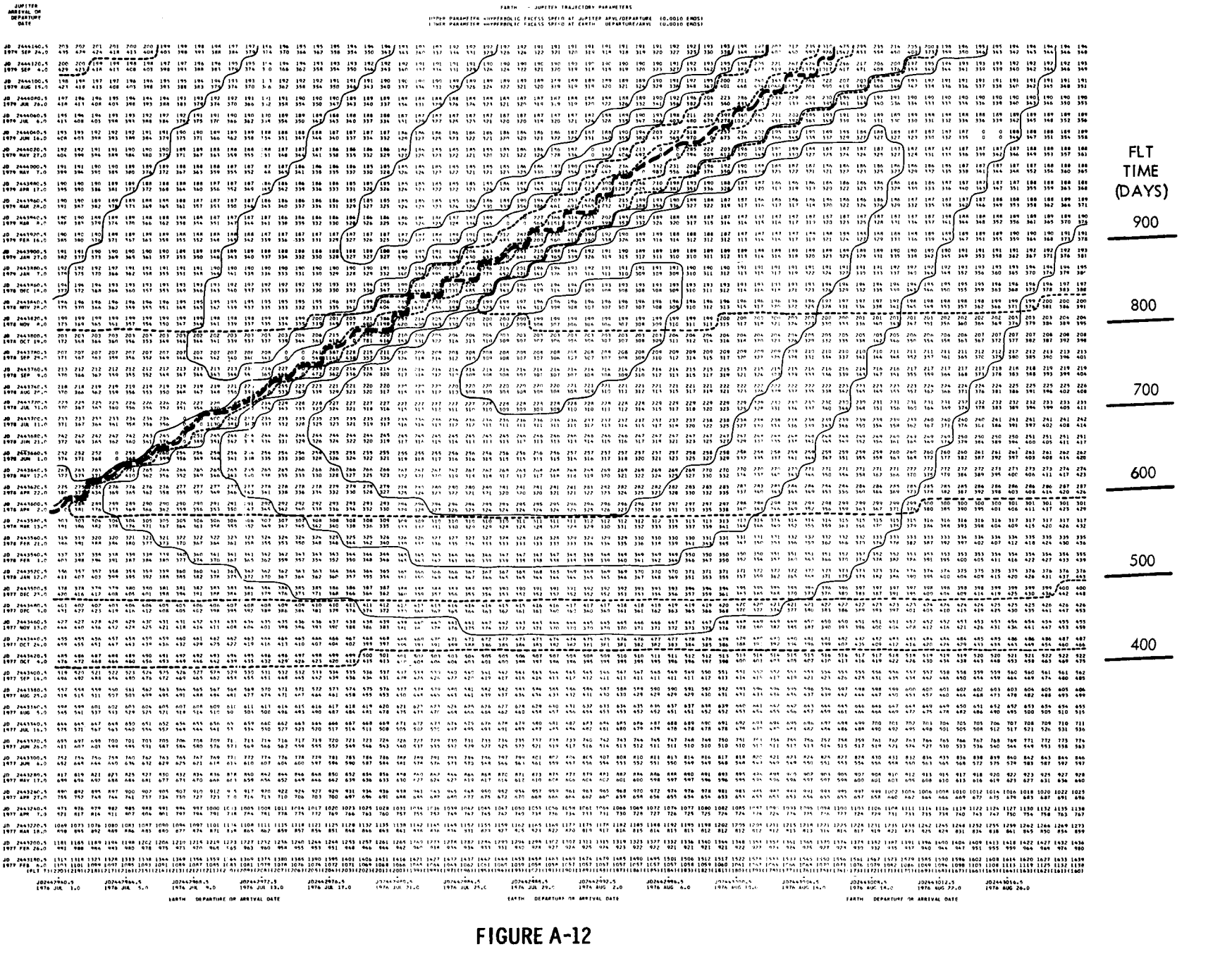
HYPERBOLIC EXCESS SPEED MISSION MAP, 1975 LAUNCH



A-12

FIGURE A-11

HYPERBOLIC EXCESS SPEED MISSION MAP, 1976 LAUNCH



A-13

FIGURE A-12

HYPERBOLIC EXCESS SPEED MISSION MAP, 1977 LAUNCH

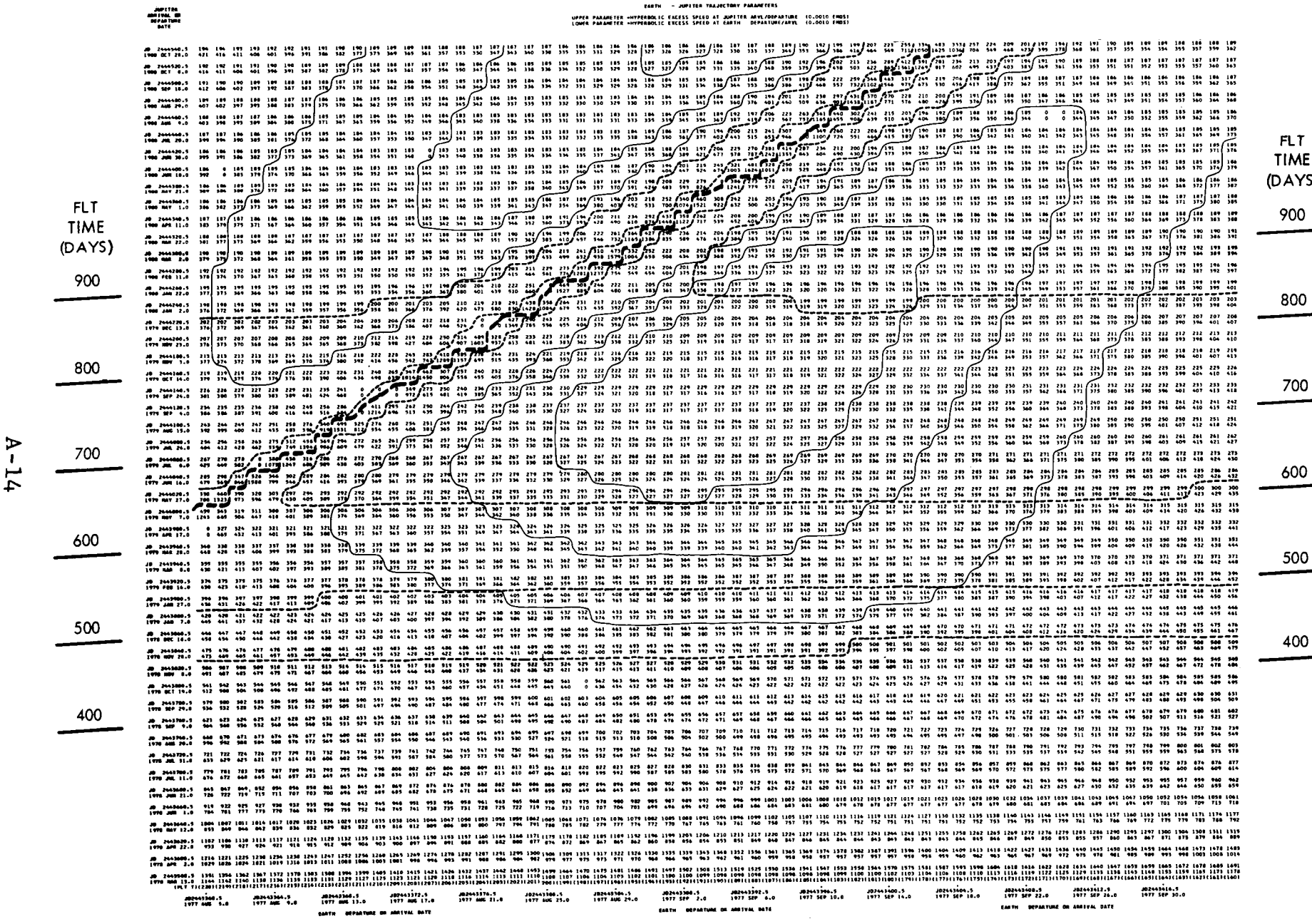


FIGURE A-13

HYPERBOLIC EXCESS SPEED MISSION MAP, 1978 LAUNCH

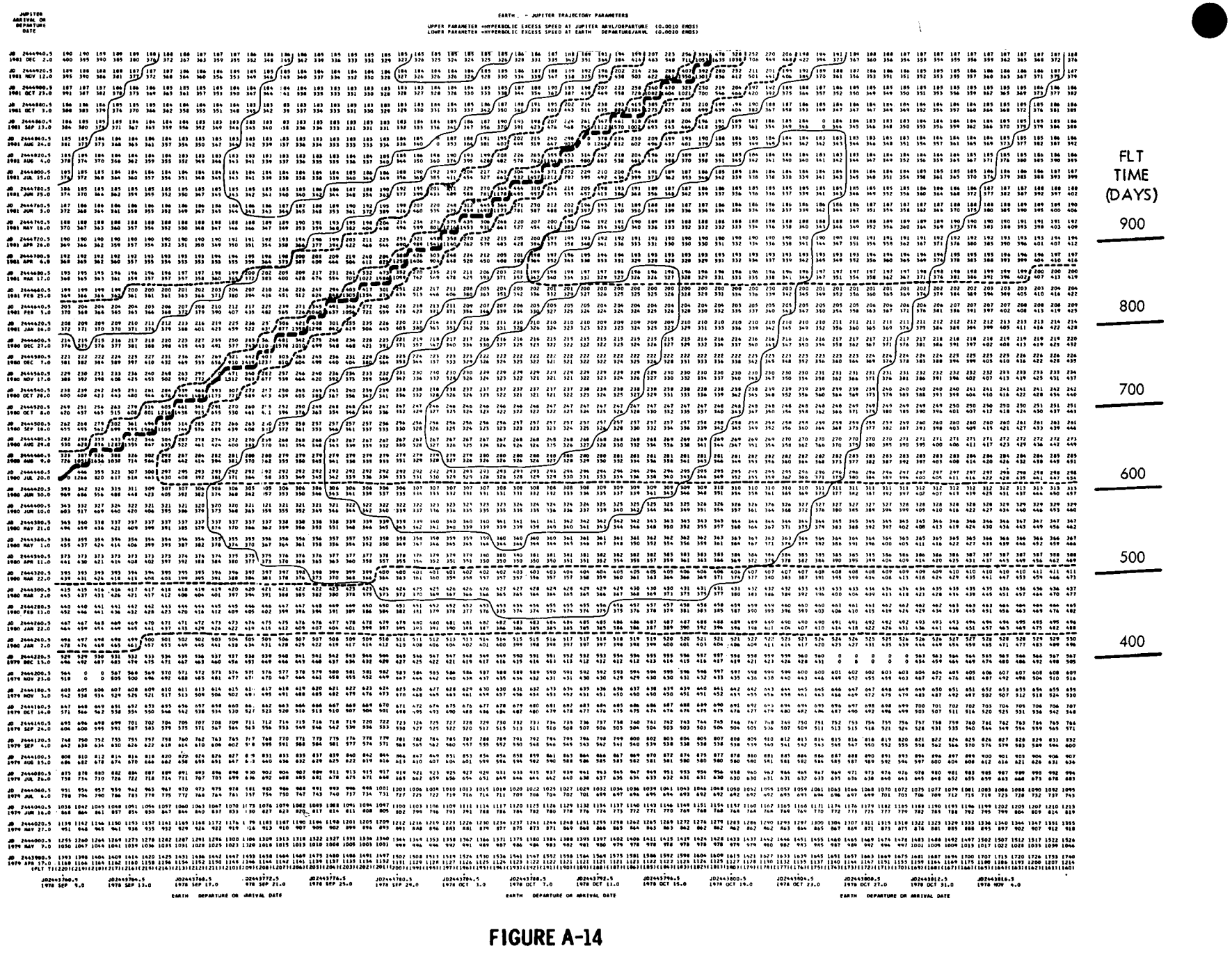


FIGURE A-14

HYPERBOLIC EXCESS SPEED MISSION MAP, 1979 LAUNCH

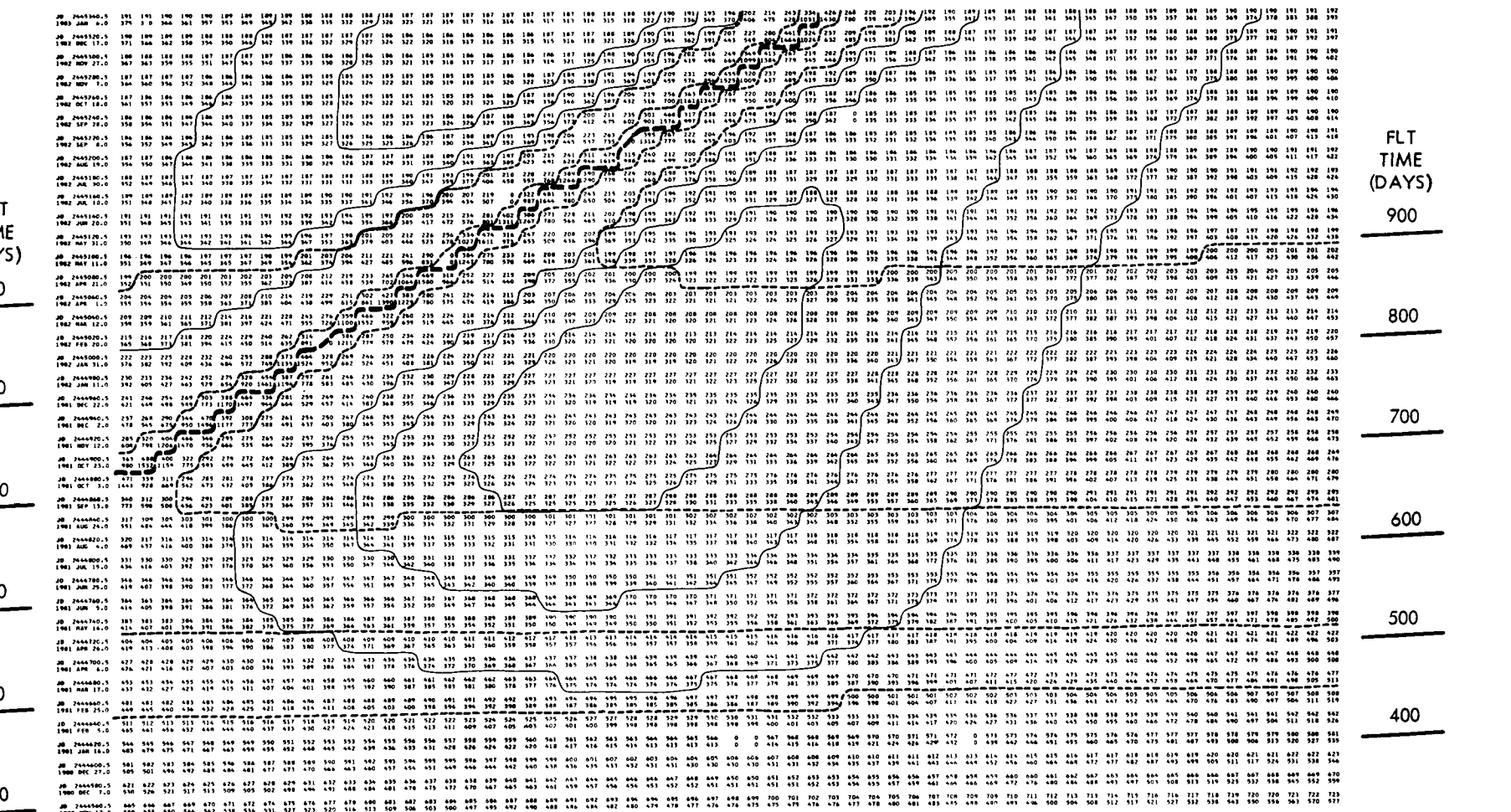


FIGURE A-15

HYPERBOLIC EXCESS SPEED MISSION MAP, 1980 LAUNCH

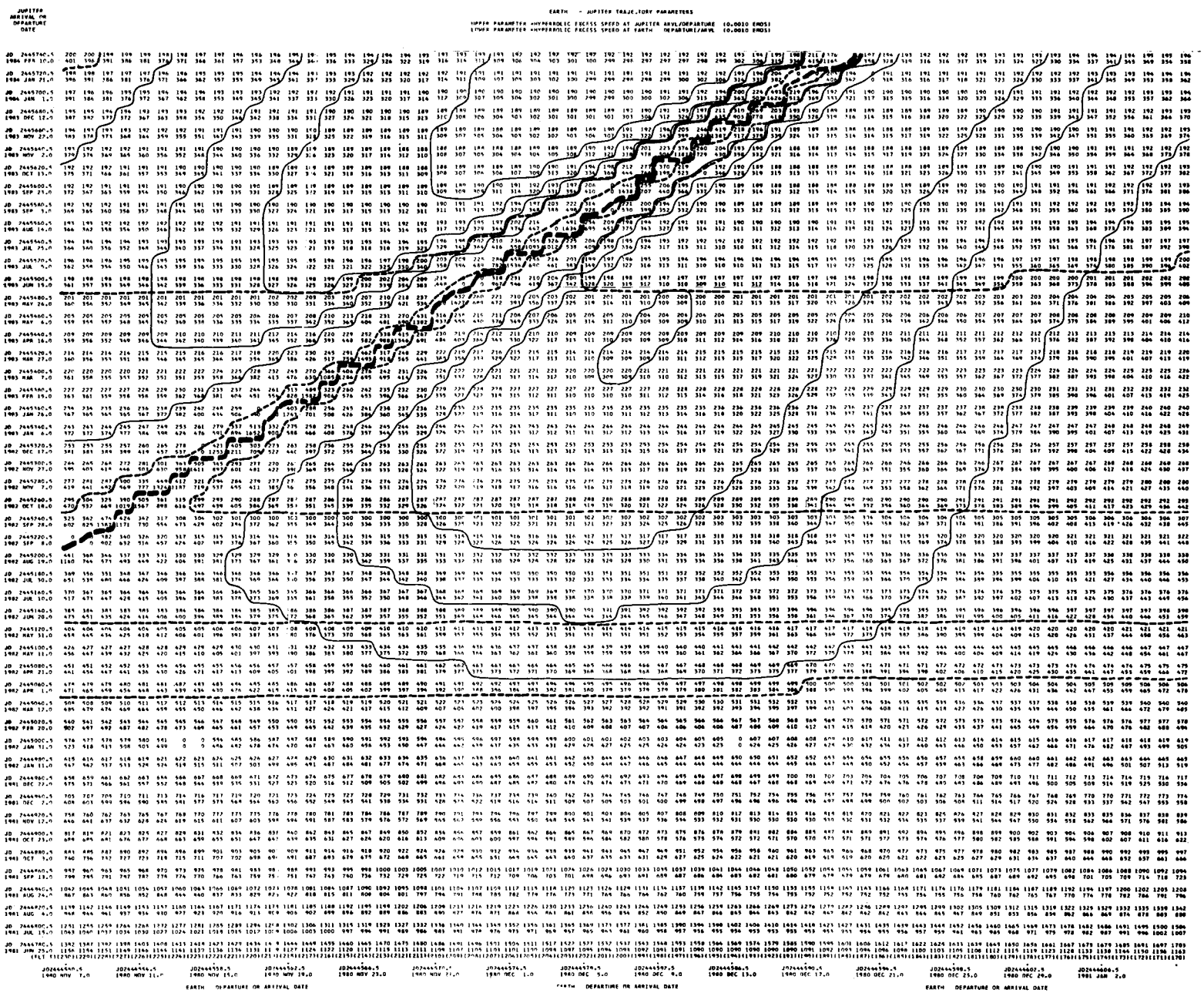


FIGURE A-16

APPENDIX B

METEOROID DAMAGE TO SPACECRAFT ANTENNAS

The following considerations are a part of the treatment of the overall problems of meteoroid damage to spacecraft antennas: (1) the types of damage which may be expected to occur, (2) the effect of each of these types of damage, (3) possible forms of protection, and (4) the effects of each of these forms of protection on the performance of the antenna.

The types of damage which seem most likely are (1) sandblasting or surface roughening due to very small particles, and (2) small holes or small deformations (Reference B-1) of not more than 2/10 wavelength (2.6 centimeter) but of sufficient size to be classed as a hole or deformation instead of surface roughness. The effect of holes and deformations is similar if the deformations are of appreciable depth. There are other types of damage that are less probable but still important enough to warrant consideration. Slits which are thin but of an appreciable wavelength (larger than 1.25 inchs) must be considered separately and are of the same class as long thin deformations. There is also the possibility of large holes or deformations of appreciable size in both dimensions with respect to a wavelength. It will be useful to speak generally of the effects of these different kinds of damage before attempting to discuss the specific impact upon the performances of the individual antennas to be considered.

Sandblasting, which causes surface roughness, chiefly affects the conductivity of the material. The skin effect causes currents to be confined to a very thin layer of conductor close to the surface, and the primary effect of surface roughness is to lengthen the conducting path, thus increasing surface resistance and resulting in losses (Reference B-2). Such an effect is important when the operation of the antenna depends upon wave conduction over a surface and is of relatively little importance when the primary function of the surface is that of a reflector or radiating

element. Small holes or deformations are individually the least effective in producing noticeable changes in antenna operation. The effects of these tend to vary as the fourth power of the "radius" or largest dimension of the hole or deformation (expressed in wavelengths), and therefore would be quite small unless a great many holes were produced (Reference B-3). Therefore, it appears desirable to allow small holes to be produced rather than to attempt to stop a meteoroid with a consequent widening of the affected area. Slits and large holes (or long and/or large deformations) can be discussed in similar ways. Their primary effect is to act as "negative" or at least differently phased sources of approximately the same strength of feed distribution. Thus, a round hole tends to produce a pattern similar to that of a parabola of the same size, and a long slit tends to produce a pattern similar to a line source of the same size (Reference B-3). The same can be said of the corresponding deformation. It is also possible for two parallel or nearly parallel slits to produce interferometer patterns with many sharp lobes.

The forms of protection against meteoroids which are considered possible are (1) conductor sheets, (2) foamed structures, (3) covering conductors with non-conducting layer, (4) metal coverings (shielding), (5) thin walls, and (6) double walls. The purpose of the first four types of protection listed is obviously to attempt to avoid as much as possible meteoroids striking the surface of all or to minimize the damage if a strike occurs. Thin walls would minimize damage by allowing the meteoroid to penetrate freely so that the smallest possible hole results. Double walls would be of primary advantage in minimizing the effect of small holes in one or the other of the walls or of slits (which even if they occurred in both walls would tend to be displaced from each other).

The effect of these different forms of protection can also be discussed generally. It will almost never be possible to use metal shielding, because such shielding will affect the performance of the antennas. Essentially, thick or thin walls used as conductors are electrically identical at the proposed frequency, almost down to the point of transluscence. The limiting factor in this case will be a mechanical one. Double layers need to be kept close (to within approximately 1/4 inch), and the selection of separating material is not critical. It is important to achieve low loss

in any covering material which will be in the antenna fields, particularly in the area close to feed points where efficiency will be materially affected. High dielectric materials can change patterns appreciably due to diffraction effects, and when these materials are used as coverings for conductors, they should be kept as thin as possible. Coverings thinner than 0.125 inch would generally be permissible. Low-loss materials, such as glasses, should be used. Low dielectric materials, such as foams, are ordinarily low loss also, and their thickness is not important. Foams can be used as fillers, inside a bicone for example, and can be used in such a way that efficiency or radiation patterns will not be noticeably affected. These overall considerations can now be applied to the types of antennas considered for the spacecraft.

In the case of a biconical horn antenna, the primary meteoroid damage problem from the standpoint of the effect on the operation of the antenna would be sandblasting. Sandblasting would increase surface resistance. Since the action of the bicone is that of a waveguide, considerations applying to waveguides are important for this antenna (Reference B-4). The losses in the wall resistance that are caused by the currents induced by the guided waves produce attenuation. This attenuation may possibly rise to quite large values, perhaps of the order of magnitude between 1 and 10 db. It would therefore be important in the case of a biconical antenna to protect the inner surfaces between the cones from such effects, particularly near the feed region, where currents are large. On the other hand, a few small holes would be of little consequence, and even large holes would not be likely to cause more difficulties than slight perturbations in the radiation patterns. A meteoroid strike which seriously damages the feed region would knock the antenna out of action. It would probably suffice to think of a spherical area of about a six-inch radius about the apices of the cone as the feed region. It is not permissible to use dielectric between the cones in this region because the high field strength there would induce loss in the dielectric. Holes of any appreciable size in the cones in this region might also seriously affect the radiation pattern. Therefore, the following methods of protecting the biconical antenna seem most appropriate.

The regions between the cones should be foamed to prevent sandblasting on the inner surfaces, except near the feed region which should be left empty. This foam could also be used to

form a lens to obtain the desired gain as discussed below. The outer region (inside each of the cones themselves) may be protected by foam or not as desired, but the small portion inside each of the cones near the feed region should be filled with a fairly dense material (perhaps even made of solid metal) in order to avoid holes which would affect the radiation pattern. The remainder of the conducting cones should probably be made of very thin material so that hole sizes would be minimized. Double-wall construction might be advisable when the effect of long slits along the circumference of the cone on the radiation patterns might be fairly important.

The next type of antenna to be considered is the round waveguide type with an array of radiating slots cut through its walls. Of the possible types of damage for such an antenna, sandblasting is the least important because it affects only the outer surface. That surface plays little role in the operation of the antenna. Holes are the most serious, particularly large holes, although holes smaller than 0.5 inches in diameter, will not have an important effect. Larger holes would radiate and thus produce side-lobes and some side effect on the main lobe of the pattern, but the radiation would be unlikely to produce important effects on the pattern. The most important effect of large holes would be to induce reflections in the waveguide. Such reflections could result in a mismatch and a consequent reduction in the power reaching the original radiating slots and a disruption of the pattern symmetry. Slits stretched around the circumference of the waveguide would also have a significant effect. This effect could be minimized by double wall construction if desired. The wall(s) should probably be thin in order to minimize the size of the holes, but not so thin as to increase the probability of deformations which would obviously affect the reflections in the waveguide. These same problems would exist with deformations produced by some cause other than meteoroids.

The next type of antenna to be discussed is the collinear array type. Such an array consists of dipole elements fed by transmission lines. About the only kind of damage which could matter would be a meteoroid strike which actually clipped one of the lead wires. This would put out a portion of the array completely, and large reductions in the gain would be caused by increasing beamwidth. Significant deformation of a portion of the array (further than 2 inches)

would also seriously effect the operation of the antenna. It is probable that any meteoroid large enough to produce a hole in a waveguide would be capable of clipping a lead.

The next type of antenna to be discussed is reflector or parabolic type. Aside from the feed element of the parabola, (which must be protected at all costs) such an antenna is almost invulnerable to meteoroid strikes. Sandblasting affects primarily the conductivity of the surface, and this conductivity is of almost no importance within very wide ranges. Holes produce effects which are easily approximated by thinking of them as "negative patterns." Thus, a large hole would tend to produce a lobe in the same direction as the main lobe, but somewhat wider. Such a lobe would not be much noticed on the pattern. Only if it took a significant portion of the energy from the main lobe and spread it in other directions would the effect be appreciable. This would not happen until a significant fraction of the dish surface was removed. Thus, a 10 percent removal of the dish surface would produce only a 1 db reduction in gain. Probably the most serious possible effect of meteoroids could come from slits. Slits would act as negative line sources which produce maximum beams in the main lobe direction. If two of these line sources were approximately parallel and separated by an appreciable distance, say a foot, they would produce an interferometer pattern which could cause ripples in the main lobe. This could seriously effect the energy density in the portion of the main lobe which actually intercepts the Earth, perhaps by as much as 3 db. While this possibility seems quite remote, it could be eliminated almost entirely by the use of a double-walled construction because slits in the back and fron faces would not be aligned.

The final types of antennas to be discussed are the electrically de-spun types. Because of the great variety of such antennas, it would certainly be possible to choose the design of the elements in such an array that meteoroid damage would be unlikely. In any case, such an array would have most of its leads, etc., interior to a well shielded region, perhaps covered by a fairly thick material sphere. In any case, it is unlikely that more than one element at a time would be removed by a meteoroid strike, and this would not be a serious problem. It is therefore not felt necessary to discuss the protection of de-spun arrays.

REFERENCES

B-1. Eichelberger, R.J. and Gehring, J.W. "Effects of Meteoroid Impacts on Space Vehicles", American Rocket Society, Space Flight Report to the Nation/New York Coliseum, 9 October, 1961.

B-2. "Skin Effect," Reference Data for Radio Engineers, 4th ed., American Book--Stratford Press, Inc., New York, New York, 1959, pp. 128-132.

B-3. Mack, R.B. and Blacksmith, P., Jr. "Some Thoughts on Scattering Cross Sections in the Resonance Region", The Modification of Electromagnetic Scattering Cross Sections in the Resonant Region, A Symposium Record, Vol. I., September 1964, AD 606106, pp. 1-9.

B-4. Schelkunoff, S., Advanced Antenna Theory, Wiley, New York, 1952., pp. 39-54.

APPENDIX C

PARAMETRIC ANALYSIS OF THE BASIC HYDRAZINE PROPULSION SUBSYSTEM

The weight of the monopropellant hydrazine system considered in this study is represented by the following equation:

$$(1)\quad W_{system} = W_H + W_{H_T} + W_{PG} + W_{PG_T} + W_B + W_{COM}$$

In the equation above, the last term, W_{COM}, represents fixed hardware, i.e., the sum of the weights of components such as valves, regulators, tubing, catalyst bed and nozzle assembly, etc., whose individual weights do not vary appreciably with total impulse. For a given thrust level, this term may be predicted from manufacturer's weight data in conjunction with an itemized listing of the system's components. The remaining five terms, however, vary directly with the total impulse requirement, or more exactly, with the weight of propellant contained within the system. Equations for these five terms are developed in the analysis which follows.

The weight of hydrazine contained within the system may be obtained from the sum of the following equations:

$$W_{H_1} = \frac{I_T}{I_{SP}} = W_{S/C}\left[1 - e^{\frac{-\Delta V}{I_{SP} g}}\right]$$ expected hydrazine consumption

$$W_{H_2} = \alpha_H W_{H_1}$$ contingency for I_{sp} degradation

$$W_{H_3} = W_{H_1}\left(\frac{\delta\Delta V}{\Delta V}\right)\frac{\left(\frac{\Delta V}{I_{SP} g}\right)}{\left(e^{\frac{\Delta V}{I_{SP} g}} - 1\right)}$$ contingency for ΔV reserve (ref. JPL TR 32-26)

$$W_{H_4} = \left(\frac{1-\epsilon}{\epsilon}\right)\left(W_{H_1} + W_{H_2} + W_{H_3}\right)$$ contingency for bladder expulsion inefficiency

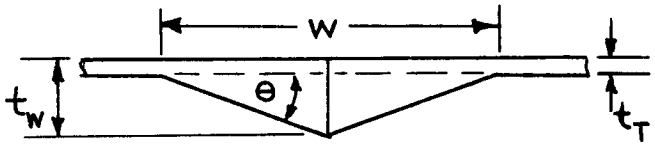
Combining these four equations and rearranging gives:

$$(2)\quad W_H = \frac{W_{S/C}}{\epsilon}\left[1 - e^{\frac{-\Delta V}{I_{SP} g}}\right]\left\{1 + \alpha_H + \left(\frac{\delta \Delta V}{\Delta V}\right)\frac{\left(\frac{\Delta V}{I_{SP} g}\right)}{\left(e^{\frac{\Delta V}{I_{SP} g}} - 1\right)}\right\}$$

The weight of a spherical hydrazine tank whose wall thickness is small compared to the tank radius, is given by:

$$(3)\quad W_{H_T} = 1.5\, P_D V_{H_T} \left(\frac{\rho}{\sigma}\right)_{MAT} (S.F.) + W_{ACC}$$

In this equation, the first term on the right-hand side represents the weight of the tank shell as determined from thin-wall stress theory. The use of this term presumes no overriding minimum gauge wall thickness considerations, which is a valid presumption for the tank diameters, design pressures, and material strengths anticipated in this study. The second term of this equation represents the weight of tank accessories such as welds, bosses, fittings, etc., which are often responsible for a significant portion of the overall delivered tank weight. This last term, unfortunately, is more difficult to describe mathematically since it is influenced by a variety of factors such as manufacturing techniques, materials, and peculiarities of the particular tank design. Nevertheless, an attempt was made to account for the weight of tank welds and fittings (and thus bring tank estimates more in line with existing hardware) by adopting the following simplified model.



Girth Weld Cross Section

In the figure to the left,

W = width of weld buildup section

t_T = nominal tank wall thickness

t_W = max. thickness of weld buildup

θ = taper angle of buildup

- Tank curvature is neglected
- Filler material density = parent material density

Weight increase due to weldment = $\left(\frac{\text{weight buildup}}{\text{linear inch}}\right)$ x(tank circumference)

Letting:

$$t_w = K_1 t_T \qquad \text{where } K_1 \text{ is some constant}$$

$$t_T = \left(\frac{P_D\ D}{2\sigma_{mat}}\right)(S.F.)$$

then:

$$\text{TAN } \theta = \frac{(t_w - t_T}{\left(\frac{w}{2}\right)}$$

and,

$$w = \frac{2(t_w - t_T)}{\text{TAN } \theta}$$

The weight of the weld buildup per linear inch is:

$$\frac{\rho_{mat} w}{2}\ (t_w - t_T) = \frac{\rho_{mat}\ (K_1 - 1)^2}{\text{TAN } \theta}\ (t_T)^2$$

Multiplying by the circumference gives:

$$W_{weld} = \frac{\rho_{mat}\ (K_1 - 1)^2}{\text{TAN } \theta}\left(\frac{P_D\ D}{2\sigma_{mat}}\right)^2\ (S.F.)^2\ \pi D$$

Since $\frac{\pi D^3}{6}$ is the tank volume, the last equation may be written:

$$W_{weld} = \frac{1.5\ (K_1 - 1)^2}{\text{TAN } \theta}\ P_D^{\ 2}\ V_{H_T}\left(\frac{\rho}{\sigma^2}\right)_{mat}\ (S.F.)^2$$

Substituting typical values, i.e., $K_1 = 3.0$, $\theta = 10^o$ gives:

$$(4)\quad W_{weld} = 1.5\ (22.7) P_D^{\ 2}\ V_{H_T}\left(\frac{\rho}{\sigma^2}\right)_{mat}\ (S.F.)^2$$

It remains now to account for the effects due to bosses, tank outlet cut-out, and buildup at the tank outlet. For these effects, an arbitrary fixed weight of 0.35 pound is assumed. The weight of tank accessories thus becomes

$$(5)\quad W_{acc} = 1.5(22.7) P_D^{\ 2}\ V_{H_T}\left(\frac{\rho}{\sigma^2}\right)_{mat}\ (S.F.)^2 + 0.35$$

Substituting Eq. (5) into Eq. (3) gives

$$(6)\quad W_{H_T} = 1.5\ P_D\ V_{H_T}\left(\frac{\rho}{\sigma}\right)_{mat}\ (S.F.)\left[1.0 + \frac{22.7\ P_D\ (S.F.)}{\sigma_{mat}}\right] + 0.35$$

The volume of the prepressurized hydrazine tank may be written as

$$(7) \quad V_{H_T} = V_H + V_B + V_{UL}$$

From previous studies, the volume of the bladder material, V_B, is conservatively estimated at 2 percent of the propellant volume, i.e., $V_B = 0.02\ V_H$. The ullage volue, V_{UL}, in a prepressurized system (with no pressure relief provision) must be ample enough to accommodate the thermal expansion of the propellant due to temperature increases, without incurring an intolerable rise in pressure in the tank due to the compression of the prepressurant gas. With an increase in temperature, the gas pressure rise in the tank is the result of (1) gas pressure increase as a result of the increase in gas temperature, and (2) gas pressure increase as a result of the reduction of the original ullage volume by an amount equivalent to the volume increase of the propellant. The ideal gas law provides an expression for the increased tank pressure in such a situation.

$$(8) \quad P_D = P_{PPG} \left(\frac{V_{UL}}{V_{UL} - \Delta V_{EXP}} \right) \left(\frac{T_{MAX}}{T_O} \right)$$

Expressing the ullage volume as a fractional part of the propellant volume gives

$$V_{UL} = \chi V_H$$

so that Eq. (8) may be written

$$(9) \quad P_D = P_{PPG} \left\{ \frac{1}{1 - \left(\frac{\Delta V}{V_o} \right) \frac{1}{\chi}} \right\} \left(\frac{T_{MAX}}{T_O} \right)$$

Eq. (7) may be rewritten as

$$(10) \quad V_{H_T} = (1.02 + \chi) V_H$$

When Eqs. (9) and (10) are substituted in the previously derived Eq. (6) for the hydrazine tank weight, the result is

$$(11) \quad W_{H_T} = 1.5\ P_{PPG} \left(\frac{T_{MAX}}{T_O} \right) \left(\frac{\rho}{\sigma} \right)_{mat} (S.F) V_H \left\{ \frac{1.02 + \chi}{1 - \left(\frac{\Delta V}{V_o} \right) \frac{1}{\chi}} \right\} \left[1.0 + \frac{22.7 (S.F.) (PPPG) \left(\frac{T_{MAX}}{T_O} \right)}{\left\{ 1 - \left(\frac{\Delta V}{V_o} \right) \frac{1}{\chi} \right\} \sigma_{mat}} \right] + 0.35$$

This last equation is plotted in modified form in Figure C-1 wherein representative design values are used. From the curve it can be seen

RATIO OF HYDRAZINE TANK WEIGHT TO HYDRAZINE VOLUME VERSUS ULLAGE FACTOR

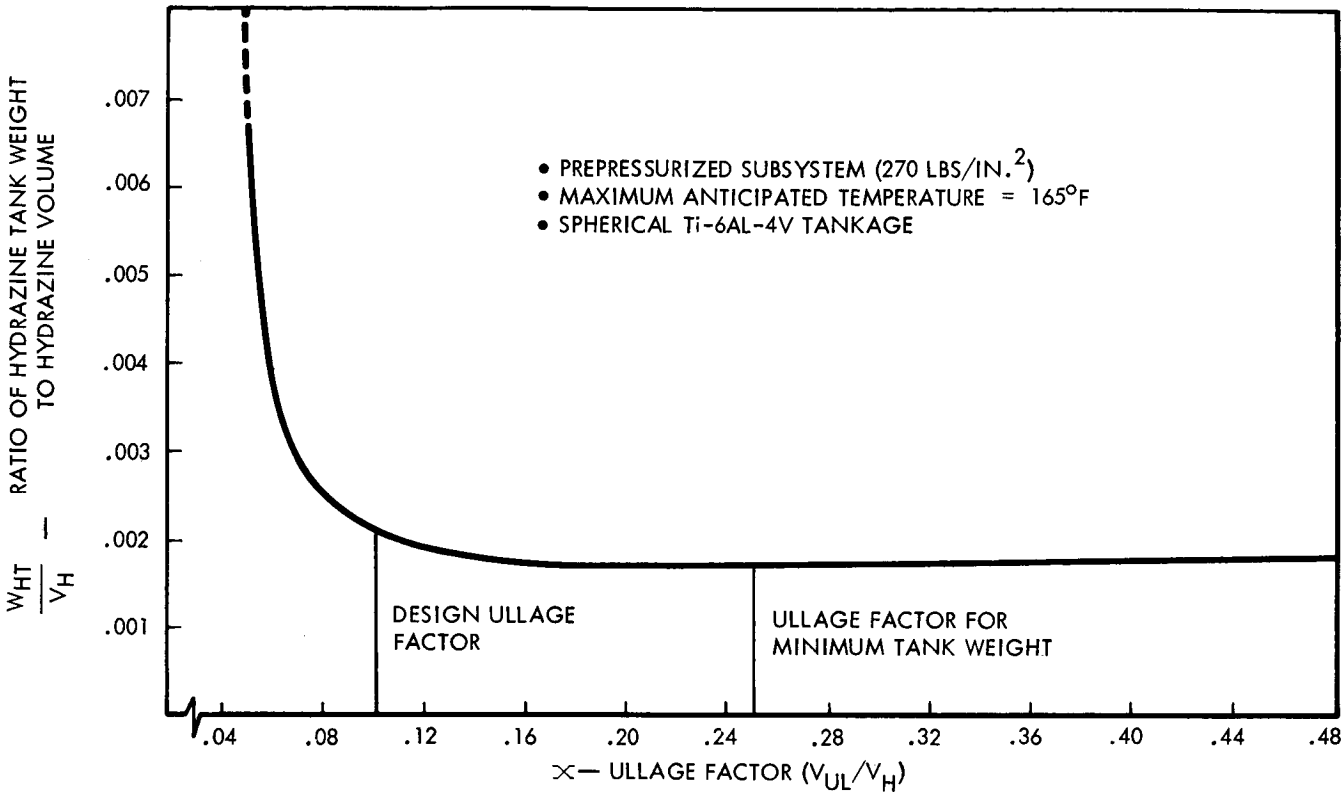


FIGURE C-1

that no appreciable savings in tank weight are attainable beyond an ullage factor of approximately 0.10. For this reason, and for the sake of reasonable tank volumes, an ullage factor of 0.10 was used in all subsequent system design calculations.

The weight of pressurant gas required for propellant expulsion may be conservatively estimated by an energy and mass balance analysis which assumed an adiabatic process and negligible line residuals. For a given weight of propellant, W_H, the weight of pressurant required becomes:

$$(12)\quad W_{PG} = \frac{P_T\, W_H}{R\, T_0\, \rho_H} \left\{ \frac{K}{1 - (P_{PG_f}/P_{PG_i})} \right\}$$

The weight of a spherical pressurant tank is given by the expression:

$$W_{PG_T} = 1.5\, P_D\, V_{PG} \left(\frac{\rho}{\sigma}\right)_{mat} (S.F.) + W_{ACC}$$

where, as before, W_{ACC} equals the weight of weldment plus the weight effect of bosses, cut-outs, fittings, etc. An argument similar to that used for determining propellant tank weight (Eq. (6)) but using $K_1 = 2.0$ gives

$$(13)\quad W_{PG_T} = 1.5\, P_D\, V_{PG} \left(\frac{\rho}{\sigma}\right)_{mat} (S.F.) \left[1.0 + \frac{8.5\, P_{PG_i}\, (S.F.)\, T_{max}}{\sigma_{mat}(T_0)} \right] + 0.35$$

which may be rewritten as

$$(14)\quad W_{PG_T} = 1.5\, W_{PG}\, R\, T_{MAX}\left(\frac{\rho}{\sigma}\right)_{mat} (S.F.)\left[1.0 + \frac{8.5\, P_{PG_i}\left(\frac{T_{MAX}}{T_O}\right)(S.F.)}{\sigma_{mat}}\right] + 0.35$$

The weight of the bladder (assumed to be essentially spherical) may be estimated from the following analysis

$$W_B = \pi D_B^2\, t_B\, \rho_B$$

$$(15)\quad W_B = 4.84\, (V_H)^{.667} (t_B)(\rho_B)$$

or alternately

$$(16)\quad W_B = 44.3\, (W_H)^{.667} (t_B)(\rho_B).$$

APPENDIX D

PARAMETRIC ANALYSIS OF A COLD GAS ATTITUDE CONTROL PROPULSION SUBSYSTEM

The weight of a typical cold gas attitude control subsystem may be represented by the following equation:

(1) $W_{system} = W_P + W_T + W_{com}$

In this equation, only the terms W_P and W_T vary appreciably with changes in the total impulse required. Expressions for these terms are derived in the treatment which follows. (Wcom, which represents the total weight of the subsystem fixed hardware, was obtained empirically and was reported in subsection 3.6.2.4.)

The weight of propellant required may be obtained from the sum of the following equations:

(a) $W_{p_1} = \frac{I_t}{I_{sp}}$ Expected Propellant Consumption

(b) $W_{p_2} = \alpha_p \; W_{p_1}$ Contingency for Isp Degradation

(c) $W_{p_3} = P_f \frac{V_{tank}}{RT_f}$ Residual Propellant at Termination of Thrust Program

The propellant tank volume may be approximated from the ideal gas law as

(2) $V_{tank} = \frac{W_p R T_i}{P_i}$ (neglects compressibility effects)

So that, Equation (c) above may be re-written as

$$W_{p_3} = \left(\frac{P_f}{P_i}\right) \left(\frac{T_i}{T_f}\right) W_p$$

Combining equations (a), (b), and (c) and rearranging them in order to derive the total weight of propellant required gives

(3) $$W_p = \left(\frac{I_t}{I_{sp}}\right) \frac{(1+\alpha_p)}{\left\{1 - \left(\frac{P_f}{P_i}\right)\left(\frac{T_i}{T_f}\right)\right\}}$$

The weight of a spherical propellant tank with a wall thickness that is small compared to the tank radius is given by the following equation:

(4) $$W_T = 1.5\ P_D\ V_{tank} \left(\frac{\rho}{\sigma}\right)_{mat} (S.F.)$$

(For the sake of brevity, the weight contribution of welds, fittings, etc. is neglected.)

The tank design pressure P_D, is defined as the pressure which would occur if the gas at the initial condition was heated to the maximum anticipated temperature. In a constant volume situation, this is:

(5) $$P_D = P_i \left(\frac{T_{MAX}}{T_i}\right)$$

Substituting equation (5) into (4) yields:

(6) $$W_T = 1.5\ P_i\ V_{TANK} \left(\frac{T_{MAX}}{T_i}\right)\left(\frac{\rho}{\sigma}\right)_{MAT} (S.F.)$$

which may be rewritten as:

(7) $$W_T = 1.5\ W_p\ R\ T_{MAX} \left(\frac{\rho}{\sigma}\right)_{MAT} (S.F.)$$

Combining equations (3) and (7) into (1) and rearranging for the total subsystem weight results in

(8) $$W_{SYSTEM} = I_T \left[\frac{(1+\alpha_p)\left\{1.0 + 1.5\ R\ T_{MAX}\left(\frac{\rho}{\sigma}\right)_{MAT} (S.F.)\right\}}{I_{sp}\left\{1 - \left(\frac{P_f}{P_i}\right)\left(\frac{T_i}{T_f}\right)\right\}}\right] + W_{COM}$$

Equation (8) is a linear equation of the slope-intercept form with the slope represented by the bracketed [ ] quantity. For a given I_T and W_{com}, the subsystem weight will be a minimum for that propellant and tank material combination which yields a minimum slope value.